frontiers | Research Topics

# Immune mechanisms of protection against Mycobacterium tuberculosis

**Edited by**
Rhea Coler, Sarah Fortune, Willem Henry Boom and JoAnne L. Flynn

**Published in**
Frontiers in Immunology

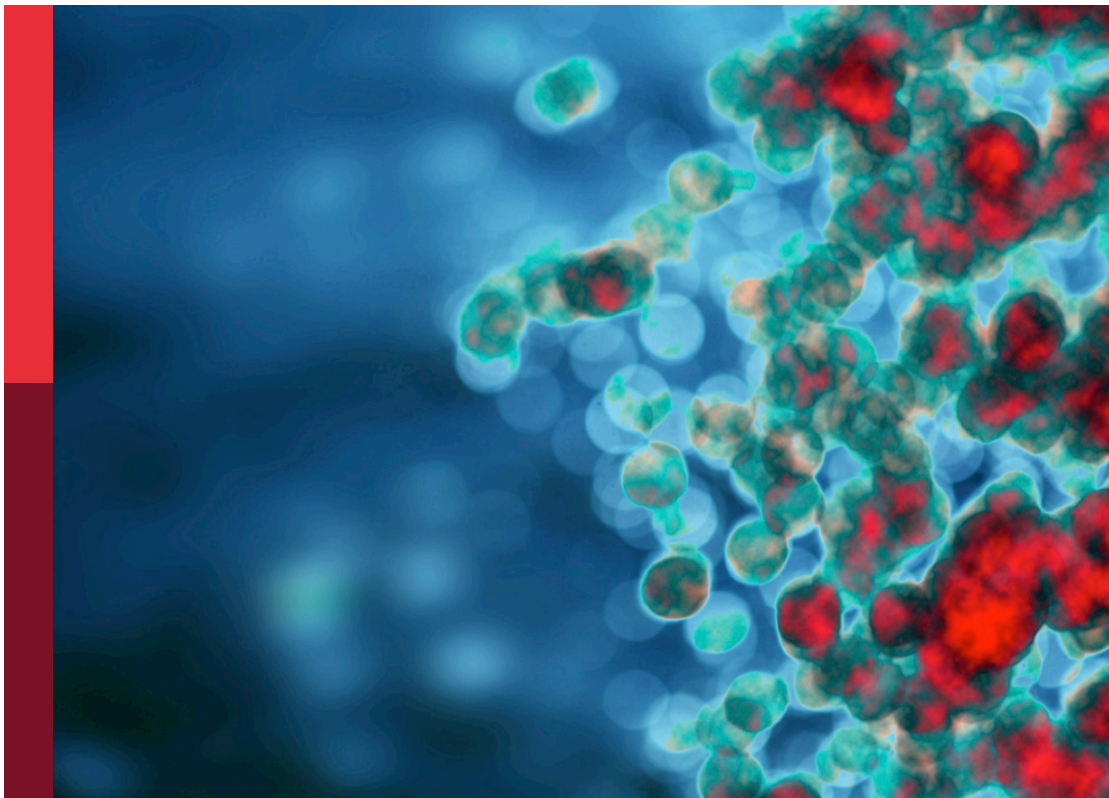

ISSN 1664-8714
ISBN 978-2-8325-6500-1
DOI 10.3389/978-2-8325-6500-1

**Generative AI statement**
Any alternative text (Alt text) provided alongside figures in the articles in this ebook has been generated by Frontiers with the support of artificial intelligence and reasonable efforts have been made to ensure accuracy, including review by the authors wherever possible. If you identify any issues, please contact us.

## About Frontiers

Frontiers is more than just an open access publisher of scholarly articles: it is a pioneering approach to the world of academia, radically improving the way scholarly research is managed. The grand vision of Frontiers is a world where all people have an equal opportunity to seek, share and generate knowledge. Frontiers provides immediate and permanent online open access to all its publications, but this alone is not enough to realize our grand goals.

## Frontiers journal series

The Frontiers journal series is a multi-tier and interdisciplinary set of open-access, online journals, promising a paradigm shift from the current review, selection and dissemination processes in academic publishing. All Frontiers journals are driven by researchers for researchers; therefore, they constitute a service to the scholarly community. At the same time, the *Frontiers journal series* operates on a revolutionary invention, the tiered publishing system, initially addressing specific communities of scholars, and gradually climbing up to broader public understanding, thus serving the interests of the lay society, too.

## Dedication to quality

Each Frontiers article is a landmark of the highest quality, thanks to genuinely collaborative interactions between authors and review editors, who include some of the world's best academicians. Research must be certified by peers before entering a stream of knowledge that may eventually reach the public - and shape society; therefore, Frontiers only applies the most rigorous and unbiased reviews. Frontiers revolutionizes research publishing by freely delivering the most outstanding research, evaluated with no bias from both the academic and social point of view. By applying the most advanced information technologies, Frontiers is catapulting scholarly publishing into a new generation.

## What are Frontiers Research Topics?

Frontiers Research Topics are very popular trademarks of the *Frontiers journals series*: they are collections of at least ten articles, all centered on a particular subject. With their unique mix of varied contributions from Original Research to Review Articles, Frontiers Research Topics unify the most influential researchers, the latest key findings and historical advances in a hot research area.

Find out more on how to host your own Frontiers Research Topic or contribute to one as an author by contacting the Frontiers editorial office: frontiersin.org/about/contact

# Immune mechanisms of protection against Mycobacterium tuberculosis

**Topic editors**

Rhea Coler — University of Washington, United States

Sarah Fortune — Harvard University, United States

Willem Henry Boom — Case Western Reserve University, United States

JoAnne L. Flynn — University of Pittsburgh, United States

**Citation**

Coler, R., Fortune, S., Boom, W. H., Flynn, J. L., eds. (2025). *Immune mechanisms of protection against Mycobacterium tuberculosis*. Lausanne: Frontiers Media SA.

doi: 10.3389/978-2-8325-6500-1

*The Topic Editors [RC, SF, WB, JF] declare that they are supported by the NIH on this IMPAc-TB collaboration.*

# Table of contents

frontiers | Frontiers in Immunology

TYPE Original Research
PUBLISHED 28 June 2024
DOI 10.3389/fimmu.2024.1427846



OPEN ACCESS

EDITED BY
Angelo Izzo,
Royal Prince Alfred Hospital, Australia

REVIEWED BY
Andreas Kupz,
James Cook University, Australia
Brian Weinrick,
Trudeau Institute, United States
Tuhina Gupta,
University of Georgia, United States

*CORRESPONDENCE
Benjamin H. Gern
benjamin.gern@seattlechildrens.org
Alan H. Diercks
alan.diercks@seattlechildrens.org
Kevin B. Urdahl
kevin.urdahl@seattlechildrens.org

†These authors share first authorship

RECEIVED 04 May 2024
ACCEPTED 13 June 2024
PUBLISHED 28 June 2024

CITATION
Cohen SB, Plumlee CR, Engels L, Mai D, Murray TA, Jahn AN, Alexander B, Delahaye JL, Cross LM, Maciag K, Schrader S, Durga K, Gold ES, Aderem A, Gerner MY, Gern BH, Diercks AH and Urdahl KB (2024) Host and pathogen genetic diversity shape vaccine-mediated protection to *Mycobacterium tuberculosis*. *Front. Immunol.* 15:1427846. doi: 10.3389/fimmu.2024.1427846



# Host and pathogen genetic diversity shape vaccine-mediated protection to *Mycobacterium tuberculosis*

Sara B. Cohen[1†], Courtney R. Plumlee[1†], Lindsay Engels[1], Dat Mai[1], Tara A. Murray[1], Ana N. Jahn[1], Bridget Alexander[1], Jared L. Delahaye[1], Lauren M. Cross[1], Karolina Maciag[1,2], Sam Schrader[1], Kaitlin Durga[1], Elizabeth S. Gold[1], Alan Aderem[1,3], Michael Y. Gerner[4], Benjamin H. Gern[1,3*], Alan H. Diercks[1*] and Kevin B. Urdahl[1,3*]

[1]Seattle Children's Research Institute, Center for Global Infectious Disease Research, Seattle, WA, United States, [2]Department of Medicine, Division of Infectious Diseases, University of Washington, Seattle, WA, United States, [3]Department of Pediatrics, University of Washington, Seattle, WA, United States, [4]Department of Immunology, University of Washington, Seattle, WA, United States

To investigate how host and pathogen diversity govern immunity against *Mycobacterium tuberculosis* (Mtb), we performed a large-scale screen of vaccine-mediated protection against aerosol Mtb infection using three inbred mouse strains [C57BL/6 (B6), C3HeB/FeJ (C3H), Balb/c x 129/SvJ (C129F1)] and three Mtb strains (H37Rv, CDC1551, SA161) representing two lineages and distinct virulence properties. We compared three protective modalities, all of which involve inoculation with live mycobacteria: Bacillus Calmette-Guérin (BCG), the only approved TB vaccine, delivered either subcutaneously or intravenously, and concomitant Mtb infection (CoMtb), a model of pre-existing immunity in which a low-level Mtb infection is established in the cervical lymph node following intradermal inoculation. We examined lung bacterial burdens at early (Day 28) and late (Day 98) time points after aerosol Mtb challenge and histopathology at Day 98. We observed substantial heterogeneity in the reduction of bacterial load afforded by these modalities at Day 28 across the combinations and noted a strong positive correlation between bacterial burden in unvaccinated mice and the degree of protection afforded by vaccination. Although we observed variation in the degree of reduction in bacterial burdens across the nine mouse/bacterium strain combinations, virtually all protective modalities performed similarly for a given strain-strain combination. We also noted dramatic variation in histopathology changes driven by both host and bacterial genetic backgrounds. Vaccination improved pathology scores for all infections except CDC1551. However, the most dramatic impact of vaccination on lesion development occurred for the C3H-SA161 combination, where vaccination entirely abrogated the development of the large necrotic lesions that arise in unvaccinated mice. In conclusion, we find that substantial TB heterogeneity can

be recapitulated by introducing variability in both host and bacterial genetics, resulting in changes in vaccine-mediated protection as measured both by bacterial burden as well as histopathology. These differences can be harnessed in future studies to identify immune correlates of vaccine efficacy.

KEYWORDS

tuberculosis, vaccine, heterogeneity, genetics, protection

## Introduction

Tuberculosis (TB), caused by the bacterium *Mycobacterium tuberculosis* (Mtb), remains a leading cause of morbidity and mortality across the globe (1), despite introduction of the Bacille Calmette-Guérin (BCG) vaccine over a century ago. BCG continues to be used in many countries due to its ability to curb disease, especially disseminated disease, in infants (2), yet it has unfortunately shown mixed efficacy at preventing pulmonary TB among adults, ranging from 0–80% (3–5). In the most commonly used mouse model of TB, C57BL/6 (B6) mice are aerosol-infected with ~50–100 colony-forming units (CFU) of lineage 4 Mtb (typically either H37Rv or Erdman). In this model, BCG immunization reliably reduces the pulmonary bacterial load by approximately 1 log at 4 weeks following infection, but this protection often wanes over time (6–8). However, the translational relevance of this pattern of protection remains unclear. Human TB disease often presents with a classic necrotizing granuloma, a feature that is notoriously absent in B6 mice, and yet pulmonary TB in humans is far more heterogeneous than often appreciated, with pathological features ranging from necrotic granulomas, non-necrotic granulomas, to pneumonia-like alveolitis (9). Despite known drawbacks of the mouse model (10), it remains an essential tool by providing opportunities for mechanistic study, and its relatively low cost enables larger scale experiments. To improve the model, we seek to better reflect the heterogeneity of human disease and provide a more robust platform for preclinical vaccine testing. To this end, we have introduced heterogeneity into the mouse model at multiple levels, including three host strains, three bacterial strains, and three protective modalities.

Host genetics are strong determinants of bacterial burden, pathology, and vaccine outcome. This has been highlighted by several studies (11–14), including a panel of subcutaneous (SC) BCG-vaccinated collaborative cross (CC) mice, where only half of the host strains showed significant reductions in lung CFU as a result of vaccination (15), and intravenous (IV) BCG-immunized diversity outbred (DO) mice, in which a wide range of CFU, survival outcomes, and pathology features was observed (16, 17). In our study, three mouse strains were included due to their broad range of responses to infection with Mtb. B6 mice can survive at least 1 year following aerosol challenge; this relative resistance to Mtb infection is thought to be at least partially due to inherent Th1 skewing and results in immunopathology characterized by diffuse lesions that lack the cellular organization of human granulomas (18). Despite this, the use of B6 mice offers an abundance of molecular tools, including transgenic and gene-knockout strains. C3HeB/FeJ (C3H) mice have high pulmonary bacterial loads and can form classical necrotizing granulomas with central caseation and hypoxia, as observed in advanced human TB disease, due at least in part to their high levels of type I interferons (19–21). The C129F1 line was generated by crossing Balb/c mice, which offer mechanistic tools, and 129/SvJ mice, which are relatively susceptible to Mtb compared to B6 mice, with poor survival outcomes (18, 22).

Mtb strain-specific properties also contribute to the heterogeneous outcomes of infection. First, different Mtb strains can elicit a range of distinct immune responses (23, 24). Second, different Mtb strains can predispose to varying patterns of cellular and tissue organization. For example, H37Rv infection of B6 mice results in disorganized lesions with intermixed macrophages and lymphocytes, while HN878 infection results in organized lesions with prominent B cell aggregates (25). Third, strains from different Mtb lineages can have varying impacts on vaccine-mediated immunity (26). We focused on lineages 2 and 4, which are considered the most pathogenic of all Mtb lineages (27). Lineage 4 (North American/European), the most geographically distributed lineage (28), is actually found on all continents, although the underlying mechanisms of its success as a human pathogen remain poorly understood. Lineage 2 (W-Beijing) strains are often associated with increased transmission and, accordingly, are growing in global distribution (29). Here, we incorporate bacterial heterogeneity by using three Mtb strains with divergent pathogenicity and immunogenicity: 1) H37Rv, a well-characterized lineage 4 strain that is commonly used for experimental studies; 2) CDC1551, a lineage 4 strain that is hyperimmunogenic but relatively low in virulence (30); and 3) SA161, a lineage 2 clinical isolate that is hypoimmunogenic and hypervirulent (31).

Finally, we examined three modes of protection (hereafter referred to as "vaccination" for simplicity). We immunized mice with BCG using two different routes: SC or IV. Despite the limitations of BCG and its varying efficacy in humans, more recent data have renewed interest in dissecting the mechanisms of protection it elicits in the limited settings where it is effective. For example, high-dose IV BCG was recently shown to confer superior

protection to intradermal (ID) BCG in non-human primates (NHP) challenged with low-dose aerosolized Mtb (32), which correlated with increased airway-resident T cells and NK cells (33). Furthermore, BCG can prevent detectable infection in a small percentage of mice infected with an ultra-low dose (ULD) of aerosolized Mtb (8). Thus, understanding how and when BCG is effective could greatly advance our understanding of TB protective immunity. The third modality of protection included in our screen is the concomitant Mtb (CoMtb) model, in which a small ($10^4$) inoculum of virulent H37Rv is administered ID to the ear (7). Inoculated bacteria are trafficked to the draining cervical lymph node where they persist for at least a year, without significant dissemination to the lung. Upon challenge with aerosolized Mtb, CoMtb mice display ~1–2 logs of protection that endures at least 4 months following infection. While not a true vaccine, this model is consistent with several observations that natural immunity induced by prior infection with Mtb itself can mediate protection against human TB disease. First, post-mortem studies observed that individuals with evidence of lymph node disease were less likely to have pulmonary TB (34). Second, nursing students who entered TB-endemic clinical settings with a positive tuberculin skin test (TST) were less likely to develop active TB disease than their classmates who were TST-negative, suggesting that pre-existing, subclinical infection with Mtb can provide protection against developing disease (35).

Altogether, this study examined 36 combinations of mouse strains, bacterial strains, and protective modalities, in which we assessed pulmonary bacterial burdens across time points (early, Day 28; and late, Day 98) and histopathology at Day 98. For most host/bacterial strain combinations, we found similar reductions in bacterial load across vaccine modalities. Histopathological analysis showed that vaccination variably impacted pathologic features, and bacterial burden at the early peak of infection was a better predictor of late pathological outcomes than bacterial burden measured at late time points. These results suggest that examination of vaccine responses in a single host/bacteria genetic background is likely insufficient to predict outcomes in heterogeneous human populations and highlight the importance of measuring both bacterial burdens and pathology when assessing the effectiveness of TB vaccines in animal models.

# Materials and methods

## Mice

C57BL/6J (B6, #000664) and C3HeB/FeJ (C3H, #000658) mice were purchased from Jackson Laboratories (Bar Harbor, ME). Balb/c x 129/SvJ (C129F1) mice were a custom breeding order from Jackson Laboratories (Bar Harbor, ME). Female mice between the ages of 9–12 weeks were used. All animals were housed and maintained in specific-pathogen-free conditions at Seattle Children's Research Institute (SCRI). All animal studies were performed in compliance with the SCRI Animal Care and Use Committee.

## BCG immunizations

BCG-Pasteur was cultured in Middlebrook 7H9 with OADC supplement and 0.05% Tween-80 at 37°C with constant agitation for five days. BCG was back diluted in 7H9 for two days and grown to an OD of 0.2–0.5. Bacteria was diluted in PBS and mice were injected subcutaneously (SC) or intravenously (IV) with 200µl of $10^6$ CFU. After immunization, mice were rested for 8 weeks prior to Mtb infection.

## Concomitant Mtb model

The CoMtb model was established as described previously (7, 36). Briefly, mice were first anesthetized by intraperitoneal injection of ketamine and xylazine diluted in PBS. Mice were placed in a lateral recumbent position, and the ear pinna was flattened with forceps and pinned onto an elevated dissection board using a 22 G needle. H37Rv Mtb grown to an OD between 0.2–0.5 over a 48-hour period was diluted to $10^6$ CFU/ml in PBS, and 10 ul ($10^4$ CFU) was administered into the dermis of the ear using a 26s G Hamilton syringe. Mice were then rested for 8 weeks prior to Mtb infection.

## Mtb aerosol infections

Infections were done with stocks of H37Rv, SA161 or CDC1551 as previously described (37). To perform aerosol Mtb infections, mice were placed in a Glas-Col aerosol infection chamber, and 50–100 CFU were deposited into their lungs. To confirm the infectious inoculum, two mice per infection were euthanized on the same day of infection, and their lungs were homogenized and plated onto 7H10 or 7H11 plates for determination of CFU.

## CFU plating

Right lungs were homogenized in M tubes (Miltenyi) containing 1mL PBS+0.05% Tween-80 (PBS-T) using a GentleMACS machine (Miltenyi). Homogenates were then diluted in PBS-T and plated onto 7H10 plates. Plates were incubated at 37°C for at least 21 days before quantification of CFU.

## Histology

Left lungs were fixed in 10% formalin for 24 hours, then dehydrated in 70% ethanol at 4°C for at least 24 hours. Samples were paraffin embedded and sectioned at the University of Washington Histology Core. Subsequently, slides were reviewed by a veterinary pathologist and scored in a blinded fashion based on the following metrics (see Supplementary Table 2): mixed granulomas (ill-formed granulomas with mixture of macrophages and lymphocytes), defined granulomas [well defined with increased separation of macrophages, epithelioid or multinucleated giant cells (MNGC) with lymphoid aggregates], perivascular lymphoid aggregates (PV LA),

peribronchiolar lymphoid aggregates (PB LA), histiocytes, foamy macrophages, MNGC, alveolar hyperplasia, neutrophils, necrosis, cholesterol clefts, edema, extent 1 (percent involvement of the lung), extent 2 (percent involvement of the lung in the worst manner).

# Results

## Most vaccine modalities provide early protection against Mtb challenge, but the durability of protection varies according to host and bacterial strain

As an initial, quantitative measure of the degree and durability of protection afforded by each vaccine modality across the strain-strain combinations, we measured lung CFU burden at Day 28 and Day 98 following infection (Figure 1). Among unvaccinated mice at Day 28, we observed a wide range of outcomes, with bacterial loads differing by over 100-fold. For example, infection with H37Rv resulted in the highest CFU burden among C129F1 mice, (Figure 1A), while infection with SA161 yielded the highest CFU burden among C3H mice (Figure 1B); however, these two strains of mice responded with similar CFU burdens after infection with CDC1551 (Figure 1C). Across Mtb strains, B6 mice developed the lowest CFU burdens among the host genotypes at Day 28 (Figures 1A–C), while C3H mice infected with SA161 developed the highest overall lung burden across both time points (Figures 1B, E). There was much less heterogeneity in burdens among unvaccinated mice at Day 98, with equivalent loads across all genotypes in response to H37Rv (Figure 1D) and SA161 (Figure 1E). Infection with CDC1551 resulted in significantly higher lung bacterial loads in C3H mice than in the other mouse

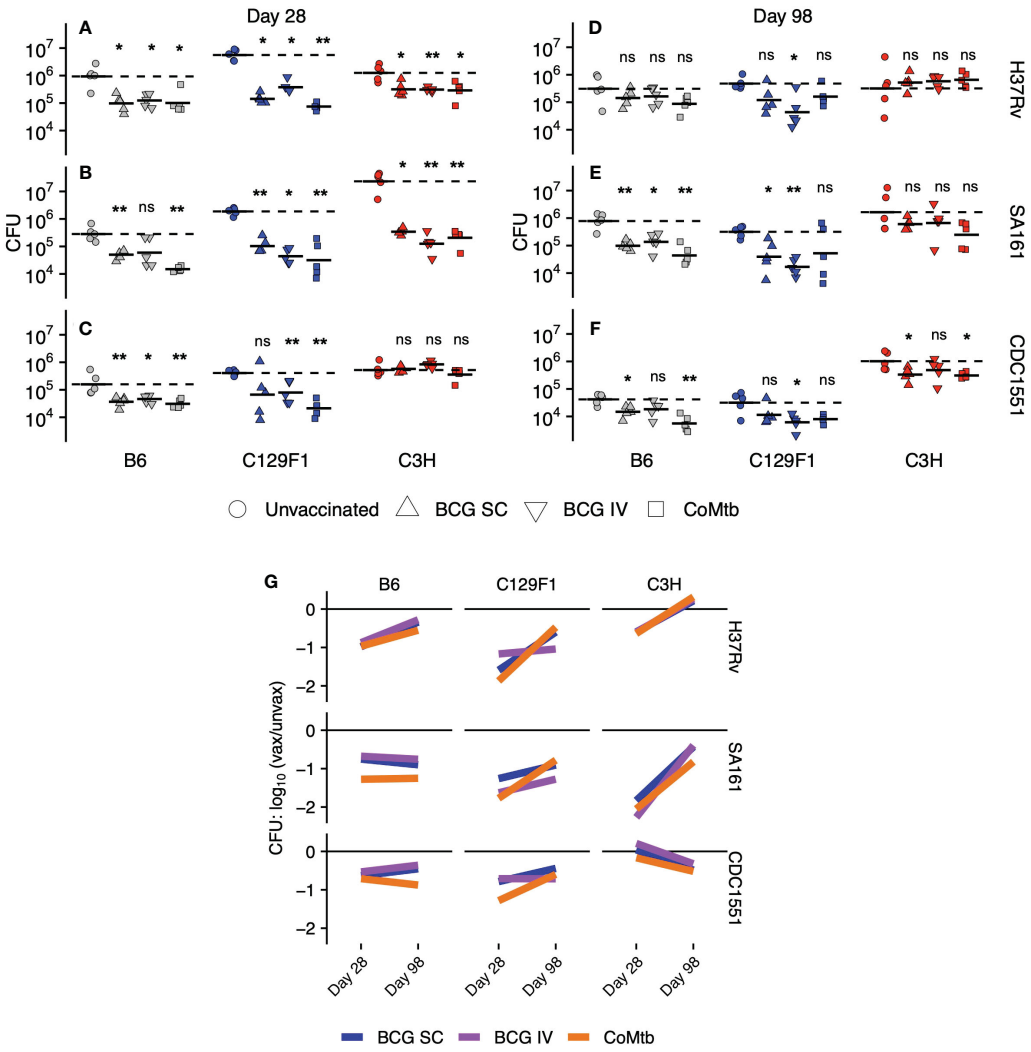


FIGURE 1
Lung bacterial burdens following vaccination across strain combinations. Right lungs were excised from C57BL/6 (B6), C3HeB/FeJ (C3H), and 129/SvJxBalb/c (C129F1) mice administered BCG [subcutaneous (SC) or intravenous (IV)] or intradermal concomitant Mtb (CoMtb) for 8 weeks and then aerosol-challenged with H37Rv, SA161, or CDC1551 Mtb for either **(A–C)** 28 days or **(D–F)** 98 days. Lungs were homogenized and plated for CFU enumeration. **(G)** Cumulative CFU data are plotted as a log change over unvaccinated for each host-bacterial strain combination over time. Statistical comparisons were performed by non-parametric Wilcoxon ranked test, with *, p<0.05; **, p<0.01; ns, not significant.

strains at the late (Figure 1F) but not early (Figure 1C) timepoint, suggesting that, even at late time points, we can identify differential responses to Mtb infection across combinations.

As expected from prior reports of vaccine-mediated immunity in the B6 mouse model (6–8, 38), lung bacterial burdens in B6 mice were significantly reduced at Day 28 by all vaccine modalities following challenge with all bacterial strains (Figures 1A–C), with the exception of IV BCG with SA161 challenge, where a high variability in CFU burden was seen (Figure 1B). The C129F1 mice behaved similarly to B6 mice based on CFU reductions following all vaccine modalities in response to all challenge strains. Unvaccinated C129F1 mice had particularly high bacterial loads, but these burdens were reduced to similar levels as B6 mice following vaccination (Figures 1A–C). In contrast to both B6 and C129F1 mice, C3H mice displayed a wide range of vaccine-mediated responses at Day 28 (Figures 1A–C). Unexpectedly, these mice were not protected from CDC1551 challenge by any vaccine modality at this time point (Figure 1C), whereas all modalities resulted in approximately 0.6-log CFU reduction upon H37Rv challenge (Figure 1A) and up to 2-log CFU reduction upon SA161 challenge (Figure 1B) (Supplementary Table 1). Overall, at Day 28, 22/27 (81.4%) strain-strain combinations resulted in significant decreases in lung CFU. At Day 98, however, CFU reduction in response to vaccination was only seen in 11/27 (40.7%) combinations. Some strain-strain combinations failed to display any vaccine-mediated reduction in bacterial load at Day 98, such as B6 and C3H mice infected with H37Rv (Figure 1D) and C3H mice infected with SA161 (Figure 1E). Among strain combinations that were protected at Day 98, there was heterogeneity associated with vaccine modality. For example, IV BCG mediated substantial protection in C129F1 mice infected with H37Rv (Figure 1D) and CDC1551 (Figure 1F), whereas SC BCG and CoMtb did not (Figures 1D, F).

We next plotted lung CFU in vaccinated vs unvaccinated mice within each strain-strain combination at each time point to visualize trends in the long-term durability of vaccine-mediated protection (Figure 1G). Among all strain-strain combinations, the magnitude of protection generally decreased over time [6/9 (B6-H37Rv, C129F1-H37Rv, C3H-H37Rv, C129F1-SA161, C3H-SA161, C129F1-CDC1551), 67%]; however, in some cases it stayed constant [2/9 (B6-SA161, B6-CDC1551), 22%] or even increased [1/9 (C3H-CDC1551), 11%]. While we noted heterogeneity in vaccine-mediated outcomes across strain-strain combinations and time points, as described in Figures 1A–F, there was a striking overlap in the behavior of the three protective modalities within most combinations. Thus, while bacterial and host strain diversity had a large overall impact on vaccine-mediated outcomes, the vaccines themselves contributed relatively little to the observed heterogeneity. For example, we observed similar initial log reductions in CFU followed by waning protection over time, as visualized by a positive slope, for B6 mice infected with H37Rv for all 3 modalities. Surprisingly, in the C3H/SA161 group, which was the most strongly protected combination at Day 28, none of the vaccines were able to mediate protective efficacy at the later time point. In contrast, durable protection across vaccine modalities, as visualized by a slope of ~0, was only seen in the B6/SA161 and B6/CDC1551 combinations. We found this was also true for almost all vaccines in C129F1 and C3H mice challenged with H37Rv (Figure 1G). The only example of improved protection over time, as indicated by a negative slope, was C3H mice challenged with CDC1551, although this combination failed to show evidence of vaccine efficacy at the early time point.

As previously noted, unvaccinated C3H mice infected with SA161 developed the highest bacterial burdens of any strain-strain combination at Day 28, peaking at loads approximately 1-log higher than in either B6 or C129F1 mice (Figure 1B). Furthermore, this combination demonstrated the strongest vaccine-mediated reduction in lung CFU at Day 28 of ~2 logs (Supplementary Table 1). To address whether early bacterial load in unvaccinated mice correlated with vaccine-mediated CFU reduction across strain-strain combinations, we plotted the log fold-change of CFU upon vaccination against the lung CFU of unvaccinated mice (Figure 2A). This analysis confirmed a

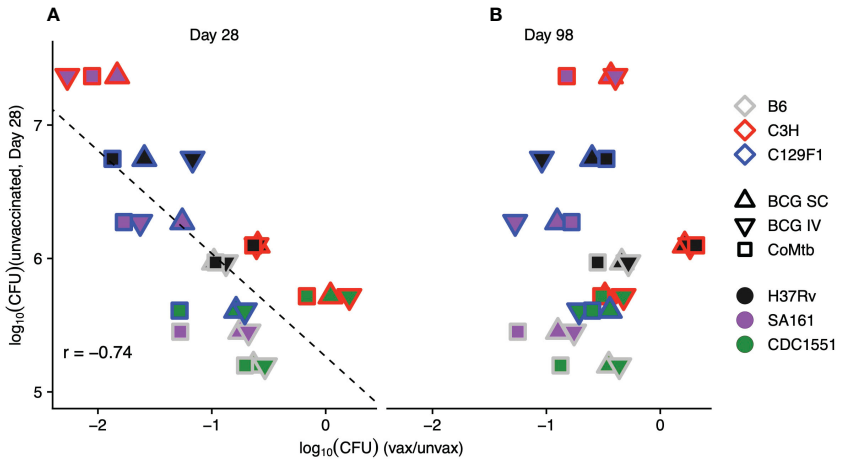


FIGURE 2
The magnitude of vaccine-induced reduction in bacterial load correlates with initial burden in unvaccinated mice. The average log reduction in CFU for each mouse strain/protective modality/bacterial strain combination at Day 28 **(A)** and Day 98 **(B)** is plotted against the bacterial burden for each mouse strain/bacterial strain combination in unvaccinated mice at Day 28. Each point represents the average of 5 mice/condition. Outline colors represent mouse strain, fill colors represent bacterial strain, and shapes represent protective modality.

correlation (r=-0.74) between the initial bacterial load at Day 28 in unvaccinated mice and vaccine-induced reduction in bacterial load. This correlation was not observed at the late, Day 98 time point (Figure 2B), suggesting that the protective mechanisms induced by vaccination may be more effective at curbing rapid bacterial growth early during infection than in reducing bacterial burden in an established infection.

We next ranked the protective efficacy of each vaccine modality in each strain-strain combination in order of its lung CFU burden in vaccinated vs unvaccinated mice at Day 28 (Figure 3A). These data underscore the broad range of magnitudes of vaccine-mediated protection at early time points across strain-strain combinations, with bacterial load reductions ranging from 0 to >2 logs, highlighting the critical role of host and pathogen diversity in modulating vaccine outcomes (Figure 3A). In contrast, the combinations at Day 98 were largely restricted to between 0 and <1 log of protection, highlighting both the limited range of responses and overall waning of protection at later time points (Figure 3B). Importantly, the disordered nature of vaccine efficacy at Day 98 (Figure 3B) when ranked by vaccine efficacy at Day 28 (Figure 3A) illustrates the inability of early protective responses to predict late vaccine-mediated protection. This heterogeneity in vaccine outcomes that emerges upon incorporating host and genetic diversity underscores the limitations of traditional animal model vaccine testing that solely relies on the standard B6/H37Rv strain combination.

## Pathological changes are driven by host and bacterial diversity

At the Day 98 time point, a time at which lesions have fully developed, the left lung was preserved in formalin for hematoxylin and eosin (H&E) staining and histopathologic analysis. The following features were assessed: extent, mixed granulomas, defined granulomas, perivascular lymphoid aggregates, peribronchial lymphoid aggregates, histiocytes, multinucleated giant cells (MNGC), neutrophils, alveolar hyperplasia, necrosis, cholesterol clefts, and edema (Supplementary Table 2). Representative H&E images from unvaccinated mice that embody clear histological patterns are shown in Figure 4. B6 mice infected with H37Rv had moderate involvement with disorganized lesions (Figure 4A), C3H mice infected with CDC1551 had extensive involvement with MNGC (Figure 4B), and C129F1 mice infected with H37Rv had a high degree of lung involvement driven by lymphoid aggregates (Figure 4C). Consistent with reports that C3H mice develop caseating granulomas more typical of primary TB granulomas seen in humans (19, 21, 39), C3H mice infected with SA161 displayed distinctive granuloma structures defined by overwhelming necrosis and neutrophil infiltration (Figure 4D). This strain combination reached the highest bacterial burdens at the Day 28 time point, nearly 1 log higher than all other combinations (Figure 1B), suggesting that early bacterial burdens can drive pathology at later time points. To gain insight into the pathological features driving lesion structure in each genotype, we performed a principal component analysis (PCA) using all scored pathology variables for all mice (Supplementary Table 2), first showing unvaccinated mice for simplicity (Figure 4E). By examining the PCA loading scores, we found that individual pathological features tended to group into 4 distinct categories: Defined, Necrosis, Extent, and Lymphoid aggregates (Figure 4F). For unvaccinated mice, we found that variation in PCA scores was largely driven by mouse strain, and to a lesser extent by bacterial strain (Figure 4E). Overall, C3H mice clustered separately from B6 and C129F1 mice, typified by a high extent of involvement and the presence of neutrophils (Figures 4B, E, F). Conversely, C129F1 mice

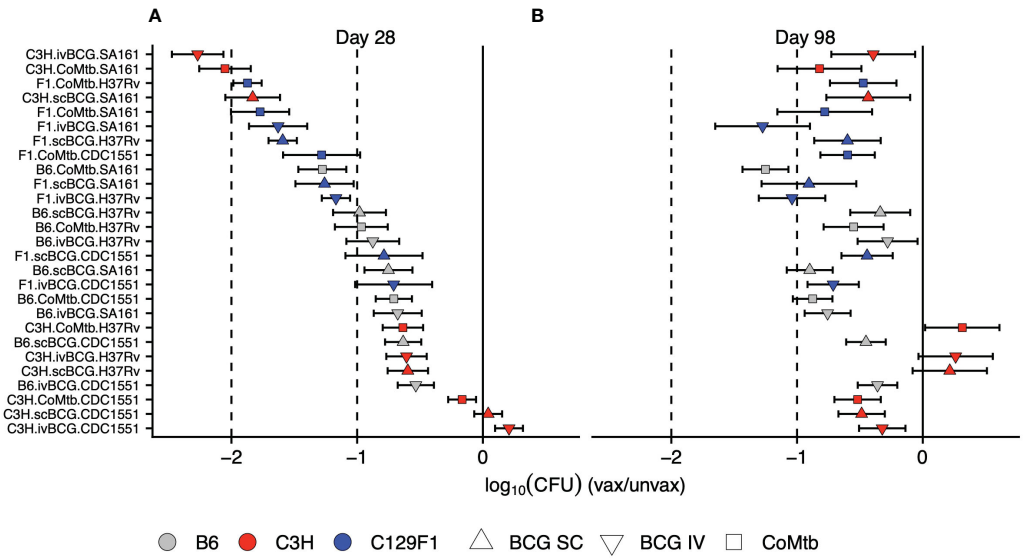


FIGURE 3
Early vaccine-mediated reductions in bacterial load do not predict late outcomes. The strain-strain combinations were ranked in order of highest vaccine-mediated reduction in bacterial load at **(A)** Day 28 post-infection. Keeping the same order, these combinations were then plotted to include the Day 98 log reductions in bacterial burden **(B)**.

10.3389/fimmu.2024.1427846

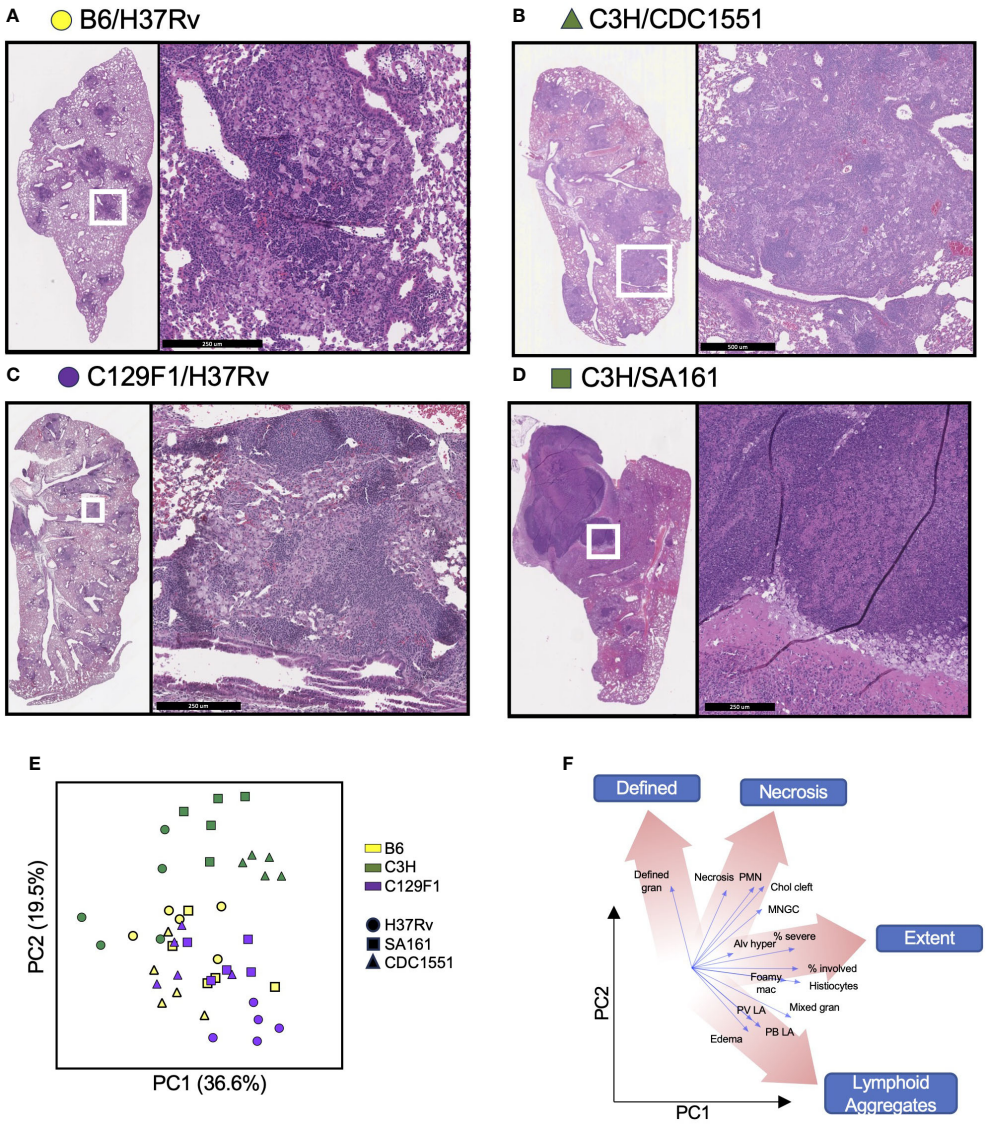


FIGURE 4
Mouse strains present a range of histopathological features upon infection with different Mtb strains. The left lung of mice was preserved in formalin at Day 98 post-Mtb infection and subjected to hematoxylin and eosin (H&E) staining to observe 14 histopathological features, which were graded in a blinded fashion by a licensed pathologist. **(A–D)** Representative sections from each strain of mouse is shown to illustrate the varying histological presentations. **(E)** Cumulative scores were used to generate a principal component analysis (PCA) encompassing all unvaccinated mice infected with each Mtb strain, with **(F)** different regions representing a predominance of certain pathological features.

contained lymphocyte-rich lesions with prominent peribronchial and perivascular aggregates (Figures 4C, E, F). Lastly, B6 mice largely fell near the center of the PCA plot, consistent with the lack of prominent scored features and the presence of disorganized lesions, with histiocytes intermixed with loose lymphoid regions (Figures 4A, E, F).

## The ability of vaccine modalities to improve pathology outcomes is dependent on both host and bacterial strain

To determine how the different vaccine modalities impacted pathology outcomes, we included data points from vaccinated mice onto the PCA plot, and separated them for each mouse strain to facilitate visualization (Figure 5A). For B6 mice, there was large overlap in pathology outcomes regardless of bacterial strain or vaccination regimen. In C3H mice, CDC1551 infection led to pathology scores that clustered in a region of the plot associated with higher lesion extent, regardless of vaccine strategy, while both H37Rv and SA161 infection resulted in a wide range in pathology scores depending on vaccination modality. In C129F1 mice, Mtb strain, but not vaccination modality, was the most significant driver of outcome along these principal components (Figure 5A). To gain insight into the vaccine-mediated changes in pathology in individual strain-strain combinations, we examined the relevant subset of data points from the PCA plot alongside representative H&E images from Day 98 (Figures 5B–E; Supplementary Figure 1; Supplementary Table 2). Several of the most striking combinations

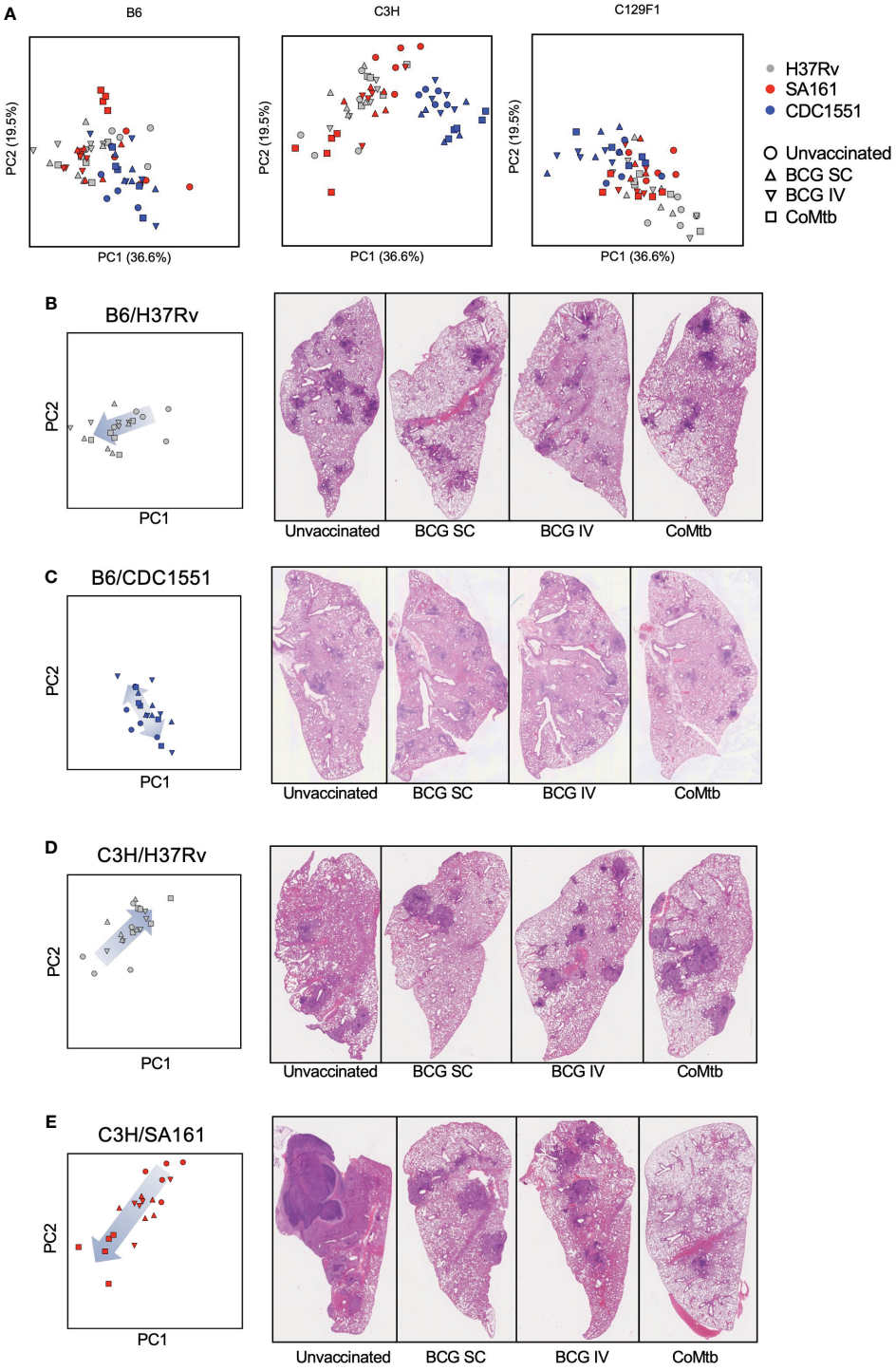


FIGURE 5
Distinct strain-strain combinations result in unique vaccine-mediated histological changes. **(A)** The same PCA plot shown in Figure 4 is now displayed separately for each mouse strain and includes vaccinated cohorts, with color depicting bacterial strain and shape depicting protective modality. **(B–E)** Shown are representative Day 98 H&E images for select strain-strain combinations of interest, alongside their associated PCA plots. The arrows indicate the change in direction of samples within the PCA plot following vaccination.

are shown in Figure 5. For the B6/H37Rv combination, all vaccine modalities resulted in modest yet clear changes in pathology scores, largely driven by decreased extent of lung involvement and lesion definition, with the arrow indicating a shift from greater to lesser involvement with vaccination (Figure 5B). For B6 mice infected with CDC1551, histologic features were similar regardless of vaccination and were marked by poorly defined lesions and abundant myeloid aggregates (Figure 5C). In the C3H/H37Rv combination, there was an unexpected increase in involvement and degree of defined granulomas in vaccinated vs unvaccinated

mice (Figure 5D). This aligns with the complete lack of protection from bacterial burden in this combination at Day 98, and even a trend toward increased CFU upon vaccination (Figure 1D). Finally, in the C3H/SA161 combination, there was dramatic overall improvement in pathology resulting from all vaccine modalities; the large necrotic granulomas observed in the unvaccinated group were absent in vaccinated mice (Figure 5E). CoMtb-inoculated C3H mice infected with SA161 had the largest reversal in degree of lesion extent, scoring lower than either BCG-immunized cohort (Figure 5E). The remaining strain-strain combinations and their respective PCA plots and H&E images are shown in Supplementary Figure 1. Together, this shows that host and bacterial genetics play a significant role in determining the effect of vaccines on pathology, and that while vaccines appeared to improve pathology in most cases, they had no effect and potentially exacerbated pathology in certain strain-strain combinations.

## Correlations of pathology features and bacterial burden vary by host strain and time point

Given the diverse histologic outcomes noted across strain-strain combinations, we sought to determine whether any of these patterns directly associated with lung bacterial burden outcomes. To address this, we overlaid a heatmap of lung CFU values at Day 98 for each mouse genotype onto their respective subset of the histopathology score PCA plot (Figure 6). In B6 mice, there was an overall lack of correlation between bacterial burden and pathology features. In contrast, while high bacterial burdens in unvaccinated C3H/SA161 mice associated with necrosis, vaccination in this strain-strain combination led to both a decrease in CFU and a shift away from necrosis. No correlation was observed between histopathology PCA scores and either CFU or vaccination status for C3H/H37Rv mice, which otherwise overlapped with C3H/SA161 mice on the PCA plot. C3H/CDC1551 infection resulted in histopathology marked by high extent regardless of vaccination status. In C129F1 mice, infection with H37Rv was associated with both higher CFU and histopathology dominated by lymphoid aggregates, regardless of vaccination status or modality.

To more clearly identify the histopathologic features that correlate with CFU outcome among mouse strains across Mtb genotypes and vaccine modalities, we performed Spearman correlation analysis of each scored feature with either the mean CFU value for all mice with that genotype at Day 28 (because matching H&E images were not collected at Day 28) (Figure 7A) or the paired CFU at Day 98 (where individual CFU values had a matching histopathology score) (Figure 7B). Consistent with the CFU heatmap overlay in Figure 6, B6 histopathology scores did not correlate with CFU at either time point, suggesting that the histological presentation of these mice is a poor indicator of bacterial control. Interestingly, in C3H mice, Day 28 CFU significantly correlated with several histological features, including necrosis, neutrophils, defined granulomas, and extent; however, these features did not correlate with Day 98 CFU burden. In C129F1 mice, on the other hand, most histopathology features correlated

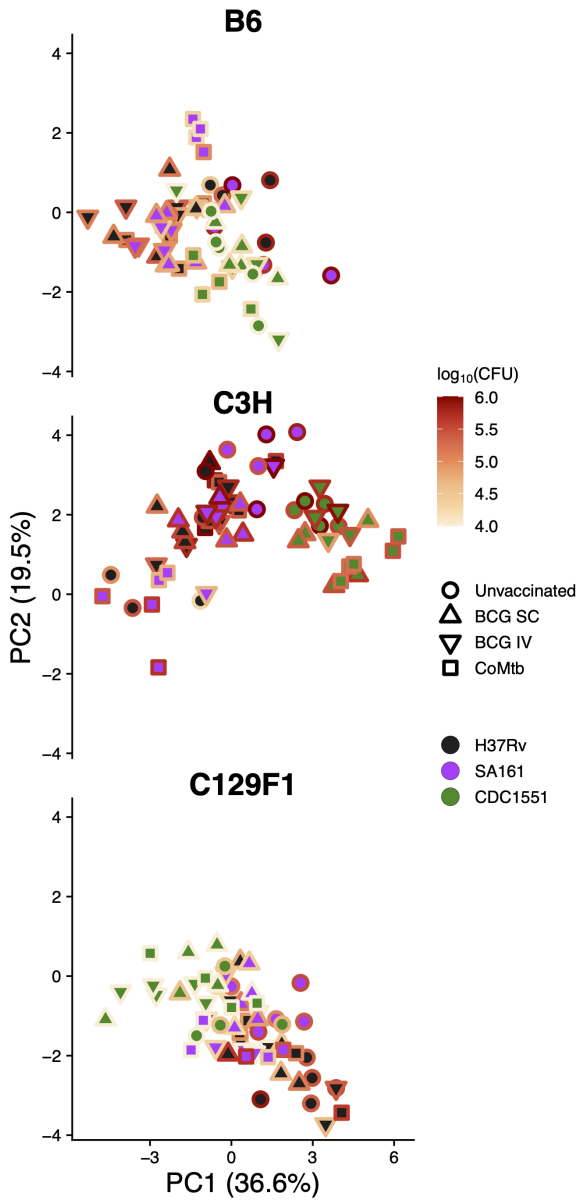


FIGURE 6
Pathology shows minimal correlation with bacterial burden late during infection. The PCA plots of histology scores separated by mouse genotype, as shown in Figure 5, were placed alongside the same plots now overlaid with the matched lung CFU value for each sample from Day 98, with dark colors representing lower bacterial CFU and bright colors representing higher bacterial CFU.

positively with CFU burden at both early and late time points, consistent with the observation that these mice retained a higher level of vaccine-induced protection at Day 98 (Figures 1D–F). Some correlative features were shared between C3H and C129F1 mice at Day 28, including mixed granulomas, MNGC, histiocytes, and extent 2, but certain features were uniquely correlated with bacterial load in each genotype. For example, burden in C3H mice uniquely correlated with neutrophils and necrosis, whereas burden in C129F1 uniquely correlated with both perivascular and peribronchial lymphocyte aggregates. Taken together, these data suggest that host genotypes display distinct pathological signatures,

10.3389/fimmu.2024.1427846

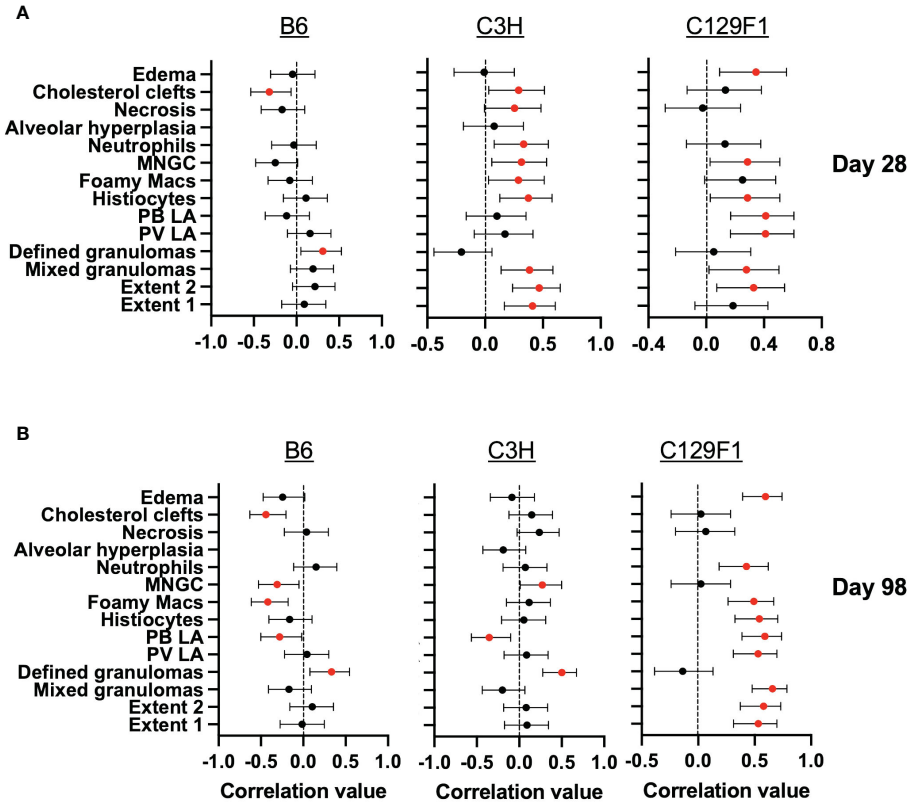


FIGURE 7
Late pathological features correlate more strongly with early than late bacterial burdens. Spearman correlation analysis was performed between histology scores for each pathology feature and lung bacterial burdens at **(A)** Day 28 and **(B)** Day 98 for each mouse genotype. For Day 98, the pathology scores and CFU values are paired, whereas for Day 28, we used the geometric mean of CFU from 5 mice per group to generate correlation values, since we did not have matched CFU values at this time point. Statistically significant correlations are shown in red ($p<0.05$).

and high CFU burden can be associated with a range of unique pathologic indicators.

## Discussion

The mouse remains the main small animal model for immunological research due to the extensive availability of molecular reagents, a large body of historical data, and relatively low cost. Much of our current understanding of TB immunology had its origins in the mouse model before subsequent validation in humans, i.e., the critical roles for CD4 T cells (40), IFNγ (41, 42), IL-12 (43), and TNFα (44). The mouse is also used extensively to test and mechanistically dissect vaccine-mediated protection against TB disease. The standard dose (SD) mouse model of Mtb infection, in which animals are infected with ~50–100 CFU, yields a highly reproducible course of disease that enables robust experimental designs using modest numbers of mice. However, the current mouse model for measuring vaccine-mediated immunity, like most experimental animal models, does not account for the extensive host and pathogen variation that is seen in humans. Another problem is that vaccine-induced reductions in bacterial burdens in mice infected with 50–100 CFU are modest (~1–2 logs) and usually transient, disappearing at later time points. In this study, we show that host and Mtb strains are more important in this model than the vaccines themselves, or their routes of delivery, in dictating outcomes. This contrasts with studies in the NHP model (32), where BCG-mediated protection was significantly enhanced upon intravenous BCG administration relative to subcutaneous. This raises questions about whether the mouse model truly is able to measure aspects of vaccine-induced immunity that are relevant to protection against human TB and may help explain why current mouse models have performed poorly in predicting vaccine efficacy outcomes in human trials. By identifying shortcomings of the mouse model, this study also provides opportunities to make adjustments for potential improvements. For example, future studies should test whether BCG given intravenously at higher doses might improve outcomes and better reflect findings in NHP. It is also possible that differences would emerge in IV BCG-immunized mice after challenge with a more physiologic Mtb challenge dose (8).

Across the 27 mouse strain/Mtb strain/vaccine combinations, the protective effect of the modalities tested, as measured by CFU burden at Day 28, ranged from over 100-fold to nil. However, protection at Day 28 did not correlate with bacterial control at Day 98, suggesting that assessing late time points in this model may be important. However, Day 98 measurements across all vaccinated conditions only reached approximately 0.5-log CFU reductions,

suggesting a limit to the achievable long-term protection in these models, and even this degree of reduction might potentially decrease further if even later time points were examined. Taken together with our observation that there were only a few instances of long-term protection and that these rarely exceeded 0.5-log CFU reduction at Day 98, the protective responses induced by BCG or CoMtb may be most effective at restraining rapidly growing bacteria during the first few weeks after infection. Indeed, across the mouse strain/Mtb strain combinations tested, the magnitude of vaccine-mediated protection at Day 28 was inversely correlated with the bacterial burden in unvaccinated mice, independent of protective modality. This is consistent with a previous finding that Mtb strains with the most robust growth *in vivo* at Day 28 were also the most restricted by BCG vaccination (45). While one interpretation of these findings is that the mouse model fails to reveal cases of remarkable vaccine-mediated immunity, one could also argue that some aspects of vaccine-induced immunity are masked by the use of a supraphysiologic Mtb challenge dose that could overwhelm the immune system. Some studies suggest that using a more physiologic challenge dose [ultra-low dose (ULD) infection with 1–3 CFU] may be able to discriminate differences in vaccine-induced immunity better than a 50–100 CFU challenge dose (8, 46). Thus, this study raises two important questions that should be addressed in future studies: 1) do mechanisms of vaccine-mediated immunity operate differently in settings of SD vs ULD? and 2) does a vaccine's ability to restrict rapid bacterial growth early during infection predict its ability to prevent disease in humans?

Our study suggests that assessing vaccine-induced histopathologic changes may be helpful in evaluating vaccine efficacy as we observed a strikingly broad range of pathologic outcomes. These ranged from a dramatic decrease in pathology due to vaccination in the C3H/SA161 combination, minimal to no changes in the majority of combinations, to even apparent exacerbation of pathology in the C3H/H37Rv combination. It was surprising that pathology outcomes at Day 98 correlated poorly with bacterial burdens at this late time point, and in fact, were more strongly associated with bacterial burdens at Day 28. This suggests that host-pathogen interactions taking place at early time points may shape developing lesions and drive pathologic differences that are perpetuated at late time points. However, in B6 mice, overall lung involvement, as measured by Extent 1 scores, did not correlate with CFU at Day 28, which was unexpected given the expectation that both of these readouts indicate poor outcomes. This may reveal a caveat of using Day 98 tissue sections to correlate with Day 28 CFU, and future studies should use paired pathology scores for each time point. Further work is needed to understand the mechanistic underpinnings of these observations, which suggest that differences in host and bacterial genetics might shape the timing, type, and/or magnitude of immune responses modulated by pre-existing immunity or vaccination, which in turn can significantly affect pathologic outcomes. Given the availability of immunologic and genetic tools available for these mouse strains, this potentially allows for the evaluation of host-pathogen interactions within various microenvironments contained in these different structures, and for the mechanistic dissection of factors driving these differences. Furthermore, our work gives insight into combinations with the greatest potential to evaluate specific pathologic features of interest, for example, the C3H/SA161 combination to evaluate lesion necrosis, and C129F1/H37Rv for lymphoid aggregates. Together with the aforementioned studies in DO and CC mice, these results suggest that the long-maligned lack of diverse structures generated during Mtb infection in the mouse model is due to a focus on models that lack genetic heterogeneity. Together, these results suggest it is important to evaluate vaccine candidates with a diverse set of genetic backgrounds, and that success or failure in one strain of mouse infected with one strain of Mtb might not be predictive of clinical success or failure (47, 48). Furthermore, while bacterial burden is the most commonly used surrogate for protection in mice, it is equally important to uncover the presence of inflammatory features and destructive tissue pathology that may provide anatomic reasons for exacerbated disease, difficulty of treatment, and/or lasting sequelae even after the infection is resolved.

Overall, our study demonstrates that host and pathogen genetic differences play a large role in dictating outcomes after vaccination. The field must continue to develop Mtb infection models that reflect this heterogeneity. However, the fact that different protective modalities performed very similarly with each host-Mtb strain combination suggests that meaningful aspects of vaccine-induced immunity may be masked in mice infected with 50–100 CFU. A physiologic challenge dose may facilitate the assessments of more clinically relevant parameters of infection, such as prevention of dissemination and prevention of detectable infection, as well as induce more discrete histopathologic features (49). Thus, future studies are needed to compare the performance of vaccines to SD vs ULD challenge and to assess whether distinct mechanisms of protection can only be assessed in response to certain doses. One limitation of this study was the inclusion of only female mice. Due to the extensive scale of the study and the already inherent variability of host and bacterial components, it was not feasible to expand the groups to incorporate both sexes. We also limited our focus to CFU and histology as the two measured parameters of protection, and additional studies will be needed to examine immune correlates relating to these findings. Performing vaccine testing using several host and Mtb strain combinations in both sexes and doing so with a more physiologic Mtb challenge dose would certainly add complexity and cost to preclinical vaccine testing in mice. However, if future studies reveal that this approach facilitates an improved ability to discriminate protective differences between vaccines and results in better correlates of outcomes in human vaccine trials, adding such complexity may be essential.

## Data availability statement

The original contributions presented in the study are included in the article/Supplementary Material. Further inquiries can be directed to the corresponding authors.

## Ethics statement

The animal study was approved by Seattle Children's Institutional Animal Care and Use Committee (IACUC). The study was conducted in accordance with the local legislation and institutional requirements.

## Author contributions

SC: Conceptualization, Formal analysis, Investigation, Writing – original draft, Writing – review & editing. CP: Conceptualization, Formal analysis, Investigation, Writing – original draft, Writing – review & editing. LE: Investigation, Writing – review & editing. DM: Investigation, Writing – review & editing. TM: Investigation, Writing – review & editing. AJ: Investigation, Writing – review & editing. BA: Investigation, Writing – review & editing. JD: Investigation, Writing – review & editing. LC: Investigation, Writing – review & editing. KM: Writing – review & editing. SS: Investigation, Writing – review & editing. KD: Investigation, Writing – review & editing. EG: Conceptualization, Writing – review & editing. AA: Funding acquisition, Writing – review & editing. MG: Conceptualization, Writing – review & editing. BG: Conceptualization, Formal analysis, Investigation, Writing – original draft, Writing – review & editing. AD: Conceptualization, Formal analysis, Supervision, Writing – original draft, Writing – review & editing. KU: Conceptualization, Funding acquisition, Supervision, Writing – original draft, Writing – review & editing.

## Funding

The author(s) declare financial support was received for the research, authorship, and/or publication of this article. This work was funded by NIH contract 75N93019C00070 (KU).

## Acknowledgments

We would like to acknowledge the Office of Animal Care at Seattle Children's Research Institute for husbandry support and the University of Washington histology core for processing tissue samples. We would also like to thank Dr. Jessica Snyder, DVM for providing pathology scores of the tissue sections for this analysis.

## Conflict of interest

The authors declare that the research was conducted in the absence of any commercial or financial relationships that could be construed as a potential conflict of interest.

## Publisher's note



## Supplementary material

The Supplementary Material for this article can be found online at: https://www.frontiersin.org/articles/10.3389/fimmu.2024.1427846/full#supplementary-material

SUPPLEMENTARY FIGURE 1
Representative H&E images of the remaining strain-strain combinations. H&E images of Day 98 lungs from the remaining combinations of mouse and bacterial strain are shown alongside their respective PCA plots.

## References

1. Global tuberculosis report 2023. Geneva: World Health Organization (2023).

2. Colditz GA, Berkey CS, Mosteller F, Brewer TF, Wilson ME, Burdick E, et al. The efficacy of bacillus Calmette-Guerin vaccination of newborns and infants in the prevention of tuberculosis: meta-analyses of the published literature. *Pediatrics*. (1995) 96:29–35. doi: 10.1542/peds.96.1.29

3. Abubakar I, Pimpin L, Ariti C, Beynon R, Mangtani P, Sterne JA, et al. Systematic review and meta-analysis of the current evidence on the duration of protection by bacillus Calmette-Guerin vaccination against tuberculosis. *Health Technol Assess*. (2013) 17:1–372, v-vi. doi: 10.3310/hta17370

4. Mangtani P, Abubakar I, Ariti C, Beynon R, Pimpin L, Fine PE, et al. Protection by BCG vaccine against tuberculosis: a systematic review of randomized controlled trials. *Clin Infect Dis*. (2014) 58:470–80. doi: 10.1093/cid/cit790

5. Trauer JM, Kawai A, Coussens AK, Datta M, Williams BM, McBryde ES, et al. Timing of Mycobacterium tuberculosis exposure explains variation in BCG effectiveness: a systematic review and meta-analysis. *Thorax*. (2021) 76:1131–41. doi: 10.1136/thoraxjnl-2020-216794

6. Lindenstrom T, Knudsen NP, Agger EM, Andersen P. Control of chronic mycobacterium tuberculosis infection by CD4 KLRG1- IL-2-secreting central memory cells. *J Immunol*. (2013) 190:6311–9. doi: 10.4049/jimmunol.1300248

7. Nemeth J, Olson GS, Rothchild AC, Jahn AN, Mai D, Duffy FJ, et al. Contained Mycobacterium tuberculosis infection induces concomitant and heterologous protection. *PloS Pathog*. (2020) 16:e1008655. doi: 10.1371/journal.ppat.1008655

8. Plumlee CR, Barrett HW, Shao DE, Lien KA, Cross LM, Cohen SB, et al. Assessing vaccine-mediated protection in an ultra-low dose Mycobacterium tuberculosis murine model. *PLoS Pathog*. 2023;19(11):e1011825.

9. Lenaerts A, Barry CE 3rd, Dartois V. Heterogeneity in tuberculosis pathology, microenvironments and therapeutic responses. *Immunol Rev*. (2015) 264:288–307. doi: 10.1111/imr.12252

10. Karp CL, Wilson CB, Stuart LM. Tuberculosis vaccines: barriers and prospects on the quest for a transformative tool. *Immunol Rev*. (2015) 264:363–81. doi: 10.1111/imr.12270

11. Gopal R, Monin L, Torres D, Slight S, Mehra S, McKenna KC, et al. S100A8/A9 proteins mediate neutrophilic inflammation and lung pathology during tuberculosis. *Am J Respir Crit Care Med*. (2013) 188:1137–46. doi: 10.1164/rccm.201304-0803OC

12. Moreira-Teixeira L, Tabone O, Graham CM, Singhania A, Stavropoulos E, Redford PS, et al. Mouse transcriptome reveals potential signatures of protection and pathogenesis in human tuberculosis. *Nat Immunol*. (2020) 21:464–76. doi: 10.1038/s41590-020-0610-z

13. Niazi MK, Dhulekar N, Schmidt D, Major S, Cooper R, Abeijon C, et al. Lung necrosis and neutrophils reflect common pathways of susceptibility to Mycobacterium tuberculosis in genetically diverse, immune-competent mice. *Dis Model Mech*. (2015) 8:1141–53. doi: 10.1242/dmm.020867

14. Smith CM, Proulx MK, Olive AJ, Laddy D, Mishra BB, Moss C, et al. Tuberculosis susceptibility and vaccine protection are independently controlled by host genotype. *mBio*. (2016) 7(5):e01516-16. doi: 10.1128/mBio.01516-16

15. Lai R, Gong DN, Williams T, Ogunsola AF, Cavallo K, Lindestam Arlehamn CS, et al. Host genetic background is a barrier to broadly effective vaccine-mediated protection against tuberculosis. *J Clin Invest*. (2023) 133(13):e167762. doi: 10.1172/JCI167762

16. Kurtz SL, Mittereder LR, Lehman CC, Khan H, Gould VA, Elkins KL. Intravenous BCG Vaccination of Diversity Outbred Mice Results in Moderately Enhanced Protection against Challenge with Mycobacterium tuberculosis Compared to Intradermal Vaccination. *Infect Immun*. (2023) 91:e0016823. doi: 10.1128/iai.00168-23

17. Kurtz SL, Rossi AP, Beamer GL, Gatti DM, Kramnik I, Elkins KL. The diversity outbred mouse population is an improved animal model of vaccination against tuberculosis that reflects heterogeneity of protection. *mSphere*. (2020) 5:e00097-20. doi: 10.1128/mSphere.00097-20

18. Soldevilla P, Vilaplana C, Cardona P-J. Mouse models for mycobacterium tuberculosis pathogenesis: show and do not tell. *Pathogens*. (2023) 12(1):49. doi: 10.3390/pathogens12010049

19. Gern BH, Klas JM, Foster KA, Cohen SB, Plumlee CR, Duffy FJ, et al. CD4-mediated immunity shapes neutrophil-driven tuberculous pathology. *BiorXiv*. (2024). doi.org/10.1101/2024.04.12.589315

20. Ji DX, Yamashiro LH, Chen KJ, Mukaida N, Kramnik I, Darwin KH, et al. Type I interferon-driven susceptibility to Mycobacterium tuberculosis is mediated by IL-1Ra. *Nat Microbiol*. (2019) 4:2128–35. doi: 10.1038/s41564-019-0578-3

21. Pan H, Yan BS, Rojas M, Shebzukhov YV, Zhou H, Kobzik L, et al. Ipr1 gene mediates innate immunity to tuberculosis. *Nature*. (2005) 434:767–72. doi: 10.1038/nature03419

22. Medina E, North RJ. Resistance ranking of some common inbred mouse strains to Mycobacterium tuberculosis and relationship to major histocompatibility complex haplotype and Nramp1 genotype. *Immunology*. (1998) 93:270–4. doi: 10.1046/j.1365-2567.1998.00419.x

23. Krishnan N, Malaga W, Constant P, Caws M, Tran TH, Salmons J, et al. Mycobacterium tuberculosis lineage influences innate immune response and virulence and is associated with distinct cell envelope lipid profiles. *PloS One*. (2011) 6:e23870. doi: 10.1371/journal.pone.0023870

24. Sarkar R, Lenders L, Wilkinson KA, Wilkinson RJ, Nicol MP. Modern lineages of Mycobacterium tuberculosis exhibit lineage-specific patterns of growth and cytokine induction in human monocyte-derived macrophages. *PloS One*. (2012) 7:e43170. doi: 10.1371/journal.pone.0043170

25. Choreno-Parra JA, Bobba S, Rangel-Moreno J, Ahmed M, Mehra S, Rosa B, et al. Mycobacterium tuberculosis HN878 infection induces human-like B-cell follicles in mice. *J Infect Dis*. (2020) 221:1636–46. doi: 10.1093/infdis/jiz663

26. Du DH, Geskus RB, Zhao Y, Codecasa LR, Cirillo DM, van Crevel R, et al. The effect of M. tuberculosis lineage on clinical phenotype. *PloS Glob Public Health*. (2023) 3:e0001788. doi: 10.1101/2023.03.14.23287284

27. Coscolla M, Gagneux S. Consequences of genomic diversity in Mycobacterium tuberculosis. *Semin Immunol*. (2014) 26:431–44. doi: 10.1016/j.smim.2014.09.012

28. Stucki D, Brites D, Jeljeli L, Coscolla M, Liu Q, Trauner A, et al. Mycobacterium tuberculosis lineage 4 comprises globally distributed and geographically restricted sublineages. *Nat Genet*. (2016) 48:1535–43. doi: 10.1038/ng.3704

29. Yang C, Luo T, Sun G, Qiao K, Sun G, DeRiemer K, et al. Mycobacterium tuberculosis Beijing strains favor transmission but not drug resistance in China. *Clin Infect Dis*. (2012) 55:1179–87. doi: 10.1093/cid/cis670

30. Manca C, Tsenova L, Barry CE 3rd, Bergtold A, Freeman S, Haslett PA, et al. Mycobacterium tuberculosis CDC1551 induces a more vigorous host response in *vivo* and in *vitro*, but is not more virulent than other clinical isolates. *J Immunol*. (1999) 162:6740–6. doi: 10.4049/jimmunol.162.11.6740

31. Palanisamy GS, DuTeau N, Eisenach KD, Cave DM, Theus SA, Kreiswirth BN, et al. Clinical strains of Mycobacterium tuberculosis display a wide range of virulence in Guinea pigs. *Tuberculosis (Edinb)*. (2009) 89:203–9. doi: 10.1016/j.tube.2009.01.005

32. Darrah PA, Zeppa JJ, Maiello P, Hackney JA, Wadsworth MH 2nd, Hughes TK, et al. Prevention of tuberculosis in macaques after intravenous BCG immunization. *Nature*. (2020) 577:95–102. doi: 10.1038/s41586-019-1817-8

33. Darrah PA, Zeppa JJ, Wang C, Irvine EB, Bucsan AN, Rodgers MA, et al. Airway T cells are a correlate of i.v. Bacille Calmette-Guerin-mediated protection against tuberculosis in rhesus macaques. *Cell Host Microbe*. (2023) 31:962–77 e8. doi: 10.1016/j.chom.2023.05.006

34. Opie EL, Aronson JD. Tubercle bacilli in latent tuberculosis lesions and in lung tissue without tuberculosis lesions. *Arch Pathol*. (1927) 4:2–21.

35. Andrews JR, Noubary F, Walensky RP, Cerda R, Losina E, Horsburgh CR. Risk of progression to active tuberculosis following reinfection with Mycobacterium tuberculosis. *Clin Infect Dis*. (2012) 54:784–91. doi: 10.1093/cid/cir951

36. Kupz A, Zedler U, Staber M, Kaufmann SH. A mouse model of latent tuberculosis infection to study intervention strategies to prevent reactivation. *PloS One*. (2016) 11:e0158849. doi: 10.1371/journal.pone.0158849

37. Urdahl KB, Liggitt D, Bevan MJ. CD8+ T cells accumulate in the lungs of Mycobacterium tuberculosis-infected Kb-/-Db-/- mice, but provide minimal protection. *J Immunol*. (2003) 170:1987–94. doi: 10.4049/jimmunol.170.4.1987

38. Delahaye JL, Gern BH, Cohen SB, Plumlee CR, Shafiani S, Gerner MY, et al. Cutting Edge: Bacillus Calmette-Guerin-Induced T Cells Shape Mycobacterium tuberculosis Infection before Reducing the Bacterial Burden. *J Immunol*. (2019) 203:807–12. doi: 10.4049/jimmunol.1900108

39. Verma S, Bhatt K, Lovey A, Ribeiro-Rodrigues R, Durbin J, Jones-Lopez EC, et al. Transmission phenotype of Mycobacterium tuberculosis strains is mechanistically linked to induction of distinct pulmonary pathology. *PloS Pathog*. (2019) 15:e1007613. doi: 10.1371/journal.ppat.1007613

40. Orme IM. Characteristics and specificity of acquired immunologic memory to Mycobacterium tuberculosis infection. *J Immunol*. (1988) 140:3589–93. doi: 10.4049/jimmunol.140.10.3589

41. Cooper AM, Dalton DK, Stewart TA, Griffin JP, Russell DG, Orme IM. Disseminated tuberculosis in interferon gamma gene-disrupted mice. *J Exp Med*. (1993) 178:2243–7. doi: 10.1084/jem.178.6.2243

42. Flynn JL, Chan J, Triebold KJ, Dalton DK, Stewart TA, Bloom BR. An essential role for interferon gamma in resistance to Mycobacterium tuberculosis infection. *J Exp Med*. (1993) 178:2249–54. doi: 10.1084/jem.178.6.2249

43. Cooper AM, Magram J, Ferrante J, Orme IM. Interleukin 12 (IL-12) is crucial to the development of protective immunity in mice intravenously infected with mycobacterium tuberculosis. *J Exp Med*. (1997) 186:39–45. doi: 10.1084/jem.186.1.39

44. Flynn JL, Goldstein MM, Chan J, Triebold KJ, Pfeffer K, Lowenstein CJ, et al. Tumor necrosis factor-alpha is required in the protective immune response against Mycobacterium tuberculosis in mice. *Immunity*. (1995) 2:561–72. doi: 10.1016/1074-7613(95)90001-2

45. Carey AF, Wang X, Cicchetti N, Spaulding CN, Liu Q, Hopkins F, et al. Multiplexed strain phenotyping defines consequences of genetic diversity in mycobacterium tuberculosis for infection and vaccination outcomes. *mSystems*. (2022) 7:e0011022. doi: 10.1128/msystems.00110-22

46. Vidal SJ, Sellers D, Yu J, Wakabayashi S, Sixsmith J, Aid M, et al. Attenuated Mycobacterium tuberculosis vaccine protection in a low-dose murine challenge model. *iScience*. (2023) 26:106963. doi: 10.1016/j.isci.2023.106963

47. Kashangura R, Sena ES, Young T, Garner P. Effects of MVA85A vaccine on tuberculosis challenge in animals: systematic review. *Int J Epidemiol*. (2015) 44:1970–81. doi: 10.1093/ije/dyv142

48. Nemes E, Geldenhuys H, Rozot V, Rutkowski KT, Ratangee F, Bilek N, et al. Prevention of M. tuberculosis infection with H4:IC31 vaccine or BCG revaccination. *N Engl J Med*. (2018) 379:138–49. doi: 10.1056/NEJMoa1714021

49. Plumlee CR, Duffy FJ, Gern BH, Delahaye JL, Cohen SB, Stoltzfus CR, et al. Ultra-low dose aerosol infection of mice with mycobacterium tuberculosis more closely models human tuberculosis. *Cell Host Microbe*. (2021) 29:68–82.e5. doi: 10.1016/j.chom.2020.10.003

frontiers | Frontiers in Immunology

TYPE Original Research
PUBLISHED 26 August 2024
DOI 10.3389/fimmu.2024.1427472



OPEN ACCESS

EDITED BY
Rhea Coler,
University of Washington, United States

REVIEWED BY
Kathirvel Maruthai,
Johns Hopkins University, United States
Mohd Saqib,
Albany Medical College, United States

*CORRESPONDENCE
Brendan K. Podell
bpodell@colostate.edu

†These authors share senior authorship

RECEIVED 03 May 2024
ACCEPTED 23 July 2024
PUBLISHED 26 August 2024

CITATION
Cooper SK, Ackart DF, Lanni F, Henao-Tamayo M, Anderson GB and Podell BK (2024) Heterogeneity in immune cell composition is associated with *Mycobacterium tuberculosis* replication at the granuloma level.
*Front. Immunol.* 15:1427472.
doi: 10.3389/fimmu.2024.1427472



# Heterogeneity in immune cell composition is associated with *Mycobacterium tuberculosis* replication at the granuloma level

Sarah K. Cooper[1,2], David Forrest Ackart[1,2], Faye Lanni[1,2], Marcela Henao-Tamayo[1,2], G. Brooke Anderson[2,3†] and Brendan K. Podell[1,2,4*†]

[1]Mycobacteria Research Laboratories, Department of Microbiology, Immunology, and Pathology, Colorado State University, Fort Collins, CO, United States, [2]Phoenix Immune Mechanisms of Protection Against Tuberculosis Center, Seattle, WA, United States, [3]Department of Environmental and Radiological Health Sciences, Colorado State University, Fort Collins, CO, United States, [4]Consortium for Applied Microbial Metrics, Aurora, CO, United States

The control of bacterial growth is key to the prevention and treatment of tuberculosis (TB). Granulomas represent independent foci of the host immune response that present heterogeneous capacity for control of bacterial growth. At the whole tissue level, B cells and CD4 or CD8 T cells have an established role in immune protection against TB. Immune cells interact within each granuloma response, but the impact of granuloma immune composition on bacterial replication remains unknown. Here we investigate the associations between immune cell composition, including B cell, CD4, and CD8 T cells, and the state of replicating *Mycobacterium tuberculosis* (*Mtb)* within the granuloma. A measure of ribosomal RNA synthesis, the RS ratio®, represents a proxy measure of *Mtb* replication at the whole tissue level. We adapted the RS ratio through use of *in situ* hybridization, to identify replicating and non-replicating *Mtb* within each designated granuloma. We applied a regression model to characterize the associations between immune cell populations and the state of *Mtb* replication within each respective granuloma. In the evaluation of nearly 200 granulomas, we identified heterogeneity in both immune cell composition and proportion of replicating bacteria. We found clear evidence of directional associations between immune cell composition and replicating *Mtb*. Controlling for vaccination status and endpoint post-infection, granulomas with lower CD4 or higher CD8 cell counts are associated with a higher percent of replicating *Mtb*. Conversely, changes in B cell proportions were associated with little change in *Mtb* replication. This study establishes heterogeneity across granulomas, demonstrating that certain immune cell types are differentially associated with control of *Mtb* replication. These data suggest that evaluation at the granuloma level may be imperative to identifying correlates of immune protection.

KEYWORDS

***Mycobacterium*, tuberculosis, granuloma, immunohistochemistry (IHC), *in situ* hybridization (ISH), image analysis**

# 1 Introduction

Tuberculosis (TB) granulomas are isolated and multifocal structures formed by the host immune response to combat *Mycobacterium tuberculosis* (*Mtb*) infection. Their role is to contain and clear the bacteria, thereby preventing further bacterial replication, disease, and transmission. However, granuloma formation plays contradictory roles in TB disease; while the formation of granulomas control *Mtb* replication, they also allow *Mtb* to persist and replicate (1). There is considerable heterogeneity in the pathology, immune cell composition and structure of granulomas (2, 3). The underlying immune mechanisms that contribute to control of *Mtb* infection across the heterogeneous population of granulomas are poorly understood. Determining natural and vaccine-mediated immune protection at the granuloma level can provide key insights into developing more effective vaccines and therapeutics.

Heterogeneity has been described in granulomas across multiple species including human, non-human primate (NHP), rabbit, guinea pig, and some strains of mice. Granulomas within the same host may appear simultaneously active and inactive by PET-CT imaging in both humans and non-human primate (NHP) models (4–6). Autopsies of human subjects show a wide diversity in granuloma morphology across disease states (7, 8), which is also reflected by NHP models (9). Some NHP granulomas demonstrate evidence of resolution by histopathology and PET-CT imaging, while others in the same host, remain active (10). While substantial heterogeneity exists across many of commonly used mouse strains (11–13), the guinea pig as a small rodent model uniquely demonstrates central caseous necrosis and granuloma organization that is characteristic of human TB (14–16). When evaluated in individual granulomas, the culturable bacterial burden used to assess protection has revealed a wide range of heterogeneity consistent with these pathology observations (17). Collectively, evidence across multiple model species and human subjects supports the presence of substantial heterogeneity in granuloma composition and function.

CD4 T cells represent the cornerstone of antimycobacterial immunity. Murine studies eliminating CD4 T cells from the immune response have demonstrated loss of protection, based on changes in culturable burden from infected lung tissue (18, 19). This protection includes both IFNγ dependent and independent mechanisms derived from CD4 T cells (18). These CD4 T cells are present in multiple states of differentiation, polarization, effector functions or memory phenotypes (20, 21). Recently, a role for B cell derived antibody and CD8 T cells has been shown in correlates of immune protection (22). Antigen-specific antibodies may exert multiple effector functions in response to *Mtb* infection including antibody-dependent cellular cytotoxicity, opsonization and facilitated phagocytosis, as well as fixation and activation of complement (23, 24). Although functions of CD8 T cells are less understood, these cells are critical to control of TB progression with links to granzymes and cytotoxic function (25–27). Although important to immune protection, the contribution of these adaptive immune cell types to granuloma success or failure remains poorly understood, primarily due to limited methods that simultaneously measure both host cell populations and individual bacterial response within a single granuloma.

Protection is typically determined by measuring differences in culturable *Mtb* from tissue via colony forming units (CFU). Although this offers important information on bacterial burden, it only measures *Mtb* capable of growth on solid agar and as such cannot provide a specific location from where the bacteria were derived. Location is particularly important in considering granuloma heterogeneity because granulomas within a single animal may exist in differing states or have differing degrees of capacity for bacterial control. Previously, observation of *Mtb* in granulomas of pathology specimens has been limited to use of either reporter strains, or cell-wall based staining through IHC or variations on the traditional acid-fast stain. These methods have limitations in both stability and reproducibility, as well as capacity to detect the total *Mtb* population (28–30). These measures also fail to provide information on the physiologic status or replicative response of the *Mtb* bacilli.

A novel adjunctive measure to CFU, the RS ratio®, measures the ratio of *Mtb* immature pre-rRNA relative to mature 23S rRNA, representing ongoing rRNA synthesis (31). We have previously shown that the RS ratio effectively serves as a proxy measure of bacterial replication status. By applying *in situ* hybridization (ISH) probes targeting these regions of rRNA, we have established the RS ratio ISH approach for detection of *Mtb* bacilli and their state of replication, thereby enabling investigation of both the host and pathogen response within a single granuloma. This approach can measure changes in response over time, and in response to vaccination, across states of both host cell populations and *Mtb* replication. Here, we measure CD4 T cell, CD8 T cell, and B cell populations using multiplexed fluorescent IHC simultaneously with the RS ratio ISH across granulomas of unvaccinated and BCG-vaccinated mice, demonstrating an association between granuloma immune cell composition and *Mtb* replication rates.

The heterogeneous nature of immune cell composition across granulomas, as demonstrated by this study, provides strong evidence that certain immune cells have a greater influence on the control of *Mtb* replication. These results emphasize the need for granuloma-focused investigations to advance the understanding of protective immunity against *Mtb* infection and inform novel vaccine and therapeutic strategies.

# 2 Materials and methods

## 2.1 Animals

Male and female C57BL/6 mice, 4–6 weeks of age, were purchased from The Jackson Laboratory. Mice were housed in a biosafety level 3 animal facility at Colorado State University (CSU), and all experimental protocols and procedures were performed in accordance with the CSU Institutional Animal Care and Use Committee under protocol number 1278. Mice were euthanized by CO2 inhalation at 56 or 114 days after exposure to *Mtb*.

## 2.2 Vaccination

Mice were mock-vaccinated with 50 µl of phosphate buffered saline (PBS) or vaccinated with the human clinical-grade Danish-1331 BCG vaccine, Lot #120005-C (AJ Vaccines), by intradermal injection at the tail base. Assuming a stock bacterial concentration of 2 x $10^6$ BCG organism per ml, as provided by the manufacturer, a targeted dose of 1 x $10^4$ CFU was administered in a 50 µl injection volume to each mouse.

## 2.3 *Mycobacterium tuberculosis* infection

150 days post-vaccination with BCG, mice were infected by low-dose aerosol with *Mtb* Erdman (BEI Resources) using a Glas-Col aerosol chamber targeting an exposure dose of 50–100 CFU, as previously described (32). Immediately post-exposure, three mice were euthanized and whole lung homogenate was plated on 7H11 agar plates to confirm aerosol delivery of expected exposure dose, achieving a mean exposure dose of 54 CFU per mouse.

## 2.4 Bacterial enumeration by CFU

At necropsy, the right caudal lung lobe of each mouse was collected and homogenized in PBS using a Bullet Blender Blue (Next Advance) device at speed 8 setting for 4 minutes, as previously described (33). Tissue homogenate was plated at serial 1:5 dilutions on 7H11 agar plates and final CFU counts were enumerated following 8 weeks of incubation.

## 2.5 Histopathology and image analysis

One third of the left lung lobe was collected at necropsy and immediately fixed in 4% paraformaldehyde for 48 hours before being paraffin embedded. 5µm tissue sections were cut and mounted on charged microscope slides, stained with hematoxylin and eosin (H&E), and scanned at 20X magnification using an Olympus VS120 scanning microscope, Hamamatsu ORCA-R2 camera, and Olympus VS-ASW 2.9 software available through the Experimental Pathology Facility at Colorado State University.

Visiopharm software was used for image analysis. Entire lung section regions of interest (ROI) were identified at 5X magnification with a custom algorithm that utilizes decision forest training to differentiate tissue from microscope slide based on color and area. An additional custom-made algorithm based on decision forest training and classification based on staining intensity, area, and morphological features at 20X magnification was created to automate granuloma detection. A final algorithm was used for quantification of area of both granulomas and healthy tissue within tissue section ROIs to calculate percent granuloma lesion burden. Identified granulomas and calculations received a final review by a pathologist (Podell BK) (34).

## 2.6 Multiplex fluorescent immunohistochemistry

Slides were deparaffinized and stained using a Leica Bond RXm automated slide stainer and associated Leica Bond reagents (Supplementary Table 1). Heat induced epitope retrieval (HIER) was performed on tissues with ER1 solution at 97°C for 30 minutes prior to quenching endogenous peroxidase activity with 3% hydrogen peroxide. Tissues were blocked using 2.5% Normal Goat Serum Blocking Solution (Vector Laboratories) then incubated with the following rat monoclonal primary antibodies: CD4 (1:100, clone 4SM95, catalog number 14–9766-82, eBioscience), CD8a (1:100, clone 4SM15, catalog number 14–0808-82, eBioscience), and CD45R/B220 (1:100, clone RA3–6B2, catalog number 103201 BD Biosciences). Sections were incubated with undiluted ImmPRESS mouse adsorbed goat anti-rat IgG-HRP polymer (Vector Laboratories) for primary antibody detection. Visualization of cell surface markers was accomplished using Opal 520 (1:200), Opal 570 (1:200), and TSA plus Cyanine 5 (1:1000) in 1X TSA Plus Automation Amplification Diluent (Akoya Biosciences). Antibody stripping was performed using HIER at 95°C and ER1 solution for 20 minutes (Leica Biosystems) between each antibody application in the following order: CD4 detected with Opal 520, CD8 detected with Opal 570, and B220 detected with Cyanine 5. Finally, nuclei were stained with Spectral DAPI (Akoya Biosciences). Whole stained lung sections were scanned at 20X magnification using an Olympus VS120 microscope, Hamamatsu ORCA-R2 camera, and Olympus VS-ASW 2.9 software at the Experimental Pathology Facility at Colorado State University. Exposure times were determined using the autoexposure function and adjusted to distinguish antibody detection of cell surface markers from erythrocyte background.

## 2.7 Multiplex fluorescent *in situ* hybridization

Slides cut in serial to those used for multiplex IHC were deparaffinized and targets hybridized using the RNAscope LS multiplex fluorescent reagents (Advanced Cell Diagnostics) according to the manufacturer's recommendations for use on the Leica Bond RXm automated slide stainer and respective Leica Bond reagents (Supplementary Table 1). HIER was performed on tissues with ER2 solution (Leica Biosystems) at 97°C for 30 minutes prior to quenching endogenous peroxidase activity with 3% hydrogen peroxide. *Mtb* was identified using RNAscope 2.5 LS Probes B-MTB-23SrRNA-1-C1 (Advanced Cell Diagnostics #471658) and B-MTB-pre-rRNA-O1-C2 (Advanced Cell Diagnostics # 507548-C2) diluted 1:50 in the C1 probe (31, 35). ISH probes were visualized using TSA plus tetramethylrhodamine (Akoya Biosciences) at a dilution of 1:750, TSA plus fluorescein (Akoya Biosciences) at a dilution of 1:1000, and TSA plus cyanine 5 (Akoya Biosciences) at a dilution of 1:750 in 1X TSA Plus Automation Amplification Diluent (Akoya Biosciences). Nuclei were counterstained with DAPI

(Advanced Cell Diagnostics). Whole stained lung sections were scanned at 40X magnification using an Olympus VS120 microscope, Hamamatsu ORCA-R2 camera, and Olympus VS-ASW 2.9 software at the Experimental Pathology Facility at CSU. Exposure times were determined using the autoexposure function and adjusted to distinguish specific probe hybridization signal from erythrocyte background.

## 2.8 Multiplex fluorescent image analysis

Whole slide images were imported into Visiopharm image analysis software. Granulomas were identified using a decision forest algorithm trained on intensity and density of all fluorophores. Granulomas identified were confirmed or corrected based on annotations acquired from detection on H&E-stained slides. Each granuloma was then automatically assigned a unique ROI number within each lobe using the enumeration function in Visiopharm. Next, using a threshold-based algorithm, nuclei were detected and annotated based on DAPI signal intensity and given margins to allow for membrane analysis. For IHC, membranes were detected based on a threshold intensity of each fluorophore and assigned to their corresponding marker. For ISH, bacilli were detected based on a threshold intensity of the fluorophore assigned to the 23S rRNA probe, and further designated as replicating or non-replicating based on intensity of the corresponding fluorophore assigned to the pre-rRNA probe. In both IHC and ISH, red blood cell autofluorescence was accounted for based on low DAPI signal intensity combined with inherent combined signals of both FITC and tetramethylrhodamine. Thresholds for all markers were adjusted for any differences in staining or imaging quality and then reviewed for accuracy. Following review, counts for each cell type were quantified using an additional Visiopharm algorithm and exported as .csv files for downstream data analysis.

## 2.9 Statistical analysis

Statistical data analysis was performed in R (version 4.3.1). Data, code, and R packages from this study can be accessed through GitHub (https://github.com/PodellLab/Granuloma_RSRatio_ISH). Data exported from Visiopharm were pre-processed to prepare for downstream analysis in R. Preliminary exploratory statistical and graphical testing were performed to evaluate data distribution and differences between treatment groups. An unpaired t-test was used as a preliminary approach to calculate differences in granuloma burden, CFUs, and ISH RS ratios across treatment groups and infection endpoints.

Next, we fit a regression model to investigate the degree to which the immune cell populations in a granuloma are associated with the number of replicating bacteria in that granuloma, adjusting for the total number of bacteria in the granuloma. To do this, we fit a regression model with the number of replicating bacteria in a granuloma as the outcome variable and with three immune cell populations as potential explanatory variables, while controlling for the timepoint and vaccination status and offsetting by the total number of bacteria. To make model coefficients more interpretable, we scaled immune cell counts by dividing by 500, based on the approximate interquartile range of each of these cell populations across the full study data. Therefore, the estimated coefficients represent an expected change per approximately one interquartile-range change in an immune cell population. Specifically, we fit the following quasi-Poisson regression model, adjusting for potential overdispersion of observed count data from each granuloma and including as an offset the log transformation of total bacterial counts measured by ISH:

$$\log(\lambda_i) = \beta_0 + \beta_1 X_{1,i} + \beta_2 X_{2,i} + \beta_3 X_{3,i} + \beta_4 X_{4,i} + \beta_5 X_{5,i} + \log(T_i)$$

Where, for each granuloma $i$:

- $\lambda_i$: Expected count of replicating *Mtb*
- $X_{1,i}$: Scaled count of B cells
- $X_{2,i}$: Scaled count of CD4 cells
- $X_{3,i}$: Scaled count of CD8 cells
- $X_{4,i}$: Indicator of vaccine status of the mouse with granuloma $i$, where unvaccinated is 0 and BCG-vaccinated is 1
- $X_{5,i}$: Indicator of infection endpoint of the mouse with granuloma $i$, where day 56 is 0 and day 114 is 1
- $T_i$: Total count of *Mtb* (replicating and non-replicating) in granuloma $i$
- $\beta_0 - \beta_5$: Model coefficients estimated from the data

# 3 Results

## 3.1 At the whole tissue level, BCG vaccination mediates reduction in culturable *Mtb* burden and total pulmonary pathology burden

Lung lobes were collected at necropsy at days 56 and 114 post-infection to assess *Mtb* burden at the level of the whole lung tissue. Colony forming units (CFU) of culturable bacteria in lung homogenate increased between day 56 and day 114 post-infection in both unvaccinated and BCG-vaccinated mice. However, BCG-vaccinated mice displayed reduced CFU burden at both days 56 and 114 post-infection compared to unvaccinated mice (Figure 1A). To establish whether the BCG vaccination offers protection from progressive pulmonary pathology at days 56 and 114 post-infection, the granuloma lesion burden was quantified histologically across the whole lung lobe using image analysis software (Figure 1B). Consistent with CFU at day 56, a significant decrease in granuloma lesion burden was observed in BCG-vaccinated mice compared to unvaccinated mice at day 56. Between day 56 and day 114 post-infection, the overall granuloma lesion burden increased in both groups. A decreased granuloma lesion burden was observed in BCG-vaccinated mice at day 114 post-infection although not statistically significant (Figure 1C).

10.3389/fimmu.2024.1427472

## 3.2 Immune protection is demonstrated in whole lung granuloma lesion burden with histologically divergent features

Regardless of differences across pulmonary pathology burden, heterogeneity could be observed in morphological structure and cell composition among individual granulomas within an individual mouse, within vaccination status, and within infection endpoints (Figures 1D-I). H&E-stained lungs demonstrated granulomas with morphology of multiple and variable subtypes as observed by the reviewing pathologist (Podell BK). Granulomas were observed that consist of large centralized lymphoid aggregates resembling *de novo* tertiary lymphoid structures, some of which contain follicular centers composed of cells with macrophage-type morphology. Lymphoid structures are surrounded by either dense and eosinophilic epithelioid macrophages that replace pulmonary architecture (Figures 1D, E), or alveolitis consisting of loose aggregates of heavily vacuolated macrophages contained within remnant alveolar spaces (Figures 1H, I). Other granulomas consisted of multiple smaller and less organized lymphoid aggregates surrounded by heavily vacuolated macrophages or have a paucity of lymphocyte cells and consist almost entirely of vacuolated macrophages. Among a proportion of the granulomas with poorly organized lymphoid structures, the heavily vacuolated macrophages were surrounded by alveolar interstitial fibrosis embedding small foci of necrosis with a high frequency of neutrophils (Figures 1F, G). While measures of granuloma lesion burden offer an indication of immune protection across the whole lung, this fails to encompass the heterogeneity of histological morphology observed across granulomas. This degree of histological heterogeneity suggests that distinct and diverse immune responses exist within and between mice, irrespective of

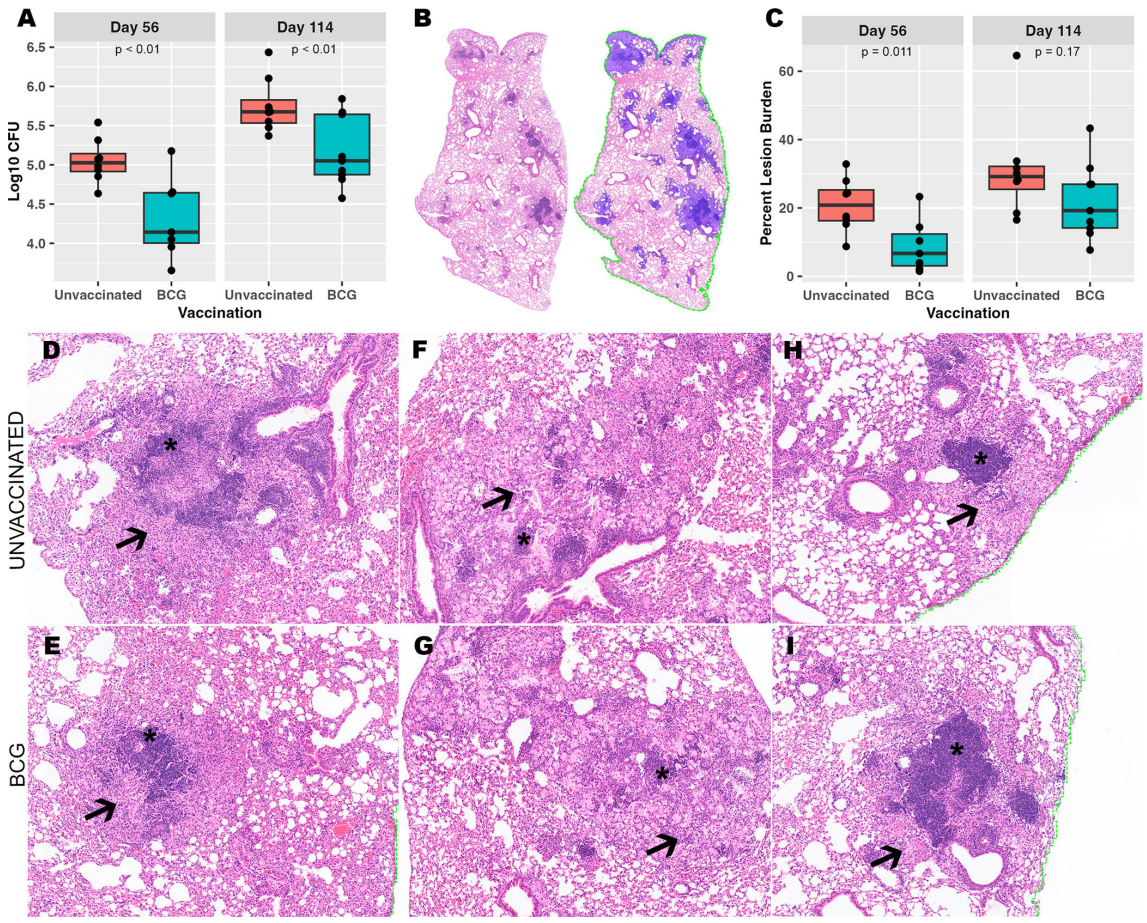


FIGURE 1
Despite BCG vaccine-mediated reduction in culturable bacterial burden, a heterogeneous granuloma response is shared across both vaccinated and unvaccinated mice. **(A)** Culturable *Mtb* colony forming units (CFU) in BCG-vaccinated and unvaccinated mice from left lung lobe tissue homogenates at day 56 and day 114 post-infection. **(B)** Right caudal lung lobes were H&E-stained after both timepoints of *Mtb* infection. A representative example is provided of a BCG-vaccinated mouse to identify and quantify granuloma lesion burden using Visiopharm image analysis software where granulomas (left) are detected across the entire lung lobe section as shown with blue overlay (right). **(C)** Percent granuloma lesion burden separated by infection endpoint and vaccination status; each point represents a lung section from an individual mouse. **(D-I)** Granulomas with diverse morphology shared between unvaccinated and BCG-vaccinated mice. **(D, E)** Loose centralized aggregates of lymphocytes (asterisk) surrounded by epithelioid macrophages (arrow). **(F, G)** Scattered small lymphocyte aggregates (asterisk) surrounded by heavily vacuolated macrophages, neutrophils and foci of necrosis embedded within areas of alveolar interstitial fibrosis (arrow). **(H, I)** Centralized dense lymphoid aggregates (asterisk) surrounded by vacuolated macrophages (arrow) and discrete granuloma boundaries. Images provided at 50X magnification.

vaccination, and that granuloma targeted analysis could offer greater insight into correlates of protection that cannot be observed through bulk tissue analyses.

## 3.3 Quantification of replicating *Mtb* by ISH RS ratio reveals heterogeneity in immune control of *Mtb* replication across granulomas

Divergent features of granuloma histomorphology suggest a more granular measure of bacterial replication may distinguish differences between granulomas. To better understand each granuloma's ability to control bacterial replication, multiplexed fluorescent *in situ* hybridization (ISH), using targets analogous to the RS ratio dPCR (31, 35), was employed to visualize individual replicating and nonreplicating *Mtb* organisms, referred to as RS ratio ISH. In this approach, a replicating bacillus was defined by colocalized detection of both ETS1/ITS1 pre-rRNA sequence and mature 23S rRNA sequence, while a non-replicating *Mtb* bacillus was defined by detection of 23S rRNA only. 191 granulomas identified on H&E-stained slides were evaluated (Table 1). The number of granulomas per mouse tended to be higher in unvaccinated mice at day 56 post-infection compared to BCG-vaccinated mice, but increased in number among BCG-vaccinated mice between day 56 and day 114 post-infection. 23S rRNA and ETS1/ITS1 pre-rRNA detection was quantified using Visiopharm image analysis software and the proportion of replicating bacteria relative to total bacteria calculated (Figures 2A–D). At both days 56 and day 114 post-infection, granulomas from unvaccinated mice displayed higher proportions of replicating *Mtb* compared to BCG-vaccinated animals (Figure 2E). Collectively, the proportions of replicating *Mtb* decreased across granulomas between day 56 and day 114, irrespective of vaccination status. Regardless of timepoint or vaccination status, a wide range of total bacterial burden and replication status was observed between and within groups and within individual animals.

Considering the heterogeneity of replicating proportions of *Mtb* observed across the granuloma, a direct comparison was made to the whole lung CFU per mouse that, as a stand-alone metric, supports vaccine-mediated protection. In comparing these metrics, it is evident that regardless of CFU value, granulomas per mouse vary in number. Within and between mice, these granulomas display an expansive range of total *Mtb* burden and proportion of replicating *Mtb* by ISH. There was no evident directional association between replicating *Mtb* by RS ratio ISH and culturable *Mtb* burden by CFU (Figure 2F). Rather, CFUs appear to more linked to the total number of granulomas in the mouse. These data suggest that total CFU burden reflects a collective contribution of diverse granuloma responses with differing capacities to control *Mtb* replication. Overall, the results from granuloma-targeted RS ratio ISH highlights that a wide range of capacity for immune control of *Mtb* replication exists across granulomas, which cannot be effectively captured by CFU. Thus, RS ratio ISH may distinguish granulomas with immune cell composition that provide greater control of *Mtb* replication.

## 3.4 Granulomas exhibit divergent composition of adaptive immune cell phenotypes by IHC

We investigated underlying spontaneous and BCG-induced adaptive immunity by multiplexed IHC in conjunction with the granuloma heterogeneity observed both histologically and in *Mtb* replication rate by RS ratio ISH. Essential adaptive immune cell phenotypes were considered because previous work shows a reduction in total lung RS ratio at the onset of adaptive immunity (31). Accordingly, CD4 cells, CD8 cells, B cells, and other host cells were targeted within granulomas in which the RS ratio ISH was

TABLE 1 Granuloma-level measures of host cells and *Mtb*.

| | Day 56 | | | Day 114 | | |
|---|---|---|---|---|---|---|
| | Unvaccinated (*n* = 59) | Vaccinated (*n* = 24) | Overall (*n* = 83) | Unvaccinated (*n* = 55) | Vaccinated (*n* = 53) | Overall (*n* = 108) |
| Host | Median Count | | | Median Count | | |
| CD4 T cell | 162 | 90 | 157 | 261 | 449 | 320 |
| CD8 T cell | 169 | 170 | 169 | 219 | 355 | 259 |
| B cell | 137 | 95 | 116 | 154 | 387 | 234 |
| Other | 2036 | 1952 | 2036 | 2407 | 2601 | 2436 |
| Total | 2441 | 2325 | 2424 | 3205 | 3538 | 3337 |
| Mtb | Median Count | | | Median Count | | |
| Replicating | 19 (22.6%) | 2.5 (5.3%) | 13 (18.3%) | 28 (7.1%) | 13 (6.8%) | 15.5 (6.6%) |
| Nonreplicating | 51 | 37 | 46 | 368 | 183 | 213.5 |
| Total | 84 | 47 | 71 | 393 | 190 | 236 |

Counts of granulomas in each group are indicated by n.

10.3389/fimmu.2024.1427472

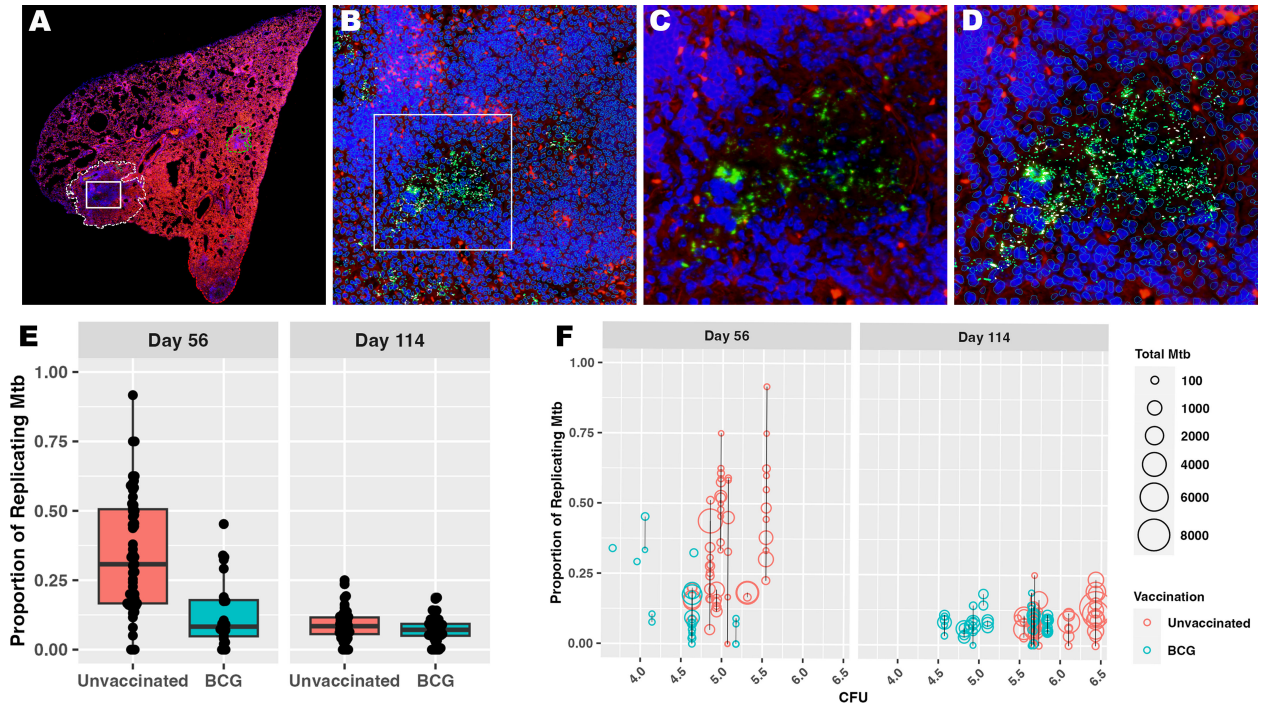


FIGURE 2
Measuring *Mtb* replication rate by ISH reveals the diversity of granuloma responses contributing to culturable bacterial burden. Populations of *Mtb* bacilli were visualized within each granuloma using RNAScope ISH. All bacteria were identified using probe pairs targeting 23S rRNA, then designated as replicating if the bacillus also contains detectable pre-rRNA with probes targeting the ETS1/ITS1 rRNA sequences. **(A)** Low magnification subgross view of a full lung section from an unvaccinated mouse shows a granuloma designated as a region of interest (ROI) by image analysis (white dotted line); white box designates the granuloma region with detected Mtb rRNA shown in panels **(B–D)**. **(B)** 100X magnification view showing the image analysis detection of all host cells and Mtb bacilli within the region designated in **(A)**. Bacilli can be observed within the inset region designated by the white box. **(C)** 400X view shows 23S rRNA detection representing the bacilli (green), some of which express pre-rRNA (white) that are designated as the replicating population. **(D)** Same field of view as in **(C)** with image analysis labeling of 23S (green) and pre-rRNA (white) among host cell nuclei (blue) **(E)** Bacterial counts (23S rRNA) and proportion of replicating bacilli (23S rRNA + pre-rRNA) are derived using Visiopharm image analysis. Each point reflects the proportion of replicating *Mtb* within a granuloma as measured by ISH and image analysis. **(F)** Proportion of replicating Mtb and total burden of *Mtb* within each granuloma by ISH are shown at the culturable pulmonary bacterial burden for each mouse measured by CFU. Each circle represents a granuloma ROI, and the size of each circle represents total *Mtb* burden by ISH. The black line connecting circles represents a single mouse, where all granulomas detected for that mouse fall along the line and share a common measure of whole lung CFU.

quantified (Table 1). Within each granuloma designated as an independent ROI, each cell subset was identified and quantified using Visiopharm image analysis software (Figures 3A-D). Granulomas displayed heterogeneous cellular composition and organization across all groups and endpoints evaluated, where total cell counts of any measured phenotype are unable to distinguish vaccine status or day of infection (Figure 3E). All measured immune cells increase in median number per granuloma between day 56 and day 114, and this increase remained similar across B cells, CD4, and CD8 cells, but these changes between infection endpoints are small in comparison to the large variability observed within each group. The most prevalent cell type at either day 56 or day 114 are those that do not belong to any of the three evaluated phenotypes and are designated by the term, “other cells”. Overall, a wide spread of cell counts was observed independent of timepoint or vaccination status, exemplifying differences across granulomas that may provide context for ability to control bacterial replication.

## 3.5 Relative rate of *Mtb* replication is inversely associated with CD4 and CD8 cell composition at the granuloma level

Having established granuloma heterogeneity in the C57BL/6 mouse model using simultaneous measures of host and bacterial response, we then performed regression analysis to identify any association with immune environments capable of controlling *Mtb* replication. To do so, a generalized linear regression model was utilized to determine associations between immune cell composition and counts of replicating *Mtb*, while accounting for total *Mtb* burden through a model offset. Based on differences between interquartile ranges (IQR) among immune cells, counts of immune cells were scaled down by a factor of 500 to approximate the IQR, which facilitates interpretation of respective comparisons. Controlling for all variables, irrespective of vaccine status or timepoint, an inverse relationship between CD4 and CD8 cells was observed with changes in the relative rate of bacterial replication. A 17.7% decrease in estimated relative rate

10.3389/fimmu.2024.1427472

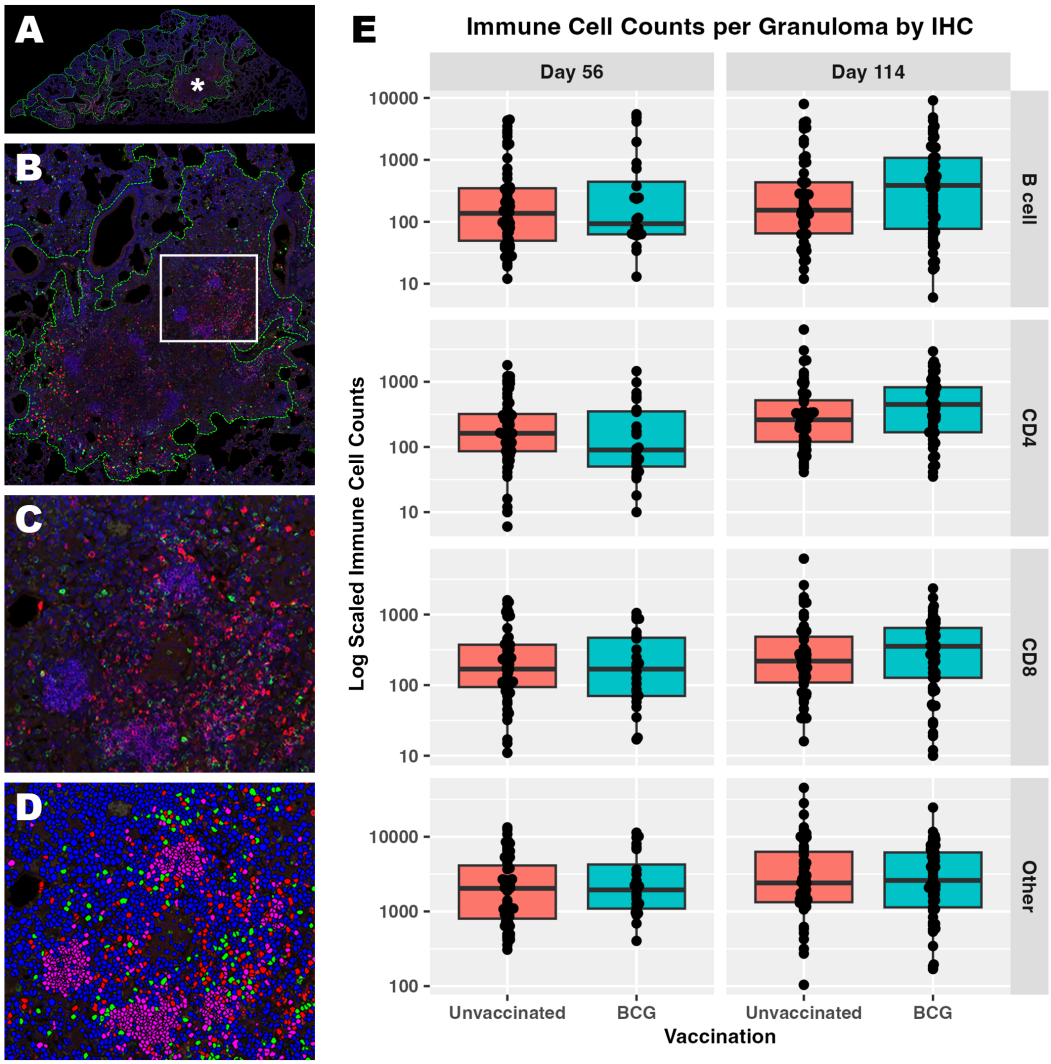


FIGURE 3
Immune cell composition of granulomas identifies a wide degree of host heterogeneity that alone cannot distinguish trends in immune protection. Populations of CD4, CD8, and B cells were visualized within each granuloma using multiplexed fluorescent IHC with a DAPI nuclear counterstain. **(A)** Low magnification subgross view of a full lung section from an unvaccinated mouse shows granulomas designated as regions of interest (ROI) by image analysis (green dotted lines). **(B)** Higher magnification view of the granuloma ROI designated by the asterisk in **(A)**. **(C)** Immune subsets are demonstrated at 200x magnification within the inset region designated by the white box in B; B cells (pink), CD4 cells (green), CD8 cells (red). **(D)** The same 200X view as in **(C)** is shown with each immune subset or 'other cell' designated using image analysis; B cells (pink), CD4 cells (green), CD8 cells (red), other cells (blue, DAPI only). Nuclei detected that do not belong to either CD4, CD8, or B cell are classified as other. **(E)** Cell counts detected at day 56 and day 114 post-infection within each granuloma ROI. Each point represents a granuloma.

of *Mtb* replication was associated with each 500-cell increase in CD4, and a 25.8% increase in relative rate of *Mtb* replication was associated with each 500-cell increase in CD8, while B cell count showed no significant association with *Mtb* replication (Figure 4). Controlling for differences in these host cell populations, BCG vaccination was associated with a 35.4% decrease in estimated relative rate of replication compared to unvaccinated, while progression to day 114 post-infection was associated with a 54.7% decrease over time compared to day 56 post-infection. Here we identify a significant association between granuloma immune cell composition and control of *Mtb* replication. Data obtained from all evaluated granulomas, including immune cell counts and replication rates are available at https://github.com/PodellLab/Granuloma_RSratio_ISH.

## 3.6 Histologic morphology of granulomas is consistent with immune cell counts and rate of Mtb replication

Based on predictions using this model, we back-translated associations between cell composition and RS ratio ISH replication rates to evaluate granuloma morphology associated with immune control of bacterial replication. Selection of two granulomas from the lung lobe of a single BCG-vaccinated mouse at day 56 post-infection highlights the observation that different degrees of bacterial replication existing between granulomas is associated with immune cell composition unique to each granuloma (Figure 5). Between these two granulomas within this

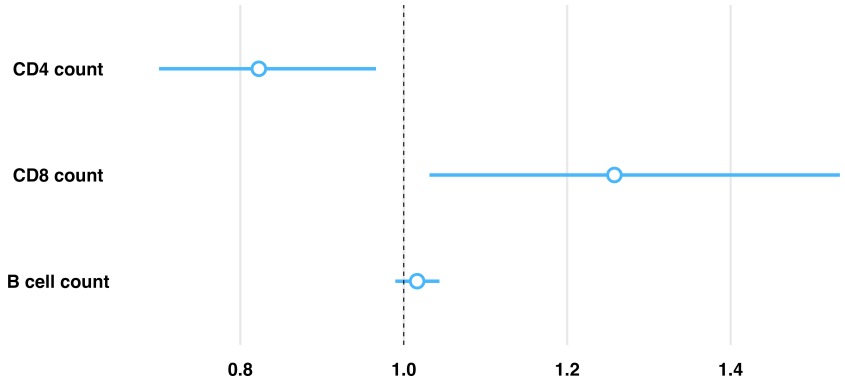


FIGURE 4
Model predictions between proportion of replicating Mtb and immune cell composition within each granuloma highlights an inverse association with CD4 and CD8 cells. Estimated relative rate of replicating Mtb is shown per 500 cell increase (approximate IQR) of each immune cell subset within an individual granuloma as estimated by a generalized linear regression model, controlling for vaccination status and infection endpoint. Controlling for all other evaluated cell phenotypes, there is an associated 17.7% reduction in the proportion of replicating Mtb for every 500 cell increase in CD4, an associated 25.8% increase in the proportion of replicating Mtb for every 500 cell increase in CD8, and no significant association in the proportion of replicating Mtb for every 500 cell increase in B cells.

single mouse, CD8 cells differ by 547 cells and Mtb replication is increased by 28.9% (Table 2). Consistent with the multiple morphologies described in Figure 1, these granulomas contain either higher proportions of vacuolated macrophages or epithelioid macrophages and B cell-rich *de novo* follicular structures. In these granulomas, the higher Mtb replication rate is localized to macrophages with vacuolated morphology, which is overrepresented in the granuloma with the higher CD8 count. These findings indicate that cell populations with a designated morphology may align with poor control of Mtb replication. Furthermore, granuloma morphology may indicate an immune environment with capacity to successfully limit, or fail to control, Mtb replication.

## 4 Discussion

In this study, we applied the RS ratio through *in situ* hybridization (RS ratio ISH) to identify the frequency of new rRNA production, which serves as a proxy measure of *Mtb* replication (31, 35). Here, we identified the replicative response of *Mtb* to immune pressure over two chronic endpoints of infection and in response to BCG vaccination. A wide range of *Mtb* replication states was demonstrated across granulomas both within individual animals, as well as between animals evaluated at the same infection endpoint, independent of respective vaccination status. These results highlight the extensive degree of heterogeneity among *Mtb* replicative states across granulomas. We found that culturable bacterial burden from whole lung homogenate, as determined by CFU, does not necessarily reflect the spectrum of *Mtb* replication states across granulomas. Although vaccination does reduce CFU, the difference in *Mtb* replication rate remains similar in some granulomas of BCG-vaccinated mice, compared to unvaccinated mice. Additionally, these data indicate that rate of replication within a granuloma and total bacterial burden do not necessarily correlate. In many instances, granulomas with the highest rate of *Mtb* replication do not have the highest burden of bacteria, as identified by detection of 23S rRNA alone. These data suggest that a differential host response may exist between granulomas with high or low replication rates, or those with high or low *Mtb* burden. We hypothesized discrimination of these immune environments and their overarching contribution to the replicative state of the *Mtb* bacilli may identify correlates of protective responses.

We identified a wide diversity of granuloma compositions, containing varying frequencies of CD4, CD8 and B cell populations, which is consistent with the highly heterogeneous replication rates of *Mtb* across granulomas. These findings are inconsistent with the constrained host immune response characteristic of the C57BL/6 mouse strain. These mice have a well-documented Th1 skewed cell-mediated immune response with granulomas described as lacking advanced pathology features (3). Despite an apparent uniformity in the immune response to *Mtb* infection, our findings indicate that granuloma heterogeneity exists in C57BL/6 mice, highlighting the importance of granuloma-targeted analysis. This approach provides an adjunctive method to distinguish granuloma-specific differences in immune response within and between animals enabling determination of the local granuloma response as opposed to whole tissue measures, such as flow cytometry.

To determine if the variability in *Mtb* replicative state is associated with differences in host response, we established a generalized linear regression model to evaluate the association between *Mtb* replication rate and CD4, CD8 and B cell populations across nearly 200 granulomas. Based on culturable CFU, these broad phenotypic categories have an established role in TB disease as a primary outcome measure. However, due to previous limitations in concurrent host and pathogen *in situ* analyses, determining associations between each immune cell subset and the *Mtb* bacterial replication state was not achievable. Using multiplexed IHC and RS ratio ISH to assess both host phenotype frequency and bacterial replication rate, we

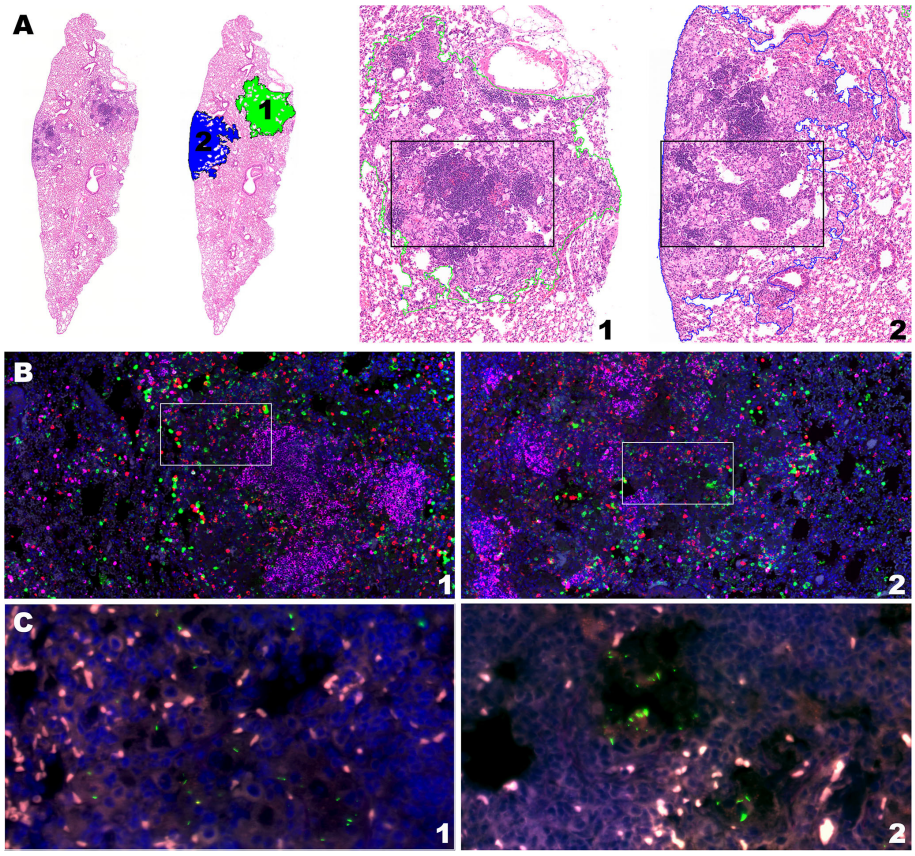


FIGURE 5
Intramouse heterogeneity in granuloma morphology, immune cell composition, and Mtb replication rate aligns with model predictions. Two neighboring granulomas within the same lung section of the same BCG-vaccinated mouse are shown by H&E stain, multiplexed IHC, and RS ratio ISH. **(A)** H&E stain at subgross showing the ROI of granuloma 1 and 2 from the BCG-vaccinated mouse (10X magnification) at day 56 post-infection and H&E morphology of each granuloma outlined by green and blue dotted lines for granulomas 1 and 2, respectively (50X magnification). **(B)** Multiplexed IHC demonstrating populations of CD4 cells (green), CD8 cells (red) and B cells (pink) in granulomas 1 and 2 (100X magnification). White boxes indicate inset regions for visualization of Mtb organisms. **(C)** Mtb bacilli detected with pre-rRNA and 23S rRNA probes by RNAScope ISH in granulomas 1 and 2.

determined the association between immune cell composition and the respective response of the bacterial population within each granuloma. Through this, a unique association between CD4 and CD8 cell frequencies and *Mtb* replication rates has been established in any individual granuloma, while a statistically significant association between B cells and *Mtb* replication rate was not observed in the evaluated granulomas.

Our model indicated that every unit increase in CD4 cells was associated with a significant decrease in *Mtb* replication rate, while every unit increase in CD8 cells was associated with a significant increase in *Mtb* replication rate. Although CD4 and CD8 cells have established roles in the constraint of *Mtb* growth in tissue, the opposing directionality of each cell type association may suggest different roles for CD4 and CD8 cells in the granuloma response. However, this relationship does not yet indicate any directional causality despite definitive associations. In this context, the RS ratio measure of replication rate may inform further investigation of granuloma response where further interventions that manipulate specific host cell phenotypes are needed to determine the mechanism by which a designated cell type contributes to immune control of *Mtb* replication.

In concordance with the granuloma-level degree of heterogeneity in both host and bacterial populations, differences in granuloma morphology based on traditional H&E-stained slides were observed. In multiple conventional inbred mouse strains, including the C57BL/6 mouse, tertiary lymphoid follicular structures are a frequent and dominant feature of the response to *Mtb* infection (36, 37). Granulomas can be distinguished as having either dense and well-structured follicles, or loosely organized lymphoid infiltration. Further, the innate populations of macrophages may be either heavily vacuolated or more epithelioid in appearance. Vacuolated macrophage populations may contain varying levels of accompanying neutrophils and cellular fragmentation consistent with multiple mechanisms of macrophage cell death. We found that intragranuloma follicular structures are heavily dominated by B cells and have limited T cell involvement. Although some granulomas have high proportions of follicle-associated B cells, our model indicated no statistical association with *Mtb* replication rate. In contrast, we histologically observed that granulomas with high CD4 T cell frequencies and lower *Mtb* replication rates contained more epithelioid macrophage populations. Granulomas with high CD8

TABLE 2 Individual granuloma measures informing histopathology morphological features.

| | BCG 24–1 | BCG 24–2 |
|---|---|---|
| Proportion replicating Mtb | 0.142 | 0.183 |
| Replicating Mtb | 27 | 43 |
| Nonreplicating Mtb | 163 | 192 |
| Total Mtb | 190 | 235 |
| CD8 count (%) | 774 | 1321 |
| CD4 count (%) | 1082 | 1027 |
| B220 count (%) | 3286 | 3485 |
| Other cell count (%) | 9097 | 11638 |
| CFU ($Log_{10}$ per g tissue) | 5.05 | 5.05 |

Examples of granulomas highlighting histopathological morphology based on GLM associations are shown in Figure 5. Characteristics of each of granuloma are identified by individual mouse-granuloma (i.e., 24–1). Data for all granulomas evaluated in this study are available on the GitHub repository.

T cells and high *Mtb* replication rates contained prominent vacuolated macrophage populations. Further *in situ* investigation of unique H&E-defined granuloma morphology may reflect critical microenvironmental differences in host response, including host immune cell composition, and subsequently constraint of *Mtb* replication (38).

The key associations in immune cell composition and bacterial replication rate revealed by our model leads us to ask the question 'does restriction of *Mtb* replication represent an ideal pathogen-targeted measure of immune protection?'. *Mtb* has an inherent capacity to enter a dormancy-like phenotype, and previous studies using progressive hypoxia models of *in vitro* grown *Mtb* suggests that dormancy onset accompanies a reduction in replication (31, 39). Such dormant phenotypes may contribute less to progressive TB disease (40, 41). Increased dormancy induced by immune pressure on the *Mtb* bacilli may be associated with an altered treatment response (42) or may reflect a temporary replicative constraint on the *Mtb* population (43), which may recover following changes in the immune environment. Alternatively, a reduced replication rate could reflect improved control of bacterial growth and an increase in bacteriostatic effect from the ongoing immune response (44–46). Distinguishing dormancy from other mechanisms of immune constraint on Mtb replication requires further investigation of the bacterial response *in situ*. This presents its own challenges but may be determined by emerging techniques, such as SearchTB, using *Mtb* enriched extracts from tissue (47).

There are limitations to this study and this method. The evaluation of only three adaptive immune cell phenotypes, B cells, CD4 and CD8 T cells, underrepresents the complexity of the TB granuloma (48). This is evident based on recent single cell RNA seq studies that have demonstrated 18 distinct lymphoid cell sub-populations involved in the pulmonary granulomatous response of murine TB models (20). We recognize the power of adjunctive immunological methods (i.e. flow cytometry, scRNAseq) in assessing host protection as well as the greater capacity of these methods to identify specific details of the host response. However, this study serves as proof-of-concept that granulomas with differing cell compositions also have distinct differences in capacity to influence *Mtb* replication. Additionally, the results presented here represent only one context of a modeled *Mtb* infection, that of unvaccinated and BCG-vaccinated C57BL/6 mice infected by low-dose aerosol exposure to the Erdman strain. The application of this approach to other model strains, species, vaccine compositions, and strains of *Mtb* will further elucidate the capacity for granuloma targeted analysis to identify correlates of immune protection. The RS ratio used here provides adjunctive value to whole tissue measures, with the distinct advantage of evaluating the concurrent host and *Mtb* bacterial response *in situ* within any given granuloma. The RS ratio ISH method is not intended to serve as an alternative or replacement for CFU determination as a measurement of TB disease outcome. Rather, this approach offers orthologous information to culturable bacterial burden by providing critical information on the *Mtb* replicative state in the native granuloma microenvironment that cannot be measured by CFU alone (31). The ongoing development and implementation of complementary granuloma and whole lung methodologies holds promise for advancing our understanding of TB and facilitating development and assessment of effective vaccines and therapeutics.

## Data availability statement

The datasets presented in this study can be found in online repositories. The names of the repository/repositories and accession number(s) can be found below: https://github.com/PodellLab/Granuloma_RSratio_ISH.

## Ethics statement

The animal study was approved by Colorado State University Institutional Animal Care and Use Committee. The study was conducted in accordance with the local legislation and institutional requirements.

## Author contributions

SC: Data curation, Formal analysis, Investigation, Methodology, Validation, Visualization, Writing – original draft, Writing – review & editing. DA: Data curation, Formal analysis, Investigation, Methodology, Writing – review & editing. FL: Conceptualization, Investigation, Resources, Supervision, Visualization, Writing – review & editing. MH-T: Conceptualization, Funding acquisition, Project administration, Resources, Supervision, Writing – review & editing. GBA: Conceptualization, Data curation, Formal analysis, Investigation, Methodology, Project administration, Resources,

Software, Supervision, Writing – original draft, Writing – review & editing. BP: Conceptualization, Formal analysis, Funding acquisition, Investigation, Methodology, Project administration, Resources, Supervision, Validation, Visualization, Writing – original draft, Writing – review & editing.

## Funding

The author(s) declare financial support was received for the research, authorship, and/or publication of this article. This project has been funded in whole or in part with federal funds from the National Institute of Allergy and Infectious Diseases, National Institutes of Health, Department of Health and Human Services, under Phoenix Immune Mechanisms of Protection Against Tuberculosis Centers (IMPAc-TB) 75N93021C00029 and by the National Institute Of Allergy And Infectious Diseases of the National Institutes of Health under Award Number T32AI162691. The content is solely the responsibility of the authors and does not necessarily represent the official views of the National Institutes of Health.

## Acknowledgments

The authors would like to acknowledge the service provided by the histology laboratory at the Veterinary Diagnostic Laboratory for their contributions to histology processing and the Experimental Pathology Facility at Colorado State University, RRID: SCR_23562, for access to automated immunostaining instrumentation and Visiopharm image analysis software.

## Conflict of interest

The authors declare that the research was conducted in the absence of any commercial or financial relationships that could be construed as a potential conflict of interest.

The author(s) declared that they were an editorial board member of Frontiers, at the time of submission. This had no impact on the peer review process and the final decision.

## Publisher's note



## Author disclaimer

The content is solely the responsibility of the authors and does not necessarily represent the official views of the National Institutes of Health.

## Supplementary material

The Supplementary Material for this article can be found online at: https://www.frontiersin.org/articles/10.3389/fimmu.2024.1427472/full#supplementary-material

## References

1. Paige C, Bishai WR. Penitentiary or penthouse condo: the tuberculous granuloma from the microbe's point of view. *Cell Microbiol.* (2010) 12:301–9. doi: 10.1111/cmi.2010.12.issue-3

2. Cadena AM, Fortune SM, Flynn JL. Heterogeneity in tuberculosis. *Nat Rev Immunol.* (2017) 17:691–702. doi: 10.1038/nri.2017.69

3. Lenaerts A, Barry CE 3rd, Dartois V. Heterogeneity in tuberculosis pathology, microenvironments and therapeutic responses. *Immunol Rev.* (2015) 264:288–307. doi: 10.1111/imr.12252

4. Chen RY, Dodd LE, Lee M, Paripati P, Hammoud DA, Mountz JM, et al. PET/CT imaging correlates with treatment outcome in patients with multidrug-resistant tuberculosis. *Sci Transl Med.* (2014) 6:265ra166. doi: 10.1126/scitranslmed.3009501

5. Coleman MT, Maiello P, Tomko J, Frye LJ, Fillmore D, Janssen C, et al. Early Changes by (18)Fluorodeoxyglucose positron emission tomography coregistered with computed tomography predict outcome after Mycobacterium tuberculosis infection in cynomolgus macaques. *Infect Immun.* (2014) 82:2400–4. doi: 10.1128/IAI.01599-13

6. Esmail H, Lai RP, Lesosky M, Wilkinson KA, Graham CM, Coussens AK, et al. Characterization of progressive HIV-associated tuberculosis using 2-deoxy-2-[(18)F] fluoro-D-glucose positron emission and computed tomography. *Nat Med.* (2016) 22:1090–3. doi: 10.1038/nm.4161

7. Wells G, Glasgow JN, Nargan K, Lumamba K, Madansein R, Maharaj K, et al. A high-resolution 3D atlas of the spectrum of tuberculous and COVID-19 lung lesions. *EMBO Mol Med.* (2022) 14:e16283. doi: 10.15252/emmm.202216283

8. Sawyer AJ, Patrick E, Edwards J, Wilmott JS, Fielder T, Yang Q, et al. Spatial mapping reveals granuloma diversity and histopathological superstructure in human tuberculosis. *J Exp Med.* (2023) 220(6):e20221392. doi: 10.1084/jem.20221392

9. Capuano SV 3rd, Croix DA, Pawar S, Zinovik A, Myers A, Lin PL, et al. Experimental Mycobacterium tuberculosis infection of cynomolgus macaques closely resembles the various manifestations of human M. tuberculosis infection. *Infect Immun.* (2003) 71:5831–44. doi: 10.1128/IAI.71.10.5831-5844.2003

10. Lin PL, Maiello P, Gideon HP, Coleman MT, Cadena AM, Rodgers MA, et al. PET CT identifies reactivation risk in cynomolgus macaques with latent M. tuberculosis. *PloS Pathog.* (2016) 12:e1005739. doi: 10.1371/journal.ppat.1005739

11. Irwin SM, Driver E, Lyon E, Schrupp C, Ryan G, Gonzalez-Juarrero M, et al. Presence of multiple lesion types with vastly different microenvironments in C3HeB/FeJ mice following aerosol infection with Mycobacterium tuberculosis. *Dis Model Mech.* (2015) 8:591–602. doi: 10.1242/dmm.019570

12. Plumlee CR, Barrett HW, Shao DE, Lien KA, Cross LM, Cohen SB, et al. Assessing vaccine-mediated protection in an ultra-low dose Mycobacterium tuberculosis murine model. *PloS Pathog.* (2023) 19:e1011825. doi: 10.1371/journal.ppat.1011825

13. Plumlee CR, Duffy FJ, Gern BH, Delahaye JL, Cohen SB, Stoltzfus CR, et al. Ultra-low dose aerosol infection of mice with mycobacterium tuberculosis more closely models human tuberculosis. *Cell Host Microbe.* (2021) 29:68–82 e5. doi: 10.1016/j.chom.2020.10.003

14. Basaraba RJ, Smith EE, Shanley CA, Orme IM. Pulmonary lymphatics are primary sites of Mycobacterium tuberculosis infection in Guinea pigs infected by aerosol. *Infect Immun.* (2006) 74:5397–401. doi: 10.1128/IAI.00332-06

15. Henao-Tamayo M, Shanley CA, Verma D, Zilavy A, Stapleton MC, Furney SK, et al. The Efficacy of the BCG Vaccine against Newly Emerging Clinical Strains of Mycobacterium tuberculosis. *PloS One.* (2015) 10:e0136500. doi: 10.1371/journal.pone.0136500

16. Palanisamy GS, DuTeau N, Eisenach KD, Cave DM, Theus SA, Kreiswirth BN, et al. Clinical strains of Mycobacterium tuberculosis display a wide range of virulence in Guinea pigs. *Tubercul (Edinb)*. (2009) 89:203–9. doi: 10.1016/j.tube.2009.01.005

17. Lin PL, Ford CB, Coleman MT, Myers AJ, Gawande R, Ioerger T, et al. Sterilization of granulomas is common in active and latent tuberculosis despite within-host variability in bacterial killing. *Nat Med*. (2014) 20:75–9. doi: 10.1038/nm.3412

18. Scanga CA, Mohan VP, Yu K, Joseph H, Tanaka K, Chan J, et al. Depletion of CD4(+) T cells causes reactivation of murine persistent tuberculosis despite continued expression of interferon gamma and nitric oxide synthase 2. *J Exp Med*. (2000) 192:347–58. doi: 10.1084/jem.192.3.347

19. Yao S, Huang D, Chen CY, Halliday L, Wang RC, Chen ZW. CD4+ T cells contain early extrapulmonary tuberculosis (TB) dissemination and rapid TB progression and sustain multieffector functions of CD8+ T and CD3- lymphocytes: mechanisms of CD4+ T cell immunity. *J Immunol*. (2014) 192:2120–32. doi: 10.4049/jimmunol.1301373

20. Akter S, Chauhan KS, Dunlap MD, Choreno-Parra JA, Lu L, Esaulova E, et al. Mycobacterium tuberculosis infection drives a type I IFN signature in lung lymphocytes. *Cell Rep*. (2022) 39:110983. doi: 10.1016/j.celrep.2022.110983

21. Esaulova E, Das S, Singh DK, Choreno-Parra JA, Swain A, Arthur L, et al. The immune landscape in tuberculosis reveals populations linked to disease and latency. *Cell Host Microbe*. (2020) 29(2):165–78.e8. doi: 10.1016/j.chom.2020.11.013

22. Chen Y, Bharrhan S, Xu J, Sharma T, Wang Y, Salgame P, et al. B cells promote granulomatous inflammation during chronic Mycobacterium tuberculosis infection in mice. *PloS Pathog*. (2023) 19:e1011187. doi: 10.1371/journal.ppat.1011187

23. Lu LL, Das J, Grace PS, Fortune SM, Restrepo BI, Alter G. Antibody fc glycosylation discriminates between latent and active tuberculosis. *J Infect Dis*. (2020) 222:2093–102. doi: 10.1093/infdis/jiz643

24. Nziza N, Cizmeci D, Davies L, Irvine EB, Jung W, Fenderson BA, et al. Defining discriminatory antibody fingerprints in active and latent tuberculosis. *Front Immunol*. (2022) 13:856906. doi: 10.3389/fimmu.2022.856906

25. Booty MG, Nunes-Alves C, Carpenter SM, Jayaraman P, Behar SM. Multiple inflammatory cytokines converge to regulate CD8+ T cell expansion and function during tuberculosis. *J Immunol*. (2016) 196:1822–31. doi: 10.4049/jimmunol.1502206

26. Gideon HP, Hughes TK, Tzouanas CN, Wadsworth MH 2nd, Tu AA, Gierahn TM, et al. Multimodal profiling of lung granulomas in macaques reveals cellular correlates of tuberculosis control. *Immunity*. (2022) 55:827–46 e10. doi: 10.1016/j.immuni.2022.04.004

27. Yang JD, Mott D, Sutiwisesak R, Lu YJ, Raso F, Stowell B, et al. Mycobacterium tuberculosis-specific CD4+ and CD8+ T cells differ in their capacity to recognize infected macrophages. *PloS Pathog*. (2018) 14:e1007060. doi: 10.1371/journal.ppat.1007060

28. Hoff DR, Ryan GJ, Driver ER, Ssemakulu CC, De Groote MA, Basaraba RJ, et al. Location of intra- and extracellular M. tuberculosis populations in lungs of mice and Guinea pigs during disease progression and after drug treatment. *PloS One*. (2011) 6:e17550. doi: 10.1371/journal.pone.0017550

29. Ryan GJ, Shapiro HM, Lenaerts AJ. Improving acid-fast fluorescent staining for the detection of mycobacteria using a new nucleic acid staining approach. *Tubercul (Edinb)*. (2014) 94:511–8. doi: 10.1016/j.tube.2014.07.004

30. Vilcheze C, Kremer L. Acid-fast positive and acid-fast negative mycobacterium tuberculosis: the koch paradox. *Microbiol Spectr*. (2017) 5(2). doi: 10.1128/microbiolspec.TBTB2-0003-2015

31. Walter ND, Born SEM, Robertson GT, Reichlen M, Dide-Agossou C, Ektnitphong VA, et al. Mycobacterium tuberculosis precursor rRNA as a measure of treatment-shortening activity of drugs and regimens. *Nat Commun*. (2021) 12:2899. doi: 10.1038/s41467-021-22833-6

32. Henao-Tamayo MI, Obregon-Henao A, Arnett K, Shanley CA, Podell B, Orme IM, et al. Effect of bacillus Calmette-Guerin vaccination on CD4+Foxp3+ T cells during acquired immune response to Mycobacterium tuberculosis infection. *J Leukoc Biol*. (2016) 99:605–17. doi: 10.1189/jlb.4A0614-308RR

33. Tiwari S, Dutt TS, Chen B, Chen M, Kim J, Dai AZ, et al. BCG-Prime and boost with Esx-5 secretion system deletion mutant leads to better protection against clinical strains of Mycobacterium tuberculosis. *Vaccine*. (2020) 38:7156–65. doi: 10.1016/j.vaccine.2020.08.004

34. Larsen SE, Reese VA, Pecor T, Berube BJ, Cooper SK, Brewer G, et al. Subunit vaccine protects against a clinical isolate of Mycobacterium avium in wild type and immunocompromised mouse models. *Sci Rep*. (2021) 11:9040. doi: 10.1038/s41598-021-88291-8

35. Robertson GT, Ramey ME, Massoudi LM, Carter CL, Zimmerman M, Kaya F, et al. Comparative analysis of pharmacodynamics in the C3HeB/feJ mouse tuberculosis model for dprE1 inhibitors TBA-7371, PBTZ169, and OPC-167832. *Antimicrob Agents Chemother*. (2021) 65:e0058321. doi: 10.1128/AAC.00583-21

36. Dutt TS, Karger BR, Fox A, Youssef N, Dadhwal R, Ali MZ, et al. Mucosal exposure to non-tuberculous mycobacteria elicits B cell-mediated immunity against pulmonary tuberculosis. *Cell Rep*. (2022) 41:111783. doi: 10.1016/j.celrep.2022.111783

37. Rijnink WF, Ottenhoff THM, Joosten SA. B-cells and antibodies as contributors to effector immune responses in tuberculosis. *Front Immunol*. (2021) 12:640168. doi: 10.3389/fimmu.2021.640168

38. Walter ND, Ernest JP, Dide-Agossou C, Bauman AA, Ramey ME, Rossmassler K, et al. Lung microenvironments harbor Mycobacterium tuberculosis phenotypes with distinct treatment responses. *Antimicrob Agents Chemother*. (2023) 67:e0028423. doi: 10.1128/aac.00284-23

39. Voskuil MI, Schnappinger D, Visconti KC, Harrell MI, Dolganov GM, Sherman DR, et al. Inhibition of respiration by nitric oxide induces a Mycobacterium tuberculosis dormancy program. *J Exp Med*. (2003) 198:705–13. doi: 10.1084/jem.20030205

40. Scanga CA, Mohan VP, Joseph H, Yu K, Chan J, Flynn JL. Reactivation of latent tuberculosis: variations on the Cornell murine model. *Infect Immun*. (1999) 67:4531–8. doi: 10.1128/IAI.67.9.4531-4538.1999

41. van Pinxteren LA, Cassidy JP, Smedegaard BH, Agger EM, Andersen P. Control of latent Mycobacterium tuberculosis infection is dependent on CD8 T cells. *Eur J Immunol*. (2000) 30:3689–98. doi: 10.1002/(ISSN)1521-4141

42. Sarathy JP, Via LE, Weiner D, Blanc L, Boshoff H, Eugenin EA, et al. Extreme drug tolerance of mycobacterium tuberculosis in caseum. *Antimicrob Agents Chemother*. (2018) 62(2):e02266-17. doi: 10.1128/AAC.02266-17

43. Smith S, Liggitt D, Jeromsky E, Tan X, Skerrett SJ, Wilson CB. Local role for tumor necrosis factor alpha in the pulmonary inflammatory response to Mycobacterium tuberculosis infection. *Infect Immun*. (2002) 70:2082–9. doi: 10.1128/IAI.70.4.2082-2089.2002

44. Gill WP, Harik NS, Whiddon MR, Liao RP, Mittler JE, Sherman DR. A replication clock for Mycobacterium tuberculosis. *Nat Med*. (2009) 15:211–4. doi: 10.1038/nm.1915

45. McDaniel MM, Krishna N, Handagama WG, Eda S, Ganusov VV. Quantifying limits on replication, death, and quiescence of mycobacterium tuberculosis in mice. *Front Microbiol*. (2016) 7:862. doi: 10.3389/fmicb.2016.00862

46. Munoz-Elias EJ, Timm J, Botha T, Chan WT, Gomez JE, McKinney JD. Replication dynamics of Mycobacterium tuberculosis in chronically infected mice. *Infect Immun*. (2005) 73:546–51. doi: 10.1128/IAI.73.1.546-551.2005

47. Wynn EA, Dide-Agossou C, Reichlen M, Rossmassler K, Al Mubarak R, Reid JJ, et al. Transcriptional adaptation of Mycobacterium tuberculosis that survives prolonged multi-drug treatment in mice. *mBio*. (2023) 14:e0236323. doi: 10.1128/mbio.02363-23

48. McCaffrey EF, Donato M, Keren L, Chen Z, Delmastro A, Fitzpatrick MB, et al. The immunoregulatory landscape of human tuberculosis granulomas. *Nat Immunol*. (2022) 23:318–29. doi: 10.1038/s41590-021-01121-x

frontiers | Frontiers in Immunology

TYPE Review
PUBLISHED 02 September 2024
DOI 10.3389/fimmu.2024.1430955



OPEN ACCESS

EDITED BY
Laurel L. Lenz,
University of Colorado, United States

REVIEWED BY
Rajko Reljic,
St George's, University of London, United Kingdom
Stephen Cose,
University of London, United Kingdom

*CORRESPONDENCE
Ryan P. McNamara
rpmcnamara@mgh.harvard.edu

RECEIVED 10 May 2024
ACCEPTED 13 August 2024
PUBLISHED 02 September 2024

CITATION
Wang Q, Nag D, Baldwin SL, Coler RN and McNamara RP (2024) Antibodies as key mediators of protection against *Mycobacterium tuberculosis*. *Front. Immunol.* 15:1430955. doi: 10.3389/fimmu.2024.1430955



# Antibodies as key mediators of protection against *Mycobacterium tuberculosis*

Qixin Wang[1], Deepika Nag[2], Susan L. Baldwin[2], Rhea N. Coler[2,3,4] and Ryan P. McNamara[1*]

[1]Ragon Institute of Massachusetts General Hospital, Massachusetts Institute of Technology, and Harvard University, Cambridge, MA, United States, [2]Seattle Children's Research Institute, Center for Global Infectious Disease Research, Seattle, WA, United States, [3]Department of Pediatrics, University of Washington School of Medicine, Seattle, WA, United States, [4]Department of Global Health, University of Washington, Seattle, WA, United States

Tuberculosis (TB) is caused by infection with the bacterial pathogen *Mycobacterium tuberculosis* (M.tb) in the respiratory tract. There was an estimated 10.6 million people newly diagnosed with TB, and there were approximately 1.3 million deaths caused by TB in 2022. Although the global prevalence of TB has remained high for decades and is an annual leading cause of death attributed to infectious diseases, only one vaccine, Bacillus Calmette–Guérin (BCG), has been approved so far to prevent/attenuate TB disease. Correlates of protection or immunological mechanisms that are needed to control M.tb remain unknown. The protective role of antibodies after BCG vaccination has also remained largely unclear; however, recent studies have provided evidence for their involvement in protection against disease, as biomarkers for the state of infection, and as potential predictors of outcomes. Interestingly, the antibodies generated post-vaccination with BCG are linked to the activation of innate immune cascades, providing further evidence that antibody effector functions are critical for protection against respiratory pathogens such as M.tb. In this review, we aim to provide current knowledge of antibody application in TB diagnosis, prevention, and treatment. Particularly, this review will focus on 1) The role of antibodies in preventing M.tb infections through preventing Mtb adherence to epithelium, antibody-mediated phagocytosis, and antibody-mediated cellular cytotoxicity; 2) The M.tb-directed antibody response generated after vaccination and how humoral profiles with different glycosylation patterns of these antibodies are linked with protection against the disease state; and 3) How antibody-mediated immunity against M.tb can be further explored as early diagnosis biomarkers and different detection methods to combat the global M.tb burden. Broadening the paradigm of differentiated antibody profiling and antibody-based detection during TB disease progression offers new directions for diagnosis, treatment, and preventative strategies. This approach involves linking the aforementioned humoral responses with the disease state, progression, and clearance.

KEYWORDS

**tuberculosis, antibody, biomarkers, LTBI (latent TB infection), active tuberculosis (ATB), systems immunology, serology**

## Introduction

Tuberculosis (TB), caused by *Mycobacterium tuberculosis* (M.tb), is an infectious disease of the respiratory tract. M.tb is a deadly and highly transmissible airborne pathogen that is passed from person to person through inhalation of respiratory secretions containing viable bacilli. Approximately 10.6 million patients were diagnosed as TB-positive and approximately 1.3 million deaths were attributed to TB in 2022 (1) The only licensed vaccine against TB, Bacillus Calmette–Guérin (BCG), which consists of attenuated *Mycobacterium bovis*, provides a protective effect in newborns and children against disseminated TB but offers less protection against pulmonary TB (2). In a systematic review including 14 reported studies and nearly 3900 children under 16, a 20% reduction in M.tb infection was attributed to BCG vaccination based on an interferon gamma (IFNγ) release assay (3). However, the protection rate may be influenced by infections that occurred prior to vaccination that were either undetectable, asymptomatic, and/or cleared. Due to the global health concern posed by TB and the lack of effective vaccines providing long-term protection against M.tb infection, novel methods for diagnosis, prevention, and therapy for TB are urgently needed.

M.tb infection occurs through the respiratory route, typically targeting the alveolar space of the lungs where alveolar macrophages recognize and engulf M.tb (4, 5). The infected alveolar macrophages provide a shelter for M.tb that shields them from extracellular antibodies and complement proteins, which could facilitate bacterial removal. Within 2-8 weeks of initial infection, if M.tb survives the formation of phagolysosomes, which is common in M.tb infection, it undergoes exponential replication and potentially infects other cells such as alveolar epithelium, endothelium, and other leukocytes present in the mucosa such as neutrophils and dendritic cells (5–8). Granulomas, aggregates of these immune cells, are the hallmark of TB and serve as a reservoir of M.tb infection. Mucosal antibodies can theoretically directly block M.tb binding to epithelial cells, while other functional antibody-mediated immune responses can occur in either serum or mucosal sites. These functional antibody responses, including antibody-dependent cellular phagocytosis (ADCP), neutrophil phagocytosis (ADNP), complement deposition (ADCD), and cellular cytotoxicity (ADCC), can play significant roles in identifying and killing infected cells, and help to clear extracellular M.tb, all of which provide additional host immune mechanisms contributing to killing the bacteria at the site of infection preventing dissemination (Figure 1).

After decades of investigation, the immune responses and infection process of M.tb have been studied, yet the role of antibodies in preventing infection or disease development remains unclear. One of the challenges that has impeded progress in this area is the variable antibody profiling among TB cohorts, further complicated by the diversity of antibody profiles generated (9–13). We previously demonstrated a positive correlation between IgM, IgA, and IgG levels against LAM, Apa, and PstS1 in serum or bronchoalveolar lavage fluid (BALF) and a decreased M.tb infection rate in non-human primates (NHP) after BCG vaccination (14). Additionally, we found that FcγR binding was higher and ADCC was more activated in patients with latent TB infection (LTBI) compared to those with active TB (ATB). Here, IgG from LTBI patients limited more M.tb surviving in macrophages than IgG from ATB patients (13). These findings suggest that a boosted humoral antibody profile could prevent M.tb infection from its onset, and antibody-mediated functions were critical in controlling the LTBI to ATBI switch in people infected with M.tb.

Advancements in understanding the role of antibodies in preventing M.tb infections, TB development, and the diagnosis of M.tb infections are crucial for developing new clinical methods to prevent the spread of M.tb and the progression of TB disease. Antibodies that protect against M.tb infection could serve as potential standards for vaccine development, while antibody-mediated immunity triggered by M.tb infection could be leveraged for post-infection treatment. Furthermore, antibodies present in the early stages of infection could serve as biomarkers to (i) improve M.tb detection, (ii) classify the disease state, and (iii) predict responses to treatment. Several antibody responses correlated with M.tb infection or after M.tb vaccination, such as opsonophagocytic clearance (ADCP, ADNP), ADCC, and the functional diversity of antibodies against M.tb are discussed (15, 16). In this review, we expand on these concepts and provide a current overview of antibody profiling and its functions in preventing TB development as well as its potential as a diagnostic marker to limit the transmission of M.tb in TB-endemic regions.

## Antibody maturation

Encounters with an antigen begin the process of antibody development and affinity maturation. A B cell receptor (BCR) can bind to an antigen and then signal for its presentation in the form of cleaved peptides to T cells through the major histocompatibility complex 2 (MHC II) on the cell surface. From there, the T cell stimulates B cell activation and proliferation through the interaction of CD40 ligand (CD40L) with CD40 on the B cell surface along with the secretion of various interleukins (ILs) such as IL-2 and IL-5. At this point, the B cell can begin the evolutionary marvel of somatic hypermutation (SHM) (17–19). The Fab domain of an antibody mediates its attachment to an antigen (Figure 1A), which is encoded within the heavy (*IgH*) and light (*IgL*) chains of the immunoglobulin genes. After stimulated expression of *IgH* and *IgL*, the B cell undergoes SHM to diversify the Fab's binding pocket and generate immunoglobins targeting specific antigens. The B cells that produce low-affinity immunoglobin undergo apoptosis (20).

Once an antibody recognizes its targeted antigen, it can mediate a number of downstream processes. One of the most recognized functions is neutralization. Antibodies can directly bind to a region of a pathogen or toxin that is used for cellular entry (Figure 1B). While neutralizing antibodies typically target the receptor binding domain (RBD) of pathogen proteins and/or pathogen toxins, they can still exert neutralization at other sites. The primary mechanism of protection by neutralizing antibodies has long been proposed to be through direct steric hindrance of the RBD with its receptor. However, there are clearly other mechanisms by which neutralizing

10.3389/fimmu.2024.1430955

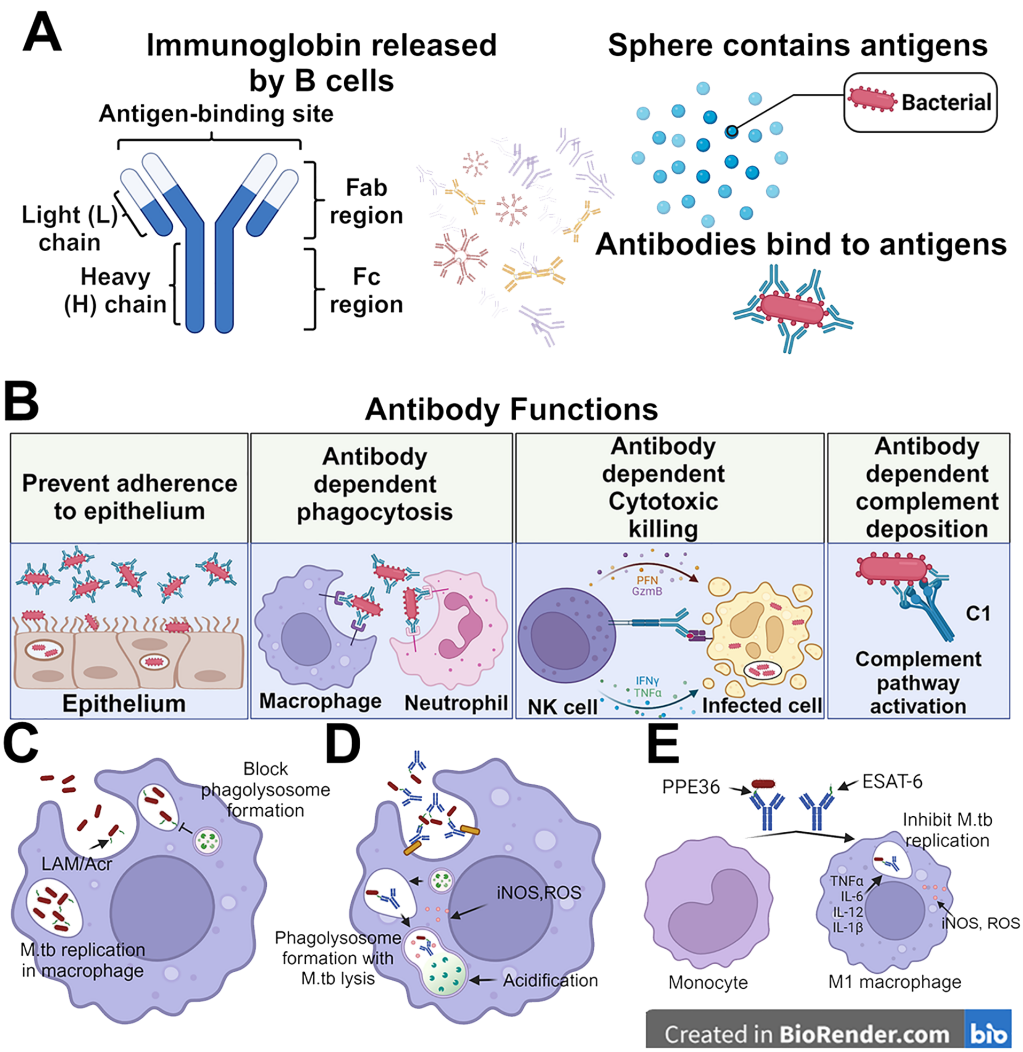


FIGURE 1
Protective roles for antibodies in M.tb control. **(A)** Antibodies consist of a Fab region which directly binds to target antigens and an Fc region which binds to cell-surfaced expressed receptors. The antibodies can bind to the surface of antigens and mediate different immunity functions. **(B)** Antibodies can leverage both their Fab and Fc domains to protect against M.tb. This can be done through direct binding of the bacteria to prevent adherence to the epithelium, opsinophagocytosis, cellular cytotoxicity activation, and complement deposition. **(C)** The M.tb not bound by the antibodies are able to replicate in the macrophages and inhibit the formation of phagolysosome. **(D)** while the antibody recognition helps the macrophage to lysis the M.tb via lysosome. **(E)** The monocytes also can be differentiated by the anti-PPE36 and anti-ESAT-6 antibodies into M1-polarized macrophages which release inflammatory cytokines to inhibit the self-replication of M.tb in the infected macrophage.

antibodies can inhibit cell entry of a toxin or whole organism/virus into a cell. Currently, no direct evidence proves that neutralizing antibodies exist in preventing M.tb infection.

## Antibody-mediated functions and Mycobacterium tuberculosis infection

### Prevention of adherence to lung epithelium

The abundance and repertoire of antibodies in the mucosa can be distinct from the serum profile within the same individual. The maturation of tissue-resident plasma cells to produce the specific antibody against M.tb antigens is in parallel with the progression of infection, which is common across most infectious diseases (21, 22). The specific mechanisms of antibody subclasses in preventing M.tb adherence to the mucosal surface may also depend on compartmentalization. Currently, although antibodies may play a role in defense against M.tb, there are no known mycobacteria-specific antibodies that can neutralize M.tb or inactivate M.tb extracellularly on their own which results in full sterilizing immunity. Immune responses to M.tb instead likely require many different cell types, representing both cellular and humoral immunity (for a review, see (23)). In BCG-immunized individuals, antibodies directed toward shared antigens should theoretically be able to inhibit or contribute to the prevention of infection. Antibodies specific for heparin-binding hemagglutinin (HBHA) as well as lipoarabinomannan (LAM), both of which are M.tb virulence factors on the surface of the bacilli, show some promise in host defense against M.tb infection. HBHA IgA

antibodies at the mucosa, for example, can block M.tb infection of lung epithelial cells (9) which in turn can help prevent dissemination of M.tb from the lungs to other organs. Interestingly, anti-HBHA IgG antibodies were shown to have the opposite effect, instead facilitating M.tb infection (9). Considering the infection route and site of M.tb, mucosal antibodies would be more likely prominent players in preventing the infection state than antibodies circulating in serum. IgA is the most abundant immunoglobins at this interface, although this antibody can also be detected in serum as well (24–26). IgA, specific to several M.tb antigens, can be observed in the pleural fluid in pleural TB patients (27). Nasal-resident IgA also showed a protective effect in inhibiting the M.tb growth and infection with the necessary activation of FcαR (22). In addition to the effective role of IgA, relevant lung epithelial cells express Fc receptors that primarily interact with IgG, providing another potential layer of humoral immunity at this site of M.tb infection.

## Opsonophagocytosis

Intracellular growth inhibition of M.tb following opsonophagocytosis, a process involving antibody-directed phagocytosis by macrophages and neutrophils (24, 26, 28–31), utilizing serum from BCG-immunized humans, has shown a potential protective role for arabinomannan-specific antibodies (32). Furthermore, the opsonophagocytosis process of killed M.tb in the presence of anti-LAM and anti-Acr (a major 16-kD a-crystallin membrane protein (33) donor-derived antibodies also results in phagosomal maturation of M.tb infected macrophages, leading to a cascade of host-mediated microbicidal responses such as the production of nitric oxide and acidification (34) (Figure 1B). Our group is currently studying the effects of adjuvants on M.tb vaccine-induced functional antibody responses against M.tb infection including opsonophagocytosis. Generating optimal antibody responses in the context of an immunotherapeutic M.tb vaccine, as an adjunct to drug treatment, could provide additional protection against persistent or recurrent M.tb (24, 26, 28–31).

For IgG subclasses, the Fc-domain can bind to FcγRs on the surface of phagocytic cells. Pro-phagocytic FcγRs include the high-affinity FcγRI (CD64) and the low-affinity FcγRIIA and FcγRIIIB (CD32a and CD16b, respectively). Phagocytosis can also occur through the recognition of complement deposited on an antigen through Fc-C1q. This deposition of complement on an antigen, or on the antibody itself bound to the antigen, can flag the complex for engulfment by phagocytes with complement receptors on their cell surface. Opsonophagocytic antibodies have been linked to protection against other intracellular bacteria as well as M.tb, including *Staphylococcus aureus*, *Escherichia coli*, *Salmonella*, and *Shigella* (35–37).

Regarding opsonophagocytosis, antibody-mediated phagocytosis is followed by phagolysosome fusion to digest antibody-bound complexes/microorganisms. This is enhanced through intracellular FcγR signaling activation (38). Interestingly, it is known that M.tb can inhibit the phagosome-lysosome fusion via a reduced $Ca^{2+}$ pathway. Thus the bacteria can be engulfed by phagocytic cells such as macrophages, but are not killed through canonical opsonophagocytosis signaling (39). This phenomenon was shown to be antigen-specific, for example in the case of M.tb, anti-LAM mediated phagocytosis presented a higher rate of M.tb killing (39). Macrophage activation, especially M1 polarization, occurs during M.tb acute infection, initiates inflammatory cytokine release, and generates oxidative species to eliminate both the intracellular and local extracellular M.tb (40). The M.tb surface protein PPE36 inhibited the M1 polarization and reduced the inflammatory cytokine production from macrophages, which enhanced the survival of M.tb (41, 42). In TB patients, the levels of IgA against PPE36 were found to be significantly higher compared to healthy control, while less elevation was noticed in either IgG or IgM (43). As mentioned above, IgA is the most dominant antibody at the site of M.tb infection, and IgA against PPE36 could inactivate the function of PPE36 and activate the M1 polarization. Another surface protein, Rv1507A, promoted the polarization of M1 macrophages, enhanced the proinflammatory cytokine release of IFN-γ and tumor necrosis factor alpha (TNF-α), and upregulated the macrophage-driven phagocytosis (44). The secreted antigen ESAT-6 also can activate the M1 macrophage polarization, and anti-ESAT-6 immunoglobin helps to inhibit the proliferation of M.tb in the infected macrophages (45–47). Taken together, antibodies targeting either M.tb surface or secreted antigens may augment their immune-evading roles, and shift the humoral response to a more functional opsonophagocytic nature against M.tb. Antibody responses to specific antigens after administration of vaccines that developed against M.tb should be further evaluated to make sure specific categories of antibodies can mediate efficient phagolysosome formation and intracellular removal of M.tb.

In addition to macrophages, neutrophils are also recruited to the site of infection by the released cytokine and chemokines. These neutrophils produce hypochlorous acid, proteases, and cytokines, and can create neutrophil extracellular traps as well as mediate phagocytosis to eliminate extracellular M.tb (48). Our previous study reported that BCG-vaccinated NHP exhibited a higher level of antibody-dependent neutrophil phagocytosis facilitated by anti-LAM immunoglobulin (14). Another study showed that IgG from LTBI patients reduced M.tb burden in infected macrophages more effectively compared to the IgG from ATB patients. On the other hand, ADCP and ADNP were more triggered by antibodies from ATB patients compared to LTBI patients (13). M.tb can block the formation of the phagolysosome which makes the macrophages an ideal environment for M.tb replication and further infection. However, there is limited research on antibody-mediated neutrophil-driven M.tb removal. Understanding how specific antibodies engage neutrophils for phagocytosis and whether phagolysosome formation occurs within these innate cells in the alveoli remains largely unexplored.

## Cellular cytotoxicity killing and natural killer cell activation

Natural killer cells (NK) are major innate lymphoid cells that play a similar role to CD8+ cytotoxic T cells. Unlike their CD8+T cell counterparts, however, NK cells do not express the T cell receptor (TCR) on their surface and can be thought of as more of a pan-cellular innate surveillance cell.

NK cells are activated by antibodies through binding of the FcγRIIIA (CD16a) on the surface (Figure 1B). Studies have shown

that this binding is correlated with the afucosylation of the Fc-domain in IgG subclasses, predominantly IgG1 and IgG3 (49–52). Downstream activation signals funnel into the secretion of IFN-γ, cellular degranulation, and secretion of other inflammatory/recruiting cytokines such as TNF-α, macrophage inflammatory protein-1β (MIP-1β), and a host of interleukins (IL) such as IL-2, IL-12, and IL-18. The combined result of activation of these signaling networks results in ADCC by the NK cells.

ADCC has been shown to play an instrumental role in combating a wide range of infectious agents including viruses, intracellular bacteria, and protozoa (53–55). The coupled degranulation and recruitment of other inflammatory cells through cytokines allow for the rapid clearance of a localized infection. This same model can be translated to a growing mass of tumor cells whereby ADCC acts to wipe out a growing malignancy (56).

The role of NK cells in protecting against M.tb infection is yet to be fully investigated. Canonical mechanism(s) of elimination of M.tb by NK cells included releasing cytotoxic chemicals (perforin and granulysin) after binding to the bacterium and interacting with macrophages or neutrophils to remove the M.tb indirectly (57, 58). The surface receptors of NK cells, NKp46 and NKp44, can be activated by the M.tb surface antigens galactan and peptidoglycan, and initiate the direct killing of M.tb by NK cells (57, 59). Unlike the opsonized phagocytosis via macrophages and neutrophils, NK cells work differently when interacting with antibody-dependent mechanisms. Directly recognized M.tb antigen by the NKp44-Fc region activates the NK cells, and BCG vaccination enhances the surface expression of NKp44 on NK cells (59). NK cells also recognize and lyse the M.tb-infected macrophages via NKp46 (60).

In terms of antibody-mediated NK cell activation, Irvine et al. showed that the serum antibody targeting LAM in BCG-vaccinated NHP presented limited NK cell activation, while the antibody targeting LAM in lavage fluid showed activation of NK cells (14). The enrichment of activated NK cells in the mucosa can later recognize either the extracellular M.tb or M.tb infected monocytes via NKp44 or TLR-2 to the peptidoglycan axis (59, 61). Abundance and maturation of NK cells within the pleural fluid are thought to be low, so many of these assays to quantify antibody-dependent effects are in artificial systems (14). That said, there is a growing body of literature implicating the role of NK cells in controlling and removing M.tb within the lower respiratory tract. Whereas some anti-M.tb immunoglobins are able to activate NK cells, including antibodies from the serum of humans immunized with ID93 +GLA-SE (62), further investigation is needed to understand the direct antibody-mediated mechanisms involved in the recognition and elimination of M.tb.

# Antibodies and Mycobacterium tuberculosis vaccines

## Antibody profiling and M.tb vaccine development

The role of antibodies in the control of M.tb has been historically controversial. The BCG vaccine has been licensed and deployed to protect against TB. While efficacy has been strong against severe TB in children and against pulmonary TB in low-endemicity regions, there is low protection against pulmonary TB in TB endemic countries. Moreover, BCG vaccination appears to offer low effectiveness in blunting onward transmission of M.tb (15, 63). The mechanism of protection against TB had been proposed to be mediated through cellular immunity, namely CD8+ and CD4+ T cells. This model was built up in large part due to the intracellular nature of M.tb and not in a cell-free state of the pathogen such as seen with respiratory viruses. However, as our appreciation for the non-neutralizing roles of antibodies has grown, we have had to revisit this long-standing dogma that cellular immunity is the sole means of controlling intracellular pathogens such as M.tb.

Several independent studies have shown that TB vaccines elicit antibody responses that correlate with protection. This includes the M72/AS01$_E$ vaccine that protects against disease progression in healthy IFN-γ release assays (IGRA)-positive M.tb exposed individuals (64, 65), pulmonary-delivered BCG in rhesus macaques (66), intravenous-delivered BCG (14), and arabinomannan-protein M.tb Ag85 conjugate vaccine (67). The ID93 vaccine candidate (made up of a fusion of 4 M.tb proteins: Rv2608, Rv3620, Rv1813, and Rv3619) administered with the TLR-4 agonist (GLA-SE), was shown to enhance vaccine-specific IgG1 and IgG3 antibody titers, NK activation, and opsonophagocytosis, in addition to an increased CD4+ T helper 1 (Th1) response (defined by IFN-γ, TNF-α, and IL-2 production from ID93-specific CD4+ T cells) (62). To that end, there is an emerging model in the field of M.tb vaccinations that cellular immunity is not solely responsible for protection against TB; similarly, antibody-mediated protection against TB is not functioning in a vacuum. Instead, both cellular and humoral immunity appear to be working in concert to limit the TB disease state (62).

The protective role of antibodies in TB disease progression has also been supported through the transfer of antibodies from an infected or vaccinated donor. In mice, high-dose IVIG attenuated bacterial growth in the lungs. This protection was lost in athymic mice, further supporting a model where antibodies and cellular immunity work in concert to limit pathogen spread and disease progression (68). Subsequent studies demonstrated that antibodies taken from individuals with high occupational exposure to M.tb could protect against aerosolized challenged mice. The antibodies were reactive towards surface-expressed M.tb antigens, and again, the protection offered by antibodies was dependent on the presence of T cells (69). Mechanistically, the glycosylation status of the Fc domain of the antibody appeared to be linked to bacterial killing. Moreover, the state of TB (active vs. latent) strongly influences the antibody response and activity (13). In ATB patients, higher levels of IgG1 to LAM and PPD, IgA1 against PPD, and IgG3 against groES were identified compared to LTBI patients (70).

## Antibody glycosylation

Antibody glycosylation including fucosylation, galactosylation digalactosylation, and sialylation, has been used as biomarkers for differentiating between LTBI and ATB (13) (Figure 2). In one study, lower levels of fucose were observed in IgG from LTBI compared to ATB patients (71). Fucosylation/afucosulation status has been shown to be linked to FcγRIIIA binding and downstream

signaling (49). Additionally, LTBI patients exhibited increased levels of di-galactosylation and sialylation, along with lower agalactosylation on IgG compared to ATB patients, indicating a heightened inflammatory state in ATB (13, 72–74). Specifically, glycosylation was predominantly observed in Fc regions rather than Fab regions and showed antigen specificity towards PPD and Ag85A (75). Furthermore, differentiated antibody glycosylation distinguishes not only between ATB and LTBI populations, but also identifies differences between ATB and treated ATB groups. Increased sialylation was found in treated ATB patients compared to untreated subjects, while no difference was observed regardless of the treatment (72). Despite extensive research into glycosylated antibodies in various M.tb infection cohorts, little work has been done to characterize the glycosylation status of antibodies following BCG vaccination, the only currently licensed vaccine (76). Notably, antibody glycosylation was only identified after M.tb infection in mice, indicating its potential as a marker of infection (76). Distinct glycosylated antibodies induced by M.tb infections could potentially aid in identifying infected macrophages and promoting phagocytosis or ADCC in cell-surfaced exposed antigens, whereas differentiated glycan removal may attenuate this process (13). RNA/DNA nucleic acid-derived M.tb vaccines expressing proteins that undergo glycosylation within the host cell may detrimentally provide 'self-glycans' on the protein masking the epitope needed for lymphocyte recognition and acquired immunity against M.tb (both humoral and cellular), whereas the mycobacterial-derived protein combined with an adjuvant may provide a more robust immune response (77).

## Antibodies as biomarkers for M.tb disease state

M.tb poses formidable challenges due to its ability to establish latent infection, leading to active disease in susceptible individuals (78). Timely and precise identification of TB plays a pivotal role in the efficient handling and containment of the disease. In recent years, there has been a growing interest in utilizing antibodies as biomarkers for assessing the disease state of TB, offering new avenues for improved diagnosis, treatment monitoring, and patient management (13, 72, 75).

## Antibodies as biomarkers to M.tb infection

Upon infection with M.tb, the host immune system mounts a complex response involving various immune cells and immune signaling moieties, including antibodies. It is well established that B cells produce antibodies in response to specific antigens derived from M.tb (79, 80). As mentioned before, antibody treatment significantly decreased the bacterial burden in mice infected with M.tb (81), and IgM responses to BCG were strongly linked with suppressed M.tb survival *in vivo* (14). Studies have also highlighted distinctions in the antibody structure between ATB and LTBI in clinical serum samples (75). This distinction in antibody features in different disease states could be an important biomarker for TB.

Biomarkers are measurable indicators of biological processes, disease states, or responses to therapeutic interventions. In the context of TB, biomarkers represent a significant avenue for enhancing diagnostic precision, evaluating treatment effectiveness, and predicting disease outcomes. Antibodies produced in response to M.tb infection offer valuable insights as biomarkers owing to their specificity and fluctuating levels across the progression of the infection. However, the application of serological tests in TB diagnosis remains debatable due to the poor sensitivity and specificity compared to existing methods (82–84). Ongoing work seeking to standardize antibody signatures as biomarkers for TB will be highly beneficial.

To date, individual antibodies, or a clustered signature of antibodies against different antigens have both been studied with varied sensitivity and specificity in identifying ATB patients. Several studies have been done to investigate the use of antibodies as biomarkers for identifying TB infection status, as summarized in the tabular form (Table 1). The use of single antibody readouts and multivariate analyses have been reported with various sensitivity and specificity readouts as biomarkers. One study using anti-PPE17 IgG showed ~70% sensitivity in identifying an LTBI cohort from non-TB patients (85). IgG and IgA to different M.tb antigens consist

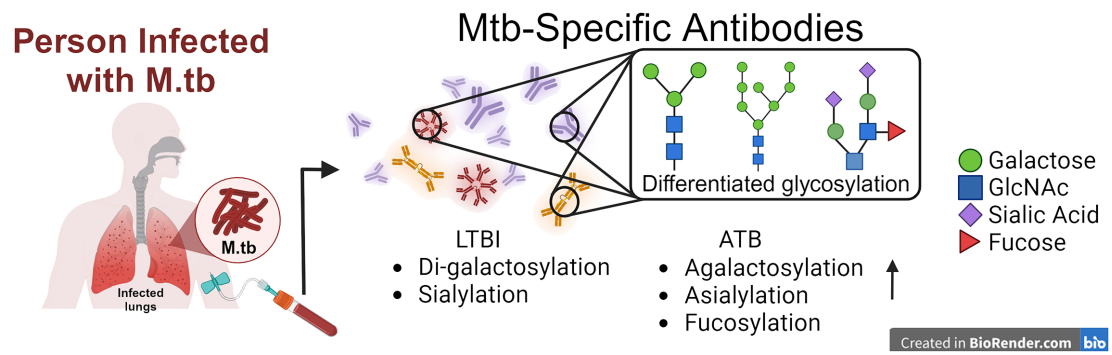


FIGURE 2
Translating antibody-based readouts novel vaccine platforms. Composite profiling of the total humoral profile can be investigated in the future with differentiated glycosylation signatures in favor of future vaccine designs against TB.

of the majority of proposed biomarker candidates in TB diagnosis (80, 83, 87, 106, 107 (86, 87),. Antibody responses to M.tb antigens, specifically IgG against TBCM and CFP-10, and IgG and IgA against Ag85B, can effectively distinguish between active tuberculosis (ATB), latent tuberculosis infection (LTBI), and non-infected individuals, providing a potential biomarker for M.tb infection (86). IgG and IgA levels against the Rv2031 antigen significantly differ among patients with active TB, their household contacts, and non-infected controls (87). An interesting marker for ongoing inflammation and severity of TB disease is IgG4 in humans. In a study including healthy, LTBI, ATB, and treated ATB cohorts, PPD-specific IgG4 as well as HspX and GroEs-specific IgG4 levels were increased in ATB, and lower levels were associated with either LTBI or treated subjects (72). Despite being linked to M.tb control (14), there is limited study on IgM as a biomarker for M.tb infection. This could be due to the inherently low affinity of IgM compared to the affinity selected IgG and IgA (88). Considering the appearance duration of IgM in the humoral antibody profile throughout the infection, IgM may serve as biomarkers for an early, albeit lower-confidence, detection method of M.tb infection. Both IgG and IgA exist both in serum and mucosa and are more likely to play crucial roles in defending against M.tb re-infection or ATB development from LTBI (89). Additionally, it is well known that affinity-matured antibody

TABLE 1 Antibodies as biomarkers to identify M.tb infection and/or different TB states.

| Sample Comparison | Antibody against antigens used | Serological assays defining M.tb infection/state; Ab levels | Sensitivity | Specificity | Reference |
|---|---|---|---|---|---|
| LTBI vs NI | IgG against PPE17 | ELISA sensitivity to Ag PPE17> ESAT-6:CFP-10 and PPD; ATB/LTBI>NI | 69.62% | N/A | (85) |
| ATB vs NI | IgG against PPE17 | | 94.93% | | |
| ATB vs Control (Non-TB+LTBI) | IgA/IgG against Mce1A | ELISA IgA/IgG anti-Mce1A; ATB>LTBI/NI | 59% (IgA), 51% (IgM), 80% (IgG) | 77%(IgA), 83% (IgM), and 84% (IgG) | (90) |
| AFB microscopy positive vs negative | Ig against Rv3881c, Rv0934, Rv0054, Rv3804c, Rv2031c, Rv1886c, Rv0129c, Rv1860 | Microbead coating with M.tb antigens; AFB(+) stain>AFB(-) stain | 92.20% | 74.70% | (91) |
| | Ig against Rv1980c, Rv3874, Rv0831c, Rv2875, Rv3841, Rv1926c, Rv3875, Rv2878c | | 93% | 79.30% | |
| ATB vs NI | IgA/IgG against A60 | ELISA anti-A60; ATB>NI | 31.3%(IgA) and 94% (IgG) | 92%(IgA) and 96% (IgG) | (94) |
| M.tb infection vs Control | IgG against M.TB48 | ELISA anti M.TB48; IgG AFB(+) stain>AFB(-) stain | 74.1% | 97.80% | (113) |
| Patients with and without culture-confirmed TB | Ig against Ag85B, Ag85A, Ag85C, Rv0934-P38, Rv3881, BfrB, Rv3873, and Rv2878c | MMIA; M.tb infection > NI | 90.6% | 88.6% | (114) |
| AFB microscopy positive vs negative | Ig against Rv3881c, Rv0934, Rv2031c, Rv1886c, Rv1860, Rv3874, Rv3875, Rv3804c, Rv3418c, Rv3507, Rv1926c, Rv3874-Rv3875 fusion, Rv2878c, Rv1099, Rv3619, Rv1677, Rv2220, Rv2032, Rv1984c, Rv3873, Rv0054, Rv3841, Rv1566c, Rv2875, Rv0129c, Rv1009, Rv1980c | MMIA; AFB(+) stain>AFB(-) stain | 91% | 93-99% | (115) |
| ATB vs healthy | IgG against Rv0310c-E and Rv3425 | ELISA; SPPT>SNPT/NI | 82.54% | 76.92% | (116) |
| | IgG against Rv1255c-E and Rv3425 | ELISA; SNPT>NI | | | |
| ATB vs Control (Non-TB+LTBI) | Ig against PstS1, Rv0831c, FbpA, EspB, bfrB, HspX and ssb | LIPS; ATB>NI/LTBI | 73.5% | 100% | (117) |
| ATB vs Patient with anti-TB treatment | IgA/IgM anti16kDa | ELISA; ATB>others | 90% for both IgA and IgM | 95% (IgA) and 90%(IgM) | (99) |
| ATB vs LTBI | Anti-LAM IgA<br>Anti-TB-LTBI IgG<br>Anti-Tpx IgG<br>Anti-MPT64 IgA | ELISA combination of Abs; ATB>LTBI | N/A | 100% accuracy | |

*(Continued)*

TABLE 1 Continued

| Sample Comparison | Antibody against antigens used | Serological assays defining M.tb infection/state; Ab levels | Sensitivity | Specificity | Reference |
|---|---|---|---|---|---|
| ATB vs LTBI/NI | Anti-16 kDa IgA, anti-MPT64 IgA | ELISA; ATB>others | 90% for Anti-16 kDa IgA, 90% for anti-MPT64 IgA | 95% for Anti-16 kDa IgA, 90% for anti-MPT64 IgA | |
| ATB vs NI | IgG against LAM | ELISA; ATB>LTBI/NI | 71.40% | 86.60% | (118) |
| ATB vs LTBI | IgG against LAM | | 83.30% | 76.40% | |
| ATB vs NI | IgA anti LAM and HSP20 with IgG anti HSP16.3, LAM, and Tpx | | 81% | 94% | |
| ATB vs LTBI | IgA anti LAM and Tpx, IgG anti LAM and TPX, IgM anti Apa | | 81% | 91.50% | |
| ATB vs LTBI vs NI | IgG against TBCM, Ag85B, CFP-10 | ELISA; ATB>LTBI>NI | N/A | N/A | (86) |
| | IgA against Ag85B | ATB>LTBI>NI | | | |
| | IgG against Ag85B | ATB>LTBI | | | |
| ATB vs Contacts vs Controls (NI) | IgA and IgG against Rv2031 | ELISA; ATB>household contacts>NI | N/A | N/A | (87) |
| ATB vs NI | IgG against Ag85 | ELISA; ATB>NI | 84.1 | 85.2% | (119) |
| | IgG against CFP-10 | | 66 | 85.2 | |
| | IgG against ESAT-6 | | 64.9 | 88.9 | |

ATB, Active TB; LTBI, Latent TB Infection; NI, Not Infected; AFB, Acid-Fast Bacillus; MMIA, Multiplex Microbead Immunoassay; SPPT, Smear-Positive Pulmonary TB; SNPT, Smear-Negative Pulmonary TB; LIPS, Luciferase Immunoprecipitation Systems.

responses to M.tb are stronger to select antigens such as those on the bacterial cell surface (4, 12, 13, 27, 64–66, 70, 80, 83, 90, 91). Therefore, a panel of IgA and IgG against multiple M.tb antigens could be considered as biomarker candidates to monitor the development of ATB from LTBI patients in TB endemic regions, which the IGRA test cannot identify (86). Figure 3 demonstrates how the immunoglobulins against antigens could be utilized not only for the detection of active TB but also for distinguishing between ATB and LTBI.

## Detection methods

Several methods are available for detecting M.tb-specific antibodies in patient samples, each with its advantages and limitations. Enzyme-linked immunosorbent assay (ELISA) is a widely used technique that allows for the quantitative measurement of antibody levels in serum, plasma, or other bodily fluids (90, 92, 93). ELISA-based assays offer high sensitivity and specificity and are amenable to high-throughput screening (94). Other approaches, such as multiplex immunoassays (95) and lateral flow assays (96–98), provide rapid and cost-effective alternatives suitable for point-of-care settings where access to laboratory facilities may be limited. Since a combination of M.tb-specific antibodies as biomarkers to evaluate the M.tb infections showed higher sensitivity and specificity than applying individual antibody approaches (99), developing high-throughput methods with multiplexed measurements may not only be more accurate, but also more cost-effective as disease incidence and/or progression biomarkers due to the long experimental duration and high cost of ELISA in detecting individual antibody isotypes/subclasses to discreet antigens, and their body fluid concentration(s). Other than ELISA and Luminex-based measurement, antibody-antigen binding activity measured by surface plasmon resonance (SPR) and total internal reflectance fluorescence (TIRF) microscopy-based biosensors (100, 101) have also been studied. While these technologies are emerging and have unique strengths, they can be limited to the detection of a single antigen or a few antigens at a time. Super-resolution microscopy-based detection methods have also been employed for M.tb protein expression and detection (102). Such a tool, which can utilize antibodies as a detector, has been employed to identify M.tb responses to drug treatments (103).

## Clinical utility

The use of antibodies as biomarkers for TB offers several advantages over traditional diagnostic methods. Antibody-based tests are non-invasive and can be performed on readily accessible samples, such as blood, saliva, or urine, making them suitable for use in diverse settings, including resource-limited areas (95, 96, 104). Moreover, antibody tests have the potential to detect TB

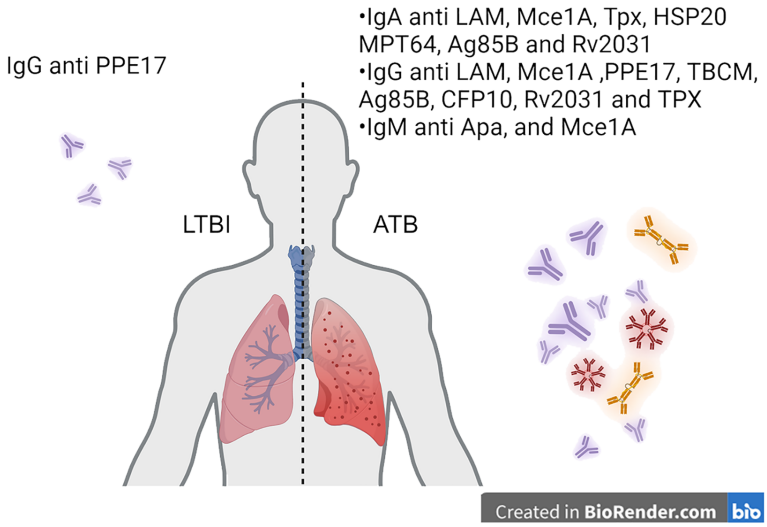


FIGURE 3
Translating antibody-based readouts to biomarkers of disease states. Antibodies specific to M.tb targets can be analyzed at the isotype and subclass level. Additionally, post-translational modifications can be identified on antigen-specific antibodies to identify signatures of disease states such as latency and active TB.

infection at an earlier stage than conventional microbiological methods, enabling prompt initiation of treatment and reducing the risk of disease transmission.

Furthermore, longitudinal monitoring of antibody levels can provide valuable insights into treatment response and disease progression. Changes in antibody titers over time may serve as indicators of treatment efficacy, allowing clinicians to tailor therapy regimens and optimize patient care. Additionally, antibody-based biomarkers hold promise for predicting treatment outcomes and identifying individuals at increased risk of disease relapse, thereby informing clinical decision-making, and improving patient outcomes. Biomarkers and antibody signatures of disease/infection are an emerging field of study that warrants further research in the areas of vaccine design, antibody-based therapies, and disease states.

## Challenges and future directions

Although studies have been conducted to understand the antibody differentiation during M.tb infection and TB development, limited vaccines have been developed to protect the adults who are exposed to M.tb, and there is still a knowledge gap in how antibody-mediated immunity controls M.tb infections. The discovery of dynamic antibody profiling at different stages of TB progression and M.tb infection is necessary to design new M.tb vaccines with better efficacy of M.tb removal after infection. Considering the principle of how NK cells participate in eliminating M.tb infected cells is not clear, further investigations are needed to understand the role of antibody-mediated NK cell activation in protecting against M.tb infection and TB development.

Despite their potential, antibody-based biomarkers for TB face several challenges that must be addressed to realize their full clinical utility. Studies show that recognition of M.tb antigens may vary among individuals, leading to the presence of different sets of antigen-specific antibody populations in samples (10), while cross-reactivity among different mycobacterial and nontuberculous mycobacterial species is also observed (105, 106). Variability in antibody responses among individuals, as well as cross-reactivity with other mycobacterial species or non-specific immune responses, may affect the accuracy of antibody-based assays. Standardization of assay protocols, validation in diverse populations, and integration into existing diagnostic algorithms are essential steps toward overcoming these challenges and ensuring the reliability and reproducibility of antibody-based tests for TB.

Furthermore, ongoing research efforts are focused on identifying novel antigen targets and developing innovative assay platforms capable of detecting multiple antibody specificities simultaneously (107). Additionally, the incorporation of antibody-based biomarkers into comprehensive diagnostic strategies, including imaging modalities and nucleic acid amplification tests, holds promise for enhancing the accuracy and efficiency of TB diagnosis and management.

Employment of therapeutic antibodies against TB is an emerging field, as is how to fine-tune humoral responses through vaccination platforms. It is known that vaccine platform and delivery route influence how antibodies leverage both Fab and Fc regions (14, 25, 88, 108–111). Given the emerging role of antibodies as mediators of protection against M.tb, further work characterizing precise mechanisms of protection at various stages within TB disease progress is needed. Such advances can reduce disease incidence and burden.

In conclusion, antibodies stand as hopeful treatments for disease and indicators for evaluating the progression of TB, presenting fresh avenues for enhanced diagnosis, treatment tracking, and patient care. Their unique specificity, ease of access,

and fluctuating patterns over the infection timeline render them invaluable instruments for early TB detection, treatment progress monitoring, and prognosis forecasting (Figure 2). Through ongoing exploration and creativity, antibody-centric examinations hold the promise to transform TB diagnostics and bolster worldwide endeavors to reduce disease burden.

## Concluding remarks

Antibody responses are not limited to pathogens that exist and/or circulate extracellularly. Moreover, antibody functions often bridge the adaptive and innate arms of the immune response. For example, an affinity-matured IgG or IgA isotype can bind to a target antigen and use its Fc domain to interact with FcRs on the surface of innate immune cells such as NK cells or neutrophils, and initiate inflammatory signaling cascades. This signaling can further recruit additional inflammatory cells to the site of the identified pathogen, helping to clear the infection.

Studies of antibody responses to M.tb have provided significant insight into how antibodies mobilize multiple aspects of the immune system to combat this pathogen. M.tb predominantly resides inside of cells which become constituents of granulomas in the lower respiratory tract. From there, the infection can spread to distant sites in the body including the spleen, kidneys, and brain (112). Antibody responses are not stagnant over time, much like disease states. Due to their adaptability, antibody signatures have been successfully used as biomarkers of disease. This approach has been successfully employed to distinguish between latent and active TB, further supporting the model of humoral fluidity.

## Author contributions

QW: Writing – review & editing, Writing – original draft, Visualization. DN: Writing – review & editing, Writing – original draft, Visualization. SB: Writing – review & editing. RC: Writing – review & editing, Supervision, Resources, Funding acquisition, Conceptualization. RM: Writing – review & editing, Writing – original draft, Supervision, Resources, Funding acquisition, Conceptualization.

## Funding

The author(s) declare that financial support was received for the research, authorship, and/or publication of this article. This project has been funded in whole or in part with Federal funds from the National Institute of Allergy and Infectious Diseases, National Institutes of Health, Department of Health and Human Services, under Contract No. 75N93021C00029, and additional funding from Seattle Tuberculosis Research Advancement Center under award P30 AI168034 (to RNC).

## Conflict of interest

The authors declare that the research was conducted in the absence of any commercial or financial relationships that could be construed as a potential conflict of interest.

The author(s) declared that they were an editorial board member of Frontiers, at the time of submission. This had no impact on the peer review process and the final decision.

## Publisher's note



## References

1. WHO. *Global tuberculosis report 2023*. World Health Organization (WHO) (2023).

2. Mangtani P, Abubakar I, Ariti C, Beynon R, Pimpin L, Fine PE, et al. Protection by BCG vaccine against tuberculosis: a systematic review of randomized controlled trials. *Clin Infect Dis*. (2014) 58(4):470–80. doi: 10.1093/cid/cit790

3. Roy A, Eisenhut M, Harris RJ, Rodrigues LC, Sridhar S, Habermann S, et al. Effect of BCG vaccination against Mycobacterium tuberculosis infection in children: systematic review and meta-analysis. *BMJ*. (2014) 349:g4643. doi: 10.1136/bmj.g4643

4. Delogu G, Sali M, Fadda G. The biology of mycobacterium tuberculosis infection. *Mediterr J Hematol Infect Dis*. (2013) 5(1):e2013070. doi: 10.4084/mjhid.2013.070

5. Haque MF, Boonhok R, Prammananan T, Chaiprasert A, Utaisincharoen P, Sattabongkot J, et al. Resistance to cellular autophagy by Mycobacterium tuberculosis Beijing strains. *Innate Immun*. (2015) 21:746–58. doi: 10.1177/1753425915594245

6. Lerner TR, Borel S, Greenwood DJ, Repnik U, Russell MR, Herbst S, et al. replicates within necrotic human macrophages. *J Cell Biol*. (2017) 216(3):583–94. doi: 10.1083/jcb.201603040

7. Huang L, Nazarova EV, Tan S, Liu Y, Russell DG. Growth of. *J Exp Med*. (2018) 215(4):1135–52. doi: 10.1084/jem.20172020

8. Toniolo C, Dhar N, McKinney JD. Uptake-independent killing of macrophages by extracellular Mycobacterium tuberculosis aggregates. *EMBO J*. (2023) 42(9):e113490. doi: 10.15252/embj.2023113490

9. Zimmermann N, Thormann V, Hu B, Köhler AB, Imai-Matsushima A, Locht C, et al. Human isotype-dependent inhibitory antibody responses against Mycobacterium tuberculosis. *EMBO Mol Med*. (2016) 8(11):1325–39. doi: 10.15252/emmm.201606330

10. Lyashchenko K, Colangeli R, Houde M, Al Jahdali H, Menzies D, Gennaro ML. Heterogeneous antibody responses in tuberculosis. *Infect Immun*. (1998) 66(8):3936–40. doi: 10.1128/IAI.66.8.3936-3940.1998

11. Mao L, LaCourse SM, Kim S, Liu C, Ning B, Bao D, et al. Evaluation of a serum-based antigen test for tuberculosis in HIV-exposed infants: a diagnostic accuracy study. *BMC Med*. (2021) 19(1):113. doi: 10.1186/s12916-021-01983-w

12. McIntyre S, Warner J, Rush C, Vanderven HA. Antibodies as clinical tools for tuberculosis. *Front Immunol*. (2023) 14:1278947. doi: 10.3389/fimmu.2023.1278947

13. Lu LL, Chung AW, Rosebrock TR, Ghebremichael M, Yu WH, Grace PS, et al. A functional role for antibodies in tuberculosis. *Cell*. (2016) 167(2):433–443.e14. doi: 10.1016/j.cell.2016.08.072

14. Irvine EB, O'Neil A, Darrah PA, Shin S, Choudhary A, Li W, et al. Robust IgM responses following intravenous vaccination with Bacille Calmette-Guérin associate

with prevention of Mycobacterium tuberculosis infection in macaques. *Nat Immunol.* (2021) 22(12):1515–23. doi: 10.1038/s41590-021-01066-1

15. Kawahara JY, Irvine EB, Alter G. A case for antibodies as mechanistic correlates of immunity in tuberculosis. *Front Immunol*. (2019) 10:996. doi: 10.3389/fimmu.2019.00996

16. Carpenter SM, Lu LL. Leveraging antibody, B cell and fc receptor interactions to understand heterogeneous immune responses in tuberculosis. *Front Immunol.* (2022) 13:830482. doi: 10.3389/fimmu.2022.830482

17. Di Noia JM, Neuberger MS. Molecular mechanisms of antibody somatic hypermutation. *Annu Rev Biochem.* (2007) 76:1–22. doi: 10.1146/annurev.biochem.76.061705.090740

18. Young C, Brink R. The unique biology of germinal center B cells. *Immunity*. (2021) 54(8):1652–64. doi: 10.1016/j.immuni.2021.07.015

19. Chaudhary N, Wesemann DR. Analyzing immunoglobulin repertoires. *Front Immunol.* (2018) 9:462. doi: 10.3389/fimmu.2018.00462

20. Feng Y, Seija N, Di Noia JM, Martin A. AID in antibody diversification: there and back again. *Trends Immunol.* (2020) 41(7):586–600. doi: 10.1016/j.it.2020.04.009

21. Freund NT, Horwitz JA, Nogueira L, Sievers SA, Scharf L, Scheid JF, et al. A new glycan-dependent CD4-binding site neutralizing antibody exerts pressure on HIV-1 *in vivo*. *PloS Pathog.* (2015) 11(10):e1005238. doi: 10.1371/journal.ppat.1005238

22. Balu S, Reljic R, Lewis MJ, Pleass RJ, McIntosh R, van Kooten C, et al. A novel human IgA monoclonal antibody protects against tuberculosis. *J Immunol.* (2011) 186 (5):3113–9. doi: 10.4049/jimmunol.1003189

23. Larsen SE, Williams BD, Rais M, Coler RN, Baldwin SL. It takes a village: the multifaceted immune response to. *Front Immunol.* (2022) 13:840225. doi: 10.3389/fimmu.2022.840225

24. Bartsch YC, Cizmeci D, Kang J, Zohar T, Periasamy S, Mehta N, et al. Antibody effector functions are associated with protection from respiratory syncytial virus. *Cell.* (2022) 185(26):4873–4886.e10. doi: 10.1016/j.cell.2022.11.012

25. Deng Y, Atyeo C, Yuan D, Chicz TM, Tibbitts T, Gorman M, et al. Beta-spike-containing boosters induce robust and functional antibody responses to SARS-CoV-2 in macaques primed with distinct vaccines. *Cell Rep*. (2023) 42(11):113292. doi: 10.1016/j.celrep.2023.113292

26. Horton RE, Vidarsson G. Antibodies and their receptors: different potential roles in mucosal defense. *Front Immunol.* (2013) 4:200. doi: 10.3389/fimmu.2013.00200

27. da Silva RJ, da Silva Corrêa R, Sardella IG, de Paulo Mulinari AC, Mafort TT, Santos AP, et al. IgA and IgG antibody detection of mycobacterial antigens in pleural fluid and serum from pleural tuberculous patients. *BMC Immunol.* (2019) 20(1):36. doi: 10.1186/s12865-019-0315-y

28. Zohar T, Hsiao JC, Mehta N, Das J, Devadhasan A, Karpinski W, et al. Upper and lower respiratory tract correlates of protection against respiratory syncytial virus following vaccination of nonhuman primates. *Cell Host Microbe*. (2022) 30(1):41–52.e5. doi: 10.1016/j.chom.2021.11.006

29. Hjelm F, Carlsson F, Getahun A, Heyman B. Antibody-mediated regulation of the immune response. *Scand J Immunol.* (2006) 64(3):177–84. doi: 10.1111/j.1365-3083.2006.01818.x

30. Vidarsson G, Dekkers G, Rispens T. IgG subclasses and allotypes: from structure to effector functions. *Front Immunol.* (2014) 5:520. doi: 10.3389/fimmu.2014.00520

31. Wang TT, Ravetch JV. Functional diversification of IgGs through Fc glycosylation. *J Clin Invest.* (2019) 129(9):3492–8. doi: 10.1172/JCI130029

32. Chen T, Blanc C, Eder AZ, Prados-Rosales R, Souza AC, Kim RS, et al. Association of human antibodies to arabinomannan with enhanced mycobacterial opsonophagocytosis and intracellular growth reduction. *J Infect Dis.* (2016) 214 (2):300–10. doi: 10.1093/infdis/jiw141

33. Yuan Y, Crane DD, Simpson RM, Zhu YQ, Hickey MJ, Sherman DR, et al. The 16-kDa alpha-crystallin (Acr) protein of Mycobacterium tuberculosis is required for growth in macrophages. *Proc Natl Acad Sci USA*. (1998) 95(16):9578–83. doi: 10.1073/pnas.95.16.9578

34. Kumar SK, Singh P, Sinha S. Naturally produced opsonizing antibodies restrict the survival of Mycobacterium tuberculosis in human macrophages by augmenting phagosome maturation. *Open Biol.* (2015) 5(12):150171. doi: 10.1098/rsob.150171

35. Chen X, Schneewind O, Missiakas D. Engineered human antibodies for the opsonization and killing of Staphylococcus aureus. *Proc Natl Acad Sci USA*. (2022) 119 (4). doi: 10.1073/pnas.2114478119

36. Vreede RW, Marcelis JH, Verhoef J. Antibodies raised against rough mutants of Escherichia coli and Salmonella strains are opsonic only in the presence of complement. *Infect Immun.* (1986) 52(3):892–6. doi: 10.1128/iai.52.3.892-896.1986

37. Mellouk N, Enninga J. Cytosolic access of intracellular bacterial pathogens: the shigella paradigm. *Front Cell Infect Microbiol*. (2016) 6:35. doi: 10.3389/fcimb.2016.00035

38. Joller N, Weber SS, Müller AJ, Spörri R, Selchow P, Sander P, et al. Antibodies protect against intracellular bacteria by Fc receptor-mediated lysosomal targeting. *Proc Natl Acad Sci USA*. (2010) 107(47):20441–6. doi: 10.1073/pnas.1013827107

39. Malik ZA, Denning GM, Kusner DJ. Inhibition of Ca(2+) signaling by Mycobacterium tuberculosis is associated with reduced phagosome-lysosome fusion and increased survival within human macrophages. *J Exp Med.* (2000) 191(2):287–302. doi: 10.1084/jem.191.2.287

40. Thiriot JD, Martinez-Martinez YB, Endsley JJ, Torres AG. Hacking the host: exploitation of macrophage polarization by intracellular bacterial pathogens. *Pathog Dis.* (2020) 78(1). doi: 10.1093/femspd/ftaa009

41. Gong Z, Yang W, Zhang H, Xiang X, Zeng J, Han S, et al. Mycobacterium tuberculosis Rv3717 enhances the survival of Mycolicibacterium smegmatis by inhibiting host innate immune and caspase-dependent apoptosis. *Infect Genet Evol.* (2020) 84:104412. doi: 10.1016/j.meegid.2020.104412

42. Peng Z, Yue Y, Xiong S. PPE36 modulates host inflammation by promoting E3 ligase smurf1-mediated myD88 degradation. *Front Immunol.* (2022) 13:690667. doi: 10.3389/fimmu.2022.690667

43. Le Moigne V, Le Moigne D, Mahana W. Antibody response to Mycobacterium tuberculosis p27-PPE36 antigen in sera of pulmonary tuberculosis patients. *Tuberculosis (Edinb).* (2013) 93(2):189–91. doi: 10.1016/j.tube.2012.10.006

44. Arora SK, Alam A, Naqvi N, Ahmad J, Sheikh JA, Rahman SA, et al. Immunodominant. *Front Immunol.* (2020) 11:1199. doi: 10.3389/fimmu.2020.01199

45. Pym AS, Brodin P, Majlessi L, Brosch R, Demangel C, Williams A, et al. Recombinant BCG exporting ESAT-6 confers enhanced protection against tuberculosis. *Nat Med.* (2003) 9(5):533–9. doi: 10.1038/nm859

46. Refai A, Gritli S, Barbouche MR, Essafi M. Virulent factor ESAT-6 drives macrophage differentiation toward the pro-inflammatory M1 phenotype and subsequently switches it to the anti-inflammatory M2 phenotype. *Front Cell Infect Microbiol.* (2018) 8:327. doi: 10.3389/fcimb.2018.00327

47. Bates TA, Trank-Greene M, Nguyenla X, Anastas A, Gurmessa SK, Merutka IR, et al. ESAT-6 undergoes self-association at phagosomal pH and an ESAT-6-specific nanobody restricts. *Elife*. (2024) 12. doi: 10.7554/eLife.91930

48. Parker HA, Forrester L, Kaldor CD, Dickerhof N, Hampton MB, et al. Antimicrobial activity of neutrophils against mycobacteria. *Front Immunol.* (2021) 12:782495. doi: 10.3389/fimmu.2021.782495

49. Tong X, McNamara RP, Avendaño MJ, Serrano EF, García-Salum T, Pardo-Roa C, et al. Waning and boosting of antibody Fc-effector functions upon SARS-CoV-2 vaccination. *Nat Commun.* (2023) 14(1):4174. doi: 10.1038/s41467-023-39189-8

50. Chakraborty S, Gonzalez J, Edwards K, Mallajosyula V, Buzzanco AS, Sherwood R, et al. Proinflammatory IgG Fc structures in patients with severe COVID-19. *Nat Immunol.* (2021) 22(1):67–73. doi: 10.1038/s41590-020-00828-7

51. Bryceson YT, Fauriat C, Nunes JM, Wood SM, Björkström NK, Long EO, et al. Functional analysis of human NK cells by flow cytometry. *Methods Mol Biol.* (2010) 612:335–52. doi: 10.1007/978-1-60761-362-6_23

52. Sakae Y, Satoh T, Yagi H, Yanaka S, Yamaguchi T, Isoda Y, et al. Conformational effects of N-glycan core fucosylation of immunoglobulin G Fc region on its interaction with Fcγ receptor IIIa. *Sci Rep.* (2017) 7(1):13780. doi: 10.1038/s41598-017-13845-8

53. Boudreau CM, Alter G. Extra-neutralizing fcR-mediated antibody functions for a universal influenza vaccine. *Front Immunol*. (2019) 10:440. doi: 10.3389/fimmu.2019.00440

54. Ackerman ME, Mikhailova A, Brown EP, Dowell KG, Walker BD, Bailey-Kellogg C, et al. Polyfunctional HIV-specific antibody responses are associated with spontaneous HIV control. *PloS Pathog.* (2016) 12(1):e1005315. doi: 10.1371/journal.ppat.1005315

55. Jegaskanda S, Weinfurter JT, Friedrich TC, Kent SJ. Antibody-dependent cellular cytotoxicity is associated with control of pandemic H1N1 influenza virus infection of macaques. *J Virol.* (2013) 87(10):5512–22. doi: 10.1128/JVI.03030-12

56. Lo Nigro C, Macagno M, Sangiolo D, Bertolaccini L, Aglietta M, Merlano MC. NK-mediated antibody-dependent cell-mediated cytotoxicity in solid tumors: biological evidence and clinical perspectives. *Ann Transl Med*. (2019) 7(5):105. doi: 10.21037/atm

57. Lu CC, Wu TS, Hsu YJ, Chang CJ, Lin CS, Chia JH, et al. NK cells kill mycobacteria directly by releasing perforin and granulysin. *J Leukoc Biol.* (2014) 96 (6):1119–29. doi: 10.1189/jlb.4A0713-363RR

58. Allen M, Bailey C, Cahatol I, Dodge L, Yim J, Kassissa C, et al. Mechanisms of control of mycobacterium tuberculosis by NK cells: role of glutathione. *Front Immunol.* (2015) 6:508. doi: 10.3389/fimmu.2015.00508

59. Esin S, Batoni G, Counoupas C, Stringaro A, Brancatisano FL, Colone M, et al. Direct binding of human NK cell natural cytotoxicity receptor NKp44 to the surfaces of mycobacteria and other bacteria. *Infect Immun.* (2008) 76(4):1719–27. doi: 10.1128/IAI.00870-07

60. Vankayalapati R, Wizel B, Weis SE, Safi H, Lakey DL, Mandelboim O, et al. The NKp46 receptor contributes to NK cell lysis of mononuclear phagocytes infected with an intracellular bacterium. *J Immunol*. (2002) 168(7):3451–7. doi: 10.4049/jimmunol.168.7.3451

61. Marcenaro E, Ferranti B, Falco M, Moretta L, Moretta A. Human NK cells directly recognize Mycobacterium bovis via TLR2 and acquire the ability to kill monocyte-derived DC. *Int Immunol.* (2008) 20(9):1155–67. doi: 10.1093/intimm/dxn073

62. Coler RN, Day TA, Ellis R, Piazza FM, Beckmann AM, Vergara J, et al. The TLR-4 agonist adjuvant, GLA-SE, improves magnitude and quality of immune responses elicited by the ID93 tuberculosis vaccine: first-in-human trial. *NPJ Vaccines.* (2018) 3:34. doi: 10.1038/s41541-018-0057-5

63. Colditz GA, Berkey CS, Mosteller F, Brewer TF, Wilson ME, Burdick E, et al. The efficacy of bacillus Calmette-Guérin vaccination of newborns and infants in the

prevention of tuberculosis: meta-analyses of the published literature. *Pediatrics*. (1995) 96(1 Pt 1):29–35. doi: 10.1542/peds.96.1.29

64. Van Der Meeren O, Hatherill M, Nduba V, Wilkinson RJ, Muyoyeta M, Van Brakel E, et al. Phase 2b controlled trial of M72/AS01. *N Engl J Med*. (2018) 379 (17):1621–34. doi: 10.1056/NEJMoa1803484

65. Penn-Nicholson A, Geldenhuys H, Burny W, van der Most R, Day CL, Jongert E, et al. Safety and immunogenicity of candidate vaccine M72/AS01E in adolescents in a TB endemic setting. *Vaccine*. (2015) 33(32):4025–34. doi: 10.1016/j.vaccine.2015.05.088

66. Dijkman K, Sombroek CC, Vervenne RAW, Hofman SO, Boot C, Remarque EJ, et al. Prevention of tuberculosis infection and disease by local BCG in repeatedly exposed rhesus macaques. *Nat Med*. (2019) 25(2):255–62. doi: 10.1038/s41591-018-0319-9

67. Prados-Rosales R, Carreño L, Cheng T, Blanc C, Weinrick B, Malek A, et al. Enhanced control of Mycobacterium tuberculosis extrapulmonary dissemination in mice by an arabinomannan-protein conjugate vaccine. *PloS Pathog*. (2017) 13(3): e1006250. doi: 10.1371/journal.ppat.1006250

68. Roy E, Stavropoulos E, Brennan J, Coade S, Grigorieva E, Walker B, et al. Therapeutic efficacy of high-dose intravenous immunoglobulin in Mycobacterium tuberculosis infection in mice. *Infect Immun*. (2005) 73(9):6101–9. doi: 10.1128/IAI.73.9.6101-6109.2005

69. Li H, Wang XX, Wang B, Fu L, Liu G, Lu Y, et al. Latently and uninfected healthcare workers exposed to TB make protective antibodies against. *Proc Natl Acad Sci USA*. (2017) 114(19):5023–8. doi: 10.1073/pnas.1611776114

70. Nziza N, Cizmeci D, Davies L, Irvine EB, Jung W, Fenderson BA, et al. Defining discriminatory antibody fingerprints in active and latent tuberculosis. *Front Immunol*. (2022) 13(46):856906. doi: 10.3389/fimmu.2022.856906

71. Zou G, Ochiai H, Huang W, Yang Q, Li C, Wang LX. Chemoenzymatic synthesis and Fcγ receptor binding of homogeneous glycoforms of antibody Fc domain. Presence of a bisecting sugar moiety enhances the affinity of Fc to FcγIIIa receptor. *J Am Chem Soc*. (2011) 133:18975–91. doi: 10.1021/ja208390n

72. Grace PS, Dolatshahi S, Lu LL, Cain A, Palmieri F, Petrone L, et al. Antibody subclass and glycosylation shift following effective TB treatment. *Front Immunol*. (2021) 12:679973. doi: 10.3389/fimmu.2021.679973

73. Anthony RM, Kobayashi T, Wermeling F, Ravetch JV. Intravenous gammaglobulin suppresses inflammation through a novel T(H)2 pathway. *Nature*. (2011) 475(7354):110–3. doi: 10.1038/nature10134

74. Jefferis R. Glycosylation as a strategy to improve antibody-based therapeutics. *Nat Rev Drug Discovery*. (2009) 8(3):226–34. doi: 10.1038/nrd2804

75. Lu LL, Das J, Grace PS, Fortune SM, Restrepo BI, Alter G. Antibody fc glycosylation discriminates between latent and active tuberculosis. *J Infect Dis*. (2020) 222(12):2093–102. doi: 10.1093/infdis/jiz643

76. Kumagai T, Palacios A, Casadevall A, García MJ, Toro C, Tiemeyer M, et al. Serum igM glycosylation associated with tuberculosis infection in mice. *mSphere*. (2019) 4(2). doi: 10.1128/mSphere.00684-18

77. Ozdilek A, Paschall AV, Dookwah M, Tiemeyer M, Avci FY. Host protein glycosylation in nucleic acid vaccines as a potential hurdle in vaccine design for nonviral pathogens. *Proc Natl Acad Sci USA*. (2020) 117(3):1280–2. doi: 10.1073/pnas.1916131117

78. Kiazyk S, Ball TB. Latent tuberculosis infection: An overview. *Can Commun Dis Rep*. (2017) 43(3–4):62–6. doi: 10.14745/ccdr.v43i34a01

79. Glatman-Freedman A, Casadevall A. Serum therapy for tuberculosis revisited: reappraisal of the role of antibody-mediated immunity against Mycobacterium tuberculosis. *Clin Microbiol Rev*. (1998) 11(3):514–32. doi: 10.1128/CMR.11.3.514

80. Achkar JM, Chan J, Casadevall A. B cells and antibodies in the defense against Mycobacterium tuberculosis infection. *Immunol Rev*. (2015) 264(1):167–81. doi: 10.1111/imr.12276

81. Watson A, Li H, Ma B, Weiss R, Bendayan D, Abramovitz L, et al. Human antibodies targeting a Mycobacterium transporter protein mediate protection against tuberculosis. *Nat Commun*. (2021) 12(1):602. doi: 10.1038/s41467-021-20930-0

82. Steingart KR, Ramsay A, Dowdy DW, Pai M. Serological tests for the diagnosis of active tuberculosis: relevance for India. *Indian J Med Res*. (2012) 135(5):695–702.

83. Achkar JM, Ziegenbalg A. Antibody responses to mycobacterial antigens in children with tuberculosis: challenges and potential diagnostic value. *Clin Vaccine Immunol*. (2012) 19(12):1898–906. doi: 10.1128/CVI.00501-12

84. Steingart KR, Flores LL, Dendukuri N, Schiller I, Laal S, Ramsay A, et al. Commercial serological tests for the diagnosis of active pulmonary and extrapulmonary tuberculosis: an updated systematic review and meta-analysis. *PloS Med*. (2011) 8(8): e1001062. doi: 10.1371/journal.pmed.1001062

85. Abraham PR, Devalraju KP, Jha V, Valluri VL, Mukhopadhyay S. PPE17 (Rv1168c) protein of Mycobacterium tuberculosis detects individuals with latent TB infection. *PloS One*. (2018) 13(11):e0207787. doi: 10.1371/journal.pone.0207787

86. Lee JY, Kim BJ, Koo HK, Kim J, Kim JM, Kook YH, et al. Diagnostic potential of igG and igA responses to. *Microorganisms*. (2020) 8(7). doi: 10.3390/microorganisms8070979

87. Abebe F, Belay M, Legesse M, K LMCF, Ottenhoff THM. IgA and IgG against Mycobacterium tuberculosis Rv2031 discriminate between pulmonary tuberculosis patients, Mycobacterium tuberculosis-infected and non-infected individuals. *PloS One*. (2018) 13(1):e0190989. doi: 10.1371/journal.pone.0190989

88. Bowman KA, Kaplonek P, McNamara RP. Understanding Fc function for rational vaccine design against pathogens. *mBio*. (2023) 15(1):e0303623. doi: 10.1128/mbio.03036-23

89. Lund FE, Randall TD. Scent of a vaccine. *Science*. (2021) 373(6553):397–9. doi: 10.1126/science.abg9857

90. Takenami I, de Oliveira CC, Lima FR, Soares J, Machado A, Riley LW, et al. Immunoglobulin G response to mammalian cell entry 1A (Mce1A) protein as biomarker of active tuberculosis. *Tuberculosis (Edinb)*. (2016) 100:82–8. doi: 10.1016/j.tube.2016.07.012

91. Khan IH, Ravindran R, Krishnan VV, Awan IN, Rizvi SK, Saqib MA, et al. Plasma antibody profiles as diagnostic biomarkers for tuberculosis. *Clin Vaccine Immunol*. (2011) 18(12):2148–53. doi: 10.1128/CVI.05304-11

92. Takenami I, de Oliveira CC, Petrilli JD, Machado A, Riley LW, Arruda S. Serum antiphospholipid antibody levels as biomarkers for diagnosis of pulmonary tuberculosis patients. *Int J Tuberc Lung Dis*. (2018) 22(9):1063–70. doi: 10.5588/ijtld.17.0874

93. Li LF, Lin MC, Chen NH, Hsieh MJ, Lee CH, Tsao TC. Serodiagnosis of tuberculosis by enzyme-linked immunosorbent assay for anti-A60 and anti-A38. *Changgeng Yi Xue Za Zhi*. (1998) 21(3):258–64.

94. Ben-selma W, Harizi H, Marzouk M, Ben Kahla I, Ben Lazreg F, Ferjeni A, et al. Evaluation of the diagnostic value of measuring IgG, IgM, and IgA antibodies to mycobacterial A60 antigen in active tuberculosis. *Diagn Microbiol Infect Dis*. (2010) 68 (1):55–9. doi: 10.1016/j.diagmicrobio.2010.05.006

95. La Manna MP, Orlando V, Li Donni P, Sireci G, Di Carlo P, Cascio A, et al. Identification of plasma biomarkers for discrimination between tuberculosis infection/disease and pulmonary non tuberculosis disease. *PloS One*. (2018) 13(3):e0192664. doi: 10.1371/journal.pone.0192664

96. Gina P, Randall PJ, Muchinga TE, Pooran A, Meldau R, Peter JG, et al. Early morning urine collection to improve urinary lateral flow LAM assay sensitivity in hospitalised patients with HIV-TB co-infection. *BMC Infect Dis*. (2017) 17:339. doi: 10.1186/s12879-017-2313-0

97. Shah M, Ssengooba W, Armstrong D, Nakiyingi L, Holshouser M, Ellner JJ, et al. Comparative performance of urinary lipoarabinomannan assays and Xpert MTB/RIF in HIV-infected individuals. *AIDS*. (2014) 28(9):1307–14. doi: 10.1097/QAD.0000000000000264

98. Hanifa Y, Fielding KL, Chihota VN, Adonis L, Charalambous S, Karstaedt A, et al. Diagnostic accuracy of lateral flow urine LAM assay for TB screening of adults with advanced immunosuppression attending routine HIV care in South Africa. *PloS One*. (2016) 11(6):e0156866. doi: 10.1371/journal.pone.0156866

99. Awoniyi DO, Baumann R, Chegou NN, Kriel B, Jacobs R, Kidd M, et al. Detection of a combination of serum IgG and IgA antibodies against selected mycobacterial targets provides promising diagnostic signatures for active TB. *Oncotarget*. (2017) 8(23):37525–37. doi: 10.18632/oncotarget.v8i23

100. Lynch HE, Stewart SM, Kepler TB, Sempowski GD, Alam SM. Surface plasmon resonance measurements of plasma antibody avidity during primary and secondary responses to anthrax protective antigen. *J Immunol Methods*. (2014) 404(5):1–12. doi: 10.1016/j.jim.2013.11.026

101. Miyoshi T, Zhang Q, Miyake T, Watanabe S, Ohnishi H, Chen J, et al. Semi-automated single-molecule microscopy screening of fast-dissociating specific antibodies directly from hybridoma cultures. *Cell Rep*. (2021) 34(5):108708. doi: 10.1016/j.celrep.2021.108708

102. Möckl L, Moerner WE. Super-resolution microscopy with single molecules in biology and beyond-essentials, current trends, and future challenges. *J Am Chem Soc*. (2020) 142(42):17828–44. doi: 10.1021/jacs.0c08178

103. Botella H, Yang G, Ouerfelli O, Ehrt S, Nathan CF, Vaubourgeix J. Distinct spatiotemporal dynamics of peptidoglycan synthesis between. *mBio*. (2017) 8(5). doi: 10.1128/mBio.01183-17

104. Estévez O, Anibarro L, Garet E, Pallares Á, Pena A, Villaverde C, et al. Identification of candidate host serum and saliva biomarkers for a better diagnosis of active and latent tuberculosis infection. *PloS One*. (2020) 15(7):e0235859. doi: 10.1371/journal.pone.0235859

105. Reyes F, Tirado Y, Puig A, Borrero R, Reyes G, Fernández S, et al. Immunogenicity and cross-reactivity against Mycobacterium tuberculosis of proteoliposomes derived from Mycobacterium bovis BCG. *BMC Immunol*. (2013) 14 (Suppl 1):S7. doi: 10.1186/1471-2172-14-S1-S7

106. Lin MY, Reddy TB, Arend SM, Friggen AH, Franken KL, van Meijgaarden KE, et al. Cross-reactive immunity to Mycobacterium tuberculosis DosR regulon-encoded antigens in individuals infected with environmental, nontuberculous mycobacteria. *Infect Immun*. (2009) 77(11):5071–9. doi: 10.1128/IAI.00457-09

107. Dai Z, Liu Z, Xiu B, Yang X, Zhao P, Zhang X, et al. A multiple-antigen detection assay for tuberculosis diagnosis based on broadly reactive polyclonal antibodies. *Iran J Basic Med Sci*. (2017) 20(4):360–7. doi: 10.22038/IJBMS.2017.8575

108. McMahan K, Wegmann F, Aid M, Sciacca M, Liu J, Hachmann NP, et al. Mucosal boosting enhances vaccine protection against SARS-CoV-2 in macaques. *Nature*. (2024) 626(7998):385–91. doi: 10.1038/s41586-023-06951-3

109. Tong X, Wang Q, Jung W, Chicz TM, Blanc R, Parker LJ, et al. *Compartment-specific antibody correlates of protection to SARS-coV-2 omicron in macaques*. *iScience* (2024) 27(9):110174. doi: 10.1016/j.isci.2024.110174

110. Jung W, Yuan D, Kellman B, Gonzalez IGDS, Clemens R, Milan EP, et al. Boosting with adjuvanted SCB-2019 elicits superior Fcγ-receptor engagement driven by IgG3 to SARS-CoV-2 spike. *NPJ Vaccines*. (2024) 9(1):7. doi: 10.1038/s41541-023-00791-y

111. Tong X, Deng Y, Cizmeci D, Fontana L, Carlock MA, Hanley HB, et al. Distinct functional humoral immune responses are induced after live attenuated and inactivated seasonal influenza vaccination. *J Immunol*. (2024) 212(1):24–34. doi: 10.4049/jimmunol.2200956

112. Manyelo CM, Solomons RS, Walzl G, Chegou NN. Tuberculous meningitis: pathogenesis, immune responses, diagnostic challenges, and the potential of biomarker-based approaches. *J Clin Microbiol*. (2021) 59(3). doi: 10.1128/JCM.01771-20

113. Lodes MJ, Dillon DC, Mohamath R, Day CH, Benson DR, Reynolds LD, et al. Serological expression cloning and immunological evaluation of MTB48, a novel Mycobacterium tuberculosis antigen. *J Clin Microbiol*. (2001) 39(7):2485–93. doi: 10.1128/JCM.39.7.2485-2493.2001

114. Shete PB, Ravindran R, Chang E, Worodria W, Chaisson LH, Andama A, et al. Evaluation of antibody responses to panels of M. tuberculosis antigens as a screening tool for active tuberculosis in Uganda. *PloS One*. (2017) 12(8):e0180122. doi: 10.1371/journal.pone.0180122

115. Khaliq A, Ravindran R, Hussainy SF, Krishnan VV, Ambreen A, Yusuf NW, et al. Field evaluation of a blood based test for active tuberculosis in endemic settings. *PloS One*. (2017) 12(4):e0173359. doi: 10.1371/journal.pone.0173359

116. Luo L, Zhu L, Yue J, Liu J, Liu G, Zhang X, et al. Antigens Rv0310c and Rv1255c are promising novel biomarkers for the diagnosis of Mycobacterium tuberculosis infection. *Emerg Microbes Infect*. (2017) 6(7):e64. doi: 10.1038/emi.2017.54

117. Burbelo PD, Keller J, Wagner J, Klimavicz JS, Bayat A, Rhodes CS, et al. Serological diagnosis of pulmonary Mycobacterium tuberculosis infection by LIPS using a multiple antigen mixture. *BMC Microbiol*. (2015) 15:205. doi: 10.1186/s12866-015-0545-y

118. Baumann R, Kaempfer S, Chegou NN, Oehlmann W, Loxton AG, Kaufmann SH, et al. Serologic diagnosis of tuberculosis by combining Ig classes against selected mycobacterial targets. *J Infect*. (2014) 69(6):581–9. doi: 10.1016/j.jinf.2014.05.014

119. Kumar G, Dagur PK, Singh PK, Shankar H, Yadav VS, Katoch VM, et al. Serodiagnostic efficacy of Mycobacterium tuberculosis 30/32-kDa mycolyl transferase complex, ESAT-6, and CFP-10 in patients with active tuberculosis. *Arch Immunol Ther Exp (Warsz)*. (2010) 58(1):57–65. doi: 10.1007/s00005-009-0055-4

frontiers | Frontiers in Immunology

TYPE Original Research
PUBLISHED 24 September 2024
DOI 10.3389/fimmu.2024.1441944



OPEN ACCESS

EDITED BY
Jagadeesh Bayry,
Indian Institute of Technology Palakkad, India

REVIEWED BY
Thomas Hagan,
Cincinnati Children's Hospital Medical Center, United States
Juraj Ivanyi,
King's College London, United Kingdom
Max Bastian,
Friedrich-Loeffler-Institute, Germany

*CORRESPONDENCE
Andrew Fiore-Gartland
agartlan@fredhutch.org

RECEIVED 31 May 2024
ACCEPTED 02 September 2024
PUBLISHED 24 September 2024

CITATION
Fiore-Gartland A, Srivastava H, Seese A, Day T, Penn-Nicholson A, Luabeya AKK, Du Plessis N, Loxton AG, Bekker L-G, Diacon A, Walzl G, Sagawa ZK, Reed SG, Scriba TJ, Hatherill M and Coler R (2024) Co-regulation of innate and adaptive immune responses induced by ID93+GLA-SE vaccination in humans. *Front. Immunol.* 15:1441944. doi: 10.3389/fimmu.2024.1441944



# Co-regulation of innate and adaptive immune responses induced by ID93+GLA-SE vaccination in humans

Andrew Fiore-Gartland[1*], Himangi Srivastava[1], Aaron Seese[1], Tracey Day[2], Adam Penn-Nicholson[3], Angelique Kany Kany Luabeya[4], Nelita Du Plessis[5], Andre G. Loxton[5], Linda-Gail Bekker[6], Andreas Diacon[7], Gerhard Walzl[5], Zachary K. Sagawa[8], Steven G. Reed[9], Thomas J. Scriba[4], Mark Hatherill[4] and Rhea Coler[10,11,12]

[1]Vaccine and Infectious Disease Division, Fred Hutchinson Cancer Center, Seattle, WA, United States, [2]Infectious Diseases and Vaccines, Innovative Medicine, Johnson & Johnson, Leiden, Netherlands, [3]Foundation for Innovative New Diagnostics (FIND), Geneva, Switzerland, [4]South African Tuberculosis Vaccine Initiative (SATVI), Institute of Infectious Disease & Molecular Medicine and Department of Pathology, University of Cape Town, Cape Town, South Africa, [5]Department of Science and Technology/National Research Foundation (DST-NRF) Centre of Excellence for Biomedical Tuberculosis Research, South African Medical Research Council Centre for Tuberculosis Research, Biomedical Research Institute, Division of Molecular Biology and Human Genetics, Faculty of Medicine and Health Sciences, Stellenbosch University, Cape Town, South Africa, [6]The Desmond Tutu Human Immunodeficiency Virus (HIV) Centre, University of Cape Town, Cape Town, South Africa, [7]TASK, Cape Town, South Africa, [8]Access to Advanced Health Institute, Seattle, WA, United States, [9]HDT Bio Corporation, Seattle, WA, United States, [10]Seattle Children's Research Institute, Center for Global Infectious Disease Research, Seattle Children's, Seattle, WA, United States, [11]Department of Pediatrics, University of Washington School of Medicine, Seattle, WA, United States, [12]Department of Global Health, University of Washington, Seattle, WA, United States

**Introduction:** Development of an effective vaccine against tuberculosis is a critical step towards reducing the global burden of disease. A therapeutic vaccine might also reduce the high rate of TB recurrence and help address the challenges of drug-resistant strains. ID93+GLA-SE is a candidate subunit vaccine that will soon be evaluated in a phase 2b efficacy trial for prevention of recurrent TB among patients undergoing TB treatment. ID93+GLA-SE vaccination was shown to elicit robust CD4+ T cell and IgG antibody responses among recently treated TB patients in the TBVPX-203 Phase 2a study (NCT02465216), but the mechanisms underlying these responses are not well understood.

**Methods:** In this study we used specimens from TBVPX-203 participants to describe the changes in peripheral blood gene expression that occur after ID93 +GLA-SE vaccination.

**Results:** Analyses revealed several distinct modules of co-varying genes that were either up- or down-regulated after vaccination, including genes associated with innate immune pathways at 3 days post-vaccination and genes associated with lymphocyte expansion and B cell activation at 7 days post-vaccination. Notably, the regulation of these gene modules was affected by the dose schedule and by participant sex, and early innate gene signatures were correlated with the ID93-specific CD4+ T cell response.

10.3389/fimmu.2024.1441944

**Discussion:** The results provide insight into the complex interplay of the innate and adaptive arms of the immune system in developing responses to vaccination with ID93+GLA-SE and demonstrate how dosing and schedule can affect vaccine responses.

KEYWORDS

**tuberculosis, vaccines, systems immunology, innate, RNA sequencing**

## Introduction

In 2022 (1), more people died from tuberculosis (TB) than from any other infectious disease (1), and although effective TB treatment is available and saves millions of lives, the impact on the global TB epidemic has been limited. This is, in part, because patients who successfully complete therapy with first-line drugs remain at high risk for TB recurrence (8% - 14%) due to relapse or reinfection (2, 3). Epidemiological modeling suggests that a vaccine targeting adolescents and young adults to prevent TB disease is a strategy that could achieve significant public health impact (4), making it imperative to accelerate the development of novel TB vaccine candidates. One candidate that showed promise in a recent phase 2b trial is the M72/AS01$_E$ vaccine, which demonstrated 50% efficacy against TB disease in South African adults (5); the vaccine is a fusion protein of two *Mycobacterium tuberculosis* (*M.tb*) antigens co-administered with a liposome formulation of the TLR4 agonist monophosphoryl lipid A (MPL) and Quillaja saponaria Molina fraction 21 (QS21). Efforts are currently underway to more fully understand the responses elicited by the vaccine and identify the immunological correlates of protection.

The ID93+GLA-SE vaccine is also a fusion protein of four *M.tb* antigens with diverse roles in pathogenesis, co-administered with the TLR4 agonist glucopyranosyl lipid A (GLA) in a stable oil-in-water emulsion (SE) formulation (6, 7). Preclinical efficacy of therapeutic immunization with ID93+GLA-SE for prevention of recurrence has been demonstrated in mouse and non-human primate models (8, 9). A recent phase 2a study (TBVPX-203, NCT02465216) of the vaccine investigated safety and immunogenicity in 60 South African adults who had recently completed multi-drug therapy for rifampicin-susceptible pulmonary TB (10). The study evaluated three dose combinations of ID93 fusion protein and GLA-SE adjuvant, as well as two dosing schedules, with the 2 μg ID93 + 5 μg GLA-SE ("2 + 5") dose combination given as either 2 injections with two-month spacing (injections on days 0 and 56), or 3 injections with one-month spacing (injection on days 0, 28 and 56; Table 1). Participants in all groups showed a robust increase in serum ID93-specific IgG. The vaccine response was also characterized by a significant increase in the ID93-specific CD4+ T cell response, with the 2-dose and 3-dose 2 + 5 regimens demonstrating comparable increases in response magnitudes after the final dose. Ultimately, the 2-dose regimen was selected for a phase 2a/2b study evaluating its efficacy in preventing TB recurrence among people living with and without HIV-1 in South Africa (NCT06205589).

In this study, we applied systems vaccinology approaches to understand better the immune responses to ID93+GLA-SE. We used RNA sequencing to examine the changes in gene expression in peripheral blood that occurred after vaccination in participants in the TBVPX-203 trial. We observed evidence of both innate and early adaptive immune pathway activation within the first seven days after vaccination and showed that specific modules of vaccine-regulated genes differentiated females and males, as well as individuals in the 2-dose vs. 3-dose treatment groups. Several response modules overlapped with responses elicited by the AS01$_E$ adjuvant in the M72 vaccine. Integration with previously published immune response data allowed us to interrogate further how changes in gene expression were associated with ID93-specific humoral and cellular responses.

TABLE 1 Study schema.

| Name | Product | ID93 dose | GLA-SE dose | Dose schedule (days) | | | Doses | N |
|---|---|---|---|---|---|---|---|---|
| 2 + 2 (x2) | ID93+GLA-SE | 2 μg | 2 μg | 0 | – | 56 | 2 | 15 |
| 10 + 2 (x2) | ID93+GLA-SE | 10 μg | 2 μg | 0 | – | 56 | 2 | 5 |
| 2 + 5 (x2) | ID93+GLA-SE | 2 μg | 5 μg | 0 | – | 56 | 2 | 15 |
| 2 + 5 (x3) | ID93+GLA-SE | 2 μg | 5 μg | 0 | 28 | 56 | 3 | 14 |
| Placebo | Placebo | – | – | 0 | – | 56 | 2 | 12 |

# Methods

## Clinical trial cohort

IDRI-TBVPX-203 (ClinicalTrials.gov Identifier: NCT02465216) was a Phase 2a, randomized, double-blind, placebo-controlled, dose-escalation evaluation ID93+GLA-SE. There were two dose levels of the ID93 antigen administered in combination with one of two dose levels of GLA-SE in two different dosing regimens. The primary objective was to describe the safety and immunogenicity profile of ID93+GLA-SE in South African, HIV-negative, healthy adults who had recently completed six months of standard, four-drug (HRZE) antibiotic therapy for drug-sensitive pulmonary TB within the last 28 days. The age range of participants was 18 to 54 with a median of 27 years old. ID93+GLA-SE was given to 48 participants and 12 received placebo; one additional participant was assigned to receive vaccine, but only provided a blood sample at day 0 (Table 1; Figure 1).

## Sample processing and RNA sequencing

Ribonucleic acid (RNA) was extracted from 298 PAXgene tube samples of whole blood from 61 participants in TBVPX203. Globin mRNA was removed using bead-based hybridization (Thermofisher GLOBINclear). DNA sequencing libraries were created from polyadenylated RNA transcripts (Ilumina TruSeq, stranded). Sequencing was performed on an Illumina NovaSeq 6000 with 100 bp paired-end reads. More than 30 million reads were generated from each sample, with 70 - 85% of reads mapping to known protein coding regions [*nextflow nf-core/rnaseq* (11), STAR (12)]. Transcripts were aggregated and quantified at the gene level using *salmon* (13).

## Identification of differentially expressed genes and statistical analyses

To identify genes that were significantly increased or decreased by vaccination we used mixed-effects models of individual gene expression at pairs of time points before and after vaccination: day 3 vs. 0, day 59 vs. 56 or day 63 vs. 56. Gene counts were normalized using the trimmed mean of M-values (TMM) method (14) and log transformed. Models were fit using R package *kimma* (15) and *lme4* (16), providing "voom" precision weights (17). Linear models to detect differentially expressed genes included participant sex and accounted for the longitudinal experimental design using a random effect for within-participant covariance; as a sensitivity analysis, participant age was considered as a covariate, with only 12 genes at day 63 having an association with age (FDR-q < 0.2). Significant differential expression was based on an unadjusted-p < 0.05, FDR-adjusted q-value < 0.2 [Benjamini and Hochberg (18)] and absolute-log2 fold-change > 0.5.

Gene modules were created from the DEGs using weighted gene correlation network analysis (WGCNA) (19). A "signed correlation" distance metric was used, meaning that gene pairs with negative correlation were assigned the largest distance prior to hierarchical clustering (soft thresholding power = 7). Gene module "eigengenes" were used for subsequent analyses of treatment effects and correlations with adaptive immune responses. Descriptive plots of gene module expression used normalized counts with a mean taken across all genes in the module; in practice there was very high correlation between the module eigengene scores and normalized counts, with normalized counts being more interpretable. For statistical inference, module eigengenes were modeled using linear mixed-effects models (LMM) fit with *lme4* (16).

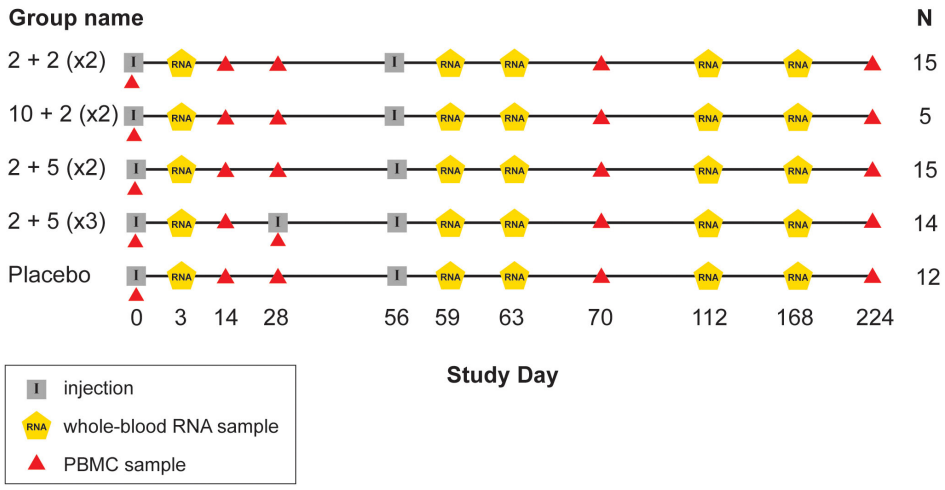


FIGURE 1
Schedule of events in TBVPX-203 study. Schematic showing the timeline of study product injections and sample collection for participants in the five study groups of TBVPX-203. The group names are defined in Table 1 based on the dose of the ID93 antigen, the dose of the GLA-SE adjuvant and the number of injections. Schematic indicates the day of each visit relative to enrollment, and whether the visit included a product injection, a blood collection for RNA extraction or a blood collection for adaptive immune response assays.

Gene set enrichment analysis (GSEA) was conducted using an over-representation analysis (ORA) and a hypergeometric test to understand functions associated with each of the modules. A hypergeometric test was conducted for each module using all DEGs as the "universe" of genes and testing all gene sets in the Blood Transcriptional Modules (BTMs (20); GSEA significance was based on FDR-q < 0.2. Cell deconvolution was conducted from the normalized gene counts using xCell (21). Longitudinal differences in the enrichment scores for each cell type were evaluated using a Wilcoxon signed-rank test.

Adaptive humoral and cellular immune response correlation analyses were conducted using rank-based Spearman correlation with significance based on FDRq < 0.2 to generate hypotheses. Multiplicity adjustment was computed across modules and module comparisons (e.g., days 3 vs. 0, 59 vs. 56 and 63 vs. 56). Predictive analyses were implemented using the Python package scikit-learn. Univariate model used non-penalized logistic regression while models of more than one variable used L1-penalized logistic regression. Area under the receiver operator curve was estimated using 5-fold cross-validation, with the AUC computed on the predicted outcomes for the "stacked folds". Delong's method (22) was used for estimating the 95% confidence interval.

## Laboratory assay data

Humoral and cellular immune response data and assay methods were previously published and described with the primary study manuscript (10). Briefly, levels of ID93-specific immunoglobulin G (IgG) in serum were measured by enzyme-linked immunosorbent assay (ELISA) using the whole fusion protein. Intracellular cytokine staining (ICS) was used to measure frequencies of ID93-specific CD4+ and CD8+ T cells from cryopreserved peripheral blood mononuclear cells (PBMCs). Antigen-specific cells were identified as those expressing at least 2 of IFNγ, IL2, TNF and/or CD154 and frequencies of these cells in the antigen stimulation condition (12-hour stimulation with whole-protein ID93) were adjusted for frequencies in the negative control condition (DMSO). There was no significant vaccine-induced increase in ID93-specific CD8+ T cells, therefore only CD4+ T cell responses were analyzed in this study. A whole-blood ICS assay (23) was also conducted with fresh whole blood and analyzed similarly to the PBMC ICS.

# Results

## Vaccination with ID93+GLA-SE induced broad changes in gene expression during the first seven days

Previously, ID93+GLA-SE was evaluated in a phase 2a trial enrolling (10) 61 volunteers who were recently diagnosed with drug-susceptible pulmonary tuberculosis and who successfully completed six months of standard TB therapy. Whole-blood samples were provided by participants at visits scheduled on the day of the first injection (day 0) and at subsequent visits including study days 3, 56, 59, 63, 112 and 168. To study the transcriptional profile of samples before and after vaccination, blood was processed and submitted for RNA sequencing, with resulting transcript sequences mapped to the human genome and quantitated at the gene level for further analysis (see Methods).

Initial analysis to identify vaccine-induced gene expression was focused on the two treatment groups that received the 2 ug ID93 + 5 ug GLA-SE dose: one group received two injections on days 0 and 56 while the other received three injections on days 0, 28 and 56. To identify genes that were differentially expressed following an injection, we modeled three pre- versus post-vaccine comparisons: days 3 vs. 0, 59 vs. 56 and 63 vs. 56. Pooling individuals from the two treatment groups, we identified differentially expressed genes (DEGs) using a linear mixed-effects model that accounted for covariation in paired samples from the same individual and adjusted for participant sex at-birth. In total the models identified 241 upregulated and 208 downregulated genes based on the pre-specified significance criteria (Figure 2; unadjusted-p < 0.05, FDR-q < 0.2, |log2-fold change| > 0.5) for a total of 426 unique DEGs. Despite receiving an identical vaccination three days earlier, participants had fewer genes with a significant change from day 0 to day 3 (12 DEGs) compared to those with a significant change from day 56 to day 59 (122 DEGs; Supplementary Figure S1); notably, nearly all of the genes that were upregulated at day 59 were also upregulated at day 3, albeit with a smaller fold-change (Supplementary Figure S1). Substantially more genes were found differentially expressed at day 63 vs. 56 with 168 genes downregulated and 145 genes upregulated (Supplementary Data Sheet 1).

To better understand the functional signaling patterns among the differentially expressed genes we used weighted gene correlation network analysis [WGCNA (19)], which identified eight distinct modules of coregulated genes that aided interpretation and enabled downstream analysis (Table 2; Supplementary Data Sheet 1). These patterns of correlated gene expression were also easily visible from rank correlation networks formed by connecting genes with a correlation coefficient, R > 0.6 (Figure 2).

## Cell-specific innate immune genes were differentially regulated three days after vaccination

Four modules contained genes typically associated with innate cell types that were differentially regulated at day 3 vs. 0, day 59 vs. 56 or both; average expression for the latter returned to pre-vaccine levels by day 63. One module contained 54 genes including several associated with innate antiviral responses and the type I interferon pathway, with OAS1, BATF2, GPB5 and SERPING1 having high centrality scores within the module network (referred to as IFN-I module, Figure 3A) (23, 24). A gene set enrichment analysis (GSEA) of genes from the IFN-I module using gene sets from the blood transcriptional modules [BTMs (20)] also detected enrichment for sets involved in complement activation (M112.0), complement and other receptors in DCs (M40), immune activation (M37.0), and activated dendritic cells (M67), in addition to the antiviral IFN signature (M75) (all with FDR-q < 0.2).

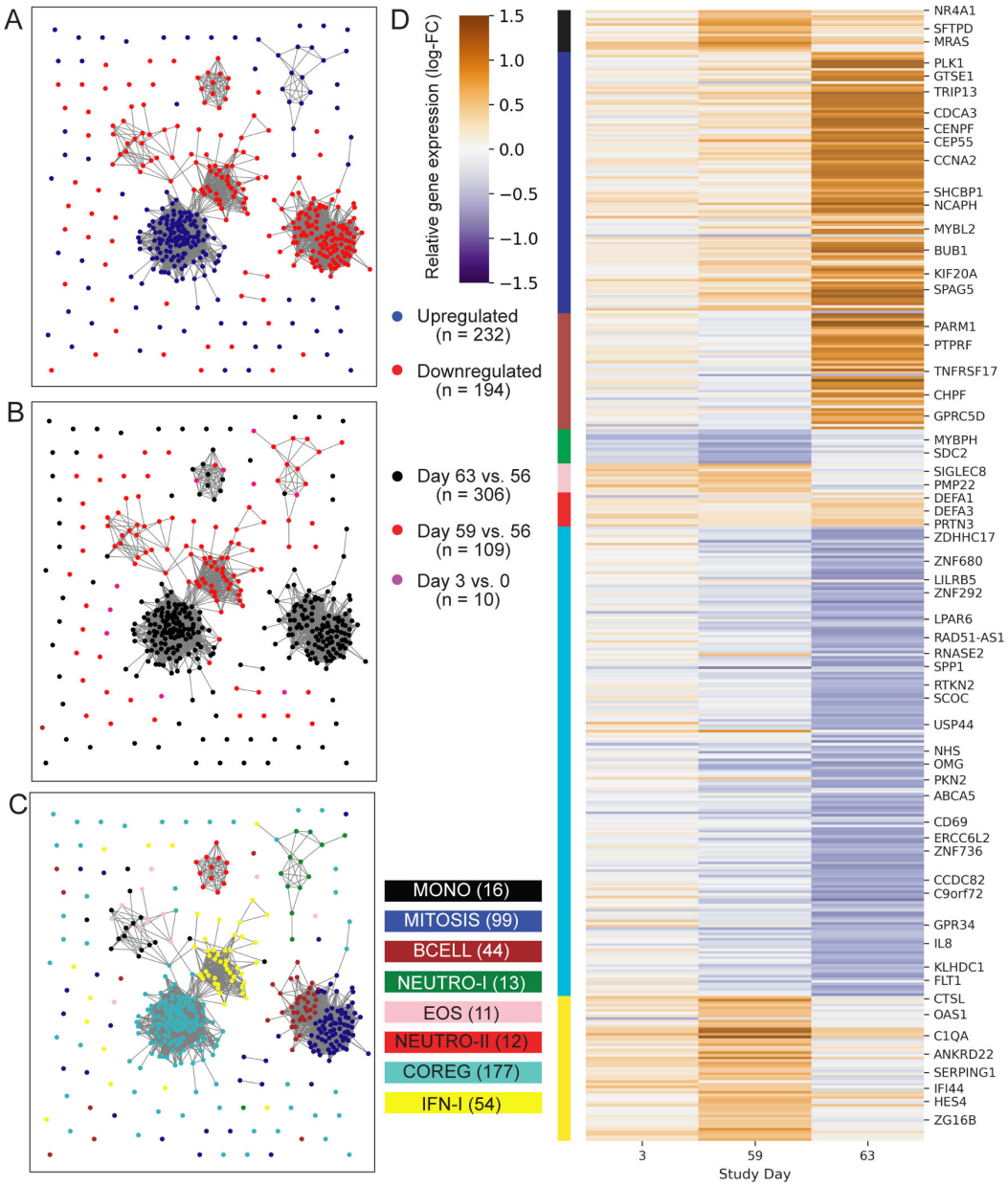


FIGURE 2
Profile of ID93+GLA-SE differentially expressed genes. Network plots represent 426 genes (nodes) that were differentially expressed after ID93+GLA-SE vaccination. Significant differential expression was based on an unadjusted-p < 0.05, FDR-adjusted q-value < 0.2 and absolute-log2 fold-change > 0.5. Edges connecting nodes represent a positive rank correlation with R > 0.6 (edge length does not convey additional information). Node color indicates **(A)** up- (red) vs. down- (blue) regulation relative to pre-vaccination, **(B)** differential regulation at one of three time points: days 3 vs. 0 (pink), 59 vs. 56 (red) or 63 vs. 56 (black), or **(C)** membership in one of eight gene modules created using WGCNA. Genes that were differentially expressed at more than one time point are colored for the time point with the largest fold-change, therefore there are fewer genes plotted than total DEGs stated in results. Each gene is in exactly one module. **(D)** Heatmap indicates log-transformed fold-change for each differentially expressed gene, relative to the most recent vaccine dose (either day 0 or day 56). Module membership is indicated by the color bar. A subset of genes are labeled by gene symbol including some of those cited in the text or found in gene sets that were significantly enriched with DEGs in the GSEA analysis.

A second module contained 12 genes, several of which were found previously to be associated with subsets of monocytes including MRAS, CDKN1C, LYPD2, LYNX1, VMO1 and SFTPD (referred to as MONO module). Notably, surfactant protein D (SFTPD) is typically expressed by alveolar macrophages in the lung and may be involved in lung defense. The MONO module was significantly upregulated at day 59 vs. day 56 (Figure 3B). A third module contained 11 coregulated genes that were upregulated 3 days after vaccination; all 11 genes were most highly expressed by eosinophils (EOS module, Figure 3C) [Human Protein Atlas (24)]. The fourth module contained 13 genes that were downregulated three days after vaccination and were almost all primarily expressed by neutrophils

TABLE 2 Summary of gene modules associated with ID93+GLA-SE vaccination.

| Module | N | Day 3 | Day 59 (+3*) | Day 63 (+7*) | Possible role |
|---|---|---|---|---|---|
| MONO | 12 | UP | UP | UP | monocyte genes, surfactant gene |
| EOS | 11 | UP | UP | – | eosinophil genes |
| IFN-I | 54 | UP | UP | – | antiviral, type I IFN, complement receptors and dendritic cells |
| NEUTRO-I | 13 | DOWN | DOWN | – | neutrophil genes |
| MITOSIS | 99 | – | – | UP | cell cycle, transcription |
| BCELL | 44 | – | – | UP | B cells, plasma cells and Ig genes |
| NEUTRO-II | 12 | – | – | UP | neutrophil granules, defensins |
| COREG | 177 | – | – | DOWN | genes coregulated other modules |

* +3 and +7 refer to the number of days post vaccination.

(HPA), including the most highly expressed genes AOC3, OTX1, SDC2 and TP35INP2 (NEUTRO-I module, Figure 3D).

With any changes in gene expression observed from whole tissues, they could be linked to a change in the cellular composition of the tissue and/or a change in regulation within cells. To address these hypotheses, we used computational cellular deconvolution, which leverages a database of cell-type specific gene expression patterns to infer enrichment scores that are proportional to the relative abundance of cells composing the sample [xCell (21)]. The output of xCell is an enrichment score that can be used for a longitudinal comparison for a given cell type, but cannot be used to infer the absolute frequency of cell types in a sample, and therefore cannot be used to compare across cell types. Generally, scores were highly variable and changes were small (Supplementary Data Sheet 1), however the analysis suggested that there was a 2.5-fold increase in the score for dendritic cells from days 56 to 59 (p=0.0012, FDRq=0.038); there was a similar trend for eosinophils and monocytes that was not significant (Supplementary Figure S2). The

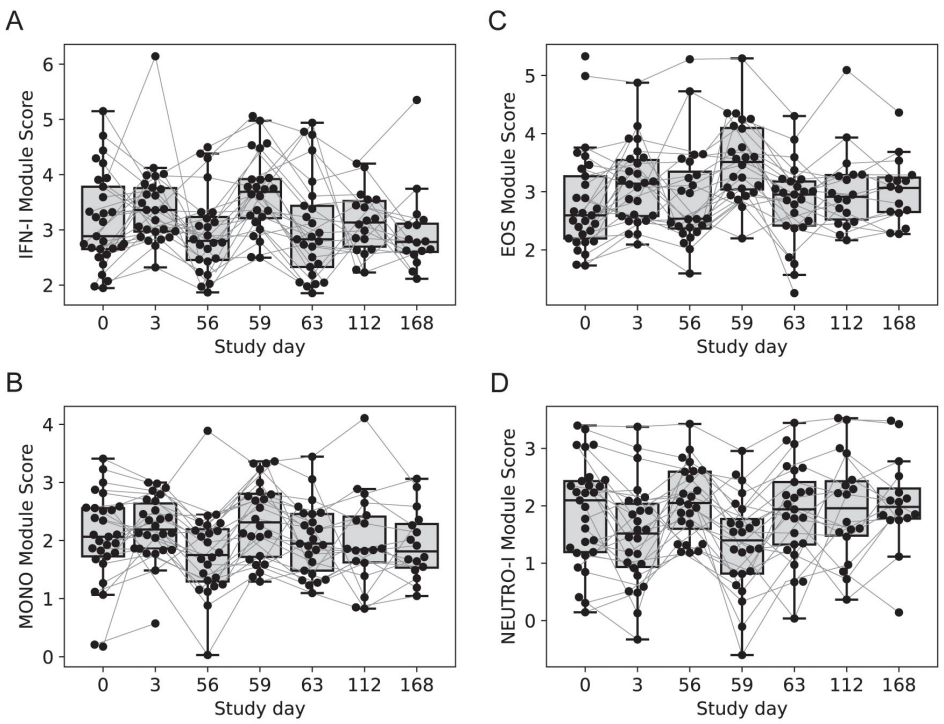


FIGURE 3
Longitudinal expression of modules with changes 3-days post-vaccination. Boxplots of the eigengene expression score for each participant in either the 2-dose or 3-dose "2 + 5" ID93+GLA-SE vaccine group (n=29). **(A)** IFN-I module, **(B)** MONOS module, **(C)** EOS module, **(D)** NEUTRO-I module. A line for each participant is overlaid, connecting longitudinal observations. Box extents indicate the interquartile range (IQR) with whiskers indicating the extent of the most extreme observation within1.5-times the IQR.

relative score for neutrophils in the blood did not substantially change across days 56 – 63 (Supplementary Figure S2), supporting the hypothesis that the decrease in expression of NEUTRO-I genes was related to downregulation of a subset of genes expressed by neutrophils. The analysis was repeated with an additional deconvolution method CIBERSORT (Supplementary Figure S3), which did not identify any cell subsets that were significantly changed by vaccination (Supplementary Data Sheet 1); this is consistent with the hypothesis that genes in transcript abundance could be attributed to changes in gene expression as opposed to changes in the abundance of specific cell types, but it remains possible that the variability associated with estimating changes in cellular composition made it difficult to detect significant changes.

## ID93+GLA-SE transiently increased expression of genes associated with TB disease progression

Many studies have demonstrated that expression levels of specific transcripts in whole-blood can be used to predict TB disease progression as well as treatment response (25–29). Given the vaccine-induced changes in the IFN-I module genes – genes that are also included in TB risk signatures – we looked at the kinetics of two leading risk signatures across study participants, through 6 months post-vaccination (Supplementary Figure S4). Both the Sweeney3 signature (GBP5, DUSP3, and KLF2) and the Darboe11 (a.k.a., RISK11: BATF2, ETV7, FCGR1C, GBP1, GBP2, GBP5, SCARF1, SERPING1, STAT1, TAP1, and TRAFD1) signatures were transiently increased 3 days after the first dose and booster dose. Expression levels returned to baseline by day 7 post-boost (i.e., day 63) and remained at consistent levels through day 168.

## Genes associated with T and B cell responses were upregulated three and seven days after vaccination

Two gene modules had similar average expression profiles showing a significant increase at day 63 vs. day 56, seven days after the last injection (Figures 4A, B; no samples were available seven days after the first injection). However, the genes formed two distinct modules based on their covariation, with a "MITOSIS" module consisting of 99 genes enriched in gene sets associated with mismatch repair, cell cycle and transcription, and a "BCELL" module containing 44 genes enriched in gene sets associated with B cells, plasma cell surface markers and immunoglobulin genes (Supplementary Data Sheet 1). The cell composition deconvolution analysis suggested that the relative frequency of class-switched memory B cells (p=0.0040, FDR-q=0.063; Supplementary Figure S2) and type-1 helper T cells (Th1, p=0.0012, FDRq=0.038), were increased at day 63 vs. day 56. A third smaller module of 12 tightly coordinated genes was also significantly increased at day 63 and contained genes associated with neutrophil cytotoxic granules

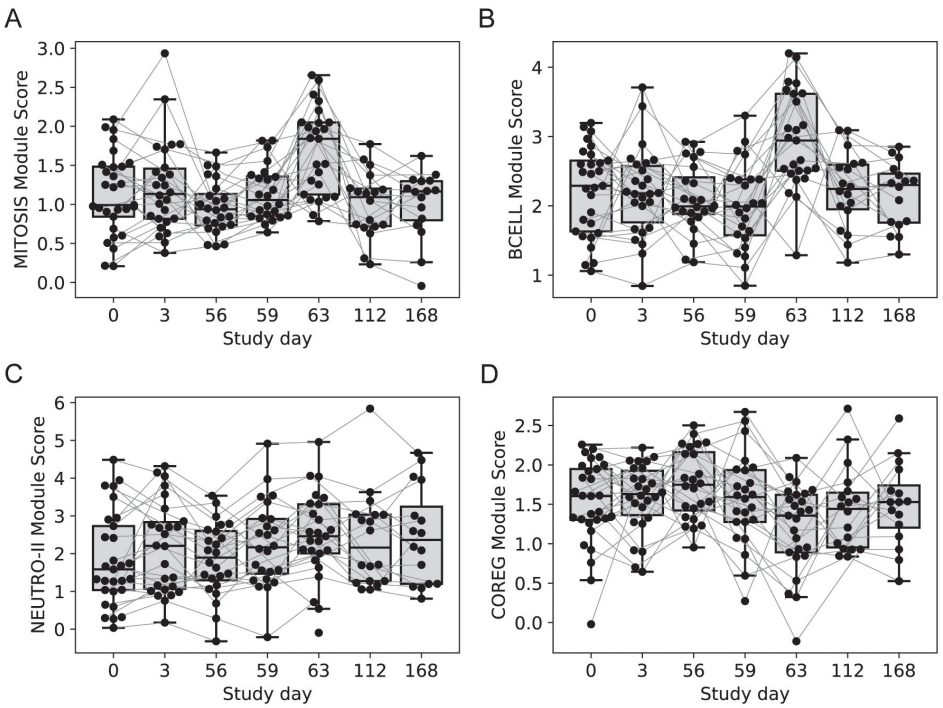


FIGURE 4
Longitudinal expression of modules with changes 7-days post-vaccination. Boxplots of the eigengene expression score for each participant in either the 2-dose or 3-dose "2 + 5" ID93+GLA-SE vaccine group (n=29). **(A)** MITOSIS module, **(B)** BCELL module, **(C)** NEUTRO-II module, **(D)** COREG module. A line for each participant is overlaid, connecting longitudinal observations. Box extents indicate the interquartile range (IQR) with whiskers indicating the extent of the most extreme observation within1.5-times the IQR.

(NEUTRO-II module; Figure 4C), including three genes encoding defensins (DEFA1, DEFA3 and DEFA4). The module also included lactotransferrin (LTF) and PRTN3, which are also expressed primarily by neutrophils.

## Genes downregulated after vaccination were negatively correlated with upregulated modules

The gene modules constructed using WGCNA have low correlation across individuals by design; genes with positively correlated expression levels were grouped into the same modules leaving relatively little correlation between modules. However, genes that were inversely/negatively correlated had large distances in the network (and module construction steps) and therefore formed distinct modules. As a result, we have two distinct modules that decreased with vaccination: NEUTRO-I which decreased 3 days after vaccination and COREG, a large module of 177 genes that decreased at day 63 (7 days post-boost; Figure 4D). While the COREG module contained several immune-related genes including (e.g., LILRB5, IL8, CD69), GSEA did not identify any significantly enriched gene sets, nor could we identify a single function that could relate all the genes. Instead, it appears that the COREG module contains genes that are coregulated with genes in other modules that were increased at day 63 (Figure 5). For example, 70 COREG genes (40%) have a negative rank correlation coefficient, R< -0.5 with at least 1 gene from the BCELL module; similarly, 33 COREG genes are negatively correlated with at least one MITOSIS gene. In comparison, only 3 genes are negatively

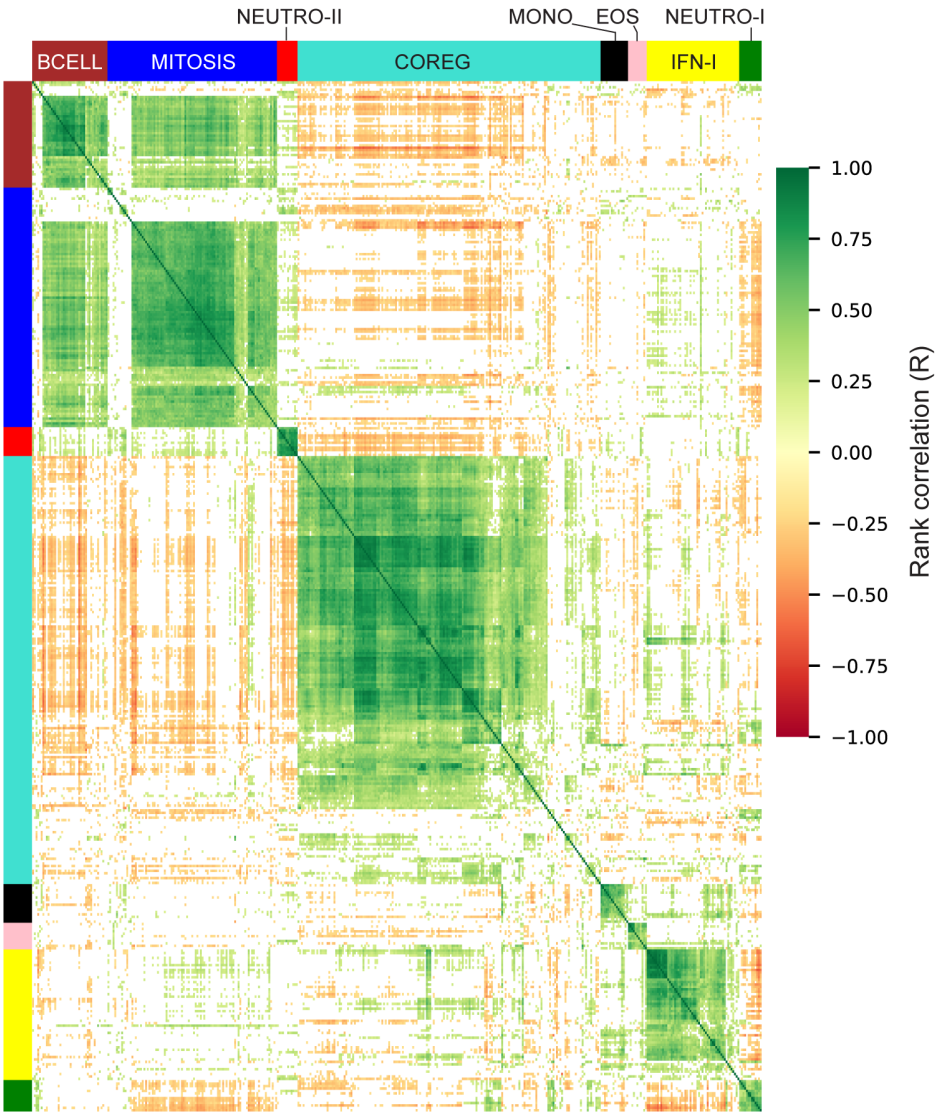


FIGURE 5
Correlation heatmap of differentially expressed genes. Rank correlations were estimated for all pairs of differentially expressed genes. Genes are organized by module and hierarchically clustered within each module. Color bars indicate module membership. Correlations with abs-R < 0.2 are censored for clarity (white).

correlated with any of the MONO, EOS or IFN-I genes, which are increased at day 3.

## IFN-I and EOS genes responded more robustly in female participants

With genes grouped into modules, we sought to understand how early vaccine-induced gene expression changes were associated with the different vaccine regimens, participant sex and ultimately, the humoral and cellular responses that were evaluated weeks later. To do this, we used the eigengene of each module as a longitudinal measure of expression for each participant and evaluated associations with additional variables using linear mixed-effects models (LMM). As an initial check, we analyzed participants in the "2 + 2 (x2)" treatment group which received lower doses of GLA-SE (2 μg, n=15). We noted similarities with the groups that received 5 μg of GLA-SE, that had been used to identify DEGs, though responses were lower (Supplementary Figure S5). For example, among participants in the "2 + 2 (x2)" group the IFN-I module was increased at days 3 and 59, while the BCELL and MITOSIS modules were increased at day 63; these were consistent with the changes seen in the 5 μg GLA-SE dose groups; these findings served as a partial validation of our approach to identify genes that were induced by vaccination.

We next evaluated the effect of participant sex on vaccine transcriptional responses; the 2-dose and 3-dose "2 + 5" groups were pooled with responses analyzed at day 3 vs. 0, since the treatment groups received identical treatments at day 0 (n=10 of 29 female). The responses of EOS and IFN-I genes at day 3 were significantly higher among females versus males (Figure 6, LMM p = 0.022 and 0.012, respectively). There was no significant effect of sex on the MONO or NETRO-I modules and we did not test the modules that were unchanged at day 3.

Testing for an effect of sex on vaccine responses was more difficult at days 59 and 63, since the treatment groups differed and were not well-balanced by sex; the 2-dose group had 8 of 15 female participants, while the 3-dose group had 2 of 14 female participants, leading us to focus on the 2-dose group. At 3 days post-2$^{nd}$ vaccination we saw an increase in EOS and IFN-I genes that tended higher among females, but was not significantly different (LMM p = 0.109 and 0.318, respectively). There was no effect of sex on the other modules at the day 59 and day 63 visits.

## Intervening day 28 vaccination blunted immune response to the booster vaccination

In the primary study, the 2-dose and 3-dose vaccine regimens had distinct cellular and humoral responses. The difference was most salient at day 70: 14 days after the 2$^{nd}$ dose for one group and 14 days after the 3$^{rd}$ dose for the other. Though the absolute levels of ID93-specific IgG and CD4+ T cells were comparable at day 70, there was a large increase from day 56 to day 70 in the 2-dose group that was not seen in the 3-dose group (reproduction of data in Supplementary Figures S6, S7). We hypothesized that there would be a similar reduction in the gene expression responses of the 3-dose group. We modeled the expression levels of each module at days 56, 59 and 63, including treatment group and sex as potential modifiers of the response; the interaction term between treatment group and day was the indicator of whether there was a difference in the 2-dose vs. 3-dose response.

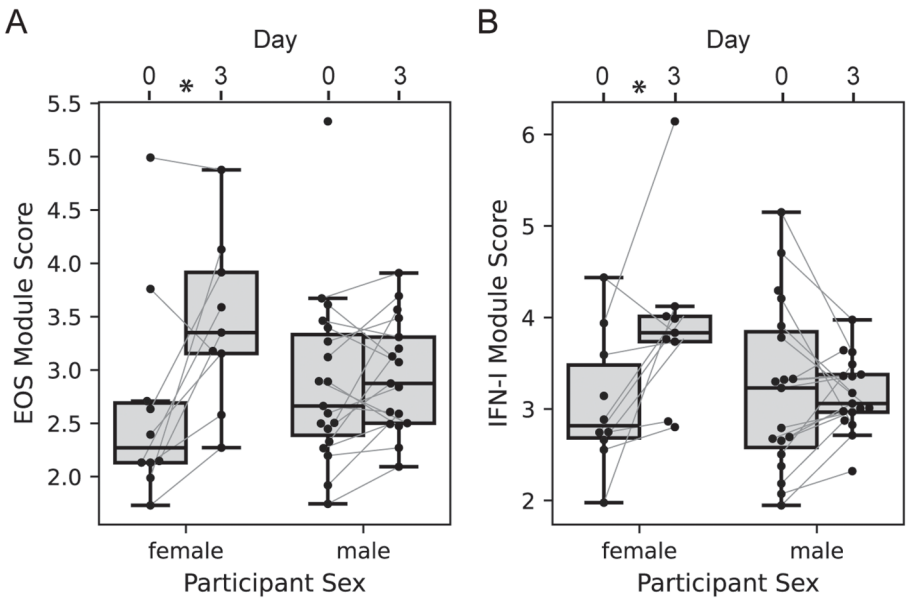


FIGURE 6
Participant sex modifies day 3 transcriptional response. Boxplots of the EOS **(A)** and IFN-I **(B)** module expression scores for each participant in either the 2-dose or 3-dose "2 + 5" ID93+GLA-SE vaccine group (n=29). Module expression score is the log-normalized transcript counts with a mean taken across all genes contained in the module. Scores are organized by visit with lines connecting the scores of an individual participant at day 0 and day 3, and by sex (n=10 of 29 female). Linear mixed modeling showed a significant modification of the vaccine-induced change by sex (EOS p = 0.022; IFN-I p=0.012).

With the model of day 59 vs. 56 we noted that the NEUTRO-I module differed significantly in the two treatment groups after adjustment for participant sex, having a 2.6-fold greater decrease in the 2-dose vs. 3-dose group (Figure 7A, p = 0.049). Similarly, the IFN-I module tended towards a greater response in the 2-dose group (Figure 7B, p = 0.094). The changes in the other modules were similar across the groups. At day 63 the MITOSIS module was increased in both groups, but the response was 2.25-fold greater in the 2-dose group (Figure 7C, p=0.0013). The BCELL group showed a similar trend, but it was not significant (p=0.115). To assess if the blunting of the vaccine response in the 3-dose group could be explained by a difference in gene expression of the modules at the time of the last vaccination, we tested for an association between module score at day 56 and the treatment group, adjusting for sex; none of the modules were significantly different across the groups at day 56 (Supplementary Data Sheet 1).

## Early innate transcriptomic signature correlated with ID93-specific CD4+ T cell responses

To better understand the orchestration of innate and adaptive immune responses after vaccination we conducted a correlation analysis to identify the gene expression modules that were associated with the magnitude of the antigen-specific CD4+ T cell and IgG antibody responses (Supplementary Data Sheet 2). The ID93-specific CD4+ T cell response was measured using two intracellular cytokine staining (ICS) assays that computed the proportion of cells expressing cytokine after ID93 stimulation: (1) PBMC-ICS using cryopreserved peripheral blood mononuclear cells (PBMC, Supplementary Figure S6) and (2) WB-ICS using fresh whole-blood. The level of ID93-specific IgG was measured by ELISA and reported as mean endpoint titers (MEPT, Supplementary Figure S7).

With the hypothesis that changes in post-vaccine gene expression were correlated with the adaptive responses we focused on the gene module changes at specific time points that were significantly increased or decreased (Table 2, 13 significant comparisons). Correlations were computed between the change in gene expression versus the absolute CD4+ T cell or IgG response level at days 14, 28, 70 or 224.

After adjusting for multiple comparisons, we found that the change in the IFN-I module at day 3 was significantly associated with ID93-specific CD4+ T-cell response at day 14 (WB-ICS, rho=0.39, FDRq=0.11), day 28 (PBMC-ICS, rho=0.44, FDRq=0.19) and day 224 (WB-ICS, rho=0.48, FDRq=0.058). Looking more broadly, these correlations were representative of a generally positive correlation between the IFN-I responses at day 3 and the CD4+ T-cell response (Figure 8). There was also a positive correlation between the day-3 IFN-I (rho=0.38) and EOS (rho=0.37) modules with the ID93-specific IgG level at day 28, though it did not reach the significance criteria (FDRq=0.212, FDRq=0.212 respectively).

Directly comparing ID93-specific CD4+ T cell and IgG responses we found that female participants had higher PBMC-ICS CD4+ T cell responses at day 28 (unadjusted-p = 0.032) and higher ELISA IgG MEPT at day 14 (unadjusted-p = 0.039), however no significant differences were observed at any other visits (Supplementary Figure S8). Computing partial correlations adjusted for participant sex reduced the correlations with the IgG response (e.g., IFN-I partial-rho=0.28), but did not consistently reduce the correlations with the CD4+ T cell response (Supplementary Figure S9). This suggests that the correlations were not primarily driven by the effect of sex on both innate and adaptive responses.

## Post-boost transcriptomic signature correlated with subsequent boosting of antibody and T-cell responses

We repeated the correlation analysis focused on responses after the boost (day 56), replacing absolute levels of CD4+ T-cell responses and IgG with relative responses, subtracting the response observed prior to the boost. While none of the correlations had FDRq < 0.2, the BCELL and MITOSIS modules at day 63 had low to moderate positive correlations with all the adaptive immune responses at days 70 and 224 (Supplementary Figure S9). This is consistent with the 3-dose vs. 2-dose treatment effect, with the 3-dose group having lower BCELL and MITOSIS responses and little or no increase in antibody and T cell responses with the 3$^{rd}$ dose. Notably, the IFN-I module was no longer associated with these adaptive responses measured relative to day 56.

A similar sensitivity analysis was conducted substituting absolute levels of CD4+ T cell and IgG at days 14 and 28 with responses relative to pre-vaccination (day 0) levels to assess if correlations were more strongly associated with relative changes in these responses (Supplementary Figure S9). All of the associations between IFN-I and the adaptive responses were weaker with the baseline-subtracted responses.

## IFN-I module responses predictive of high CD4+ T-cell responders at day 224

To complement the correlation analysis we also conducted a predictive analysis, employing multivariate regularized logistic regression modules to predict high and low responders. High versus low response was defined as above or below the median response. Predictor sets included, (1) Prime: all modules with a day 3 response (see Table 2, 4 variables), (2) Boost: all modules with a day 59 or day 63 response (9 variables), (3) IFN-I: day 3 and day 59 (2 variables) and (4) Prime + Boost (13 variables). Performance was quantified using the area under the receiver operator curve in 5-fold cross-validation (CV-AUC). Analysis was focused on prediction of the CD4+ T-cell response at day 224 measured by PBMC-ICS and WB-ICS. Consistent with the correlation analysis, prediction of high responders could be predicted by the IFN-I responses 3 days after the prime and boost vaccinations (Figure 9). For WB-ICS the IFN-I variables had a CV-AUC = 0.91 (95% CI 0.78 – 1.00) and the

10.3389/fimmu.2024.1441944

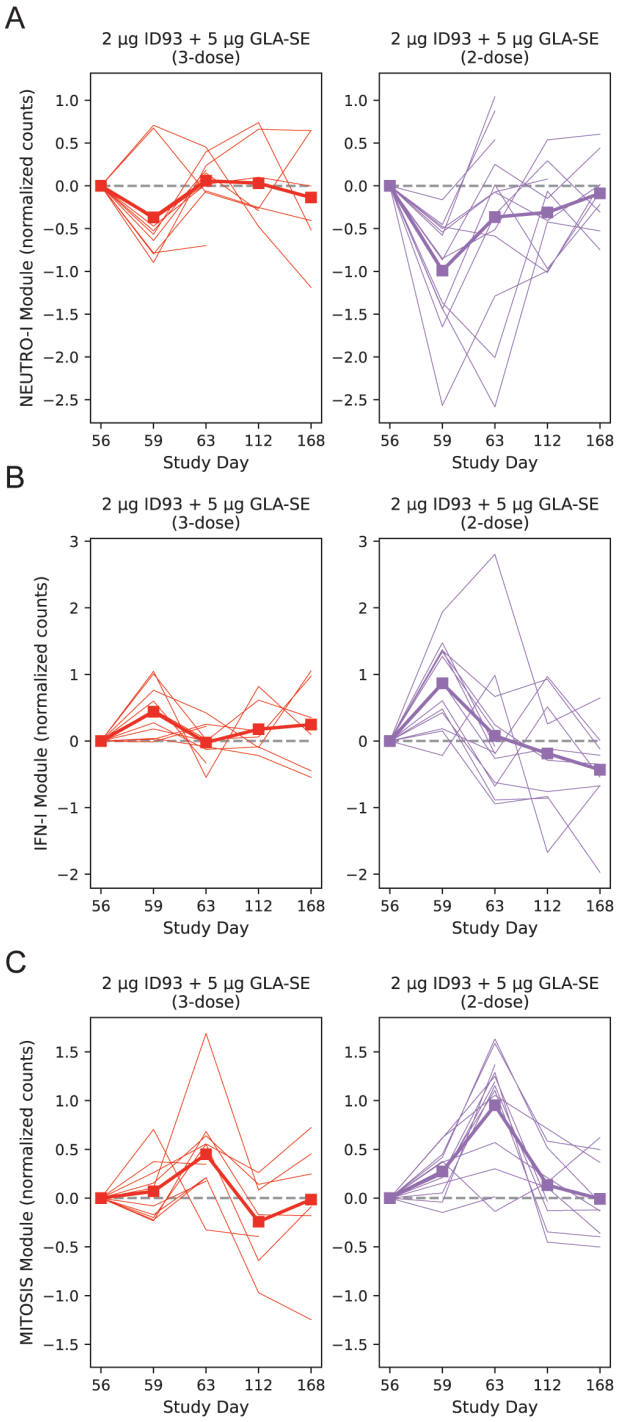


FIGURE 7
Post-boost transcriptional changes by treatment group. Baseline-subtracted normalized expression level plotted for the NEUTRO-I **(A)**, IFN-I **(B)** and MITOSIS **(C)** modules, organized by participant and day. A module's expression is the log-normalized transcript counts with a mean taken across all genes contained in the module; each participant's module expression at day 0 is subtracted from the time series for that individual. Module expression values are plotted longitudinally with each participant represented by a single line and the group mean represented by a thick line and square symbols (treatment group indicated at the top of each panel). Linear mixed modeling showed that the 2-dose group had a greater change at day 59 vs. 56 for the NEUTRO-I module ($p=0.049$) with a trend for the IFN-I module ($p=0.094$). At day 63 vs. day 56 the MITOSIS module had a larger response in the 2-dose group ($p=0.0013$). Dashed line on each plot indicates zero change from day 0 (i.e., pre-vaccine) expression. Broken lines represent missing data that result from missing samples.

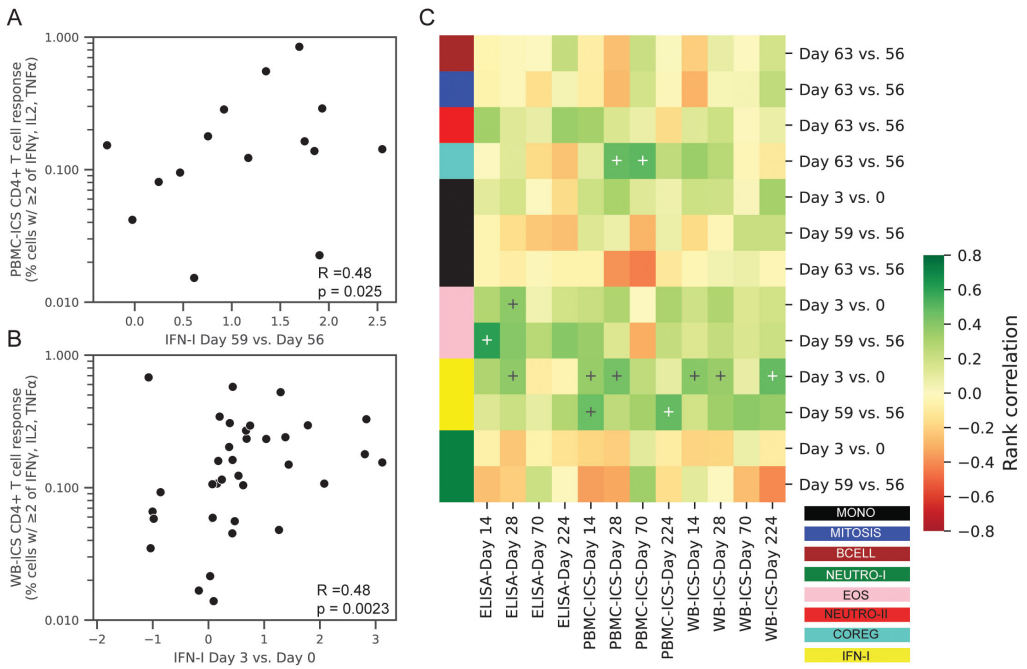


FIGURE 8
Correlations between transcriptional responses and ID93-specific adaptive responses. Rank correlations between pairs of gene module expression changes and absolute levels of ID93-specific CD4+ T-cell responses and IgG antibody levels in the blood. Transcriptional changes were expressed as changes in the eigengene score between two days (e.g., day 3 vs. 0). CD4+ T-cell responses were measured by PBMC-ICS or WB-ICS while IgG was measured by ID93 ELISA. Significant correlations (FDRq < 0.2 and p<0.05) included **(A)** PBMC-ICS at day 224 with IFN-I at day 59 vs. 56 and **(B)** WB-ICS at day 224 and IFN-I at day 3 vs. 0 (rank correlation coefficient R and unadjusted p-valued indicated in lower left corner of panel). **(C)** Heatmap of all tested correlations organized by module color (see Figure 1 for key). Modules were only tested for correlation at the day that they showed a significant change post-vaccination (13 comparisons). Crosses on heatmap indicate an unadjusted p < 0.05 (black and white for visual clarity).

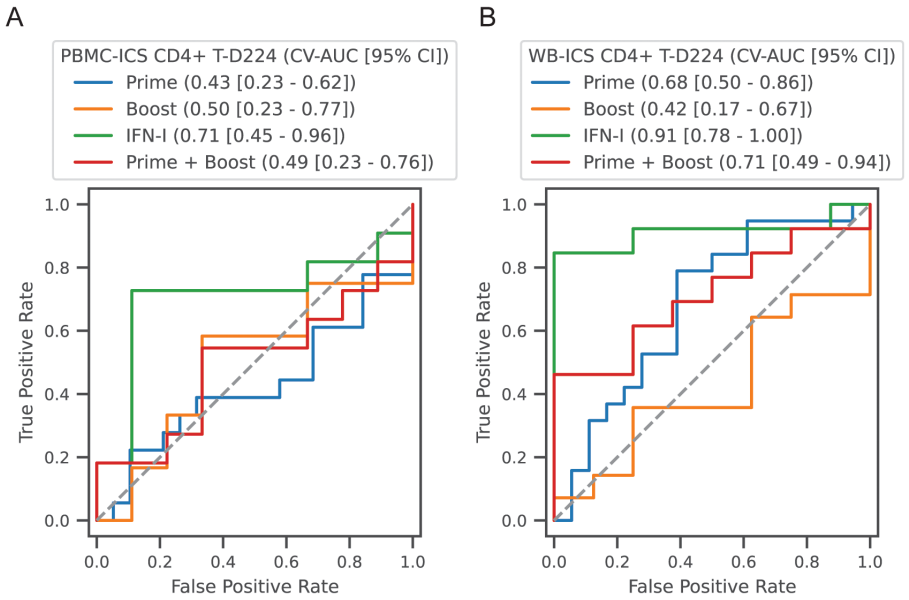


FIGURE 9
Classification of high versus low CD4+ T-cell responders. Participants in all vaccine groups were categorized as high or low based on the median of the CD4+ T-cell response; **(A)** PBMC-ICS and **(B)** WB-ICS responses were analyzed separately. Regularized logistic regression (L1 penalty) was used to train a classifier based on feature sets: (1) Prime: modules that responded after the 1st dose (4 features), (2) Boost: modules that responded after boost dose (i.e., day 56, 9 features), (3) IFN-I modules after the prime and boost (2 features), (4) Combination of all prime and boost modules (13 features). Classifier performance was evaluated in 5-fold cross-validation (CV). Receiver operator curves (ROC) are plotted for each feature set, with cross-validated area under the ROC curve (CV-AUC) and 95% confidence interval (CI) indicated above the plot. Gray dashed line indicates performance equivalent to uninformed guessing.

addition of other variables did not improve prediction. The IFN-I variable set was also predictive of the PBMC-ICS CD4+ T-cell response with CV-AUC = 0.71 (95% CI 0.45 – 0.96).

## Discussion

ID93+GLA-SE elicits a multitude of immune responses that can be detected as differentially regulated genes in peripheral blood, 3 and 7 days after vaccination. Using a modular gene analysis approach we mapped modules of correlated genes to their associated cell types and functions. From the vaccine response signature it was apparent that a diverse population of cells was responding, with innate immune populations, such as eosinophils, neutrophils, and monocytes responding 3 days post-vaccination and a mix of innate and adaptive populations responding by day 7. The gene expression responses seemed to be attributable to both changes in the relative composition of immune cell types in the blood as well as changes in their gene expression; for example, while dendritic cells and memory B cells were increased 3 and 7 days after vaccination (respectively), several modules contained a relatively select set of genes with increased expression that could be more easily explained by a changed gene expression pattern. To our knowledge this is the first human transcriptomic analysis of the GLA-SE adjuvant and the ID93+GLA-SE vaccine.

Pre-clinical studies have previously demonstrated the efficacy of therapeutic immunization with ID93+GLA-SE to improve TB treatment outcomes (30, 31); many of the innate and adaptive signatures we observed in this study are consistent with the immune responses observed in model systems. A prior study of GLA-SE in mice at 6 hours, 1 day, 3 days and 7 days post-injection identified DEGs that were enriched for genes involved in innate antiviral responses and the type-I IFN pathway as early as 6 hours post-vaccination (32). Adaptive responses in the mouse related to T cells, cytokines, antigen presentation and cell cycle were evident from day 3 through day 7, earlier than we observed in humans.

It was notable that the responses of innate modules 3 days after the booster dose (day 59) were stronger than the responses 3 days after the prime (day 3); this was evidenced by the larger number of differentially expressed genes, and larger shifts in expression. A similar phenomenon was observed in studies of the adjuvant $AS01_B$ and $AS01_E$, which contain the TLR4-agonist MPL (33–35). In those studies, blood transcriptomic responses 1 day after vaccination were characterized by an increase in genes associated with dendritic cells (DCs), monocytes, neutrophils and IFN signaling; responses 1 day after the 2$^{nd}$ dose were greater than responses 1 day after the 1$^{st}$ dose. This could be an effect of trained immunity, which refers to long-term epigenetic reprogramming of innate cells that can alter responsiveness for months. Effects of trained immunity have been demonstrated with live-attenuated vaccines and hypothesized with TLR-stimulating adjuvants such as GLA-SE (36). Alternatively, the mechanism could involve CD4+ memory T cells that respond quickly after the boost or prime-induced antibody immune complexes that help to enhance the innate response (34). Notably, participants in this study had some level of pre-existing ID93-specific T-cell memory at baseline, whereas participants in the AS01 studies were naïve to the antigen (hepatitis B surface antigen, HBs).

Prior work has established that vaccine-induced immune responses are typically more robust among females; this has been shown for a variety of vaccine platforms and applies to both adaptive as well as innate responses (37). Among others, genes associated with viral sensing and the type-I IFN response are often enhanced in females, demonstrated recently in a study of replication defective herpes simplex virus 2 vaccine (38). In this study, the vaccine-induced increase in the IFN-I and EOS modules at day 3 was more robust among the female vaccine recipients. Female participants had higher ID93-specific IgG and CD4+ T cell responses after the first dose, consistent with the increased type-I IFN response and the correlations between the two. After subsequent doses sex was no longer associated with higher CD4+ T cell and IgG responses; it is possible that multiple vaccine doses reduced the effects, however a limitation of the study was the sex-imbalance in the three-dose vaccine group, among those that had samples available for transcriptional analysis. This reduced our ability to measure the effects of sex on late adaptive responses.

Our correlative analysis of the transcriptomic and adaptive responses revealed a moderate positive association between the day 3 IFN-I and EOS modules and the antigen-specific CD4+ T-cell response; remarkably the correlation was consistent across two samples/assays (PBMC or whole-blood ICS) and from 2 weeks to 7 months after the 1$^{st}$ dose. The IFN-I response at day 59 also showed a similar trend suggesting that each participant's ability to mount a type-I IFN response was generally a predictor of their CD4 + T cell response. The correlations of IFN-I with CD4+ T cell and IgG responses were weaker when we analyzed baseline-subtracted measures for these responses; it suggests that it's not the pre-existing T cell response that is driving the IFN-I vaccine response, but all these results require validation in a larger cohort.

With our attempt to classify high versus low CD4+ T-cell responders we found that the innate IFN-I response could predict the Day 224 CD4+ T cell responders with an AUC of 0.91 (WB-ICS) and 0.71 (PBMC-ICS), and outperformed combinations of the other transcriptional response modules. The ability to predict a durable and robust T cell response from an innate gene signature is quite promising; such a signature could be used to accelerate the design or selection of adjuvants with improved durability. As this study enrolled a relatively small, geographically specific cohort, future studies will be needed to validate the predictive performance and understand the immune mechanisms. The prior studies of AS01 with hepatitis B virus surface antigen (HBs antigen) similarly showed a positive correlation between the innate response and the HBs-specific CD4+ T cell response (39). A study of RTS,S/AS01 in malaria-naïve adults also reported similar transcriptomic responses with type-I IFN related genes increased at day 1 and plasmablast and cell-cycling genes increased at day 6, however correlations with the CD4+ T cell response were only observed within a group that received an initial dose of an Ad35-vectored immunogen (35).

In the AS01 studies, plasmablast-associated genes peaked at day 7 (or day 6 with RTS,S), yet both the HBs/AS01 and RTS,S/AS01 studies found a positive correlation between expression of plasmablast-associated genes at day 1 with the antibody response two weeks later. The BCELL module we identified was not upregulated at day 3, nor was it correlated with the absolute level of ID93-specific IgG (we did not measure gene expression at day 1). However, we did observe that

the response of the BCELL module 7 days after the boost was positively associated with the relative increase in IgG following the boost. This positive association of a plasmablast gene signature with the magnitude of the antibody response has been seen with several other vaccines (40), including the influenza tetravalent inactivated vaccine (TIV) (41) and yellow fever YF-17D (42).

A unique feature of the TBVPX-203 study was that it provided a direct comparison of immune responses after a final boost dose at day 56, with or without an intervening dose at day 28. We found that the response of the MITOSIS module at day 59 was significantly diminished in the 3-dose compared to the 2-dose group. The module, which was enriched for cell cycling and mismatch repair genes, was similar to responses observed 7 days after vaccination with AS01 (34, 35) and a variety of other vaccine adjuvants and platforms (40), and seemed to be associated with expansion of the T and B lymphocytes. In this study the decrease in response with the 3-dose schedule is consistent with the small or negligible subsequent increase in antibody titers and frequency of CD4+ T cells. Trends for a similar pattern in the NEUTRO-I and IFN-I modules 3 days after the boost (day 59) suggest that the innate response was also diminished with the 3-dose schedule. These data further bolster the decision that was made to advance the 2-dose regimen for further clinical testing. The lack of samples after the intervening boost at day 28 and at day 7 post-prime were limitations of the study that prevented us from more fully characterizing the effect of the vaccine schedule on immunogenicity. Though further experiments would be needed to describe the mechanisms underlying the effects of dose interval on immunogenicity, our observation is consistent with a recent review of vaccine RCTs that compared dose schedules; the review showed that longer dose intervals have been associated with increased antibody responses in trials of mRNA COVID-19, AS04-adjuvanted HPV and inactivated poliovirus vaccines (43).

The IFN-I module in this study included several genes that also appear in gene signatures used to predict risk of TB disease progression (26, 28). As expected, the risk signature scores in these participants track closely with the IFN-I module, with a transient increase 3 days post-vaccination and subsequent resolution by day 7. A recent study of H56:IC31, a subunit vaccine with a TLR9-stimulating adjuvant, assessed immunogenicity of the vaccine administered as adjunctive immunotherapy during TB treatment (44). In that study the TB risk signature genes increased expression two months after treatment completion and the increase was greater among placebo recipients compared to H56:IC31; samples were not available to establish when the gene signature initially increased or whether or not it ever resolved. With ID93+GLA-SE vaccination within 28 days after treatment completion we see only transient vaccine-induced increases and no evidence of long-term changes in TB risk scores over 18 months, suggesting there may not have been a similar post-treatment increase, however we have no population-matched healthy controls with which we can directly evaluate absolute TB risk scores.

Our data provide a window into how the innate and adaptive responses are orchestrated after vaccination with ID93+GLA-SE in a population that was recently treated for TB disease. The transcriptional responses provided an opportunity to dissect the combined effects of host sex, vaccine schedule and adjuvant dose on immunogenicity. A limitation of this study and many vaccine studies is the lack of an adjuvant-only or empty-vector group that would allow for further dissection of the innate and adaptive responses; determining the role of recall responses was particularly challenging in this study since participants were not naïve to the *M.tb* antigens in the vaccine, even at baseline. Though we have dissected and described the immune responses to ID93+GLA-SE, we provide no new evidence about which aspects of the immune response may or may not be protective; an ongoing phase 2b study of therapeutic vaccination with ID93+GLA-SE for prevention of TB recurrence could be an opportunity to validate the response modules we observed and potentially evaluate them as correlates of protection (HVTN603/ACTG5397, NCT06205589). There may also be an opportunity to identify common correlates of protection with M72/$AS01_E$, since the two evidently induce similar innate responses; identifying correlates of protection for a disease can accelerate clinical development through greater understanding of mechanism, and by establishing surrogate immunogenicity endpoints for smaller, faster trials (45). Beyond TB, the response signatures of ID93+GLA-SE and the effects of dose schedule may be informative for the continued development of GLA and GLA-SE as an adjuvant for other vaccines such as those for preventing HIV-1 (46), leishmaniasis (47), leprosy (48), schistosomiasis (49), and malaria (50).

## Data availability statement

The datasets presented in this study can be found in online repositories. The transcriptomic dataset generated for this study can be found in the NIH SRA with Accession (PRJNA1101039). Analysis datasets have been made public at: https://figshare.com/s/5e70a07df9bd2c359520. All analysis code for this manuscript can be accessed at https://github.com/agartland/TBVPX203_RNA.

## Ethics statement

The studies involving humans were approved by University of Cape Town and University of Stellenbosch. The studies were conducted in accordance with the local legislation and institutional requirements. The participants provided their written informed consent to participate in this study.

## Author contributions

AF-G: Writing – review & editing, Writing – original draft, Supervision, Methodology, Formal analysis, Conceptualization. HS: Writing – review & editing, Writing – original draft, Visualization, Formal analysis. AS: Writing – review & editing, Investigation. TD: Writing – review & editing, Conceptualization. AP-N: Writing – review & editing. AKL: Writing – review & editing. NP: Writing – review & editing. AGL: Writing – review & editing. L-GB: Writing – review & editing. AD: Writing – review & editing. GW: Writing – review & editing. ZS: Writing – review & editing. SR: Writing – review & editing. TS: Writing – review & editing. MH: Writing – review & editing. RC: Writing – review & editing.

## Funding

The author(s) declare financial support was received for the research, authorship, and/or publication of this article. Funded in part by the Wellcome Trust (UNS31744) and with Federal funds from the National Institute of Allergy and Infectious Diseases, National Institutes of Health, Department of Health and Human Services, under the Seattle Tuberculosis Research Advancement Center (P30 AI168034) and Contract No. 75N93021C00029. The content is solely the responsibility of the authors and does not necessarily represent the official views of the National Institutes of Health.

## Acknowledgments

We thank the participants and their families for volunteering and participating in this study.

## Conflict of interest

Author SR was employed by the company HDT Bio Corporation.

The remaining authors declare that the research was conducted in the absence of any commercial or financial relationships that could be construed as a potential conflict of interest.

The author(s) declared that they were an editorial board member of Frontiers, at the time of submission. This had no impact on the peer review process and the final decision.

## Publisher's note



## Supplementary material

The Supplementary Material for this article can be found online at: https://www.frontiersin.org/articles/10.3389/fimmu.2024.1441944/full#supplementary-material

## References

1. World Health Organization. *Global Tuberculosis Report 2023* . Available online at: https://www.who.int/teams/global-tuberculosis-programme/tb-reports/global-tuberculosis-report-2023 (Accessed May 4, 2024).

2. Evans TG, Churchyard GJ, Penn-Nicholson A, Chen C, Gao X, Tait DR, et al. Epidemiologic studies and novel clinical research approaches that impact TB vaccine development. *Tuberculosis (Edinb).* (2016) 99 Suppl 1:S21–5. doi: 10.1016/J.TUBE.2016.05.008

3. Verver S, Warren RM, Beyers N, Richardson M, van der Spuy GD, Borgdorff MW, et al. Rate of reinfection tuberculosis after successful treatment is higher than rate of new tuberculosis. *Am J Respir Crit Care Med.* (2005) 171:1430–5. doi: 10.1164/RCCM.200409-1200OC

4. Knight GM, Griffiths UK, Sumner T, Laurence YV, Gheorghe A, Vassall A, et al. Impact and cost-effectiveness of new tuberculosis vaccines in low- and middle-income countries. *Proc Natl Acad Sci USA.* (2014) 111:15520–5. doi: 10.1073/PNAS.1404386111

5. Tait DR, Hatherill M, van der Meeren O, Ginsberg AM, Van Brakel E, Salaun B, et al. Final analysis of a trial of M72/AS01E vaccine to prevent tuberculosis. *N Engl J Med.* (2019) 381:2429–39. doi: 10.1056/NEJMOA1909953

6. Bertholet S, Ireton GC, Kahn M, Guderian J, Mohamath R, Stride N, et al. Identification of human T cell antigens for the development of vaccines against Mycobacterium tuberculosis. *J Immunol.* (2008) 181:7948–57. doi: 10.4049/jimmunol.181.11.7948

7. Coler RN, Day TA, Ellis R, Piazza FM, Beckmann AM, Vergara J, et al. The TLR-4 agonist adjuvant, GLA-SE, improves magnitude and quality of immune responses elicited by the ID93 tuberculosis vaccine: first-in-human trial. *NPJ Vaccines.* (2018) 3. doi: 10.1038/S41541-018-0057-5

8. Baldwin SL, Reese VA, Larsen SE, Pecor T, Brown BP, Granger B, et al. Therapeutic efficacy against Mycobacterium tuberculosis using ID93 and liposomal adjuvant formulations. *Front Microbiol.* (2022) 13:935444. doi: 10.3389/fmicb.2022.935444

9. Baldwin SL, Reese VA, Larsen SE, Beebe E, Guderian J, Orr MT, et al. Prophylactic efficacy against Mycobacterium tuberculosis using ID93 and lipid-based adjuvant formulations in the mouse model. *PloS One.* (2021) 16. doi: 10.1371/JOURNAL.PONE.0247990

10. Day TA, Penn-Nicholson A, Luabeya AKK, Fiore-Gartland A, Du Plessis N, Loxton AG, et al. Safety and immunogenicity of the adjunct therapeutic vaccine ID93 + GLA-SE in adults who have completed treatment for tuberculosis: a randomised, double-blind, placebo-controlled, phase 2a trial. *Lancet Respir Med.* (2020) 2600:1–14. doi: 10.1016/S2213-2600(20)30319-2

11. Ewels PA, Peltzer A, Fillinger S, Patel H, Alneberg J, Wilm A, et al. The nf-core framework for community-curated bioinformatics pipelines. *Nat Biotechnol.* (2020) 38:276–8. doi: 10.1038/S41587-020-0439-X

12. Dobin A, Davis CA, Schlesinger F, Drenkow J, Zaleski C, Jha S, et al. STAR: Ultrafast universal RNA-seq aligner. *Bioinformatics.* (2013) 29. doi: 10.1093/bioinformatics/bts635

13. Patro R, Duggal G, Love MI, Irizarry RA, Kingsford C. Salmon provides fast and bias-aware quantification of transcript expression. *Nat Methods.* (2017) 14. doi: 10.1038/nmeth.4197

14. Robinson MD, Oshlack A. A scaling normalization method for differential expression analysis of RNA-seq data. *Genome Biol.* (2010) 11. doi: 10.1186/gb-2010-11-3-r25

15. Dill-McFarland KA, Mitchell K, Batchu S, Segnitz RM, Benson B, Janczyk T, et al. Kimma: flexible linear mixed effects modeling with kinship covariance for RNA-seq data. *Bioinformatics.* (2023) 39. doi: 10.1093/BIOINFORMATICS/BTAD279

16. Bates D, Mächler M, Bolker BM, Walker SC. Fitting linear mixed-effects models using lme4. *J Stat Softw.* (2015) 67:1–48. doi: 10.18637/JSS.V067.I01

17. Law CW, Chen Y, Shi W, Smyth GK. voom: Precision weights unlock linear model analysis tools for RNA-seq read counts. *Genome Biol.* (2014) 15:R29. doi: 10.1186/gb-2014-15-2-r29

18. Benjamini Y, Hochberg Y. Multiple hypotheses testing with weights. *Scandinavian J Stat.* (1997) 24. doi: 10.1111/1467-9469.00072

19. Zhang B, Horvath S. A general framework for weighted gene co-expression network analysis. *Stat Appl Genet Mol Biol.* (2005) 4:Article17. doi: 10.2202/1544-6115.1128

20. Li S, Rouphael N, Duraisingham S, Romero-Steiner S, Presnell S, Davis C, et al. Molecular signatures of antibody responses derived from a systems biology study of five human vaccines. *Nat Immunol.* (2013) 15. doi: 10.1038/ni.2789

21. Aran D. Cell-type enrichment analysis of bulk transcriptomes using xCell. *Methods Mol Biol.* (2020) 2120:263–76. doi: 10.1007/978-1-0716-0327-7_19

22. DeLong ER, DeLong DM, Clarke-Pearson DL. Comparing the areas under two or more correlated receiver operating characteristic curves: A nonparametric approach. *Biometrics.* (1988) 44. doi: 10.2307/2531595

23. Kagina BM, Mansoor N, Kpamegan EP, Penn-Nicholson A, Nemes E, Smit E, et al. Qualification of a whole blood intracellular cytokine staining assay to measure mycobacteria-specific CD4 and CD8 T cell immunity by flow cytometry. *J Immunol Methods.* (2015) 417:22–33. doi: 10.1016/J.JIM.2014.12.003

24. Uhlen M, Karlsson MJ, Zhong W, Tebani A, Pou C, Mikes J, et al. A genome-wide transcriptomic analysis of protein-coding genes in human blood cells. *Science.* (2019) 366. doi: 10.1126/SCIENCE.AAX9198

25. Thompson EG, Du Y, Malherbe ST, Shankar S, Braun J, Valvo J, et al. Host blood RNA signatures predict the outcome of tuberculosis treatment. *Tuberculosis*. (2017) 107:48–58. doi: 10.1016/j.tube.2017.08.004

26. Darboe F, Mbandi SK, Thompson EG, Fisher M, Rodo M, van Rooyen M, et al. Diagnostic performance of an optimized transcriptomic signature of risk of tuberculosis in cryopreserved peripheral blood mononuclear cells. *Tuberculosis*. (2018) 108:124–6. doi: 10.1016/j.tube.2017.11.001

27. Zak DE, Penn-Nicholson A, Scriba TJ, Thompson E, Suliman S, Amon LM, et al. A blood RNA signature for tuberculosis disease risk: a prospective cohort study. *Lancet*. (2016) 6736:1–11. doi: 10.1016/S0140-6736(15)01316-1

28. Sweeney TE, Braviak L, Tato CM, Khatri P. Genome-wide expression for diagnosis of pulmonary tuberculosis: a multicohort analysis. *Lancet Respir Med*. (2016) 4:213–24. doi: 10.1016/S2213-2600(16)00048-5

29. Warsinske H, Vashisht R, Khatri P. Host-response-based gene signatures for tuberculosis diagnosis: A systematic comparison of 16 signatures. *PloS Med*. (2019) 16. doi: 10.1371/JOURNAL.PMED.1002786

30. Coler RN, Bertholet S, Pine SO, Orr MT, Reese V, Windish HP, et al. Therapeutic immunization against Mycobacterium tuberculosis is an effective adjunct to antibiotic treatment. *J Infect Dis*. (2013) 207:1242–52. doi: 10.1093/INFDIS/JIS425

31. Larsen SE, Baldwin SL, Orr MT, Reese VA, Pecor T, Granger B, et al. Enhanced Anti- Mycobacterium tuberculosis Immunity over Time with Combined Drug and Immunotherapy Treatment. *Vaccines (Basel)*. (2018) 6. doi: 10.3390/VACCINES6020030

32. Olafsdottir TA, Lindqvist M, Nookaew I, Andersen P, Maertzdorf J, Persson J, et al. Comparative systems analyses reveal molecular signatures of clinically tested vaccine adjuvants. *Sci Rep*. (2016) 6:1–14. doi: 10.1038/srep39097

33. van den Berg RA, De Mot L, Leroux-Roels G, Bechtold V, Clement F, Coccia M, et al. Adjuvant-associated peripheral blood mRNA profiles and kinetics induced by the adjuvanted recombinant protein candidate tuberculosis vaccine M72/AS01 in Bacillus Calmette-Guérin-vaccinated adults. *Front Immunol*. (2018) 9:564. doi: 10.3389/fimmu.2018.00564

34. de Mot L, Bechtold V, Bol V, Callegaro A, Coccia M, Essaghir A, et al. Transcriptional profiles of adjuvanted hepatitis B vaccines display variable interindividual homogeneity but a shared core signature. *Sci Transl Med*. (2020) 12:1–13. doi: 10.1126/scitranslmed.aay8618

35. Kazmin D, Nakaya HI, Lee EK, Johnson MJ, van der Most R, Van Den Berg RA, et al. Systems analysis of protective immune responses to RTS,S malaria vaccination in humans. *Proc Natl Acad Sci USA*. (2017) 114:2425–30. doi: 10.1073/pnas.1621489114

36. Ziogas A, Netea MG. Trained immunity-related vaccines: innate immune memory and heterologous protection against infections. *Trends Mol Med*. (2022) 28:497–512. doi: 10.1016/j.molmed.2022.03.009

37. Klein SL, Jedlicka A, Pekosz A. The Xs and Y of immune responses to viral vaccines. *Lancet Infect Dis*. (2010) 10:338–49. doi: 10.1016/S1473-3099(10)70049-9

38. Cheung F, Apps R, Dropulic L, Kotliarov Y, Chen J, Jordan T, et al. Sex and prior exposure jointly shape innate immune responses to a live herpesvirus vaccine. *Elife*. (2023) 12:1–21. doi: 10.7554/eLife.80652

39. Burny W, Callegaro A, Bechtold V, Clement F, Delhaye S, Fissette L, et al. Different adjuvants induce common innate pathways that are associated with enhanced adaptive responses against a model antigen in humans. *Front Immunol*. (2017) 8:943. doi: 10.3389/fimmu.2017.00943

40. Hagan T, Gerritsen B, Tomalin LE, Fourati S, Mulè MP, Chawla DG, et al. Transcriptional atlas of the human immune response to 13 vaccines reveals a common predictor of vaccine-induced antibody responses. *Nat Immunol*. (2022) 23:1788–98. doi: 10.1038/S41590-022-01328-6

41. Nakaya HI, Wrammert J, Lee EK, Racioppi L, Marie-Kunze S, Haining WN, et al. Systems biology of vaccination for seasonal influenza in humans. *Nat Immunol*. (2011) 12:786–95. doi: 10.1038/ni.2067

42. Querec TD, Akondy RS, Lee EK, Cao W, Nakaya HI, Teuwen D, et al. Systems biology approach predicts immunogenicity of the yellow fever vaccine in humans. *Nat Immunol*. (2009) 10:116–25. doi: 10.1038/ni.1688

43. Rodrigues CMC, Plotkin SA. The influence of interval between doses on response to vaccines. *Vaccine*. (2021) 39:7123–7. doi: 10.1016/j.vaccine.2021.10.050

44. Alonso-Rodríguez N, Vianello E, van Veen S, Jenum S, Tonby K, van Riessen R, et al. Whole blood RNA signatures in tuberculosis patients receiving H56:IC31 vaccine as adjunctive therapy. *Front Immunol*. (2024) 15:1350593. doi: 10.3389/FIMMU.2024.1350593

45. Nemes E, Fiore-Gartland A, Boggiano C, Coccia M, D'Souza P, Gilbert P, et al. The quest for vaccine-induced immune correlates of protection against tuberculosis. *Vaccine Insights*. (2022) 1:165–81. doi: 10.18609/VAC/2022.027

46. Phillips B, Van Rompay KKA, Rodriguez-Nieves J, Lorin C, Koutsoukos M, Tomai M, et al. Adjuvant-dependent enhancement of HIV env-specific antibody responses in infant rhesus macaques. *J Virol*. (2018) 92. doi: 10.1128/JVI.01051-18

47. Coler RN, Duthie MS, Hofmeyer KA, Guderian J, Jayashankar L, Vergara J, et al. From mouse to man: safety, immunogenicity and efficacy of a candidate leishmaniasis vaccine LEISH-F3+GLA-SE. *Clin Transl Immunol*. (2015) 4. doi: 10.1038/cti.2015.6

48. Duthie MS, Frevol A, Day T, Coler RN, Vergara J, Rolf T, et al. A phase 1 antigen dose escalation trial to evaluate safety, tolerability and immunogenicity of the leprosy vaccine candidate LepVax (LEP-F1 + GLA–SE) in healthy adults. *Vaccine*. (2020) 38:1700–7. doi: 10.1016/j.vaccine.2019.12.050

49. Tendler M, Almeida MS, Vilar MM, Pinto PM, Limaverde-Sousa G. Current status of the sm14/GLA-SE schistosomiasis vaccine: overcoming barriers and paradigms towards the first anti-parasitic human(itarian) vaccine. *Trop Med Infect Dis*. (2018) 3. doi: 10.3390/tropicalmed3040121

50. Sirima SB, Richert L, Chêne A, Konate AT, Campion C, Dechavanne S, et al. PRIMVAC vaccine adjuvanted with Alhydrogel or GLA-SE to prevent placental malaria: a first-in-human, randomised, double-blind, placebo-controlled study. *Lancet Infect Dis*. (2020) 20:585–97. doi: 10.1016/S1473-3099(19)30739-X

frontiers | Frontiers in Immunology

TYPE Methods
PUBLISHED 02 October 2024
DOI 10.3389/fimmu.2024.1427526



OPEN ACCESS

EDITED BY
José Roberto Mineo,
Federal University of Uberlandia, Brazil

REVIEWED BY
Sunil Joshi,
University of Miami, United States
Rajko Reljic,
St George's University of London,
United Kingdom

*CORRESPONDENCE
Taru S. Dutt
tarudutt@colostate.edu
Marcela Henao-Tamayo
marcela.henao_tamayo@colostate.edu

RECEIVED 03 May 2024
ACCEPTED 13 September 2024
PUBLISHED 02 October 2024

CITATION
Dutt TS, Spencer JS, Karger BR, Fox A, Obregon-Henao A, Podell BK, Anderson GB and Henao-Tamayo M (2024) ELISA-R: an R-based method for robust ELISA data analysis. *Front. Immunol.* 15:1427526. doi: 10.3389/fimmu.2024.1427526



# ELISA-R: an R-based method for robust ELISA data analysis

Taru S. Dutt[1,2]*, John S. Spencer[1,2], Burton R. Karger[3], Amy Fox[1], Andres Obregon-Henao[1,2], Brendan K. Podell[1,2], G. Brooke Anderson[4] and Marcela Henao-Tamayo[1,2]*

[1]Department of Microbiology, Immunology, and Pathology, Colorado State University, Fort Collins, CO, United States, [2]Mycobacterial Research Laboratories, Colorado State University, Fort Collins, CO, United States, [3]College of Osteopathic Medicine, University of New England, Biddeford, ME, United States, [4]Environmental and Radiological Health Sciences, Colorado State University, Fort Collins, CO, United States

Enzyme-linked immunosorbent assay (ELISA) is a technique to detect the presence of an antigen or antibody in a sample. ELISA is a simple and cost-effective method that has been used for evaluating vaccine efficacy by detecting the presence of antibodies against viral/bacterial antigens and diagnosis of disease stages. Traditional ELISA data analysis utilizes a standard curve of known analyte, and the concentration of the unknown sample is determined by comparing its observed optical density against the standard curve. However, in the case of vaccine research for complicated bacteria such as *Mycobacterium tuberculosis* (Mtb), there is no prior information regarding the antigen against which high-affinity antibodies are generated and therefore plotting a standard curve is not feasible. Consequently, the analysis of ELISA data in this instance is based on a comparison between vaccinated and unvaccinated groups. However, to the best of our knowledge, no robust data analysis method exists for "non-standard curve" ELISA. In this paper, we provide a straightforward R-based ELISA data analysis method with open access that incorporates end-point titer determination and curve-fitting models. Our modified method allows for direct measurement data input from the instrument, cleaning and arranging the dataset in the required format, and preparing the final report with calculations while leaving the raw data file unchanged. As an illustration of our method, we provide an example from our published data in which we successfully used our method to compare anti-Mtb antibodies in vaccinated vs non-vaccinated mice.

KEYWORDS

**ELISA, *Mycobacterium tuberculosis*, *Mycobacterium leprae*, antibodies, data analysis, curve-fitting, endpoint titer**

## 1 Introduction

Enzyme-linked Immunosorbent assay (ELISA) has been widely used over the years as a serodiagnostic tool in infectious diseases, including tuberculosis (TB) and leprosy (1–12). After getting infected with a pathogen, our immune system starts producing antibodies to fight the infection. ELISA has been used to detect the presence of these antibodies for either

diagnostic purposes or for evaluating vaccine efficacy (13). When assessing vaccine efficacy, ELISA can provide us with precise information regarding whether the candidate vaccine is inducing potent antibody responses, the number of antibodies produced in vaccinated and non-vaccinated groups, the specific antigen targeted by the antibodies, and the type of antibody isotype generated. ELISA is a cost-effective and efficient method for the initial evaluation of vaccine effectiveness, particularly in human subjects (14, 15).

TB, caused by *Mycobacterium tuberculosis* (Mtb), continues to be a significant global health challenge. The current vaccine, Bacille Calmette-Guerin (BCG), shows variable efficacy, necessitating better vaccination strategies (16, 17). ELISA is a powerful tool for measuring immune responses, particularly antibodies or cytokines in the blood, which are essential for determining the efficacy of a vaccine or comprehending the various stages of TB (9, 18–20). In our study, we explored how mucosal exposure to non-tuberculous mycobacterium (NTM) affects B cell-mediated immunity and the efficacy of BCG vaccination against pulmonary TB, leveraging ELISA to quantify these immune responses (21). NTMs are mycobacterium that do not cause TB but are ubiquitous in the environment (22–26). Therefore, most populations in the low-middle income countries and even high-income countries are exposed to NTMs almost daily. However, how continuous NTM exposure affect the immune response to Mtb is largely unknown. Previous research has highlighted the potential of NTMs to modulate immune responses to TB due to shared antigens with Mtb and BCG (27–30). Studies using ELISA have shown mixed results: some report that NTM exposure can mask BCG-induced protection, while others suggest enhanced protection. While the role of NTMs in modulating BCG efficacy has been studied, the exact mechanisms, remain unclear. Therefore, there is a need for comprehensive studies. Here we used ELISA to measure the specific antibody responses induced by NTMs against Mtb. In our study, we investigated how mucosal exposure to NTMs affects B cell-mediated immunity and enhances the protective efficacy of BCG vaccination against pulmonary TB. We hypothesized that NTM exposure increases B cell influx and anti-Mtb antibody production in the lungs (due to ~85% genetic similarity between NTM and Mtb), leading to reduced bacterial burden and improved protection, as measured by ELISA. This study developed a mouse model mimicking human BCG vaccination followed by continuous NTM exposure via drinking water. Mice were divided into four groups: BCG only, NTM only, BCG plus low-dose NTM, and BCG plus high-dose NTM. After BCG vaccination and NTM exposure, mice were challenged with Mtb. ELISA was used to quantify anti-Mtb IgG and IgA antibodies in serum and bronchoalveolar lavage fluid (BALF). This data has been employed to develop our ELISA-R method and to quantify the anti-Mtb immune response in mice that were exposed to NTM versus those that were not.

ELISA data analysis is as critical as conducting the assay itself. The correct data analysis ensures the accuracy, reliability, and interpretability of results. In the case of well-characterized viruses or known analytes, data analysis is generally uncomplicated and adheres to the standard curve method (31). In the standard curve method, the known antigen or antibody is plotted against varying concentrations of known antibody/antigen. The concentration of the unknown analyte is subsequently determined by comparing the observed value of the unknown analyte against this standard curve (Figure 1).

On the contrary, vaccine research, particularly that involving complex microorganisms like Mtb having 4000 genes coding for ~4000 proteins, typically entails examining the existence of antibodies directed against unidentified vaccine antigens. Consequently, the generation of a standard curve is not possible due to the lack of information regarding the antigen and antibody type. Antibody quantification is accomplished for this type of ELISA through the utilization of serial dilution of the samples and a non-standard curve method. As a result, the analysis of ELISA data in this instance is based on a comparison between vaccinated and unvaccinated groups. However, to the best of our knowledge, no robust data analysis method exists for "non-standard curve" ELISA.

The three common methods that have been used previously for ELISA data analysis without a standard curve are:

1. Fitting a sigmoid model curve: With this method, the sigmoidal curve is fit for each sample, and then estimated key parameters are compared to the points of maximum growth (PMG) (Figure 2A). When a sample has a higher concentration of protein to be measured, all dilutions of this sample have higher absorbance; the sigmoidal curve shifts towards a more diluted end (32, 33). While this method has high sensitivity and specificity, it requires complex algorithms and computational resources, needs sufficient

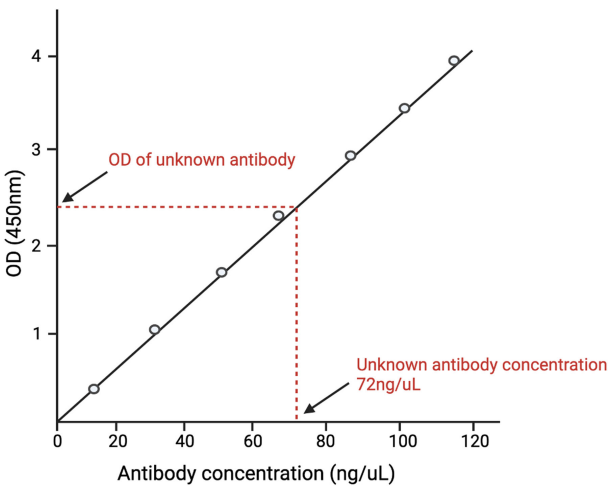


FIGURE 1
A depiction of the standard curve method of analyzing ELISA data. A standard curve is generated by plotting different concentrations of known antigens against the optical density (O.D.) of each concentration. The O.D. of the unknown antigen is then measured. The concentration of the unknown antigen is then determined by matching the O.D. of the unknown antigen with the O.D. of the known antigen and finding its respective concentration.

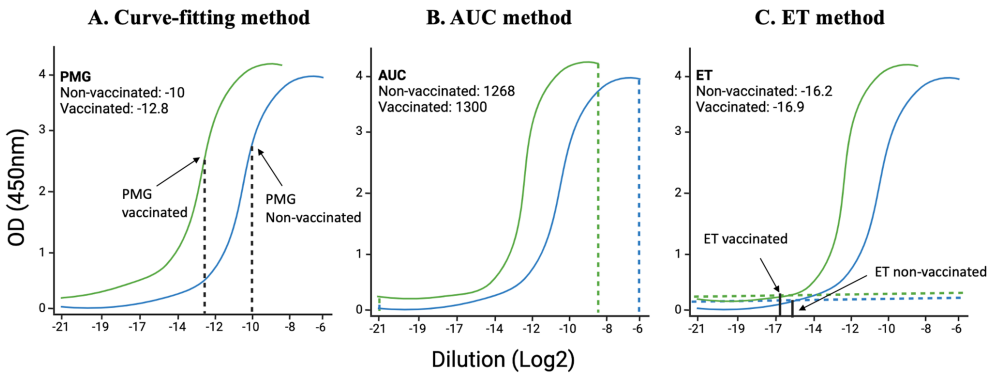


FIGURE 2
Illustration of curve-fitting, an area under the curve (AUC), and endpoint titer (ET) methods: Using data from Dutt et al., 2022, we have analyzed data using already established methods. **(A)** the previous curve-fitting method that calculates the point of maximum growth, **(B)** the AUC method that calculates the total area covered by each sample at different dilutions, and **(C)** the ET method that takes into consideration the least dilution at which the curve starts above the background.

data points for reliable curve fitting and low concentration samples may not yield accurate parameter estimates.

2. Area under the curve (AUC) method: AUC is defined as the definite integral between the two points in a curve (34–36). AUC for ELISA is calculated by estimating the parameters in a curve and then integrating the curve from the lowest concentration to the highest dilution (Figure 2B). AUC method offers the advantage of providing a comprehensive measure of the overall antibody response across all dilutions, making it useful for assessing the total immunogenicity in a sample. Its calculation is relatively simple compared to fitting a sigmoidal curve, involving straightforward integration of the absorbance data, which reduces computational demands. However, the AUC method has significant drawbacks. It cannot determine the endpoint titer, the maximum dilution at which the antibody remains detectable, thereby missing critical quantitative information. Additionally, the accuracy of the AUC is highly dependent on the correct estimation of curve parameters, which can be influenced by noise and variability in the data, potentially leading to less reliable results.
3. Endpoint titer (ET) method: The ET method in ELISA relies on selecting a cutoff absorbance level above the noise background (Figure 2C) (37, 38). The ET method in ELISA is advantageous due to its simplicity and ease of implementation. It quickly identifies the presence of antibodies by determining the highest dilution at which the antibody is still detectable, making it suitable for high-throughput screening. This method does not require complex computational tools or advanced expertise, allowing for rapid and straightforward analysis. However, the ET method produces discrete, less precise data, as dilutions are limited to specific values, potentially overlooking subtle differences in antibody concentrations. Additionally, the method is susceptible to background variability across different samples and wells, which can introduce bias and affect the accuracy of the cutoff determination. The lack of detailed quantitative information about antibody concentrations further limits its utility in comprehensive immunological studies.

Here, we have developed a comprehensive R-based ELISA method (ELISA-R) by integrating the fitting of a sigmoid model with the endpoint titer method to leverage the strengths of both approaches. The sigmoid model fitting provides high sensitivity and specificity by accurately modeling the concentration-absorbance relationship across a range of dilutions, allowing for precise quantification of protein levels. Meanwhile, the endpoint titer method offers simplicity and rapid identification of the highest dilution at which antibodies are still detectable, providing a clear and easily interpretable measure. Our ELISA-R method begins with the direct input of measurement data (O.D. values and sample information) from the instrument, ensuring a seamless transition from raw data to analysis. The data is then cleaned and arranged into the "tidy" format, preparing it for subsequent analysis steps. The sigmoid model fitting is applied to generate a detailed absorbance-concentration curve, extracting key parameters that represent the sample's response. Simultaneously, the endpoint titer is determined by identifying the dilution level where the absorbance exceeds a predefined cutoff, indicating the presence of antibodies.

By combining these two methods, ELISA-R generates a single, specific value for each sample that reflects both the detailed quantitative information from the curve fitting and the practical, easily comparable endpoint titer. This dual approach enhances the robustness and reliability of the analysis, allowing for meaningful comparisons across different samples and groups. Additionally, ELISA-R ensures that the raw data file remains unchanged, preserving data integrity while producing a comprehensive final report with all necessary calculations and visualizations. This integrated method offers an accessible, efficient, and reproducible solution for ELISA data analysis, supporting a wide range of immunological research applications.

# 2 Methods

## 2.1 Data used for ELISA-R data analysis method development

For the ELISA-R development, we used our published data from Cell Reports (21). In this data, ELISA was performed to evaluate the presence of anti-Mtb IgA antibodies in the bronchoalveolar fluid (BALF) and serum of BCG vaccinated and BCG vaccinated-and non-tuberculous mycobacteria (NTM) exposed mice at 120 days post-Mtb infection. A detailed ELISA method has been described in the paper. But briefly, high binding 96-half-well microplates (Corning Life Sciences, cat#3690) were coated with 100 ng of Mtb HN878 lysate (BEI, cat# NR-14824) prepared in PBS and incubated overnight at 4°C. The next day, plates were washed five times with 180 µL of wash buffer (PBS + 0.05% Tween-20), and non-specific interactions were blocked using 180 µL of blocking buffer (PBS + 0.05% Tween-20 + 2% BSA + 2% normal goat serum [Jackson ImmunoResearch Inc., cat#005-000-121 West Grove, PA, USA]). After 2 hours, plates were washed, and different dilutions of serum and BAL prepared in blocking buffer (1:50, 1:100, 1:200, 1:400, 1:800, 1:1600, 1:3200, 1:6400, 1:12800, and 1:25600) were added to the wells and incubated for one hour. Plates were then washed and incubated for 1 hour with horseradish peroxidase (HRP)-conjugated anti-mouse IgA secondary antibodies (Southern Biotech, cat# 1040-05) prepared in the blocking buffer. The colorimetric substrate was developed with the addition of 100 µl of TMB substrate (Thermo Fisher Scientific, Rockford, cat# ENN301), and the reaction was stopped by adding 50 µl of 1 M sulphuric acid. Absorbance was measured at 450 nm using a BioTek Synergy 2 plate reader (BioTek Instruments Inc., Winooski, VT, USA).

## 2.2 Creating a function for curve fitting model

To develop a more robust way of ELISA data analysis, we created a curve-fitting model function using the *nlsLM* function of the *minpack.lm* R package (39). nlsLM function from the minpack.lm package, is a powerful technique for fitting non-linear models to data. This approach is especially advantageous for ELISA data analysis, where the relationship between dilution and absorbance often follows a non-linear pattern. The nlsLM function in R is used for non-linear least squares fitting, a process that minimizes the sum of the squares of the residuals (the differences between observed and predicted values). This function is an enhancement of the traditional Levenberg-Marquardt algorithm, designed for more robust performance, particularly with complex, non-linear data (27). In the early 1960s, the Levenberg-Marquardt algorithm was developed to solve nonlinear least squares problems. Least squares problems arise in the context of fitting a parameterized mathematical model to a set of data points by minimizing an objective expressed as the sum of the squares of the errors between the model function and a set of data points. By minimizing the sum of squared residuals, non-linear models fitted using nlsLM will provide a better fit to the data, leading to more accurate predictions and inferences.

Hence, we used the following equation for curve fitting sigmoid model:

$$f(x) = (a - d)/(1 + (\log\_dilution/c)\ b)) + d \quad (1)$$

Where,

a = maximum absorbance;

d = minimum absorbance;

c = point of maximum growth; and

b = slope at c.

This method takes into account the minimum and maximum absorbance values, the point of maximum growth, and the slope of the curve. This comprehensive approach ensures that all critical aspects of the data are considered.

## 2.3 Applying the values obtained from the curve-fitting model function as an input for the endpoint titer function

The traditional ET method, despite its widespread use in vaccinology for measuring antibody levels, has notable limitations that restrict its comprehensiveness. The method's reliance on twofold serial dilutions, while generally adequate for distinguishing markedly different responses, may lack sensitivity in detecting subtle yet significant variations in antibody levels. Furthermore, the reproducibility and standardization of ET can be problematic due to variability in protocols and interpretation across different laboratories. Therefore, we created the function for endpoint titer (ET) evaluation. Our ET function is not based on the traditional minimum background for each sample but rather takes into account the minimum and maximum absorbance of each sample, the shape of the curve, and the slope of the curve. The input values for these parameters are taken from the output of the curve-fitting model.

$$ET = c * (((a - d)/(0.2 - d)) - 1)^{(1/b)} \quad (2)$$

Traditional endpoint titer calculations often rely on a fixed threshold, which may not be optimal for all samples. By using the fitted parameters from the curve, this method provides a more accurate and sample-specific endpoint titer.

## 2.4 Statistical analysis

Statistical significance between the two groups was determined using unpaired t-tests ($p < 0.05$) using the *ggpubr* package. If there are more than two groups, then Analysis of Variance (ANOVA) was applied. All codes have been generated and plotted using R (Version 4.1).

# 3 Results

## 3.1 Create the curve-fitting model using the NTM dataset

Using the NTM datasets, we first applied the approach of fitting a sigmoid model to each mouse in the Saline, BCG, NTM, and BCG +NTM groups. For this, we read the data obtained from Dutt et al., 2022 (21) (also provided in Supplementary Table 1) in R and reformatted the data to follow the principles of tidy data (40). We converted the dilutions to log base 2 to simplify the values and converted the data to a dataframe. We then applied the curve fitting model equation to each mouse in the group and evaluated the values for maximum absorbance, the slope at c, the point of maximum growth, and minimum absorbance (the values of the coefficients a, b, c, and d, respectively, in Equation 1. This function then results in a sigmoid curve of absorbance versus dilution (log2) for each mouse (Figure 3) and the values for a, b, c, and d for each mouse (Supplementary Table 1). We will then use the values of a, b, c, and d as input for the endpoint titer function.

## 3.2 Applying the curve-fitting model values to the endpoint titer function

Traditionally, ET has been calculated using $O.D._{50,}$ which is the reciprocal of the highest sample dilution that gives a reading at O.D. of 50% of that sample. However, it does not take into account the minimum and maximum absorbance of each sample, the shape of the curve, and the slope of the curve. In our method, we are taking these important factors into account by combining the curve-fitting model with the ET function. We applied the values of a, b, c, and d to the above-mentioned ET equation and obtained the ET value of each mouse (Supplementary Table 2). We employed both the traditional Endpoint Titration (ET) method and the advanced ELISA-R method to analyze our data, as shown in Figures 4A, B, respectively. The comparison reveals significant differences between these two approaches. Using the traditional ET method, the endpoint titer values, analyzed with $O.D._{50}$, ranged from 0 to 1200 dilutions. These values failed to accurately represent antibody strength and titer. Conversely, the ELISA-R method demonstrated superior performance by pinpointing the highest

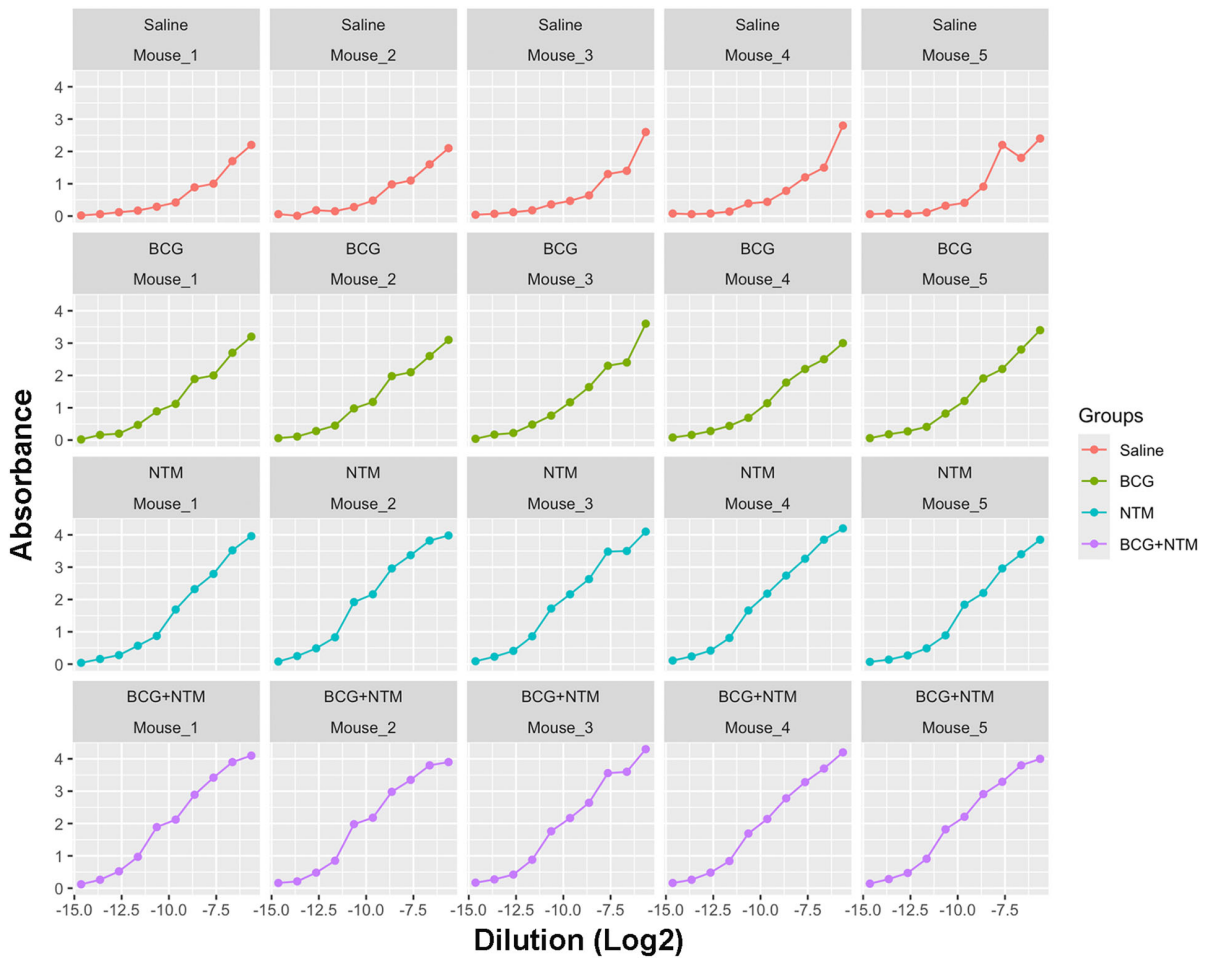


FIGURE 3
Curves generated for each mouse using a modified curve fitting model. After applying the curve-fitting model to our Dutt et al., 2022 dataset, our model generated the curves against dilution versus absorbance for each mouse. These curves then allow our modified curve fitting model to identify the average maximum absorbance, minimum absorbance, background, and slope of the curve based on each sample to enter into our method.

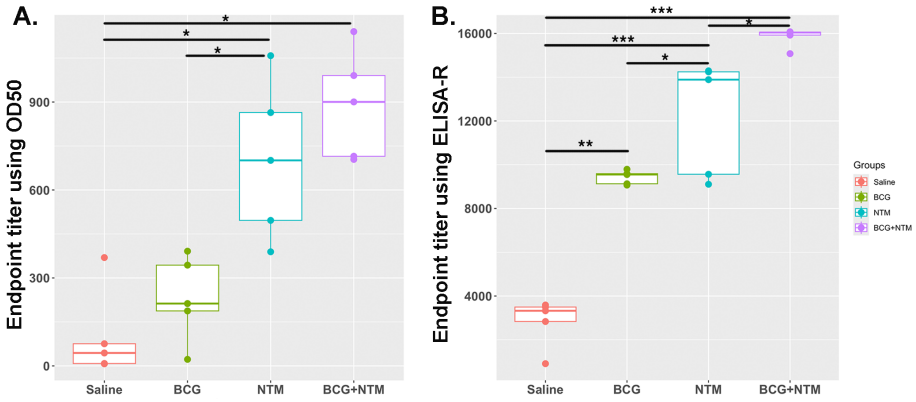


FIGURE 4
Comparative analysis of ELISA data analysis using traditional endpoint titer using $O.D._{50}$ vs. endpoint titer calculated using ELISA-R. **(A)** Analysis of BCG-NTM mouse study ELISA data using traditional endpoint titer method that used $O.D._{50}$ as a cut-off point. Data is plotted as the dilution of a sample that produces an O.D. value equal to 50% of the maximum O.D. observed for that sample. **(B)** Plot for Endpoint titer calculation using ELISA-R. In these graphs, the endpoint titer of IgA antibodies in the BALF of each mouse in the Saline, BCG, NTM, and BCG-NTM groups was compared with each other. We found that the BALF of BCG-NTM mice has a higher titer of IgA antibodies than the BALF of mice in Saline, BCG, or NTM groups. Statistical significance was calculated using ANOVA. *p<0.05, **p<0.005, ***p<0.0005.

dilution at which the antibody effectively binds to the antigen. Furthermore, the ELISA-R method significantly reduced sample variability, providing more consistent and reliable results. This highlights ELISA-R's ability to deliver precise and meaningful insights into antibody-antigen interactions, making it a more robust and dependable choice for ELISA data analysis.

## 3.3 Testing ELISA-R with clinical human serum samples

We developed ELISA-R using a dataset from a mouse model that is in a highly controlled environment with fewer variables. However, it is crucial to evaluate our method to other datasets, especially from human settings. Therefore, we have used the ELISA raw dataset with serial two-fold titration of the human serum from 1:100 to 1:102,400 with three antigens of *Mycobacterium leprae* (rAg85B, PGL-I, and LAM). There are 50 lepromatous patient sera, which are further divided into borderline lepromatous (BL, n = 13) or polar lepromatous (LL, n = 37), and 20 tuberculoid sera that are also divided into polar tuberculoid (TT, n = 10) and borderline tuberculoid (BT, n = 10). The information about these leprosy patient serum samples was previously published (41). The O.D. values for each dilution are plotted to go across each serum sample [Supplementary Tables 3 (rAg85B), 4 (PGL-I), and 5 (LAM)]. We applied our ELISA-R method for the analysis of this dataset by taking into consideration each patient. We first read the data stored in Excel format in R, subtracted the baseline values of the patients from the respective wells, and arranged the data in a tidy format. We then applied ELISA-R to the data for antibodies against all three antigens, namely, rAg85B, PGL-I, and LAM. In addition, we applied the traditional ET method using $O.D._{50}$ values to compare the difference between these two methods in human samples (with more variability). We found that anti-Ag85B, PGL-I, and LAM antibodies are highest in LL patients, followed by BL, BT, and TT, which were consistent with Spencer et al.'s published findings (Figure 5). In our analysis of human samples as well, the ELISA-R method consistently outperformed the traditional ET method, delivering cleaner, more accurate data with significantly reduced variability. This demonstrates ELISA-R's superior reliability and precision in detecting and quantifying our target analytes.

# 4 Discussion

Quantifying and assessing the presence of antibodies directed against the bacterial or viral antigens that the vaccine targets is an essential element of vaccine research (42–44). However, quantifying antibodies and comparing them among different populations and vaccination groups can be challenging and time-consuming. Different methods are available to quantify antibodies and compare them among samples. However, all these methods have certain flaws that can misinterpret the data; for example, when we directly plot graphs based on optical density (O.D.), then we are not taking into consideration the baseline differences of each sample, the shape of the curve of the sample, and all the dilutions into consideration. Similarly, in the AUC method, there is a possibility that two or three samples can have similar AUC values. However, the antibody titers can be different. Therefore, the analysis of ELISA data should be more focused and consider all the crucial parameters into account, such as the background signal of each sample, O.D. values of samples at each dilution, and the slope of the sample curve.

Here, we have created ELISA-R, a robust R programming-based method for the analysis of ELISA data that takes into consideration all the above-mentioned challenges of ELISA data analysis. ELISA-R utilizes an advanced non-linear least squares curve-fitting model, enhanced with the Levenberg-Marquardt modification, to precisely identify critical parameters such as minimum and maximum absorption, background, and slope for each sample. These parameters are then used to compute accurate endpoint titer

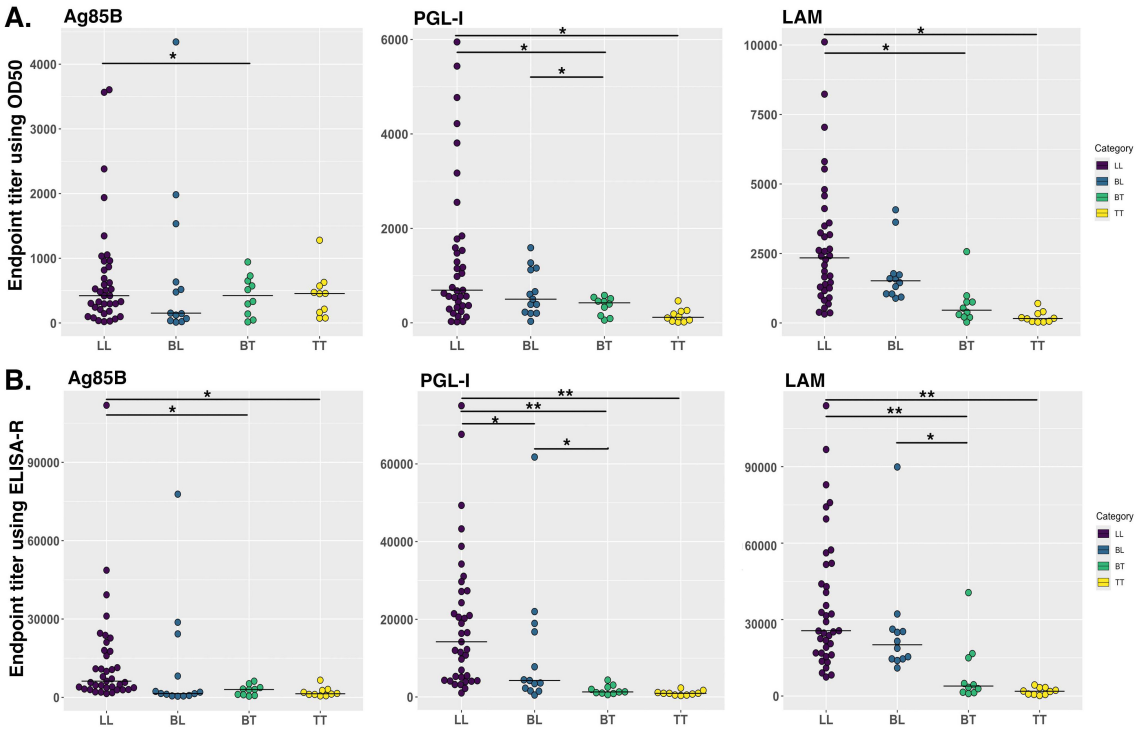


FIGURE 5
Comparison of human antibodies against *Mycobacterium leprae* antigens in different stages of leprosy patient cohorts. IgG antibodies against Ag85B and LAM and IgM antibodies against PGL-I were evaluated using indirect ELISA by Spencer et al. (41). We re-analyzed this data by using our ELISA-R for anti-Ag85B IgG, anti-PGL-I IgM and anti-LAM IgG in LL, BL, BT and TT patients. **(A)** Data was analyzed using the traditional ET method. **(B)** Data analyzed using ELISA-R. LL, polar lepromatous; BL, borderline lepromatous; BT, borderline tuberculoid; and TT, polar tuberculoid. Statistical significance has been calculated using ANOVA. *p<0.05, **p<0.005.

values, ensuring robust and reliable analysis. What sets ELISA-R apart is its exceptional time efficiency. ELISA-R seamlessly imports data directly from Excel, subtracts the blank of each sample, processes the data, and generates comprehensive graphs in under 15 minutes. This rapid processing time significantly enhances productivity, allowing researchers to focus on interpreting results rather than managing data. ELISA-R is designed with user-friendliness in mind, making it accessible to non-R programmers. We are also currently developing a graphical user interface to further simplify its use, ensuring that even those with minimal programming experience can easily navigate the software. Unlike traditional methods that consider only one or two parameters, ELISA-R takes into account five crucial parameters for each sample, resulting in a more robust and comprehensive analysis. Additionally, ELISA-R is free and open-source, making it an invaluable tool for researchers worldwide.

We developed ELISA-R using our published well-optimized ELISA data, as this data has been acquired using inbred mouse strain and, therefore, has less variability. Nonetheless, we have also applied our ELISA-R method to complicated datasets with larger variability, such as human patient data derived from different clinical forms of leprosy (Figure 5). ELISA-R worked successfully for both datasets and provided the same trend as we were getting by analyzing data manually (as confirmed by Dr. John Spencer, who analyzed the results manually). However, ELISA-R took significantly less time than the manual analysis. In addition, the results provided by our method are more robust as it takes different variables into account. All in all, ELISA-R is a robust and faster method of analyzing ELISA data, which is not limited to ELISA data alone but may be widely utilized for assays that involve optical density, dilutions, and curves, such as cytokine data.

## 4.1 Limitation of the ELISA-R

One significant challenge in ELISA data analysis is the potential for batch effects, which occur when assays for different groups of samples are conducted on different days, leading to variations in results due to technical inconsistencies rather than true biological differences. Factors such as changes in plate reader settings, the use of different plates, and other technical variations can introduce batch effects, complicating the analysis and interpretation of ELISA data. Currently, ELISA-R does not include methods to correct for batch effects and normalize the data, a limitation that impacts the accuracy and reliability of our analyses. To address this, we propose incorporating robust statistical methods for batch effect correction and data normalization in future versions of ELISA-R. One approach is to use mixed-effects models to account for both fixed effects (such as biological conditions) and random effects (such as batch variations), partitioning the variability attributable to batch

differences and isolating the true biological signal. Another method is the empirical Bayes approach, such as the ComBat algorithm, which adjusts for batch effects by modeling batch-specific parameters and harmonizing the data across batches. Additionally, normalization techniques like quantile normalization can be used to make the distribution of absorbance values consistent across different batches, reducing the impact of batch-specific variations. By integrating these methods into ELISA-R, we aim to enhance its utility, making it a more powerful tool for ELISA data analysis, and ensuring that the results reflect true biological differences rather than technical artifacts. This will contribute to the reproducibility and reliability of ELISA experiments, leading to more accurate scientific discoveries.

### 4.2 Future prospective

We are currently developing a graphical user interface (GUI) for the ELISA-R method, utilizing the Shiny package in R. Our goal is to empower every researcher to analyze their ELISA data with greater accuracy and speed, all without the need for programming expertise. This user-friendly tool will make advanced ELISA data analysis accessible to all.

## Data availability statement

The original contributions presented in the study are included in the article/Supplementary Material. Further inquiries can be directed to the corresponding authors.

## Ethics statement

The studies involving humans were approved by Institutional Review Board CSU. The studies were conducted in accordance with the local legislation and institutional requirements. The participants provided their written informed consent to participate in this study. The animal study was approved by Institutional Animal Care and Use Committee (IACUC). The study was conducted in accordance with the local legislation and institutional requirements.

## Author contributions

TSD: Conceptualization, Data curation, Formal analysis, Investigation, Methodology, Software, Validation, Visualization, Writing – original draft, Writing – review & editing. JSS: Data curation, Formal analysis, Investigation, Validation, Writing – review & editing. BKP: Data curation, Investigation, Writing – review & editing. AF: Data curation, Investigation, Writing – review & editing. AO-H: Data curation, Investigation, Methodology, Writing – review & editing. BKP: Funding acquisition, Writing – review & editing. GBA: Conceptualization, Formal analysis, Methodology, Software, Supervision, Validation, Visualization, Writing – review & editing. MH-T: Conceptualization, Funding acquisition, Investigation, Methodology, Resources, Supervision, Validation, Visualization, Writing – review & editing.

## Funding

The author(s) declare financial support was received for the research, authorship, and/or publication of this article. This research was supported by NIH grants R01AI127475 and R21AI121099 (NIH-NIAID) to MH-T. In addition, this project has been funded in whole or in part with Federal funds from the NIH-NIAID under Contract No. 75N93021C00029 to BP and MH-T.

## Acknowledgments

The authors would like to acknowledge Colorado State University's (CSU) Lab Animal Resources staff for taking great care of animals. In addition, TD would like to thank Dr. Michael Lyons, an associate professor at CSU, for the scientific conversations and constructive input that improved this work.

## Conflict of interest

The authors declare that the research was conducted in the absence of any commercial or financial relationships that could be construed as a potential conflict of interest.

## Publisher's note



## Supplementary material

The Supplementary Material for this article can be found online at: https://www.frontiersin.org/articles/10.3389/fimmu.2024.1427526/full#supplementary-material

# References


1. Ragan IK, Hartson LM, Dutt TS, Obregon-Henao A, Maison RM, Gordy P, et al. A whole virion vaccine for COVID-19 produced via a novel inactivation method and preliminary demonstration of efficacy in an animal challenge model. *Vaccines*. (2021) 9:340. doi: 10.3390/vaccines9040340

2. Kuno G, Gómez I, Gubler DJ. An ELISA procedure for the diagnosis of dengue infections. *J Virol Methods*. (1991) 33:101–13. doi: 10.1016/0166-0934(91)90011-N

3. *Diagnosis of tuberculosis in an Indian population by an indirect ELISA protocol based on detection of Antigen 85 complex: a prospective cohort study | BMC Infectious Diseases | Full Text* (Accessed May 2, 2024).

4. Yoshihara N. ELISA for diagnosis of infections by viruses. *Nihon Rinsho Jpn J Clin Med*. (1995) 53:2277–82.

5. Ksiazek TG, West CP, Rollin PE, Jahrling PB, Peters CJ. ELISA for the detection of antibodies to ebola viruses. *J Infect Dis*. (1999) 179:S192–8. doi: 10.1086/514313

6. Longoni SS, Beltrame A, Prato M, Spencer JS, Bergamaschi N, Clapasson A, et al. ELISA test based on the phenolic glycolipid-I (PGL-I) of mycobacterium leprae: A reality of a laboratory from a non-endemic country. *Pathog Basel Switz*. (2022) 11:894. doi: 10.3390/pathogens11080894

7. Wernike K, Aebischer A, Michelitsch A, Hoffmann D, Freuling C, Balkema-Buschmann A, et al. Multi-species ELISA for the detection of antibodies against SARS-CoV-2 in animals. *Transbound Emerg Dis*. (2021) 68:1779–85. doi: 10.1111/tbed.13926

8. Hasan R, Dockrell HM, Chiang T, Hussain R. Quantitative antibody ELISA for leprosy. *Int J Lepr Mycobact Dis Off Organ Int Lepr Assoc*. (1989) 57:766–76.

9. Banerjee S, Gupta S, Shende N, Kumar S, Harinath BC. Serodiagnosis of tuberculosis using two ELISA systems. *Indian J Clin Biochem*. (2003) 18:48–53. doi: 10.1007/BF02867367

10. Wright PF, Nilsson E, Van Rooij EM, Lelenta M, Jeggo MH. Standardisation and validation of enzyme-linked immunosorbent assay techniques for the detection of antibody in infectious disease diagnosis. *Rev Sci Tech Int Off Epizoot*. (1993) 12:435–50. doi: 10.20506/rst.12.2.691

11. Melkie ST, Arias L, Farroni C, Jankovic Makek M, Goletti D, Vilaplana C. The role of antibodies in tuberculosis diagnosis, prophylaxis and therapy: a review from the ESGMYC study group. *Eur Respir Rev*. (2022) 31:210218. doi: 10.1183/16000617.0218-2021

12. Frade MAC, de Paula NA, Gomes CM, Vernal S, Filho FB, Lugão HB, et al. Unexpectedly high leprosy seroprevalence detected using a random surveillance strategy in midwestern Brazil: A comparison of ELISA and a rapid diagnostic test. *PloS Negl Trop Dis*. (2017) 11:e0005375. doi: 10.1371/journal.pntd.0005375

13. Prevention I of M (US) B on HP and D. Immune response to vaccine antigens, in: *Vaccine safety forum: summaries of two workshops* (1997). US: National Academies Press. Available online at: https://www.ncbi.nlm.nih.gov/books/NBK233000/ (Accessed May 2, 2024).

14. Sadarangani M, Marchant A, Kollmann TR. Immunological mechanisms of vaccine-induced protection against COVID-19 in humans. *Nat Rev Immunol*. (2021) 21:475–84. doi: 10.1038/s41577-021-00578-z

15. Wen G-P, He L, Tang Z-M, Wang S-L, Zhang X, Chen Y-Z, et al. Quantitative evaluation of protective antibody response induced by hepatitis E vaccine in humans. *Nat Commun*. (2020) 11:3971. doi: 10.1038/s41467-020-17737-w

16. Andersen P, Doherty TM. The success and failure of BCG — implications for a novel tuberculosis vaccine. *Nat Rev Microbiol*. (2005) 3:656–62. doi: 10.1038/nrmicro1211

17. Dockrell HM, Smith SG. What have we learnt about BCG vaccination in the last 20 Years? *Front Immunol*. (2017) 8:1134. doi: 10.3389/fimmu.2017.01134

18. Kozakiewicz L, Phuah J, Flynn J, Chan J. The role of B cells and humoral immunity in Mycobacterium tuberculosis infection. *Adv Exp Med Biol*. (2013) 783:225–50. doi: 10.1007/978-1-4614-6111-1_12

19. Glatman-Freedman A. The role of antibody-mediated immunity in defense against Mycobacterium tuberculosis: advances toward a novel vaccine strategy. *Tuberc Edinb Scotl*. (2006) 86:191–7. doi: 10.1016/j.tube.2006.01.008

20. Abebe F, Bjune G. The protective role of antibody responses during Mycobacterium tuberculosis infection. *Clin Exp Immunol*. (2009) 157:235–43. doi: 10.1111/j.1365-2249.2009.03967.x

21. Dutt TS, Karger BR, Fox A, Youssef N, Dadhwal R, Ali MZ, et al. Mucosal exposure to non-tuberculous mycobacteria elicits B cell-mediated immunity against pulmonary tuberculosis. *Cell Rep*. (2022) 41:111783. doi: 10.1016/j.celrep.2022.111783

22. Hoefsloot W, van Ingen J, Andrejak C, Angeby K, Bauriaud R, Bemer P, et al. The geographic diversity of nontuberculous mycobacteria isolated from pulmonary samples: an NTM-NET collaborative study. *Eur Respir J*. (2013) 42:1604–13. doi: 10.1183/09031936.00149212

23. Hilborn ED, Covert TC, Yakrus MA, Harris SI, Donnelly SF, Rice EW, et al. Persistence of nontuberculous mycobacteria in a drinking water system after addition of filtration treatment. *Appl Environ Microbiol*. (2006) 72(9):5864–9. doi: 10.1128/AEM.00759-06

24. Black GF, Dockrell HM, Crampin AC, Floyd S, Weir RE, Bliss L, et al. Patterns and implications of naturally acquired immune responses to environmental and tuberculous mycobacterial antigens in northern Malawi. *J Infect Dis*. (2001) 184:322–9. doi: 10.1086/322042

25. Covert TC, Rodgers MR, Reyes AL, Stelma GN. Occurrence of nontuberculous mycobacteria in environmental samples. *Appl Environ Microbiol*. (1999) 65:2492–6. doi: 10.1128/AEM.65.6.2492-2496.1999

26. Zulu M, Monde N, Nkhoma P, Malama S, Munyeme M. Nontuberculous mycobacteria in humans, animals, and water in Zambia: A systematic review. *Front Trop Dis*. (2021) 2:679501. doi: 10.3389/fitd.2021.679501

27. Verma D, Chan ED, Ordway DJ. Non-tuberculous mycobacteria interference with BCG-current controversies and future directions. *Vaccines*. (2020) 8:688. doi: 10.3390/vaccines8040688

28. Poyntz HC, Stylianou E, Griffiths KL, Marsay L, Checkley AM, McShane H. Non-tuberculous mycobacteria have diverse effects on BCG efficacy against Mycobacterium tuberculosis. *Tuberc Edinb Scotl*. (2014) 94:226–37. doi: 10.1016/j.tube.2013.12.006

29. Abate G, Hamzabegovic F, Eickhoff CS, Hoft DF. BCG Vaccination Induces M. avium and M. abscessus Cross-Protective Immunity. *Front Immunol*. (2019) 10:234. doi: 10.3389/fimmu.2019.00234

30. Zimmermann P, Finn A, Curtis N. Does BCG vaccination protect against nontuberculous mycobacterial infection? A systematic review and meta-analysis. *J Infect Dis*. (2018) 218:679–87. doi: 10.1093/infdis/jiy207

31. Nummer SA, Weeden AJ, Shaw C, Snyder BK, Bridgeman TB, Qian SS. Updating the ELISA standard curve fitting process to reduce uncertainty in estimated microcystin concentrations. *MethodsX*. (2018) 5:304–11. doi: 10.1016/j.mex.2018.03.011

32. Findlay JWA, Dillard RF. Appropriate calibration curve fitting in ligand binding assays. *AAPS J*. (2007) 9:E260–267. doi: 10.1208/aapsj0902029

33. Dunn J, Wild D. Chapter 3.6 - Calibration Curve Fitting. In: Wild D, editor. *The Immunoassay Handbook, 4th ed.* Elsevier, Oxford (2013). p. 323–36. doi: 10.1016/B978-0-08-097037-0.00022-1

34. Fernandez Z, de Arruda Rodrigues R, Torres JM, Marcon GEB, de Castro Ferreira E, de Souza VF, et al. Development and validity assessment of ELISA test with recombinant chimeric protein of SARS-CoV-2. *J Immunol Methods*. (2023) 519:113489. doi: 10.1016/j.jim.2023.113489

35. Wouters E, Verbrugghe C, Devloo R, Debruyne I, De Clippel D, Van Heddegem L, et al. A novel competition ELISA for the rapid quantification of SARS-CoV-2 neutralizing antibodies in convalescent plasma. *Transfusion (Paris)*. (2021) 61:2981–90. doi: 10.1111/trf.16652

36. Bliss CM, Parsons AJ, Nachbagauer R, Hamilton JR, Cappuccini F, Ulaszewska M, et al. Targeting antigen to the surface of EVs improves the *in vivo* immunogenicity of human and non-human adenoviral vaccines in mice. *Mol Ther Methods Clin Dev*. (2020) 16:108–25. doi: 10.1016/j.omtm.2019.12.003

37. Frey A, Di Canzio J, Zurakowski D. A statistically defined endpoint titer determination method for immunoassays. *J Immunol Methods*. (1998) 221:35–41. doi: 10.1016/s0022-1759(98)00170-7

38. Stowe RP, Ruiz RJ, Fagundes CP, Stowe RH, Chen M, Glaser R. An ELISA method to compute endpoint titers to epstein-barr virus and cytomegalovirus: application to population-based studies. *J Immunol Methods*. (2014) 408:64–9. doi: 10.1016/j.jim.2014.05.006

39. Elzhov TV, Mullen KM, Spiess A-N, Bolker B. minpack.lm: R interface to the levenberg-marquardt nonlinear least-squares algorithm found in MINPACK, plus support for bounds (2023). Available online at: https://cran.r-project.org/web/packages/minpack.lm/index.html (Accessed May 2, 2024).

40. Wickham H. Tidy data. *J Stat Softw*. (2014) 59:1–23. doi: 10.18637/jss.v059.i10

41. Spencer JS, Kim HJ, Wheat WH, Chatterjee D, Balagon MV, Cellona RV, et al. Analysis of antibody responses to Mycobacterium leprae phenolic glycolipid I, lipoarabinomannan, and recombinant proteins to define disease subtype-specific antigenic profiles in leprosy. *Clin Vaccine Immunol CVI*. (2011) 18:260–7. doi: 10.1128/CVI.00472-10

42. Bates TA, McBride SK, Leier HC, Guzman G, Lyski ZL, Schoen D, et al. Vaccination before or after SARS-CoV-2 infection leads to robust humoral response and antibodies that effectively neutralize variants. *Sci Immunol*. (2022) 7:eabn8014. doi: 10.1126/sciimmunol.abn8014

43. Pollard AJ, Bijker EM. A guide to vaccinology: from basic principles to new developments. *Nat Rev Immunol*. (2021) 21(2):83–100. doi: 10.1038/s41577-020-00479-7

44. Mascola JR, Montefiori DC. The role of antibodies in HIV vaccines. *Annu Rev Immunol*. (2010) 28:413–44. doi: 10.1146/annurev-immunol-030409-101256

frontiers | Frontiers in Immunology

TYPE Opinion
PUBLISHED 08 October 2024
DOI 10.3389/fimmu.2024.1429250



OPEN ACCESS

EDITED BY
Igor Kramnik,
Boston University, United States

REVIEWED BY
Giovanni Delogu,
Catholic University of the Sacred Heart, Italy

*CORRESPONDENCE
Que Dang
que.dang@nih.gov

†These authors share first authorship

RECEIVED 07 May 2024
ACCEPTED 26 August 2024
PUBLISHED 08 October 2024

CITATION
Dang Q, Eichelberg K, Vázquez-Maldonado N, Boggiano C, Leitner WW, Ramachandra L, Deckhut-Augustine A and Read SW (2024) Immune mechanisms of protection against *Mycobacterium tuberculosis*-centers. *Front. Immunol.* 15:1429250. doi: 10.3389/fimmu.2024.1429250



# Immune mechanisms of protection against *Mycobacterium tuberculosis*-centers

Que Dang[1*†], Katrin Eichelberg[2†], Nancy Vázquez-Maldonado[3†], César Boggiano[1], Wolfgang W. Leitner[3], Lakshmi Ramachandra[2], Alison Deckhut-Augustine[3] and Sarah W. Read[1]

[1]Division of AIDS, National Institute of Allergy and Infectious Diseases, National Institutes of Health, Rockville, MD, United States, [2]Division of Microbiology and Infectious Diseases, National Institute of Allergy and Infectious Diseases, National Institutes of Health, Rockville, MD, United States, [3]Division of Allergy, Immunology, and Transplantation, National Institute of Allergy and Infectious Diseases, National Institutes of Health, Rockville, MD, United States

KEYWORDS

***Mycobacterium tuberculosis*, TB vaccine, IMPAc-TB, TB immune responses, mechanisms of protection**

Tuberculosis (TB), caused by *Mycobacterium tuberculosis* (*Mtb*), is one of the world's leading infectious disease killers and is second only to COVID-19 deaths. TB has been found to be present in all countries and age groups. Although TB is a preventable and curable disease, an estimated 10.6 million people in 2022 developed TB worldwide. This included 5.8 million men, 3.5 million women, and 1.3 million children. Of these individuals, 1.3 million people died, including 167,000 people with HIV (1). Notably, TB is the leading cause of death among people living with HIV.

As one of the world's largest funders of biomedical research on TB, the National Institute of Allergy and Infectious Diseases (NIAID) at the National Institutes of Health (NIH) has prioritized investing in TB to save lives. Specifically, NIAID supports and conducts basic, translational, and clinical research to better understand TB and expedite the development of innovative new tools and strategies to improve diagnosis, prevention, and treatment of TB.

In 2016, NIAID convened a workshop on "The Impact of *Mtb* Immune Evasion on Protective Immunity: Implications for TB Vaccine Design". This workshop brought together global experts with the goal of defining immune mechanisms that could be targeted through novel research approaches and to inform vaccine design and immune therapeutic interventions for the prevention of TB. The meeting identified scientific gaps and influenced the initiative that led to the establishment of the Immune Mechanisms of Protection Against *Mycobacterium tuberculosis* Centers (IMPAc-TB) program (2). The

overarching goal of the IMPAc-TB program is to understand the nature, location, and timing of immune responses required to prevent initial *Mtb* infection and to develop a comprehensive understanding of the immune responses required to prevent progression along the continuum of TB disease. Other goals of the IMPAc-TB program include understanding the effects of co-infections such as HIV on immune responses to *Mtb* infection or TB vaccination and improving the value of animal models in predicting TB vaccine efficacy in humans. These goals align with those of the NIAID Strategic Plan for Tuberculosis Research.

To accomplish these objectives, three contracts were awarded to multi-disciplinary research teams: HI-IMPAc-TB: Principal Investigators: Sarah Fortune, M.D. (Harvard); Henry Boom, M.D. (Case Western Reserve University); and JoAnne Flynn, Ph.D. (University of Pittsburgh); Phoenix: Principal investigator: Rhea Coler, Ph.D. (Seattle Children's Research Institute); and Cascade: Principal investigator: Kevin Urdahl, M.D., Ph.D. (Seattle Children's Research Institute) (3). The goals of the three centers can be viewed at IMPAc-TB.

Figure 1 briefly illustrates the unique aspects of each IMPAc-TB center.

Although all three centers are pursuing distinct goals and addressing different research questions, collectively they conduct analyses on tissue-specific and systemic immune responses in small animals, nonhuman primates (NHPs), and humans to identify and to characterize the immunological space associated with protection and susceptibility to *Mtb*. Interestingly, the different approaches used by the centers lead to the identification of converging themes that may play a role in protection and/or susceptibility.

Other select highlights and contributions by the centers are as follows:

- Development of the first clinical trial employing a controlled human infection model to test the efficacy of a TB vaccine candidate. Participants will be challenged with aerosolized Bacille Calmette-Guerin (BCG). This clinical trial is expected to start at the end of 2024.
- Cross-species comparison to define immune mechanisms for the prevention of infection or disease using mice, including Collaborative Cross mice, guinea pigs, NHPs, and humans.
- Ultra-low dose challenge model in small animals and in NHPs.
- Back-translation, refinement, and validation of preclinical models with human data to improve their predictive value.
- Validation of newly developed guinea pig-specific immunological reagents to be offered to the field.
- Development of novel analytical frameworks for the integration of complex and multi-modal profiling data sets that will advance the identification of correlates of protection across species.

The subsequent articles in this issue of *Frontiers* exemplify additional work by the three centers.

The IMPAc-TB program is one of NIAID's largest investments in TB vaccine research. Additionally, NIAID supports other TB vaccine-related programs such as Innovation for TB Vaccine Discovery (ITVD) and Advancing Vaccine Adjuvant Research for TB (AVAR-T). The 2024 NIAID Strategic Plan for Tuberculosis

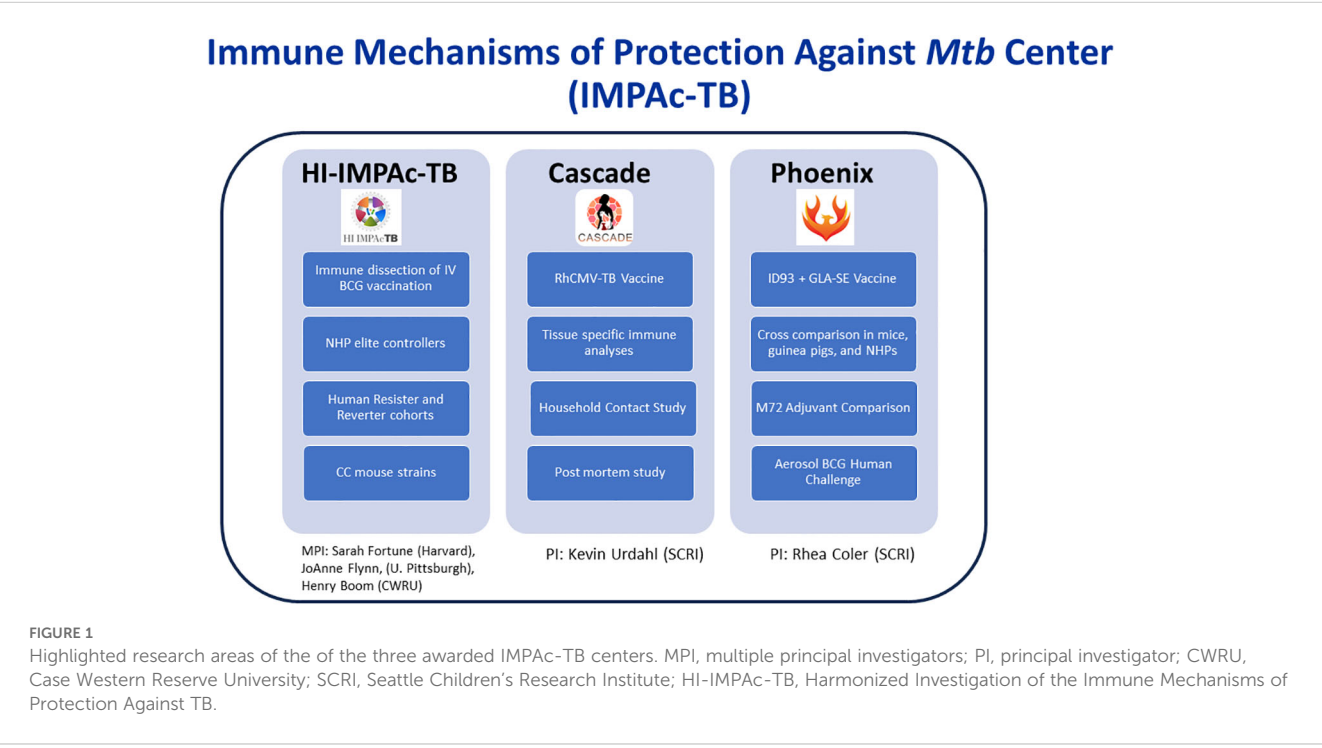


FIGURE 1
Highlighted research areas of the of the three awarded IMPAc-TB centers. MPI, multiple principal investigators; PI, principal investigator; CWRU, Case Western Reserve University; SCRI, Seattle Children's Research Institute; HI-IMPAc-TB, Harmonized Investigation of the Immune Mechanisms of Protection Against TB.

Research Update reaffirms the commitment of NIAID to accelerate basic and preclinical, translational, and clinical research and to expedite the development of innovative tools and new strategies to end the TB pandemic.

We hope you enjoy reading the articles in this special issue!

## Author contributions

QD: Project administration, Writing – original draft, Writing – review & editing, Conceptualization, Funding acquisition. KE: Conceptualization, Funding acquisition, Project administration, Writing – original draft, Writing – review & editing. NV-M: Conceptualization, Funding acquisition, Project administration, Writing – original draft, Writing – review & editing. CB: Funding acquisition, Supervision, Writing – original draft, Writing – review & editing. WL: Funding acquisition, Supervision, Writing – original draft, Writing – review & editing. LR: Funding acquisition, Supervision, Writing – original draft, Writing – review & editing. AD-A: Funding acquisition, Supervision, Writing – original draft, Writing – review & editing. SR: Funding acquisition, Supervision, Writing – original draft, Writing – review & editing.

## Funding

The author(s) declare that no financial support was received for the research, authorship, and/or publication of this article.

## Conflict of interest

The authors declare that the research was conducted in the absence of any commercial or financial relationships that could be construed as a potential conflict of interest.

## Publisher's note



## References

1. *Tuberculosis (who.int)*. (2023).
2. NIAID. NIH awards contracts to advance tuberculosis immunology research. *Vaccine*. (2017) 35(27):3433–40. doi: 10.1016/j.vaccine.2017.04.007
3. *Immune mechanisms of protection against mycobacterium tuberculosis centers (IMPAc-TB)*. (NIH/National Allergy and Infectious Diseases/Research: NIAID: National Institute of Allergy and Infectious Diseases). (2019).

frontiers | Frontiers in Immunology

TYPE Original Research
PUBLISHED 15 October 2024
DOI 10.3389/fimmu.2024.1460344



OPEN ACCESS

EDITED BY
Sarah Fortune,
Harvard University, United States

REVIEWED BY
Taru S. Dutt,
Colorado State University, United States
Alasdair Leslie,
Africa Health Research Institute (AHRI), South Africa

*CORRESPONDENCE
Michael Gale Jr
mgale@uw.edu

RECEIVED 05 July 2024
ACCEPTED 26 September 2024
PUBLISHED 15 October 2024

CITATION
Sung C-J, Whitmore LS, Smith E, Chang J, Tisoncik-Go J, Barber-Axthelm A, Selseth A, Feltham S, Ojha S, Hansen SG, Picker LJ and Gale Jr M (2024) Functional genomic analysis of the 68-1 RhCMV-*Mycobacteria tuberculosis* vaccine reveals an IL-15 response signature that is conserved with vector attenuation.
*Front. Immunol.* 15:1460344.
doi: 10.3389/fimmu.2024.1460344



# Functional genomic analysis of the 68-1 RhCMV-*Mycobacteria tuberculosis* vaccine reveals an IL-15 response signature that is conserved with vector attenuation

Cheng-Jung Sung[1], Leanne S. Whitmore[1], Elise Smith[1], Jean Chang[1], Jennifer Tisoncik-Go[1,2], Aaron Barber-Axthelm[3], Andrea Selseth[3], Shana Feltham[3], Sohita Ojha[3], Scott G. Hansen[3], Louis J. Picker[3] and Michael Gale Jr[1,2]*

[1]Center for Innate Immunity and Immune Disease, Department of Immunology, University of Washington, Seattle, WA, United States, [2]Washington National Primate Research Center, Seattle, WA, United States, [3]Vaccine and Gene Therapy Institute and Oregon National Primate Research Center, Oregon Health and Science University, Beaverton, OR, United States

Tuberculosis (TB), caused by *Mycobacterium tuberculosis* (*Mtb*) is a deadly infectious disease having a major impact on global health. Using the CMV vector for development of novel vaccines is a promising new strategy that elicits strong and durable, high frequency memory T cell responses against heterologous immunogens. We conducted functional transcriptomic analysis of whole blood samples collected from cohorts of rhesus (Rh) macaques that were administered RhCMV/TB vector using a prime-boost strategy. Two modified CMV vectors were used in this study, including 68-1 RhCMV/TB-6Ag (encoding 6 *Mtb* protein immunogens, including Ag85A, ESAT-6, Rv3407, Rv2626, Rpf A, and Rpf D) and its attenuated variant, 68-1 RhCMV/Δpp71-TB-6Ag (a cell-to-cell spread-deficient vaccine vector lacking the Rh110 gene encoding the pp71 tegument protein). Bulk mRNA sequencing, differential gene expression, and functional enrichment analyses showed that these RhCMV/TB vaccines induce the innate and adaptive immune responses with specific transcriptomic signatures, including the IL-15-induced protective gene signature previously defined to be linked with protection against simian immunodeficiency virus (SIV) by the 68-1 RhCMV/SIV vaccine. While both vectors exhibited a transcriptomic response of the IL-15 protective signature in whole blood, we show that lack of pp71 does not maintain induction of the protective signature for

the full duration of the study compared to the parental non-attenuated vector. Our observations indicate that RhCMV vector vaccines induce a transcriptomic response in whole blood that include a conserved IL-15 signature of which vector-encoded pp71 is an important component of response durability that upon future *Mtb* challenge may define specific vaccine protection outcomes against *Mtb* infection.

KEYWORDS

**tuberculosis, cytomegalovirus, rhesus macaque, vaccine, spread-deficient, IL-15, innate immunity, transcriptomic analysis**

# 1 Introduction

*Mycobacterium tuberculosis* (*Mtb*) primarily infects the lungs causing tuberculosis (TB) with an estimated 1.3 million deaths in 2022 and a death rate of around 50% if untreated (1). For individuals who are human immunodeficiency virus (HIV)-positive, TB is particularly devastating as it is the leading cause of death for people infected with both pathogens. With the increasing prevalence of drug-resistant TB strains, finding a protective vaccine solution is essential for reducing the global infection and disease rates (2). Currently, there is only one licensed vaccine in use for TB control, Bacillus Calmette-Guérin (BCG) vaccine, underscoring the need for investigation of novel vaccines to prevent pulmonary TB disease.

HIV causes disease by infecting and depleting $CD4^+$ T cells. $CD8^+$ T cells play a crucial role to control HIV by facilitating cytolytic mechanism to remove infected $CD4^+$ T cells. The cytomegalovirus (CMV) vector with its unique ability to elicit a strong and durable $CD8^+$ T cell response has shown great promise for use as a novel vaccine vector, particularly for HIV. Simian immunodeficiency virus (SIV), a lentivirus that infects nonhuman primates such as rhesus macaques (RMs), exhibits infection and pathogenic response similar to HIV with $CD4^+$ T cell depletion. The 68-1 derived RhCMV/SIV vector has the unique ability to control and clear SIV (3–5) in RMs by quickly eliciting and maintaining a high level of effector T cells with SIV-specific recognition by T cells occurring through MHC-Ia, MHC-II, or MHC-E antigens. Specifically, MHC-E restricted $CD8^+$ cells facilitate clearance of SIV (5). This SIV control and clearance behavior was also observed in the attenuated version of the 68-1 RhCMV/SIV vaccine (68-1 RhCMV/SIV Δpp71) that lacks expression of viral protein that facilitates CMV spread and dissemination through the body, thereby enhancing vector safety (6). $CD8^+$ T cells induction and regulation can be triggered by multiple factors, including specific antigens and cytokines such as IL-12, IL-18, and IL-15. Many studies have shown that IL-15 promotes memory $CD8^+$ T cells homeostatic proliferation to expand $CD8^+$ T cells, resulting in enhanced immunity against diseases including SIV and TB. Functional genomic analysis via mRNA-sequencing (Seq) of whole blood in 68-1 RhCMV/SIV-vaccinated RMs identified an IL-15-mediated transcriptional response that linked with vaccine protection against multiple SIV challenges (4).

This RhCMV vaccine backbone has also shown promising results in the prevention of *Mtb* infection and disease. Previous *Mtb* challenge studies have demonstrated that RhCMV/TB vaccination resulted in circulating *Mtb*-specific $CD4^+$ and $CD8^+$ T cells, and RMs with subcutaneous RhCMV/TB vaccination showed reduced *Mtb* infection and disease (based on both *Mtb* culture and pathologic score) by nearly 70% compared to unvaccinated controls (7). In these studies, functional transcriptomic analysis of whole blood post *Mtb* challenge revealed vaccine-induced innate immune responses linked with reduced disease (7). Here, we administered a prime plus two boosts regimen of the 68-1 RhCMV/TB-6Ag and 68-1 RhCMV/Δpp71-TB-6Ag vaccines to independent cohorts of 12 and eight RMs, respectively. These vaccines with RhCMV vectors encoding a single six-antigen-expressing polyprotein insert consist of two antigens from each of these three classes: acute-phase (ESAT-6 and Ag85A), latency (Rv3407 and Rv2626), and resuscitation (Rpf A and Rpf D; GenBank KY611405). These six antigens were selected by Hansen et al. in 2018 (7) using a mouse challenge model in which each antigen was shown to be at least partially protective. We conducted mRNA-sequencing of whole blood to define gene expression correlates of the response elicited by each vaccine. Differential gene expression and functional enrichment analyses of the transcriptomic signature of whole blood show that both vectors induce specific innate and adaptive immune response signatures of myeloid cell function, T cell receptor signaling, and lymphocyte activation. Unique signatures are linked with each vaccine. We show that the RhCMV/Δpp71-TB-6Ag vaccine transcriptional response wanes after the second boost. Direct comparison of RhCMV/TB vaccine signatures with the RhCMV/SIV vaccine signature (4) revealed similar transcriptional responses featuring IL-15-linked protective signature response. Our study shows that IL-15 signature is a major component of immune programming by 68-1 RhCMV vectored vaccines.

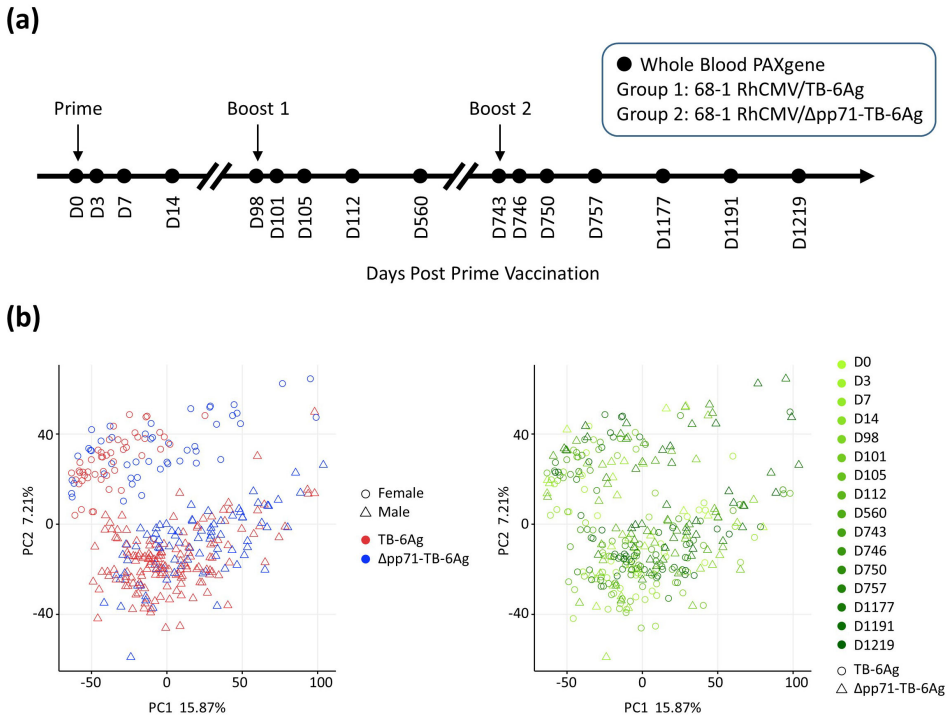


FIGURE 1
NHP vaccine study design and PCA describing the general variance. **(A)** Schematic overview of the two vaccine groups, vaccination time, and the 16 time points for which whole blood samples were collected for RNA-seq analysis in this study. Arrows indicated time points when RMs were administered with either the 68-1 RhCMV/TB-6Ag or the 68-1 RhCMV/Δpp71-TB-6Ag vectors set at D0 (prime), D98 (boost 1), and D743 (boost 2). **(B)** PCA biplots showing transcriptomic variation across all samples in this study. Each point on the plot represented an RNA-seq sample from an animal at each time point during vaccination regimen, for the visualization of vaccine group versus sex (left) and vaccine group versus time point (right). In the left panel, shape denoted sex (circle for female; triangle for male) and color denoted vaccine type (red for 68-1 RhCMV/TB-6Ag; blue for 68-1 RhCMV/Δpp71-TB-6Ag). In the right panel, color denoted time point (light to dark green for D0 to D1219) and shape denoted vaccine type (circle for 68-1 RhCMV/TB-6Ag; triangle for 68-1 RhCMV/Δpp71-TB-6Ag).

# 2 Results

## 2.1 Initial examination of sample variation across vaccine cohorts

To examine the differences in the vaccine signatures between RhCMV/TB vaccines, we conducted a functional genomic analysis of whole blood collected from immunized RM (*Macaca mulatta*) using bulk mRNA sequencing (mRNA-Seq). A total of 24 RMs (males and females) were randomized and assigned to one of two vaccine groups (n=12 per group). Animals received a prime-boost vaccine regimen of 68-1 RhCMV/TB-6Ag (n=12) or 68-1 RhCMV/Δpp71-TB-6Ag vector (n=12) spaced 14 weeks apart that was followed by a second boost administered 92 weeks later (Figure 1A, Supplementary Table S1). Four RMs of 68-1 RhCMV/Δpp71-TB-6Ag group were not included for the further transcriptional analyses due to lack of second boost data. Herein, we refer to these RhCMV vaccine vectors as non-attenuated (68-1 RhCMV/TB-6Ag) and attenuated (68-1 RhCMV/Δpp71-TB-6Ag) vectors, respectively. Whole blood samples collected at pre-vaccination day 0 (D0) and 15 additional time points following prime and boost immunization during the vaccination phase of the study were processed for bulk mRNA-Seq analyses.

To initially assess the major sources of variation within the resulting mRNA-Seq dataset, principal component analysis (PCA) was performed using all 15,399 expressed genes for 320 samples (20 RMs, each with 16 time points). A major source of variation was the sex of the animals, along principal component (PC)2 (Figure 1B). We accounted for this variation in downstream differential gene expression analysis by making sex a covariate in our linear model, thus removing batch effects due to sex in order to increase overall power of our study. Analysis of sex-specific vaccine response differences will be directly addressed in a subsequent study. PCA also revealed that samples neither segregated by time point nor by vaccine type (Figure 1B), reflecting a conserved response across vaccines.

## 2.2 Complete blood count and deconvolution analysis

Initially we examined complete blood count (CBC) data collected from across the vaccine time course for an overview of blood cell count dynamics of the different vaccine vector groups (Figure 2A). Generally, lymphocytes and neutrophils showed a separation of cell proportions between the two vaccine vector

10.3389/fimmu.2024.1460344

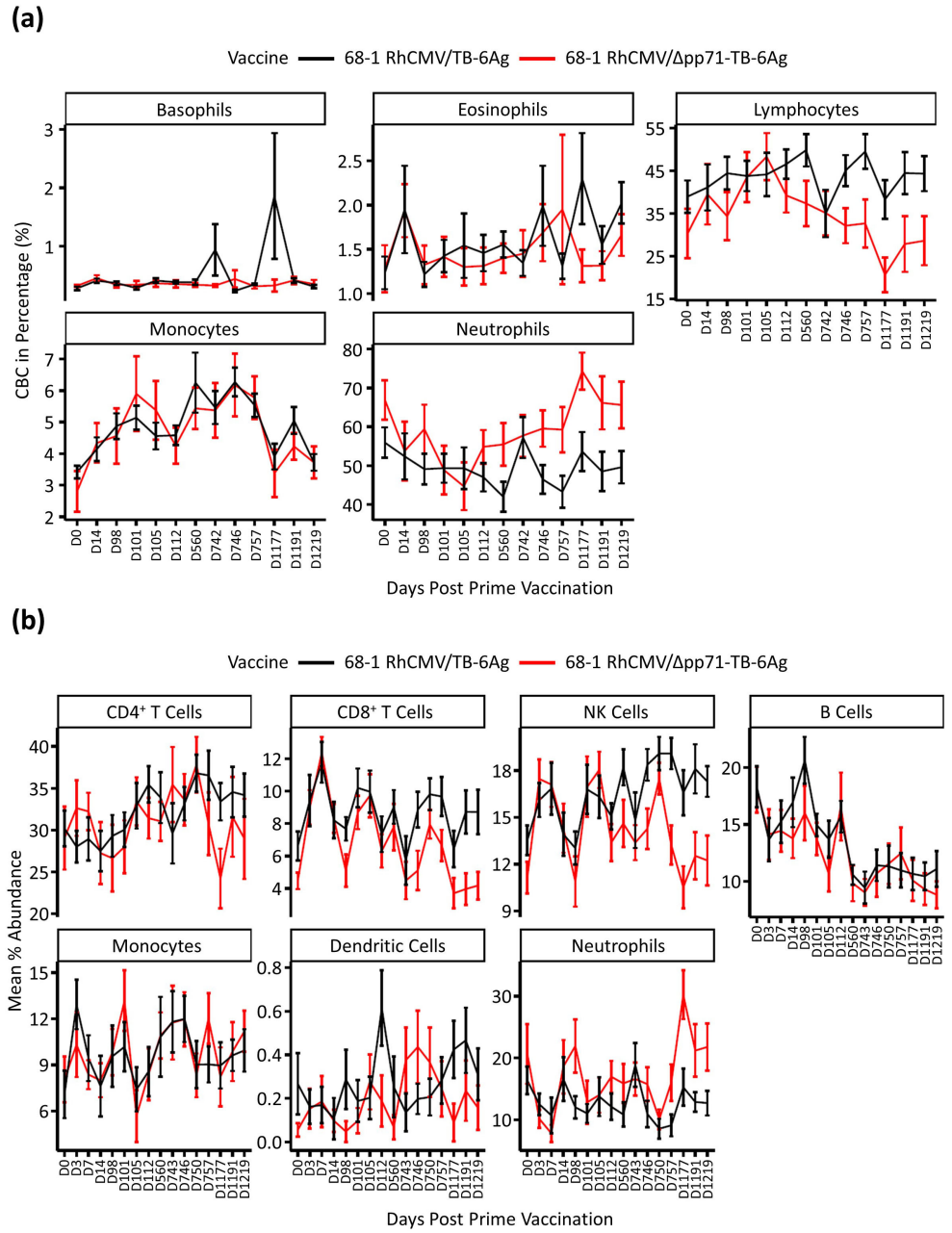


FIGURE 2
Cell type abundance analysis. **(A)** Complete blood count (CBC) test in percentage of five cell types, including basophil, eosinophil, lymphocyte, monocyte, and neutrophil. Vaccine groups were labeled in two colors, where black represented 68-1 RhCMV/TB-6Ag and red represented 68-1 RhCMV/Δpp71-TB-6Ag. Plots were made using mean data with standard error bars for each group at 13 time points post prime vaccination. **(B)** Deconvolution analysis of RNA sequencing data by CIBERSORTx to predict cell type abundance. Vaccine groups were labeled in the same way as described above in **(A)**, and plots were made using mean data with standard error bars for each group at all 16 time points post prime vaccination.

groups after the second boost vaccination at day (D)743. Specifically, compared to baseline, lymphocytes (including T, B, and NK cells) showed a decreasing trend in abundance in the attenuated vaccine vector group while staying stable in the non-attenuated vaccine vector group, with increased neutrophils in the attenuated vaccine group. We also performed a deconvolution analysis of the whole blood transcriptional dataset using CIBERSORTx with the LM22 signature (8, 9) to predict the abundance of different cell types in each sample and to interrogate differences observed across time points and vaccine vector groups. Cell abundance averages and standard error were calculated for each time point within the two groups (Figure 2B). We observed an initial increase in $CD8^+$ T and NK cells following prime and the first boost administrations in both vaccine groups. Following the second boost, NK and $CD8^+$ T cells in the attenuated group decreased to D0 abundance levels while remaining elevated in animals who received the non-attenuated vaccine vector. These observations show that the non-attenuated vaccine vector caused more

10.3389/fimmu.2024.1460344

persistent and sustained change in NK and $CD8^+$ T cell abundances compared to the attenuated vaccine vector.

## 2.3 Global analysis of whole blood transcriptomic signature induced by RhCMV/TB vaccination across vector types

To identify the whole blood gene expression responses to the RhCMV/TB vaccines, we performed differentially expressed (DE) analyses to define genes with statistically significant expression changes from D0 at each time point in both vaccine vector groups. A total of 4,816 significant DE genes were defined in at least one time point post-vaccination, with a false discovery rate (FDR; Benjamini-Hochberg (BH) procedure)-adjusted *p*-value less than 0.05 and an absolute $\log_2$ fold change (LFC) value greater than 0.58 (equivalent to fold change 1.5). Transcriptional changes strongly increased after each immunization (prime, boost 1, and boost 2) which then decreased over time (Figure 3A, Supplementary Table S2). This outcome shows that the vaccine responses induced by the RhCMV/TB vaccine vectors are rapidly induced. All 4,816 significant DE genes were assessed by cluster analysis using Pearson correlation and Ward.D2 hierarchical clustering methods which revealed six distinct gene modules. Overall, the whole blood transcriptional kinetics of the response of both vaccine vector groups appeared similar, except that the non-attenuated vaccine vector induced a stronger response that was prolonged and maintained over 92 weeks through D1219 following prime immunization as compared to the response elicited by the attenuated vaccine vector group that was less durable and diminished at D1177 post-prime immunization. Compared to the non-attenuated vaccine vector group, many DE genes from clusters 1, 5, and 6 lost their expression signatures after approximately three years following the prime immunization (D1177, D1191, and D1219) in the attenuated vaccine vector group. These results demonstrated the durability differences of the vaccine vector responses, revealing that the durability of the 68-1 RhCMV/Δpp71-TB-6Ag-induced response wanes within 3-years post-vaccination. Thus, the RhCMV pp71 protein is important for long-term maintenance of the vaccine transcriptional response.

Previously, we identified a RhCMV/SIV vaccine whole blood protective transcriptomic signature of 186 genes that were part of the response to IL-15, expressed in vaccinated RMs who were protected against SIV infection (4). We evaluated if any of the genes in this protection signature were present in the DE genes of each RhCMV/TB vaccine vector examined in this study. Of the 186 protection signature genes featuring the response to IL-15, 131 (70.43%) were identified as significant DE genes across the vaccine vectors in this study (Figure 3A, right hand side, Supplementary Table S3), showing that the 68-1 RhCMV vaccine vector generates a

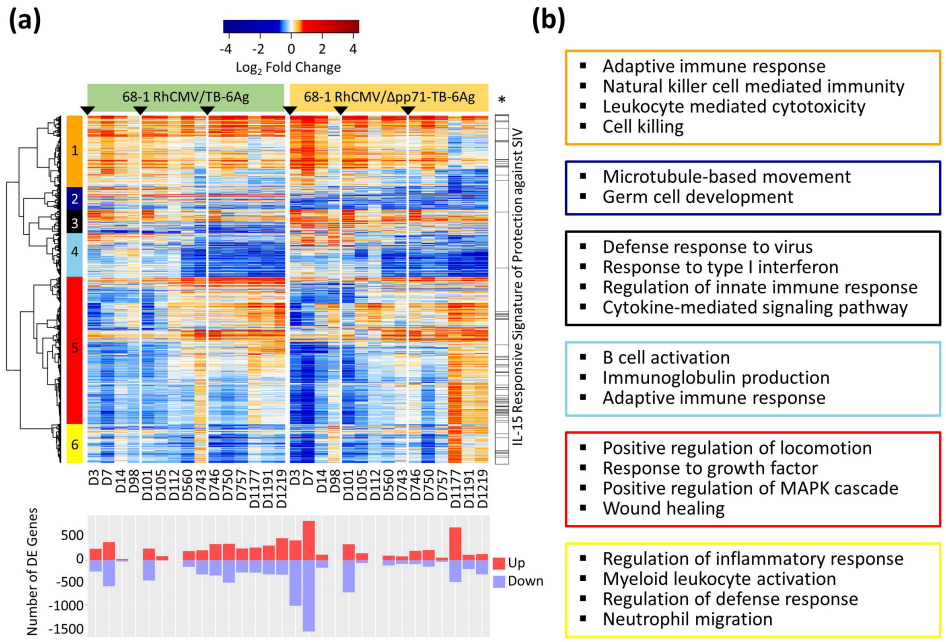


FIGURE 3
Whole blood mRNA-Seq analysis of RhCMV/TB vaccine response in RMs. **(A)** Heatmap of LFC values of all 4,816 significant (FDR-adjusted *p*-value < 0.05 and $|\log_2 FC| > 0.58$) DE genes identified in at least one vaccine group and one time point for both the non-attenuated (left side) and the attenuated (right side) vaccine groups with a gradient color intensity bar above the heatmap indicating the LFC values where red and blue depicted as up- and down-regulated, respectively. Barplot below the heatmap showed the total number of significant DE genes at each time point relative to baseline (D0), with up- and down-regulated genes labeled separately. Six gene modules were defined using Pearson correlation followed by Ward.D2 hierarchical clustering method. The bar on the right of the heatmap with an asterisk label (*) showed the genes overlapping the previously published protection signature. **(B)** Functional enrichment analyses on DE gene modules were performed for each cluster in heatmap. Select significant biological processes for each cluster were listed in colored boxes matching to the clusters in the heatmap (orange, darkblue, black, skyblue, red, and yellow, for clusters 1 to 6, respectively).

conserved signature that includes an IL-15 response program in whole blood.

Other relevant biological processes associated with these DE genes were investigated using over-representation analysis (ORA) performed on each of the six modules of genes identified by clustering. Select significant biological processes are shown in Figure 3B (the full set of significant enrichments are shown in Supplementary Table S4). Genes that were induced after prime immunization with both RhCMV/TB vaccine vectors were mostly found in cluster 1, with specific gene expression then variably reduced at late time points (D1177, D1191, and D1219) especially for the attenuated vaccine vector group. We found enrichment for genes in cluster 1 related to adaptive immune response programming (e.g., *CX3CR1*, *GATA3*, *IFNG*, *IL10*, *IL18*, *IL23A*, *PRF1*, and *TBX21*), NK cell-mediated immunity, and leukocyte-mediated cytotoxicity. Cluster 5 included the greatest number of co-expressed genes. Notably, most of these genes were reduced in expression compared to baseline levels (down-regulated) after the prime vaccination with the expression increasing over time for both vaccine groups. For this cluster, the attenuated vaccine vector group showed a stronger magnitude of expression increase at D1177, D1191, and D1219 that linked to the reduced expression of the otherwise induced module 1 genes. Cluster 5 genes were enriched for fundamental cellular processes including regulation of MAPK signaling and featuring *CCR1*, *MAP3K5*, *MYD88*, *PIK3CG*, and *TLR4*. Cluster 6 genes were typically down-regulated from baseline following vaccination but for animals who received the attenuated vaccine vector the expression of these genes shifted at the later time points to levels of induction/up-regulation compared to baseline. Module 6 genes were significantly associated with defense related innate immune response and regulation (e.g., *CASP4*, *IL1RL1*, *MAPK13*, *STAT5B*, and *TRIM5*), including myeloid leukocyte activation and neutrophil migration. Many of the DE genes in clusters 1, 5, and 6 showed differences between the attenuated and non-attenuated vaccine groups three years following the prime immunization (D1177, D1191, and D1219) and linked with the protection signature defined by Barrenäs et al. in 2021 (4; see Figure 3A, right), showing that the genes in the protection signature were similarly regulated during the prime and boost 1 phases for both vaccine vectors but this response became dysregulated during the boost 2 phase in animals who received the attenuated vaccine vector.

We also found that genes in cluster 2 (see Figure 3A) were associated with cilium movement and microtubule-based movement defining regulation of cell motility, and cell trafficking (e.g., *CFAP45*, *DNAH1*, *KIF14*, *RNASE10*, *TSSK4*, and *TTC21A*). Cluster 2 genes were variably expressed in animals who received the non-attenuated vaccine vector but were down-regulated in the attenuated vaccine vector animals across time points. Genes in cluster 3, including *CXCL9*, *CXCL10*, *IRF7*, *IRF9*, *STAT1*, *STAT2*, and *TRIM21*, were enriched for antiviral innate immune response related biological processes, such as response to type I interferon (IFNs) and cytokine-mediated signaling pathway, and these genes were rapidly induced in response to administration of both RhCMV/TB vaccine vectors. Enrichment for cluster 4, with significant genes such as *CD19*, *CD40*, *CXCR5*, *IGHE*, and *TLR9*, included humoral immune responses and were strongly down-regulated late in the vaccine phase for both groups.

## 2.4 Upstream regulator analysis and network of target genes

We performed upstream regulator analyses on the DE genes across the vaccine vector time series using Ingenuity Pathway Analysis (IPA). In particular, we included a focus to assess the upstream regulators linked with programming each vaccine vector whole blood gene expression signature, including those linked with signature durability. Upstream regulators were identified and sorted by both the sum of absolute z-scores compared to baseline and the sum of $-\log_{10}$ (*p*-value) across time points in each vaccine vector group. The top 12 significant upstream regulators identified from both vaccine vector groups are shown in Figure 4A and Supplementary Table S5. Among these upstream regulators, IFNG (gamma), STAT1, interferon alpha, IL-21, IL-2, IL-18, TBX21, STING, and IL-15 were predicted to be actively signaling at multiple points in the time course. STAT3 and IL-4 were predicted to be inhibited compared to baseline. TNF showed inconsistent activation patterns across the two vaccine groups. During the prime and boost 1 phases, upstream regulators of the attenuated/68-1 RhCMV/Δpp71-TB-6Ag group maintained significant activation or inhibition throughout both phases while the non-attenuated/68-1 RhCMV/TB-6Ag group had a relative decrease in activation/inhibition of upstream regulators after D7 and D105, for the prime and boost 1 phases respectively. Conversely, the attenuated/68-1 RhCMV/Δpp71-TB-6Ag group during boost 2 (D746-D1219) exhibited little to no significant regulation of these upstream regulators at late time points following the boost 2 phase while the regulation of the same upstream regulators in the non-attenuated/68-1 RhCMV/TB-6Ag group was maintained. The distinct dynamics of upstream regulators including loss of activation in the attenuated/68-1 RhCMV/Δpp71-TB-6Ag group therefore underscores the vaccine vector signature durability differences of DE gene expression particularly during the second boost phase.

To reveal the gene networks and their expression dynamics linked with these upstream regulators, we made network plots showing upstream regulators (*p*-value less than 0.05) and their DE target genes at D7 (Figure 4B) and D750 with LFCs for both vaccine groups (Figure 4C). The networks displayed the most DE genes at D7, revealing consistent up- and down-regulation of target genes across both vaccine groups. Unique to D7, genes *AQP9*, *CST7*, *CXCL8*, *IFI27*, *ISG15*, *KIT*, *NCR1*, *OASL*, *PROK2*, and *PTG2* were all induced/up-regulated compared to baseline reflecting an innate immune and adaptive immune activation state that links with the response to *Mtb* antigens (10). At D750, genes *AICDA*, *BCL2A1*, *CCR5*, *CD72*, *CLIC5*, *CRISPLD2*, *CXCR1*, *FPR2*, *GFI1*, *IL12RB2*, *KLRB1*, *KLRG1*, *S100A9*, *TNFAIP6*, and *WLS* were uniquely all targets of upstream regulators and mark a TH1-polarized adaptive immune response (11, 12).

For each vaccine vector and in both networks, IL-15 was identified as an active upstream regulator. Expression and

10.3389/fimmu.2024.1460344

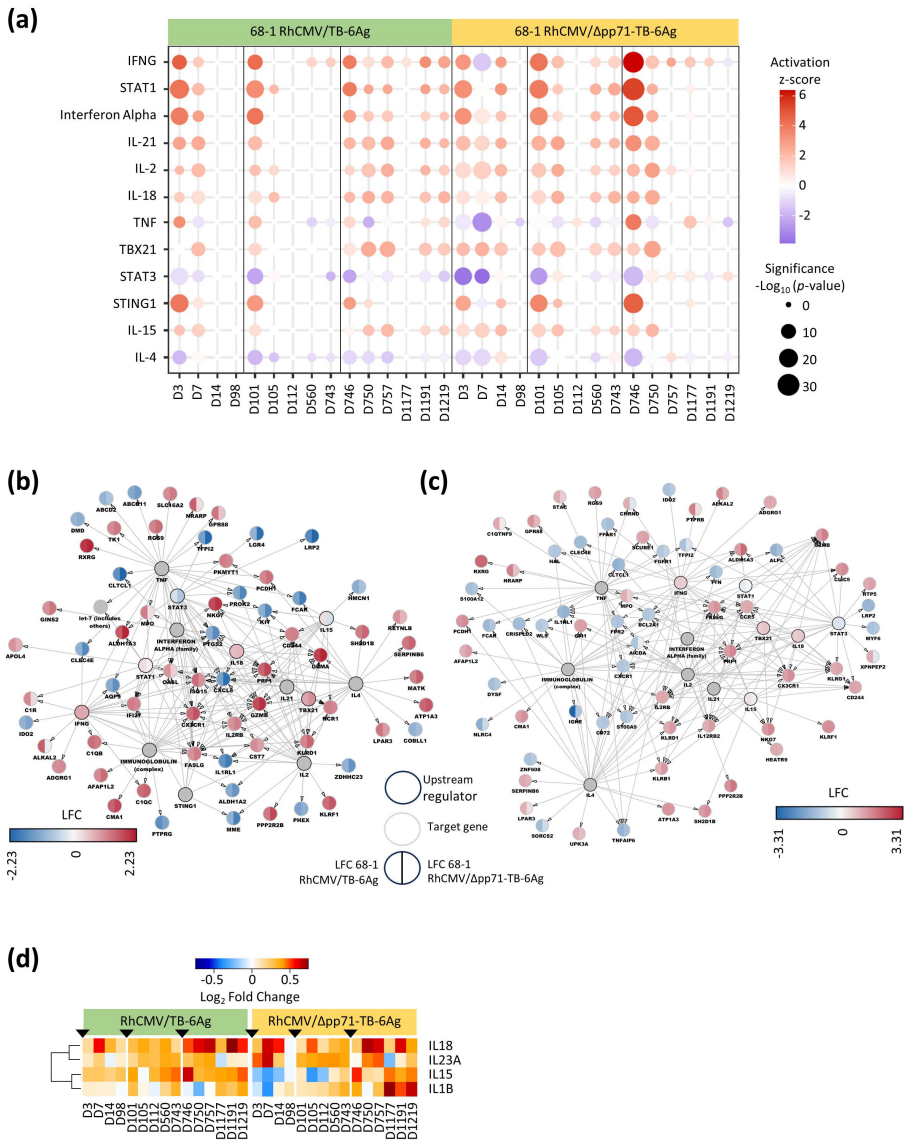


FIGURE 4
Upstream analysis and regulation networks in RhCMV/TB-vaccinated RMs. **(A)** Dot plot delineated select top upstream regulators identified through Ingenuity Pathway Analysis (IPA). The colors represented z-scores (> 2 for activation in red and < -2 for inhibition in blue) and dot size was proportional to the significance of $\log_{10}$ *p*-value as per the legend. **(B, C)** Networks showing LFC levels of downstream targeted genes and the major upstream regulators (circles with black lines) in 68-1 RhCMV/TB-6Ag (left half of each circle) and 68-1 RhCMV/Δpp71-TB-6Ag (right half of each circle) vaccine groups at D7 **(B)** and D750 **(C)**. **(D)** Heatmap showing the significant (FDR-adjusted *p*-value < 0.05 and $|\log_2 FC| > 0.58$) gene expression changes from baseline of *IL15* and the other important interleukin upstream regulator genes (*IL18*, *IL23A*, and *IL1B*) for both the non-attenuated (left side) and the attenuated (right side) vaccine groups, with a gradient color intensity bar above the heatmap indicating the LFC values where red and blue depicted as up- and down-regulated, respectively.

signaling of IL-15 was shown to be linked to RhCMV/SIV vaccine protection in previous study (4). We identified IL-15 and four additional cytokines that were significantly DE in our vaccine vector groups, which included *IL15*, *IL18*, *IL23A*, and *IL1B* (Figure 4D, Supplementary Table S6). IL-15 was induced, and expression was typically maintained across the time course in the non-attenuated/68-1 RhCMV/TB-6Ag group but its expression was low and variable across prime and boost-1 time series in the attenuated/68-1 RhCMV/Δpp71-TB-6Ag group. We also found that IL-18 expression was consistently induced across the time series for both vaccine vector groups, and that IL-1β was induced to high levels at the end of the time series following boost-2 in the attenuated/68-1 RhCMV/Δpp71-TB-6Ag group.

## 2.5 Conservation of IL-15 signature between 68-1 RhCMV vector vaccines

We previously defined a 186 gene expression signature associated with RhCMV/SIV vaccine protection, all of which were shown to be regulated in response to IL-15 (4). Importantly, 131 of these genes were significantly DE across RhCMV/TB vaccine vectors (see

10.3389/fimmu.2024.1460344

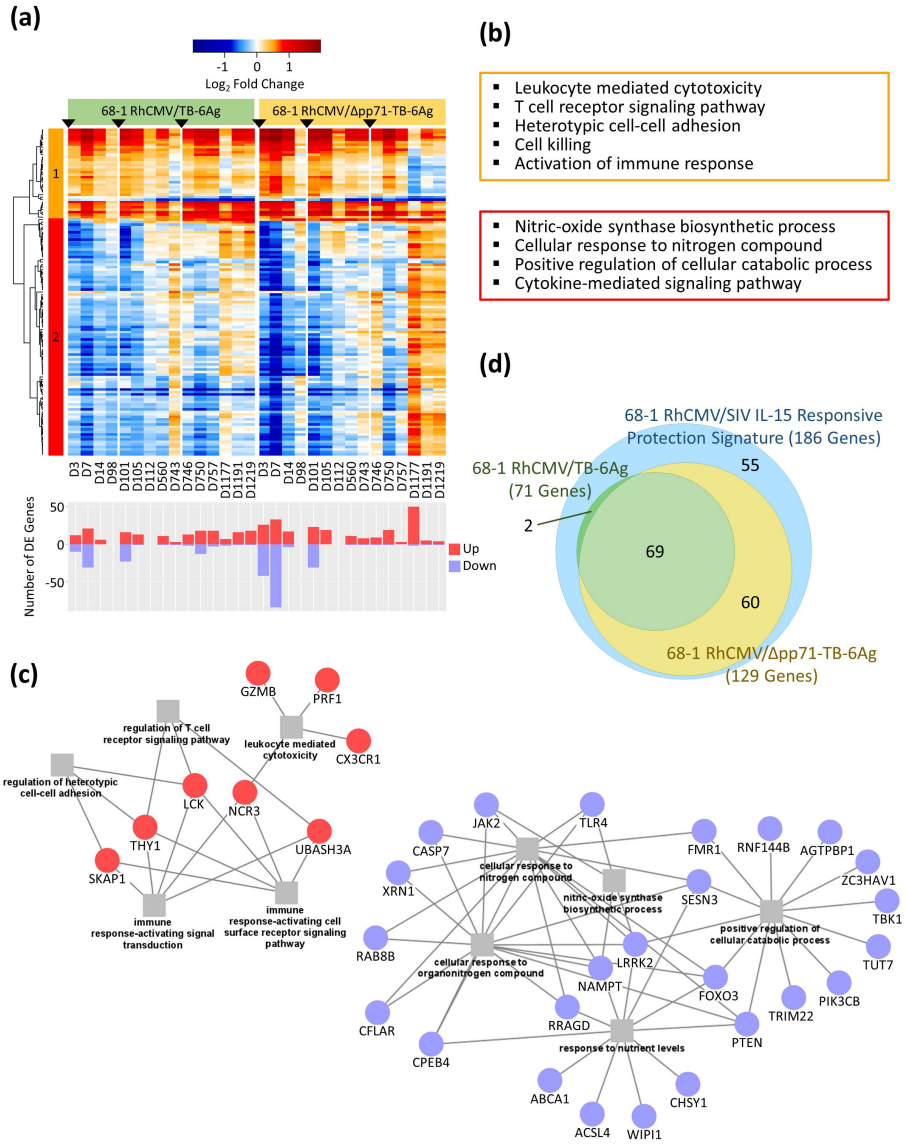


FIGURE 5
Conserved transcriptional profiles overlapping the IL-15 response signature of SIV protection. **(A)** Heatmap of the LFC values of 131 significant (FDR-adjusted $p$-value < 0.05 and $|\log_2 FC| > 0.58$) DE genes overlapping the previously published IL-15 protection signature genes for both the non-attenuated (left side) and the attenuated (right side) vaccine groups, with a gradient color intensity bar above the heatmap indicating the LFC values where red and blue depicted as up- and down-regulated, respectively. Barplot below the heatmap showed the total number of significant DE genes at each time point relative to baseline (D0), with up- and down-regulated genes labeled separately. Genes were clustered into two modules using Pearson correlation followed by Ward.D2 hierarchical clustering method. **(B)** Functional enrichment analyses identified biological processes of genes significantly over-represented for each cluster according to colors of the clusters in the heatmap (orange for cluster 1; red for cluster 2). **(C)** Network showing select biological processes with significant overlapping genes for cluster 1 (left) and cluster 2 (right), with squares representing biological processes and circles showing the enriched DE genes. **(D)** Proportional Venn diagram of three circles, showing the overlap between the previously published IL-15 protection signature (186 genes in blue), overlapped 68-1 RhCMV/TB-6Ag vaccine signature (71 genes in green), and overlapped 68-1 RhCMV/Δpp71-TB-6Ag vaccine signature (129 genes in yellow).

Figure 3A). We evaluated the expression dynamics of this gene signature across the 68-1 RhCMV/SIV, non-attenuated/68-1 RhCMV/TB-6Ag and the attenuated/68-1 RhCMV/Δpp71-TB-6Ag vaccine vector responses (Figure 5A, Supplementary Table S7). Two gene modules were identified based on Pearson correlation and Ward.D2 hierarchical clustering including 36 genes in cluster 1 that were induced/up-regulated and 95 genes in cluster 2 that were typically suppressed/down-regulated compared to baseline. Genes in cluster 1 represented immune activation and immune effector functions and were immediately induced following prime vaccination. Expression of cluster 1 genes was typically maintained in the non-attenuated/68-1 RhCMV/TB-6Ag group but a subset of these genes demonstrated a transient down-regulation prior to boost 2, after which boost 2 restored their induced expression pattern. These genes underwent sustained reduction in expression in the attenuated/68-1 RhCMV/Δpp71-TB-6Ag group at late time points following boost 2. The down-regulated cluster 2 gene expression pattern shifted to increased levels of expression for a large subset of

genes at late time points after each boost wherein this expression shift was more extensive and enhanced in the attenuated/68-1 RhCMV/Δpp71-TB-6Ag group. These results show that the non-attenuated/68-1 RhCMV/TB-6Ag and attenuated/68-1 RhCMV/Δpp71-TB-6Ag vaccine vectors each immediately induce the IL-15 response gene expression profile in blood. This signature is sustained and reengaged following boost but can wane in late time points following boost 2. Moreover, lack of vector-encoded pp71 impacts the longer-term durability and breadth of this gene expression signature.

We conducted enrichment tests using over representation analysis (ORA) methodology (13) to identify the biological processes associated with the 131 IL-15 response genes in our data sets. ORA of cluster 1 demonstrated an up-regulated enrichment of cell-mediated immune response related to immune signaling including leukocyte mediated cytotoxicity and the T cell receptor signaling pathway (Figure 5B, Supplementary Table S8), and produced gene networks with key genes such as *CX3CR1*, *GZMB*, *LCK*, *NCR3*, *PRF1*, *SKAP1*, *TBX21*, *THY1*, and *UBASH3A* (Figure 5C). The down-regulated genes in cluster 2 were significantly enriched for cellular response to oxygen levels, cytokine signaling, cell death, and catabolic processes, including genes such as *CASP7*, *FOXO3*, *JAK2*, *NAMPT*, *PIK3CB*, and *TRIM22* (Figure 5C; see Supplementary Table S8 for the complete list of genes). Specifically, among these 131 RhCMV vector-induced signature genes, 71 were significantly DE in the non-attenuated/68-1 RhCMV/TB-6Ag group while 129 were significantly DE in the attenuated/68-1 RhCMV/Δpp71-TB-6Ag group, with 69 highly conserved genes identified to be significant in all three groups (protection signature, 68-1 RhCMV/TB-6Ag, and 68-1 RhCMV/Δpp71-TB-6Ag; Figure 5D, Supplementary Table S3). Importantly, these observations demonstrate that the IL-15 response protection signature identified by Barrenäs et al. in 2021 (4) was also induced in 68-1 RhCMV/TB vectors. Vaccine-induced regulation of these genes therefore links the functionality of RhCMV vaccines and could be important for vaccine efficacy.

## 3 Discussion

Here we present a functional genomic analysis of the RhCMV vaccine vectors including a non-attenuated/68-1 RhCMV/TB-6Ag vaccine vector and an attenuated/68-1 RhCMV/Δpp71-TB-6Ag vaccine vector with direct comparison to the RhCMV/SIV vaccine vector across prime/boost vaccination regimen. Both RhCMV/TB vectors express 6 specific *Mtb* antigens and were designed as vaccines to protect against infection and disease by *Mtb* (7), whereas the RhCMV/SIV vaccine expresses specific SIV antigens as a preclinical vaccine design for protection against SIV/HIV infection (14, 15). We found that similar to the RhCMV/SIV vaccine vector, the RhCMV/TB vaccine vectors (both 68-1 strain) rapidly induce the expression of genes that impart regulation of key immunological pathways programming cellular responses that impact both innate and adaptive immunity. Remarkably, the RhCMV vaccine vector whole blood signature is conserved across the three vectors analyzed here to feature a common IL-15 response signature that we previously linked with vaccine protection against SIV (4). While this vaccine vector signature exhibited fluctuating durability beyond three years for the non-attenuated/68-1 RhCMV/TB-6Ag vaccine vector, the vaccine signature was found to decrease following the second boost more strongly for the attenuated/68-1 RhCMV/Δpp71-TB-6Ag vaccine vector. These results indicate that the two *Mtb* vaccine vectors elicit similar responses of immune programming but with differential dynamics and overall durability linked with the RhCMV pp71 protein. Importantly, the non-attenuated/68-1 RhCMV/TB-6Ag vaccine vector can protect against infection and disease by *Mtb* (7).

We identified enriched upstream regulators from significantly DE genes in response to the 68-1 RhCMV/TB vaccines, including cytokines (e.g., IL-15, IL-2, IL-21, IL-18, and IL-4, IFN gamma) and transcription factors (e.g., STAT1, TNF, TBX21, STAT5, and STAT3). In focusing on target genes at D7 and D750, we identified innate immune genes (for example *IFI27* and *ISG15*) induced by more than three upstream regulators specifically at D7. This pattern of gene expression suggests that the vaccine elicited innate immune activation and responses through multiple pathways during the prime phase of the vaccination. Our data sets show that deletion of Rh110 encoding pp71 links with an inability of the attenuated vector to maintain the persistent activation of the upstream regulators and subsequent expression of specific target genes that support vaccine signature durability. RhCMV with pp71 deletion has an inhibited ability to undergo cell-to-cell spread, making it a possible safer option to be applied as a future vaccine. Our observations suggest that this spread-deficient phenotype impacts vaccine signature durability. We also note that we observed an increase in polymorphonuclear leukocytes (PMNs) in the attenuated vaccine group compared to the non-attenuated vector group, linking this difference to vaccine attenuation and possibly differences in vector spread in tissue. This attenuation could likely drive a differential inflammatory response that recruits increased PMNs thus displayed as increased circulating neutrophils as they transit from bone marrow to blood to tissue. However, whether maintaining these vaccine-induced cellular and gene expression changes for three years will underlie a differential protection outcome against *Mtb* disease remains unknown until challenge studies with pathological analyses are conducted and completed. A previous RhCMV/SIV study showed that the attenuated pp71-deleted 68-1 RhCMV/SIV vaccine had the same efficacy to protect against SIV infection as the non-attenuated vaccine following virus challenge at approximately three years after last vaccination (6). Ongoing *Mtb* challenge studies of vaccinated cohorts will ascertain vaccine efficacy to protect against *Mtb* disease.

Of particular interest in vaccine response signatures is the presence of the IL-15 response, as previously identified protection signature to RhCMV/SIV vaccination included a robust IL-15 response program that was induced rapidly and persisted in RMs protected from SIV challenge (4, 5, 16, 17). Here we provide the first comparison of RhCMV/TB with RhCMV/SIV vaccine whole blood signatures, revealing that more than 70% of the RhCMV/SIV protection signature genes were also significantly DE in the RhCMV/TB vaccine signatures. These analyses demonstrate that 68-1 RhCMV/SIV and 68-1 RhCMV/TB vector vaccines induce a conserved IL-15 signaling response signature across studies. During the first two years of vaccine phase (for time points D3 through

D757) in the current study, our analyses revealed that both the attenuated and non-attenuated 68-1 RhCMV/TB vaccines elicited rapid and stable transcriptional responses after prime administration. This vaccine-induced transcriptional whole blood signature gradually waned during the third year of vaccine phase in RMs administered the attenuated vaccine vector, while the signature induced by the non-attenuated vaccine vector was maintained. Thus, vector persistence with differential cell-to-cell spread may alter the durability of RhCMV whole blood vaccine signatures. An important consideration for the current study is that our observations are limited to whole blood, and the RhCMV vaccine vector induces tissue responses that link with blood cell signatures and effector function to mediate vaccine efficacy. A limitation of our study is that we did not examine the tissue response to vaccination. Importantly, the whole blood vaccine response signature featured the induction of genes involved in cell motility and trafficking, implicating a process in which immune cells are being programmed to migrate into tissues. Thus, tissue responses can occur as an additional component of RhCMV/TB vaccine immune programming that might also impart vaccine efficacy. Our ongoing *Mtb* challenge studies will directly address the tissue response to vaccination to link whole blood and tissue response signature with vaccine efficacy for protection against *Mtb* infection and disease.

IL-15, expressed primarily in myeloid cells (dendritic cells, monocytes, and macrophages), plays an important role in $CD8^+$ T cell and NK cell activation (18–22). Previous studies have demonstrated the importance of induction of the unconventionally MHC-E restricted $CD8^+$ T cell responses by 68-1 RhCMV vector vaccines for efficacy against SIV (4–6, 17), whereas protection mediated by RhCMV/TB does not specifically require MHC-E restriction (7). We propose that the IL-15 signature is an important component of overall immune programming to promote myeloid cell activation, and NK and $CD8^+$ T cell function induced by RhCMV vaccine vectors. Indeed, cell deconvolution analysis showed a vaccination-induced acute increase of NK and $CD8^+$ T cells in our vaccine cohorts. We observed a decrease in percentages of these cell types specifically in the attenuated group at later time points (post second boost) concomitant with reduction of the IL-15 signature. Furthermore, the CBC results revealed a similar pattern for the lymphocyte percentage, which supported our transcriptional cell abundance analyses, indicating that maintenance of the IL-15 signature links with vaccine vector-induced NK and T cell abundance in whole blood and could be a determinant of vaccine durability and efficacy.

In conclusion this work shows that the RhCMV/TB vectors elicit a whole blood transcriptional signature with different timing dynamics. Additionally, we link RhCMV vectors with a conserved IL-15 response signature. Future exploration with challenge outcome data and validation will be necessary to examine whether the 68-1 RhCMV/Δpp71-TB-6Ag and other attenuated vaccines protect against TB disease with a strong and stable long-term signature. It is noteworthy that many studies have suggested to use IL-15 as an adjuvant for TB vaccines (4, 23–25) and thus it will be interesting to further investigate the use of 68-1 RhCMV/Δpp71-TB-6Ag vaccine along with IL-15 as an adjuvant to enhance both the protection signature and durability of the vaccine, making it a possible promising vaccine against pulmonary TB disease.

# 4 Material and methods

## 4.1 Rhesus macaques

A total of 24 purpose-bred, pedigreed, RMs (*Macaca mulatta*) of Indian genetic background were included in this non-human primate (NHP) study. Four RMs of 68-1 RhCMV/Δpp71-TB-6Ag group were not included for the further transcriptional analyses due to lack of second boost data. Among these 20 study animals (ten were from the ONPRC colony and the other ten were from the Puerto Rico (PR) colony), 14 were males and six were females, with age ranging from 4 to 7 years old. At assignment, all study RMs were free of *Cercopithecine herpesvirus 1*, D-type simian retrovirus, simian T-lymphotropic virus type 1, simian immunodeficiency virus, and *Mycobacterium tuberculosis*, however, all were naturally RhCMV-infected. All study RMs were housed in Animal Biosafety level (ABSL)-2 rooms during vaccine phase with autonomously controlled temperature, humidity and lighting. Study RMs were both single- and pair-cage housed. Animals were only paired with one another during the vaccine phase if they belonged to the same vaccination group. Regardless of their pairing, all animals had visual, auditory and olfactory contact with other animals. Single cage-housed RMs received an enhanced enrichment plan that was designed and overseen by RM behavior specialists. RMs received commercially prepared primate chow twice daily and received supplemental fresh fruit or vegetables daily. Fresh, potable water was provided via automatic water systems. Physical exams, including body weight and complete blood counts, were performed at scheduled protocol time points. RMs were sedated with ketamine HCl or Telazol for procedures, including subcutaneous vaccine administration and venipuncture.

## 4.2 RhCMV vectors and vaccination

A total of 20 RMs that were included in this transcriptional study were assigned to each of two vaccine groups and vaccinated three times, receiving a prime, a week 14 homologous boost, and followed by a second boost 92 weeks after the first boost. The two vaccines used in this study were 68-1 RhCMV/TB-6Ag vector (n=12) expressing a single six-antigen *Mtb* polyprotein (Ag85A, ESAT-6, Rv3407, Rv2626, Rpf A, and Rpf D) and an analogous RhCMV/TB-6Ag vector (68-1 RhCMV/Δpp71-TB-6Ag; n=8) lacking tegument protein pp71 encoded by RhCMV Rh110 gene (6, 7). The spread-deficient RhCMV/TB vector (ΔRh110) is unable to disseminate from the injection site to distant sites *in vivo*, but it remains immunogenic for T cell responses (26). The 68-1 RhCMV/TB vector was constructed by bacterial artificial chromosome (BAC) recombineering, and the vector preparations and characterization have been previously described (3, 6, 27–29). In this study, RMs were

vaccinated subcutaneously at a dose of $5\times10^6$ plaque-forming units (PFU) of each of the assigned 68-1 RhCMV/TB vectors.

## 4.3 Sample collection, library prep, and RNA sequencing

Longitudinal whole blood samples were collected into PAXgene RNA tubes (PreAnalytiX) following the manufacturer's instructions. RNA was isolated using RNAdvance Blood Kit (Beckman) on a Biomek i7 Automated Workstation (Beckman) following the validated protocol provided with the kit that included an on-column DNase treatment. Total RNA was quantified using Qubit™ RNA Assay kit, and RNA integrity assessed using the Agilent 4200 TapeStation instrumentation. mRNA-seq libraries were constructed using the KAPA HyperPrep Kit with RiboErase (HMR) Globin + mRNA Capture Kit (Roche Diagnostics) following the manufacturer's recommended protocol that was adapted for the Biomek i7. Samples were randomized across the project, including internal plate controls to protect against batch effects. Qubit™ DNA Assay Kit was used to determine library DNA concentration and Agilent TapeStation assay was used to determine library size distribution and quality. Libraries were sequenced on an Illumina NovaSeq X sequencer at Northwest Genomics Center (University of Washington) using an Illumina NovaSeq S2 v2 200 cycle kit following the manufacturer's protocol for sample handling and loading. Sequencing run metrics were visualized for quality assurance followed by demultiplexing using bcl2fastq. A total of 640 fastq files were generated for downstream transcriptomic analyses, and the quality were assessed using FastQC.

## 4.4 Sequence data pre-processing and preparation for analysis of differential expression

Raw sequence reads were processed to digitally remove residual adapters and low-quality bases by using Trim Galore v0.6.4 (powered by Cutadapt v3.7 (30);), along with quality check using FastQC v0.11.2 (31). Trimmed reads were then filtered to remove globin and ribosomal sequences using Bowtie2 v2.3.4 (32). Paired reads were aligned to the Mmul_10 *Macaca mulatta* genome (Ensembl v109 (33);) and gene expression was quantified with STAR v2.7.10b (34) using the –quantMode GeneCounts flag to generate raw gene counts. After removing lowly expressed genes with mean gene counts below 4, trimmed mean of M-values (TMM (35);) normalization was performed using the calcNormFactors function in edgeR (36) to calculate the scaling factor for the adjusted library sizes. Gene counts were then transformed into $\log_2$-counts per million (log-CPM) values by limma package (37) with the voom function (38) for subsequent analyses.

## 4.5 Principal component analysis

Principal component analysis (PCA) was performed on the transformed normalized count matrix for an initial inspection of the whole transcriptome. This allows visualization of samples to determine sources of variation across samples within a dataset to include as a covariate in the final model. Eigenvalues were computed using the built-in R function prcomp (39–41) with all expressed genes, and the top two eigenvectors represent the two dimensions on the PCA plot. Biplots with the top two principal components, PC1 and PC2, were generated using data points from all 320 samples (including 20 RMs, with 16 time points each) with the label of vaccine group, sex, and time point.

## 4.6 Deconvolution analysis

To further impute the gene expression profiles with an estimation of cell type proportions, we input normalized gene expression values for all samples into CIBERSORTx (9), a machine learning tool, to predict cell abundance levels. We represented similar cell types together by summing predicted cell percentages as the following: B cells naive and B cells memory as B cells, T cells CD4 naive, T cells CD4 memory resting and T cells CD4 memory activated as CD4 cells, NK cells resting and NK cells activated as NK cells, and dendritic cells resting and dendritic cells activated as dendritic cells.

## 4.7 Differential gene expression analysis and visualization

Differential gene expression analysis was performed for each time point using D0 as the common baseline comparator of each vaccine group. To determine the significant differentially expressed (DE) genes in the RhCMV/TB vector-vaccinated cohort, normalized counts were utilized for linear modeling across contrasts for each gene using the limma package in R and Bioconductor (42). Significant DE genes were identified with a false discovery rate (FDR; BH procedure)-adjusted $p$-value less than 0.05 and an absolute $\text{Log}_2$ fold change (LFC) value greater than 0.58. These genes were then organized by Pearson correlation method for the calculation of correlation-based distance metrics, followed by grouping into co-expression modules using the Ward.D2 hierarchical clustering method. Heatmaps were generated for the visualization of the LFC values of clustered DE genes using the WGCNA (43, 44), heatmap.2 (codes on GitHub) with gplots, and edgeR (36). Further graphics were made using R packages, including ggplot2 (45) for barplots to display the numbers of DE genes at each time point, and eulerr (46, 47) for the proportional Venn diagram.

### 4.8 Over representation analysis

Functional enrichment analysis was performed for each module of DE genes using over representation analysis (ORA) with the enrichGO function in the clusterProfiler package (48) to determine whether genes that were pre-defined to be associated with certain annotations are statistically more prevalent in our gene sets of interest than would be expected by chance. The biological process subontology of Gene Ontology (GO: BP) annotations used in this study were retrieved from org.Hs.eg.db (49). After converting the RM Ensembl gene IDs to Human Genome Organisation Gene Nomenclature Committee (HGNC) gene symbols, significantly over-represented genes were identified using a threshold of FDR-adjusted *p*-value less than 0.05. Network plots were generated using Cytoscape (50) for the visualization of representative biological processes and the significantly enriched DE genes.

### 4.9 Upstream regulator analysis

Upstream regulator analysis was performed using Ingenuity Pathway Analysis (IPA; QIAGEN Inc (51).;). The LFC values and FDR-adjusted *p*-values of all the significant DE genes were input for the analyses, and the information of the top identified upstream transcriptional regulators and cytokines that were common across time points in both vaccine groups were collected for making dot plots using ggplot2 in R. Networks were generated through Cytoscape from IPA results. We extracted the significant upstream regulators and their target genes, generate a network file for each time point and mapped the LFCs for each vaccine vector to the corresponding genes using the Omics Visualizer app within Cytoscape.

## Data availability statement

The raw data is available on GEO GSE273911. The R codes applied to these analyses can be accessed at https://github.com/galelab/Sung_RhCMV_TB_IL15_Attenuation.

## Ethics statement

The animal studies were approved by RM care and all experimental protocols and procedures were approved by the ONPRC Institutional Animal Care and Use Committee (IACUC). The ONPRC is a Category I facility and the Laboratory Animal Care and Use Program at the ONPRC is fully accredited by the American Association for Accreditation of Laboratory Animal Care (AAALAC) and has an approved Assurance (#A3304-01) for the care and use of animals on file with the NIH Office for Protection from Research Risks. The IACUC adheres to national guidelines established in the Animal Welfare Act (7 U.S.C. Sections 2131-2159) and the Guide for the Care and Use of Laboratory Animals (8th Edition) as mandated by the U.S. Public Health Service Policy. The studies were conducted in accordance with the local legislation and institutional requirements. Written informed consent was obtained from the owners for the participation of their animals in this study.

## Author contributions

C-JS: Data curation, Formal analysis, Software, Visualization, Writing – original draft, Writing – review & editing. LW: Data curation, Formal analysis, Software, Supervision, Visualization, Writing – original draft, Writing – review & editing. ES: Data curation, Resources, Writing – review & editing. JC: Resources, Writing – review & editing. JT-G: Data curation, Project administration, Supervision, Writing – original draft, Writing – review & editing. AB-A: Resources, Writing – review & editing. AS: Resources, Writing – review & editing. SF: Resources, Writing – review & editing. SO: Resources, Writing – review & editing. SH: Conceptualization, Project administration, Writing – original draft, Writing – review & editing. LP: Conceptualization, Project administration, Writing – original draft, Writing – review & editing. MG: Conceptualization, Project administration, Supervision, Writing – original draft, Writing – review & editing.

## Funding

The author(s) declare financial support was received for the research, authorship, and/or publication of this article. This study was supported by grant P51 OD-011092 (Oregon National Primate Research Center), NIAID contract 75N93019C00070, Bill & Melinda Gates Foundation grants OPP1188079 and OPP1193500, grant P51 OD011425 to the Washington National Primate Research Center, with infrastructure support from NIAID contract HHSN272201800008C.

## Conflict of interest

OHSU and LP and SH have a significant financial interest in Vir Biotechnology, Inc., a company that may have a financial interest in the results of CMV-based vector research and technology. This potential individual and institutional conflict of interest has been reviewed and managed by OHSU.

The remaining authors declare that the research was conducted in the absence of any commercial or financial relationships that could be construed as a potential conflict of interest.

## Publisher's note

reviewers. Any product that may be evaluated in this article, or claim that may be made by its manufacturer, is not guaranteed or endorsed by the publisher.

## Supplementary material

The Supplementary Material for this article can be found online at: https://www.frontiersin.org/articles/10.3389/fimmu.2024.1460344/full#supplementary-material

SUPPLEMENTARY TABLE 1
Animal information (vaccine, sex, and age).

SUPPLEMENTARY TABLE 2
Global DE genes information (LFC, adjusted *p*-value, and cluster numbers).

SUPPLEMENTARY TABLE 3
IL-15 responsive protection signature and the overlapping genes.

SUPPLEMENTARY TABLE 4
Global enrichment information with associated genes.

SUPPLEMENTARY TABLE 5
Top upstream regulators information (z-score and *p*-value).

SUPPLEMENTARY TABLE 6
Four interleukin genes information (LFC and adjusted *p*-value).

SUPPLEMENTARY TABLE 7
Conserved DE genes information (LFC, adjusted *p*-value, and cluster numbers).

SUPPLEMENTARY TABLE 8
Conserved enrichment information with associated genes.

## References

1. World Health Organization. Global Tuberculosis Report 2023 (2023). Available online at: https://www.who.int/teams/global-tuberculosis-programme/tb-reports/global-tuberculosis-report-2023 (Accessed August 6, 2024).

2. Bu Q, Qiang R, Fang L, Peng X, Zhang H, Cheng H. Global trends in the incidence rates of MDR and XDR tuberculosis: Findings from the global burden of disease study 2019. *Front Pharmacol.* (2023) 14:1156249. doi: 10.3389/fphar.2023.1156249

3. Hansen SG, Piatak M Jr, Ventura AB, Hughes CM, Gilbride RM, Ford JC, et al. Immune clearance of highly pathogenic SIV infection. *Nature.* (2013) 502:100–4. doi: 10.1038/nature12519

4. Barrenäs F, Hansen SG, Law L, Driscoll C, Green RR, Smith E, et al. Interleukin-15 response signature predicts RhCMV/SIV vaccine efficacy. *PLoS Pathog.* (2021) 17: e1009278. doi: 10.1371/journal.ppat.1009278

5. Picker LJ, Lifson JD, Gale M Jr, Hansen SG, Früh K. Programming cytomegalovirus as an HIV vaccine. *Trends Immunol.* (2023) 44:287–304. doi: 10.1016/j.it.2023.02.001

6. Hansen SG, Marshall EE, Malouli D, Ventura AB, Hughes CM, Ainslie E, et al. A live-attenuated RhCMV/SIV vaccine shows long-term efficacy against heterologous SIV challenge. *Sci Transl Med.* (2019) 11:eaaw2607. doi: 10.1126/scitranslmed.aaw2607

7. Hansen SG, Zak DE, Xu G, Ford JC, Marshall EE, Malouli D, et al. Prevention of tuberculosis in rhesus macaques by a cytomegalovirus-based vaccine. *Nat Med.* (2018) 24:130–43. doi: 10.1038/nm.4473

8. Newman AM, Liu CL, Green MR, Gentles AJ, Feng W, Xu Y, et al. Robust enumeration of cell subsets from tissue expression profiles. *Nat Methods.* (2015) 12:453–7. doi: 10.1038/nmeth.3337

9. Newman AM, Steen CB, Liu CL, Gentles AJ, Chaudhuri AA, Scherer F, et al. Determining cell type abundance and expression from bulk tissues with digital cytometry. *Nat Biotechnol.* (2019) 37:773–82. doi: 10.1038/s41587-019-0114-2

10. Yi F, Hu J, Zhu X, Wang Y, Yu Q, Deng J, et al. Transcriptional profiling of human peripheral blood mononuclear cells stimulated by mycobacterium tuberculosis PPE57 identifies characteristic genes associated with type I interferon signaling. *Front Cell Infect Microbiol.* (2021) 11:716809. doi: 10.3389/fcimb.2021.716809

11. Szabo SJ, Kim ST, Costa GL, Zhang X, Fathman CG, Glimcher LH. A novel transcription factor, T-bet, directs Th1 lineage commitment. *Cell.* (2000) 100:655–69. doi: 10.1016/S0092-8674(00)80702-3

12. Zhang Y, Zhang Y, Gu W, Sun B. TH1/TH2 cell differentiation and molecular signals. *Adv Exp Med Biol.* (2014) 841:15–44. doi: 10.1007/978-94-017-9487-9_2

13. Fernandes M, Husi HORA. FCS, and PT strategies in functional enrichment analysis. *Methods Mol Biol.* (2021) 2361:163–78. doi: 10.1007/978-1-0716-1641-3_10

14. Masopust D, Picker LJ. Hidden memories: frontline memory T cells and early pathogen interception. *J Immunol.* (2012) 188:5811–7. doi: 10.4049/jimmunol.1102695

15. Picker LJ, Hansen SG, Lifson JD. New paradigms for HIV/AIDS vaccine development. *Annu Rev Med.* (2012) 63:95–111. doi: 10.1146/annurev-med-042010-085643

16. Méndez-Lagares G, Chin N, Chang WLW, Lee J, Rosás-Umbert M, Kieu HT, et al. Cytomegalovirus mediates expansion of IL-15-responsive innate-memory cells with SIV killing function. *J Clin Invest.* (2021) 131:e148542. doi: 10.1172/JCI148542

17. Malouli D, Gilbride RM, Wu HL, Hwang JM, Maier N, Hughes CM, et al. Cytomegalovirus-vaccine-induced unconventional T cell priming and control of SIV replication is conserved between primate species. *Cell Host Microbe.* (2022) 30:1207–1218.e7. doi: 10.1016/j.chom.2022.07.013

18. Picker LJ, Reed-Inderbitzin EF, Hagen SI, Edgar JB, Hansen SG, Legasse A, et al. IL-15 induces CD4+ effector memory T cell production and tissue emigration in nonhuman primates. *J Clin Invest.* (2006) 116:1514–24. doi: 10.1172/JCI27564

19. Verbist KC, Klonowski KD. Functions of IL-15 in anti-viral immunity: multiplicity and variety. *Cytokine.* (2012) 59:467–78. doi: 10.1016/j.cyto.2012.05.020

20. Jabri B, Abadie V. IL-15 functions as a danger signal to regulate tissue-resident T cells and tissue destruction. *Nat Rev Immunol.* (2015) 15:771–83. doi: 10.1038/nri3919

21. Guo Y, Luan L, Patil NK, Sherwood ER. Immunobiology of the IL-15/IL-15Ralpha complex as an antitumor and antiviral agent. *Cytokine Growth Factor Rev.* (2017) 38:10–21. doi: 10.1016/j.cytogfr.2017.08.002

22. Waldmann TA, Miljkovic MD, Conlon KC. Interleukin-15 (dys)regulation of lymphoid homeostasis: Implications for therapy of autoimmunity and cancer. *J Exp Med.* (2020) 217. doi: 10.1084/jem.20191062

23. Umemura M, Nishimura H, Saito K, Yajima T, Matsuzaki G, Mizuno S, et al. Interleukin-15 as an immune adjuvant to increase the efficacy of Mycobacterium bovis bacillus Calmette-Guérin vaccination. *Infect Immun.* (2003) 71:6045–8. doi: 10.1128/IAI.71.10.6045-6048.2003

24. Kolibab K, Yang A, Derrick SC, Waldmann TA, Perera LP, Morris SL. Highly persistent and effective prime/boost regimens against tuberculosis that use a multivalent modified vaccine virus ankara-based tuberculosis vaccine with interleukin-15 as a molecular adjuvant. *Clin Vaccine Immunol.* (2010) 17:793–801. doi: 10.1128/CVI.00006-10

25. Winchell CG, Nyquist SK, Chao MC, Maiello P, Myers AJ, Hopkins F, et al. CD8 + lymphocytes are critical for early control of tuberculosis in macaques. *J Exp Med.* (2023) 220:e20230707. doi: 10.1084/jem.20230707

26. Marshall E, Malouli D, Hansen SG, Gilbride RM, Hughes CM, Ventura AB, et al. Enhancing safety of cytomegalovirus vaccine vectors by engaging host intrinsic immunity. *Sci Transl Med.* (2019) 11:eaaw2603. doi: 10.1126/scitranslmed.aaw2603

27. Hansen SG, Vieville C, Whizin N, Coyne-Johnson L, Siess DC, Drummond DD, et al. Effector memory T cell responses are associated with protection of rhesus monkeys from mucosal simian immunodeficiency virus challenge. *Nat Med.* (2009) 15:293–9. doi: 10.1038/nm.1935

28. Hansen SG, Ford JC, Lewis MS, Ventura AB, Hughes CM, Coyne-Johnson L, et al. Profound early control of highly pathogenic SIV by an effector memory T cell vaccine. *Nature.* (2011) 473:523–7. doi: 10.1038/nature10003

29. Hansen SG, Sacha JB, Hughes CM, Ford JC, Burwitz BJ, Scholz I, et al. Cytomegalovirus vectors violate CD8+ T cell epitope recognition paradigms. *Science.* (2013) 340:1237874. doi: 10.1126/science.1237874

30. Martin M. Cutadapt removes adapter sequences from high-throughput sequencing reads. *EMBnet J.* (2011) 17:10–2. doi: 10.14806/ej.17.1.200

31. Andrews S. FastQC: A Quality Control Tool for High Throughput Sequence Data. Available online at: http://www.bioinformatics.babraham.ac.uk/projects/fastqc/ (Accessed May 1, 2024).

32. Langmead B, Salzberg SL. Fast gapped-read alignment with Bowtie 2. *Nat Methods.* (2012) 9:357–9. doi: 10.1038/nmeth.1923

33. Warren WC, Harris RA, Haukness M, Fiddes IT, Murali SC, Fernandes J, et al. Sequence diversity analyses of an improved rhesus macaque genome enhance its biomedical utility. *Science.* (2020) 370:eabc6617. doi: 10.1126/science.abc6617

34. Dobin A, Davis CA, Schlesinger F, Drenkow J, Zaleski C, Jha S, et al. STAR: ultrafast universal RNA-seq aligner. *Bioinformatics*. (2013) 29:15–21. doi: 10.1093/bioinformatics/bts635

35. Robinson MD, Oshlack A. A scaling normalization method for differential expression analysis of RNA-seq data. *Genome Biol*. (2010) 11:R25. doi: 10.1186/gb-2010-11-3-r25

36. Robinson MD, McCarthy DJ, Smyth GK. edgeR: a Bioconductor package for differential expression analysis of digital gene expression data. *Bioinformatics*. (2010) 26:139–40. doi: 10.1093/bioinformatics/btp616

37. Ritchie ME, Phipson B, Wu D, Hu Y, Law CW, Shi W, et al. limma powers differential expression analyses for RNA-sequencing and microarray studies. *Nucleic Acids Res*. (2015) 43:e47. doi: 10.1093/nar/gkv007

38. Law CW, Chen Y, Shi W, Smyth GK. voom: Precision weights unlock linear model analysis tools for RNA-seq read counts. *Genome Biol*. (2014) 15:R29. doi: 10.1186/gb-2014-15-2-r29

39. Mardia KV, Kent JT, Bibby JM. Multivariate analysis. *Acad Press*. (1979).

40. Becker RA, Chambers JM, Wilks AR. *The New S Language*. Monterey: Wadsworth & Brooks/Cole (1988).

41. Venables WN, Ripley BD. Modern applied statistics with S. *Stat Computing (SCO) Springer-Verlag*. (2002).

42. Gentleman RC, Carey VJ, Bates DM, Bolstad B, Dettling M, Dudoit S, et al. Bioconductor: open software development for computational biology and bioinformatics. *Genome Biol*. (2004) 5:R80. doi: 10.1186/gb-2004-5-10-r80

43. Langfelder P, Horvath S. WGCNA: an R package for weighted correlation network analysis. *BMC Bioinf*. (2008) 9:559. doi: 10.1186/1471-2105-9-559

44. Wan Q, Tang J, Han Y, Wang D. Co-expression modules construction by WGCNA and identify potential prognostic markers of uveal melanoma. *Exp Eye Res*. (2018) 166:13–20. doi: 10.1016/j.exer.2017.10.007

45. Wickham H. *ggplot2: Elegant Graphics for Data Analysis*. New York: Springer-Verlag (2016), ISBN: .

46. Larsson J, Gustafsson P. (2018). A case study in fitting area-proportional euler diagrams with ellipses using eulerr, in: *Proceedings of International Workshop on Set Visualization and Reasoning*. Edinburgh, United Kingdom: CEUR Workshop Proceedings. Vol. 2116. pp. 84–91.

47. Larsson J. *eulerr: Area-Proportional Euler and Venn Diagrams with Ellipses*. R package (2024). https://CRAN.R-project.org/package=eulerr (Accessed May 1, 2024).

48. Yu G, Wang LG, Han Y, He QY. clusterProfiler: an R package for comparing biological themes among gene clusters. *OMICS*. (2012) 16:284–7. doi: 10.1089/omi.2011.0118

49. Carlson M. *org.Hs.eg.db: Genome wide annotation for Human*. R package (2019). doi: 10.18129/B9.bioc.org.Hs.eg.db.

50. Shannon P, Markiel A, Ozier O, Baliga NS, Wang JT, Ramage D, et al. Cytoscape: a software environment for integrated models of biomolecular interaction networks. *Genome Res*. (2003) 13:2498–504. doi: 10.1101/gr.1239303

51. Krämer A, Green J, Pollard J Jr, Tugendreich S. Causal analysis approaches in Ingenuity Pathway Analysis. *Bioinformatics*. (2014) 30:523–30. doi: 10.1093/bioinformatics/btt703

frontiers | Frontiers in Immunology

TYPE Brief Research Report
PUBLISHED 28 October 2024
DOI 10.3389/fimmu.2024.1427510



OPEN ACCESS

EDITED BY
Anna Kathleen Coussens,
The University of Melbourne, Australia

REVIEWED BY
Suraj B. Sable,
Centers for Disease Control and Prevention (CDC), United States
Ben Gold,
Weill Cornell Medicine, United States
Brian Weinrick,
Trudeau Institute, United States

*CORRESPONDENCE
Rhea N. Coler
Rhea.Coler@Seattlechildrens.org

RECEIVED 03 May 2024
ACCEPTED 06 September 2024
PUBLISHED 28 October 2024

CITATION
Larsen SE, Abdelaal HFM, Plumlee CR, Cohen SB, Kim HD, Barrett HW, Liu Q, Harband MH, Berube BJ, Baldwin SL, Fortune SM, Urdahl KB and Coler RN (2024) The chosen few: *Mycobacterium tuberculosis* isolates for IMPAc-TB.
*Front. Immunol.* 15:1427510.
doi: 10.3389/fimmu.2024.1427510



# The chosen few: *Mycobacterium tuberculosis* isolates for IMPAc-TB

Sasha E. Larsen[1], Hazem F. M. Abdelaal[1], Courtney R. Plumlee[1], Sara B. Cohen[1], Ho D. Kim[1], Holly W. Barrett[1,2], Qingyun Liu[3], Matthew H. Harband[1], Bryan J. Berube[1], Susan L. Baldwin[1], Sarah M. Fortune[4,5], Kevin B. Urdahl[1,6,7] and Rhea N. Coler[1,2,7]*

[1]Seattle Children's Research Institute, Center for Global Infectious Disease Research, Seattle Children's, Seattle, WA, United States, [2]Department of Global Health, University of Washington, Seattle, WA, United States, [3]Department of Genetics, University of North Carolina at Chapel Hill, Chapel Hill, NC, United States, [4]Department of Immunology and Infectious Diseases, Harvard T. H. Chan School of Public Health, Boston, MA, United States, [5]Broad Institute of Massachusetts Institute of Technology (MIT), and Harvard, Cambridge, MA, United States, [6]Department of Immunology, University of Washington, Seattle, WA, United States, [7]Department of Pediatrics, University of Washington School of Medicine, Seattle, WA, United States

The three programs that make up the Immune Mechanisms of Protection Against *Mycobacterium tuberculosis* Centers (IMPAc-TB) had to prioritize and select strains to be leveraged for this work. The CASCADE team based at Seattle Children's Research Institute are leveraging M.tb H37Rv, M.tb CDC1551, and M.tb SA161. The HI-IMPACT team based at Harvard T.H. Chan School of Public Health, Boston, have selected M.tb Erdman as well as a novel clinical isolate recently characterized during a longitudinal study in Peru. The PHOENIX team also based at Seattle Children's Research Institute have selected M.tb HN878 and M.tb Erdman as their isolates of choice. Here, we describe original source isolation, genomic references, key virulence characteristics, and relevant tools that make these isolates attractive for use. The global context for M.tb lineage 2 and 4 selection is reviewed including what is known about their relative abundance and acquisition of drug resistance. Host–pathogen interactions seem driven by genomic differences on each side, and these play an important role in pathogenesis and immunity. The few M.tb strains chosen for this work do not reflect the vast genomic diversity within this species. They do, however, provide specific virulence, pathology, and growth kinetics of interest to the consortium. The strains selected should not be considered as "representative" of the growing available array of M.tb isolates, but rather tools that are being used to address key outstanding questions in the field.

KEYWORDS

***Mycobacterium tuberculosis*, tuberculosis, TB, lineages, diversity, isolates, IMPAc-TB**

# 1 Introduction

Across each of the Immune Mechanisms of Protection Against *Mycobacterium tuberculosis* Centers (IMPAc-TB), there are mechanistic questions of special focus. The CASCADE team at Seattle Children's Research Institute are examining the stages of infection through detailed interrogation of pulmonary pathology and natural or vaccine-induced protection across this continuum in mice, non-human primates, and human studies. The HI-IMPACT team based at Harvard T.H. Chan School of Public Health, Boston, are leveraging key immune correlates of protection from their seminal intravenous (IV) bacillus Calmette–Guérin (BCG) vaccination strategy in rhesus macaques (1, 2) and comparing those with human cohort responses with computational modeling to better design vaccines against tuberculosis (TB). The PHOENIX team based at Seattle Children's Research Institute are focused on a cross-species analysis of candidate vaccine-induced immunity and efficacy for prevention of disease or infection in preclinical mouse, guinea pig, and non-human primates as well as a human aerosol challenge model using BCG as a representative mycobacteria.

While these centers are focused on discrete but complementary work, each are using modeling, escalating from *in vitro* or *in silico* through *in vivo* preclinical and first-in-man experimental medicine studies. In the TB research field, we challenge *in vitro* or *in vivo* models with "representative" isolates of *Mycobacterium tuberculosis* (M.tb) that fit some categorical aspect of what we would like to examine or that provide continuity with previous work to continue a specific story. Recent data are challenging the use of "representative" to define our M.tb isolates of choice and instead suggest there is an underrepresentation of the breadth of biological diversity that exists in M.tb (3–5). Indeed, even preclinical drug therapy studies have demonstrated significant differences in *in vivo* sensitivity between M.tb strains (6). Next-generation tools and use of big data pipelines may allow us to better profile huge arrays of M.tb isolates or lineages in the near future, as groups within this consortium are already leveraging artificial intelligence and systems biology for complex data and predictive modeling.

In the absence of current or established tools that allow us to readily select challenge isolates spanning a vast array of M.tb lineages, it was necessary for each of the IMPAc-TB consortiums to choose the few they would study across their programs. The six strains used in the CASCADE (SCRI), HI-IMPACT (Harvard), or PHOENIX (SCRI) centers are described here (Table 1). We outline the source of each isolate, reference the sequenced genome if available, include specific tools in that background, give a summary of models using that strain, and provide seminal aspects of the isolate including virulence or kinetics if known and key historical work using that isolate. These basic features helped define the selection of isolates for specific consortium endpoints.

TABLE 1 M.tb isolates being used across the three IMPAc-TB consortiums.

| Program | Lineage 2 | Lineage 4 |
|---|---|---|
| CASCADE | SA161 | H37Rv, CDC1551 |
| HI-IMPACT | Clinical Peru Isolate | Erdman |
| PHOENIX | HN878 | Erdman |

# 2 Materials and methods

## 2.1 M.tb genome sequencing

### 2.1.1 Genomic DNA extraction

In order to obtain high-quality genomic DNA (gDNA) from M.tb cultures of all of the isolates except the g2g clinical isolate described above, we followed the methodology described previously (7). In summary, mycobacterial cultures (M.tb SA161, H37Rv, CDC1551, Erdman, and HN878) were grown to an optical density 600 nm (O.D. 600) of 1.5. Subsequently, the cultures were harvested by centrifugation, washed in PBS, and dissolved in TE buffer. To lyse the mycobacteria, the bacterial suspension was subjected to 80°C for 20 min. After allowing the tubes to cool to room temperature, lysozyme solution (100 mg/ml) was added to each tube, followed by incubation at 37°C for 3 h with intermittent mixing. Next, a mixture of SDS (10%) and proteinase K (20 mg/ml) was added to each tube in an 88:12 ratio. The tubes were then incubated at 65°C for 2 h. Following this incubation period, 100 µl of 5 M NaCl was added to each tube and incubated at 65°C for an additional 10 min. Subsequently, an 80 µl aliquot of 10% cetyl trimethyl ammonium bromide (CTAB) solution (Sigma-Aldrich, St. Louis, MO) was added, mixed thoroughly, and incubated at 65°C for another 10 min. The DNA was then extracted first with an equal volume of phenol/chloroform/isoamyl alcohol (25:24:1 v/v/v) and then with chloroform/isoamyl alcohol (24:1 v/v). The DNA was precipitated by adding 0.6 volumes of ice-cold isopropanol. The precipitated DNA was pelleted by centrifugation at 10,000 rpm and 4°C for 15 min. The resulting DNA pellets were washed with cold 75% ethanol and dried using a SpeedVac for 5 min. Finally, the genomic DNA was resuspended in 50 µl of sterile distilled water. The quality of the gDNA was assessed using a NanoDrop spectrophotometer (Thermo Scientific, Wilmington, DE).

### 2.1.2 Library production

Starting with a minimum of 750 ng of DNA, samples are sheared in a 96-well format using a Covaris LE220 focused ultrasonicator targeting 380-bp inserts. This insert size improves overall library performance and allows the longer sequencing read lengths on Illumina sequencing platforms (150 bp) to be efficiently used without producing a significant number of overlapping reads. The resulting sheared DNA was cleaned with Agencourt AMPure XP beads to remove sample impurities prior to library construction. Shearing was followed by size selection performed using the KAPA Hyper Prep kit (KR0961 v1.14). End-repair, A-tailing, and ligation are performed as directed. Two final AMPure cleanups are performed after ligation to remove excess adapter dimers from the library. All library construction steps are automated on the Perkin Elmer Janus platform. Library yield

was quantified using Quant-IT dsDNA High Sensitivity kit (Invitrogen Q33120). Libraries were validated in triplicate using the Bio-Rad CFX384 Real-Time System and KAPA Library Quantification Kit (KK4824).

#### 2.1.3 Whole-genome sequencing

Massively parallel sequencing-by-synthesis with fluorescently labeled, reversibly terminating nucleotides was carried out using the Illumina NovaSeq 6000 platform (RTA 3.1.5) and was performed at the University of Washington Center for Rare Disease Research (UW-CRDR). Barcoded genome libraries were pooled with liquid handling robotics prior to loading. Raw sequence reads with an average read length of 150 bp were assembled against the sequence of the reference strain M.tb H37Rv (NCBI accession number: NC_018143.2) using SPADES v3.15.4 (8). Whole-genome sequences were deposited into GenBank BioProject: PRJNA1051793, as described with specific accession numbers stated.

### 2.2 *In vivo* mouse challenge and survival studies

In all studies, mice were housed in the Seattle Children's Research Institute (SCRI) biosafety level 3 (BSL-3) animal facility under pathogen-free conditions and were handled in accordance with approved protocols from the SCRI Institutional Animal Care and Use Committee (IACUC). All methods were carried out in accordance with animal welfare guidelines and regulations. For survival studies, breeding pairs of C57BL/6 bg/bg (beige) mice were originally purchased through Jackson Laboratories. In-house bred male beige mice were used for experiments at 4–6 weeks of age and had not been previously used for breeding purposes. Mice were maintained at four animals per cage. Mice were challenged with a low-dose aerosol (target 25–100 CFU per mouse upon infection) of either M.tb SA161 or M.tb HN878 using a Glas-Col whole-body aerosol infection chamber. Bacterial burden was evaluated at 24 h and 4 weeks post challenge as previously described (9). Survival was monitored in 10 mice per group following M.tb infection. Animals with greater than 20% weight loss, or moribund condition, were euthanized. For ultra-low dose aerosol (targets 1–3 CFU per mouse upon infection) studies, female C57BL/6 mice purchased from Jackson Laboratories (age 8–27 weeks old) were challenged with either M.tb Erdman or M.tb H37Rv also using a Glas-Col whole-body aerosol infection chamber. Pulmonary bacterial burden was evaluated 35–42 days post challenge.

### 2.3 Statistical analysis

For *ex vivo* plating of organ homogenate to enumerate bacterial CFU in a single organ and timepoint (24 h, 4 weeks, or 6 weeks post-challenge), we used a two-tailed unpaired Student's t test to compare between M.tb challenge strains. For probability of survival, cohorts were compared using the log-rank Mantel–Cox test. All statistical analysis was performed using GraphPad Prism version 10.2.2.

## 3 Results

### 3.1 M.tb isolates

As the consortium matures, we are reflecting on opportunities to cross-validate or harmonize so the discrete but complimentary data being generated can have the largest impact for the TB pathogenesis, immunology, and vaccine communities. Interestingly, and without prior discussions, each of the programs focused their M.tb isolates across two modern lineages, 2 and 4. Lineage 2 is notable in its expanding global distribution, "hypervirulence," correlations with relapse, and enriched acquisition of antibiotic drug resistance (10–16). *In vitro*, lineage 2 Beijing isolates persist and grow normally within macrophages compared with other lineages that are relatively more inhibited once they are intracellular (17). These features make lineage 2 high-priority in preclinical studies for evaluation of disease progression and efficacy of vaccine candidates. M.tb isolates SA161 and HN878 and the clinical isolate from Peru are lineage 2 isolates represented in the IMPAc-TB consortiums. Lineage 4, the Euro-American lineage, is also well distributed globally and can be associated with unique features of disease pathology and treatment failure in humans (18–21). M.tb H37Rv, Erdman, and CDC1551 are each lineage 4 isolates being leveraged by one or more of the IMPAc-TB programs. Each isolates' key features and rationale for selection are described below.

### 3.2 M.tb HN878 (lineage 2)

M.tb HN878, a W-Beijing lineage isolate, was sourced by the PHOENIX consortium directly from BEI Resources (NR-13647). This clinical isolate was derived from a patient sample in Houston, Texas, in a 1990s outbreak and has been well studied since (22) with the parental genome sequence available on GenBank: ADNF01000000.1. Many other M.tb-derived materials including M.tb HN878 whole-cell lysate (NR-14824), derived lipid fraction (NR-14839), and genomic DNA (NR-14867) are available within the BEI Resources Repository. Defined as hypervirulent (23), M.tb HN878 induces a waning host T helper 1 (Th1) response and rapid expansion of regulatory T cells in chronic preclinical settings (22), as well as progressive pulmonary pathology and morbidity in C57BL/6 mice (24, 25). Interestingly, this isolate can acquire large genetic duplications with serial *in vitro* passage dramatically reducing virulence *in vivo* (25, 26). For the PHOENIX consortium, we generated a large batch single passage culture in 2019 to avoid the duplication issue and ensure continuity across studies, and we confirmed virulence of our stock culture in mouse survival studies (25). The single passage PHOENIX batch of M.tb HN878 was sequenced, and that genome can be found at GenBank: SAMN38797941.

The M.tb HN878 strain has been evaluated extensively *in vitro* as well as in preclinical mouse and guinea pig models of aerosol challenge. This includes recent examinations of single-cell preparations and of the influence of detergents on the

mycobacterial cell wall and their impacts on interactions with innate immune cells (27). *In vivo*, M.tb HN878 induces more granulomatous-like structures in preclinical models that better reflect human pathology than other well-used isolates (22, 23, 28). This includes induction of a blood-based TB transcriptional signature in C3HeB/FeJ mice by M.tb HN878 infection, whereas similar studies using less virulent M.tb H37Rv to infect C57BL/6 mice did not result in production of this human-derived biomarker of TB disease (29). Recent evidence suggests that while aerosol infection with a high dose of M.tb HN878 does induce bone-marrow-derived myelopoiesis, there is a concomitant reduction in trained innate immune responses in a mouse model (30). A key feature which led to the selection of this strain is that the high virulence of M.tb HN878 may be due to the preferential recruitment of pathology-inducing neutrophils and relatively damped adaptive responses (29). Despite the observed virulence and immune skewing from clinical M.tb HN878 isolate infection, prophylactic vaccination with BCG provides protection from bacterial burden and pulmonary pathology and enhances survival in several preclinical models (31–33). M.tb HN878 was selected by the PHOENIX consortium due to its well profiled virulence discussed above and its membership in lineage 2, which has high global prevalence. This M.tb isolate serves as a suitable strain to evaluate vaccine-specific efficacy in both prevention of infection (POI) and prevention of disease (POD) contexts, key components of the PHOENIX goals for the program. To our knowledge, this will also be the first time M.tb HN878 is used as a challenge strain in nonhuman primates.

## 3.3 M.tb SA161 (lineage 2)

M.tb SA161 is also a W-Beijing-type Lineage 2 isolate (34). SA161 is derived from a cluster of cases in Arkansas and was originally sourced by the CASCADE team from Dr. Ian Orme at Colorado State University (34). The M.tb SA161 being used by the Urdahl Lab in the CASCADE program was sequenced, and the genome sequence is deposited at GenBank: SAMN38797942.

Like M.tb HN878, SA161 is a highly virulent W-Beijing strain of M.tb (35). Historical data suggest that lineage 2 Beijing isolates may associate with TB infections in persons living with human immunodeficiency virus (PLWHIV) (35). As such, M.tb SA161 has been evaluated in several models with seminal features of HIV infection including mice transgenic for HIV transcription protein Tat (35). M.tb SA161 is frequently paired with highly susceptible mouse strains like C3HeB/FeJ to model high frequencies of pulmonary pathology and use survival as primary endpoints (32, 35). Despite the highly virulent M.tb—highly susceptible mouse strain pairing—prophylactic vaccination with BCG still affords protection from bacterial burden and pathology in both mouse and guinea pig infections at intermediate timepoints (32, 36). At later timepoints post challenge, W-Beijing strains M.tb HN878 and M.tb SA161 upregulate regulatory T-cell responses and the early protection wanes as mice succumb to high bacterial burden (> 6 Log10 CFU) and pathology in a more resistant C57BL/6 mouse strain (31), which was a key feature for its selection in this consortium.

At the start of the IMPAc-TB contract, the PHOENIX and CASCADE consortiums performed a head-to-head virulence survival study of M.tb SA161 and M.tb HN878 to both compare their relative virulence as lineage 2 members as well as infer any similarities or differences worth noting for future comparisons across programs. In this study, male Beige mice were challenged with a low-dose aerosol (25–100 CFU) of either lineage 2 isolate. Beige mice were used in this study because they are highly susceptible to mycobacterial infections and offered a compressed survival timeline (<200 days) for this exploratory head-to-head study. In addition, both in human epidemiology and in mouse preclinical studies, males are more sensitive to TB disease [well reviewed here (37)], which also afforded an accelerated assessment between M.tb isolates. Samples were collected 24 h post challenge to confirm deposition in lungs, and for HN878, we observed 23, 67, and 52 CFU per mouse (averaging 47 CFU) and 14, 31, and 59 CFU were observed for SA161 challenge (average 35 CFU; n=3 per group). At 4 weeks post challenge, lung and spleen bacterial burden were evaluated (n=6–7) with no significant difference in either site between the two challenge strains at this timepoint observed (Figures 1A, B). A cohort of mice (n=10 each) was followed for morbidity endpoints resulting in probability of survival over time (Figure 1C). The median survival for mice challenged with M.tb HN878 was 165 days, whereas the median survival for M.tb SA161 infected mice was 119.5 days.

In this comparative study, we observed a different survival profile in a Beige mouse background between M.tb HN878 and M.tb SA161 low-dose aerosol challenges, despite relatively equivalent bacterial burden at 4 week post challenge in both the lung and spleen. Interestingly, M.tb SA161 induces an earlier initiation of morbidity (day 88 to 151, 63 days of group decline) but the overall group mortality is more heterogeneous over time when compared with M.tb HN878 (day 144 to 172, 28 days of group decline), which seems to have a relatively delayed but more uniform morbidity of the total group. To our knowledge, this is the first report in male Beige mice for either M.tb isolate with these endpoints. This different pattern of morbidity between isolates in highly sensitive Beige mice mirrors that observed in the literature in more resistant C57BL/6 mice (31); however, the data reported here are less virulent in Beige mice comparatively by survival presumably due to the lower challenge dose at infection. In the context of the PHOENIX program where differences between vaccine groups are being evaluated, M.tb HN878 is a preferred isolate, but if, in contrast, interest is in the mechanism of disease progression and host variability in progressions to disease, then M.tb SA161 is a more reasonable strain to select. In the context of the CASCADE program, M.tb SA161 has been the primary isolate used to characterize pathological and immunological disease outcomes following vaccination due to its ability to generate large necrotic granulomas in the C3HeB/FeJ background. These profiles and specific endpoints of interest are well tailored to the overall objectives of the PHOENIX and CASCADE programs.

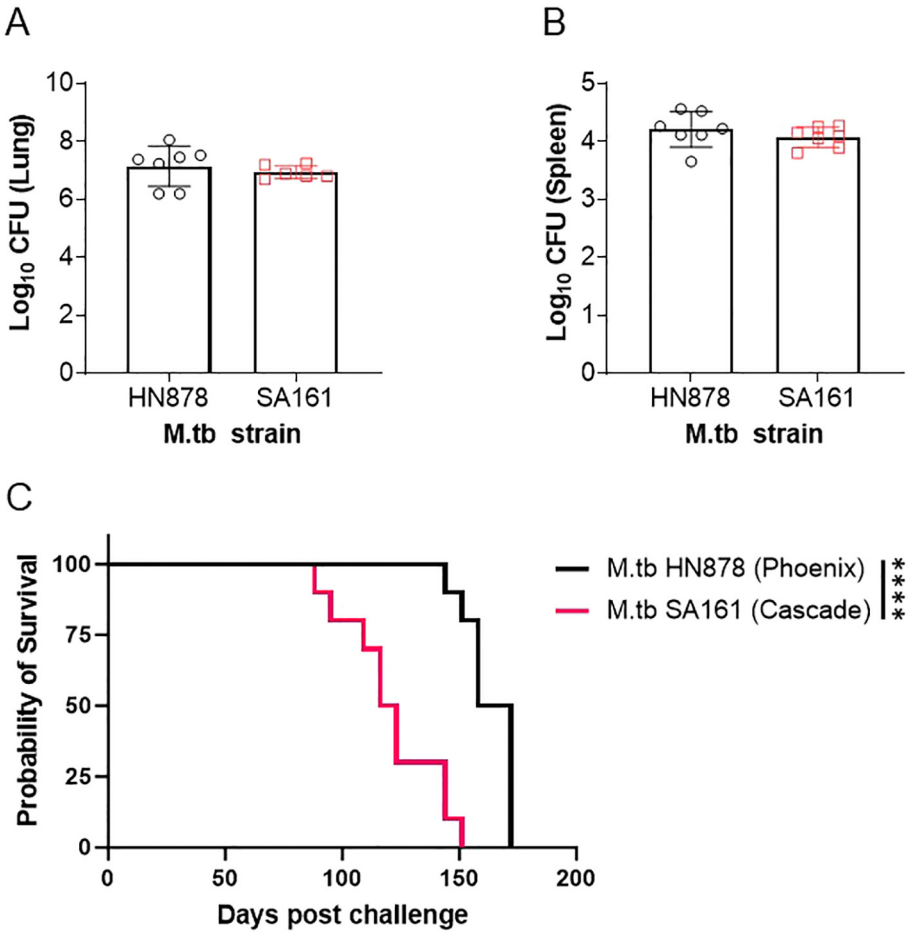


FIGURE 1
Survival of mice challenged with Beijing isolates of M.tb. Male Beige mice were challenged with a low-dose aerosol of either M.tb HN878 (open black circles) or M.tb SA161 (open red squares). At 4 weeks post-challenge, **(A)** lung and **(B)** spleen bacterial burden were evaluated in n=6-7. Two-tailed unpaired Student's t test found no significant differences between lung ($p = 0.4997$) or spleen ($p = 0.3365$) groups. Mean $Log_{10}$ CFU for lung = 7.1 HN878 and 6.9 for SA161. Mean $Log_{10}$ CFU for spleen = 4.2 HN878 and 4.0 for SA161 **(C)** Cohorts of = 10 mice per challenge (M.tb HN878 = black line or M.tb SA161 = red line) isolate were followed over time with weekly or more frequent weighing as a measure of morbidity due to infection. When mice reached 20% weight loss, they were considered moribund and humanely euthanized. Asterisks represent significance ($p < 0.0001$) between the groups using a Log-rank Mantel–Cox test comparing survival curves. Data representative of one experiment.

## 3.4 Clinical Peru isolate (lineage 2)

A distinct clinical isolate was recently discovered after the initiation of the IMPAc-TB program during a genome-to-genome (G2G) study conducted in Lima, Peru (38) (manuscript accepted, pending publication, SRA accession codes referenced there). This G2G study was designed to identify the genetic interaction between host genetic background and M.tb genetic background. The researchers discovered a single host variant (located in a non-coding region of the FLOT1 gene) that was associated with infection by a particular M.tb strain they called g2g-L2. They found the g2g-L2 strain locally emerged in Peru around 60 years ago but has since undergone rapid expansion. In a 2010 cohort, the g2g-L2 strain accounted for 6.6% of all M.tb strains circulating in Lima, Peru, but by 2020, the prevalence had almost doubled (12.6%). Additionally, it was shown that 87% of the g2g-L2 strains were in genomic clusters, whereas the clustering rates for the neighboring L2 clades were only 18% to 28%. These data indicate that the g2g-L2 strain has increased transmissibility in the local population. While the g2g-L2 strain can transmit successfully in Lima, Peru, it was not found elsewhere in the world. The authors also showed that g2g-L2 strains have a distinctive redox state compared with their nearest neighbor strains, manifested as a more oxidative cell state and resistance to reductive stress. The authors narrowed down a mutation (Thr2Asn) in trxB2 that was specific to the g2g-L2 strain, and they found that this trxB2 mutation can lead to higher activity of thioredoxin reductase and a significant shift in the NAD+/NADH ratio toward the oxidized state.

The authors delved into the underlying interaction between Mtb strains (g2g-L2 vs. nearest-neighbor strains, termed non-g2g-L2) and host immune cells with differing genetic backgrounds (FLOT1, AT vs. TT). RNA-seq analysis was employed to profile the innate immune response to M.tb infection, with the expression of 20 infection-responsive genes used to gauge the "infection score," where higher expression indicated a stronger response. The study revealed that overall, AT host cells exhibited an elevated infection

response compared with TT host cells. However, within the AT host cells, g2g-L2 infection blunted this response relative to non-g2g-L2 infection. Specifically, FLOT1-AT cells exhibited increased expression of genes associated with type 1 and type 2 interferon pro-inflammatory signaling, MHC-I antigen processing and presentation, IL-1B signaling, cytosolic DNA sensing, and zinc homeostasis. The authors posited that FLOT1-AT donors mount a robust transcriptional response to infection, potentially due to increased sensitivity in inducing innate responses. However, this response was skewed toward interferon following non-g2g-L2 infection, contrasting with IL-1B dominant responses observed after g2g-L2 infection. As the most recently isolated M.tb within the consortium, this g2g strain helps ground the clinical relevance of findings back to human epidemiologic data, a feature unique to the HI-IMPACT program.

## 3.5 M.tb Erdman (lineage 4)

M.tb Erdman K01 was sourced by the PHOENIX consortium directly from BEI Resources (NR-15404). This original clinical isolate was derived from human sputum at the Mayo Clinic in 1945 and is noted to be highly virulent (39). A low passage culture of M.tb Erdman was generated by the Coler Lab in the PHOENIX program. The stock material was sequenced and the assembled genome deposited at GenBank: SAMN38797939. A notable feature of M.tb Erdman was the development of a barcoded library (BEI Resources NR-50781) where each bacterium contains a unique and trackable sequence, enabling the profiling of a single cells' longitudinal fate *in vivo*. This library has been leveraged in non-human primate models coupled with pathology and imaging to interrogate individual lesion-level disease progression and infection dynamics (40).

M.tb Erdman has been extensively used for aerosol challenge with diversity outbred mice to identify critical gene loci (41–44), innate cell influx, pulmonary necrosis (45), and age-related influences (46) that correlate with a spectrum of disease in this model. In mice, prophylactic BCG vaccination provides protection from early pulmonary and peripheral bacterial burden after challenge with M.tb Erdman (33). Studies in cynomolgus macaques infected with M.tb Erdman identified peripheral blood transcriptional changes occurring early (<6 months) post infection (47), which share similarities with human risk signatures predicting advancement to active TB disease. The similarities in risk signatures between M.tb Erdman-infected macaques and humans highlights the usefulness of this model to predict vaccine outcomes in humans.

## 3.6 M.tb H37Rv (lineage 4)

M.tb H37 was isolated from a human lung sample at the Trudeau Laboratory in 1905. M.tb H37Rv was derived from this isolate after selection for rough colony morphology and virulence in 1934 (48) and is one of the most widely used strains of M.tb available. Despite researchers identifying notable polymorphisms between M.tb H37Rv isolates maintained in different laboratories (49), the M.tb H37Rv genome is commonly used as the base reference. Indeed, antigens included in high-priority clinical vaccine candidates are sourced from the H37Rv genome, including ID93 (50), M72 (51), GamTBvac (52), and H107e (53). The M.tb H37Rv being leveraged by the CASCADE consortium was a gift from the lab of Dr. Joel Ernst. This isolate was derived from ATCC TMC 102 (catalog #27294), and the genome was partially sequenced and published in 1998. Despite this isolate serving as the *de facto* M.tb genome reference, the full genome sequence was only recently completed, comprising over 6,000 novel base pair regions, using a new paradigm of assembly called Bact-Builder (54). The CASCADE program M.tb H37Rv strain has been serially passaged through mice and has maintained virulence properties compared with other lab-adapted strains, perhaps through retention of the virulence factor PDIM, which is rapidly lost upon *in vitro* passage (55). The CASCADE M.tb H37Rv isolate was sequenced, and that assembled genome can be found at GenBank: SAMN38797937.

Like M.tb Erdman, M.tb H37Rv has been developed as a barcoded strain, allowing for the individual tracking and monitoring of deposited bacteria at the time of challenge and through chronic timepoints of infection and disease (56). This is an especially useful tool in the context of ultra-low-dose aerosol infections where as few as one bacterium per mouse is inhaled and monitored over time (56), better reflecting the conditions of human challenge. In general, M.tb H37Rv laboratory isolates are notably less virulent across models, with higher rates of survival and less necrotic lesions in the translational guinea pig preclinical model compared with other strains being used in this program including M.tb Erdman, M.tb HN878, or M.tb CDC1551 (23). Lower virulence of M.tb H37Rv compared with M.tb Erdman has also been observed in a New Zealand White rabbit model of aerosol challenge by 5 weeks post infection (57). Despite these reports, the CASCADE M.tb H37Rv isolate has similar virulence to M.tb Erdman and is more virulent than M.tb CDC1551, in studies by the group in C57BL/6 mice (Figure 2 and article by some of these same authors presented in this special issue (58), respectively). These patterns of virulence align with prior studies using the CASCADE programs' M.tb H37Rv in C57BL/6 mice (56, 59). As such, the CASCADE program has used H37Rv as the primary lineage 4 strain to draw direct comparisons with M.tb SA161. Interestingly, in a BALB/c drug therapy model, different isolates of M.tb H37Rv were similarly sensitive to front-line drug treatment with rifampicin, isoniazid, and pyrazinamide as M.tb Erdman (6). However, M.tb H37Rv has been the strain of choice to date when assessing genetic components influencing host susceptibility in the context of the collaborative cross mice (60–63).

## 3.7 M.tb CDC1551 (lineage 4)

M.tb CDC1551 is a clinical isolate collected in the mid-1990s amid an outbreak with uncharacteristically highly positive tuberculin skin testing rates in rural Kentucky and Tennessee (64). The CASCADE M.tb CDC1551 isolate, originally a gift from W.R. Bishai, was sequenced, and that assembled genome can be found at GenBank: SAMN38797940. The BEI repository hosts numerous M.tb CDC1551-derived materials including cell lysate (NR-14835), polyclonal anti-sera from a guinea pig infection (NR-

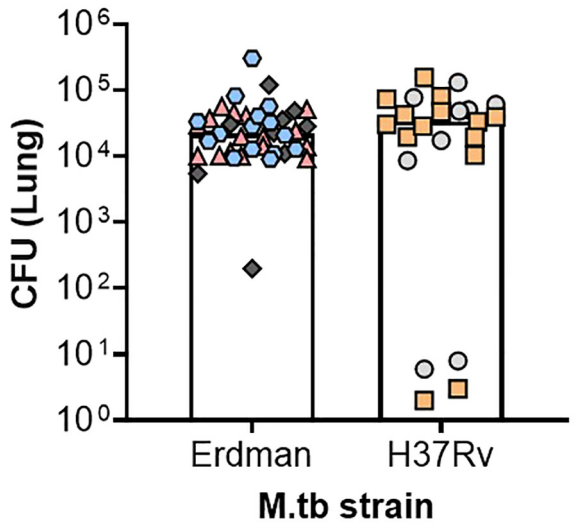


FIGURE 2
Comparable pulmonary bacterial burden between M.tb H37Rv and Erdman after ultra-low-dose challenge. Female C57BL/6 mice were challenged between 8 and 27 weeks of age with an ultra-low-dose challenge of either M.tb Erdman or M.tb H37Rv. At 35–42 days post-infection, lung bacterial burden was evaluated. Data depict six different challenge experiments, denoted in the figure as different-colored shapes, where each shape represents an individual mouse whose CFU was over 1. Two-tailed unpaired Student's t test found no significant differences between the challenged groups ($p = 0.5196$) where the mean CFU for M.tb Erdman was $3.4 \times 10^4$ and for M.tb H37Rv was $4.2 \times 10^4$.

13818), genomic DNA (NR-48981), and a large assortment of transposon mutants. Live-attenuated vaccines are gaining traction in the TB research community, and one notable vaccine based in a parent CD1551 background is M.tbΔsigH (65).

M.tb H37Rv, M.tb Erdman, and M.tb CDC1551 contain a frame-shift deletion in a gene cluster responsible for phenolic glycolipid (PGL) production, resulting in a relatively reduced virulence compared with lineage 2 isolates (including M.tb HN878) which do not contain this deletion (66). Furthermore, prophylactic BCG vaccination provides better protection against these lineage 4 isolates compared with lineage 2 isolates in an intravenous infectious challenge of pooled barcoded M.tb in a C57BL/6 mouse model (67). Although the initial paper describing this strain in an *in vivo* mouse model found that, when compared with M.tb Erdman, M.tb CDC1551 expanded rapidly and notably reached two logs higher lung bacterial burden by day 20 (64), curiously, the M.tb Erdman peaked at ~$10^4$, which is ~2 logs lower than the typical CFU load following infection with virulent M.tb strains, such as M.tb Erdman or M.tb H37Rv. A subsequent study found that M.tb CDC1551 was actually less virulent than several other M.tb strains tested, including M.tb H37Rv, M.tb Erdman, and M.tb HN878, while inducing a more hyperinflammatory immune response (68). Consistent with the more recent study, the CASCADE M.tb CDC1551 isolate is less virulent in C57BL/6 mice than the CASCADE M.tb H37Rv isolate, with an approximately 1-log reduction in the peak lung bacterial burden.

# 4 Discussion

Aside from strain identity and genome sequence, there are many factors that influence how M.tb can behave both *in vitro* and *in vivo*. This includes culture conditions like the presence, absence, or concentration of Tween which directly changes the cell wall and some subsequent interactions with host cells (69–71) or growth medium albumin choice. Large first stock batches are made for each consortium where M.tb were grown in 10% OADC, 0.05% Tween, and in the absence of $C0_2$. For enumeration for mouse infection studies, the CASCADE program uses OD600nm of 1.0 and Phoenix uses direct CFU plating of aliquots and both programs combine these results with empirical titration experiments to determine nebulizer stock dilutions to attain the infection range per mouse desired. The Coler, Fortune, and Urdahl labs serve as distributor partners for each consortium where large low-passage batches (>900 1.0-ml aliquots in the case of the PHOENIX program) are made and stocks are distributed to contract partners to reduce the influence of strain passage on results obtained within each consortium. Annual CFU plating by all partners is a contract deliverable for some of the consortiums as a simple and direct check that stocks remain viable and at or near expected CFU. The status of specific lipids, like phthiocerol dimycocerosates (PDIMs) on the bacterial cell envelope, which have been observed to affect pathogenesis and virulence, is a similar factor important for understanding and comparing M.tb strain outcomes (72). The mouse-passaged M.tb H37Rv used by the CASCADE program recently confirmed PDIM status (73), and M.tb Erdman was similarly confirmed prior to DNA barcoding (40) and no subsequent colony purification occurred. PDIM status was not a planned screen throughout the program, although we acknowledge that this could affect results.

While each program is using different isolates, they are consistently from lineages 2 and 4, which provides some harmony of interest. Importantly, each isolate suits the needs of each consortium; for example, CASCADE is mechanistically interrogating the diversity of the immune response including pathology endpoints and the variability within an M.tb SA161 infection, possibly identifying key differences in disease progression. Conversely, PHOENIX is interested in vaccine efficacy endpoints and M.tb HN878 provides a more homologous response and disease progression that affords resolution between immunization strategies. The ability of HI-IMPACT to leverage a recent clinical isolate with a direct relationship to epidemiological data and human genetic variabilities make their work in preclinical models highly translational and informative. However, this collective work has excluded other lineages, including 1 and 3 which are found in Southeast Asian countries like Indonesia and the Philippines, which are among the top eight high-TB burden countries globally (74). Should these consortiums find critical disparities in relative immune responses or protection from vaccinations, it would be necessary to perform similar analyses using lineages 1 and 3. Other *ex vivo* tools like the mycobacterial growth inhibition assay (75–77), which allow for multiple challenge isolates to be used, are also being integrated into specific programs

and may help address this need for an increased breadth of M.tb challenges to increase the scope of findings and areas of follow-up.

By identifying salient differences between strains being used across the three programs, we aim to transparently identify what may be common findings versus those that may be unique due to model organism selection. It is clear from the literature that whole-genome sequencing can reveal key genes involved in drug resistance, adaptations to stress conditions, and virulence of M.tb isolates (78–80). The sequences reported here aim to contribute to those efforts and provide pathogen genomic comparators for phenotypic outcomes across the consortium. Future work will align the sequences reported here to parent lineage-specific reference genomes available, clinical isolates, and an ancestral, non-lineage-specific, M.tb complex genome (termed $MTBC_0$) (81). We expect that placing these isolates in the advanced phylogeny available for M.tb, through a number of platforms such as TB-Annotator (82) or MAGMA (83), will provide more opportunities to further link protection or pathogenic outcomes derived from IMPAc-TB with existing literature and clinical trends. In addition to M.tb isolate identity, the consortium is actively discussing challenge doses and how this directly influences outcomes in the preclinical models being studied. Furthermore, use of diversity outbred and collaborative cross mouse strains is an acknowledgement that host diversity plays a significant role in TB outcomes and may help uncover critical immune correlates of immunity.

## Data availability statement

The datasets presented in this study can be found in online repositories. The names of the repository/repositories and accession number(s) can be found below: https://www.ncbi.nlm.nih.gov/genbank/, BioProject: PRJNA1051793.

## Ethics statement

The animal study was approved by Seattle Childrens' Research Institute Animal Care and Use Committee. The study was conducted in accordance with the local legislation and institutional requirements.

## Author contributions

SL: Conceptualization, Formal analysis, Investigation, Project administration, Resources, Visualization, Writing – original draft. HA: Data curation, Investigation, Software, Writing – original draft. CP: Resources, Writing – review & editing. SC: Writing – review & editing. HK: Investigation, Resources, Writing – review & editing. QL: Writing – original draft. MH: Investigation, Resources, Writing – review & editing. BB: Writing – review & editing. SB: Writing – review & editing. SF: Funding acquisition, Writing – review & editing. KU: Funding acquisition, Writing – review & editing. RC: Funding acquisition, Project administration, Supervision, Writing – review & editing. HB: Investigation, Visualization, Writing – review & editing.

## Funding

The author(s) declare financial support was received for the research, authorship, and/or publication of this article. This project has been funded in whole or in part with Federal funds from the National Institute of Allergy and Infectious Diseases, National Institutes of Health, Department of Health and Human Services, under Contract Nos. 75N93021C00029 (to RC), 75N93019C00070 (to KU), and 75N93019C00071 (to SF). Additional support was from the National Institute of Allergy and Infectious Diseases, National Institutes of Health, under contract number P30AI168023 for the Seattle Tuberculosis Research Advancement Center - SEATRAC. The content is solely the responsibility of the authors and does not necessarily represent the official views of the National Institutes of Health.

## Acknowledgments

The authors would like to thank all consortium partner institutions for their collaboration and dedication to advancing our knowledge about protective mechanisms against M.tb. The following reagents were obtained through BEI Resources by the Coler Lab, NIAID, NIH: *Mycobacterium tuberculosis*, Strain HN878, NR-13647, and Strain Erdman K01, NR-15404. The authors acknowledge Research Scientific Computing at Seattle Children's Research Institute for providing HPC resources that have contributed to the research results reported within this paper. The authors would also like to thank the SCRI Office of Animal Care (OAC) for their management of animal resources.

## Conflict of interest

The authors declare that the research was conducted in the absence of any commercial or financial relationships that could be construed as a potential conflict of interest.

The author(s) declared that they were an editorial board member of Frontiers, at the time of submission. This had no impact on the peer review process and the final decision.

## Publisher's note

# References


1. Darrah PA, Zeppa JJ, Maiello P, Hackney JA, Wadsworth MH 2nd, Hughes TK, et al. Prevention of tuberculosis in macaques after intravenous BCG immunization. *Nature*. (2020) 577(7788):95–102. doi: 10.1038/s41586-019-1817-8

2. Larson EC, Ellis-Connell AL, Rodgers MA, Gubernat AK, Gleim JL, Moriarty RV, et al. Intravenous bacille calmette-guérin vaccination protects simian immunodeficiency virus-infected macaques from tuberculosis. *Nat Microbiol*. (2023) 8(11):2080–92. doi: 10.1038/s41564-023-01503-x

3. O'Neill MB, Mortimer TD, Pepperell CS. Diversity of Mycobacterium tuberculosis across evolutionary scales. *PloS Pathog*. (2015) 11(11):e1005257. doi: 10.1371/journal.ppat.1005257

4. Stanley S, Spaulding CN, Liu Q, Chase MR, Ha DTM, Thai PVK, et al. High-throughput phenogenotyping of Mycobacteria tuberculosis clinical strains reveals bacterial determinants of treatment outcomes. *bioRxiv*. (2023). doi: 10.1101/2023.04.09.536166

5. Smith CM, Sassetti CM. Modeling diversity: Do homogeneous laboratory strains limit discovery? *Trends Microbiol*. (2018) 26(11):892–5. doi: 10.1016/j.tim.2018.08.002

6. De Groote MA, Gruppo V, Woolhiser LK, Orme IM, Gilliland JC, Lenaerts AJ. Importance of confirming data on the *in vivo* efficacy of novel antibacterial drug regimens against various strains of Mycobacterium tuberculosis. *Antimicrob Agents Chemother*. (2012) 56(2):731–8. doi: 10.1128/aac.05701-11

7. Abdelaal HFM, Spalink D, Amer A, Steinberg H, Hashish EA, Nasr EA, et al. Genomic polymorphism associated with the emergence of virulent isolates of mycobacterium bovis in the nile delta. *Sci Rep*. (2019) 9(1):11657. doi: 10.1038/s41598-019-48106-3

8. Bankevich A, Nurk S, Antipov D, Gurevich AA, Dvorkin M, Kulikov AS, et al. Spades: A new genome assembly algorithm and its applications to single-cell sequencing. *J Comput Biol*. (2012) 19(5):455–77. doi: 10.1089/cmb.2012.0021

9. Larsen SE, Erasmus JH, Reese VA, Pecor T, Archer J, Kandahar A, et al. An RNA-based vaccine platform for use against Mycobacterium tuberculosis. *Vaccines (Basel)*. (2023) 11(1):130. doi: 10.3390/vaccines11010130

10. Merker M, Blin C, Mona S, Duforet-Frebourg N, Lecher S, Willery E, et al. Evolutionary history and global spread of the Mycobacterium tuberculosis beijing lineage. *Nat Genet*. (2015) 47(3):242–9. doi: 10.1038/ng.3195

11. Glynn JR, Whiteley J, Bifani PJ, Kremer K, van Soolingen D. Worldwide occurrence of Beijing/W strains of Mycobacterium tuberculosis: A systematic review. *Emerg Infect Dis*. (2002) 8(8):843–9. doi: 10.3201/eid0805.020002

12. Kikuchi T, Nakamura M, Hachisu Y, Hirai S, Yokoyama E. Molecular epidemiological analysis of Mycobacterium tuberculosis modern beijing genotype strains isolated in chiba prefecture over 10 years. *J Infect Chemother*. (2022) 28(4):521–5. doi: 10.1016/j.jiac.2021.12.020

13. Shaik J, Pillay M, Moodley J, Jeena P. Predominance of the Mycobacterium tuberculosis beijing strain amongst children from a high tuberculosis burden township in South Africa. *Tuberculosis (Edinb)*. (2022) 136:102250. doi: 10.1016/j.tube.2022.102250

14. Barbier M, Wirth T. The evolutionary history, demography, and spread of the Mycobacterium tuberculosis complex. *Microbiol Spectr*. (2016) 4(4). doi: 10.1128/microbiolspec.TBTB2-0008-2016

15. Tsolaki AG, Gagneux S, Pym AS, Goguet de la Salmoniere YO, Kreiswirth BN, Van Soolingen D, et al. Genomic deletions classify the Beijing/W strains as a distinct genetic lineage of Mycobacterium tuberculosis. *J Clin Microbiol*. (2005) 43(7):3185–91. doi: 10.1128/jcm.43.7.3185-3191.2005

16. He C, Cheng X, Kaisaier A, Wan J, Luo S, Ren J, et al. Effects of Mycobacterium tuberculosis lineages and regions of difference (Rd) virulence gene variation on tuberculosis recurrence. *Ann Transl Med*. (2022) 10(2):49. doi: 10.21037/atm-21-6863

17. Adams KN, Verma AK, Gopalaswamy R, Adikesavalu H, Singhal DK, Tripathy S, et al. Diverse clinical isolates of Mycobacterium tuberculosis develop macrophage-induced rifampin tolerance. *J Infect Dis*. (2019) 219(10):1554–8. doi: 10.1093/infdis/jiy710

18. Stucki D, Brites D, Jeljeli L, Coscolla M, Liu Q, Trauner A, et al. Mycobacterium tuberculosis lineage 4 comprises globally distributed and geographically restricted sublineages. *Nat Genet*. (2016) 48(12):1535–43. doi: 10.1038/ng.3704

19. Nahid P, Bliven EE, Kim EY, Mac Kenzie WR, Stout JE, Diem L, et al. Influence of M. tuberculosis lineage variability within a clinical trial for pulmonary tuberculosis. *PloS One*. (2010) 5(5):e10753. doi: 10.1371/journal.pone.0010753

20. He CJ, Wan JL, Luo SF, Guo RJ, Paerhati P, Cheng X, et al. Comparative study on tuberculosis drug resistance and molecular detection methods among different Mycobacterium tuberculosis lineages. *Infect Drug Resist*. (2023) 16:5941–51. doi: 10.2147/idr.S423390

21. Du DH, Geskus RB, Zhao Y, Codecasa LR, Cirillo DM, van Crevel R, et al. The effect of M. tuberculosis lineage on clinical phenotype. *PloS Glob Public Health*. (2023) 3(12):e0001788. doi: 10.1371/journal.pgph.0001788

22. Ordway D, Henao-Tamayo M, Harton M, Palanisamy G, Troudt J, Shanley C, et al. The hypervirulent Mycobacterium tuberculosis strain HN878 induces a potent TH1 response followed by rapid down-regulation. *J Immunol*. (2007) 179(1):522–31. doi: 10.4049/jimmunol.179.1.522

23. Palanisamy GS, Smith EE, Shanley CA, Ordway DJ, Orme IM, Basaraba RJ. Disseminated disease severity as a measure of virulence of Mycobacterium tuberculosis in the guinea pig model. *Tuberculosis (Edinb)*. (2008) 88(4):295–306. doi: 10.1016/j.tube.2007.12.003

24. Baldwin SL, Reese VA, Huang PW, Beebe EA, Podell BK, Reed SG, et al. Protection and long-lived immunity induced by the Id93/Gla-se vaccine candidate against a clinical Mycobacterium tuberculosis isolate. *Clin Vaccine Immunol*. (2016) 23(2):137–47. doi: 10.1128/cvi.00458-15

25. Berube BJ, Larsen SE, McNeil MB, Reese VA, Pecor T, Kaur S, et al. Characterizing *in vivo* loss of virulence of an Hn878 Mycobacterium tuberculosis isolate from a genetic duplication event. *Tuberculosis (Edinb)*. (2022) 137:102272. doi: 10.1016/j.tube.2022.102272

26. Domenech P, Rog A, Moolji JU, Radomski N, Fallow A, Leon-Solis L, et al. Origins of a 350-kilobase genomic duplication in Mycobacterium tuberculosis and its impact on virulence. *Infect Immun*. (2014) 82(7):2902–12. doi: 10.1128/iai.01791-14

27. Mittal E, Roth AT, Seth A, Singamaneni S, Beatty W, Philips JA. Single cell preparations of Mycobacterium tuberculosis damage the mycobacterial envelope and disrupt macrophage interactions. *Elife*. (2023) 12:e85416. doi: 10.7554/eLife.85416

28. Choreño-Parra JA, Bobba S, Rangel-Moreno J, Ahmed M, Mehra S, Rosa B, et al. Mycobacterium tuberculosis Hn878 infection induces human-like B-cell follicles in mice. *J Infect Dis*. (2020) 221(10):1636–46. doi: 10.1093/infdis/jiz663

29. Moreira-Teixeira L, Tabone O, Graham CM, Singhania A, Stavropoulos E, Redford PS, et al. Mouse transcriptome reveals potential signatures of protection and pathogenesis in human tuberculosis. *Nat Immunol*. (2020) 21(4):464–76. doi: 10.1038/s41590-020-0610-z

30. Maceiras AR, Silvério D, Gonçalves R, Cardoso MS, Saraiva M. Infection with hypervirulent Mycobacterium tuberculosis triggers emergency myelopoiesis but not trained immunity. *Front Immunol*. (2023) 14:1211404. doi: 10.3389/fimmu.2023.1211404

31. Ordway DJ, Shang S, Henao-Tamayo M, Obregon-Henao A, Nold L, Caraway M, et al. Mycobacterium bovis BCG-mediated protection against W-Beijing strains of Mycobacterium tuberculosis is diminished concomitant with the emergence of regulatory T cells. *Clin Vaccine Immunol*. (2011) 18(9):1527–35. doi: 10.1128/cvi.05127-11

32. Henao-Tamayo M, Obregón-Henao A, Creissen E, Shanley C, Orme I, Ordway DJ. Differential mycobacterium bovis BCG vaccine-derived efficacy in C3heb/Fej and C3h/Heouj mice exposed to a clinical strain of Mycobacterium tuberculosis. *Clin Vaccine Immunol*. (2015) 22(1):91–8. doi: 10.1128/cvi.00466-14

33. Jeon BY, Derrick SC, Lim J, Kolibab K, Dheenadhayalan V, Yang AL, et al. Mycobacterium bovis BCG immunization induces protective immunity against nine different Mycobacterium tuberculosis strains in mice. *Infect Immun*. (2008) 76(11):5173–80. doi: 10.1128/iai.00019-08

34. Palanisamy GS, DuTeau N, Eisenach KD, Cave DM, Theus SA, Kreiswirth BN, et al. Clinical strains of Mycobacterium tuberculosis display a wide range of virulence in guinea pigs. *Tuberculosis (Edinb)*. (2009) 89(3):203–9. doi: 10.1016/j.tube.2009.01.005

35. Honda JR, Shang S, Shanley CA, Caraway ML, Henao-Tamayo M, Chan ED, et al. Immune responses of HIV-1 tat transgenic mice to Mycobacterium tuberculosis W-Beijing SA161. *Open AIDS J*. (2011) 5:86–95. doi: 10.2174/1874613601105010086

36. Obregón-Henao A, Shanley C, Bianco MV, Cataldi AA, Basaraba RJ, Orme IM, et al. Vaccination of guinea pigs using mce operon mutants of Mycobacterium tuberculosis. *Vaccine*. (2011) 29(26):4302–7. doi: 10.1016/j.vaccine.2011.04.027

37. Gupta M, Srikrishna G, Klein SL, Bishai WR. Genetic and hormonal mechanisms underlying sex-specific immune responses in tuberculosis. *Trends Immunol*. (2022) 43(8):640–56. doi: 10.1016/j.it.2022.06.004

38. Luo Y, Huang C-C, Liu Q, Howard N, Li X, Zhu J, et al. A Flot1 host regulatory allele is associated with a recently expanded mtb clade in patients with tuberculosis. *medRxiv*. (2022) 2022.02.07.22270622. doi: 10.1101/2022.02.07.22270622

39. Miyoshi-Akiyama T, Matsumura K, Iwai H, Funatogawa K, Kirikae T. Complete annotated genome sequence of Mycobacterium tuberculosis erdman. *J Bacteriol*. (2012) 194(10):2770. doi: 10.1128/jb.00353-12

40. Martin CJ, Cadena AM, Leung VW, Lin PL, Maiello P, Hicks N, et al. Digitally barcoding Mycobacterium tuberculosis reveals *in vivo* infection dynamics in the macaque model of tuberculosis. *mBio*. (2017) 8(3):e00312–17. doi: 10.1128/mBio.00312-17

41. Gatti DM, Tyler AL, Mahoney JM, Churchill GA, Yener B, Koyuncu D, et al. Systems genetics uncover new loci containing functional gene candidates in Mycobacterium tuberculosis-infected diversity outbred mice. *bioRxiv*. (2023). doi: 10.1101/2023.12.21.572738

42. Kurtz SL, Mittereder LR, Lehman CC, Khan H, Gould VA, Elkins KL. Intravenous BCG vaccination of diversity outbred mice results in moderately enhanced protection against challenge with Mycobacterium tuberculosis compared to intradermal vaccination. *Infect Immun*. (2023) 91(7):e0016823. doi: 10.1128/iai.00168-23

43. Koyuncu D, Niazi MKK, Tavolara T, Abeijon C, Ginese ML, Liao Y, et al. Cxcl1: A new diagnostic biomarker for human tuberculosis discovered using diversity outbred mice. *PloS Pathog*. (2021) 17(8):e1009773. doi: 10.1371/journal.ppat.1009773

44. Tavolara TE, Niazi MKK, Gower AC, Ginese M, Beamer G, Gurcan MN. Deep learning predicts gene expression as an intermediate data modality to identify susceptibility patterns in Mycobacterium tuberculosis infected diversity outbred mice. *EBioMedicine*. (2021) 67:103388. doi: 10.1016/j.ebiom.2021.103388

45. Niazi MK, Dhulekar N, Schmidt D, Major S, Cooper R, Abeijon C, et al. Lung necrosis and neutrophils reflect common pathways of susceptibility to Mycobacterium tuberculosis in genetically diverse, immune-competent mice. *Dis Model Mech*. (2015) 8 (9):1141–53. doi: 10.1242/dmm.020867

46. Harrison DE, Astle CM, Niazi MKK, Major S, Beamer GL. Genetically diverse mice are novel and valuable models of age-associated susceptibility to Mycobacterium tuberculosis. *Immun Ageing*. (2014) 11(1):24. doi: 10.1186/s12979-014-0024-6

47. Gideon HP, Skinner JA, Baldwin N, Flynn JL, Lin PL. Early whole blood transcriptional signatures are associated with severity of lung inflammation in cynomolgus macaques with Mycobacterium tuberculosis infection. *J Immunol (Baltimore Md 1950)*. (2016) 197(12):4817–28. doi: 10.4049/jimmunol.1601138

48. Steenken W, Oatway WH, Petroff SA. Biological studies of the tubercle bacillus : III. dissociation and pathogenicity of the R and S variants of the human tubercle bacillus (H(37)). *J Exp Med*. (1934) 60(4):515–40. doi: 10.1084/jem.60.4.515

49. Ioerger TR, Feng Y, Ganesula K, Chen X, Dobos KM, Fortune S, et al. Variation among genome sequences of H37Rv strains of Mycobacterium tuberculosis from multiple laboratories. *J Bacteriol*. (2010) 192(14):3645–53. doi: 10.1128/jb.00166-10

50. Baldwin SL, Reese V, Granger B, Orr MT, Ireton GC, Coler RN, et al. The Id93 tuberculosis vaccine candidate does not induce sensitivity to purified protein derivative. *Clin Vaccine Immunol*. (2014) 21(9):1309–13. doi: 10.1128/CVI.00372-14

51. Skeiky YA, Lodes MJ, Guderian JA, Mohamath R, Bement T, Alderson MR, et al. Cloning, expression, and immunological evaluation of two putative secreted serine protease antigens of Mycobacterium tuberculosis. *Infect Immun*. (1999) 67(8):3998–4007. doi: 10.1128/iai.67.8.3998-4007.1999

52. Tkachuk AP, Gushchin VA, Potapov VD, Demidenko AV, Lunin VG, Gintsburg AL. Multi-subunit BCG booster vaccine GamTBvac: Assessment of immunogenicity and protective efficacy in murine and guinea pig TB models. *PloS One*. (2017) 12(4): e0176784. doi: 10.1371/journal.pone.0176784

53. Woodworth JS, Clemmensen HS, Battey H, Dijkman K, Lindenstrøm T, Laureano RS, et al. A Mycobacterium tuberculosis-specific subunit vaccine that provides synergistic immunity upon co-administration with Bacillus Calmette-Guérin. *Nat Commun*. (2021) 12(1):6658. doi: 10.1038/s41467-021-26934-0

54. Chitale P, Lemenze AD, Fogarty EC, Shah A, Grady C, Odom-Mabey AR, et al. A comprehensive update to the Mycobacterium tuberculosis H37Rv reference genome. *Nat Commun*. (2022) 13(1):7068. doi: 10.1038/s41467-022-34853-x

55. Domenech P, Reed MB. Rapid and spontaneous loss of phthiocerol dimycocerosate (PDIM) from Mycobacterium tuberculosis grown *in vitro*: Implications for virulence studies. *Microbiol (Reading)*. (2009) 155(Pt 11):3532–43. doi: 10.1099/mic.0.029199-0

56. Plumlee CR, Duffy FJ, Gern BH, Delahaye JL, Cohen SB, Stoltzfus CR, et al. Ultra-low dose aerosol infection of mice with Mycobacterium tuberculosis more closely models human tuberculosis. *Cell Host Microbe*. (2021) 29(1):68–82.e5. doi: 10.1016/j.chom.2020.10.003

57. Manabe YC, Dannenberg AM Jr., Tyagi SK, Hatem CL, Yoder M, Woolwine SC, et al. Different strains of Mycobacterium tuberculosis cause various spectrums of disease in the rabbit model of tuberculosis. *Infect Immun*. (2003) 71(10):6004–11. doi: 10.1128/iai.71.10.6004-6011.2003

58. Cohen SB, Plumlee CR, Engels L, Mai D, Murray TA, Jahn AN, et al. Host and pathogen genetic diversity shape vaccine-mediated protection to Mycobacterium tuberculosis. *Front Immunol*. (2024) 15:1427846. doi: 10.3389/fimmu.2024.1427846

59. Plumlee CR, Barrett HW, Shao DE, Lien KA, Cross LM, Cohen SB, et al. Assessing vaccine-mediated protection in an ultra-low dose Mycobacterium tuberculosis murine model. *PloS Pathog*. (2023) 19(11):e1011825. doi: 10.1371/journal.ppat.1011825

60. Smith CM, Proulx MK, Lai R, Kiritsy MC, Bell TA, Hock P, et al. Functionally overlapping variants control tuberculosis susceptibility in collaborative cross mice. *mBio*. (2019) 10(6):e02791–19. doi: 10.1128/mbio.02791-19

61. Smith CM, Proulx MK, Olive AJ, Laddy D, Mishra BB, Moss C, et al. Tuberculosis susceptibility and vaccine protection are independently controlled by host genotype. *mBio*. (2016) 7(5):01516–16. doi: 10.1128/mbio.01516-16

62. Lai R, Gong DN, Williams T, Ogunsola AF, Cavallo K, Lindestam Arlehamn CS, et al. Host genetic background is a barrier to broadly effective vaccine–mediated protection against tuberculosis. *J Clin Invest*. (2024) 133(13):e167762. doi: 10.1172/JCI167762

63. Smith CM, Baker RE, Proulx MK, Mishra BB, Long JE, Park SW, et al. Host-pathogen genetic interactions underlie tuberculosis susceptibility in genetically diverse mice. *eLife*. (2022) 11:e74419. doi: 10.7554/eLife.74419

64. Valway SE, Sanchez MP, Shinnick TF, Orme I, Agerton T, Hoy D, et al. An outbreak involving extensive transmission of a virulent strain of Mycobacterium tuberculosis. *N Engl J Med*. (1998) 338(10):633–9. doi: 10.1056/nejm199803053381001

65. Kaushal D, Foreman TW, Gautam US, Alvarez X, Adekambi T, Rangel-Moreno J, et al. Mucosal vaccination with attenuated Mycobacterium tuberculosis induces strong central memory responses and protects against tuberculosis. *Nat Commun*. (2015) 6:8533. doi: 10.1038/ncomms9533

66. Reed MB, Domenech P, Manca C, Su H, Barczak AK, Kreiswirth BN, et al. A glycolipid of hypervirulent tuberculosis strains that inhibits the innate immune response. *Nature*. (2004) 431(7004):84–7. doi: 10.1038/nature02837

67. Carey AF, Wang X, Cicchetti N, Spaulding CN, Liu Q, Hopkins F, et al. Multiplexed strain phenotyping defines consequences of genetic diversity in Mycobacterium tuberculosis for infection and vaccination outcomes. *mSystems*. (2022) 7(3):e0011022. doi: 10.1128/msystems.00110-22

68. Manca C, Tsenova L, Barry CE 3rd, Bergtold A, Freeman S, Haslett PA, et al. Mycobacterium tuberculosis CDC1551 induces a more vigorous host response *in vivo* and *in vitro*, but is not more virulent than other clinical isolates. *J Immunol*. (1999) 162 (11):6740–6. doi: 10.4049/jimmunol.162.11.6740

69. Leisching G, Pietersen RD, Mpongoshe V, van Heerden C, van Helden P, Wiid I, et al. The host response to a clinical MDR mycobacterial strain cultured in a detergent-free environment: A global transcriptomics approach. *PloS One*. (2016) 11(4):e0153079. doi: 10.1371/journal.pone.0153079

70. Sani M, Houben EN, Geurtsen J, Pierson J, de Punder K, van Zon M, et al. Direct visualization by cryo-EM of the mycobacterial capsular layer: A labile structure containing ESX-1-Secreted proteins. *PloS Pathog*. (2010) 6(3):e1000794. doi: 10.1371/journal.ppat.1000794

71. Pietersen RD, du Preez I, Loots DT, van Reenen M, Beukes D, Leisching G, et al. Tween 80 induces a carbon flux rerouting in Mycobacterium tuberculosis. *J Microbiol Methods*. (2020) 170:105795. doi: 10.1016/j.mimet.2019.105795

72. Rens C, Chao JD, Sexton DL, Tocheva EI, Av-Gay Y. Roles for phthiocerol dimycocerosate lipids in Mycobacterium tuberculosis pathogenesis. *Microbiol (Reading)*. (2021) 167(3). doi: 10.1099/mic.0.001042

73. Cohen SB, Gern BH, Delahaye JL, Adams KN, Plumlee CR, Winkler JK, et al. Alveolar macrophages provide an early Mycobacterium tuberculosis niche and initiate dissemination. *Cell Host Microbe*. (2018) 24(3):439–46.e4. doi: 10.1016/j.chom.2018.08.001

74. World Health Organization. *Global tuberculosis report*. (2023).

75. Painter H PS, Cia F, Stockdale L, Tanner R, Willcocks S, Reljic R, et al. Adaption of the ex vivo mycobacterial growth inhibition assay for use with murine lung cells. *Sci Rep*. (2020) 10:1–9. doi: 10.1038/s41598-020-60223-y

76. Painter H, Willcocks S, Zelmer A, Reljic R, Tanner R, Fletcher H. Demonstrating the utility of the ex vivo murine mycobacterial growth inhibition assay (MGIA) for high-throughput screening of tuberculosis vaccine candidates against multiple Mycobacterium tuberculosis complex strains. *Tuberculosis (Edinb)*. (2024) 146:102494. doi: 10.1016/j.tube.2024.102494

77. Painter H, Harriss E, Fletcher HA, McShane H, Tanner R. Development and application of the direct mycobacterial growth inhibition assay: A systematic review. *Front Immunol*. (2024) 15:1355983. doi: 10.3389/fimmu.2024.1355983

78. Stanley S, Spaulding CN, Liu Q, Chase MR, Ha DTM, Thai PVK, et al. Identification of bacterial determinants of tuberculosis infection and treatment outcomes: A phenogenomic analysis of clinical strains. *Lancet Microbe*. (2024) 5(6): e570–e80. doi: 10.1016/s2666-5247(24)00022-3

79. Atavliyeva S, Auganova D, Tarlykov P. Genetic diversity, evolution and drug resistance of Mycobacterium tuberculosis lineage 2. *Front Microbiol*. (2024) 15:1384791. doi: 10.3389/fmicb.2024.1384791

80. Billows N, Phelan J, Xia D, Peng Y, Clark TG, Chang YM. Large-scale statistical analysis of Mycobacterium tuberculosis genome sequences identifies compensatory mutations associated with multi-drug resistance. *Sci Rep*. (2024) 14(1):12312. doi: 10.1038/s41598-024-62946-8

81. Harrison LB, Kapur V, Behr MA. An imputed ancestral reference genome for the Mycobacterium tuberculosis complex better captures structural genomic diversity for reference-based alignment workflows. *Microb Genom*. (2024) 10(1). doi: 10.1099/mgen.0.001165

82. Senelle G, Sahal MR, La K, Billard-Pomares T, Marin J, Mougari F, et al. Towards the reconstruction of a global TB history using a new pipeline "TB-Annotator". *Tuberculosis (Edinb)*. (2023) 143s:102376. doi: 10.1016/j.tube.2023.102376

83. Heupink TH, Verboven L, Sharma A, Rennie V, de Diego Fuertes M, Warren RM, et al. The MAGMA pipeline for comprehensive genomic analyses of clinical Mycobacterium tuberculosis samples. *PloS Comput Biol*. (2023) 19(11):e1011648. doi: 10.1371/journal.pcbi.1011648

frontiers | Frontiers in Immunology

TYPE Clinical Trial
PUBLISHED 14 November 2024
DOI 10.3389/fimmu.2024.1427371



OPEN ACCESS

EDITED BY
Sarah Fortune,
Harvard University, United States

REVIEWED BY
Paul Ogongo,
University of California San Francisco, United States
Aneesh Vijayan,
Independent researcher, Leiden, Netherlands

*CORRESPONDENCE
Helen McShane
helen.mcshane@ndm.ox.ac.uk

†These authors share first authorship

RECEIVED 03 May 2024
ACCEPTED 14 October 2024
PUBLISHED 14 November 2024

CITATION
Fredsgaard-Jones T, Harris SA, Morrison H, Ateere A, Nassanga B, Ramon RL, Mitton C, Fletcher E, Decker J, Preston-Jones H, Jackson S, Mawer A, Satti I, Barer M, Hinks T, Bettinson H and McShane H (2024) A dose escalation study to evaluate the safety of an aerosol BCG infection in previously BCG-vaccinated healthy human UK adults. *Front. Immunol.* 15:1427371. doi: 10.3389/fimmu.2024.1427371



# A dose escalation study to evaluate the safety of an aerosol BCG infection in previously BCG-vaccinated healthy human UK adults

Timothy Fredsgaard-Jones[1†], Stephanie A. Harris[1†], Hazel Morrison[1], Alberta Ateere[1], Beatrice Nassanga[1], Raquel Lopez Ramon[1], Celia Mitton[1], Eve Fletcher[2], Jonathan Decker[2], Hannah Preston-Jones[1], Susan Jackson[1], Andrew Mawer[1], Iman Satti[1], Michael Barer[2], Timothy Hinks[3], Henry Bettinson[3] and Helen McShane[1*]

[1]The Jenner Institute, University of Oxford, Oxford, United Kingdom, [2]Department of Respiratory Science, University of Leicester, Leicester, United Kingdom, [3]Oxford Centre for Respiratory Medicine, Nuffield Department of Clinical Medicine, University of Oxford, Oxford, United Kingdom

**Introduction:** Tuberculosis (TB) is the leading cause of death worldwide from a single infectious agent. Bacillus Calmette-Guérin (BCG), the only licensed vaccine, provides limited protection. Controlled human infection models (CHIMs) are useful in accelerating vaccine development for pathogens with no correlates of protection; however, the need for prolonged treatment makes *Mycobacterium tuberculosis* an unethical challenge agent. Aerosolised BCG provides a potential safe surrogate of infection. A CHIM in BCG-vaccinated as well as BCG-naïve individuals would allow identification of novel BCG-booster vaccine candidates and facilitate CHIM studies in populations with high TB endemicity. The purpose of this study was to evaluate the safety and utility of an aerosol BCG CHIM in historically BCG-vaccinated volunteers.

**Methods:** There were 12 healthy, historically BCG-vaccinated UK adults sequentially enrolled into dose-escalating groups. The first three received $1 \times 10^4$ CFU aerosol BCG Danish 1331 via a nebuliser. After safety review, subsequent groups received doses of $1 \times 10^5$ CFU, $1 \times 10^6$ CFU, or $1 \times 10^7$ CFU. Safety was monitored through self-reported adverse events (AEs), laboratory tests, and lung function testing. Immunology blood samples were taken pre-infection and at multiple timepoints post-infection. A bronchoalveolar lavage (BAL) taken 14 days post-infection was analysed for presence of live BCG.

**Results:** No serious AEs occurred during the study. Solicited systemic and respiratory AEs were frequent in all groups, but generally short-lived and mild in severity. There was a trend for more reported AEs in the highest-dose group. No live BCG was detected in BAL from any volunteers. Aerosol BCG induced potent systemic cellular immune responses in the highest-dose group 7 days post-infection.

**Discussion:** Aerosol BCG infection up to a dose of $1 \times 10^7$ CFU was well-tolerated in historically BCG-vaccinated healthy, UK adults. No live BCG was detected in the BAL fluid 14 days post-infection despite potent systemic responses, suggesting early clearance. Further work is needed to expand the number of volunteers receiving BCG via the aerosol route to refine and establish utility of this aerosol BCG CHIM.

**Clinical trial registration:** https://clinicaltrials.gov/, identifier NCT04777721.

KEYWORDS

**tuberculosis, BCG, CHIM, vaccine, aerosol**

## Introduction

Globally, tuberculosis (TB) remains the leading cause of death from a single infectious agent (1), and even in survivors, it exerts a significant impact on the quality of their health (2). The WHO has set ambitious targets to curb the impact of TB, with an aim to reduce mortality to 95% of the numbers seen in 2015 (3). Integral to the success of this strategy will be the development and deployment of a more efficacious vaccine than BCG (3, 4), which provides limited protection to *Mycobacterium tuberculosis* (*M.tb*) infection in adults and has variable efficacy against pulmonary disease (5). To date, the lack of defined correlates of protection and a robust model for assessing efficacy and immunogenicity for candidate vaccines has frustrated vaccine development (6). There is an urgent need for other tools to identify at an early stage which vaccine candidates have the greatest chance of success. Controlled human infection models (CHIMs) have been successfully utilised in the development of vaccine strategies for other globally important diseases including malaria, influenza, cholera, and typhoid (7–10). CHIMs also provide the opportunity to interrogate the immunological responses to early infection (11), something which is challenging in *M.tb* field studies where infection often predates symptoms by months or years. A functioning TB CHIM could also be utilised to directly assess the vaccine efficacy of a novel vaccine as part of early-stage clinical trials on healthy volunteers, by providing a head-to-head comparison with unvaccinated controls. Given the high costs of phase 3 trials for TB vaccines (12), this would be invaluable in ensuring that only the most promising candidates are taken forward.

Developing a CHIM for TB vaccines is complex, as the duration and toxicity of treatment as well as lack of a definitive proof of cure mean that virulent *M.tb* would not be an ethical challenge agent. In the absence of an attenuated form of *M.tb*, Bacillus Calmette-Guérin (BCG) provides an attractive alternative challenge agent due to its low pathogenic potential and excellent safety record as a vaccine (13). We have previously developed an intradermal BCG CHIM (14–16); however, using a respiratory CHIM would be beneficial, as it accurately mimics the natural route of *M.tb* infection and allows for the characterisation of local mucosal immune responses.

Instilling BCG directly into the lungs has previously been shown to be safe and well tolerated (17); however, aerosol delivery provides a less invasive approach and logistical and operational benefits in a low-resource setting. We have previously shown that aerosol BCG can be safely administered to BCG-naïve healthy adult volunteers and that viable BCG can be successfully recovered from bronchoalveolar lavage (BAL) samples taken 14 days after initial challenge (18). Ongoing work has focussed on evaluating the local respiratory and systemic responses to aerosol challenge (ClinicalTrials.gov NCT03912207). As the majority of the world's population are vaccinated with BCG as part of routine childhood vaccine schedules, it is important that any TB CHIM could also be conducted on historically BCG-vaccinated volunteers. Not only would this allow for CHIMs to be conducted on more varied populations including settings where TB is endemic, but also it would allow for the evaluation of future TB vaccine candidates in a prime-boost regimen with intradermal BCG. Prime-boost approaches have been shown to enhance *M.tb* immunity in animal models (19), and heterologous vaccine programs have recently shown promise in providing protection against COVID-19 (20).

Evaluation of the safety of aerosol BCG infection in historically BCG-vaccinated humans is prudent given the large surface area of the respiratory mucosa. Intradermal BCG revaccination has not been associated with an increased side effect profile in large randomised controlled trials (21), whereas studies involving non-human primates are reassuring, showing that an aerosol vaccination boost of historically intradermally vaccinated animals can also be achieved safely (22). The results of another respiratory BCG human challenge model via bronchoscopic instillation included some participants with previous BCG vaccination and also showed a favourable side effect profile (17), albeit at a lower dose to a single lobe of the lung.

Here, we present the results of a dose escalation study investigating the safety and tolerability of aerosol BCG infection in historically BCG-vaccinated healthy adult volunteers from an

area with low *M.tb* prevalence. We also present data on BCG recovery from bronchoalveolar lavage fluid and face mask sampling post-infection and exploratory immunological data to characterise the response to aerosol BCG infection, and to further inform the immunological response to mycobacteria.

# Materials and methods

## Study design

We designed a controlled human infection study using BCG delivered via the aerosol route. The study, along with associated documents, was approved by the Oxford A Research Ethics Committee (Ref. 20/SC/0059) and was registered with ClinicalTrials.gov prior to study commencement (ClinicalTrials.gov ID: NCT04777721). All aspects of the study were conducted according to the principle of the Declaration of Helsinki and Good Clinical Practice.

## Trial participants

Healthy, historically BCG-vaccinated UK adults aged 18–50 residing in the Oxford area were recruited by use of approved adverts. Following written informed consent, volunteers were screened for eligibility at the Centre for Clinical Vaccinology and Tropical Medicine, University of Oxford. Volunteers were screened for previous exposure to *M.tb* through clinical history, physical examination, chest radiographs, and a negative interferon gamma release assay (QuantiFERON-TB Gold Plus (Qiagen, Hilden, Germany)) on fresh blood. BCG vaccination status was confirmed via occupational health/medical records or evidence of a BCG scar, whereas to be eligible, previous intradermal BCG vaccination must have occurred at least 12 months prior to enrolment.

Volunteers were screened for evidence of an underlying immunodeficiency, including HIV, through serological and haematological testing and medical history. Volunteers with underlying asthma or other significant respiratory disease evidenced through medical history or clinically significant abnormalities in pulmonary function tests or chest radiograph were excluded. Volunteers who were current smokers, pregnant, or breastfeeding and those who had a medical history, which was deemed by the study physicians to be clinically relevant, were also excluded. The full eligibility criteria can be found in the study protocol (Supplementary Document 1). Volunteers who fulfilled the inclusion criteria were invited to participate.

## Group allocation

Volunteers were sequentially enrolled into one of four study groups, starting at the lowest aerosol BCG dose until each study group was full (three volunteers per group). Volunteers were not blinded to their dose. A review of the safety data taken from volunteers was completed at least 7 days after the final volunteer in each group had been enrolled. Safety data assessment included solicited and unsolicited adverse events (AEs) reported in electronic diaries (eDiaries), safety blood tests, pulmonary function tests, bronchoscopy reports, and physical observations from study visits. Data were discussed with an independent safety monitoring committee (SMC). The decision to continue dose escalation was at the discretion of the committee, and only after agreement with the SMC was enrolment to the next dosing group initiated.

## Challenge agent

BCG Danish 1331 (AJV Vaccines, Denmark) was used for all groups. According to the manufacturer, lyophilised vials contain 2–$8 \times 10^6$ CFU; therefore, the median of $5 \times 10^6$ CFU was assumed for dosing. All vials were mixed with BCG solvent (AJV vaccines) and diluted with 0.9% normal saline as appropriate for the dose in each study group. The total volume of fluid aerosolised for each volunteer was 1 mL. Aerosolisation was achieved using the handheld Omron MicroAir U22 ultrasonic mesh nebuliser (OMRON Healthcare Ltd., UK). Volunteers were instructed to breathe at a normal rate and the device set in a continuous aerosolisation mode.

## Clinical interventions

All volunteers received one dose of aerosolised BCG (either $1 \times 10^4$, $1 \times 10^5$, $1 \times 10^6$, or $1 \times 10^7$ CFU) on D0 of the study. Blood was obtained on all study visits (D0, D2, D7, D14, D28, D56, D84, and D168) whereas bronchoscopy was completed on D14, and induced sputum was an optional investigation on D168.

After challenge, the volunteers were provided with an eDiary to record solicited respiratory AEs (cough, sputum production, haemoptysis, sore throat, wheeze, dyspnoea, chest tightness, and chest pain) and systemic AEs (fever, feverishness, fatigue, malaise, myalgia, arthralgia, headache, and nausea) for 28 days. Volunteers were also asked to record any other unlisted AEs. All AEs were scored between 0 (not present) and 3 (severe) based on predefined criteria (see Supplementary Figure 1). The inclusion of systemic AEs was identified based on SmPC for BCG (23), whereas respiratory AEs were based on previous experience from aerosol vaccine trials including previous trials completed using aerosol BCG (18, 24). AEs (solicited and unsolicited) were also recorded at all study visits where durations of AEs and their severity were collected retrospectively.

Basic vital signs were recorded at all study visits. Spirometry was completed immediately after administration of aerosol BCG on D0 and repeated on D2 and D7 visits, and Transfer Factor of the lung for Carbon Dioxide ($TL_{CO}$) was completed on the D7 visit. Any volunteers with potentially significant drops in $TL_{CO}$ at D7 (≥15% compared with baseline or a $TL_{CO}$ below the predicted lower limit of normal adjusted for age, height, gender, and ethnicity) had repeat measurement undertaken at D84. Further lung function was also repeated where deemed clinically indicated.

Volunteers reporting any grade 3 AEs during eDiary attended for an additional clinic visit. Volunteers with a fever (≥37.5°C) were investigated with physical examination and history and underwent

blood tests and microbiological investigation including throat swabs for respiratory pathogens and mycobacterial blood cultures as appropriate.

A single bronchoscopy was completed on D14 following aerosol challenge by an experienced respiratory physician. Volunteers were offered intravenous sedation (midazolam and fentanyl). After local anaesthesia was administered to the oropharynx, above and below the vocal cords, a fibreoptic bronchoscope was used to macroscopically inspect respiratory mucosa and to obtain a bronchoalveolar lavage of the right middle lobe using 150 mL of sterile 0.9% saline.

Face mask sampling was completed using an adapted duckbill face mask (Integrity® 600-3004) containing four 3D-printed polyvinyl alcohol (PVA) sampling matrix strips to detect any exhaled BCG. Masks were worn for 30 min on several study visits: D0, both before and immediately after aerosol challenge, D2, D7, D14, and D28. Masks were positioned to avoid any contact with face and sampling strips. Volunteers were asked to avoid touching the internal components of the masks but were permitted to talk and cough while wearing the masks. Volunteers were not permitted to eat while wearing the mask; however, if they felt the need to expectorate sputum or required a drink during the procedure, they were permitted to briefly remove the mask before replacing. Masks were placed in a sampling bag and allowed to dry before sealing for transport at room temperature.

## Detection and quantification of BCG

### BCG infection dose

The infection dose was verified by generating serial dilutions of BCG from the diluted vaccine vials and adding the appropriate dilution to a BACTEC™ Mycobacterial Growth Indicator Tube (MGIT) containing Middlebrook 7H9 media, supplemented with 800 µL of BBL MGIT OADC (oleic acid, albumin, dextrose, and catalase) and PANTA (polymyxin B, amphotericin B, nalidixic acid, trimethoprim, and azlocillin) mixture (Becton Dickinson, UK) (BD). Tubes were added to the BACTEC™ MGIT instrument (Becton Dickinson, UK) and time to positivity (TTP) by fluorescence recorded. TTP is inversely correlated with the number of CFU present and was converted to CFU by means of a standard curve, where serial dilutions of a BCG vaccine vial were generated and an aliquot of each dilution plated onto solid M7H11 agar and an aliquot added to a supplemented MGIT tube. Resulting TTP was plotted against log10 CFU and a linear regression performed to obtain an equation for the line. Results are reported as CFU/vaccine vial and CFU/dose for each group.

### Detection of BCG in BAL and induced sputum samples

BCG detection was performed on the entire BAL sample volume from all 12 volunteers in the study, as previously described (18). Briefly, BAL samples were centrifuged at 3,000 g for 17 min and the supernatant decanted into fresh 50 mL centrifuge tubes and stored at −80°C. The pellet was decontaminated using the BBL® MycoPrep™ Specimen Digestion/Decontamination Kit (Becton Dickinson, UK) according to the manufacturer's instructions. Briefly, the ampule in the MycoPrep™ Reagent bottle was broken and N-acetyl-L-cysteine (NALC) was dissolved by gentle shaking to activate the NALC-sodium hydroxide (NALC-NaOH) solution. 5 mL was added to the BAL pellet and incubated for 15 min at room temperature with occasional gentle mixing. Phosphate-buffered saline (PBS) was then added to 50 mL, and the solution was centrifuged at 3,000 g for 17 min. Supernatant was discarded and the pellet resuspended in supplemented media from the corresponding MGIT tube and returned to the tube. The MGIT tube was added to the BACTEC™ MGIT instrument (Becton Dickinson, UK), as above, and TTP was recorded.

Induced sputum samples were obtained from 11/12 volunteers at D168 post-aerosol BCG. Induced sputum samples were decontaminated by adding an equal volume of activated BBL® MycoPrep™ following the above procedure for BCG detection in the BAL.

### Processing of adapted PVA masks

For groups 3 and 4 ($1 \times 10^6$ and $1 \times 10^7$ CFU aerosol BCG), facemasks from D0 pre- and post-aerosol BCG, D2, and D7 were processed for detection of live BCG. Under sterile conditions, the two PVA strips from one side of the face mask were removed and placed into a stomacher bag. The remainder of the mask containing the other two PVA strips was repackaged and stored at RT for later qPCR. 4.5 mL of molecular-grade water was added to the strips in the stomacher bag and the bag manipulated by hand for 5 min to dissolve the strips. Once dissolved, the solution was transferred to a 50 mL Falcon tube and an equal volume of BBL® MycoPrep™ was added and processed as above for detection of BCG. All facemasks from all time points were processed for qPCR.

For qPCR analysis, the remaining two PVA strips were removed from the face mask and dissolved in 4 mL Tris buffer (25 mM, pH 8.0) using a multifunction tube rotator for 60 min. After dissolution, samples were pelleted using centrifugation (15,000 x *g* for 10 min). The pellet was resuspended in 100 µL Tris–EDTA (20 mM Tris, 2 mM EDTA, pH 8.0) before being transferred to a screwcap tube. 0.25 g of lysing matrix B and 100 µL Chelex suspension (50% w/v Chelex 100, 1% w/v Nonidet P-40, 1% w/v Tween 20) were added to the resuspended pellet. Cells were disrupted in a FastPrep-24 5G homogeniser (MP Biomedicals, CA, USA) at 6.5 m/s for 45 s (4 rounds with a 2 min incubation on ice between each round). Samples were centrifuged at 15,000 x *g* for 2 min and the supernatant collected for qPCR analysis. Sample DNA was initially detected using SensiFAST™ Probe No-ROX (Bioline, UK) following the manufacturer's instructions, with primers and probes targeting the IS1081 gene: forward primer: 5′-CTG CTC TCG ACG TTC ATC GCC C-3′ (final concentration: 333 nM); reverse primer: 5′-GGC TAG CAG ACC TCA CCT ATG TGT-3′ (final concentration: 333 nM); probe: 5′-6-FAM GGC TGA AGC/ZEN/CGA CGC CCT GTG CGG G-3′-IABFQ (final concentration: 167 nM). Thermal cycling conditions for the IS1081 assay was as follows: incubation at 50°C for 2 min, incubation at 95°C for 10

min, followed by 45 PCR cycles (denaturation: 95°C for 15 s; combined annealing/extension: 60°C for 60 s). Positive samples were re-assayed for detection of the IS6110 gene using SensiFAST™ SYBR® No-Rox (Bioline, UK) according to the manufacturer's instructions. Primers used to target the IS6110 gene: forward primer: 5′-AGC GTA GGC GTC GGT GAC-3′ (final concentration: 400 nM); reverse primer: 5′-GGG TAG CAG ACC TCA CCT ATG TGT-3′ (final concentration: 400 nM) (25). Thermal cycling for the IS6110 assay was performed with the conditions as follows: incubation at 95°C for 15 min, followed by 40 PCR cycles (denaturation: 95°C for 15 s; annealing: 68°C for 30 s; extension: 72°C for 20 s; additional extension step: 82°C for 20 s). All thermal cycling was performed using a Rotor-Gene Q thermocycler (Qiagen, Cat N: 9001590).

### Genotyping of mycobacteria isolated from BAL and induced sputum

After a minimum of 42 days on the BACTEC™ MGIT instrument (when the manufacturer's protocol considers the sample negative), the contents of positive MGIT tubes were transferred to a 50 mL centrifuge tube and centrifuged at 3,000 g for 17 min. Supernatant was discarded and the pellet resuspended in 200 µL PBS and stored at −80°C for batched DNA extraction. DNA extraction was carried out as previously described (26). Briefly, DNA was released from 200 µL of thawed homogenate using the tough microorganism lysing kit (Precellys) in a Precellys 24 machine at 6,500 rpm for 3 × 30 s. Homogenate was transferred to a separate tube and 50 µL PBS used to wash the remaining homogenate from the beads. 180 µL of ATL buffer and 20 µL of proteinase K (Qiagen) were added, vortexed, and incubated at 56°C for 4 h. From this point, the extractions were carried out following the manufacturer's instructions (Qiagen DNeasy Blood and Tissue Kit).

Genotyping was carried out using the HAIN™ GenoType MTBC VER 1.X kit (Bruker) according to the manufacturer's instructions for use. Briefly, DNA extracted from BAL and induced sputum was amplified using kit-specific primers and PCR conditions. 20 µL of the PCR product was chemically denatured and hybridised to the kit-specific DNA•STRIP, which contains specific probes complementary to the amplified PCR products. The bound amplicon is detected by addition of streptavidin–alkaline phosphatase and made visible by a colorimetric reaction. This results in a specific banding pattern on the strip, corresponding to a particular mycobacterium species, determined by comparing with the kit-specific insert.

## Immunology

### *Ex vivo* enzyme-linked immunospot

Fresh peripheral blood mononuclear cells (PBMC) separated from whole blood (WB) were used to measure *ex vivo* IFN-γ enzyme-linked immunospot (ELISpot) responses as previously described on samples collected at D0, D7, D14, D28, D56, D84, and D168 of the study (27). Briefly, cells were stimulated in triplicate at $3 \times 10^5$ PBMC/well with 20 µg/mL of PPD from *M.tb* (AJ Vaccines, Denmark), $2 \times 10^5$ CFU/mL BCG Danish (AJ Vaccines, Denmark), 1 µg/mL of MTB300, a pool comprising 300 peptides from *M.tb* (Sette, La Jolla), and anti-human CD3 mAb (positive control; Mabtech AB) or left unstimulated as a negative control for the assay. Background (unstimulated) subtracted antigen-specific responses are presented as spot-forming cells (SFC) per $1 \times 10^6$ PBMC.

### Concentration of BAL fluid

Frozen BAL fluid (BALF) was thawed and duplicate 20 µL volumes used to determine the phospholipid concentration by means of a phospholipid assay kit (Sigma-Aldrich). The manufacturer's instructions were followed and the concentration obtained in µM converted to concentration in µg/mL using the molecular weight of phosphatidyl-choline (28).

The physiological concentration of phospholipid in the lung is estimated to be 1 mg/mL, so it would have been desirable to concentrate BALF to this physiological concentration; however, samples were normalised to 0.5 mg/mL of phospholipid to ensure sufficient volume remained for enzyme-linked immunosorbent assay (ELISA) analysis, while still increasing the likelihood that the antibody concentration would rise above the limit of detection (29). BAL antibody arbitrary units were then multiplied by 2 in order to present BAL antibody per 1 mg/mL phospholipid. BAL samples were concentrated by adding 15 mL volumes to separate Amicon® Ultra-15 Centrifugal Filter Units—10-kDa cutoff (Millipore) and centrifuging at 3,000 g for between 5 min and 30 min, depending on the extent of concentration required. When the desired volume was achieved, the portion of sample remaining above the filter was transferred to a 2 mL cryovial and stored at −80°C for later analysis.

### Enzyme-linked immunosorbent assay

ELISAs, measuring PPD-specific IgG and IgA, were performed on serum taken at D0 and at days 2, 7, 14, 28, 56, 84, and 168 post-aerosol BCG infection and on concentrated BALF taken at D14. ELISA plates (Nunc-Immuno MaxiSorp) were coated with 50 µL/well of 5 µg/mL PPD in PBS and incubated overnight at 4°C. Plates were washed and blocked with 100 µL/well casein for 1 h at room temperature. Serum samples were diluted 1 in 50 (or repeated with a higher dilution if necessary) in casein and standards prepared by serial 1 in 2 dilutions of a reference pool of serum. Blocking solution was discarded, and 50 µL of samples and standard curve dilutions were added to duplicate wells and plates incubated at room temperature for 2 h. Plates were washed, and 50 µL of a 1 in 1,000 dilution of anti-human goat IgG (γ-chain-specific)-alkaline phosphatase antibody (Sigma-Aldrich) or a 1 in 500 dilution of anti-human goat IgA (α-chain-specific)-alkaline phosphatase antibody (Sigma-Aldrich) was added. Plates were incubated for 1 h at room temperature. Plates were washed and developed by adding 50 µL/well of p-nitrophenyl phosphate and disodium salt (pNPP) substrate (Sigma-Aldrich). After 5 min, plates were read at 405 nm using Gen5 software (v2.0.7, BioTek) and read approx. every 30 min to ensure a read where the standards produced a curve

with parameters within the specified range. Plates passed if average optical density values for the blank wells were <0.15, the standard curve was within predefined parameters and if the optical density of replicate sample values had a coefficient of variation <20%. BAL antibody values are presented as arbitrary units based on the standard curve and multiplied by 2, based on the phospholipid physiological concentration of 1 mg/mL.

### Direct PBMC mycobacterial growth inhibition assay

The direct PBMC Mycobacterial growth inhibition assay (MGIA) was carried out on frozen PBMC from all 12 volunteers, collected at D0 and at days 7, 28, and 56 post-aerosol BCG, as previously described (30). Briefly, 3 $\times 10^6$ PBMC and ~500 CFU BCG Pasteur were combined in a total volume of 600 µL RPMI (containing 25 mM HEPES, 2 mM L-glutamine 20% foetal calf serum, and 1% v/v sodium pyruvate) in a 48-well plate. Plates were incubated at 37°C and 5% $CO_2$ for 96 h, and then contents of each well were added to separate 2 mL screw-cap tubes and centrifuged at 12,000 rpm for 10 min. 500 µL sterile water was added to each well and left for a minimum of 5 min to lyse adherent monocytes. Supernatants were carefully removed from the 2 mL tubes and discarded, and water from a corresponding well was added to the pellet. Tubes were vortexed for 1 s and the contents added to BACTEC™ MGIT tubes supplemented as above and added to the BACTEC™ MGIT instrument until TTP was detected. On day 0, duplicate viability control tubes were set up by adding the same volume of BCG Pasteur stock directly to supplemented BACTEC™ MGIT tubes, as was added to each well containing the PBMC sample. TTP readout was converted to $\log_{10}$ CFU using a standard curve of TTP against CFU (enumerated by growth on solid M7H11 agar). Results are presented as growth ratio (log10 CFU sample/log10 CFU control).

## Statistical analysis

All statistical analysis was performed using GraphPad Prism (v10). Prism calculates exact p-values, which takes into account tied values. Non-parametric tests were applied as data were not normally distributed. Differences in medians between two groups were calculated using the Mann–Whitney test and the Wilcoxon signed rank test for paired data. Correction for multiple comparisons was done using Friedman test. For comparison of non-continuous safety data, chi-squared tests were used. In all cases, significant differences are presented with their p value; the significance level was set as $p < 0.05$.

# Results

## Participants

The first volunteer was enrolled into group 1 ($1 \times 10^4$ CFU) on 06/07/2022; volunteers were sequentially enrolled until each study group was full (three volunteers per group). After a satisfactory SMC outcome was reached, enrolment continued in this way until enrolment into the final group (group 4) was completed on 04/01/2023.

In total, 20 volunteers were assessed for eligibility in the trial, and 12 volunteers were enrolled across 4 groups (Figure 1). In total, eight women and four men were enrolled; the median age of the volunteers was 35 years (range 23 to 49). The baseline demographics of the volunteers are displayed in Table 1.

## Safety

No serious adverse events of any kind occurred during the study. All volunteer visits were completed as per the protocol and were performed within the specified window.

Solicited symptoms reported by the volunteers are presented below. Few unsolicited symptoms deemed to be possibly, probably, or definitely related were reported throughout the study. These were generally mild and of short duration and are outlined in Supplementary Table 1.

## Solicited adverse events in 14 days following aerosol BCG administration

Solicited symptoms were frequent in all groups, but generally mild in severity. The median duration of AEs first reported within 72 hours of challenge was between 1 and 3 days for all systemic AEs and 2 and 4 days for respiratory AEs (Table 2). There were no grade 3 AEs of any type in the first 14 days after challenge.

The maximum grade and frequency of each solicited systemic and respiratory AEs reported in the first 14 days after aerosol BCG challenge are shown in Figure 2.

The most frequently reported systemic AEs after challenge were fatigue and headache, whereas the most frequently reported respiratory AEs were cough and tickly throat. There were no solicited AEs which were reported in the 14 days after aerosol BCG challenge, and not reported by any volunteers after bronchoscopy. One individual in group 4 reported a cough from D1 which continued throughout the diary and remained present at the end of the study, albeit at significantly reduced intensity. This volunteer also reported 2 days of grade 2 fever and an increased frequency of symptoms in the first 72 h following BCG challenge compared with other volunteers. Figure 1 Supplementary Appendix details the duration and severity of all solicited symptoms for this individual. Investigations including chest radiographs, blood cultures (conventional and mycobacterial), respiratory culture, and PCR were completed to rule out alternative causes. An initial chest radiograph taken on D2 revealed nodularity in the right middle lobe, spirometry on the same day was normal, and $TL_{CO}$ on D7 was not significantly different from baseline. Macroscopic appearances of the bronchial mucosa inspected at the D14 bronchoscopy were unremarkable. Repeat chest radiograph 7 weeks later showed complete resolution of radiological changes. No alternative causative organisms were identified, and mycobacterial blood cultures were negative as was induced sputum at the day D168 visit.

10.3389/fimmu.2024.1427371

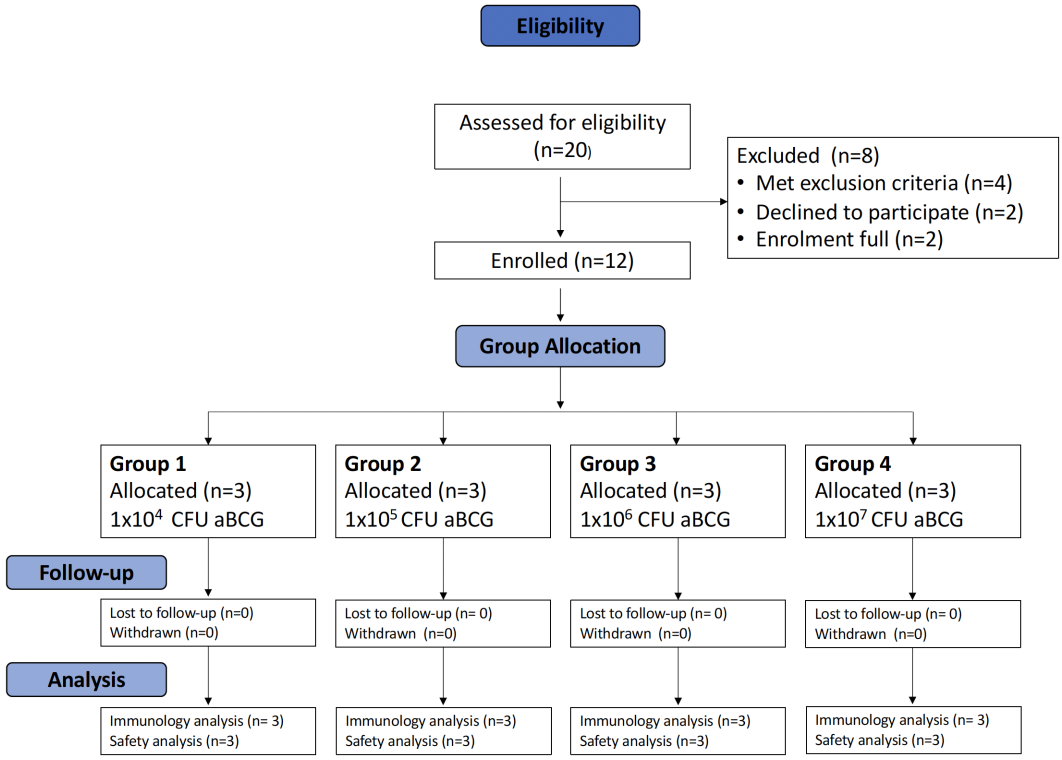


FIGURE 1
Consort diagram for TB044.

TABLE 1 Demographics and baseline respiratory function of all enrolled volunteers.

| Characteristic | |
|---|---|
| **Female, n (%)** | 8 (67) |
| **Median age in years (range)** | 35 (23–49) |
| **BMI (kg/m$^2$) median (range)** | 26.6 (21.4–35.4) |
| Country of birth | |
| **UK** | 7 |
| **South Africa** | 2 |
| **Chile** | 1 |
| **Pakistan** | 1 |
| **Portugal** | 1 |
| **Time since first BCG vaccination in years, median (range)** | 28 (16–37) |
| Baseline spirometry | |
| **Mean % predicter FEV1 (range)** | 109 (87–124) |
| **Mean % predicted FVC (range)** | 107 (90–123) |
| **Mean % predicted $TL_{CO}$ (range)** | 100 (87–116) |
| **Mean % predicted $K_{CO}$ (range)** | 103 (87–113) |
| **Median baseline % $SaO_2$ (range)** | 98 (97–100) |

More AEs were reported in volunteers in group 4 compared with groups 1 to 3, both for days of reported systemic AEs (68/335 vs. 36/1007 p<0.0001) and for respiratory AEs (18/1134 vs. 63/378 p<0.0001).

## Solicited adverse events reported in the 14 days following bronchoscopy

All bronchoscopies were completed without complication, and all were reported macroscopically as showing normal mucosa by the conducting consultant physician. Solicited AEs occurred in all study groups after bronchoscopy. Symptoms were consistent with those expected following all bronchoscopies. The most frequently reported AEs were cough, sore throat, tickly throat, and fatigue.

The median duration of AEs starting within the first 72 h of bronchoscopy was between 1 and 3 days in all cases (Supplementary Table 2). The frequency of AEs reported was similar between groups, and the increased frequency of AEs reported in group 4 compared with groups 1–3 after BCG challenge was not evident after bronchoscopy (53/714 vs. 171/2141 p=0.63).

The maximum grade for AEs after bronchoscopy was 2, apart from one individual who reported 2 days of grade 3 fever on D15 and D16 of the study. Upon PCR testing, this individual was found to have a nasopharyngeal swab which was positive for influenza A. Mycobacterial blood cultures were negative for growth after 6 weeks

10.3389/fimmu.2024.1427371

TABLE 2 Median duration of solicited AEs reported within 72 h of aerosol BCG challenge.

| Solicited AE | Number of volunteers (proportion, max grade) | | | | Total n=12 | Median duration of AE in days (range) | |
|---|---|---|---|---|---|---|---|
| | Group 1 n=3 | Group 2 n=3 | Group 3 n=3 | Group 4 n=3 | | | |
| **Temperature** | 0 | 0 | 0 | 1 (0.33, 2) | 1 | 2 | – |
| **Arthralgia** | 0 | 0 | 0 | 2 (0.66, 2) | 2 | 2.5 | (2–3) |
| **Myalgia** | 0 | 1 (0.33, 1) | 2 (0.66, 1) | 3 (1, 2) | 6 | 1.5 | (1–4) |
| **Feverishness** | 0 | 0 | 0 | 3 (1, 2) | 3 | 2 | (1–5) |
| **Headache** | 2 (0.66, 2) | 0 | 0 | 3 (1, 1) | 5 | 2 | (1–4) |
| **Fatigue** | 1 (0.33, 1) | 1 (0.33, 1) | 1 (0.33, 1) | 3 (1, 2) | 6 | 2.5 | (1–13) |
| **Nausea** | 0 | 0 | 0 | 0 | 0 | – | – |
| **Malaise** | 0 | 0 | 0 | 3 (1, 1) | 3 | 1 | (1–14) |
| **Cough** | 0 | 0 | 1 (0.33, 1) | 3 (1, 2) | 4 | 2.5 | (1–162) |
| **Sore throat** | 0 | 1 (0.33, 1) | 0 | 2 (0.66, 1) | 3 | 2 | (2–5) |
| **Tickly throat** | 1 (0.33, 1) | 1 (0.33, 1) | 2 (0.66, 1) | 1 (0.33, 1) | 5 | 1 | (1–6) |
| **Wheeze** | 0 | 0 | 0 | 2 (0.66,1) | 2 | 1.5 | (1–2) |
| **SOB** | 0 | 0 | 0 | 1 (0.33, 1) | 1 | 4 | – |
| **Cough phlegm** | 0 | 0 | 0 | 2 (0.66,1) | 2 | 1.5 | (1–2) |
| **Cough blood** | 0 | 0 | 0 | 0 | 0 | – | – |
| **Chest tightness** | 0 | 0 | 0 | 2 (0.66, 1) | 2 | 2.5 | (2–3) |
| **Chest pain** | 0 | 0 | 0 | 0 | 0 | – | – |

Grading range 1–3, AE presented here started within the first 72 h of e-Diary self-reporting. Group 1 = $1 \times 10^4$ CFU; group 2 = $1 \times 10^5$ CFU; group 3 = $1 \times 10^6$ CFU; group 4 = $1 \times 10^7$ CFU BCG SSI. SOB, shortness of breath.

of incubation, and induced sputum at D168 was negative for BCG. One other volunteer had a grade 1 fever following bronchoscopy; as previously discussed, this individual also had negative mycobacterial blood cultures.

Overall, a greater number of AEs were reported in the 14 days after bronchoscopy than after aerosol BCG challenge (224/2,855 vs. 185/2,854 p=0.046). Separate analysis of each group showed the same association for groups 1 to 3; however, the trend was reversed in group 4 where significantly fewer AEs were reported after bronchoscopy than after aerosol BCG challenge (53/714 vs. 131/713 p<0.0001).

## Lung function tests

None of the volunteers were found to have a clinically significant drop in Transfer Factor for carbon monoxide ($TL_{CO}$) or transfer coefficient of the lung for carbon monoxide ($K_{CO}$) at D7 after administration of BCG. Although the sample size was too small for statistical tests to be completed, there was a trend for greater drops in $TL_{CO}$ and $K_{CO}$ in group 4 compared with groups 1 to 3 (−11.7% vs. −2.3%, −8.3% vs. −2.5% mean change for $TL_{CO}$ and $K_{CO}$, respectively. Oxygen saturations were within the normal range at all study visits. Repeat $TL_{CO}$ and $K_{CO}$ at D84 remained within the expected variability of the test for all volunteers. Figure 3 shows the $TL_{CO}$ adjusted for haemoglobin ($TL_{COADJ}$) for each group.

Forced vital capacity (FVC) and forced expiratory volume in one second (FEV1) were similar across all groups and are shown in Figure 4. No significant drops in FVC or FEV1 were seen at any timepoint.

## Adverse safety blood tests

Haematology and biochemistry adverse events were rare. Four cases of hypokalaemia were identified after enrolment (grade 1: n=2, grade 2: n=1, grade 3: n=1); these were found to be normal on repeat testing and thought likely to be related delays in processing and raised ambient temperature, as described in other studies based at the same site (31). One individual was found to have an elevated eosinophil count (grade 1) on D14, which normalised by the time of repeat testing on D28. Another volunteer was found to have a transient rise in urea on D7 which normalised by D14; this individual reported use of protein supplements which were thought to have contributed to this result. Two volunteers were found to have grade 1 anaemia during follow-up. These were found after day 14 of the study and were static on repeat testing. They did not necessitate changes to the protocolised blood draws.

One volunteer in the high-dose group 4, previously discussed as having a larger number of AEs after aerosol BCG-challenge, was found to have a transient raise in bilirubin (grade 2) and alanine transaminase (grade 1) on D2 of the study; this was accompanied by

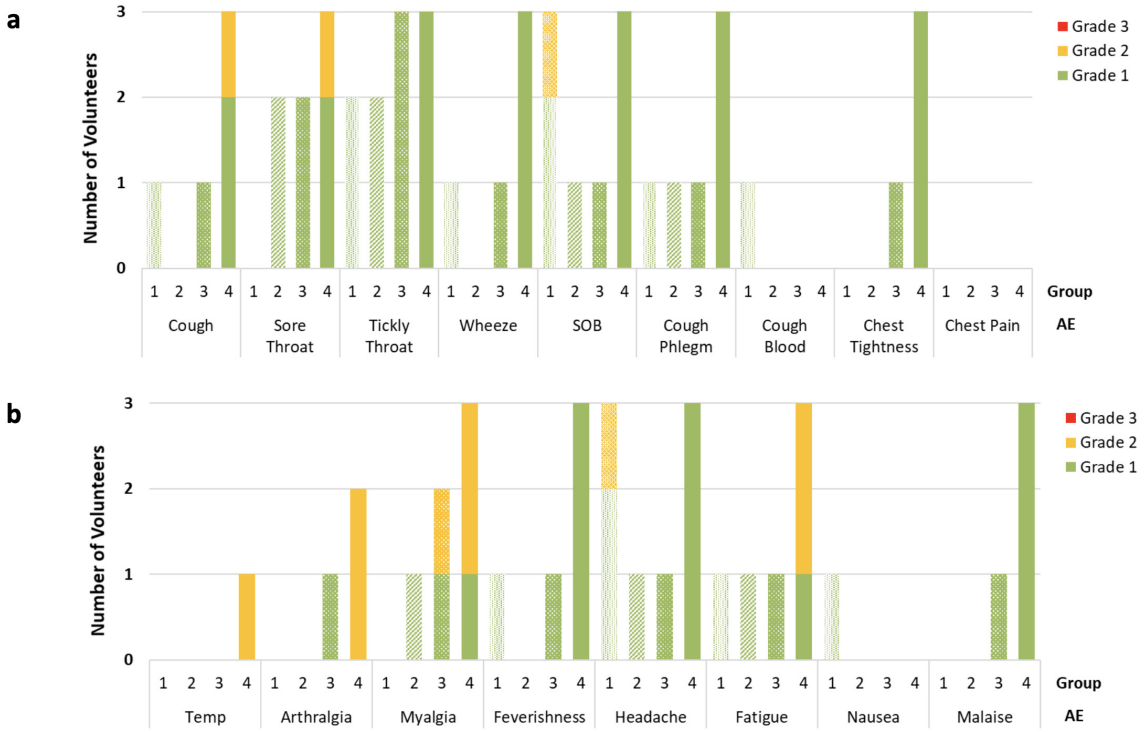


FIGURE 2
Number and maximum grade reported of respiratory **(A)** and systemic **(B)** adverse (AE) occurrence on daily volunteer diary in the 2 weeks following BCG aerosol challenge. AE's reported split by group, dose of aerosol BCG delivered; Group 1 = 1 × $10^4$ CFU; Group 2 = 1 × $10^5$ CFU; Group 3 = 1 × $10^6$ CFU; Group 4 = 1 × $10^7$ CFU. Data obtained once daily in all cases, and volunteers in each group n=3. SOB, Shortness Breath.

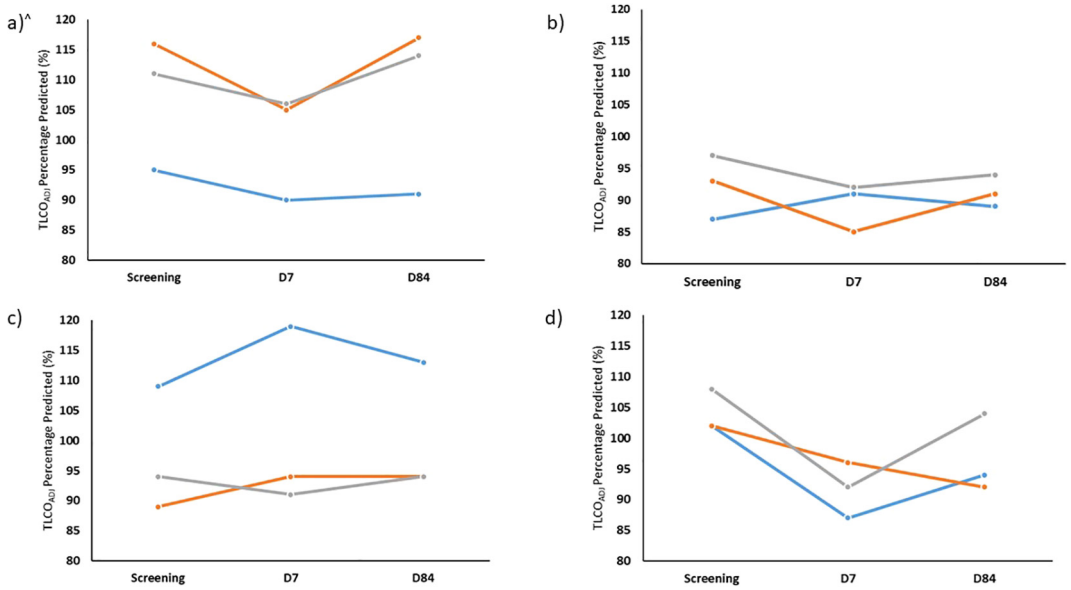


FIGURE 3
Percentage of predicted TLCO (TLCO$_{ADJ}$) at screening and also 7 days (D7) and 84 days (D84) after aerosol BCG for Group 1 **(A)**, Group 2 **(B)**, Group 3 **(C)** and Group 4 **(D)** for each volunteer enrolled. TLCO, transfer capacity of the lung, for the carbon monoxide. All percentage predicted accounting for age, sex, ethnicity and height and adjusted for most recent laboratory haemoglobin. N.B. volunteer in blue TLCO repeated at D168 rather than D84.

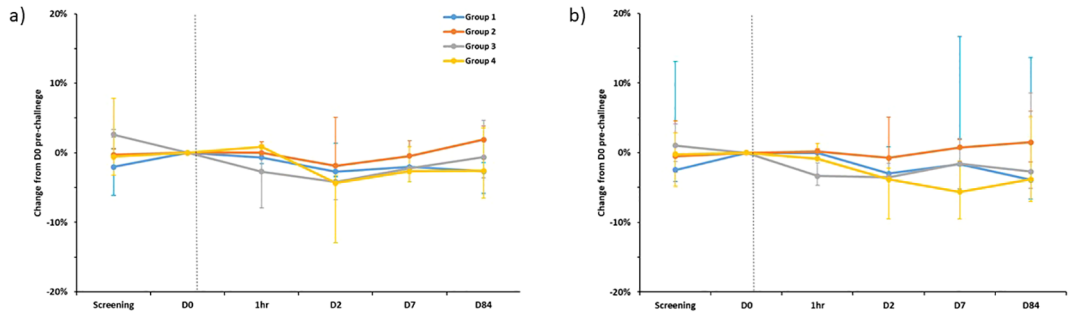


FIGURE 4
Percentage change in FEV1 **(A)** and FVC **(B)** compared to pre-challenge (D0) testing, separated by group. Plotted points are the median percentage change for each group. Bars show range. FEV1 - Forced Expiratory Volume in 1$^{st}$ second, FVC, Forced Vital Capacity. Dotted line is time of BCG administration. D0 spirometry was completed on the day of enrolment immediately prior to challenge. 1hr- repeated spirometry taken one hour after challenge with BCG was completed. N.B Spirometry for one individual in group 1 completed at D168 rather than D84 visit.

a raised white cell count (grade 1) and grade 1 hyponatraemia. These AEs all normalised on repeat testing by D14. This individual also had a raised C-reactive protein measured at D2 of 209.2 mg/L (normal laboratory range 0 mg/L–5 mg/L), which gradually reduced on repeat testing to 19.2 mg/L by D7 and 6.2 mg/L by D28.

## BCG infection dose

BCG was quantified, by BACTEC$^{TM}$ MGIT, from the diluted vaccine vials used to prepare the dose for nebulisation. The same batch of BCG was used for 11/12 volunteers; a new batch was used for the final volunteer enrolled due to the first batch having passed its expiry date. The number of BCG CFU/vial and number of BCG CFU/dose were calculated for each volunteer (Figure 5). The number of BCG CFU/vial ranged from $2.24 \times 10^6$– $6.11 \times 10^6$ (median $3.71 \times 10^6$), with some variation between vials used for different groups; however, all were within the range stated by the manufacturer ($2–8 \times 10^6$ CFU/vial). The median dose given to volunteers in groups 1–4 was $5.01 \times 10^3$, $5.60 \times 10^4$, $1.12 \times 10^6$, and $8.12 \times 10^6$ CFU/vial, respectively. This was within 0.5 logs of the intended dose for each group.

## BCG was not detectable in BAL and sputum samples

BAL samples were pelleted, decontaminated, and added to BACTEC$^{TM}$ MGIT tubes for detection of live BCG 14 days post-aerosol BCG. No growth was detected in 11/12 BAL samples; one sample in group 2 became positive after 813 h. Out of the 12 volunteers in the study, 11 gave an induced sputum sample at D168 post-aerosol BCG; these samples were processed in the same way as the BAL samples for detection of growth. No growth was detected in 8/11 samples, with the other 3 becoming positive at 56 h, 545 h, and 636 h. DNA extraction and use of HAIN MTBC genotyping on all positive samples found that this growth was not BCG but identified as "High GC Gram Positive Bacterium".

## BCG identified from PVA strips from face mask sampling

Two PVA strips from each mask, worn pre- and immediately post-aerosol BCG and 2 and 7 days post-aerosol BCG, in the two high-dose groups were dissolved, decontaminated, and added to

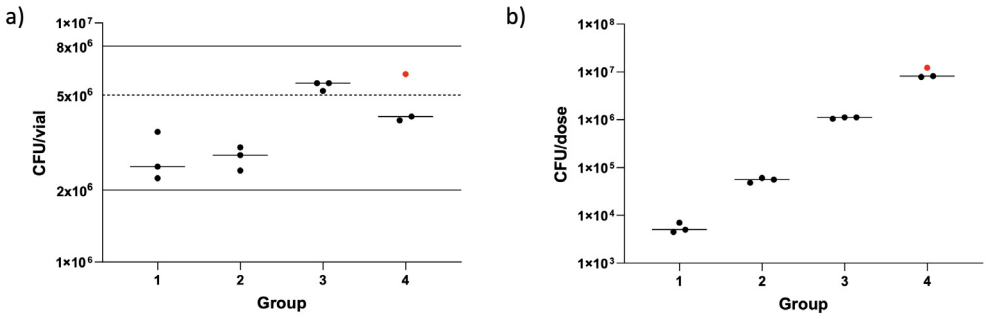


FIGURE 5
Enumeration of BCG from clinical vaccine vials **(A)** and dose loaded into the nebulizer **(B)**. Dots represent individual vaccine vials/dose per volunteer. Red dot shows a different batch of BCG used. Lines show median numbers per group, solid lines show the manufacture's stated range for amount of BCG contained in a vaccine vial and the dotted line shows value used for dose calculations.

BACTEC™ MGIT tubes for detection of live BCG. No growth of BCG was detected in any of the samples processed.

qPCR performed on the remaining PVA strips showed detectable evidence of the *Mycobacterium bovis* BCG in 5/60 samples taken after infection in two target genes, whereas a further five post-infection samples were positive using a single BCG target gene. None of the pre-infection samples were positive for BCG. Seven out of 10 of the samples with detectable BCG were from volunteers in group 4, two out of 12 were detected in group 3, and one other sample was positive at D0 in group 1. Figure 6 shows a heat map of the Ct values calculated for all mask samples processed, by volunteer and time point.

## *Ex vivo* IFN-γ ELISpot responses

Fresh PBMC IFN-γ ELISpot responses to PPD, BCG, and a pool of MTB300 peptides were measured at D0 and at days 7, 14, 28, 56, 84, and 168 post-aerosol BCG. Due to only having three volunteers per dose group, it was not possible to perform statistical comparisons between them. However, a clear dose effect could be seen, with volunteers in the highest dose group having the biggest increase in responses between baseline and the peak of the response at D7 (Table 3). All groups were combined to compare responses at each time point to baseline (Figure 7). PPD, BCG, and MTB300 responses at D7 were all significantly higher than baseline ($p = 0.020$, 0.021, and 0.0034 respectively, Wilcoxon matched-pairs); only BCG responses remained significantly higher than baseline at D14 ($p = 0.016$), and no other time points were significantly different from baseline.

## PPD-specific IgA and IgG antibody responses

PPD-specific IgA and IgG were measured in the serum of all volunteers at D0 and 2, 7, 14, 28, 56, 84, and 168 days post-aerosol BCG and in concentrated BAL fluid at D14 for 11/12 volunteers (one volunteer's BAL fluid was lost due to a processing error; Figure 7). There was no noticeable dose effect in the serum, so all 12 volunteers were combined for analysis; there was no significant increase in either IgA or IgG over time compared with baseline (Friedman test). Levels of PPD-specific IgA and IgG in the BAL fluid were generally lower than those in the serum, with no noticeable dose effect, but with only three samples in each group, it was not possible to do a statistical comparison.

## Direct PBMC mycobacterial growth inhibition assay

The direct MGIA was performed in one batch on PBMC frozen at baseline and at 7, 28, and 56 days post-aerosol BCG from all volunteers. PBMC from 19 BCG naïve volunteers were run alongside to act as a control for the assay, and there was a significant reduction in the log10 CFU growth ratio in the

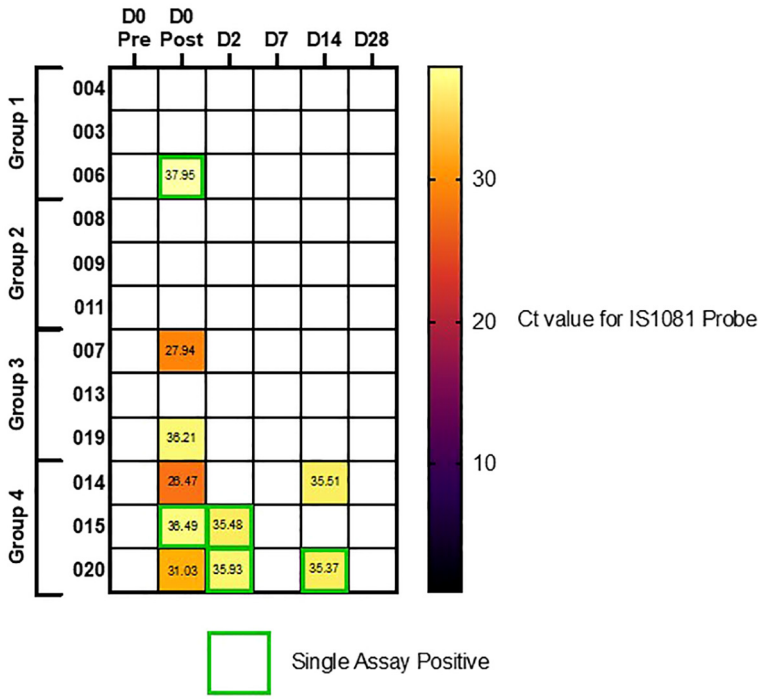


FIGURE 6
Heatmap of qPCR results using IS1081 probe, from PVA masks. Volunteers separated by dosing group (Group 1 = 1 x $10^4$ CFU, Group 2 = 1 x $10^5$ CFU, Group 3 = 1 x $10^6$ CFU and group 4 = 1 x $10^7$ CFU). Single assay positive probes highlighted in green boxes, where secondary IS6110 probe was not also positive.

TABLE 3 Median IFN-γ ELISpot responses per million PBMC by dose group.

| | PPD | | | | BCG | | | | MTB300 | | | |
|---|---|---|---|---|---|---|---|---|---|---|---|---|
| Time point (days) | Group 1 | Group 2 | Group 3 | Group 4 | Group 1 | Group 2 | Group 3 | Group 4 | Group 1 | Group 2 | Group 3 | Group 4 |
| **0** | 343 | 228 | 91 | 477 | 213 | 266 | 123 | 1,028 | 68 | 72 | 83 | 450 |
| **7** | 401 | 280 | 149 | 4,943 | 192 | 209 | 206 | 4,943 | 117 | 114 | 79 | 3,077 |
| **14** | 291 | 194 | 132 | 2,313 | 90 | 373 | 181 | 1,723 | 53 | 74 | 34 | 1,373 |
| **28** | 279 | 204 | 260 | 1,627 | 138 | 59 | 214 | 1,242 | 67 | 144 | 49 | 406 |
| **56** | 326 | 234 | 153 | 766 | 229 | 204 | 318 | 584 | 54 | 80 | 114 | 471 |
| **84** | 300 | 247 | 172 | 508 | 188 | 86 | 136 | 651 | 44 | 57 | 40 | 467 |
| **168** | 372 | 451 | 160 | 626 | 322 | 203 | 338 | 532 | 76 | 117 | 91 | 314 |

Group 1 = 1 × $10^4$ CFU; group 2 = 1 × $10^5$ CFU; group 3 = 1 × $10^6$ CFU; group 4 = 1 × $10^7$ CFU BCG SSI.

historically BCG-vaccinated group at baseline compared with the naïve group (p = 0.023, Mann–Whitney; Figure 8). There was a trend towards better control of BCG growth after aerosol BCG, with lower median growth ratios at D7 and D28 compared with baseline, but this did not reach statistical significance.

## Discussion

This is the first aerosol-BCG CHIM to be completed on historically BCG-vaccinated volunteers. We have shown that aerosol challenge, which closely mimics the route of infection of *M.tb*, can be safely performed up to a loaded dose of 1 × $10^7$ CFU BCG Danish. Despite some variability in the frequency and severity of AEs between volunteers, this route of challenge and the following bronchoscopy was well-tolerated by volunteers.

All volunteers experienced some systemic and respiratory symptoms during the 28-day eDiary; however, no volunteers experienced severe (grade 3) symptoms as a direct result of BCG challenge and there were no serious adverse events in this study. The number of AEs reported within the first 72 h of challenge was greater in the highest-dose group (group 4), where both the frequency and maximum severity of systemic and respiratory symptoms increased. Despite the dose effect, even at the highest dose, the duration of AEs was generally short. Symptoms were predictable, with few unsolicited AEs recorded, and the most commonly reported AEs of cough, sore, or tickly throat and fatigue were generally mild, with only 10.4% of reported AEs

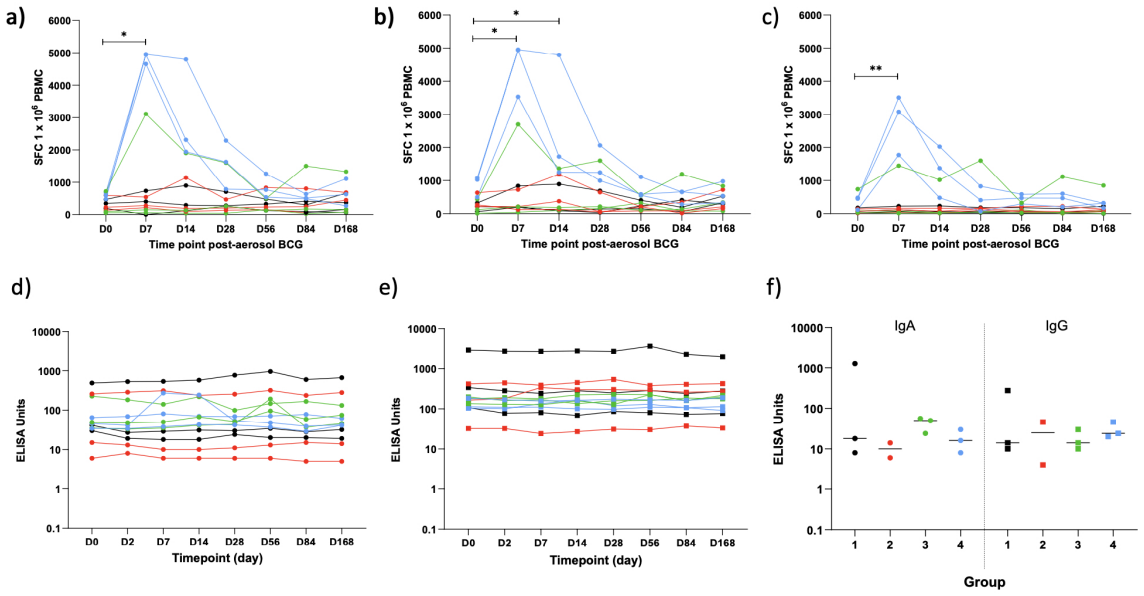


FIGURE 7
IFN-γ ELISpot responses to PPD **(A)**, BCG **(B)** and a pool of *M.tb* peptides - MTB300 **(C)** and ELISA PPD-specific IgA **(D)** and IgG **(E)** in serum at baseline and multiple time points post-aerosol BCG and in concentrated BAL fluid 14 days post-aerosol BCG **(F)**. Dots represent individual values, lines represent a volunteers response over time. Colours represent the different dose groups - black = 1 x $10^4$ CFU, red = 1 x $10^5$ CFU, green = 1 x $10^6$ CFU and blue = 1 x $10^7$ CFU. Stars denote significance *p = <0.05, **p = <0.01.

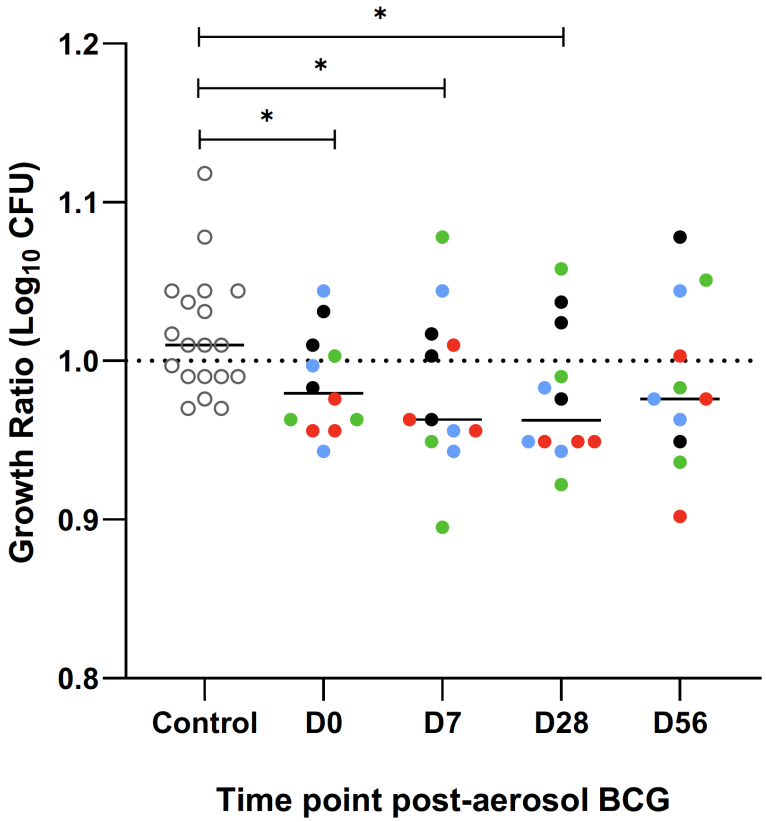


FIGURE 8
Ratio of BCG growth after a 96 hour incubation with PBMC, collected and frozen on day of aerosol BCG and 7, 28 and 56 days post-aerosol BCG, in the mycobacterial growth inhibition assay (MGIA). A group of BCG naïve volunteers (open circles) were run as a control for the assay. Colours represent the different dose groups - black = 1 x $10^4$ CFU, red = 1 x $10^5$ CFU, green = 1 x $10^6$ CFU and blue = 1 x $10^7$ CFU. Stars denote significance *p = <0.05.

more severe than grade 1. Compared with a previous aerosol BCG CHIM, which we have completed on BCG-naïve volunteers (18), the most commonly reported AEs were similar in type. Although the sample size of groups in this study are small, there does appear to be a trend for more symptoms in the 72 h following challenge in historically BCG vaccinated individuals than was seen previously in BCG-naïve volunteers (18). It is credible that a stronger and more rapid adaptive immunological response secondary to immunological memory meant that historically vaccinated individuals had a larger symptom burden. However, it is also important to note that this study was not blinded, whereas some aspects of our previous BCG-naïve study were, and this may have affected the rate of reporting.

AEs reported following bronchoscopy were also predictable and of a similar frequency to those reported in another healthy volunteer cohort (32). It was reassuring that we did not see a dose effect on the frequency of AEs post bronchoscopy, suggesting that BAL sampling at day 14 does not pose a significant risk of potentiating BCG infection after challenge; this is also in keeping with results from previous work in BCG naive volunteers, where there was no difference in the proportion of AEs reported by aerosol BCG and control groups (18, 33).

Comparison of symptom burden to another BCG respiratory challenge study published by Davids et al. is pertinent, as this study was also conducted on individuals who were historically BCG vaccinated, although some also had evidence of *M.tb* infection or previous disease (17). There are significant differences in methodology which make comparisons challenging, foremost that BCG was administered via bronchoscopy and only to one lobe of the lung and at a different dose (1 × $10^4$ CFU). The authors of this study state that 70% of individuals reported an AE deemed to be related to their bronchoscopy, whereas they concluded that there were no AEs definitively related to BCG (17). Making a clear distinction on causality, when the two events occur at the same timepoint, is challenging. We have shown that AEs related to BCG challenge and bronchoscopy are similar and we found no symptoms unique to each phase of our study. While aerosol BCG has historically been trialled as a treatment for lung carcinoma, the underlying pathology and concurrent use of other treatment make comparison difficult (34, 35).

One individual in group 4 of this study had markedly more symptoms within the first 72 h of challenge than were reported by other volunteers. This included several grade 2 symptoms: fever lasting 2 days, cough, arthralgia, myalgia, and fatigue as well as night sweats lasting 11 days. Symptoms were accompanied by a significantly raised C-reactive protein on day 2. It is difficult to be certain why this individual had such marked symptoms. Baseline characteristics, including time since initial BCG vaccination, was not significantly different to other volunteers. We considered whether this individual could have developed a BCGosis;

however, serial mycobacterial blood cultures were negative, and the acuity of symptoms and speed of recovery, without the need for additional treatment, did not support this. Although we did not find microbiological evidence for a concurrent viral or bacterial infection, we cannot entirely rule out this possibility as routine diagnostics for respiratory infections do not yield a causative organism in the majority of cases (36). Given the similarity in time course of symptom onset, it is likely that a major driver was a systemic response triggered by BCG re-exposure. This is supported by the large BCG-specific ELISpot response seen for this individual, and the transitory chest radiograph changes. Although this volunteer had a mild ongoing cough even at final visit on day 168, this was significantly improved, with the volunteer reporting only an occasional non-productive cough occurring very intermittently which was not affecting any of their normal activities. Causality in this regard is also difficult as this volunteer had been given a diagnosis of gastric reflux prior to starting the study, which is a common cause of chronic cough (37). The volunteer had elected not to initiate any preventative therapy offered for their diagnosis of reflux, and therefore we cannot rule out this co-existing diagnosis as contributory. Given the small number of volunteers recruited to the highest BCG dose, recruitment of more volunteers would be of benefit to evaluate the spectrum of symptoms experienced after aerosol BCG challenge in historically vaccinated individuals at a dose of $1 \times 10^7$ CFU/dose. There is significant heterogeneity in the side effect profile of those who receive intravesicular BCG for the treatment of bladder neoplasms (38), and it is likely that the same is true of BCG administered through the respiratory system.

We found no evidence of Koch phenomenon (39) after re-exposure to BCG, and despite frequent monitoring of lung function tests, there were no clinically significant drops in any of the functional tests. We did note a trend for larger drops from baseline of $TL_{CO}$ and $K_{CO}$ at day 7 in group 4. Measurement of $TL_{CO}$ is known to be highly variable; even after appropriate adjustment for demographics and haemoglobin, it has been shown to be affected by recent exercise and food intake as well as diurnal variations and timing of the menstrual cycle (40–42). Pulmonary function tests are also well established to be effort dependent (43), and this may explain some of the trend seen when compared with screening results. Given the inflammatory responses observed in volunteers, modest changes to lung $TL_{CO}$ could be expected. $TL_{CO}$ is not routinely used in clinical practice to assess response to infection; however, a study of adult patients admitted with acute varicella zoster infection showed that the transfer factor was significantly reduced in the majority of individuals following infection, even in the absence of a diagnosis of pneumonia (44). Volunteers with small reductions in $TL_{CO}$ in our study did not report associated clinical symptoms of breathlessness and had normal observations recorded and unremarkable physical examination at study visits. Reassuringly, we noted that the size of differences from baseline diminished upon retesting at day 84.

No BCG was detectable by BACTEC™ MGIT in BAL samples 14 days post-BCG challenge in any of the volunteers. The reasons for this are not immediately clear. We have previously shown that viable BCG can be consistently cultured from BCG-naïve healthy UK adults following challenge with a dose as low as $1 \times 10^4$ CFU BCG Bulgaria (18). It is conceivable that the immunological memory afforded by historic intradermal BCG vaccination for these individuals aided clearance prior to D14 or that there is a BCG strain affect. BCG conferred 80% protection in the British MRC study, and this potential demonstration of a known BCG vaccine effect in our aerosol BCG infection model provides data to support the biological validity of this model (45). In a different respiratory BCG CHIM, Davids et al. instilled a dose of $1 \times 10^4$ CFU BCG SSI (Danish) into a single lung segment of historically BCG-vaccinated volunteers, some of whom also had evidence of *M.tb* infection or previous disease (17). BCG was only recovered in 6 of 54 volunteers from a BAL completed 3 days after initial BCG challenge. Despite differences both in the modes of delivery, dose of BCG, and timing of bronchoscopy, it is credible in both studies that enhanced clearance was afforded from immunological memory of primary vaccination. As the sample size in each dosing group of our study was small, we cannot discount the possibility of successfully recovering BCG in a significant proportion of individuals. It is possible that the sensitivity to detect BCG in our study was hampered by the processing of BAL fluid samples. To reduce the risk of contamination by other typical bacteria, lavage samples underwent decontamination with MycoPrep™. NALC-NaOH-based approaches to decontamination such as MycoPrep™ are known to significantly reduce the viability of *M.tb* (46)., and it is credible that the same would be the case for BCG. Alternative processing techniques may improve the sensitivity of culture but would run a significant risk of contamination with other bacteria from the lung or oropharynx.

qPCR evidence of exhaled BCG was detected from face mask sampling in all three volunteers from group 4 immediately after challenge and from 2/3 volunteers in group 3. Previous studies have used this technology for identification of cases of incipient *M.tb* infections in those with subclinical disease, where it has been shown to have the potential to provide earlier diagnosis than sampling sputum (47), and an improved predictor of transmissibility (48). The larger proportion of positive samples in group 4 suggests a dose effect and provides support for the use of higher inoculums of BCG in this aerosol challenge model. It is notable that we were not able to isolate live BCG on any exhaled PVA strip samples after incubation in MGIT. As previously discussed, the sensitivity of culture is also likely to be reduced by the decontamination of samples with MycoPrep™, as has previously been reported during development of these adapted face masks (49). However, these data do provide a reassuring safety signal as it suggests that volunteers in this study do not pose a significant risk to close contacts even immediately after administration of aerosol BCG.

Two volunteers in group 4 also had positive PCRs on D14, despite having no culturable BCG in their BAL sample. This may be related to issues with sensitivity, but it is also credible that this constitutes genetic material from non-viable bacilli. Equally masks were worn for a relatively short time period (30 min) during which volunteers breathed normally. Although few studies have focussed directly on means to optimise sampling of infectious agents from adapted facemasks, the optimal duration of sampling is not established (50).

Previous experience of face mask sampling with *M.tb* has highlighted that sensitivity of this tool is likely to be improved with prolonged durations of mask wearing (49). Further work is needed to optimise the sensitivity of this emerging technology.

All volunteers in this study were shown to elicit significant adaptive immune responses to BCG infection. ELISpot responses were significantly increased compared with baseline. There was also evidence of a dose effect with volunteers in group 4 showing greater fold change compared with baseline when stimulated with PPD, BCG, and the MTB300 peptide pool. This time course is similar to what we have previously shown in BCG-naïve volunteers (18), and in an aerosol delivery study of the *M.tb* viral vector vaccine MVA85A (24), with peak responses occurring at day 7. Although we did not directly compare ELISpot responses between BCG-naïve and historically vaccinated individuals in this study, heightened ELISpot responses following revaccination with intradermal BCG have been reported in other studies (51). Further work to directly compare the magnitude of immunological responses between intradermal and aerosol routes after re-challenge would be valuable.

We did not see a significant increase in PPD-specific IgA and IgG responses compared with baseline in the serum of challenged volunteers, nor was there a significant difference in IgA and IgG levels in the BAL fluid between the different dose groups. The importance of antibodies in the clearance of mycobacteria remains contested and the results inconsistent (52). Data from a small study in Turkey showed that intradermal BCG causes increases in PPD-specific serum IgG after primary intradermal vaccination (53). There is evidence for increasing titres of antibodies to components of the cell wall in revaccination studies which may be more pertinent to our results. One group showed a detectable increase in IgG to lipoarabinomannan after primary intradermal BCG vaccination which increased again following intradermal re-vaccination 6 months later (54). It is possible that the time interval between primary and secondary exposure is important, as another group showed that while both primary and secondary vaccination resulted in transient increases from baseline antibody titres against arabinomannan, there was no difference in the maximal antibody responses between those who were BCG-naïve and those who had been vaccinated in childhood (55). Whether the aerosol route of delivery is important is not entirely clear. NHPs given primary aerosol BCG vaccination were shown to have a significant rise in serum PPD-specific IgG following primary aerosol vaccination (56). We have previously shown that there are significant increases from baseline in PPD-specific IgG and IgA responses in the serum after aerosol BCG (Bulgaria) vaccination, although IgG responses were short lived falling to baseline by day 14 (18). We are unaware of data reporting humoral responses to BCG revaccination through the aerosol route in animal or human models.

It is interesting that there was a trend towards better control in the MGIA assay after aerosol BCG, and that this was more marked in the highest-dosing group even though these data did not reach statistical significance. The MGIA is a functional sum-of-the-parts assay designed to establish whether the control of the combined immunological response to mycobacteria is enhanced (57). In this study, we completed the MGIA on frozen PBMC and did not include paired serum samples to minimise variability; this comes at the cost of negating the role of neutrophils and antibodies present in whole blood. The small sample size means that this study was not powered to draw clear conclusions but provides a basis to explore the role for aerosolised BCG as a vaccine candidate in its own right given non-human primate data, suggesting that mucosal BCG is more protective than intradermal BCG (58).

Guided by our previous work developing a BCG CHIM, we elected to utilise the entire BAL pellet for culture in order to improve the sensitivity of viable BCG detection (18). This has limited the ability to characterise the local pulmonary immunological responses to aerosol BCG in this study. Previous works conducted by our group and others have highlighted that local immune response kinetics can be very different to those seen in circulation after administration of BCG (17, 18). Given the successful dose escalation in this study, we plan to extensively interrogate the local immunological responses after challenge in the future cohort of historically BCG-vaccinated healthy adults. This is a key role for CHIM studies in accelerating vaccine research, providing an opportunity to identify novel corelates of protection and to identify novel vaccination targets and approaches (11).

In this study, we have shown that the aerosol BCG challenge is safe in historically BCG-vaccinated healthy adults up to a dose of $1 \times 10^7$ CFU. Although we showed subjects mounted significant BCG-specific immunological responses, we were not able to culture BCG from BAL samples taken 14 days after challenge. Future work should focus on exploring ways to maximise sensitivity of culture techniques in large cohorts to investigate whether aerosol BCG CHIMs are useful in assessing prime-boost vaccine regimes involving historically BCG-vaccinated individuals. Aerosol BCG CHIMs remain a promising tool to accelerate TB vaccine development and as an avenue to further appraise the role of aerosolised vaccines for respiratory infections, which could provide advantages over more conventional routes.

## Data availability statement

The original contributions presented in the study are included in the article/Supplementary Material. Further inquiries can be directed to the corresponding author.

## Ethics statement

The studies involving humans were approved by South Central - Oxford A Research Ethics Committee. The studies were conducted in accordance with the local legislation and institutional requirements. The participants provided their written informed consent to participate in this study.

## Author contributions

TF-J: Methodology, Data Curation, Investigation, Formal analysis, Visualization, Writing – review & editing, Writing – original draft. SH: Methodology, Investigation, Formal analysis,

Visualization, Writing – review & editing, Writing – original draft. HMo: Methodology, Investigation, Writing – review & editing. AA: Investigation, Writing – review & editing. BN: Investigation, Writing – review & editing. RR: Supervision, Writing – review & editing. CM: Investigation. Writing – review & editing. EF: Investigation, Writing – review & editing. JD: Investigation, Writing – review & editing. HP-J: Project Administration, Writing – review & editing. SJ: Methodology, Investigation, Writing – review & editing. AM: Investigation, Writing – review & editing. IS: Methodology, Investigation, Writing – review & editing. MB: Supervision, Validation. Writing – review & editing. TH: Investigation, Writing – review & editing. HB: Investigation, Writing – review & editing. HMc: Conceptualization, Methodology, Supervision, Writing – review & editing.

## Funding

The authors declare financial support was received for the research, authorship, and/or publication of this article. This project has been funded in whole or in part with Federal funds from the National Institute of Allergy and Infectious Diseases, National Institutes of Health, Department of Health and Human Services, under Contract No. 75N93021C00029. We thank the study volunteers for their time and commitment. The research was supported by the National Institute for Health Research (NIHR) Oxford Biomedical Research Centre (BRC). The views expressed are those of the authors and not necessarily those of the NHS, the NIHR or the Department of Health and Social Care.

## Acknowledgments

This study was completed as part of a IMPAC-TB consortium. We are grateful to the members of our Safety Monitoring Committee: Dr Hassan Mahomed (University of Stellenbosch, SA, Chair), Dr Francesca Little, University of Cape Town, SA), and Professor Stephen Gordon (Liverpool School of Tropical Medicine, UK). We would also like to thank the wider support from the Jenner Institute Vaccine Trials Team for wider aspects of the running of the clinical trial.

## Conflict of interest

The handling editor SF declared a past co-authorship with the author HM.

The authors declare that the research was conducted in the absence of any commercial or financial relationships that could be construed as a potential conflict of interest.

## Publisher's note



## Author disclaimer

The content is solely the responsibility of the authors and does not necessarily represent the official views of the National Institutes of Health. The views expressed are those of the author(s) and not necessarily those of the NHS, the NIHR, or the Department of Health.

## Supplementary material

The Supplementary Material for this article can be found online at: https://www.frontiersin.org/articles/10.3389/fimmu.2024.1427371/full#supplementary-material

## References

1. Organization WH. Global tuberculosis report 2023: Licence: CC BY-NC-SA 3.0 IGO. (2023).

2. Miller TL, McNabb SJ, Hilsenrath P, Pasipanodya J, Weis SE. Personal and societal health quality lost to tuberculosis. *PloS One*. (2009) 4:e5080. doi: 10.1371/journal.pone.0005080

3. Uplekar M, Weil D, Lonnroth K, Jaramillo E, Lienhardt C, Dias HM, et al. WHO's new end TB strategy. *Lancet*. (2015) 385:1799–801. doi: 10.1016/S0140-6736(15)60570-0

4. World Health O. *The Initiative for Vaccine Research strategic plan 2010-2020*. Geneva: World Health Organization (2010).

5. Mangtani P, Abubakar I, Ariti C, Beynon R, Pimpin L, Fine PE, et al. Protection by BCG vaccine against tuberculosis: a systematic review of randomized controlled trials. *Clin Infect Dis*. (2014) 58:470–80. doi: 10.1093/cid/cit790

6. Morven EMW, Helen M. TB vaccine development: where are we and why is it so difficult? *Thorax*. (2015) 70:299. doi: 10.1136/thoraxjnl-2014-205202

7. Chen WH, Cohen MB, Kirkpatrick BD, Brady RC, Galloway D, Gurwith M, et al. Single-dose live oral cholera vaccine CVD 103-hgR protects against human experimental infection with vibrio cholerae O1 el tor. *Clin Infect Dis*. (2016) 62:1329–35. doi: 10.1093/cid/ciw145

8. Kester KE, Cummings JF, Ofori-Anyinam O, Ockenhouse CF, Krzych U, Moris P, et al. Randomized, double-blind, phase 2a trial of falciparum malaria vaccines RTS,S/AS01B and RTS,S/AS02A in malaria-naive adults: safety, efficacy, and immunologic associates of protection. *J Infect Dis*. (2009) 200:337–46. doi: 10.1086/600120

9. Jin C, Gibani MM, Moore M, Juel HB, Jones E, Meiring J, et al. Efficacy and immunogenicity of a Vi-tetanus toxoid conjugate vaccine in the prevention of typhoid fever using a controlled human infection model of Salmonella Typhi: a randomised controlled, phase 2b trial. *Lancet*. (2017) 390:2472–80. doi: 10.1016/S0140-6736(17)32149-9

10. Clements ML, Betts RF, Murphy BR. Advantage of live attenuated cold-adapted influenza A virus over inactivated vaccine for A/Washington/80 (H3N2) wild-type virus infection. *Lancet*. (1984) 1:705–8. doi: 10.1016/S0140-6736(84)92222-0

11. Morrison H, Jackson S, McShane H. Controlled human infection models in COVID-19 and tuberculosis: current progress and future challenges. *Front Immunol*. (2023) 14:1211388. doi: 10.3389/fimmu.2023.1211388

12. Burki T. Pivotal tuberculosis vaccine trial begins. *Lancet*. (2024) 403:1125. doi: 10.1016/S0140-6736(24)00579-8

13. Villanueva P, Crawford NW, Garcia Croda M, Collopy S, Araújo Jardim B, de Almeida Pinto Jardim T, et al. Safety of BCG vaccination and revaccination in healthcare workers. *Hum Vaccin Immunother*. (2023) 19:2239088. doi: 10.1080/21645515.2023.2239088

14. Minassian AM, Ronan EO, Poyntz H, Hill AV, McShane H. Preclinical development of an in *vivo* BCG challenge model for testing candidate TB vaccine efficacy. *PloS One*. (2011) 6:e19840. doi: 10.1371/journal.pone.0019840

15. Harris SA, Meyer J, Satti I, Marsay L, Poulton ID, Tanner R, et al. Evaluation of a human BCG challenge model to assess antimycobacterial immunity induced by BCG and a candidate tuberculosis vaccine, MVA85A, alone and in combination. *J Infect Dis*. (2014) 209:1259–68. doi: 10.1093/infdis/jit647

16. Minhinnick A, Harris S, Wilkie M, Peter J, Stockdale L, Manjaly-Thomas ZR, et al. Optimization of a human bacille calmette-guérin challenge model: A tool to evaluate antimycobacterial immunity. *J Infect Dis*. (2016) 213:824–30. doi: 10.1093/infdis/jiv482

17. Davids M, Pooran A, Hermann C, Mottay L, Thompson F, Cardenas J, et al. A human lung challenge model to evaluate the safety and immunogenicity of PPD and live bacillus calmette-guérin. *Am J Respir Crit Care Med*. (2020) 201:1277–91. doi: 10.1164/rccm.201908-1580OC

18. Satti I, Marshall JL, Harris SA, Wittenberg R, Tanner R, Lopez Ramon R, et al. Safety of a controlled human infection model of tuberculosis with aerosolised, live-attenuated Mycobacterium bovis BCG versus intradermal BCG in BCG-naive adults in the UK: a dose-escalation, randomised, controlled, phase 1 trial. *Lancet Infect Dis*. (2024) 24:909-21. doi: 10.1016/S1473-3099(24)00143-9

19. Wu J, Hu Z, Lu SH, Fan XY. Heterologous prime-boost BCG with DNA vaccine expressing fusion antigens Rv2299c and Ag85A improves protective efficacy against Mycobacterium tuberculosis in mice. *Front Microbiol*. (2022) 13:927031. doi: 10.3389/fmicb.2022.927031

20. Andersson NW, Thiesson EM, Baum U, Pihlström N, Starrfelt J, Faksová K, et al. Comparative effectiveness of heterologous third dose vaccine schedules against severe covid-19 during omicron predominance in Nordic countries: population based cohort analyses. *BMJ*. (2023) 382:e074325. doi: 10.1136/bmj-2022-074325

21. Bannister S, Sudbury E, Villanueva P, Perrett K, Curtis N. The safety of BCG revaccination: A systematic review. *Vaccine*. (2021) 39:2736–45. doi: 10.1016/j.vaccine.2020.08.016

22. Morrison AL, Sarfas C, Sibley L, Williams J, Mabbutt A, Dennis MJ, et al. IV BCG Vaccination and Aerosol BCG Revaccination Induce Mycobacteria-Responsive γδ T Cells Associated with Protective Efficacy against M. tb Challenge. *Vaccines (Basel)*. (2023) 11. doi: 10.3390/vaccines11101604

23. BCG vaccine AJV smPC. Available online at: https://www.medicines.org.uk/emc/product/9890/smpcgref (Accessed April 15, 2024).

24. Satti I, Meyer J, Harris SA, Manjaly Thomas ZR, Griffiths K, Antrobus RD, et al. Safety and immunogenicity of a candidate tuberculosis vaccine MVA85A delivered by aerosol in BCG-vaccinated healthy adults: a phase 1, double-blind, randomised controlled trial. *Lancet Infect Dis*. (2014) 14:939–46. doi: 10.1016/S1473-3099(14)70845-X

25. Akkerman OW, Werf T, Boer Md, Beer J, Rahim Z, Rossen JWA, et al. Comparison of 14 molecular assays for detection of mycobacterium tuberculosis complex in bronchoalveolar lavage fluid. *J Clin Microbiol*. (2013) 51:3505–11. doi: 10.1128/JCM.00843-13

26. Minassian AM, Satti I, Poulton ID, Meyer J, Hill AV, McShane H. A human challenge model for Mycobacterium tuberculosis using Mycobacterium bovis bacille Calmette-Guerin. *J Infect Dis*. (2012) 205:1035–42. doi: 10.1093/infdis/jis012

27. Meyer J, Harris SA, Satti I, Poulton ID, Poyntz HC, Tanner R, et al. Comparing the safety and immunogenicity of a candidate TB vaccine MVA85A administered by intramuscular and intradermal delivery. *Vaccine*. (2013) 31:1026–33. doi: 10.1016/j.vaccine.2012.12.042

28. Moliva JI, Rajaram MV, Sidiki S, Sasindran SJ, Guirado E, Pan XJ, et al. Molecular composition of the alveolar lining fluid in the aging lung. *Age (Dordr)*. (2014) 36:9633. doi: 10.1007/s11357-014-9633-4

29. Arcos J, Sasindran SJ, Fujiwara N, Turner J, Schlesinger LS, Torrelles JB. Human lung hydrolases delineate Mycobacterium tuberculosis-macrophage interactions and the capacity to control infection. *J Immunol*. (2011) 187:372–81. doi: 10.4049/jimmunol.1100823

30. Tanner R, Satti I, Harris SA, O'Shea MK, Cizmeci D, O'Connor D, et al. Tools for Assessing the Protective Efficacy of TB Vaccines in Humans: in vitro Mycobacterial Growth Inhibition Predicts Outcome of in *vivo* Mycobacterial Infection. *Front Immunol*. (2020) 10. doi: 10.3389/fimmu.2019.02983

31. Hodgson SH, Iveson P, Larwood J, Roche S, Morrison H, Cosgrove C, et al. Incidental findings in UK healthy volunteers screened for a COVID-19 vaccine trial. *Clin Trans Science*. (2022) 15:524–34. doi: 10.1111/cts.13170

32. Leiten EO, Eagan TML, Martinsen EMH, Nordeide E, Husebø GR, Knudsen KS, et al. Complications and discomfort after research bronchoscopy in the MicroCOPD study. *BMJ Open Respir Res*. (2020) 7:e000449. doi: 10.1136/bmjresp-2019-000449

33. Morrison H, Jackson S, Marshall J, Mitton C, Lopez Ramon R, Fredsgaard-Jones T, et al. Healthy volunteer symptom profile following research bronchoscopy. *Eur Respir J*. (2023) 62:PA4628. doi: 10.1183/13993003.congress-2023.PA4628

34. Cusumano CL, Jernigan JA, Waldman RH. Aerosolized BCG (Tice strain) treatment of bronchogenic carcinoma: phase I study. *J Natl Cancer Inst*. (1975) 55:275–9.

35. Garner FB, Meyer CA, White DS, Lipton A. Aerosol BCG treatment of carcinoma metastatic to the lung: a phase I study. *Cancer*. (1975) 35:1088–94. doi: 10.1002/1097-0142(197504)35:4<1088::AID-CNCR2820350411>3.0.CO;2-2

36. Jain S, Self WH, Wunderink RG, Fakhran S, Balk R, Bramley AM, et al. Community-acquired pneumonia requiring hospitalization among U.S. Adults. *New Engl J Med*. (2015) 373:415–27. doi: 10.1056/NEJMoa1500245

37. Chang AB, Lasserson TJ, Gaffney J, Connor FL, Garske LA. Gastro-oesophageal reflux treatment for prolonged non-specific cough in children and adults. *Cochrane Database Systematic Rev*. (2011) 1). doi: 10.1002/14651858.CD004823.pub4

38. Liu Y, Lu J, Huang Y, Ma L. Clinical spectrum of complications induced by intravesical immunotherapy of bacillus calmette-guérin for bladder cancer. *J Oncol*. (2019) 2019:6230409. doi: 10.1155/2019/6230409

39. Taylor JL, Turner OC, Basaraba RJ, Belisle JT, Huygen K, Orme IM. Pulmonary necrosis resulting from DNA vaccination against tuberculosis. *Infect Immun*. (2003) 71:2192–8. doi: 10.1128/IAI.71.4.2192-2198.2003

40. Medarov BI, Pavlov VA, Rossoff L. Diurnal variations in human pulmonary function. *Int J Clin Exp Med*. (2008) 1:267–73.

41. Sansores RH, Abboud RT, Kennell C, Haynes N. The effect of menstruation on the pulmonary carbon monoxide diffusing capacity. *Am J Respir Crit Care Med*. (1995) 152:381–4. doi: 10.1164/ajrccm.152.1.7599851

42. Brian LG, Vito B, Felip B, Brendan GC, Robert J, Adrian K, et al. 2017 ERS/ATS standards for single-breath carbon monoxide uptake in the lung. *Eur Respir J*. (2017) 49:1600016. doi: 10.1183/13993003.00016-2016

43. Gregg LR, Paul LE. Pulmonary function testing. *Respir Care*. (2012) 57:165. doi: 10.4187/respcare.01640

44. Mohsen AH, Peck RJ, Mason Z, Mattock L, McKendrick MW. Lung function tests and risk factors for pneumonia in adults with chickenpox. *Thorax*. (2001) 56:796–9. doi: 10.1136/thorax.56.10.796

45. Hart PD, Sutherland I. BCG and vole bacillus vaccines in the prevention of tuberculosis in adolescence and early adult life. *Br Med J*. (1977) 2:293–5. doi: 10.1136/bmj.2.6082.293

46. Mtafya B, Sabiiti W, Sabi I, John J, Sichone E, Ntinginya Nyanda E, et al. Molecular bacterial load assay concurs with culture on naOH-induced loss of mycobacterium tuberculosis viability. *J Clin Microbiol*. (2019) 57. doi: 10.1128/jcm.01992-18

47. Williams CM, Abdulwhhab M, Birring SS, De Kock E, Garton NJ, Townsend E, et al. Exhaled Mycobacterium tuberculosis output and detection of subclinical disease by face-mask sampling: prospective observational studies. *Lancet Infect Dis*. (2020) 20:607–17. doi: 10.1016/S1473-3099(19)30707-8

48. Williams CM, Muhammad AK, Sambou B, Bojang A, Jobe A, Daffeh GK, et al. Exhaled mycobacterium tuberculosis predicts incident infection in household contacts. *Clin Infect Dis*. (2023) 76:e957–e64. doi: 10.1093/cid/ciac455

49. Williams CM, Cheah ES, Malkin J, Patel H, Otu J, Mlaga K, et al. Face mask sampling for the detection of Mycobacterium tuberculosis in expelled aerosols. *PloS One*. (2014) 9:e104921. doi: 10.1371/journal.pone.0104921

50. Hu B. Recent advances in facemask devices for in *vivo* sampling of human exhaled breath aerosols and inhalable environmental exposures. *Trends Analyt Chem*. (2022) 151:116600. doi: 10.1016/j.trac.2022.116600

51. Whelan KT, Pathan AA, Sander CR, Fletcher HA, Poulton I, Alder NC, et al. Safety and immunogenicity of boosting BCG vaccinated subjects with BCG: comparison with boosting with a new TB vaccine, MVA85A. *PloS One*. (2009) 4:e5934. doi: 10.1371/journal.pone.0005934

52. Tanner R, Villarreal-Ramos B, Vordermeier HM, McShane H. The humoral immune response to BCG vaccination. *Front Immunol*. (2019) 10:1317. doi: 10.3389/fimmu.2019.01317

53. Beyazova U, Rota S, Cevheroğlu C, Karsligil T. Humoral immune response in infants after BCG vaccination. *Tubercle Lung Disease*. (1995) 76:248–53. doi: 10.1016/s0962-8479(05)80013-9

54. de Vallière S, Abate G, Blazevic A, Heuertz RM, Hoft DF. Enhancement of innate and cell-mediated immunity by antimycobacterial antibodies. *Infection Immunity*. (2005) 73:6711–20. doi: 10.1128/IAI.73.10.6711-6720.2005

55. Chen T, Blanc C, Eder AZ, Prados-Rosales R, Souza AC, Kim RS, et al. Association of human antibodies to arabinomannan with enhanced mycobacterial opsonophagocytosis and intracellular growth reduction. *J Infect Dis*. (2016) 214:300–10. doi: 10.1093/infdis/jiw141

56. White AD, Sarfas C, West K, Sibley LS, Wareham AS, Clark S, et al. Evaluation of the immunogenicity of mycobacterium bovis BCG delivered by aerosol to the lungs of macaques. *Clin Vaccine Immunol*. (2015) 22:992–1003. doi: 10.1128/CVI.00289-15

57. Tanner R, Hoogkamer E, Bitencourt J, White A, Boot C, Sombroek CC, et al. The in *vitro* direct mycobacterial growth inhibition assay (MGIA) for the early evaluation of TB vaccine candidates and assessment of protective immunity: a protocol for non-human primate cells. *F1000Res*. (2021) 10:257. doi: 10.12688/f1000research

58. Dijkman K, Sombroek CC, Vervenne RAW, Hofman SO, Boot C, Remarque EJ, et al. Prevention of tuberculosis infection and disease by local BCG in repeatedly exposed rhesus macaques. *Nat Med*. (2019) 25:255–62. doi: 10.1038/s41591-018-0319-9

frontiers | Frontiers in Immunology

TYPE Review
PUBLISHED 09 December 2024
DOI 10.3389/fimmu.2024.1427559



OPEN ACCESS

EDITED BY
Angelo Izzo,
Royal Prince Alfred Hospital, Australia

REVIEWED BY
Jayne Hope,
University of Edinburgh, United Kingdom
Mohd Saqib,
Albany Medical College, United States
Taru S. Dutt,
Colorado State University, United States

*CORRESPONDENCE
Edward D. Chan
chane@njhealth.org

RECEIVED 04 May 2024
ACCEPTED 18 November 2024
PUBLISHED 09 December 2024

CITATION
Lyu J, Narum DE, Baldwin SL, Larsen SE, Bai X, Griffith DE, Dartois V, Naidoo T, Steyn AJC, Coler RN and Chan ED (2024) Understanding the development of tuberculous granulomas: insights into host protection and pathogenesis, a review in humans and animals.
*Front. Immunol.* 15:1427559.
doi: 10.3389/fimmu.2024.1427559



# Understanding the development of tuberculous granulomas: insights into host protection and pathogenesis, a review in humans and animals

Jiwon Lyu[1,2], Drew E. Narum[2], Susan L. Baldwin[3], Sasha E. Larsen[3], Xiyuan Bai[2,4], David E. Griffith[5], Véronique Dartois[6], Threnesan Naidoo[7], Adrie J. C. Steyn[8,9], Rhea N. Coler[3,10,11] and Edward D. Chan[2,4,12]*

[1]Division of Pulmonary and Critical Medicine, Soon Chun Hyang University Cheonan Hospital, Seoul, Republic of Korea, [2]Department of Academic Affairs, National Jewish Health, Denver, CO, United States, [3]Center for Global Infectious Diseases, Seattle Children's Research Institute, Seattle, WA, United States, [4]Division of Pulmonary Sciences and Critical Care Medicine, University of Colorado School of Medicine, Aurora, CO, United States, [5]Department of Medicine, National Jewish Health, Denver, CO, United States, [6]Center for Discovery and Innovation, Hackensack Meridian School of Medicine, Nutley, NJ, United States, [7]Departments of Forensic & Legal Medicine and Laboratory Medicine & Pathology, Faculty of Medicine & Health Sciences, Walter Sisulu University, Mthatha, South Africa, [8]Africa Health Research Institute, University of KwaZulu-Natal, Durban, South Africa, [9]Department of Microbiology and Centers for AIDS Research and Free Radical Biology, University of Alabama at Birmingham, Birmingham, AL, United States, [10]Department of Pediatrics, University of Washington School of Medicine, Seattle, WA, United States, [11]Department of Global Health, University of Washington, Seattle, WA, United States, [12]Department of Medicine, Rocky Mountain Regional Veterans Affairs Medical Center, Aurora, CO, United States

Granulomas, organized aggregates of immune cells which form in response to *Mycobacterium tuberculosis* (*Mtb*), are characteristic but not exclusive of tuberculosis (TB). Despite existing investigations on TB granulomas, the determinants that differentiate host-protective granulomas from granulomas that contribute to TB pathogenesis are often disputed. Thus, the goal of this narrative review is to help clarify the existing literature on such determinants. We adopt the *a priori* view that TB granulomas are host-protective organelles and discuss the molecular and cellular determinants that induce protective granulomas and those that promote their failure. While reports about protective TB granulomas and their failure may initially seem contradictory, it is increasingly recognized that either deficiencies or excesses of the molecular and cellular components in TB granuloma formation may be detrimental to the host. More specifically, insufficient or excessive expression/representation of the following components have been reported to skew granulomas toward the less protective phenotype: *(i)* epithelioid macrophages; *(ii)* type 1 adaptive immune response; *(iii)* type 2 adaptive immune response; *(iv)* tumor necrosis factor; *(v)* interleukin-12; *(vi)* interleukin-17; *(vii)* matrix metalloproteinases; *(viii)* hypoxia in the TB granulomas; *(ix)* hypoxia inducible factor-1 alpha; *(x)* aerobic glycolysis; *(xi)* indoleamine 2,3-dioxygenase activity; *(xii)* heme oxygenase-1 activity; *(xiii)* immune checkpoint; *(xiv)* leukotriene A4 hydrolase activity; *(xv)* nuclear-factor-kappa B; and *(xvi)* transforming growth factor-beta. Rather, more precise and timely coordinated immune responses appear essential for eradication or containment of *Mtb* infection. Since there are several animal

models of infection with *Mtb*, other species within the *Mtb* complex, and the surrogate *Mycobacterium marinum* – whether natural (cattle, elephants) or experimental (zebrafish, mouse, guinea pig, rabbit, mini pig, goat, non-human primate) infections – we also compared the TB granulomatous response and other pathologic lung lesions in various animals infected with one of these mycobacteria with that of human pulmonary TB. Identifying components that dictate the formation of host-protective granulomas and the circumstances that result in their failure can enhance our understanding of the macrocosm of human TB and facilitate the development of novel remedies – whether they be direct therapeutics or indirect interventions – to efficiently eliminate *Mtb* infection and prevent its pathologic sequelae.

KEYWORDS

**tuberculosis, pathology, animal models, immunology, lung, mycobacteria, granuloma**

# 1 Introduction

Granulomas are aggregates of immune cells that form in response to repetitive exposure to various stimuli that include infectious agents (*e.g.*, bacteria, fungi, protozoa, helminths, and viruses), non-infectious foreign bodies (*e.g.*, talc, starch, sutures), or an unknown inciting agent (*e.g.*, sarcoidosis, Crohn's enteritis, granulomatosis with polyangiitis, polyarteritis nodosa, *etc.*) (1–3). While granulomas are typically regarded as a host-protective response against microbial agents, they may also lead to pathologic consequences, especially if the granulomas are unable to eradicate the microbes (2). In the context of tuberculosis (TB), granulomas are well documented in both humans and experimental animals (4).

The objective of this narrative review is to describe the factors that provide a host-protective granulomatous response with TB and the circumstances which cause granulomas fail. To help shed light on determinants of protective and non-protective TB granulomas, we also compared the TB granulomatous response and other pathologic lung lesions in various animals naturally or experimentally infected with *Mycobacterium tuberculosis* (*Mtb*), other *Mtb* complex species, or a mycobacterial surrogate with that of human pulmonary TB.

**Abbreviations:** AFB, acid-fast bacilli; BCG, Bacillus Calmette Guérin; CT, computed tomography; CTLA-4, cytotoxic T lymphocyte-associated protein 4; ESAT-6, early secreted antigenic target 6; FDG, deoxy-2-[$^{18}$F]-fluoro-D-glucose; iBALT, inducible bronchus-associated lymphoid tissue; IDO-1, indoleamine 2,3-dioxygenase; IFNγ, interferon-gamma; HIF-1α, hypoxia inducible factor-1-alpha; HO-1, heme oxygenase-1; IL-12, interleukin-12; IL-17, interleukin-17; LDL, low density lipoprotein; LTA4H, leukotriene A4 hydrolase; $LTA_4$, leukotriene $A_4$; $LTB_4$, leukotriene $B_4$; $LXA_4$, lipoxin $A_4$; MGC, multinucleated giant cell; MIBI-TOF, multiplexed ion beam imaging by time-of-flight; μCT, micro-computed tomography; MMP-1, matrix metalloproteinase-1; MMP-9, matrix metalloproteinase-9; *Mtb, Mycobacterium tuberculosis*; NET, neutrophil extracellular trap; NFκB, nuclear factor kappa-B; NHP, non-human primates; PD-1, programmed cell death protein-1; PD-L1, programmed death-ligand 1; PET, positron emission tomography; PPARγ, peroxisome proliferator-gamma; RIP1, receptor-interacting serine/threonine kinase 1; RIP3, receptor-interacting protein interacting serine/threonine kinase 3; RIPK-3, receptor interacting protein kinase 3; ROS, reactive oxygen species; STAT6, signal transducer and activator of transcription 6; TB, tuberculosis; TCR, T cell receptor; TDM, trehalose 6,6'-dimycolate; TIM3, T cell immunoglobin and mucin domain-containing protein-3; TLO, tertiary lymphoid organs; TGFβ, transforming growth factor-beta; TNF, tumor necrosis factor; TR4, testicular receiver 4.

# 2 Cellular composition and functions of the TB granuloma

## 2.1 Overall structure of granulomas

Granulomas are considered a key histopathologic feature of TB. Classically, the spatial organization of TB granulomas is comprised of a central region populated with macrophages (epithelioid, activated, and foamy macrophages) with an innermost zone that may become necrotic. Other myeloid cell types (dendritic cells, neutrophils, eosinophils, multinucleated giant cells, and/or mast cells) may be interspersed with the macrophages. Surrounding the macrophages are lymphocytes (T cells, B cells, natural killer cells, and innate lymphoid cells), forming a cuff in the outer zone of the granulomas (Figures 1A, B). Granulomas may also contain endothelial and epithelial cells from blood vessels and airways, respectively, as well as be encapsulated by collagen secreted by fibroblasts. However, granulomas may display great diversity with regards to certain immunological characteristics even within a single individual (5). In more protective granulomas, the concentric cell layers are gradually organized along with the

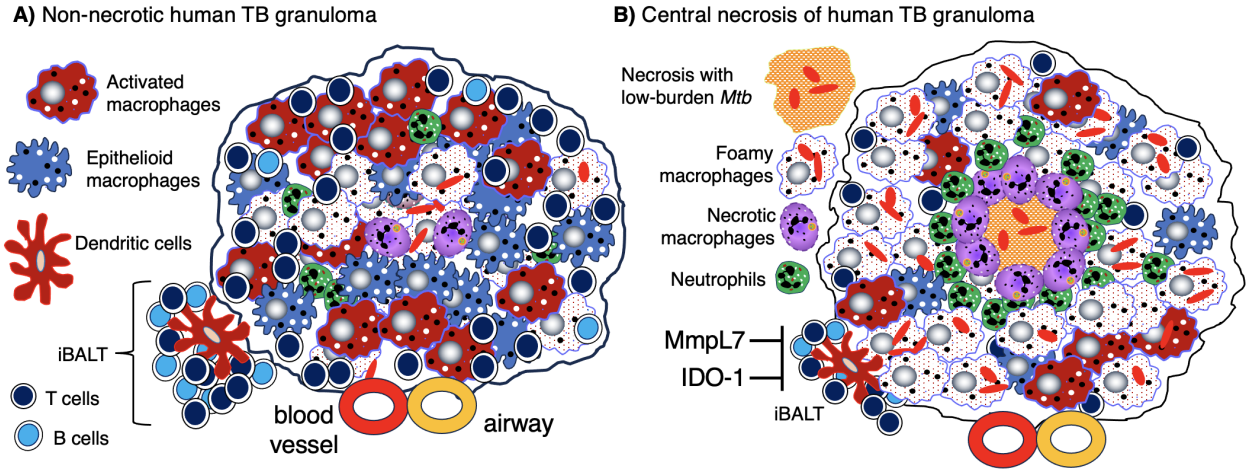


FIGURE 1
Human TB granulomas may be non-necrotic or necrotic. Several different fates of granulomas occur and such heterogeneity may present in the same individual. **(A)** A non-necrotic TB granuloma is characterized by the presence of epithelioid macrophages and activated macrophages as well as fewer foamy macrophages, necrotic macrophages, neutrophils, and more or less a rim of host-protective T cells and B cells along with relatively few bacilli. iBALT may be considered an "appendage" of granulomas typically comprised of dendritic cells, B cells, and T cells and may serve as a ready supply of immune cells for the neighboring granuloma. This granuloma is protective as shown by the relatively few *Mtb* (red-colored rod-shaped structures. **(B)** A granuloma with central necrosis characterized by fewer epithelioid and activated macrophages and more foamy macrophages, necrotic macrophages, and neutrophils along with an area of central necrosis. There are also fewer host-protective T cells and B cells. Due to the fewer number of host-protective innate and adaptive immune cells, there is overall a greater *Mtb* burden. However, in the central necrotic area of this human granuloma, there is active killing of *Mtb* resulting in fewer viable *Mtb* in this region. Higher levels of MmpL7 and IDO-1 inhibit iBALT formation. IDO-1, indoleamine 2,3-dioxygenase; iBALT, inducible bronchus-associated lymphoid tissue; MmpL7, Mycobacterial membrane protein Large 7; *Mtb*, *Mycobacterium tuberculosis*; TB, tuberculosis.

presence of fibrosis, which suppresses necrosis, strengthens the lymphocytic rim, and leads to pathologic resolution (Figure 1A). These resolved granulomas can be identified radiologically and histologically by dystrophic calcification of the necrotic debris within these structures (6). In cases of active and progressive TB, granulomas have higher number of foamy macrophages and neutrophils as well as exhibit necrotic centers (Figure 1B).

Granulomas can be classified by several different morphological characteristics. One is whether cells within the central regions of granulomas are necrotic, which may be found in human TB, in natural TB in animals, and experimental TB in some laboratory animals. Caseation is the gross pathological term which alludes to the "cheese-like" material found when sufficient number of macrophages in the granuloma core undergo necrotic cell death. Caseating granulomas typically are consisted of necrotic, acellular core surrounded by epithelioid macrophages, and an outer lymphocytic cuff comprised of B and T cells (7). While the presence or absence of granuloma necrosis is often linked, respectively, to infectious (*e.g.*, TB) or non-infectious (*e.g.*, sarcoidosis) etiology for the granuloma, this dichotomy is not absolute. For example, necrosis may be seen in some non-infectious granulomas (2) and TB granulomas may not show any necrosis (Figure 2) (8).

Granulomas can show other morphological characteristics. Some granulomas may display fibrosis, characterized by collagen deposit either peripherally (those with a cuff of collagen surrounding them) or centrally (those with collagen throughout the entire granuloma) (9). Another subtype of granulomas is known as suppurative or neutrophil-rich granuloma. These granulomas arise when neutrophils infiltrate the center of the granuloma. Overall, high concentrations of neutrophils within *Mtb* granulomas have shown to be host destructive (enable spread of infection, higher levels of inflammation, and result in poorer host outcomes) (10). A calcified granuloma is typically regarded as the "final" stage of infection, and a sign of a successful host-immune response. The calcification (or mineralization) process typically begins within the caseous center (7, 11).

## 2.2 Selected immune cells that comprise granulomas

### 2.2.1 Macrophages

Lung macrophages are ubiquitous in granulomas and along with dendritic cells are likely the first cell types in the nascent granuloma. These phagocytes engulf *Mtb* and orchestrate the influx of other cell types (2). After being engulfed, *Mtb* are killed when *Mtb*-containing phagosomes fuse with lysosomes. However, the bacilli may avoid this fate by inhibiting phagosome and autophagosome maturation (12–16). Ingested *Mtb* may also escape from arrested phagosomes by disrupting the phagosome membrane – *via* the release of *Mtb* pore-forming protein ESAT-6 (early secreted antigenic target-6) utilizing the ESX-1 (type VII) secretion system – and translocating into the cytoplasm (17, 18). In

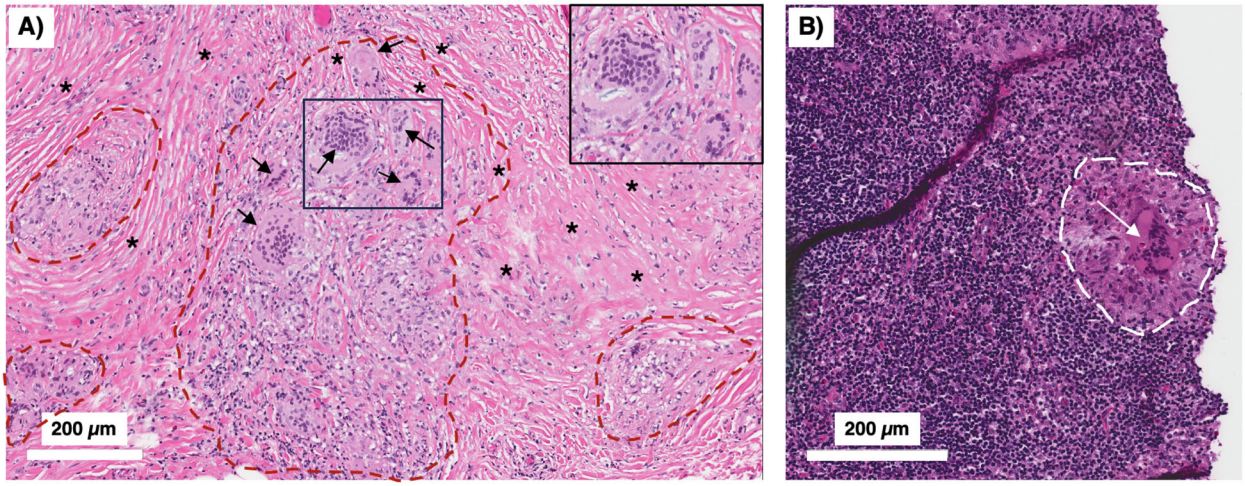


FIGURE 2
Peritoneal TB with non-necrotizing granulomas. A 51-year-old man from the Philippines presented with a two-year history of early satiety, intractable abdominal pain, and weight loss exceeding 60 pounds. Abdominal CT showed evidence of "peritoneal carcinomatosis." **(A)** Peritoneal biopsy showed no evidence of malignancy. Instead, there were multiple non-necrotizing granulomas (demarcated by red dashed lines) with prominent Langhans-type multinucleated giant cells (arrows) and surrounding fibrosis (asterisks) (H&E). The boxed inset shows a magnified view of the smaller box demonstrating the multinucleated giant cells. **(B)** A peritoneal lymph node biopsy showed similar non-necrotizing granulomatous inflammation (white dashed line) with a conspicuous multinucleated giant cells (white arrow) (H&E). The acid-fast stain in both the peritoneal and lymph node biopsies were negative. With standard treatment for drug-susceptible TB, his symptoms abated and he regained his lost body weight. TB, tuberculosis.

the cytosol, *Mtb* replicates, precipitating both necrosis of the phagocytes and release of bacilli extracellularly. Neighboring macrophages then phagocytose the released *Mtb* and the infection cycle repeats. During this cycle of suboptimal control of infection, the infected and subsequent necrotic macrophages release both inflammatory chemokines and mycobacterial cell wall components that induce influx of neutrophils and monocytes to the infection site, forming the early granuloma (19).

Infected macrophages and dendritic cells also migrate to the regional mediastinal lymph nodes to help differentiate and recruit antigen-specific T cells (*e.g.*, $T_H1$ and $T_H17$), which then migrate to the infection site, activate monocytes and macrophages, and participate in the formation of evolving granulomas (15, 16, 19–21). This delayed influx of recruited T cells to the site of the infection may allow *Mtb* to persist if the initial macrophages encountered are of the more "permissive" phenotype (22). However, with sufficient recruitment of *Mtb*-specific and activated T cells to the granulomas, containment or eradication of *Mtb* within the granulomas is possible. Macrophages in evolving granulomas may be comprised of various phenotypes, including "classically activated"/inflammatory (M1) macrophages and various subsets of "alternatively activated" (M2) macrophages as well as other morphologically distinct macrophages (epithelioid macrophages, foamy macrophages) that likely have overlapping features with M1 or M2 macrophages, and multinucleated Langhans giant cells (23, 24).

M1 macrophages are activated in response to $T_H1$ T-cell signals (interferon-gamma [IFNγ] and tumor necrosis factor [TNF]) as well as lipopolysaccharide (LPS) (7). Once activated, M1 macrophages secrete pro-inflammatory cytokines (TNF, interleukin-1 [IL-1], IL-6) and inducible nitric oxide synthase (iNOS). Whereas the M1 response is important in TB control, an excessive response can lead to chronic inflammation as well as inflammatory diseases (25). On the other hand, M2 macrophages are known to inhibit the inflammatory response, playing an important role in wound healing and tissue repair. These macrophages are activated by $T_H2$ T-cell cytokines (IL-4 and IL-13). In response, they produce anti-inflammatory cytokines (IL-10, transforming growth factor-beta [TGFβ]), IL-6, and arginase (7, 25). However, this binary categorization is likely an oversimplification to fully describe the function of these subtypes, especially M2 macrophages which are divided into at least three sub-phenotypes (26, 27). We expound below two distinct macrophage phenotypes given their preponderance in granulomas: "epithelioid macrophages" and "foamy macrophages" (2, 28).

#### 2.2.1.1 Epithelioid macrophages

Epithelioid macrophages are so named due to their cellular characteristics that resemble epithelial cells: spread morphology, elongated nuclei, high cytoplasm-to-nucleus ratio, and contact interaction with neighboring macrophages. Epithelioid macrophages are also less phagocytic and more secretive than activated macrophages (29, 30). Additional characteristics of epithelioid macrophages are discussed in Table 1.

#### 2.2.1.2 Foamy macrophages

Macrophages in some TB granulomas appear foamy due to the accumulation of various intracellular lipids (cholesterol, triglycerides, and phospholipids) (31). In foamy macrophages, bacilli are observed in proximity to lipid droplets, posited to be a nutrient source for *Mtb* (29). Foamy macrophages are typically found around the edge of the necrotic core of caseating granulomas

TABLE 1 Epithelioid and foamy macrophages in TB granulomas.

| Cell Type | Location in granuloma | Role in mycobacterial infection | Stimulus that drives production |
|---|---|---|---|
| **Epithelioid macrophages** | Surrounding the necrotic center and interspersed in the cellular rim (34) | Depletion leads to increased intracellular bacillary numbers (35) whereas excessive formation "walls off" infection site from other immune cells and antibiotics (36, 37) | IL-4 activation of STAT6, which mediates expression of E-cadherin, adhesion molecule that is crucial in transforming cytoskeletal structure of epithelioid macrophages through production of adherens junctions, desmosomes, & tight junctions (11, 35, 37) |
| **Foamy macrophages** | Surrounding the necrotic center; rarely found in non-necrotic granulomas (32) | Contributes to caseous necrosis (by discharging intracellular lipids & *Mtb*) & have less bactericidal/phagocytic compared to other macrophages due to fat accumulation, creating long-term persistence of *Mtb* in these cells (31, 38); fat accumulation occurs due to ESX-1 driven metabolic shift from glycolysis to ketogenic pathway synthesis, inducing expression of G-protein coupled receptor GPR109A which inhibits lipolysis (39) (Figure 3); fat accumulation decreases autophagy due to lower expression of lactate (byproduct of glycolysis), which normally increases autophagy by *lactylation* of class III phosphatidylinositol 3 kinase) (39–42); reduced autophagy further attenuates glycolysis and ketogenic pathway (*i.e.*, oxidative phosphorylation), the latter via autophagy mediated metabolism of triglycerides into fatty acids, which are then broken down into acetyl Co A in the mitochondria for ATP production (43–45). | *Mtb* derived oxygenated mycolic acids bind to host lipid sensing nuclear receptors PPARγ and TR4, inducing production of host derived LDL receptors (scavenger receptor A and CD36) (31, 38, 46, 47); these receptors bind and mediate influx of host derived LDL intracellularly (Figure 3); ESX-1 drives foamy macrophage formation in *M. marinum*-zebrafish model (48); IL-10 also shown to induce differentiation to foamy macrophages (49) |

ESX-1, ESAT-6 protein family secretion system (ESAT-6, 6 KDa early secretory antigenic target); IL-4, interleukin-4; LDL, low density lipoprotein; PPARγ, peroxisome proliferator-gamma; TR4, testicular receiver 4.

and rarely found in non-necrotic granulomas (Figures 1, 3) (32). In human autopsy cases of TB, foamy DEC-205$^+$ dendritic cells were more common in lipoid pneumonia and cavitary lesions than in granulomas (33). Additional characteristics of foamy macrophages are discussed in Table 1.

#### 2.2.1.3 Apoptotic vs. necrotic cell death of phagocytes in granulomas

Death of *Mtb*-containing phagocytes may either be a mechanism of restricting *Mtb* replication or spreading the infection. Apoptosis of *Mtb*-infected cells is a mechanism by which phagocytosed intracellular bacilli are killed (50–58). In addition, macrophage phagocytosis of apoptotic bodies – a process known as efferocytosis – can further enhance the killing of *Mtb* contained within the apoptotic bodies (59). Thus, apoptosis is a host protective mechanism to not only dispose of phagocytosed *Mtb* but to limit excessive inflammation associated with necrosis (58). In contrast, in the zebrafish-*M. marinum* model, phagocytosis of apoptotic macrophages infected with *M. marinum* promoted the spread of mycobacteria (60).

In contrast, cell necrosis permits survival and release of *Mtb* to infect neighboring cells (58, 61–63). Necrosis may be dictated, in part, by the *Mtb* strain and thus an immune evasive virulence phenomenon. Divangahi et al. (64) demonstrated that the more virulent *Mtb* H37Rv, in contrast to the less virulent *Mtb* H37Ra, induced the lipoxin A4 ($LXA_4$) production, which then blocks both synthesis of prostaglandin $E_2$ ($PGE_2$) and activation of synaptotagmin 7. Since $PGE_2$ prevents necrosis of *Mtb*-infected macrophages (61, 64–66) and synaptotagmin 7 (a calcium ion sensor) is involved with lysosome-mediated repair mechanism (64), $LXA_4$ induced by the more virulent *Mtb* prevents repair of the injured plasma membrane caused by *Mtb*, resulting in cellular necrosis. Another mechanism by which *Mtb* induces necrosis is *via* activation of the cytosolic receptor-interacting protein kinase 3 (RIPK-3) pathway, preventing apoptosis of *Mtb*-infected macrophages through Bcl-xL and promoting reactive oxygen species (ROS)-mediated cell necrosis (67).

### 2.2.2 Neutrophils

Neutrophils can phagocytose *Mtb* as well as release neutrophil extracellular traps (NETs), which are comprised of chromatin (DNA) decorated with neutrophil-derived proteins (elastase, histones) that entrap the extracellular bacilli. NETs have antimicrobial activity and the NET-induced inflammatory response may promote migration of activated dendritic cells to the draining lymph nodes to activate naïve T cells; however, excessive NET-associated inflammation also causes tissue injury (68, 69). In addition, type 1 interferon-induced NET formation was found to promote *Mtb* growth and disease severity in mice genetically susceptible to TB (65). Neutrophils may also be present at the interface between the necrotic center and epithelioid macrophages as well be a source of immunoregulatory cytokines TNF and IL-10 (70). In C3HeB/FeJ mice, a fulminant necrotizing alveolitis with uncontrolled neutrophilic response in the lungs is associated with greater *Mtb* burden and mortality (34). Neutrophils may also provide a niche for mycobacterial growth, and this ability was associated with increased mitochondrial metabolic activity (71, 72).

### 2.2.3 Lymphocytes

#### 2.2.3.1 CD4$^+$ T effector cells

CD4$^+$IFNγ$^+$ T cells are critical in the formation of granulomas with early containment of *Mtb* (73–75). However, excessive amounts of CD4$^+$IFNγ$^+$ T cells, in conjunction with increased TNF, can also cause macrophage necrosis and poorer control of *Mtb* (76, 77). Similarly, either excessive or insufficient CD4$^+$IL-13$^+$ T cells (37, 78) impairs host control of *Mtb* (79–81). However, BALB/c mice with genetic disruption of IL-4 were more proficient in controlling *Mtb* (82), indicating that attenuating $T_H2$ (IL-4, IL-13) immunity in more

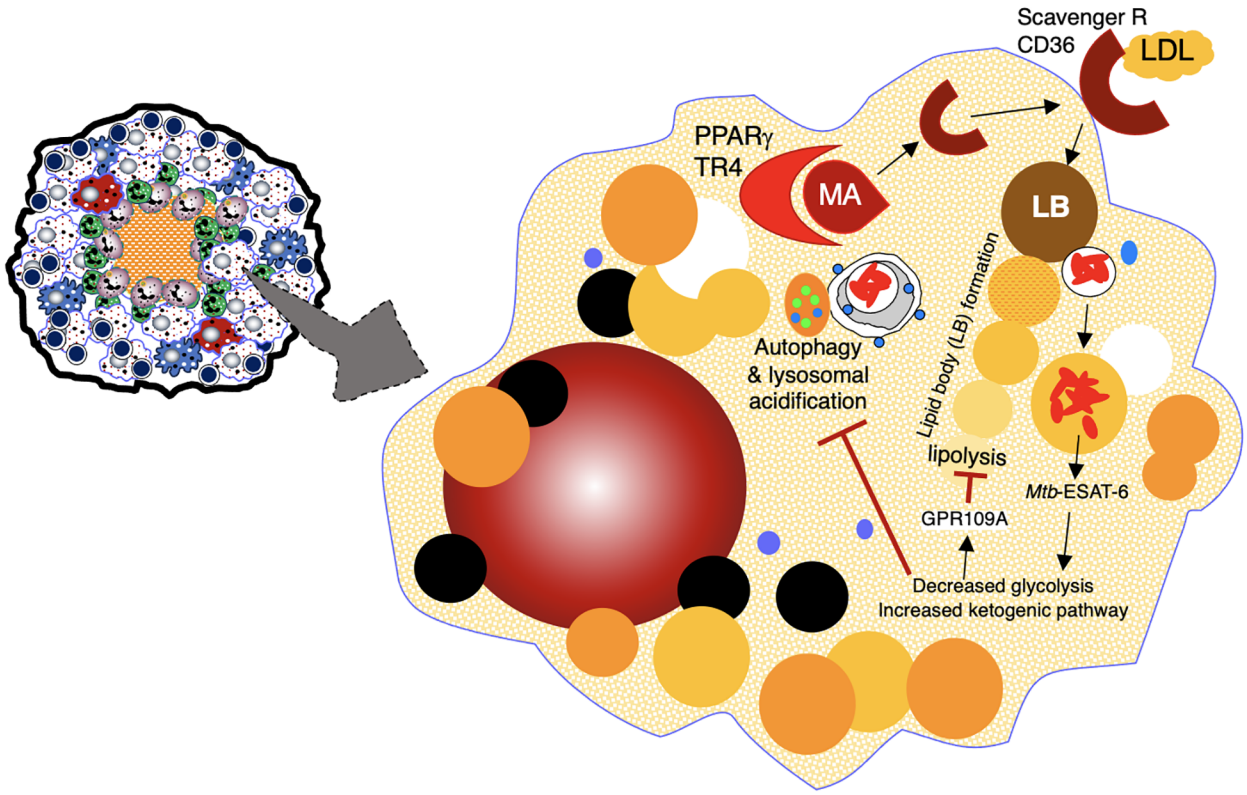


FIGURE 3
Formation of foamy macrophages and their role in TB pathogenesis. Foamy macrophages play a key role in the formation of caseous necrosis. They are formed when macrophages acquire cholesterol-containing LDL particles into lipid bodies. See text for discussion. ESAT-6, 6 kDa early secretory antigenic target; GPR109A, a specific G-protein coupled receptor; LB, lipid bodies; LDL, low density lipoprotein; MA, mycolic acids; PPARγ, peroxisome proliferator-gamma; TR4, testicular receiver 4.

immunocompromised mice is host-protective. TGFβ produced by macrophages and T regulatory cells (Tregs) predisposes to *Mtb* in a computer simulated TB granuloma model, in experimental animals, and in humans (83–85). However, TGFβ combined with IL-23 promotes the expansion of $T_H17$ cells, which are important in the control of *Mtb* during earlier stages of infection (86). IL-17 secreted by $T_H17$ cells has other host-protective functions (limiting excessive granuloma hypoxia, inducing iBALT formation, recruiting $CD4^+IFN\gamma^+$ T cells) (87–90) but also host-deleterious properties (inducing excessive influx of neutrophils that may limit the formation of protective granulomas) (91, 92). Serum IL-9 (produced by $T_H9$ cells) was found to be significantly higher in pulmonary TB subjects than individuals with sarcoidosis, a granulomatous disorder of unknown etiology (93).

### 2.2.3.2 $CD8^+$ T effector cells

$CD8^+$ T cells, through their cytotoxic response, help limit bacterial replication in the later stage of disease (6, 94). Following aerosol *Mtb* infection of mice, $CD8^+$ cells were not considered to play a major protective role (95) whereas with high intravenous inoculum, they were more essential for protection (96–98). $CD8^+$ T-cells are able to recognize and induce apoptosis of infected macrophages (99). In mice, $CD8^+$ T cells were found to be important in maintaining stable latent phase of infection, in part through production of IFNγ (100). However, increased TGFβ and IL-10 expression and reduced granzyme B production by $CD8^+$ T cells are associated with poorer control in patients with active TB (101).

### 2.2.3.3 T regulatory cells

Tregs are $CD4^+$ T cells (or less frequently $CD8^+$ marker) characterized by the phenotypic markers $Foxp3^+CD25^{hi}CD127^{dim/-}$. Tregs develop from naïve T cells in the presence of TGFβ and dampen the function of M1 macrophages and T effector cells through expression of immunosuppressive cytokines TGFβ, IL-10, and IL-35 (102–104). Tregs were more commonly present in cavities than in the lipoid pneumonia or granulomas of human post-primary TB in the lungs (33) Within granuloma-infiltrating T cells of both *Mtb*-infected mice and rhesus macaques, TGFβ signaling antagonized activity of IFNγ-producing $CD4^+$ T cells and impaired control of *Mtb* (83).

### 2.2.3.4 B cells

B cells also play an important role in the granulomatous and iBALT response against *Mtb* (105, 106). B cells found in granulomas produce the chemokine CXCL13, which recruits specific T cells to the infection site, promoting follicle-like structure formation within granulomas (107). B cells also function as antigen-presenting cells

within granulomas, enhancing proliferation of a host-protective T cells and plasma cells against *Mtb* infection (108). Studies in mice have shown that B cells decrease neutrophil motility (109–111).

Three distinct populations of B cells exist: B effector 1 cells (Be1), B effector 2 cells (Be2), and regulatory IL-10 producing B cells (B10). Be1 cells are produced when naïve B cells are primed by $T_H1$ cytokines. These cells then produce IFNγ, IL-12, TNF, IL-10, and IL-6. On the other hand, Be2 cells are differentiated in the presence of $T_H2$ cytokines, and, in turn, are producers of IL-2, lymphotoxin, IL-4, IL-13, IL-10 and IL-6 (105, 112, 113). Once produced, Be1 and Be2 cells are able to influence the differentiation of naïve $CD4^+$ T cells into $T_H1$ or $T_H2$, respectively (112). Regulatory B cells are known to downregulate the T cell response through production of IL-10 or TGFβ (112, 113). Thus, whereas effector B cells induce the inflammatory T cell response, regulatory B cells downregulate this pathway. Due to the crucial role that $CD4^+$ T cells play in the formation of TB granulomas, the ability of B cells to induce or block this pathway illustrates their importance in granuloma formation. Indeed, clusters of B cells are found in human TB granulomas (114).

## 2.3 Inducible bronchus-associated lymphoid tissue, an accessory organoid to granulomas

Tertiary lymphoid organs (TLOs) are organized lymphoid structures that form in non-lymphoid tissues in response to injury, inflammation, or chronic infection (115). These structures have been shown to surround granulomas during mycobacterial infection (116, 117). While TLOs and granulomas are generally regarded as discrete structures, they have been shown to share similar biological processes (118). One such TLO that is associated with granuloma formation is inducible bronchus-associated lymphoid tissue (iBALT). iBALT are comprised of B cells, T cells, and antigen-presenting cells (*e.g.*, dendritic cells) and are juxtaposed to granulomas (Figures 1A, B) (119–121). The immune cell inflammation that accompanies *Mtb* infection: *(i)* induces "stromal lymphoid tissue organizer cells" (fibroblasts, myofibroblasts, and endothelial cells) to transform into follicular dendritic cells; *(ii)* triggers them to produce chemokines (CXCL13, CXCL12, CCL21, CCL19), which recruit and organize T cells, B cells, and dendritic cells into iBALT; and *(iii)* supports high endothelial venule formation to allow lymphocyte trafficking into the infection site (122). Interleukin-17 (IL-17), IL-23, and group 3 innate lymphoid cells (ILC3s) also promote the differentiation and activation of lymphoid cells that participate in iBALT formation (89, 90, 123–125).

iBALT has been described with pulmonary TB in humans (75, 121, 126), non-human primates (NHP) (75, 121, 126), rabbits (127), guinea pigs (127), and mice (75, 125). iBALTs are considered to be protective against *Mtb* for several reasons: *(i)* they can serve as a site for local antibody production (128, 129); *(ii)* they can render support to neighboring granulomas as a ready supply of additional immune cells (119, 130); *(iii)* the presence of iBALT can be associated with the maintenance of latency and containment of infection, whereas its absence is associated with active disease (75, 121). However, in the context of sustained and unresolved TB, iBALT may become pathogenic and contribute to lung injury, especially with sustained IL-17 expression and neutrophil recruitment (119).

Certain molecules can have an impact on iBALT formation. For example, NHP infected with *Mtb* that lacked MmpL7 (Mycobacterial membrane protein Large 7) showed an increase in granulomas containing iBALT, suggesting that *Mtb*-derived MmpL7 prevents the formation of host-protective iBALT (Figure 1B) (131). Another study found in both *in vitro* (macrophage) and *in vivo* (murine and NHP) *Mtb* models that inhibition of indoleamine 2,3-dioxygenase (IDO-1) activity resulted in a greater host protective response as well as increased iBALT, indicating that IDO-1 also inhibits iBALT formation (Figure 1B) (132).

# 3 The granuloma paradox

## 3.1 Granulomas may be viewed from different perspectives

One overarching paradox of TB is that despite being the most lethal infectious disease globally, most who are infected with *Mtb* do not ever develop disease, consistent with pathologic studies that most human TB lesions are regressive (133, 134). Because humans and *Mtb* have co-existed for a long time, it is likely that the genetics of both humans and *Mtb* are important in determining who are at risk for developing latent infection or active TB disease (135, 136). The battle between *Mtb* and host immunity may be viewed from either the perspective of the bacilli or the host. When the host is unable to completely eradicate the *Mtb* upon initial infection – due to immune evasive strategies of *Mtb* such as arrest of phagosome maturation (137) – the next best recourse is to contain the infection through the formation of granulomas. While granulomas are generally regarded as a host-protective response by controlling the *Mtb* infection, they also provide a niche that allows *Mtb* survival by limiting the trafficking of immune cells (4). Some newly infected macrophages may also escape from the original granuloma to form a secondary granuloma, albeit this was observed in the *M. marinum*-zebrafish model (60).

Drawing from epidemiological evidence indicating that the majority of individuals with latent TB infection do not progress to active TB but remain at risk, our discussion framework centers on the host-protective nature of TB granulomas. We explore the multifaceted circumstances leading to their occasional failure in protecting the host. There are many factors that determine whether TB granulomas are protective or harmful. One plausible explanation for variability in the protective efficacy of granulomas lies in the existence of different granuloma phenotypes – a heterogenous spectrum of lesions – within the same individual. These distinct granuloma types emerge due to a complex interplay between the host immune response and *Mtb* components, reflecting varying endotypes (138). However, a glaring limitation emerges

when assigning a specific granuloma phenotype as detrimental to the host: the challenge of discerning whether a particular granuloma phenotype fails to protect or if it arises as a consequence of such failure or an attempt to correct the failure. In essence, our comprehension of granulomas is significantly hindered by our inability to observe the temporal evolution of individual granulomas in the context of live bacilli burden. Nevertheless, we have organized below the descriptions of granulomas in the context of host-protection or not.

## 3.2 Evidence that granulomas serve host-protective function

### 3.2.1 Epidemiological and clinical observations

The notion that TB granulomas are host-protective is evinced indirectly from the observation that most individuals infected with *Mtb* – identified through positive tuberculin skin tests or IFNγ release assays – do not progress to active TB and commonly exhibit calcified granulomas. Indeed, global data show a much greater preponderance of individuals infected with *Mtb* without disease (by ~200-fold) than those with active TB (139).

A stronger piece of clinical evidence that granulomas serve a host-protective function is that individuals with severe immunodeficiency (such as those with AIDS or immune suppression by pharmacologic TNF blocking agents) are highly susceptible to *Mtb* and have poorly-formed or absent granulomas (140–145). On a cellular level, TNF is necessary for macrophage-mediated control of mycobacterial infection (146). The requirement of TNF in forming a host-protective TB granuloma is evinced by the finding that mice knocked out for TNF or neutralized of TNF function were unable to form granulomas in response to *Mtb* infection and showed greater *Mtb* burden (147). One novel function of TNF in granuloma formation is the induction of a T cell receptor (TCR) αβ-based recombinatorial immune receptor in subpopulations of monocytes/macrophages (148). As macrophage-TCRαβ was found to induce the release of CCL2 (monocyte chemoattractant protein 1), which recruits monocytes, dendritic cells, and memory T cells, deletion of this variable macrophage-TCRαβ or TNF results in structurally compromised TB granulomas (148). Yet, there are case reports of caseating granulomas (often a sign of high *Mtb* burden) found in active TB in the presence of TNF blocking agents, indicating that granulomas that form despite TNF deficiency are not protective (149, 150). One possible scenario for this finding is that latent TB granulomas previously existed but with the introduction of an anti-TNF agent, there was proliferation of dormant *Mtb*, causing disruption of the intact, protective granuloma with secondary necrosis. An alternative explanation is that during treatment with an anti-TNF agent, a new *Mtb* infection occurred (plausible in TB endemic countries), resulting in inadequate control of the initial infection and the recruitment of other cell types such as neutrophils, resulting in caseating necrosis of the poorly protective granulomas. The observation that most of the *Mtb* are extracellular within necrotic granulomas, with lesser number located in the macrophage-rich region surrounding the core would support either scenario (151).

### 3.2.2 HIF-1α, a response to granuloma hypoxia, is largely host-protective

In non-necrotic, cellular granulomas, *Mtb* exists mainly intracellularly in the infected macrophage population within the core of the intact granuloma (11, 151, 152). One likely factor that allows granulomas to remain intact and non-necrotic is the prevention of a hypoxic environment within granulomas. More specifically, if cellular hypoxia occurs, one thwarting response is through increased production of hypoxia inducible factor-1 alpha (HIF-1α) by innate immune cells (macrophages, dendritic cells, and neutrophils) and lymphocytes (153). HIF-1α, which combines with constitutive HIF-1β to form HIF1, increases angiogenesis to the granuloma *via* induction of vascular endothelial growth factor, which allows oxygen and nutrient transport to the cells within granulomas (154). HIF-1α also aids cell survival in the hypoxic environment by augmenting glycolysis to generate quickly available ATP (155–157).

Several studies have shown that inducible HIF-1α is host-protective against *Mtb* infection. HIF-1α enhances the *Mtb*-killing abilities of both phagocytes and monocytes by several effector mechanisms including apoptosis of *Mtb*-infected phagocytes and enhanced production of cellular anti-microbial elements (nitric oxide, granule proteases, and anti-microbial peptides) (154, 158–160). Live *Mtb* alone has been shown to induce HIF-1α (154, 161) but this effect was especially seen in conjunction with IFNγ (162). In turn, HIF-1α augments IFNγ-induced genes that play important roles in effector functions against *Mtb* such as inflammatory cytokines and chemokines (IL-1α, IL-1β, and IL-6) (154, 162, 163). Hypoxia-induced HIF-1α also induces expression of CXCR4 – the receptor for the lymphocyte chemokine (and pro-angiogenic) CXCL12; thus, HIF-1α maintains both the influx of potentially host-protective immune cells to granulomas and the viability of these cells (164, 165). These findings are supported by studies of mice with conditional genetic disruption of HIF-1α in myeloid cells wherein with *Mycobacterium avium* infection, there was greater granuloma necrosis (perhaps due in part to impaired neovascularization of the granulomas) and impaired clearance of the mycobacteria (166). In the *M. marinum*-zebrafish model, stabilization of HIF-1α at the early stages of infection enhanced the levels of nitric oxide and reduced mycobacterial burden (167). Furthermore, suppression of granuloma-associated angiogenesis – which would be expected to cause hypoxia and induce the expression of HIF-1α – decreased *M. marinum* burden (168). While the ability of HIF-1α to enhance host immune cells against mycobacteria may be mediated by NFκB activation (169), HIF-1α may also attenuate an excessive NFκB response to prevent injurious inflammation (170).

## 3.3 Evidence that granulomas serve to propagate *Mtb*

### 3.3.1 Is bacillary patience a survival factor for Mtb? A teleological perspective

The first observation that certain granulomas – depending on the model used – benefit *Mtb* growth is that *Mtb* has adapted to

remain quiescent for long periods with the opportunity to propagate at later times. Unlike pathogens that do not develop latency in the host and evade host immunity by antigenic variation, *Mtb* is capable of surviving (in a latent form), paradoxically, *because* of its recognition by host immune cells. The notion that *Mtb* has exploited recognition by the host as a survival mechanism is supported by the extensive diversity of *Mtb* antigens and epitopes that are recognized by $CD4^+$ and $CD8^+$ T cells of both active TB subjects and healthy controls (171–173). Hence, a potential interpretation is that T-cell recruitment to the site of infection, although initially a host-protective mechanism, could inadvertently aid *Mtb* by facilitating the establishment of a latent infection within an organized granuloma. This arrangement extends the bacilli's survival, enabling them to lay dormant until conditions conducive to their reactivation arise, such as during immune senescence, thereby facilitating their dissemination to other individuals (6, 174, 175). Therefore, a teleological perspective suggests that *Mtb*, by exhibiting remarkable "patience" in remaining quiescent after encountering host immune cells within granulomas, ensures a higher probability of long-term survival for its species.

### 3.3.2 The co-evolution of Mtb with its host to survive within granulomas

The second observation that granulomas benefit *Mtb* is that the bacilli have developed survival mechanisms within the host phagocytes. A denouement of such survival capability is that the bacilli can spread between phagocytes within either quiescent or disruptive stages of granulomas. Mechanisms for this intracellular survival and spread to other cells are *Mtb*-mediated rupture of the phagosome membrane to escape into the cytoplasm, evading phagosome-lysosome fusion (17) as well as apoptosis-mediated cell-to-cell spread (60, 176). This intracellular movement of mycobacteria is likely an immune evasive mechanism because pathogenic mycobacteria are more capable of translocating from the intra-phagosome compartment to the cytosol *via* pore-inducing mycobacterial ESAT-6 protein than non-pathogenic mycobacteria (discussed in Section II.2.1 above) (17, 18). A connection between this intracellular immune evasive mechanism and the earlier-discussed *Mtb* latency survival strategy within organized granulomas emerges. ESAT-6, known to contain multiple T-cell epitopes (both CD4 and CD8), plays a pivotal role (177). Interestingly, just before *Mtb* burden plateaued post-infection in mice, the mRNA levels of both ESAT-6 and Ag85B decreased by 10-fold (178). This decline, reflecting little turnover of *Mtb* during the stationary phase, allows for *Mtb* to be still recognized by T cells but prevented its complete eradication by the immune system.

ESAT-6 secretion systems (ESX), particularly ESX-1 and ESX-5, have been shown to be virulence factors during mycobacterial infection. The importance of ESX-1 in mycobacterial pathogenesis is evinced by the finding that *Mtb* strains lacking ESX-1 have decreased pathogenesis and intracellular replication compared to wild-type strains (179). In humans, ESX-1 induction of the chemokine fractalkine (CX3CL1) mediates the recruitment of monocytes to the expanding granuloma (180). In contrast, the ESX-1 of *M. marinum* induced expression of matrix metalloproteinase 9 (MMP-9), which facilitates influx of uninfected macrophages, expanding the granulomatous lesions that may contain viable mycobacteria (181, 182). ESX-5 of *M. marinum* has been shown to inhibit induction of proinflammatory cytokines (IL-12p40, TNF, IL-6) (183) as well as induce both inflammasome/IL-1β activation and caspase-independent cell death (184).

*Mtb* also secretes lipids that affect the host immune response and caseous granuloma formation. These include mycolic acids, specifically trehalose 6,6'-dimycolate (TDM, aka cord factor), a toxic lipid that induces epithelioid macrophage transformation, pro-inflammatory cytokine production, and necrosis of the granulomas (185–187). Experimentally, the largest oil droplets of oil-water emulsions containing TDM were the most granulomagenic (188). In contrast, de-lipidated BCG – where TDM was stripped from the outer cell wall – induced more of an acute (neutrophilic-like) infiltration and reduced delayed hypersensitivity (granulomatous) response along with more rapid clearance of de-lipidated BCG in mice, indicating that TDM is both a virulence factor and responsible for granuloma formation (189). The programming *Mtb* into a dormancy state by the dormancy survival regulon (DosR) is induced by carbon monoxide and hydrogen sulfide as well as a local environment that is hypoxic, acidic, and contains high nitric oxide levels (190–195). This induced dormancy of *Mtb* results in reduced metabolic activities of the bacilli, but they are also able to dysregulate host-lipid synthesis resulting in the production of lipid bodies (39). This process transforms macrophages into the foamy phenotype capable of not only sustaining the dormant *Mtb* but contributing to the caseous necrosis when granulomas breakdown (31).

*Mtb* has the capacity to import and catabolize host-derived cholesterol (an integral part of cellular membranes) – *via* proteins encoded by the mycobacterial gene cluster *mce4* and by the *igr* locus, respectively – and use it as a carbon and energy source to survive for prolonged periods in caseous granulomas (196, 197). The catabolism of cholesterol in host-cells requires a shift from aerobic to anaerobic metabolism within the hypoxic and necrotic granuloma core which contributes to the dormant state of *Mtb*. In this state, *Mtb* remodels the cell wall and produces intracellular triglycerides (comprised of three long-chain fatty acids esterified to glycerol). β-oxidation of even-chain fatty acids produces acetyl-Co-A, which can be used for either synthesizing triglycerides (a lipid relevant for dormancy) or fueling the tricarboxylic acid (TCA) cycle (for ATP production) (198). Odd chain fatty acids undergo β-oxidation to produce the 3-carbon propionyl-CoA, which can be further metabolized to products that enter the TCA cycle or produce methyl-branched lipids to synthesize the mycobacterial cell wall (198). The mycobacterial enzyme isocitrate lyase (Icl) serves two functions for *Mtb*: *(i)* it is essential for conversion of even-chain fatty acids under nutrient limitation; *i.e.*, Icl metabolizes isocitrate (6C) to glyoxylate (2C) and succinate (4C) with subsequent combining of glyoxylate with acetyl-Co-A (2C, a product of β-oxidation of fatty acids) to form malate (4C), which enters and fuels the tricarboxylic acid cycle and *(ii)* by fueling the TCA cycle, it activates the events that occur downstream of the initial steps in the metabolism of the toxic propionyl-CoA. In addition, the gene that encodes the lipid transporter also plays an important role in *Mtb* growth (6, 199).

### 3.3.3 What causes necrosis and caseation of TB granulomas?

The root cause of the necrotic cell death and subsequent caseation in TB granulomas is not precisely known. Within TB granulomas, macrophage necrosis occurs by various and not necessarily mutually exclusive mechanisms. The first mechanism is dysregulation of the pro-inflammatory cytokine TNF. On the one hand, either deficiency or antagonism of TNF impairs macrophage control of *Mtb* (and of *M. marinum*), increases mycobacterial burden in macrophages, and results in necrotic macrophage death with subsequent tissue spread of *Mtb* (4, 76, 146, 200). This TNF deficiency may also occur endogenously in certain individuals due to decreased leukotriene A4 hydrolase (LTA4H) activity (CC genotype of *LTA4H* gene), resulting in a decrease ratio of the pro-inflammatory leukotriene B4 ($LTB_4$) to the anti-inflammatory $LXA_4$ (201, 202). On the other hand, TNF excess due to high LTA4H activity (TT genotype), resulting in increased $LTB_4$:$LXA_4$ ratio), leads to activation of the TNF receptor-interacting serine/threonine kinases 1 and 3 (RIP1 and RIP3), mitochondrial reactive oxygen species (ROS), and initiated programmed necrosis (necroptosis) of the macrophages (76). Thus, both the hypoinflammatory (CC) and hyperinflammatory (TT) genotypes of $LTA_4H$ were associated with poorer outcomes compared to the heterozygous (CT) genotype (201, 202).

The second mechanism for macrophage necrosis is the insufficient clearance of *Mtb*-infected apoptotic phagocytes. *Mtb*-infected macrophages that undergo apoptosis are further phagocytosed by (recruited) uninfected macrophages, a process known as efferocytosis (60). However, if the influx of these uninfected macrophages is insufficient, apoptotic *Mtb*-infected macrophages are not cleared, leading to necrosis (203). While apoptosis of *Mtb*-infected macrophages is known to kill the intracellular bacilli, any surviving bacilli in apoptotic bodies that are not efferocytosed are released during secondary necrosis of the apoptotic bodies (51, 204).

The third hypothesized mechanism for the development of caseous necrosis is related to a deficiency or an excess of $CD4^+$ T cell response. Deficiency of $CD4^+IFN\gamma^+$ T cells and insufficient formation of host-protective granulomas (147, 205, 206) results in increased IL-17-mediated neutrophilic influx and overwhelming *Mtb* infection of the macrophages, with both events leading to necrosis of the phagocytes (Figure 4A). The mechanism by which an excess of $CD4^+$ T cells contribute to necrosis is not clear, but based on experimental evidence, the exuberant IFNγ response induces TNF and other downstream inflammatory mediators (207), causing activation of the aforementioned RIP1 and RIP3, necrotic macrophage death (necroptosis), and release and proliferation of mycobacteria (Figure 4B) (76, 208–210). IFNγ also increases CXCR3 (a receptor for several angiostatic chemokines) that may result in granuloma hypoxia and necrosis (Figure 4B) (211). Another supporting clue that excess IFNγ (and its downstream effects) may contribute to a detrimental immune response to the host is based on a study showing that IFNγ production by $T_H1$ cells is far more important for TB control in the spleen than in the lungs and that increasing the IFNγ-producing capacity by the $T_H1$ cells actually exacerbated the lung infection and led to more rapid mortality (77). In contrast to these two extremes of $CD4^+IFN\gamma^+$ T cell deficiency and excess, we posit that a more precise $CD4^+$ T cell response would be more optimal (Figure 4C).

A fourth mechanism for the development of caseous necrosis, related to an excess of $CD4^+IFN\gamma^+$ T cells discussed above, is insufficient negative regulation of IFNγ. *Mtb* induction of IFNγ upregulates the immune checkpoint PD-1 (programmed cell death protein-1), which, in turn, inhibits $IFN\gamma^+$ $T_H1$ cells, a form of negative feedback mechanism to prevent excessive IFNγ production (212). The importance of dampening an excessive IFNγ production is evinced by studies showing that PD-1 knockout mice are paradoxically more susceptible to *Mtb* infection (213–216).

A fifth proposed mechanism for the development of necrosis in TB granulomas is the inability of the granuloma to overcome excessive hypoxia (described above), causing cell death and central necrosis in the granuloma. TB granulomas are hypoxic in guinea pigs, rabbits, and NHP (217). Employing dynamic PET imaging using the tracer [$^{18}$F]-fluoromisonidazole, heterogenous degrees of tissue hypoxia were found in the TB pneumonia and around cavities (218). In contrast to the host-protective function of HIF-1α against TB (discussed in Section III.2.2 above), excessive HIF-1α may be harmful. Domingo-Gonzalez et al. (87) showed that when IL-17 was neutralized in *Mtb*-infected mice, there was higher production of HIF-1α, more hypoxic necrotic granulomas, exacerbated inflammation, and increased *Mtb* burden. They further showed that restricting HIF-1α activity in the mice by neutralizing IL-17 reversed both the excessive inflammation and the increased *Mtb* burden (87). While it is not clear how HIF-1α may induce hypoxic necrotic granulomas – since it has known properties that mitigates hypoxia and its detrimental sequelae such as induction angiogenesis and switch to glycolytic metabolism – one possible mechanism is that HIF-1α can induce mucin production and transepithelial resorption of sodium ion and water, resulting in increased mucus in the airways and thus indirectly worsening hypoxia to the lungs and the granulomas (219). Either *Mtb* or hypoxia-induced HIF-1α is known to individually and synergistically induce MMP-1, which can lead to lung tissue destruction and cavity formation *via* its collagenase activity (218). Baay-Guzman et al. (154) found a dual opposing roles for HIF-1α in mice: *(i)* a protective role in early stage TB (≤28 days after infection) through macrophage activation in conjunction with IFNγ and *(ii)* a detrimental role at a later stage of infection through HIF-1α inhibition of apoptosis of foamy macrophages, impairing an effector mechanism by which intracellular *Mtb* are killed.

Finally, type-1 interferons, produced by interstitial macrophages and plasmacytoid dendritic cells, have been found to exacerbate *Mtb* infection, recruit neutrophils, NETs formation, and promote tissue necrosis (220, 221). Not only have type-1 interferons been found to inhibit protective cytokines (IFNγ, TNF, IL-12, IL-1α, IL-1β), but they also contribute to spread of infection and lung inflammation by increasing accumulation of myeloid cells (66, 222). Type-1 interferons have been shown to contribute to necrosis through inhibition of $PGE_2$. As noted above, $PGE_2$ is known to prevent necrosis of *Mtb*-infected macrophages (61, 64–66). In turn, $PGE_2$ (and IL-1) were found to inhibit expression of type-1 interferons (65, 223). It has also been shown that type-1 interferon induction of interleukin-1 receptor

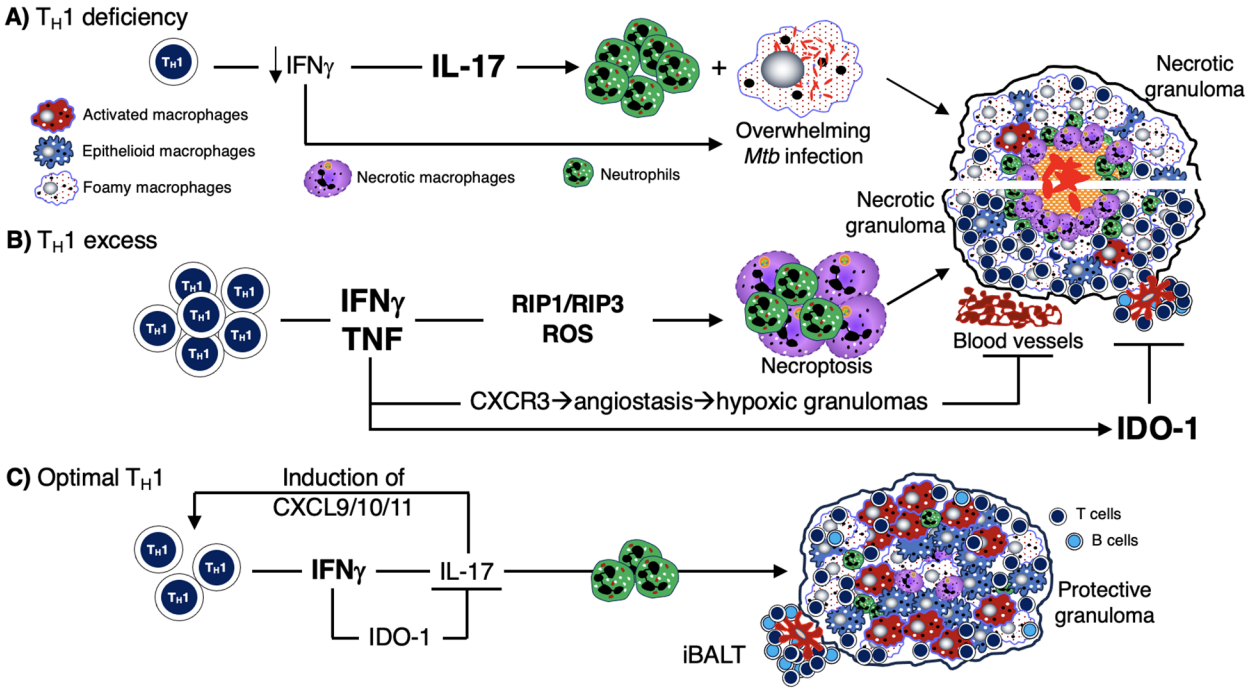


FIGURE 4
Mechanisms by which deficiency or excess $CD4^+IFN\gamma^+$ T cells predispose to TB. **(A)** Deficiency of $T_H1$ ($CD4^+IFN\gamma^+$) T cells – as seen in advanced AIDS, genetic defects in the IFNγ-IL-12 axis, and in animal models – has been shown to increase the risk of TB and other mycobacterial infections. This IFNγ deficiency leads to an increase in IL-17 and neutrophilic influx. This combined with a lack of macrophage activation (due to insufficient number of $CD4^+IFN\gamma^+$ T cells) leads to an overwhelming *Mtb* infection of phagocytes, resulting in an unprotective, necrotic granuloma. **(B)** Excess $T_H1$ cell activation and numbers lead to a secondary increase in TNF, which can then induce RIP1 and RIP3 activation, excessive ROS formation, and macrophage necroptosis. The sequence of these events leads to over-inflamed, necrotic, and unprotective granulomas. **(C)** There is ample evidence in both humans and experimental animal models that optimal quantity and temporal influx of *Mtb*-specific $CD4^+IFN\gamma^+$ T cells are necessary for control ± eradication of *Mtb* infection, in part through activation of macrophages. IFNγ also inhibits IL-17 production from $T_H17$ cells which can induce chemokines for $CD4^+IFN\gamma^+$ T cells. In non-hematopoietic cells, IFNγ also induces IDO-1 production that inhibit excessive IL-17 production (via the catabolized products of tryptophan by the actions of IDO). Hence, IL-17 production is kept in check, limiting the amount of potentially harmful neutrophilic influx. IDO-1, indoleamine 2,3-dioxygenase; IFNγ, interferon-gamma; IL-12, interleukin-12; IL-17, interleukin-17; *Mtb*, *Mycobacterium tuberculosis*; RIP, receptor-interacting serine-threonine kinases; ROS, reactive oxygen species; TB, tuberculosis; TNF, tumor necrosis factor.

antagonist IL-1Ra mediated susceptibility to *Mtb* (224). Despite these host-harmful effects of type 1 interferons during *Mtb* infection, they have also been shown to exhibit host-protective properties in certain conditions; *(i)* co-administration with antimycobacterial chemotherapy; *(ii)* lack of IFNγ signaling from the host; *(iii)* BCG vaccination in certain animal models (65).

## 3.4 Lesion heterogeneity

The physical makeup and host-protective abilities of granulomas can vary greatly. When granulomas form in response to an infection, it gives rise to a trajectory that varies across a spectrum between complete bacterial clearance to uncontrolled infection. Distinct types of TB granulomas exist, all potentially coexisting within a single host infected with *Mtb* (Table 2) (138, 152, 225). Several factors can affect granuloma heterogeneity, such as host inflammatory/immune responses as well as differences in physiological-chemical properties of the different regions of the lungs (discussed in Section IV.3 below). Consequently, spatially grouped bacilli may encounter diverse granuloma environments depending on factors such as granuloma type, age, and regional immune response; in turn, *Mtb* can display different phenotypes depending on the microenvironment they are being enveloped (225). This variability leads to a dynamic landscape where some granulomas progress while others regress, even within a single infected individual. This notion of lesion heterogeneity is also supported by reports that sterile (mainly calcified) lesions may coexist with active TB lesions (226).

More supporting evidence for this claim comes from a study in which cynomolgus macaques were infected with *Mtb* and their developing granulomas were tracked using computed tomography (CT) combined with deoxy-2-[$^{18}$F]-fluoro-D-glucose (FDG) positron emission tomography (PET) scans before necropsy was performed (226). Based on the PET-CT findings, the metabolic state of individual granulomas showed a dynamic pattern, even within the same animal. Remarkably, their findings revealed that individual granulomas mostly arise from one bacillus of *Mtb* (226). Furthermore, the number of culturable bacteria in the granulomas decreased significantly after time (~15-fold decrease from 4 to 11 weeks). Interestingly, compared to lesions of the NHP at 4 and 11 weeks after infection, animals with latent infection and

TABLE 2 Heterogeneity of granulomas and other TB lesions.

| Heterogeneity characteristic | Examples |
|---|---|
| **Morphology** | Lesions can be necrotic, caseous, fibrocaseous, non-necrotizing, neutrophil rich, mineralized, completely fibrotic, or cavitary (7, 138). |
| **Cellular composition** | Typically macrophages as well as CD4 and CD8 T cells surrounding a necrotic core, but there can also be multinucleated giant cells, neutrophils, dendritic cells, and fibroblasts (4, 138). |
| **Immune cell response** | Early forming granulomas demonstrate type-2 immune response whereas later forming granulomas demonstrate adaptive $T_H1$, $T_H17$ and cytotoxic T cell responses (227). Huge variability in numbers and phenotypes of T cells, and range of cytokine profiles and bacterial burdens (138, 234). |
| **Inflammation** | Proper balance of pro/anti-inflammatory responses is needed to control *Mtb* infection. A more pro-inflammatory response can lead to liquefaction or softening of the caseum (235). A more anti-inflammatory response tends to be associated with an overall better outcome in terms of reactivation as well as long-term prognosis (232). Various inflammatory signatures and killing potentials can be found even within the same granuloma (138, 226, 236). Limitations in the interpretation of these findings include: *(i)* inability to follow the inflammatory phenotype and correlate with culturable *Mtb* in single lesions over time and *(ii)* incapacity to determine whether the inflammation type observed is the cause or effect of the ability or inability of the host to control the infection. |

those with active TB (defined as clinical disease and *Mtb* culture positivity ≥ 3 months after infection) had 10-100–fold less culturable bacteria (226). While the CFU count modestly correlated directly with FDG uptake – a sign of increased glycolysis – it does not necessarily implicate glycolysis as a cause of impaired disposal of *Mtb*; *i.e.*, increased FDG uptake may be a marker for increases of either glycolysis alone or of both glycolysis plus mitochondrial oxidative phosphorylation. Another study using the cynomolgus macaque *Mtb* model found that the lesions showed different immune cell responses based on whether the lesions formed earlier *vs* later (227). Consistent with the prior *Mtb* culture results, earlier forming granulomas in *Mtb*-infected cynomolgus macaques displayed type-2 immune responses, which tend to allow for the survival of *Mtb* within the granuloma, whereas later forming granulomas demonstrate adaptive $T_H1$, $T_H17$ and cytotoxic T cell responses, which tend to be more effective at killing *Mtb* bacilli and controlling the infection (227). This heterogeneity not only underpins the diversity in infection outcomes between lesions but also complicates treatment efforts. Individual lesions may exhibit varying responses to antibiotics, posing challenges in achieving consistent therapeutic outcomes.

TB is classically divided into "active" vs. "latent" forms, although the current paradigm acknowledges a clinical continuum that also include incipient and subclinical TB (228). Perhaps reflecting these clinical phenotypes is the presence of a spectrum of pathologic lesions that may be seen in human and experimental TB. Following low-dose (~25 bacilli) infection of cynomolgus macaque, about 40% develop active disease whereas 60% develop latent infection (229, 230). In those macaques with active TB, some lesions showed replicating high-burden mycobacteria and necrotic granuloma whereas others showed fewer mycobacteria, more fibrosis, and resolved granulomas, mirrored by PET-CT imaging that demonstrated both metabolically active and metabolically inactive granulomas. Interestingly, even with culture confirmed negativity of NHP with latent infection, both PET-positive and PET-negative lesions may be seen with the caveat that the degree of PET-CT positivity correlates with glucose uptake by the cells and does not necessarily inform the level of control of the *Mtb* infection. In an antibiotic treatment study of pulmonary TB in cynomolgus macaques and in humans, decline in PET activity correlated with reduced bacterial load in both treatment groups and at necropsy in the NHP, with also a reduction in pulmonary pathology (231). Another study showed that a substantial number of humans treated for active drug-susceptible TB remained PET-positive along with positive *Mtb* mRNA in sputa, indicating either subclinical active disease or resolved TB with residual dead *Mtb* (232). These findings show that dividing clinical TB into "active" or "latent" is an oversimplification, and that the dominant type among a spectrum of lesions is likely to dictate the clinical disease (6, 152). Indeed, a recent review categorized TB into eight different states, ranging from elimination by various mechanisms to disseminated disease (233).

## 3.5 Does aerobic glycolysis in TB lesions–granulomas protect against or predispose to TB?

Answering this question is challenging because it is difficult to know in any distinct granuloma that is failing – defined as unopposed *Mtb* replication and worsening pathology – whether the presence of aerobic glycolysis is the cause of the failure or an attempt to rectify the failure. Furthermore, since it has been shown that seemingly distinct granulomas may in fact be different "branches" of the same granuloma (237, 238), the task in answering this question is even more daunting. Nevertheless, we will summarize the reported data.

On the one hand, there are indirect evidence that aerobic glycolysis increases host-susceptibility to TB: *(i)* PET-CT is commonly employed to detect TB lesions in NHP because this avoids the need to sacrifice the animal while obtaining more data in a temporal fashion. While PET-CT has been cited as a radiographic marker of aerobic glycolysis (a Warburg effect) (239), it is not specific for aerobic glycolysis alone since it is only a marker for glucose uptake, which can be seen with increased glycolysis (either aerobic or anaerobic) alone or with increase of both glycolysis and oxidative phosphorylation. Compared to the more TB-susceptible rhesus macaques, the more TB-resistant cynomolgus macaques infected with *Mtb* showed reduced dissemination of infectious granulomas and fewer PET-positive/necrotic lymph nodes (240). While this finding may suggest that aerobic glycolysis increases host susceptibility to TB in the rhesus macaques, one could contrarily argue that the increased PET-CT positivity (increased glycolysis) was an attempt to control the *Mtb* infection in the lymph nodes (240); *(ii)* in cancer cells, there is generally an inverse relationship

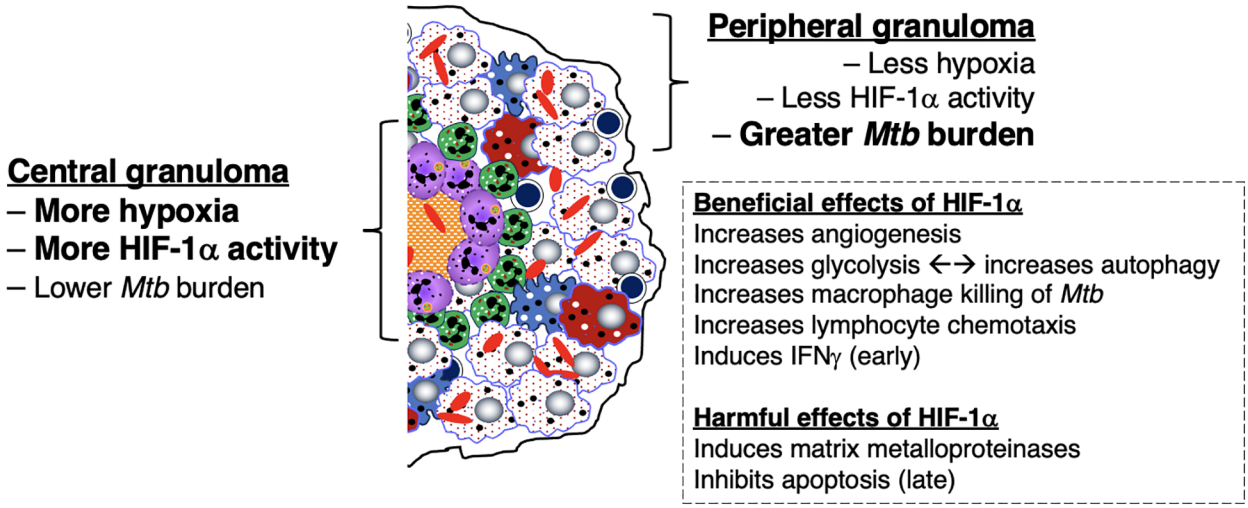


FIGURE 5
Differential expression of hypoxia, HIF-1α, and downstream effects in the central and peripheral regions of the necrotic granuloma. The central region of a necrotic granuloma is more hypoxic. As a result, there is greater HIF-1α expression with a panoply of downstream effects due to HIF-1 activity. One immune mechanism induced by HIF-1 is aerobic glycolysis, which in turn induces autophagy through the byproduct lactate. Hence, the central necrotic area of an intact human TB granuloma is usually sterile or with low bacterial burden. In contrast, the peripheral region of the granuloma less hypoxic with less HIF-1α induction. In the presence of macrophages that are less effective in killing *Mtb* (as shown by the foamy macrophages), there is less ability to kill *Mtb*, as shown by the greater bacilli number. However, in the presence of activated macrophages and T cells, the peripheral granuloma may also be efficient in either killing or controlling the *Mtb* infection. HIF-1α, hypoxia-inducible factor 1-alpha; IFNγ, interferon-gamma; *Mtb*, *Mycobacterium tuberculosis*; TB=tuberculosis;.

between glycolysis and autophagy; *i.e.*, increased glycolysis contributes to decreased autophagy (241) and loss of autophagy switches energy metabolism to glycolysis (242); in contrast to cancer cells, the glycolytic byproduct lactate increases autophagy in macrophages (see below); *(iii)* since the lung apices are more alkalotic in upright humans and alkalosis drives aerobic glycolysis (due to increased activity of hexokinase and phosphofructokinase activity (243, 244), key enzymes in the glycolytic pathway), one could also posit that perhaps an increase in glycolysis in the upper lung zones is (partly) responsible for the increased involvement of the upper lung zones in post-primary TB.

On the other hand, there is a collective strong argument that aerobic glycolysis of macrophages is host-protective against TB: *(i)* *Mtb* infection of macrophages inhibits aerobic glycolysis and increases fatty acid metabolism by mitochondria; this inhibition of aerobic glycolysis increased mycobacterial growth and decreased the production of certain pro-inflammatory mediators (40, 245–247); *(ii)* phagocytosis is augmented by glycolysis (40, 248); *(iii)* using live *Mtb*, HIF-1α switches macrophage metabolism to aerobic glycolysis which polarizes macrophages to the M1 phenotype (and secondarily to the $T_H1$ phenotype) against *Mtb* (162, 163) (Figure 5); *(iv)* since the ability of mycobacterial ESX-1 to convert glycolysis to ketosis induces the formation of foamy macrophages – which are known be impaired in controlling intracellular mycobacteria due to decrease of both autophagy and lysosomal acidification (39) – lending credence that glycolysis is host-protective; *(v)* lactate, the byproduct of glycolysis, increases autophagy, possibly through hyperlactylation of PI3 kinase (39, 41, 42); *(vi)* while the aforementioned inverse relationship between protection and aerobic glycolysis in *Mtb*-infected macaques (240) suggests that aerobic glycolysis confers susceptibility, one could argue that the greater protection against TB in the cynomolgus macaques prevented the need for an increase in host-protective aerobic glycolysis; *(vii)* indirect evidence that aerobic glycolysis is host-protective is that calcification of granulomas – a sign of well-controlled TB lesions – is more likely to occur in an alkaline environment, which would also promote aerobic glycolysis; *(viii)* the central parts of necrotic granulomas are considered to be more hypoxic and have greater HIF-1α expression; since HIF-1α increases glycolysis, whose byproduct lactate augments autophagy, this may account for the low *Mtb* number in the central necrotic area of granulomas (Figure 5, left-hand side) (161, 163). Because immune cells at the granuloma periphery are less hypoxic and have less HIF-1α activity, there is greater burden of *Mtb* in the outer regions of the granulomas (Figure 5, right-hand side). Interestingly, increased aerobic glycolysis may participate in a positive feedback phenomenon as increased autophagy – due to greater macrophage activation – also promotes aerobic glycolysis (43, 44). However, analyzing for the presence of aerobic glycolysis is challenging and requires more testing than simply measuring lactate levels and transcriptional analysis of glycolytic enzymes (40).

## 3.6 Either insufficient or excessive immune response impairs the ability of host granulomas/lesions in controlling *Mtb* infection

There is strong evidence that lack of $CD4^+IFN\gamma^+$ T cells or IFNγ signaling, as seen in advanced AIDS patients (73, 249) and

individuals with genetic mutations of various components IFNγ-IL-12 axis (250–253), respectively are vulnerable to TB and non-tuberculous mycobacterial infections. These clinical evidences are supported experimentally by increased susceptibility of IFNγ-knockout mice to TB (254, 255). Thus, one would predict that genetic disruption of the immune checkpoint PD-1, which increases $CD4^+IFN\gamma^+$ T cell activation, would enhance the ability of the host to control an *Mtb* infection. Yet, three studies have shown that mice with the *PD-1* gene knocked out, which would increase $CD4^+IFN\gamma^+$ T cell activation, are more susceptible to *Mtb* infection with not only more severe pathology but greater *Mtb* burden (213, 214, 216). In contrast to the findings with the *PD-1* gene knockout mice, wild type mice that were administered blocking antibody to TIM3 (another immune checkpoint) or the *TIM3* knockout mice were more resistant to *Mtb* with reduced the bacilli burden in the lungs compared to their respective control mice (256). Similarly, administration of an anti-CTLA-4 antibody decreased *Mycobacterium bovis* (*M. bovis*) Bacillus Calmette Guérin (BCG) burden by one-half log at 6 weeks post-infection (257). Plausible mechanistic explanations for these differences include: *(i)* differential capacity among the various immune checkpoints (PD-1 *vs.* TIM3) to inhibit T effector cell function; *(ii)* the disparity between partial inhibition of immune checkpoints with an antibody *vs.* complete genetic disruption of an immune checkpoint; and *(iii)* separate background strains of mice used (C57BL/6 *vs.* BALB/c) wherein mice that are intrinsically and relatively more immunosuppressed (*e.g.*, the BALB/c background in the *TIM3* gene knockout mice) may be more likely to benefit from immune checkpoint inhibitors.

Either deficiency or excess of other molecular and cellular components that impair the host's ability to control *Mtb* infections are listed in Table 3. Thus, we posit that a "modest" activation of these components, at the appropriate times in the course of the *Mtb* infection, are necessary for optimal control of the infection. This "Goldilocks principle" – illustrating the concept of finding the "optimal middle ground" based on the English fairy tale *Goldilocks and the Three Bears* – is also shown graphically (Figure 6).

## 4 Characteristics of human TB and granulomas

In humans, active TB is classically divided into primary TB and post-primary TB, the latter known as reactivation TB, usually located in the lungs after establishment of systemic host-protective immunity in primary TB (283). Since *Mtb* is acquired through inhalation of *Mtb*-containing droplet nuclei less than 5 μm that reach the terminal bronchioles and alveoli, the granulomas in primary TB are located more commonly in the lower lung zones where the ventilation is greater (284). In contrast, the location of post-primary TB is typically more prevalent in the upper lung zones, especially the lung apices but also the superior segments of the lower lobes. These differences suggest that the immunological correlates of protection of primary TB and post-primary TB may be quite different as perhaps evinced by BCG protection against primary TB but less successfully with post-primary TB (285).

TABLE 3 Deficiency or excess of specific components that impairs host control of *Mtb*.

| Component | Deficiency (component beneficial to host) | Excess (component harmful) |
|---|---|---|
| **Epithelioid macrophages** | Absolute Stat 6 depletion prevents epithelioid macrophage differentiation, increasing *Mtb* growth in granulomas (36, 37). | Excessive formation may create a "wall" that prevents immune cell influx into granulomas whereas some disruption increases immune access and promote host survival (35). |
| **$T_H1$ (IFNγ)** | Natural examples are individuals with advanced HIV infection (73, 249) or with genetic defect in IFNγ-IL-12 axis (Medelian Susceptibility to Mycobacterial Diseases) who are vulnerable to systemic mycobacterial infections (250, 253) due to $CD4^+IFN\gamma^+$ deficiency resulting in massive *Mtb* burden and necrotic macrophage death (Figure 4A). Deficiency of IFNγ may also augment IL-17 production, inducing neutrophil influx (258). Appropriate IFNγ production induces IDO-1 that inhibits excessive IL-17 production, limiting excessive neutrophil influx (91) (Figure 4C). | Excess $T_H1$ (IFNγ) results in secondary excess in TNF (207). TNF activates RIP1 and RIP3, induces robust reactive oxygen species, programmed necrosis (necroptosis), and TB cavitation (76, 77) (Figure 4B). IFNγ also increases CXCR3 (a receptor for several angiostatic chemokines), causing hypoxia and granuloma necrosis (211). Excess IFNγ-induced IDO-1 (259) can also inhibit iBALT formation. |
| **$T_H2$/Stat6** | $T_H2$ cells are required for granuloma formation as $T_H2$ deficiency results in failed epithelioid transformation and increased *Mtb* burden (37, 78). | Excess $T_H2$ results in insufficient host-protective immunity causing granuloma necrosis, increased delayed-type hypersensitivity to TNF, cavitation, perinecrotic fibrotic capsule, and *Mtb* transmission (79–81). |
| **TNF** | Mice in which either TNF is neutralized by a monoclonal antibody or have genetic disruption of the 55 kDa TNF receptor are more susceptible to *Mtb* (147, 260). Humans treated with anti-TNF antibody for autoimmune are highly susceptible to TB (141–143). | TNF activates RIP1 and RIP3 and induces production of reactive oxygen intermediates, resulting in activation of BAX, and initiation of a mitochondrial mediated cascade that induces cyclophilin-D-mediated necroptosis (76, 261). TNF also causes anorexia and cachexia (262). |
| **IL-12** | Deficiency of IL-12 or defect in IL-12 receptor subunit is associated with predisposition to mycobacterial infections (250–253). | Depending on the *Mtb* lineage, the ancestral human IL-12B allele may be associated with more severe TB (suggesting co-evolution of humans and *Mtb*) (136). |

*(Continued)*

TABLE 3 Continued

| Component | Deficiency (component beneficial to host) | Excess (component harmful) |
|---|---|---|
| **IL-17** | Insufficient IL-17 increases (sequentially) HIF-1α expression, hypoxic necrotic granuloma formation, & severity of TB (87). IL-17 also required for initial formation of protective iBALT (89, 90, 119). IL-17 triggers the production of chemokines that recruit $CD4^+IFN\gamma^+$ T cells (88). | Excess $T_H17$ and IL-17 production increases influx of neutrophils, augmenting granuloma necrosis (91, 92). Sustained & prolonged IL-17 production in iBALT lesions could result in chronic inflammatory & pathologic iBALT (119). |
| **MMPs** | MMPs facilitate leucocyte recruitment, cytokine and chemokine processing, defensin activation and matrix remodeling (181). Inhibition of MMPs in BALB/c mice was deleterious, resulting in decreased IL-1 and IL-2 expression, premature increase in IL-4, delayed granuloma formation, & more rapid progression of TB (263). In contrast, inhibition of MMPs in C57BL/6 mice was salubrious, resulting in increased fibrosis of the granulomas, decreased leukocyte recruitment (to the granulomas), & decreased numbers of *Mtb* in the lungs & blood in early disease (264). | Excess MMP may lead to immunopathology that leads to *Mtb* dissemination or persistence (181). MMP-9 helps mediate intercellular spread of *M. marinum* (60, 182). |
| **Hypoxia** | The beneficial, seemingly paradoxical, effects of hypoxia to the host are that hypoxia can: *(i)* impair the growth of *Mtb* as evinced by *Mtb*-infected mice, guinea pigs, & rabbits controlled the TB significantly better when breathing 10% $O_2$ (vs. 21% $O_2$) (265); *(ii)* induce expression of HIF-1α, augmenting phagocytes to kill *Mtb* in part through impaired ability to activate autophagy (158, 162) (see also HIF-1α below); *(iii)* recruit immune cells to infection site through induction of the chemokine receptor CXCR4 for $CD4^+$ T cells (164) & neovascularization (165). | Hypoxia induces necrosis of immune cells in granulomas & of pulmonary tissues (211, 266), causing increased disease severity and provide a niche for *Mtb* (87). Hypoxia also induces secretion of MMP-1 causing lung destruction and cavities (218). |
| **HIF-1α** | Hypoxia-induced HIF-1α enhances glycolysis to generate ATP quickly, increases angiogenesis (267), coordinates antimicrobial responses of macrophages such as production of inflammatory cytokines (268), and induces greater M1 macrophage and $T_H1$ cell phenotypes (154, 162, 163) to kill *Mtb* and other bacteria including pyogenic bacteria and *Mycobacterium avium* (159, 160, 166). | HIF-1α, although induced by hypoxia, has also been shown to induce hypoxic TB granulomas (87), to inhibit apoptosis of *Mtb*-infected foamy macrophages (impairing killing of intracellular *Mtb*) (154), and induce MMP-1 (a collagenase that may cause tissue destruction) (218). |
| **Aerobic glycolysis** | Aerobic glycolysis skews macrophages and T cells toward the M1 and $T_H1$ (IFNγ-producing) phenotypes, augmenting immune cells to control *Mtb* infection (161, 163). Lactate produced from glycolysis increases autophagy and killing of *Mtb* (39, 41) | Indirect evidence that the more TB-resistant cynomolgus macaques have less positive PET-CT lesions (see above discussions). Post-translational modification of proteins by lactate may also lead to excessive inflammation (269). |
| **IDO-1 activity** | IDO-1 expression in granulomas is found mainly in the rim that surrounds the central necrosis (270). IDO-1 catabolizes tryptophan into kynurenine. Since tryptophan is normally required for *Mtb* growth, absence of IDO-1 would theoretically provide excess fuel for *Mtb* growth (271). Insufficient IDO-1 would increase IL-17, resulting in increased neutrophil influx into and cause necrosis of the granulomas (Figure 7). | Increased IDO-1 activity is a predictor of death in *Mtb*-infected hosts (272). Excess IDO-1 activity would decreased proliferation of $CD4^+$ and $CD8^+$ T cells (132). Reduced remodeling of granuloma resulting in decreased influx of $CD4^+$ T cells to the granuloma core (Figure 7) (132, 271).. Nevertheless, in the NHP model, (modest) inhibition of IDO-1 results in both reduced *Mtb* burden and disease severity (Figure 7) (132, 271). |
| **HO-1 activity** | HO-1 is protective and promotes granuloma formation in *M. avium* infection (273). In mice, HO-1 deficiency leads to increased susceptibility to *Mtb* infection with increased bacterial loads and mortality due, in part, to failure to mount a protective $T_H1$-mediated granulomatous response (274, 275). HO-1 catalyzes the oxidation of heme (as seen with TB hemorrhage) to produce iron, biliverdin, and carbon monoxide that have anti-oxidant, anti-inflammatory, and anti-apoptotic properties to attenuate TB immunopathology (276, 277). | Treatment of macrophages or mice with a HO-1 inhibitor leads to enhanced control of mycobacterial replication (278, 279); it is believed that HO-1 expression increases iron availability in activated macrophages, which benefits *Mtb* growth (276). HO-1 levels correlate directly with the level of active TB but this relationship by itself does not inform whether HO-1 is host-protective or not (280). |
| **Immune checkpoint** | C57BL/6 mice with genetic disruption of the *PD-1* gene are more susceptible to *Mtb* infection with both severe pathology and greater *Mtb* burden (213, 214, 216). The *PD-L1* gene knockout mice do not have as severe TB than the *PD-1* knockout mice, perhaps because *PD-L2* gene is still intact (Figure 6) (213, 281). See above for more detailed discussion. | BALB/c mice with genetic disruption of *TIM3* gene were more resistant to *Mtb* (256). Similarly, administration of an anti-CTLA-4 antibody enhanced mycobacterium-specific T cell proliferation as well as a decrease in *M. bovis*-BCG burden (257). |
| **LTA4H activity** | Individuals with the CC genotype of *LTA4H* possess an anti-inflammatory (decreased $LTB_4$:$LXA_4$ ratio) and have poorer TB outcome. See above for more detailed discussion. | Individuals with the TT genotype of *LTA4H* possess a pro-inflammatory phenotype (increased $LTB_4$:$LXA_4$ ratio) and have poorer TB outcome. |
| **NFκB** | NFκB-mediated responses are critical for restricting bacterial growth in a granuloma (282). | In excess, NFκB may also cause injurious inflammation and cell necrosis (282) and may inhibit apoptosis and autophagy of *Mtb*-infected macrophages (50). |
| **TGFβ** | In conjunction with IL-23, TGFβ promotes the expansion of $T_H17$ cells, which are important for early control of *Mtb* infection (86). | TGFβ negatively impacts IFNγ-producing $CD4^+$ T cells in granulomas, impairing control of *Mtb* (83, 101). |

CTA-4, cytotoxic T lymphocyte-associated protein 4; HIF-1α, hypoxia-inducible factor-1 alpha; HO-1, heme oxygenase-1; IDO-1, indoleamine 2,3-dioxygenase; IL-12, interleukin-12; IL-17, interleukin-17; LTA4H, leukotriene $A_4$ hydrolase; $LTB_4$, leukotriene $B_4$; $LXA_4$, lipoxin $A_4$; MMPs, matrix metalloproteinases; NFκB, nuclear factor-kappa B; PD-1, programmed cell death protein-1; TGFβ, transforming growth factor-beta; TIM3, T cell immunoglobulin and mucin domain-containing protein 3; TNF, tumor necrosis factor.

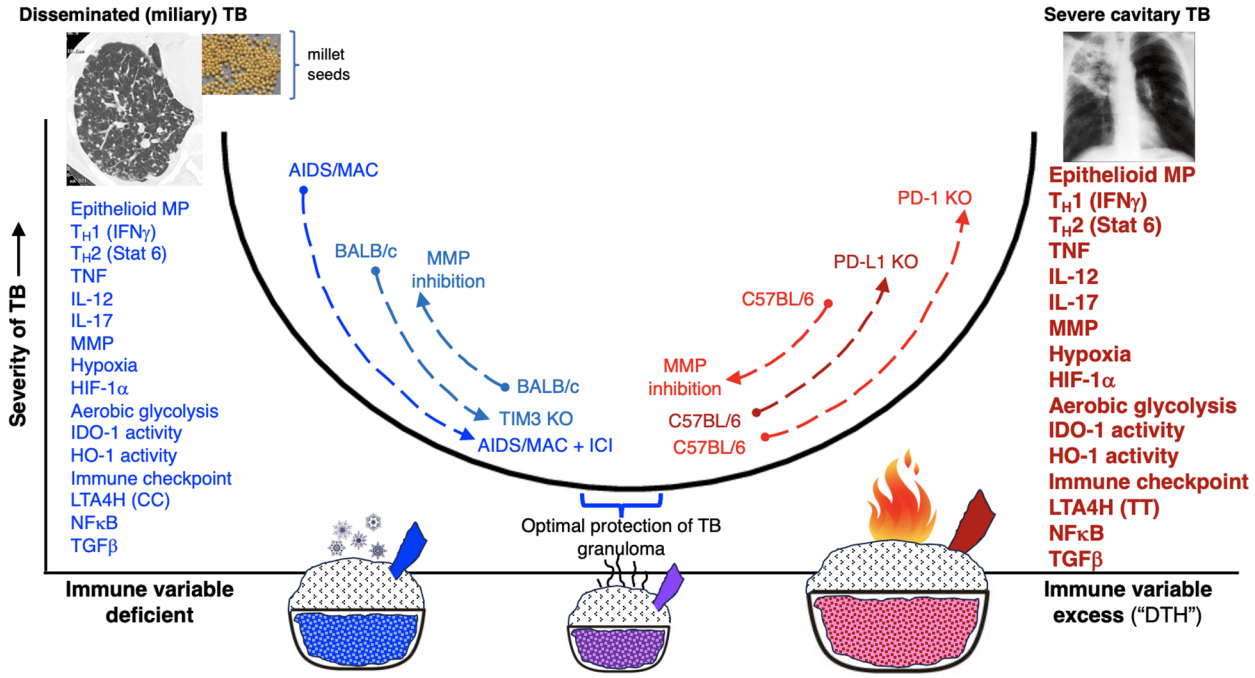


FIGURE 6
Either excessive or deficiency of molecular or cellular immune elements may predispose to unprotective granuloma or defense against *Mtb*. The diagram illustrates that either deficiency or excessive of specific immune components (x-axis) may result in increased susceptibility and severity of TB (y-axis). Using the immune checkpoint inhibitors as an example, we posit that in conditions where the host is either severely immunocompromised, immune checkpoint inhibition would be beneficial against mycobacterial infection, as exemplified by: *(i)* advanced AIDS patient with severe mycobacterial infection that improved with an anti-PD-1 antibody and *(ii)* TIM3 antagonism or *TIM3* gene knockout mice are protected against mycobacteria in the less immunocompetent BALB/c mice. In contrast, in hosts with better preserved immune function, immune checkpoint inhibition results in a hyperinflammatory state, worsening control of mycobacterial infections, as exemplified by the mice with genetic disruption for *PD-1* or *PD-L1* gene. Perhaps the severity of TB is not as severe in the PD-L1 knockout mice than the PD-1 knockouts because in the PD-L1 knockout mice, PD-L2 is still intact and thus the enhanced immune activation with the genetic disruption of PD-L1 is not as severe as of PD-1. We have also shown other molecular and cellular components in which deficiency or excess predispose to TB. See also text and Table 2 for further discussion. AIDS, acquired immunodeficiency syndrome; HIF-1α, hypoxia-inducible factor 1-alpha; HO-1, heme oxygenase-1; ICI, immune checkpoint inhibitor; IDO-1, indoleamine 2,3-dioxygenase; IFNγ, interferon-gamma; IL-12, interleukin-12; IL-17, interleukin-17; LTA4H, leukotriene $A_4$ hydrolase; MAC, *Mycobacterium avium* complex; MP, macrophages; MMP, matrix *Mtb*, *Mycobacterium tuberculosis*; NFκB, nuclear factor-kappa B; PD-1, programmed cell death protein-1; PD-L1, programmed death-ligand-1; TB, tuberculosis; TGFβ, transforming growth factor-beta; TNF, tumor necrosis factor.

## 4.1 Self-limiting primary TB and primary progressive TB

In immunocompetent individuals, primary TB – most commonly affecting the lungs but may present as extrapulmonary TB – typically remains asymptomatic and resolves spontaneously. It is most often detected radiographically as a Ghon lesion (a sequela of untreated primary TB characterized by a lung nodule comprised of caseous granulomas surrounded by a fibroblastic rim), a Ghon complex (the combination of a nodule with associated draining mediastinal lymphadenopathy), or a Ranke complex (characterized by calcification of the Ghon complex) (286). On imaging, such lesions may be suspicious for lung cancer prompting surgical removal, but diagnosed histopathologically as TB-related (287). A relatively small number of bacilli adapt to the granuloma micro-environment and persist as asymptomatic latent infection. Autopsy studies revealed that granulomas in latent TB tissues exhibited lower cellularity and inflammation but displayed more prominent sclerosis, fibrous encapsulation, and calcification compared to their active counterparts (152). Histological analysis of latent TB lesions from individuals who died of non-TB-related causes has revealed caseous and fibrocaseous characteristics (288).

Ghesani and co-workers (289) reported the PET-CT findings of five household contacts of active TB patients before and during treatment for latent TB infection. These five individuals had no evidence of active TB and asymptomatic ("latent") TB infection was established based on positive QuantiFERON testing and negative chest radiographs. This report showed that: *(i)* FDG uptake was increased in the thoracic lymph nodes in four of the five contacts; *(ii)* on repeat PET-CT testing while on treatment for latent TB infection, the FDG uptake decreased or became negative in three of the four and no change in one with initial mild FDG uptake; *(iii)* in the one patient with initial negative FDG uptake in the chest, there was evidence of remote latent TB infection as evinced by calcified granuloma in the lung parenchyma and ipsilateral calcified hilar lymph node (Ranke complex); *(iv)* the QuantiFERON results correlated highly with the intensity of the FDG uptake, indicating the PET positivity likely reflected a type 1 ($CD4^+IFN\gamma^+$) immune response (289).

Some individuals, perhaps with sub-optimal and not necessarily severely immunocompromised immune function may develop

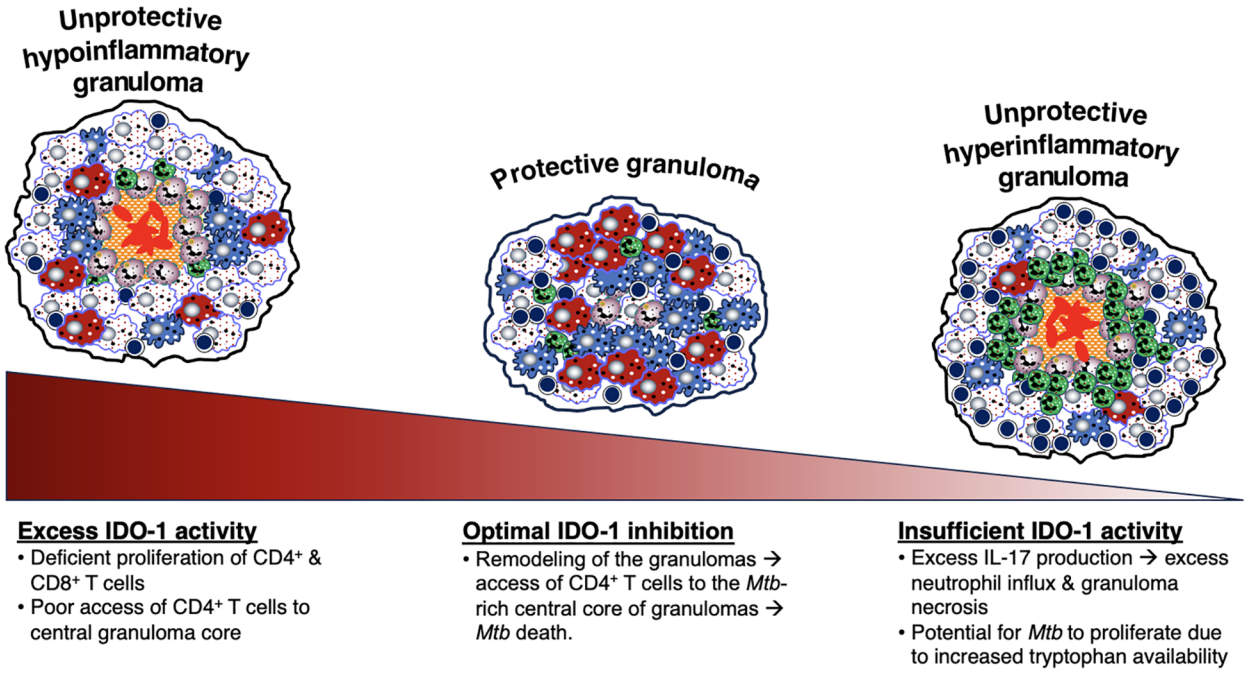


FIGURE 7
Relative IDO-1 activity helps dictate the level of protection by TB granulomas. IDO-1 activity can also be an indicator of the protectiveness of a granuloma. When there is an optimal level of IDO-1 inhibition, the remodeling of the granulomas allows access of $CD4^+$ T cells to the central core of the granuloma, resulting in *Mtb* death. However, excessive or insufficient IDO-1 activity leads to an unprotective granuloma. An excess of IDO activity results in an unprotective, hypoinflammatory granuloma, characterized by deficient proliferation of $CD4^+$ and $CD8^+$ T cells and poor access of $CD4^+$ T cells to the granuloma core, allowing *Mtb* to grow within the center. On the other hand, an insufficient level of IDO-1 activity leads to an unprotective, hyperinflammatory granuloma, characterized by excess IL-17 production and excess neutrophil influx and granuloma necrosis. IDO-1 is also responsible for the catabolization of tryptophan (a molecule necessary for *Mtb* growth) into kynurenine. A deficiency of IDO-1 would in turn increase levels of tryptophan and allow for more *Mtb* growth. IDO-1, indoleamine 2,3-dioxygenase; IL-17, interleukin-17; *Mtb*, *Mycobacterium tuberculosis*;.

primary progressive TB. Except for a history of a relatively recent active TB exposure and the location of disease (more likely to be mid to lower lung zones), such patients are essentially indistinguishable from those with post-primary TB.

## 4.2 Post-primary TB

Post-primary TB accounts for the majority (≥80%) of active TB cases. In the 19th and early 20th centuries, pathologic analyses of human TB tissues were commonly performed on subjects with varying profiles of disease severity. These studies were conducted prior to the discovery of effective antibiotic therapy and thus also reflect the natural history of TB (134, 288, 290–292). Dr. Robert Hunter and his colleagues have critically reviewed these older literature as well as microscopically examined treatment-naïve TB lung specimens (287, 293–297). Two characteristic lesions of human pulmonary TB emerged: caseating granulomas and tuberculous pneumonia (Figures 8A, B) (293). Caseating granulomas were reflective of primary TB, which may be self-limiting or progressive (Figure 8A). While post-primary TB may begin with degeneration of primary granulomas (Figure 8A), some contend that it starts as a nascent pneumonic process which then spreads endobronchially resulting in airway obstruction and lipoid pneumonia, the latter due to the presence of lipid-laden ("foamy") macrophages and DEC-$205^+$ dendritic cells infiltrating the airway lumina and alveolar spaces (Figure 8B) (33). However, because most surgically resected or autopsy TB cases represent advanced disease, it is challenging to determine with certainty whether endobronchial spread is a primary or secondary process, or a combination of both. The early inflammation that occurs with this post-primary pneumonic process was largely attributed to a Type IV hypersensitivity reaction to *Mtb* antigen and not to an increase in the number of viable *Mtb* since the early stages of this pneumonic process were very often paucibacillary (133, 298, 299). The formation of necrotic granulomas due to host-mediated bacillary destruction rather than proliferation is supported by recent RNAscope and immunohistochemistry studies (300). In this study, a significant amount of *Mtb* mRNA and Ag85B was detected in human necrotic granulomas in the lungs and lymph nodes of a confirmed TB patient, despite being Ziehl-Nielsen-negative (300).

These findings are further corroborated by another study that characterized the micro-anatomical environment of human TB lung tissues using micro-computed tomography (μCT), histopathology, and immunohistochemistry to determine the three-dimensional shape of the TB granulomas and their spatial relationship to airway and vascular structures (237, 238, 301). Consequently, unlike the typical two-dimensional description of TB granulomas as round discrete structures, they found that human

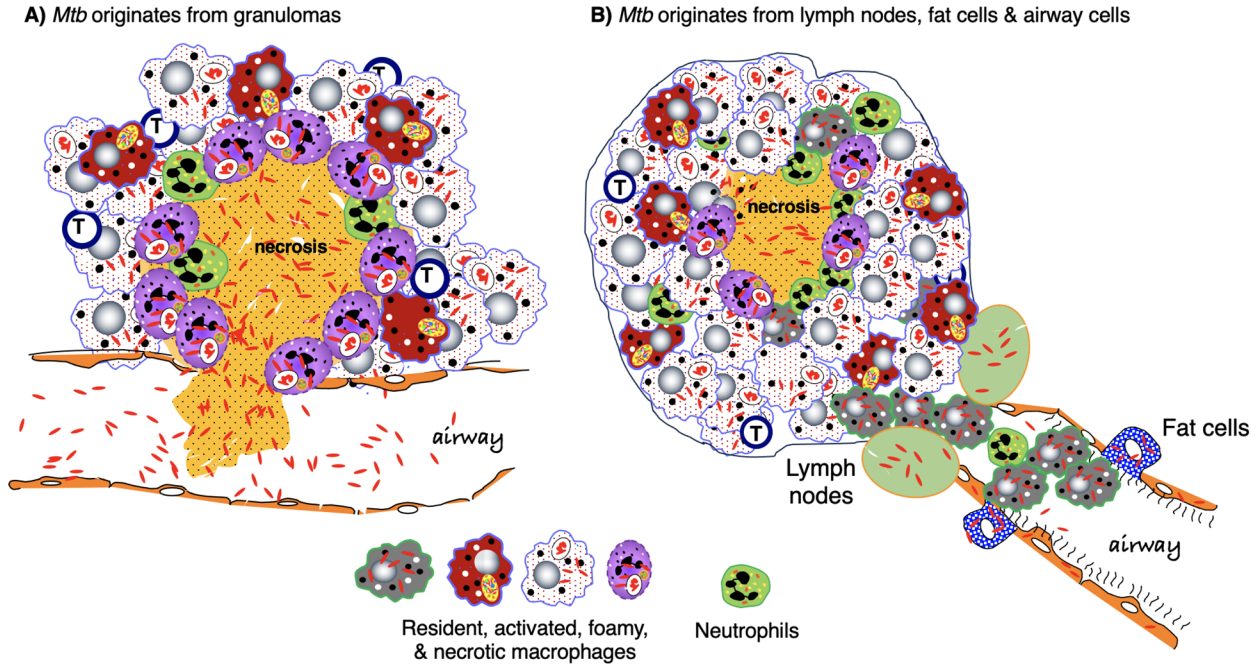


FIGURE 8
Origin of *Mtb* and early events in the development of post-primary TB. **(A)** An often-cited description for the evolution of post-primary (reactivation) TB is that immune dysfunction results in progressive necrosis and liquefaction of the granuloma, exuberant multiplication of dormant *Mtb*, disruption of the integrity of the granuloma wall, and spillage *Mtb*-filled necrotic granulomatous content into the airways. Pneumonia forms due to endobronchial spread of granuloma content. **(B)** An alternative description of post-primary TB is based on the paradigm chronic stable granulomas are mostly sterile and that the dormant *Mtb* that "reawaken" originated from lymph nodes. fat cells, and airway epithelial cells causing a bronchogenic lipoid pneumonia. Granulomas may form around pockets of necrotizing pneumonia. As discussed in the text, it is plausible that both reactivation models occur. *Mtb*, *Mycobacterium tuberculosis*; TB, tuberculosis.

necrotic TB granulomas demonstrated cylindrical, branched morphologies which are connected to the airways and shaped by the bronchi, supporting the bronchogenic spread of *Mtb*. Another clinically relevant finding is that the lack of vascularization within obstructed bronchi likely resulted in further necrosis poor antimicrobial penetration of affected lung segments, and the development of functional drug resistance (237). Additionally, utilizing histopathology and genome-wide transcriptomic analysis, immunological profiling of human lungs surgically resected for recalcitrant active TB showed considerable variation in T cell influx in different granulomas as well as significant differences in gene expression of the inflammatory response, immune cell trafficking, and cell mediated immune response (5).

The post-primary pneumonic process can either resolve spontaneously with resolution of the airway obstruction (thought to occur in the majority of cases) or develop necrosis and a caseating pneumonia (in ~5% of cases) (Figure 8B). One *Mtb* component that may be responsible for the caseating pneumonia is the glycolipid TDM (185, 188). If caseous necrosis develops – often linked to a rapid surge in *Mtb* numbers (133, 297) – the infection may progress in one of two ways: either through the formation of a post-primary granuloma around the caseous pneumonia, attempting to contain the infection, or through cavitation, which leads to even greater *Mtb* replication and facilitates their expulsion into the airways, enabling person-to-person transmission. The pathogenesis of cavitary disease may arise not only from the caseating necrosis associated with the pneumonic process but also from the degradation of fibrous tissue at the periphery of secondary granuloma by MMP-1 and MMP-9 (302–306). Additional factors for cavitation include pulmonary infarction resulting from vasculitis (287, 294), and an excessive immune response (285, 307, 308). Interestingly, the lack of necrotizing granulomas in most standard mouse strains may be linked to the absence of lung expression of the mouse ortholog of MMP-1 (303, 304).

## 4.3 Where do the *Mtb* originate from in post-primary TB?

The precise location of dormant *Mtb* before their reactivation, leading to post-primary TB, remains a topic of debate. Some argue that dormant *Mtb* residing within primary granulomas break out as the integrity of the granulomas declines due to waning immunity (Figure 9A). Subsequently, *Mtb* enters the airway lumina, leading to endobronchial spread. Alternative evidence suggests that *Mtb* originates from normal-appearing lung tissues, fat cells, and thoracic lymph nodes since primary granulomas are noted to be sterile after five years (21, 294, 309). However, unless all innumerable microscopic granulomas in the lungs of primary TB can be individually dissected and cultured – logistically an untenable task – it is impossible to exclude primary TB granulomas as potential sources of reactivated *Mtb* during

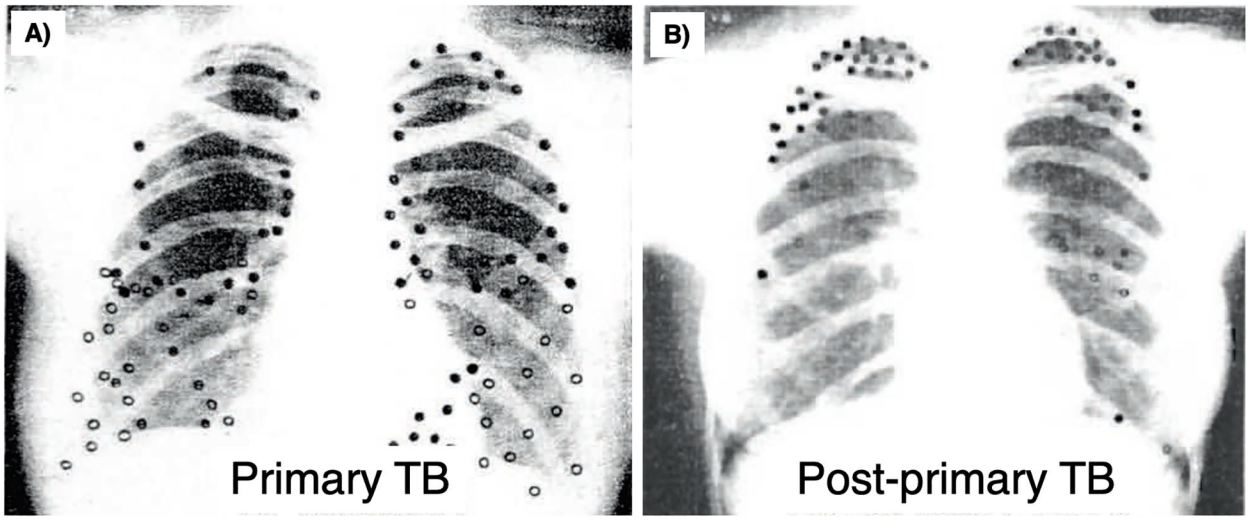


FIGURE 9
Distribution of lesions in primary and post primary TB. The localization of lesions of **(A)** primary and **(B)** post-primary TB of several people were plotted on an X-ray. Each dot marks the location of an individual's lesion. The distribution of primary TB is consistent with chance distribution of airborne infection while most post-primary lesions were in the upper lobes, especially the apical segments. Reprinted with permission of the American Thoracic Society. Copyright © 2024 American Thoracic Society. All rights reserved. Medlar E.M. The pathogenesis of minimal pulmonary tuberculosis: A study of 1,225 necropsies in cases of sudden and unexpected death. Am Rev Tuberc 1948; 58: 583-611. The American Journal of Respiratory and Critical Care Medicine is an official journal of the American Thoracic Society. TB, tuberculosis.

development of post-primary TB. Furthermore, both hypotheses are not necessarily mutually exclusive, leading to a reasonable supposition that both quiescent lung granulomas and other tissues (fat cells, lymph nodes) are potential sources of reactivated *Mtb*. Following cavitation, endobronchial spread may occur to all other parts of the lungs (310).

Most primary TB lesions reside in the lower lung zone (Figures 9A, 10A) because inhaled *Mtb* are preferentially deposited in the more ventilated lower lung zones. However, primary TB lesions can also form in the upper lung zones, albeit less frequently (Figure 9A) (294, 298). Nonetheless, post-primary TB is more common in the upper lobes (especially apices) and superior segments of the lower lobes (Figures 9B, 10A). The exact reason for the differing lung distribution between primary TB and post-primary TB remains unclear, as it seems unlikely to be solely attributed to the initial residence of dormant *Mtb*. We suggest that

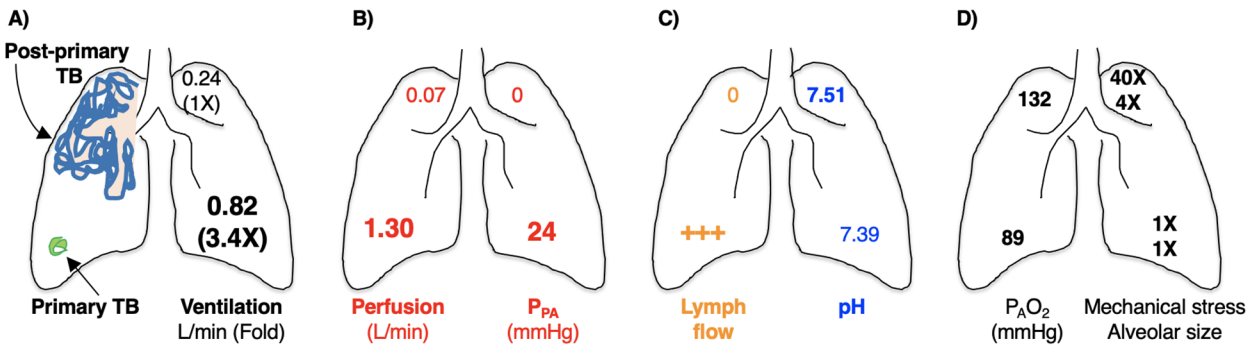


FIGURE 10
Anatomical-physiological-chemical mechanisms by which post-primary TB is more common in the upper lobes of the lungs. Based on differences in the physiological-chemical properties between the upper lobes and lower lobes, primary *Mtb* lesions located in the upper lobes, while fewer than that in the lower lobes, are more likely to reactivate. **(A)** Diagram showing that primary TB is located mostly in the lower lung zone (green circular structure that represents a calcified granuloma – Ghon complex). This distribution of primary TB is due to greater (3.4X) ventilation in the lower lobes than the upper lobes of an upright human. **(B)** In the upright human, there is decreased lung perfusion pressure due to lower pulmonary artery pressure in the upper lobes. This decreased perfusion will result in decreased influx of immune cells and soluble mediators to the upper lobes in the upright position. **(C)** Lymph formation and flow are also significantly decreased in the upper lobes, resulting in increased accumulation of mycobacteria and antigens in the upper lobes and contributing to increased hypersensitivity reactions and lung damage. pH in the upper lobes is more alkalotic which induces glycolysis and, in turn, increases autophagic clearance of *Mtb* by the macrophages. **(D)** The $P_AO_2$ is also significantly greater in the upper lobes than the lower lobes, which favors *Mtb* growth. The mechanical stress and alveolar size of the upper lobes are also greater (by 40X and 4X, respectively) than the lower lobes, predisposing this area to the development of cavities, especially with large inspiratory efforts. *Mtb*, *Mycobacterium tuberculosis*; $P_AO_2$, partial pressure of alveolar oxygen; TB, tuberculosis.

this locational disparity arises from the preferential reactivation of primary lesions in the upper lung zones, influenced by fundamental physiological and chemical principles.

First, while there is less ventilation to the upper lung zones in the upright position in humans, there is much less perfusion in the upper lung zones (Figure 10B). The relative overall decrease in blood perfusion to the upper lung zones will also result in decreased influx of both immune cells and soluble factors such as antibodies and complement components (311, 312). Second, because the lung apices have decreased capillary perfusion pressure in the upright human, there is decreased lymphatic fluid formation in the upper lung zones, resulting in reduced lymphatic drainage of *Mtb* antigen/debris removal to lymph nodes and reduced T cell priming (Figure 10C) (313). Third, there is relative alkalosis in the upper lung zones compared to the lung bases (~pH 7.51 vs. 7.39, respectively) due to increased ventilation:perfusion ratio in the upper lung zones (314). Alkalosis promotes aerobic glycolysis over oxidative phosphorylation (315, 316) and this increase in glycolysis can hinder autophagic flux (241), impairing a key mechanism for killing intracellular *Mtb*. Supporting this hypothesis, experimental TB in rabbits predominantly affects the dorsal regions of the lungs; however, when the rabbits are kept in a vertical position, the infection primarily targets the superior parts of the lungs (317, 318). Fourth, the relatively greater $O_2$ delivery to the upper lung zones (Figure 10D) creates a more hospitable environment for *Mtb* replication (313, 319). The reason that there is greater $O_2$ tension in the upper lobes is that perfusion by deoxygenated blood arising from the pulmonary artery in a low pressure right ventricular circulation is surpassed by oxygenated blood flow from the bronchial artery, which is a high-pressure left ventricular circulation; *i.e.*, compared to the lower lobes, there is relatively less $O_2$ extracted from the upper lobe alveoli by the red blood cells in the upright human. This notion is supported by evidence that in marginal human donor lungs, there is significantly better oxygenation to the upper lobes than the remaining lungs, as measured by the ratio $PaO_2$:$FiO_2$ (partial pressure of $O_2$ in the blood:inspired $O_2$ concentration) (320). One piece of supporting evidence for this mechanism is that *Mtb*-infected guinea pigs breathing 10% oxygen exhibit less severe TB pathology compared to control animals breathing ambient air (265, 317). Conversely, *Mtb*-infected mice breathing 60% $O_2$ had significantly higher burden of viable *Mtb* in the lungs than control mice breathing 20% $O_2$ (317).

## 4.4 What causes pulmonary cavitation?

There are two prevailing models regarding the formation of TB cavities in the lungs, each corresponding to the two main models of post-primary TB development. It is likely that both models occur with varying frequencies within individuals. The first model suggests that a stable granuloma harboring dormant *Mtb* becomes destabilized due to "immunosuppression," leading to liquefaction of the central caseous necrosis and subsequent multiplication of *Mtb*. The contents of the cavity then erode into an airway, allowing air to enter the emptying granuloma and expanding the space. The second model proposes that post-primary TB initially presents as bronchogenic lipoid pneumonia, which then undergoes necrosis. This triggers a secondary granulomatous reaction, which forms around the necrotizing pneumonia, resulting in cavitation due to the necrosis and expectoration of the necrotic material. One finding that challenges both models is that air analysis reveals most cavities contain lower oxygen levels and higher carbon dioxide levels than those measured in the airway lumen (321). However, it is plausible that intermittent or progressive obstruction of the airway emanating from the cavity could lead to hypoxia and hypercarbia within the cavity lumina. Once cavities form, further necrosis and disruption of the cavitary walls may allow extracellular mycobacteria to access the blood and lymphatic vessels, as well as the airways, facilitating their spread to other individuals through aerosolization (322). Tuberculous cavities typically harbor high concentrations of bacilli, and their presence heightens infectiousness due to their communication to the airways and subsequent aerosol transmission of *Mtb*. While necrosis is a prerequisite for cavitation, it alone is insufficient to ensure its development.

Recently, a study compared the cell-specific gene expression profiles of sarcoidosis granuloma (usually not associated with necrosis) and human TB granuloma (often associated with necrosis). Compared to sarcoidosis, the most upregulated gene in TB was the collagenase matrix metalloproteinase-1 (MMP-1) (305). MMP-1 is a collagenase that is essential for cavity formation through the degradation of the fibrous extracellular matrix that surrounds granulomas (304). Infection with *Mtb* induces MMP-1 and MMP-9 production in macrophages (302). During the early stages of granuloma formation, MMP-1 expression increases in the surrounding epithelial cells and leukocytes (181). While MMPs facilitate leucocyte recruitment, cytokine/chemokine processing, and defensin activation, excess MMP activity may lead to damaging immunopathology including granuloma destruction and pathogen dissemination or persistence (181, 303). Inhibition of MMP with a broad spectrum MMP inhibitor yielded conflicting results, but this may be due to timing of the inhibition in relation to the *Mtb* infection (263, 264). Early MMP inhibition (at the time of *Mtb* infection) with a broad spectrum MMP inhibitor (BB-94) in mice resulted in decrease in pro-inflammatory cytokines (IL-1 and IL-2), premature increase in IL-4, delayed and smaller granuloma formation, and more rapid progression of disease characterized by small lung nodules suggestive of miliary TB (263). In contrast, delayed administration of BB-94 (18 days after *Mtb* inoculation) resulted in increased collagen deposition within early granulomas with decreased *Mtb* burden (264).

Mechanical factors may also account for why TB cavities are more common the upper lung zones. In the upright human, there is significant increase in both physical stress and alveolar sizes in the upper lung zones during inspiration, ~40 times and ~4 times greater, respectively, than the lower lung zones (Figure 10D). These physical differences may subject the upper lung zones to increased physical stress and along with actions of various metalloproteinases produced by immune cells that degrade lung

tissues, increase vulnerability to cavitary formation. Based on these plausible pathogenic mechanisms, it has been suggested that historical TB treatment of enforced bed rest may be an effective adjunctive remedy for TB (312).

Animal models are essential for studying TB pathogenesis and developing treatments and vaccines. As with all disease models, it is vital to select species that replicate key characteristics of human TB, including the development of caseous necrosis surrounded by a collagen rim, hypoxia, both intracellular and extracellular populations of bacilli, liquefaction, and cavity formation (152). In this context, we will first discuss select animals with natural *Mtb* complex infections, such as cattle and elephants, followed by a review of experimental animal models including zebrafish, mice, guinea pigs, rabbits, and non-human primates (152, 266, 323–327).

# 5 Characteristics of natural TB infections of animals

## 5.1 Cattle

Cattle are a natural host of *Mycobacterium bovis*, an *Mtb* complex organism (328). While cattle can be experimentally infected with *Mtb*, TB is less severe (329). *M. bovis* also infects many other domesticated and wild animal species (328, 330). Cattle have several advantages in TB vaccine research – the disease progresses slowly, the granulomatous reaction are similar to that seen in humans, and vaccination in neonatal calves confers protection but wanes over time (331–334). Disadvantages include their large size/high cost in experimental housing (326) and post-primary TB is not a characteristic of them (294).

Granulomas in tuberculin reacting cattle (due to *M. bovis*) may be uncommon to rare (1-2%) when tissues are examined in a slaughterhouse but are commonly found (>70%) when analyzed using 5 mm lung slices (335). Wangoo et al. (336) have classified bovine TB granulomas in experimentally infected calves with *M. bovis* into four separate stages of severity based on size and microscopic morphological characteristics such as cellular composition, necrosis and fibrosis. Similar to humans and NHP, all stages of granulomas in this *M. bovis* infection model may be seen simultaneously in the same animal (336, 337).

As in human TB, $CD4^+$ and $CD8^+$ T cells are important in host immunity to bovine TB. In most stage I/II lesions of bovine TB, $CD8^+$ and $CD25^+$ T cells were found in the rim of the granulomas whereas $CD4^+$ T cells were distributed in both the lymphocytic rim and center of the granulomas (337). γδ T cells were interspersed among the macrophages, leading to the speculation that $CD4^+$ and γδ T cells – observed in granulomas within the first 21 days after experimental *M. bovis* infection in cattle (338, 339) – both play a role in the maintenance and the maturation of the granulomas as well as a host-protective role in respiratory mucosal immunity (340, 341). In stage III/IV lesions, all the examined T cell populations were present among the mononuclear component of the granulomas. The clinical and pathologic features of *M. bovis*-infected cattle that mimic human pulmonary TB are described in Table 4.

## 5.2 Elephants

Elephants are divided into African elephants (*Loxodonta africana*) and Asian (Indian) elephants (*Elephas maximus*). While TB in elephants is mostly due to *Mtb*, *M. bovis* (342–345) and *M. caprae* (346) have been reported. TB in elephants has been identified more commonly in Asian elephants than African elephants, possibly due to greater contact between the former and humans. However, it is not known whether Asian elephants are intrinsically more susceptible (347, 348).

TB has been observed in both wild (349–351) and captive elephants (344, 352). Spread among elephants and inter-species infection between humans and elephants (likely bidirectional) have been either strongly suspected or well-documented (353–357).

Heterogenous TB granulomas are also found in elephant TB. The main pathological lesions of elephant TB occur in the lungs and thoracic lymph nodes (358). Gross anatomical features include non-caseating and caseating granulomatous nodules as well as calcified caseous and cavitary lesions. Histopathologic features include epithelioid granulomas with giant cells in both lymph nodes and lung lesions as well as caseous and necrotizing granulomatous pneumonia in more severe cases (358). One study showed that of nine Asian elephants that died from TB, six had poorly-formed granulomas in the lungs with low to moderate number of lymphocytes, comprised mostly of B cells (359). However, the other two elephants had discrete and well-demarcated granulomas and greater number of T cells. The clinical and pathologic features of *Mtb*-infected elephants that mimic human pulmonary TB are described in Table 4.

# 6 TB Granulomas associated with experimental infections

## 6.1 Zebrafish

The primary limitations of zebrafish in experimental TB are that they do not have lungs and cannot be infected in a sustained fashion with *Mtb* due to lower temperature requirements of zebrafish. Instead, *M. marinum* is used as a surrogate because it naturally inhabits zebrafish, is genetically similar to *Mtb*, and causes TB-like diseases in poikilothermic animals (76, 261, 360, 361). Nevertheless, both the embryonic-larval and adult zebrafish models have several advantages in understanding mycobacterial pathogenesis: *(i)* large-scale screening studies can be attempted since they are small and easy to reproduce and raise; *(ii)* their transparency in the embryonic and larval stages allows their internal structures to be visualized temporally without the need to sacrifice them; *(iii)* zebrafish embryos have a temporal separation between the earlier development of innate immunity (macrophages and neutrophils) and later development of adaptive immunity (lymphocytes), allowing the study of only innate immunity during the initial stages of mycobacterial infections; *(iv)* hypoxic or non-hypoxic granulomas can be induced according to the infection site – *via* inoculation of *M. marinum* in poorly or richly vascularized areas,

TABLE 4 Comparison of the features of natural and experimental animal TB with human pulmonary TB.

| Present in animals? | Human TB Features | | | | | | |
|---|---|---|---|---|---|---|---|
| | Clinical features | | | Pathologic features | | | |
| | Latent infection | Primary progressive TB | Reactivation TB | TB pneumonia | Non-caseating granuloma | Caseating granuloma | Cavitary disease |
| **Cattle** | Yes (461–465) | Yes (334, 336–340, 461) | Not reported "naturally" but experimentally with recovery of *M. bovis* with or without treatment of animals with the "mycobacterial promoter resuscitation factor B (RpfB) protein" (462–464). | Yes (lipoid pneumonia) (29) | Not reported | Yes (336) | No (29, 266, 323) |
| **Elephants** | Yes (352, 357, 359, 466) | Possible but unable to distinguish readily with reactivation TB. | Yes (352, 467) | Yes (349, 358) | Not reported | Yes (345, 347, 348, 354, 358) | Yes (348, 358) |
| **Zebrafish** | Yes, with low-dose *M. marinum* infection (468) | Yes, with high-dose *M. marinum* (369) or with "cluster I" strain (isolated from humans with fish tank granuloma). Chronic disease with longer survival of the zebrafish is seen with infection with "cluster II" strain of *M. marinum* (469). | Yes, of latent infection with gamma-irradiation (468) | N/A | Yes (361) | Yes. With time, the central necrosis of the granulomas may be surrounded by a cellular and/or fibrotic cuff (168, 369). | N/A |
| **Mice** | Used antibiotics to suppress *Mtb* but not kill them with ability to reactivate (Cornell model) (384). | Yes (34, 185, 374, 376, 383, 386). | Yes, with use of non-sterilizing antibiotic regimen (384) and with (premature) termination of antibiotic regimen (376). | Yes (295, 387). | Yes (383). | Yes, with the C3HeB/FeJ (Kramnik) mouse strain (34, 376), the CBA/J strain (470), or intraperitoneal immunization with *Mtb* and rechallenge (185). | Yes, in certain strains (C3HeB/FeJ and CBA/J) (386, 387). |
| **Guinea pigs** | Yes, with use of antibiotics to suppress *Mtb* (402, 403). | Yes (325, 395, 401, 407, 471, 472). | Yes (405). | Yes (406, 473). | Yes (472). | Yes (325, 472). | Yes, sporadically (325, 372, 471). |
| **Rabbits** | Yes, in the TB-resistant New Zealand white rabbits infected with *Mtb* CDC1551 (425). | Yes (420, 474). | Yes, glucocorticoid was used to cause reactivation TB in New Zealand white rabbits with latent TB infection (425). | Yes (474). | Yes (425). | Yes (323, 475). | Yes (323, 420, 431). |
| **Mini pigs** | Yes (435, 436). | Yes (435, 436). | Unknown but potentially yes. | None reported | Yes (435, 436). | Yes (435, 436). | None reported. |

*(Continued)*





10.3389/fimmu.2024.1427559

TABLE 4 Continued

| Present in animals? | Human TB Features | | | | | | |
|---|---|---|---|---|---|---|---|
| | Clinical features | | | Pathologic features | | | |
| | Latent infection | Primary progressive TB | Reactivation TB | TB pneumonia | Non-caseating granuloma | Caseating granuloma | Cavitary disease |
| **Goats** | Yes. Goats inoculated with *M. bovis* in the airways did not develop clinical signs of infection when euthanized 5 months later; there were also *M. bovis* cultured from thoracic lymph nodes, calcified lesions in the lungs, and skin test confirmed bovine TB (438). | Yes (437, 476). | Yes (477). | Yes, with foamy macrophages (478). | None found. | Yes (437, 438, 477, 479). | Yes (437, 477). |
| **NHP** | Yes, in rhesus and cynomolgus macaques (229, 452, 480). | Yes, in rhesus and cynomolgus macaques (226, 240, 451, 481–485). Yes, in marmosets (447, 486). | Yes, in both rhesus and cynomolgus macaques (229, 452, 480). Reactivation from latent infection can occur but is rare (<5%) (487). | Yes, in rhesus and cynomolgus macaques (226, 483, 487). Yes in marmosets (447). | Yes, in rhesus and cynomolgus macaques (482, 487).<br>Yes, in marmosets (447). | Yes, in rhesus and cynomolgus macaques (451, 452, 484).<br>Yes, in marmosets (447). | Yes, in rhesus and cynomolgus macaques (229, 451, 452, 485). Yes, in marmosets (447, 486). |

| Differences between Rhesus and Philippine cynomolgus macaques with TB | |
|---|---|
| Rhesus macaques | Cynomolgus macaques |
| More susceptible to *Mtb* with higher bacterial burden, greater signs of clinical disease, and slower progression of TB (240). | More resistant to *Mtb* with fewer symptoms, reduced dissemination of granulomas and slower progression of disease (240). |
| More gross pathology (240). | PET-CT shows reduced dissemination of granulomas, slower increase in lung inflammation, and fewer PET-positive/necrotic lymph nodes than rhesus macaques (240). Immunohistochemistry showed greater influx of macrophages, B cells, and T cells in most of the granuloma types than rhesus macaques (488). |
| More reliable model for active disease (240). | More reliable model for latent infection (452). |





10.3389/fimmu.2024.1427559

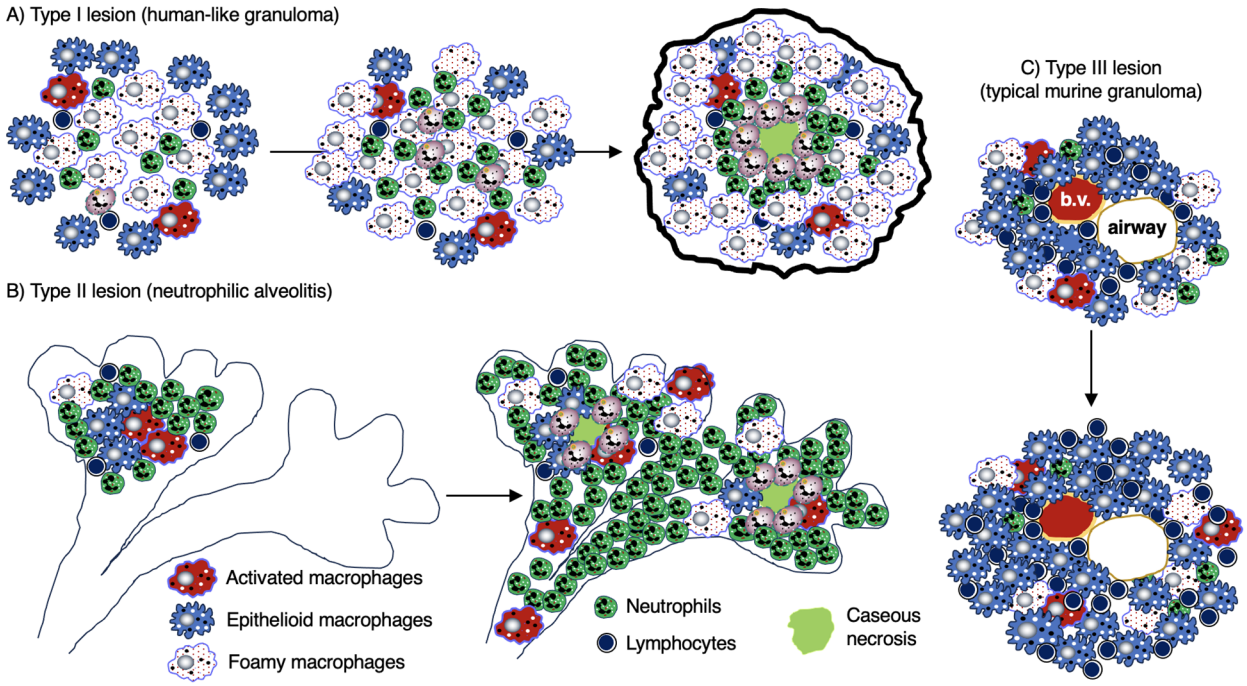


FIGURE 11
Different types of TB lung lesions in the C3HeB/FeJ mice. Three types of histopathologic TB lesions are seen in the C3HeB/FeJ mice. **(A)** Type 1 lesion is mainly comprised of foamy macrophages, few epithelioid macrophages and lymphocytes, and a caseous center surrounded by neutrophils. This lesion most resembles to that seen in human TB. **(B)** Type 2 lesion is the most severe form and is characterized by a neutrophilic, necrotizing alveolitis with occlusion of the terminal bronchioles and caseous necrosis. **(C)** Type 3 lesion is comprised mainly of infiltration of epithelioid macrophages and lymphocytes, smaller numbers of foamy and activated macrophages and neutrophils around the airway and blood vessel pair. This is the typical lesion seen in most other mouse strains. TB, tuberculosis.

respectively – in the larva model; *(v)* in the advanced model, acute or chronic/latent infection may be induced based on the infectious dose (4, 362–370). The clinical and pathologic features of *M. marinum*-infected zebrafish that mimic human pulmonary TB are described in Table 4.

## 6.2 Mice

Mice are a tractable animal model for TB because they are relatively easy to handle, inexpensive, require little space, have similar immune components to humans, and there is an expansive array of immunological reagents available. Furthermore, there is the ability to genetically engineer mouse strains to elucidate the role of specific genes with *Mtb* infection; *i.e.*, "knock-out" and "knock-in" mouse strains through targeted disruption of specific genes (266, 323, 326, 371, 372). These advantages allow for assessment of large-scale drug screening and vaccine efficacy testing, in addition to monitoring disease endpoints following *Mtb* infection.

While susceptibility to TB can be affected by the virulence of *Mtb* strain used, route of infection, and the inoculum dose (373), the genetic background of mice plays a critical role with *Mtb* infection. Many distinct mouse lineages exist with varying genetic backgrounds. Historically, these lineages are divided into two main categories: "resistant" or "susceptible" strains. Currently, the most common mouse lineages used in TB research are the BALB/c and C57BL/6 mice ("resistant" strains) and the C3HeB/FeJ, DBA/2, and 129/Sv mice ("susceptible" strains). The C3HeB/FeJ strain is regarded as a valuable resource for host-pathogen and drug response characterization since it better mimics histopathologic features of human TB: well-formed, hypoxic TB granulomas with central necrosis and liquefaction, elements not seen in other inbred strains (34, 326, 374, 375). Indeed, C3HeB/FeJ mice infected with *Mtb* may develop three morphologically distinct lesion types in the lungs (Figures 11A–C) (34). The unique susceptibility of C3HeB/FeJ mice to TB is due to *de novo* mutation and defective expression of the *Ipr1* gene located within the sst1 (super-susceptibility-to-tuberculosis 1) locus (376, 377). The *sst1* locus from C3HeB/FeJ has been engineered into a C57BL/6 background, termed congenic B6.C3H-*sst1* which harbored a 10–fold higher bacterial burden at four weeks post-infection and displayed large necrotic lesions in histopathology evaluations (376, 378). The B6.C3H-sst1 strain has helped demonstrate that the sst1 locus independently defines necrotic lesion progression in the mouse model (376).

The Collaborative Cross (CC) mice are a multi-parental mouse genetic reference population characterized by genetic polymorphism with a spectrum of sensitivity to *Mtb* infection (379–381). Bacterial burden after intravenous infection with *Mtb* ranges over 1000-fold across these strains (379). This CC strain catalog has advanced our understanding of the interplay of different

genes on host susceptibility to TB by enabling the ability to reference and isolate key genetic loci influencing that sensitivity. For example, CC042 strains exhibit deficient IFNγ production which correlated with fewer macrophages and T cells being recruited to the lungs but enhanced neutrophil infiltration and necrotic lesions compared to C57BL/6 mice (380). In addition to informing which immune components provide host protection, the CC or diversity outbred (DO) mouse strains have also been shown to impact the effectiveness of TB vaccines and thus more likely to be more informative and a better alternative to inbred mouse strains. A DO model inherently lowers the power available to decipher key genetic components as each genotype is only present in a single animal, whereas the CC model retains diversity of the DO model while powering studies with repeatable and well powered "n" per genotype (382). Both CC and DO modeling better recapitulates the diversity and spectrum of TB disease observed in human clinical cases, including interrogation of pulmonary lesions and granuloma formation.

One notable disadvantage of the TB mouse model is that *Mtb* infection results in a slowly progressive infection that eventually leads to death, a model of primary progressive TB rather than post-primary TB or latent TB infection (323, 383). However, two models have been reported for latent TB in mice (with potential for reactivation): *(i)* the use of antibiotics to eliminate actively replicating *Mtb* but not sterilizing all *Mtb* (the Cornell model) (384) and *(ii)* intradermal (ear) inoculation of mice that produced a long-term clinical state characterized by the presence of *Mtb*-specific T cells but no overt signs of active TB (385). Major gaps in the field also include understanding subclinical TB disease and biological features that promote *Mtb* transmission, which remain outside the capacity of the present mouse models.

Other shortcomings of mice in TB research include: *(i)* their inability to form caseating granulomas and lung cavitation except in the C3HeB/FeJ mouse (386, 387) or as part of an experimental condition, such as mice that received intraperitoneal injection with TDM in oil prior to infection with *Mtb* (185, 295); *(ii)* predominance of loosely formed granulomatous lesion (Type III lesions mentioned in Figure 11), whereas humans form discrete granulomas (34, 266); *(iii)* absence of hypoxia in mouse granulomas (with the exception of the C3HeB/FeJ strain) and thus murine macrophages may be more likely to undergo apoptosis rather than necrosis (266, 388); *(iv)* localization of *Mtb* intracellularly in non-necrotic lesions in commonly used mouse strains (389), whereas in human and other animal models, *Mtb* primarily resides extracellularly (372, 387, 390); thus, the sterilizing activity of new TB drug/regimen seen in mice may not be observed in other animal models or human clinical trials (391); *(v)* alterations in how the CC mouse strains with genetic polymorphisms respond to TB vaccines (392); and *(vi)* differences in antigen clusters between mice and humans that may impact host immunity to *Mtb*; *e.g.*, mice do not possess a homolog of human IL-32, a cytokine associated with host protection in human macrophages and in a transgenic murine model that expresses human IL-32γ (393, 394). The clinical and pathologic features of *Mtb*-infected mice that mimic human pulmonary TB are described in Table 4.

## 6.3 Guinea pigs

Guinea pigs were one of the first experimental animals used to study TB. Some of the earliest studies using this model were conducted by Robert Koch and Max Lurie in the late 19$^{th}$ and early 20$^{th}$ centuries, respectively (395–397). Currently, the outbred Dunkin-Hartley strain is the most common strain used in research (398). Guinea pigs display many features during *Mtb* infection that are similar to humans: *(i)* newborn guinea pigs have mature lympho-myeloid system like that found in human infants; *(ii)* their hormonal and immunological phenotypes; *(iii)* guinea pigs also do not synthesize vitamin C but must obtain it from their diet; *(iv)* guineas pigs are glucocorticoid-resistant (324); and *(v)* presence of necrotic primary granuloma after low-dose *Mtb* infection (323–325).

Guinea pigs are also highly susceptible to *Mtb*, making them good models for primary progressive disease. They develop pulmonary TB with very low doses of *Mtb* (as low as 2-4 CFU per animal) (399) as well as with exposure to exhaust ambient air from human TB patients (400) or to neighboring *Mtb*-infected guinea pigs within the same room but in different cages (397). Lurie also showed that concomitant respiratory and enteric infection with *Mtb* of guinea pigs resulted in more chronic respiratory TB whereas only respiratory inoculation with *Mtb* resulted in more acute respiratory TB (396). Although it has been argued for many years that a latent TB model and thus post-primary (reactivation) TB are not possible in guinea pigs due to their increased susceptibility (325, 395, 401), some have found it possible to do so (402, 403). Because guinea pigs are also well protected by the BCG vaccine and respond well to anti-TB antibiotics, they are useful for drug and vaccine studies (399, 404–411).

Disadvantages of guinea pigs in TB research include: *(i)* greater expense than mice; *(ii)* most *Mtb* infections of guinea pigs model primary progressive disease than post-primary TB; *(iii)* more limited immunologic reagents than for mice. However, successful cloning of various cytokines (IFNγ, IL-4, IL-10, and IL-17) from guinea pigs expands the ability to characterize the immune response to *Mtb* (412–415). The clinical and pathologic features of *Mtb*-infected guinea pigs that mimic human pulmonary TB are described in Table 4.

## 6.4 Rabbits

Nearly 100 years ago, Lurie and colleagues developed a rabbit model of TB, wherein rabbits with varying levels of *Mtb* resistance were developed (416–418). Rabbits are useful to model both human latent TB infection and active TB, developing caseating granulomas that may liquify and cavitate (323, 395, 419–425). It has also been used to distinguish between protective cellular immunity and potentially damaging mechanisms of "delayed type hypersensitivity" (426–428).

The severity of rabbit TB lung pathology can be influenced by two main factors: the specific *Mtb* strain used; *e.g.*, Erdman *Mtb* was found to cause more severe pathology and worse outcomes than *Mtb* CDC1551 and H37Rv (424, 429) and the rabbit genotype; *e.g.*,

inbred rabbits are more susceptible to *Mtb*, resulting in the formation of lung granulomas and cavities, than outbred rabbit strains (395, 424).

Another way that rabbits mimic human TB infection is that they show a spectrum of disease outcome, including the development of latent TB infection in the TB-resistant outbred strain of New Zealand white rabbits (424, 425, 430). Lung cavities are also common with serial low-dose *Mtb* infection of rabbits (431–433). Serial CT scans demonstrated that the cavities developed from areas of necrotizing pneumonia in the dorsal-caudal region of the rabbit lungs – anatomically analogous to the apical region of the human lung – pulmonary segments with the greatest mechanical stress, decreased blood flow, and highest partial pressure of alveolar $O_2$ in the normal position of rabbits (311–313, 319, 431). Disadvantages of rabbits include larger housing requirements, greater expense, more difficulty in handling, greater challenge in gene manipulation, and lesser repertoire of immunologic reagents compared to mouse models (323, 434). The clinical and pathologic features of *Mtb*-infected rabbits that mimic human pulmonary TB are described in Table 4.

## 6.5 Mini pigs

Mini pigs have been used to model primary progressive TB (435, 436). Like guinea pigs, spread of *Mtb* may occur between infected mini pigs and their previously uninfected neighbors (436). The advantage of the mini pig model is that the anatomical structure of the lungs is like that seen in humans, with the normal presence of intralobular septae that become thickened following encapsulation of granulomas, which prevents the development of new lesions (435). This encapsulation – present in humans but not in rodents or NHP – makes the mini pigs a promising model to study latency because drainage of latent bacilli into the airways or alveolar spaces (435, 436). However, mini pigs also have the disadvantage of being expensive and large (up to 150 pounds). The clinical and pathologic features of *Mtb*-infected mini pigs that mimic human pulmonary TB are described in Table 4.

## 6.6 Goats

Goats are natural hosts of *M. caprae* and *M. bovis* and have been used to study bacillary load, pathology, and vaccine efficiency. Their high susceptibility and the fact that they mimic human infection by developing caseous necrotizing granulomas as well as cavities make them good models for studying TB (437). Compared to other experimental animals, goats are also more like humans in terms of size, body weight, and respiratory anatomy (266, 438). In goats, it was shown that the immune response varied depending on the route of BCG vaccination; *i.e.*, a negative intradermal or interferon-gamma release assay test for latent TB infection was more likely to be observed following oral administration of heat-inactivated *M. bovis* vaccine compared to the intramuscular route (439). Given that goats may develop TB lesions like that seen in humans and that either heat-inactivated *M. bovis* vaccine and BCG vaccine showed efficacy against *M. caprae* (440), goats are potential models to study vaccine efficacy. The clinical and pathologic features of *Mtb*-infected goats that mimic human pulmonary TB are described in Table 4.

## 6.7 Non-human primates

In early 1900's, rhesus macaques were used in experimental TB by Dr. Gerald B. Webb and his colleagues at his home in Colorado Springs, Colorado (441, 442). Their work was involved subcutaneous injections of *Mtb* in the NHPs. Subsequent experimental TB work with rhesus macaques from ~1950-1970 also involved vaccination with intravenous BCG (443, 444). Since 1996, the Philippine cynomolgus macaque was utilized for experimental TB, showing that depending on the dose, either active TB or latent TB infection may develop (229, 445). Cynomolgus macaques primed with BCG and then boosted with the *Mtb72F/AS02A* vaccine showed long-term protection against TB (446). Whereas the control monkeys showed granulomas with caseous centers, extensive edema, and were fused, the granulomas of the NHP vaccinated sequentially with BCG and *Mtb*72F/AS02A were discrete lesions with no necrosis or edema (446). More recently, marmosets, which are much smaller than the macaques, have been used in experimental TB (447).

NHPs are likely the most accurate model in human TB research because of their similarities to humans genetically, immunologically (*e.g.*, functional MHC regions, T-cell antigen receptors, and other cellular features that are relevant for vaccine testing), clinically (manifesting a spectrum of TB from latent infection to active disease), pathologically (including pneumonia, various forms of granulomas, and cavitary disease) and pharmacokinetically (with relevance for testing new drugs) (229, 326, 448–457). Limitations of the NHP model are more logistical – smaller sample sizes and time points due to cost and more difficulty in handling (456). However, serial radiographic imaging of a relatively large animal – namely, chest radiograph, CT, magnetic resistance imaging, and $^{18}$FDG-PET-CT to detect areas of increased metabolic activity to indicate host immune response to the infection (458–460) – have been highly informative. The clinical and pathologic features of *Mtb*-infected NHP that mimic human pulmonary TB are described in Table 4. The key clinical, radiographic, and pathological differences between the rhesus and cynomolgus macaques relevant for TB are shown in Table 4.

# 7 Summary and future perspective

Substantial progress has been made in our understanding of the host immune responses that either protect against TB or contribute to TB pathogenesis. Much of the work have focused on the granulomas and the molecular and cellular components that participate in their formation in experimental animals as well as re-analysis of archived and more contemporaneous human TB tissues. While descriptive analyses of the different cell types in the granuloma architecture have been dominating, the role of soluble

mediators (cytokines, chemokines, growth factors) and metabolic studies (hypoxia, aerobic glycolysis, and activity of various cellular enzymes such as MMPs, IDO-1, and HO-1) have enriched our understanding of TB granulomas but have also raised new avenues of research. One emerging paradigm is that either a deficiency or excess of certain host-derived molecular and cellular components may be harmful to the host which, in turn, allow for the proliferation and persistence of *Mtb*. While new imaging techniques such as MIBI-TOF (multiplexed ion beam imaging by time of flight) and PET-CT using the radioactive tracers deoxy-2-[$^{18}$F]-fluoro-D-glucose and [$^{18}$F]- fluoromisonidazole have contributed to our understanding of TB, it is important to understand their limitations. For example, one overarching limitation is our inability to analyze immunological and microbiological data simultaneously in individual granulomatous TB lesions *in vivo* over time. Rather, "snapshots" of events limits our ability to interpret whether the myriad of molecular and cellular components that can be found in active TB are: *(i)* the main drivers of TB pathogenesis (causing loss of host protection), *(ii)* attempts to correct an inadequate initial immune response, or *(iii)* possibly both depending on the temporality of the responses. While some of these limitations can be overcome by targeted genetic disruption of specific molecular or genetic components, inherent limitations of these models to human TB remain. A better understanding of the immune correlates of protection may also help guide the development of antimicrobial agents that can target privileged sites of *Mtb* and of host-directed therapies. While "high-tech" approaches to better understand granulomas and other TB lesions are occurring, we ought not lose sight of the value of "low-tech" foundational principles of anatomy, physiology, and chemistry that should be included in both the experimental studies and care of TB patients.

## Author contributions

JL: Writing – original draft, Writing – review & editing. DN: Writing – review & editing. SB: Writing – review & editing. SL: Writing – review & editing. XB: Writing – review & editing. DG: Writing – review & editing. VD: Writing – review & editing. TN: Writing – review & editing. AS: Writing – review & editing. RC: Writing – review & editing. EC: Writing – original draft, Writing – review & editing.

## Funding

The author(s) declare financial support was received for the research, authorship, and/or publication of this article. This project has been funded in whole or in part with Federal funds from the National Institute of Allergy and Infectious Diseases, National Institutes of Health, Department of Health and Human Services, under Contract No. 75N93021C00029.

## Acknowledgments

We are grateful to Lorelenn Fornis for help with the initial literature search.

## Conflict of interest

The authors declare that the research was conducted in the absence of any commercial or financial relationships that could be construed as a potential conflict of interest.

## Publisher's note



## Author disclaimer

The content is solely the responsibility of the authors and does not necessarily represent the official views of the National Institutes of Health.

## References

1. Mehta AC, Ali SR. Mnemonic for the differential diagnosis of non-caseating granulomas. *Sarcoidosis Vasc Diffuse Lung Dis*. (2017) 34:200–7. doi: 10.36141/svdld.v34i2.5674

2. Pagan AJ, Ramakrishnan L. The formation and function of granulomas. *Annu Rev Immunol*. (2018) 36:639–65. doi: 10.1146/annurev-immunol-032712-100022

3. Shah KK, Pritt BS, Alexander MP. Histopathologic review of granulomatous inflammation. *J Clin Tuberc Other Mycobact Dis*. (2017) 7:1–12. doi: 10.1016/j.jctube.2017.02.001

4. Ramakrishnan L. Revisiting the role of the granuloma in tuberculosis. *Nat Rev Immunol*. (2012) 12:352–66. doi: 10.1038/nri3211

5. Subbian S, Tsenova L, Kim MJ, Wainwright HC, Visser A, Bandyopadhyay N, et al. Lesion-specific immune response in granulomas of patients with pulmonary tuberculosis: A pilot study. *PloS One*. (2015) 10:e0132249. doi: 10.1371/journal.pone.0132249

6. Martinot AJ. Microbial offense vs host defense: who controls the TB granuloma? *Vet Pathol*. (2018) 55:14–26. doi: 10.1177/0300985817705177

7. Flynn JL, Chan J, Lin PL. Macrophages and control of granulomatous inflammation in tuberculosis. *Mucosal Immunol*. (2011) 4:271–8. doi: 10.1038/mi.2011.14

8. Anonymous. *Granulomatous Infections and Inflammations: Cellular and Molecular Mechanisms*. Boros DL, editor. Washington, D.C: ASM Press (2003). doi: 10.1128/9781555817879

9. Warsinske HC, DiFazio RM, Linderman JJ, Flynn JL, Kirschner DE. Identifying mechanisms driving formation of granuloma-associated fibrosis during *Mycobacterium tuberculosis* infection. *J Theor Biol*. (2017) 429:1–17. doi: 10.1016/j.jtbi.2017.06.017

10. Hult C, Mattila JT, Gideon HP, Linderman JJ, Kirschner DE. Neutrophil dynamics affect *mycobacterium tuberculosis* granuloma outcomes and dissemination. *Front Immunol*. (2021) 12:712457. doi: 10.3389/fimmu.2021.712457

11. Cronan MR. In the thick of it: formation of the tuberculous granuloma and its effects on host and therapeutic responses. *Front Immunol*. (2022) 13:820134. doi: 10.3389/fimmu.2022.820134

12. Deretic V, Singh S, Master S, Harris J, Roberts E, Kyei G, et al. *Mycobacterium tuberculosis* inhibition of phagolysosome biogenesis and autophagy as a host defence mechanism. *Cell Microbiol*. (2006) 8:719–27. doi: 10.1111/j.1462-5822.2006.00705.x

13. Russell DG. *Mycobacterium tuberculosis*: here today, and here tomorrow. *Nat Rev Mol Cell Biol*. (2001) 2:569–77. doi: 10.1038/35085034

14. Russell DG, Purdy GE, Owens RM, Rohde KH, Yates RM. *Mycobacterium tuberculosis* and the four-minute phagosome. *ASM News*. (2005) 71:459–63.

15. Ehrt S, Schnappinger D. Mycobacterial survival strategies in the phagosome: defence against host stresses. *Cell Microbiol*. (2009) 11:1170–8. doi: 10.1111/j.1462-5822.2009.01335.x

16. Meena LS. Rajni. Survival mechanisms of pathogenic *Mycobacterium tuberculosis* H37Rv. *FEBS J*. (2010) 277:2416–27. doi: 10.1111/j.1742-4658.2010.07666.x

17. Houben D, Demangel C, van Ingen J, Perez J, Baldeón L, Abdallah AM, et al. ESX-1-mediated translocation to the cytosol controls virulence of mycobacteria. *Cell Microbiol*. (2012) 14:1287–98. doi: 10.1111/j.1462-5822.2012.01799.x

18. Peng X, Sun J. Mechanism of ESAT-6 membrane interaction and its roles in pathogenesis of *Mycobacterium tuberculosis*. *Toxicon*. (2016) 116:29–34. doi: 10.1016/j.toxicon.2015.10.003

19. Russell DG. *Mycobacterium tuberculosis* and the intimate discourse of a chronic infection. *Immunol Rev*. (2011) 240:252–68. doi: 10.1111/j.1600-065X.2010.00984.x

20. Cohen SB, Gern BH, Delahaye JL, Adams KN, Plumlee CR, Winkler JK, et al. Alveolar macrophages provide an early *mycobacterium tuberculosis* niche and initiate dissemination. *Cell Host Microbe*. (2018) 24:439–446.e4. doi: 10.1016/j.chom.2018.08.001

21. Ganchua SKC, White AG, Klein EC, Flynn JL. Lymph nodes-The neglected battlefield in tuberculosis. *PloS Pathog*. (2020) 16:e1008632. doi: 10.1371/journal.ppat.1008632

22. McCaffrey EF, Donato M, Keren L, Chen Z, Delmastro A, Fitzpatrick MB, et al. The immunoregulatory landscape of human tuberculosis granulomas. *Nat Immunol*. (2022) 23:318–29. doi: 10.1038/s41590-021-01121-x

23. Marakalala MJ, Martinez FO, Plüddemann A, Gordon S. Macrophage heterogeneity in the immunopathogenesis of tuberculosis. *Front Microbiol*. (2018) 9:1028. doi: 10.3389/fmicb.2018.01028

24. McClean CM, Tobin DM. Macrophage form, function, and phenotype in mycobacterial infection: lessons from tuberculosis and other diseases. *Pathog Dis*. (2016) 74:ftw068. doi: 10.1093/femspd/ftw068

25. Kadomoto S, Izumi K, Mizokami A. Macrophage polarity and disease control. *Int J Mol Sci*. (2021) 23:144. doi: 10.3390/ijms23010144

26. Martinez FO, Gordon S. The M1 and M2 paradigm of macrophage activation: time for reassessment. *F1000Prime Rep*. (2014) 6:13. doi: 10.12703/P6-13

27. Murray PJ, Allen JE, Biswas SK, Fisher EA, Gilroy DW, Goerdt S, et al. Macrophage activation and polarization: nomenclature and experimental guidelines. *Immunity*. (2014) 41:14–20. doi: 10.1016/j.immuni.2014.06.008

28. Adams DO. The granulomatous inflammatory response: a review. *Am J Pathol*. (1976) 84:164–92.

29. Palmer MV, Kanipe C, Boggiatto PM. The bovine tuberculoid granuloma. *Pathogens*. (2022) 11:61. doi: 10.3390/pathogens11010061

30. Mariano M, Malucelli BE. Defective phagocytic ability of epithelioid cells reversed by levamisole. *J Pathol*. (1980) 130:33–6. doi: 10.1002/path.1711300105

31. Russell DG, Cardona PJ, Kim MJ, Allain S, Altare F. Foamy macrophages and the progression of the human tuberculosis granuloma. *Nat Immunol*. (2009) 10:943–948. doi: 10.1038/ni.1781

32. Caceres N, Tapia G, Ojanguren I, Altare F, Gil O, Pinto S, et al. Evolution of foamy macrophages in the pulmonary granulomas of experimental tuberculosis models. *Tuberculosis (Edinb)*. (2009) 89:175–82. doi: 10.1016/j.tube.2008.11.001

33. Welsh KJ, Risin SA, Actor JK, Hunter RL. Immunopathology of postprimary tuberculosis: increased T-regulatory cells and DEC-205-positive foamy macrophages in cavitary lesions. *Clin Dev Immunol*. (2011) 2011:307631. doi: 10.1155/2011/307631

34. Irwin SM, Driver E, Lyon E, Schrupp C, Ryan G, Gonzalez-Juarrero M, et al. Presence of multiple lesion types with vastly different microenvironments in C3HeB/FeJ mice following aerosol infection with *Mycobacterium tuberculosis*. *Dis Model Mech*. (2015) 8:591–602. doi: 10.1242/dmm.019570

35. Cronan MR, Beerman RW, Rosenberg AF, Saelens JW, Johnson MG, Oehlers SH, et al. Macrophage epithelial reprogramming underlies mycobacterial granuloma formation and promotes infection. *Immunity*. (2016) 45:861–76. doi: 10.1016/j.immuni.2016.09.014

36. Cohen SB, Gern BH, Urdahl KB. The tuberculous granuloma and preexisting immunity. *Annu Rev Immunol*. (2022) 40:589–614. doi: 10.1146/annurev-immunol-093019-125148

37. Cronan MR, Hughes EJ, Brewer WJ, Viswanathan G, Hunt EG, Singh B, et al. A non-canonical type 2 immune response coordinates tuberculous granuloma formation and epithelialization. *Cell*. (2021) 184:1757–1774.e14. doi: 10.1016/j.cell.2021.02.046

38. Peyron P, Vaubourgeix J, Poquet Y, Levillain F, Botanch C, Bardou F, et al. Foamy macrophages from tuberculous patients' granulomas constitute a nutrient-rich reservoir for *M. tuberculosis* persistence. *PloS Pathog*. (2008) 4:e1000204. doi: 10.1371/journal.ppat.1000204

39. Singh V, Jamwal S, Jain R, Verma P, Gokhale R, Rao KV. *Mycobacterium tuberculosis*-driven targeted recalibration of macrophage lipid homeostasis promotes the foamy phenotype. *Cell Host Microbe*. (2012) 12:669 –681. doi: 10.1016/j.chom.2012.09.012

40. Cumming BM, Pacl HT, Steyn AJC. Relevance of the warburg effect in tuberculosis for host-directed therapy. *Front Cell Infect Microbiol*. (2020) 10:576596. doi: 10.3389/fcimb.2020.576596

41. Maoldomhnaigh C, Cox DJ, Phelan JJ, Mitermite M, Murphy DM, Leisching G, et al. Lactate alters metabolism in human macrophages and improves their ability to kill *mycobacterium tuberculosis*. *Front Immunol*. (2021) 12:663695. doi: 10.3389/fimmu.2021.663695

42. Sun W, Jia M, Feng Y, Cheng X. Lactate is a bridge linking glycolysis and autophagy through lactylation. *Autophagy*. (2023) 19:3240–1. doi: 10.1080/15548627.2023.2246356

43. Fan Q, Yang L, Zhang X, Ma Y, Li Y, Dong L, et al. Autophagy promotes metastasis and glycolysis by upregulating MCT1 expression and Wnt/β-catenin signaling pathway activation in hepatocellular carcinoma cells. *J Exp Clin Cancer Res*. (2018) 37:9. doi: 10.1186/s13046-018-0673-y

44. Lee YR, Wu SY, Chen RY, Lin YS, Yeh TM, Liu HS. Regulation of autophagy, glucose uptake, and glycolysis under dengue virus infection. *Kaohsiung J Med Sci*. (2020) 36:911–9. doi: 10.1002/kjm2.v36.11

45. Singh R, Kaushik S, Wang Y, Xiang Y, Novak I, Komatsu M, et al. Autophagy regulates lipid metabolism. *Nature*. (2009) 458:1131–5. doi: 10.1038/nature07976

46. Dkhar HK, Nanduri R, Mahajan S, Dave S, Saini A, Somavarapu AK, et al. *Mycobacterium tuberculosis* keto-mycolic acid and macrophage nuclear receptor TR4 modulate foamy biogenesis in granulomas: a case of a heterologous and noncanonical ligand-receptor pair. *J Immunol*. (2014) 193:295–305. doi: 10.4049/jimmunol.1400092

47. Mahajan S, Dkhar HK, Chandra V, Dave S, Nanduri R, Janmeja AK, et al. *Mycobacterium tuberculosis* modulates macrophage lipid-sensing nuclear receptors PPARγ and TR4 for survival. *J Immunol*. (2012) 188:5593–603. doi: 10.4049/jimmunol.1103038

48. Johansen MD, Kasparian JA, Hortle E, Britton WJ, Purdie AC, Oehlers SH. *Mycobacterium marinum* infection drives foam cell differentiation in zebrafish infection models. *Dev Comp Immunol*. (2018) 88:169–72. doi: 10.1016/j.dci.2018.07.022

49. Genoula M, Marín Franco JL, Dupont M, Kviatcovsky D, Milillo A, Schierloh P, et al. Formation of foamy macrophages by tuberculous pleural effusions is triggered by the interleukin-10/signal transducer and activator of transcription 3 axis through ACAT upregulation. *Front Immunol*. (2018) 9:459. doi: 10.3389/fimmu.2018.00459

50. Bai X, Feldman NE, Chmura K, Ovrutsky AR, Su WL, Griffin L, et al. Inhibition of nuclear factor-kappa B activation decreases survival of *Mycobacterium tuberculosis* in human macrophages. *PloS One*. (2013) 8:e61925. doi: 10.1371/journal.pone.0061925

51. Divangahi M, Desjardins D, Nunes-Alves C, Remold HG, Behar SM. Eicosanoid pathways regulate adaptive immunity to *Mycobacterium tuberculosis*. *Nat Immunol*. (2010) 11:751–8. doi: 10.1038/ni.1904

52. Keane J, Balcewicz-Sablinska MK, Remold HG, Chupp GL, Meek BB, Fenton MJ, et al. Infection by *Mycobacterium tuberculosis* promotes human alveolar macrophage apoptosis. *Infect Immun*. (1997) 65:298–304. doi: 10.1128/iai.65.1.298-304.1997

53. Keane J, Remold HG, Kornfeld H. Virulent *Mycobacterium tuberculosis* strains evade apoptosis of infected alveolar macrophages. *J Immunol*. (2000) 164:2016–20. doi: 10.4049/jimmunol.164.4.2016

54. Keane J, Shurtleff B, Kornfeld H. TNF-dependent BALB/c murine macrophage apoptosis following *Mycobacterium tuberculosis* infection inhibits bacillary growth in an IFN-gamma independent manner. *Tuberculosis (Edinb)*. (2002) 82:55–61. doi: 10.1054/tube.2002.0322

55. Lam A, Prabhu R, Gross CM, Riesenberg LA, Singh V, Aggarwal S. Role of apoptosis and autophagy in tuberculosis. *Am J Physiol Lung Cell Mol Physiol*. (2017) 313:L218–29. doi: 10.1152/ajplung.00162.2017

56. Oddo M, Renno T, Attinger A, Bakker T, MacDonald HR, Meylan PR. Fas ligand-induced apoptosis of infected human macrophages reduces the viability of intracellular *Mycobacterium tuberculosis*. *J Immunol*. (1998) 160:5448–54. doi: 10.4049/jimmunol.160.11.5448

57. Rojas M, Barrera LF, Puzo G, Garcia LF. Differential induction of apoptosis by virulent *Mycobacterium tuberculosis* in resistant and susceptible murine macrophages: role of nitric oxide and mycobacterial products. *J Immunol*. (1997) 159:1352–61. doi: 10.4049/jimmunol.159.3.1352

58. Sia JK, Rengarajan J. Immunology of *mycobacterium tuberculosis* infections. *Microbiol Spectr*. (2019) 7:1–37. doi: 10.1128/microbiolspec.GPP3-0022-201

59. Martin CJ, Booty MG, Rosebrock TR, Nunes-Alves C, Desjardins DM, Keren I, et al. Efferocytosis is an innate antibacterial mechanism. *Cell Host Microbe*. (2012) 12:289–300. doi: 10.1016/j.chom.2012.06.010

60. Davis JM, Ramakrishnan L. The role of the granuloma in expansion and dissemination of early tuberculous infection. *Cell*. (2009) 136:37–49. doi: 10.1016/j.cell.2008.11.014

61. Chen M, Divangahi M, Gan H, Shin DS, Hong S, Lee DM, et al. Lipid mediators in innate immunity against tuberculosis: opposing roles of PGE2 and LXA4 in the

induction of macrophage death. *J Exp Med*. (2008) 205:2791–801. doi: 10.1084/jem.20080767

62. Chen M, Gan H, Remold HG. A mechanism of virulence: virulent *Mycobacterium tuberculosis* strain H37Rv, but not attenuated H37Ra, causes significant mitochondrial inner membrane disruption in macrophages leading to necrosis. *J Immunol*. (2006) 176:3707–16. doi: 10.4049/jimmunol.176.6.3707

63. Gan H, Lee J, Ren F, Chen M, Kornfeld H, Remold HG. *Mycobacterium tuberculosis* blocks crosslinking of annexin-1 and apoptotic envelope formation on infected macrophages to maintain virulence. *Nat Immunol*. (2008) 9:1189–97. doi: 10.1038/ni.1654

64. Divangahi M, Chen M, Gan H, Desjardins D, Hickman TT, Lee DM, et al. *Mycobacterium tuberculosis* evades macrophage defenses by inhibiting plasma membrane repair. *Nat Immunol*. (2009) 10:899–906. doi: 10.1038/ni.1758

65. Moreira-Teixeira L, Mayer-Barber K, Sher A, O'Garra A. Type I interferons in tuberculosis: Foe and occasionally friend. *J Exp Med*. (2018) 215:1273–85. doi: 10.1084/jem.20180325

66. Mundra A, Yegiazaryan A, Karsian H, Alsaigh D, Bonavida V, Frame M, et al. Pathogenicity of type I interferons in *mycobacterium tuberculosis*. *Int J Mol Sci*. (2023) 24:3919. doi: 10.3390/ijms24043919

67. Zhao X, Khan N, Gan H, Tzelepis F, Nishimura T, Park SY, et al. Bcl-xL mediates RIPK3-dependent necrosis in M. tuberculosis-infected macrophages. *Mucosal Immunol*. (2017) 10:1553–68. doi: 10.1038/mi.2017.12

68. Soldevilla P, Vilaplana C, Cardona P-J. Mouse models for *mycobacterium tuberculosis* pathogenesis: show and do not tell. *Pathogens*. (2022) 12:49. doi: 10.3390/pathogens12010049

69. Papayannopoulos V. Neutrophil extracellular traps in immunity and disease. *Nat Rev Immunol*. (2017) 18:134–47. doi: 10.1038/nri.2017.105

70. Gideon HP, Phuah J, Junecko BA, Mattila JT. Neutrophils express pro- and anti-inflammatory cytokines in granulomas from *Mycobacterium tuberculosis*-infected cynomolgus macaques. *Mucosal Immunol*. (2019) 12:1370–81. doi: 10.1038/s41385-019-0195-8

71. Lovewell RR, Baer CE, Mishra BB, Smith CM, Sassetti CM. Granulocytes act as a niche for *Mycobacterium tuberculosis* growth. *Mucosal Immunol*. (2021) 14:229–41. doi: 10.1038/s41385-020-0300-z

72. Andrews JT, Zhang Z, Prasad GVRK, Huey F, Nazarova EV, Wang J, et al. Metabolically active neutrophils represent a permissive niche for. *Mycobacterium tuberculosis*. *Mucosal Immunol*. (2024) 17:825–42. doi: 10.1016/j.mucimm.2024.05.007

73. Bhatt A, Quazi Syed Z, Singh H. Converging epidemics: A narrative review of tuberculosis (TB) and human immunodeficiency virus (HIV) coinfection. *Cureus*. (2023) 15:e47624. doi: 10.7759/cureus.47624

74. Saunders BM, Frank AA, Orme IM, Cooper AM. CD4 is required for the development of a protective granulomatous response to pulmonary tuberculosis. *Cell Immunol*. (2002) 216:65–72. doi: 10.1016/S0008-8749(02)00510-5

75. Slight SR, Rangel-Moreno J, Gopal R, Lin Y, Fallert Junecko BA, Mehra S, et al. CXCR5+ T helper cells mediate protective immunity against tuberculosis. *J Clin Invest*. (2013) 123:712–26. doi: 10.1172/JCI65728

76. Roca FJ, Ramakrishnan L. TNF dually mediates resistance and susceptibility to mycobacteria via mitochondrial reactive oxygen species. *Cell*. (2013) 153:521–34. doi: 10.1016/j.cell.2013.03.022

77. Sakai S, Kauffman KD, Sallin MA, Sharpe AH, Young HA, Ganusov VV, et al. CD4 T cell-derived IFN-γ Plays a minimal role in control of pulmonary *mycobacterium tuberculosis* infection and must be actively repressed by PD-1 to prevent lethal disease. *PloS Pathog*. (2016) 12:e1005667. doi: 10.1371/journal.ppat.1005667

78. Hammarén MM, Oksanen KE, Nisula HM, Luukinen BV, Pesu M, Rämet M, et al. Adequate Th2-type response associates with restricted bacterial growth in latent mycobacterial infection of zebrafish. *PloS Pathog*. (2014) 26:e1004190. doi: 10.1371/journal.ppat.1004190

79. Heitmann L, Abad Dar M, Schreiber T, Erdmann H, Behrends J, Mckenzie ANJ, et al. The IL-13/IL-4Rα axis is involved in tuberculosis-associated pathology. *J Pathol*. (2014) 234:338–50. doi: 10.1002/path.2014.234.issue-3

80. Mazzarella G, Bianco A, Perna F, D'Auria D, Grella E, Moscariello E, et al. T lymphocyte phenotypic profile in lung segments affected by cavitary and non-cavitary tuberculosis. *Clin Exp Immunol*. (2003) 132:283–8. doi: 10.1046/j.1365-2249.2003.02121.x

81. Hernandez-Pando R, Aguilar D, Hernandez ML, Orozco H, Rook G. Pulmonary tuberculosis in BALB/c mice with non-functional IL-4 genes: changes in the inflammatory effects of TNF-alpha and in the regulation of fibrosis. *Eur J Immunol*. (2004) 34:174–83. doi: 10.1002/eji.200324253

82. Buccheri S, Reljic R, Caccamo N, Ivanyi J, Singh M, Salerno A, et al. IL-4 depletion enhances host resistance and passive IgA protection against tuberculosis infection in BALB/c mice. *Eur J Immunol*. (2007) 37:729–37. doi: 10.1002/eji.200636764

83. Gern BH, Adams KN, Plumlee CR, Stoltzfus CR, Shehata L, Moguche AO, et al. TGFβ restricts expansion, survival, and function of T cells within the tuberculous granuloma. *Cell Host Microbe*. (2021) 29:594–606.e6. doi: 10.1016/j.chom.2021.02.005

84. Hirsch CS, Hussain R, Toossi Z, Dawood G, Shahid F, Ellner JJ. Cross-modulation by transforming growth factor beta in human tuberculosis: suppression of antigen-driven blastogenesis and interferon gamma production. *Proc Natl Acad Sci U.S.A*. (1996) 93:3193–8. doi: 10.1073/pnas.93.8.3193

85. Warsinske HC, Pienaar E, Linderman JJ, Mattila JT, Kirschner DE. Deletion of TGF-β1 increases bacterial clearance by cytotoxic T cells in a tuberculosis granuloma model. *Front Immunol*. (2017) 8:1843. doi: 10.3389/fimmu.2017.01843

86. Basile JI, Kviatcovsky D, Romero MM, Balboa L, Monteserin J, Ritacco V, et al. *Mycobacterium tuberculosis* multi-drug-resistant strain M induces IL-17+ IFNγ- CD4+ T cell expansion through an IL-23 and TGF-β-dependent mechanism in patients with MDR-TB tuberculosis. *Clin Exp Immunol*. (2017) 187:160–73. doi: 10.1111/cei.12873

87. Domingo-Gonzalez R, Das S, Griffiths KL, Ahmed M, Bambouskova M, Gopal R, et al. Interleukin-17 limits hypoxia-inducible factor 1α and development of hypoxic granulomas during tuberculosis. *JCI Insight*. (2017) 2:e92973. doi: 10.1172/jci.insight.92973

88. Khader SA, Bell GK, Pearl JE, Fountain JJ, Rangel-Moreno J, Cilley GE, et al. IL-23 and IL-17 in the establishment of protective pulmonary CD4+ T cell responses after vaccination and during *Mycobacterium tuberculosis* challenge. *Nat Immunol*. (2007) 8:369–77. doi: 10.1038/ni1449

89. Rangel-Moreno J, Carragher DM, de la Luz Garcia-Hernandez M, Hwang JY, Kusser K, Hartson L, et al. The development of inducible bronchus-associated lymphoid tissue depends on IL-17. *Nat Immunol*. (2011) 12:639–46. doi: 10.1038/ni.2053

90. Zhu M, Fu Y. Proinflammatory IL-17 induces iBALT development. *Cell Mol Immunol*. (2012) 9:101–2. doi: 10.1038/cmi.2011.46

91. Desvignes L, Ernst JD. Interferon-gamma-responsive nonhematopoietic cells regulate the immune response to *Mycobacterium tuberculosis*. *Immunity*. (2009) 31:974–85. doi: 10.1016/j.immuni.2009.10.007

92. Nandi B, Behar SM. Regulation of neutrophils by interferon-γ limits lung inflammation during tuberculosis infection. *J Exp Med*. (2011) 208:2251–62. doi: 10.1084/jem.20110919

93. Jain R, Kumari R, Chakraborty S, Mitra DK, Mohan A, Hadda V, et al. T-cell signature cytokines distinguish pulmonary sarcoidosis from pulmonary tuberculosis. *Eur J Immunol*. (2023) 53:e2250255. doi: 10.1002/eji.202250255

94. Lin PL, Flynn JL. CD8 T cells and *Mycobacterium tuberculosis* infection. *Semin Immunopathol*. (2015) 37:239–49. doi: 10.1007/s00281-015-0490-8

95. Mogues T, Goodrich ME, Ryan L, LaCourse R, North RJ. The relative importance of T cell subsets in immunity and immunopathology of airborne *Mycobacterium tuberculosis* infection in mice. *J Exp Med*. (2001) 193:271–80. doi: 10.1084/jem.193.3.271

96. Flynn J, Goldstein MM, Triebold KJ, Koller B, Bloom B. Major histocompatibility complex class I-restricted T cells are required for resistance to *Mycobacterium tuberculosis* infection. *Proc Natl Acad Sci USA*. (1992) 89:12013–7. doi: 10.1073/pnas.89.24.12013

97. Behar SM, Dascher CC, Grusby MJ, Wang CR, Brenner MB. Susceptibility of mice deficient in CD1D or TAP1 to infection with *Mycobacterium tuberculosis*. *J Exp Med*. (1999) 189:1973–80. doi: 10.1084/jem.189.12.1973

98. Sousa AO, Mazzaccaro RC, Russell RG, Lee FK, Turner OC, Hong S, et al. Relative contributions of distinct MHC class I-dependent cell populations in protection to tuberculosis infection in mice. *Proc Natl Acad Sci USA*. (2000) 97:4204–8. doi: 10.1073/pnas.97.8.4204

99. Lazarevic V, Flynn J. CD8+ T cells in tuberculosis. *Am J Respir Crit Care Med*. (2002) 166:1116–21. doi: 10.1164/rccm.2204027

100. van Pinxteren LA, Cassidy JP, Smedegaard BH, Agger EM, Andersen P. Control of latent *mycobacterium tuberculosis* infection is dependent on CD8 T cells. *Eur J Immunol*. (2000) 30:3689–98. doi: 10.1002/1521-4141(200012)30:12<3689::AID-IMMU3689>3.0.CO;2-4

101. Silva BDS, Trentini MM, da Costa AC, Kipnis A, Junqueira-Kipnis AP. Different phenotypes of CD8+ T cells associated with bacterial load in active tuberculosis. *Immunol Lett*. (2014) 160:23–32. doi: 10.1016/j.imlet.2014.03.009

102. Cavassani KA, Carson WF, Moreira AP, Wen H, Schaller MA, Ishii M, et al. The post sepsis-induced expansion and enhanced function of regulatory T cells create an environment to potentiate tumor growth. *Blood*. (2010) 115:4403–11. doi: 10.1182/blood-2009-09-241083

103. Shevach EM. Mechanisms of Foxp3+ T regulatory cell-mediated suppression. *Immunity*. (2009) 30:636–45. doi: 10.1016/j.immuni.2009.04.010

104. Vignali DA, Collison LW, Workman CJ. How regulatory T cells work. *Nat Rev Immunol*. (2008) 8:523–32. doi: 10.1038/nri2343

105. Chan J, Mehta S, Bharrhan S, Chen Y, Achkar JM, Casadevall A, et al. The role of B cells and humoral immunity in *Mycobacterium tuberculosis* infection. *Semin Immunol*. (2014) 26:588–600. doi: 10.1016/j.smim.2014.10.005:588-600

106. Achkar JM, Chan J, Casadevall A. B cells and antibodies in the defense against *Mycobacterium tuberculosis* infection. *Immunol Rev*. (2015) 264:167–81. doi: 10.1111/imr.2015.264.issue-1

107. Choreño-Parra JA, Bobba S, Rangel-Moreno J, Ahmed M, Mehra S, Rosa B, et al. *Mycobacterium tuberculosis* HN878 infection induces human-like B-cell follicles in mice. *J Infect Dis*. (2020) 221:1636–46. doi: 10.1093/infdis/jiz663

108. Stewart P, Patel S, Comer A, Muneer S, Nawaz U, Quann V, et al. Role of B cells in *mycobacterium tuberculosis* infection. *Vaccines (Basel)*. (2023) 11:955. doi: 10.3390/vaccines11050955

109. Achkar JM, Chan J, Casadevall A. Role of B cells and antibodies in acquired immunity against *Mycobacterium tuberculosis*. *Cold Spring Harb Perspect Med*. (2014) 5:a018432. doi: 10.1101/cshperspect.a018432

110. Maglione PJ, Xu J, Chan J. B cells moderate inflammatory progression and enhance bacterial containment upon pulmonary challenge with *Mycobacterium tuberculosis*. *J Immunol*. (2007) 178:7222–34. doi: 10.4049/jimmunol.178.11.7222

111. Kondratieva TK, Rubakova EI, Linge IA, Evstifeev VV, Majorov KB, Apt AS. B cells delay neutrophil migration toward the site of stimulus: tardiness critical for effective bacillus Calmette-Guérin vaccination against tuberculosis infection in mice. *J Immunol*. (2010) 184:1227–34. doi: 10.4049/jimmunol.0902011

112. Kozakiewicz L, Phuah J, Flynn J, Chan J. The role of B cells and humoral immunity in *Mycobacterium tuberculosis* infection. *Adv Exp Med Biol*. (2013) 783:225–50. doi: 10.1007/978-1-4614-6111-1_12

113. Lund FE, Randall TD. Effector and regulatory B cells: modulators of CD4+ T cell immunity. *Nat Rev Immunol*. (2010) 10:236–47. doi: 10.1038/nri2729

114. Choi HS, Rai PR, Chu HW, Cool C, Chan ED. Analysis of nitric oxide synthase and nitrotyrosine expression in human pulmonary tuberculosis. *Am J Respir Crit Care Med*. (2002) 166:178–86. doi: 10.1164/rccm.2201023

115. Bery AI, Shepherd HM, Li W, Krupnick AS, Gelman AE, Kreisel D. Role of tertiary lymphoid organs in the regulation of immune responses in the periphery. *Cell Mol Life Sci*. (2022) 79:359. doi: 10.1007/s00018-022-04388-x

116. Schinköthe J, Köhler H, Liebler-Tenorio EM. Characterization of tuberculous granulomas in different stages of progression and associated tertiary lymphoid tissue in goats experimentally infected with Mycobacterium avium subsp. hominissuis. *Comp Immunol Microbiol Infect Dis*. (2016) 47:41–51. doi: 10.1016/j.cimid.2016.05.006

117. Ogbonna E. Deep spatial characterization of tertiary lymphoid structures in pulmonary tuberculosis granulomas. *Open Forum Infect Dis*. (2023) 10:ofad500.1715. doi: 10.1093/ofid/ofad500.1715

118. Krausgruber T, Redl A, Barreca D, Doberer K, Romanovskaia D, Dobnikar L, et al. Single-cell and spatial transcriptomics reveal aberrant lymphoid developmental programs driving granuloma formation. *Immunity*. (2023) 56:289–306.e7. doi: 10.1016/j.immuni.2023.01.014

119. Marin ND, Dunlap MD, Kaushal D, Khader SA. Friend or foe: the protective and pathological roles of inducible bronchus-associated lymphoid tissue in pulmonary diseases. *J Immunol*. (2019) 202:2519–2526. doi: 10.4049/jimmunol.1801135

120. Silva-Sanchez A, Randall TD. Role of iBALT in respiratory immunity. *Curr Top Microbiol Immunol*. (2020) 426:21–43. doi: 10.1007/82_2019_191

121. Ulrichs T, Kosmiadi GA, Trusov V, Jorg S, Pradl L, Titukhina M, et al. Human tuberculous granulomas induce peripheral lymphoid follicle-like structures to orchestrate local host defence in the lung. *J Pathol*. (2004) 204:217–28. doi: 10.1002/path.v204:2

122. Jones GW, Hill DG, Jones SA. Understanding immune cells in tertiary lymphoid organ development: It is all starting to come together. *Front Immunol*. (2016) 7:401. doi: 10.3389/fimmu.2016.00401

123. Ardain A, Domingo-Gonzalez R, Das S, Kazer SW, Howard NC, Singh A, et al. Group 3 innate lymphoid cells mediate early protective immunity against tuberculosis. *Nature*. (2019) 570:528–32. doi: 10.1038/s41586-019-1276-2

124. Gopal R, Rangel-Moreno J, Slight S, Lin Y, Nawar HF, Fallert Junecko BA, et al. Interleukin-17-dependent CXCL13 mediates mucosal vaccine-induced immunity against tuberculosis. *Mucosal Immunol*. (2013) 6:972–84. doi: 10.1038/mi.2012.135

125. Khader SA, Guglani L, Rangel-Moreno J, Gopal R, Junecko BA, Fountain JJ, et al. IL-23 is required for long-term control of *Mycobacterium tuberculosis* and B cell follicle formation in the infected lung. *J Immunol*. (2011) 187:5402–7. doi: 10.4049/jimmunol.1101377

126. Zhang M, Wang Z, Graner MW, Yang L, Liao M, Yang Q, et al. B cell infiltration is associated with the increased IL-17 and IL-22 expression in the lungs of patients with tuberculosis. *Cell Immunol*. (2011) 270:217–23. doi: 10.1016/j.cellimm.2011.05.009

127. Pabst R, Gehrke I. Is the bronchus-associated lymphoid tissue (BALT) an integral structure of the lung in normal mammals, including humans? *Am J Respir Cell Mol Biol*. (1990) 3:131–5. doi: 10.1165/ajrcmb/3.2.131

128. Hughes CE, Benson RA, Bedaj M, Maffia P. Antigen-presenting cells and antigen presentation in tertiary lymphoid organs. *Front Immunol*. (2016) 7:481. doi: 10.3389/fimmu.2016.00481

129. Foo SY, Phipps S. Regulation of inducible BALT formation and contribution to immunity and pathology. *Mucosal Immunol*. (2010) 3:537–44. doi: 10.1038/mi.2010.52

130. Jones GW, Jones SA. Ectopic lymphoid follicles: inducible centres for generating antigen-specific immune responses within tissues. *Immunology*. (2016) 147:141–51. doi: 10.1111/imm.2016.147.issue-2

131. Dunlap MD, Prince OA, Rangel-Moreno J, Thomas KA, Scordo JM, Torrelles JB, et al. Formation of lung inducible bronchus associated lymphoid tissue is regulated by *mycobacterium tuberculosis* expressed determinants. *Front Immunol*. (2020) 11:1325. doi: 10.3389/fimmu.2020.01325

132. Gautam US, Foreman TW, Bucsan AN, Veatch AV, Alvarez X, Adekambi T, et al. *In vivo* inhibition of tryptophan catabolism reorganizes the tuberculoma and augments immune-mediated control of *Mycobacterium tuberculosis*. *Proc Natl Acad Sci U.S.A*. (2018) 115:E62–71. doi: 10.1073/pnas.1711373114

133. Canetti G. The tubercle bacillus in the pulmonary lesion of man. In: *Histobacteriology and Its Bearing on the Therapy of Pulmonary Tuberculosis*. Springer Publishing Company Inc, New York (1955).

134. Rich AR. *The Pathogenesis of Tuberculosis*. Springfield, IL: Thomas (1944).

135. McHenry ML, Williams SM, Stein CM. Genetics and evolution of tuberculosis pathogenesis: New perspectives and approaches. *Infect Genet Evol*. (2020) 81:104204. doi: 10.1016/j.meegid.2020.104204

136. McHenry ML, Bartlett J, Igo RP Jr., Wampande EM, Benchek P, Mayanja-Kizza H, et al. Interaction between host genes and *Mycobacterium tuberculosis* lineage can affect tuberculosis severity: Evidence for coevolution? *PloS Genet*. (2020) 16:e1008728. doi: 10.1371/journal.pgen.1008728

137. Goldberg MF, Saini NK, Porcelli SA. Evasion of innate and adaptive immunity by *mycobacterium tuberculosis*. *Microbiol Spectr*. (2014) 2:MGM2–0005-2013. doi: 10.1128/microbiolspec.MGM2-0005-2013

138. Cadena AM, Fortune SM, Flynn JL. Heterogeneity in tuberculosis. *Nat Rev Immunol*. (2017) 17:691–702. doi: 10.1038/nri.2017.69

139. Anonymous. *Global Tuberculosis Report*. Geneva: Organization WH (2023).

140. Diedrich CR, O'Hern J, Wilkinson RJ. HIV-1 and the *Mycobacterium tuberculosis* granuloma: A systematic review and meta-analysis. *Tuberculosis (Edinb)*. (2016) 98:62–76. doi: 10.1016/j.tube.2016.02.010

141. Harris J, Keane J. How tumour necrosis factor blockers interfere with tuberculosis immunity. *Clin Exp Immunol*. (2010) 161:1–9. doi: 10.1111/j.1365-2249.2010.04146.x

142. Keane J. TNF-blocking agents and tuberculosis: new drugs illuminate an old topic. *Rheumatol (Oxford)*. (2005) 44:714–20. doi: 10.1093/rheumatology/keh567

143. Keane J, Gershon S, Wise RP, Mirabile-Levens E, Kasznica J, Schwieterman WD, et al. Tuberculosis associated with infliximab, a tumor necrosis factor alpha-neutralizing agent. *N Engl J Med*. (2001) 345:1098–104. doi: 10.1056/NEJMoa011110

144. Horsburgh CR Jr., O'Donnell M, Chamblee S, Moreland JL, Johnson J, Marsh BJ, et al. Revisiting rates of reactivation tuberculosis: a population-based approach. *Am J Respir Crit Care Med*. (2010) 182:420–5. doi: 10.1164/rccm.200909-1355OC

145. Solovic I, Sester M, Gomez-Reino JJ, Rieder HL, Ehlers S, Milburn HJ, et al. The risk of tuberculosis related to tumour necrosis factor antagonist therapies: a TBNET consensus statement. *Eur Respir J*. (2010) 36:1185–206. doi: 10.1183/09031936.00028510

146. Clay H, Volkman HE, Ramakrishnan L. Tumor necrosis factor signaling mediates resistance to mycobacteria by inhibiting bacterial growth and macrophage death. *Immunity*. (2008) 29:283–94. doi: 10.1016/j.immuni.2008.06.011

147. Saunders BM, Cooper AM. Restraining mycobacteria: role of granulomas in mycobacterial infections. *Immunol Cell Biol*. (2000) 78:334–41. doi: 10.1046/j.1440-1711.2000.00933.x

148. Beham AW, Puellmann K, Laird R, Fuchs T, Streich R, Breysach C, et al. A TNF-regulated recombinatorial macrophage immune receptor implicated in granuloma formation in tuberculosis. *PloS Pathog*. (2011) 7:e1002375. doi: 10.1371/journal.ppat.1002375

149. Garcia Vidal C, Rodríguez Fernández S, Martínez Lacasa J, Salavert M, Vidal R, Rodríguez Carballeira M, et al. Paradoxical response to antituberculous therapy in infliximab-treated patients with disseminated tuberculosis. *Clin Infect Dis*. (2005) 40:756–9. doi: 10.1086/427941

150. Iliopoulos A, Psathakis K, Aslanidis S, Skagias L, Sfikakis PP. Tuberculosis and granuloma formation in patients receiving anti-TNF therapy. *Int J Tuberc Lung Dis*. (2006) 10:588–90.

151. Mattila JT, Ojo OO, Kepka-Lenhart D, Marino S, Kim JH, Eum SY, et al. Microenvironments in tuberculous granulomas are delineated by distinct populations of macrophage subsets and expression of nitric oxide synthase and arginase isoforms. *J Immunol*. (2013) 191:773–84. doi: 10.4049/jimmunol.1300113

152. Lenaerts A, Barry CE 3rd., Dartois V. Heterogeneity in tuberculosis pathology, microenvironments and therapeutic responses. *Immunol Rev*. (2015) 264:288–307. doi: 10.1111/imr.2015.264.issue-1

153. Palazon A, Goldrath AW, Nizet V, Johnson RS. HIF transcription factors, inflammation, and immunity. *Immunity*. (2014) 41:518–28. doi: 10.1016/j.immuni.2014.09.008

154. Baay-Guzman GJ, Duran-Padilla MA, Rangel-Santiago J, Tirado-Rodriguez B, Antonio-Andres G, Barrios-Payan J, et al. Dual role of hypoxia-inducible factor 1 α in experimental pulmonary tuberculosis: its implication as a new therapeutic target. *Future Microbiol*. (2018) 13:785–98. doi: 10.2217/fmb-2017-0168

155. Cramer T, Yamanishi Y, Clausen BE, Förster I, Pawlinski R, Mackman N, et al. HIF-1 alpha is essential for myeloid cell-mediated inflammation. *Cell*. (2003) 112:645–57. doi: 10.1016/S0092-8674(03)00154-5

156. Roiniotis J, Dinh H, Masendycz P, Turner A, Elsegood CL, Scholz GM, et al. Hypoxia prolongs monocyte/macrophage survival and enhanced glycolysis is associated with their maturation under aerobic conditions. *J Immunol*. (2009) 182:7974–81. doi: 10.4049/jimmunol.0804216

157. Strehl C, Fangradt M, Fearon U, Gaber T, Buttgereit F, Veale DJ. Hypoxia: how does the monocyte-macrophage system respond to changes in oxygen availability? *J Leukoc Biol*. (2014) 95:233–41. doi: 10.1189/jlb.1212627

158. Li Q, Xie Y, Cui Z, Huang H, Yang C, Yuan B, et al. Activation of hypoxia-inducible factor 1 (Hif-1) enhanced bactericidal effects of macrophages to *Mycobacterium tuberculosis*. *Tuberculosis (Edinb)*. (2021) 126:102044. doi: 10.1016/j.tube.2020.102044

159. Nizet V, Johnson RS. Interdependence of hypoxic and innate immune responses. *Nat Rev Immunol*. (2009) 9:609–17. doi: 10.1038/nri2607

160. Peyssonnaux C, Datta V, Cramer T, Doedens A, Theodorakis EA, Gallo RL, et al. HIF-1alpha expression regulates the bactericidal capacity of phagocytes. *J Clin Invest*. (2005) 115:1806–15. doi: 10.1172/JCI23865

161. Shi L, Salamon H, Eugenin EA, Pine R, Cooper A, Gennaro ML. Infection with *Mycobacterium tuberculosis* induces the Warburg effect in mouse lungs. *Sci Rep*. (2015) 5:18176. doi: 10.1038/srep18176

162. Braverman J, Sogi KM, Benjamin D, Nomura DK, Stanley SA. HIF-1α Is an essential mediator of IFN-γ-dependent immunity to *mycobacterium tuberculosis*. *J Immunol*. (2016) 197:1287–97. doi: 10.4049/jimmunol.1600266

163. Shi L, Eugenin EA, Subbian S. Immunometabolism in tuberculosis. *Front Immunol*. (2016) 7:150. doi: 10.3389/fimmu.2016.00150

164. Schioppa T, Uranchimeg B, Saccani A, Biswas SK, Doni A, Rapisarda A, et al. Regulation of the chemokine receptor CXCR4 by hypoxia. *J Exp Med*. (2003) 198:1391–402. doi: 10.1084/jem.20030267

165. Schutyser E, Su Y, Yu Y, Gouwy M, Zaja-Milatovic S, Van Damme J, et al. Hypoxia enhances CXCR4 expression in human microvascular endothelial cells and human melanoma cells. *Eur Cytokine Netw*. (2007) 18:59–70. doi: 10.1684/ecn.2007.0087

166. Cardoso MS, Silva TM, Resende M, Appelberg R, Borges M. Lack of the transcription factor hypoxia-inducible factor 1α (HIF-1α) in macrophages accelerates the necrosis of *mycobacterium avium*-induced granulomas. *Infect Immun*. (2015) 83:3534–44. doi: 10.1128/IAI.00144-15

167. Elks PM, Brizee S, van der Vaart M, Walmsley SR, van Eeden FJ, Renshaw SA, et al. Hypoxia inducible factor signaling modulates susceptibility to mycobacterial infection via a nitric oxide dependent mechanism. *PloS Pathog*. (2013) 9:e1003789. doi: 10.1371/journal.ppat.1003789

168. Oehlers SH, Cronan MR, Scott NR, Thomas MI, Okuda KS, Walton EM, et al. Interception of host angiogenic signalling limits mycobacterial growth. *Nature*. (2015) 517:612–5. doi: 10.1038/nature13967

169. de Oliveira Rezende A, Sabóia RS, da Costa AC, da Silva Monteiro DMP, Zagmignan A, Santiago LÂM, et al. Restricted activation of the NF-κB pathway in individuals with latent tuberculosis infection after HIF-1α Blockade. *Biomedicines*. (2022) 10:817. doi: 10.3390/biomedicines10040817

170. Bandarra D, Biddlestone J, Mudie S, Müller HA, Rocha S. HIF-1α restricts NF-κB-dependent gene expression to control innate immunity signals. *Dis Model Mech*. (2015) 8:169–81. doi: 10.1242/dmm.017285

171. Panda S, Morgan J, Cheng C, Saito M, Gilman RH, Ciobanu N, et al. Identification of differentially recognized T cell epitopes in the spectrum of tuberculosis infection. *Nat Commun*. (2024) 15:765. doi: 10.1038/s41467-024-45058-9

172. Lindestam Arlehamn CS, Paul S, Mele F, Huang C, Greenbaum JA, Vita R, et al. Immunological consequences of intragenus conservation of *Mycobacterium tuberculosis* T-cell epitopes. *Proc Natl Acad Sci U.S.A*. (2015) 112:E147–155. doi: 10.1073/pnas.1416537112

173. Lindestam Arlehamn CS, Lewinsohn D, Sette A, Lewinsohn D. Antigens for CD4 and CD8 T cells in tuberculosis. *Cold Spring Harb Perspect Med*. (2014) 4:a018465. doi: 10.1101/cshperspect.a018465

174. Comas I, Chakravartti J, Small PM, Galagan J, Niemann S, Kremer K, et al. Human T cell epitopes of *Mycobacterium tuberculosis* are evolutionarily hyperconserved. *Nat Genet*. (2010) 42:498–503. doi: 10.1038/ng.590

175. Coscolla M, Copin R, Sutherland J, Gehre F, de Jong B, Owolabi O, et al. *M. tuberculosis* T cell epitope analysis reveals paucity of antigenic variation and identifies rare variable TB antigens. *Cell Host Microbe*. (2015) 18:538–48. doi: 10.1016/j.chom.2015.10.008

176. Aguilo JI, Alonso H, Uranga S, Marinova D, Arbués A, de Martino A, et al. ESX-1-induced apoptosis is involved in cell-to-cell spread of *Mycobacterium tuberculosis*. *Cell Microbiol*. (2013) 15:1994–2005. doi: 10.1111/cmi.12169

177. Mustafa AS. Immunological characterization of proteins expressed by genes located in *mycobacterium tuberculosis*-specific genomic regions encoding the ESAT6-like proteins. *Vaccines (Basel)*. (2021) 9:27. doi: 10.3390/vaccines9010027

178. Rogerson BJ, Jung YJ, LaCourse R, Ryan L, Enright N, North RJ. Expression levels of *Mycobacterium tuberculosis* antigen-encoding genes versus production levels of antigen specific T cells during stationary level lung infection in mice. *Immunology*. (2006) 118:195–201. doi: 10.1111/j.1365-2567.2006.02355.x

179. Gröschel MI, Sayes F, Simeone R, Majlessi L, Brosch R. ESX secretion systems: mycobacterial evolution to counter host immunity. *Nat Rev Microbiol*. (2016) 14:677–91. doi: 10.1038/nrmicro.2016.131

180. Hingley-Wilson SM, Connell D, Pollock K, Hsu T, Tchilian E, Sykes A, et al. ESX1-dependent fractalkine mediates chemotaxis and *Mycobacterium tuberculosis* infection in humans. *Tuberculosis (Edinb)*. (2014) 94:262–70. doi: 10.1016/j.tube.2014.01.004

181. Elkington PT, O'Kane CM, Friedland JS. The paradox of matrix metalloproteinases in infectious disease. *Clin Exp Immunol*. (2005) 142:12–20. doi: 10.1111/j.1365-2249.2005.02840.x

182. Volkman HE, Pozos TC, Zheng J, Davis JM, Rawls JF, Ramakrishnan L. Tuberculous granuloma induction via interaction of a bacterial secreted protein with host epithelium. *Science*. (2010) 327:466–9. doi: 10.1126/science.1179663

183. Abdallah AM, Savage ND, van Zon M, Wilson L, Vandenbroucke-Grauls CM, van der Wel NN, et al. The ESX-5 secretion system of *Mycobacterium marinum* modulates the macrophage response. *J Immunol*. (2008) 181:7166–75. doi: 10.4049/jimmunol.181.10.7166

184. Abdallah AM, Bestebroer J, Savage ND, de Punder K, van Zon M, Wilson L, et al. Mycobacterial secretion systems ESX-1 and ESX-5 play distinct roles in host cell death and inflammasome activation. *J Immunol*. (2011) 187:4744–53. doi: 10.4049/jimmunol.1101457

185. Hunter RL, Olsen M, Jagannath C, Actor JK. Trehalose 6,6'-dimycolate and lipid in the pathogenesis of caseating granulomas of tuberculosis in mice. *Am J Pathol*. (2006) 168:1249–61. doi: 10.2353/ajpath.2006.050848

186. Bekierkunst A. Acute granulomatous response produced in mice by trehalose-6,6-dimycolate. *J Bacteriol*. (1968) 96:958–61. doi: 10.1128/jb.96.4.958-961.1968

187. Geisel RE, Sakamoto K, Russell DG, Rhoades ER. *In vivo* activity of released cell wall lipids of *mycobacterium bovis* bacillus calmette guerin is due principally to trehalose mycolates. *J Immunol*. (2005) 174:5007–15. doi: 10.4049/jimmunol.174.8.5007

188. Yarkoni E, Rapp HJ. Granuloma formation in lungs of mice after intravenous administration of emulsified trehalose-6,6'-dimycolate (Cord factor): reaction intensity depends on size distribution of the oil droplets. *Infect Immun*. (1977) 18:552–4. doi: 10.1128/iai.18.2.552-554.1977

189. Silva CL, Ekizlerian SM, Fazioli RA. Role of cord factor in the modulation of infection caused by mycobacteria. *Am J Pathol*. (1985) 118:238–47.

190. Chen T, He L, Deng W, Xie J. The *Mycobacterium* DosR regulon structure and diversity revealed by comparative genomic analysis. *J Cell Biochem*. (2013) 114:1–6. doi: 10.1002/jcb.v114.1

191. Sherman DR, Voskuil M, Schnappinger D, Liao R, Harrell MI, Schoolnik GK. Regulation of the *Mycobacterium tuberculosis* hypoxic response gene encoding alpha -crystallin. *Proc Natl Acad Sci USA*. (2001) 98:7534–9. doi: 10.1073/pnas.121172498

192. Shiloh MU, Manzanillo P, Cox JS. *Mycobacterium tuberculosis* senses host-derived carbon monoxide during macrophage infection. *Cell Host Microbe*. (2008) 3:323–30. doi: 10.1016/j.chom.2008.03.007

193. Voskuil MI, Schnappinger D, Visconti KC, Harrell MI, Dolganov GM, Sherman DR, et al. Inhibition of respiration by nitric oxide induces a Mycobacterium tuberculosis dormancy program. *J Exp Med*. (2003) 198:705–13. doi: 10.1084/jem.20030205

194. Sevalkar RR, Glasgow JN, Pettinati M, Marti MA, Reddy VP, Basu S, et al. *Mycobacterium tuberculosis* DosS binds H2S through its Fe3+ heme iron to regulate the DosR dormancy regulon. *Redox Biol*. (2022) 52:102316. doi: 10.1016/j.redox.2022.102316

195. Saini V, Chinta KC, Reddy VP, Glasgow JN, Stein A, Lamprecht DA, et al. Hydrogen sulfide stimulates Mycobacterium tuberculosis respiration, growth and pathogenesis. *Nat Commun*. (2020) 11:557. doi: 10.1038/s41467-019-14132-y

196. Pandey AK, Sassetti CM. Mycobacterial persistence requires the utilization of host cholesterol. *Proc Natl Acad Sci U.S.A*. (2008) 105:4376–80. doi: 10.1073/pnas.0711159105

197. Miner MD, Chang JC, Pandey AK, Sassetti CM, Sherman DR. Role of cholesterol in *Mycobacterium tuberculosis* infection. *Indian J Exp Biol*. (2009) 47:407–11.

198. Gengenbacher M, Kaufmann SHE. *Mycobacterium tuberculosis*: success through dormancy. *FEMS Microbiol Rev*. (2012) 36:514–32. doi: 10.1111/j.1574-6976.2012.00331.x

199. Martinot AJ, Farrow M, Bai L, Layre E, Cheng TY, Tsai JH, et al. Mycobacterial metabolic syndrome: lprG and rv1410 regulate triacylglyceride levels, growth rate and virulence in *mycobacterium tuberculosis*. *PloS Pathog*. (2016) 12:e1005351. doi: 10.1371/journal.ppat.1005351

200. Clay H, Davis JM, Beery D, Huttenlocher A, Lyons SE, Ramakrishnan L. Dichotomous role of the macrophage in early *Mycobacterium marinum* infection of the zebrafish. *Cell Host Microbe*. (2007) 2:29–39. doi: 10.1016/j.chom.2007.06.004

201. Tobin DM, Roca FJ, Oh SF, McFarland R, Vickery TW, Ray JP, et al. Host genotype-specific therapies can optimize the inflammatory response to mycobacterial infections. *Cell*. (2012) 148:434–46. doi: 10.1016/j.cell.2011.12.023

202. Tobin DM, Vary JCJr., Ray JP, Walsh GS, Dunstan SJ, Bang ND, et al. The lta4h locus modulates susceptibility to mycobacterial infection in zebrafish and humans. *Cell*. (2010) 140:717–30. doi: 10.1016/j.cell.2010.02.013

203. Pagan AJ, Yang CT, Cameron J, Swaim LE, Ellett F, Lieschke GJ, et al. Myeloid growth factors promote resistance to mycobacterial infection by curtailing granuloma necrosis through macrophage replenishment. *Cell Host Microbe*. (2015) 18:15–26. doi: 10.1016/j.chom.2015.06.008

204. Berg RD, Levitte S, O'Sullivan MP, O'Leary SM, Cambier CJ, Cameron J, et al. Lysosomal disorders drive susceptibility to tuberculosis by compromising macrophage migration. *Cell*. (2016) 165:139–52. doi: 10.1016/j.cell.2016.02.034

205. Caruso AM, Serbina N, Klein E, Triebold K, Bloom BR, Flynn JL. Mice deficient in CD4 T cells have only transiently diminished levels of IFN-gamma, yet succumb to tuberculosis. *J Immunol*. (1999) 162:5407–16. doi: 10.4049/jimmunol.162.9.5407

206. Kwan CK, Ernst JD. HIV and tuberculosis: A deadly human syndemic. *Clin Microbiol Rev*. (2011) 24:351–76. doi: 10.1128/CMR.00042-10

207. Vila-del Sol V, Punzón C, Fresno M. IFN-gamma-induced TNF-alpha expression is regulated by interferon regulatory factors 1 and 8 in mouse macrophages. *J Immunol*. (2008) 181:4461–70. doi: 10.4049/jimmunol.181.7.4461

208. Ahmed M, Tezera LB, Elkington PT, Leslie AJ. The paradox of immune checkpoint inhibition re-activating tuberculosis. *Eur Respir J*. (2022) 60:2102512. doi: 10.1183/13993003.02512-2021

209. Pagán AJ, Ramakrishnan L. Immunity and immunopathology in the tuberculous granuloma. *Cold Spring Harb Perspect Med*. (2014) 5:a018499. doi: 10.1101/cshperspect.a018499

210. Tezera LB, Bielecka MK, Ogongo P, Walker NF, Ellis M, Garay-Baquero DJ, et al. Anti-PD-1 immunotherapy leads to tuberculosis reactivation via dysregulation of TNF-α. *Elife*. (2020) 9:e52668. doi: 10.7554/eLife.52668

211. Aly S, Laskay T, Mages J, Malzan A, Lang R, Ehlers S. Interferon-gamma-dependent mechanisms of mycobacteria-induced pulmonary immunopathology: the role of angiostasis and CXCR3-targeted chemokines for granuloma necrosis. *J Pathol*. (2007) 212:295–305. doi: 10.1002/path.v212:3

212. Jurado JO, Alvarez IB, Pasquinelli V, Martínez GJ, Quiroga MF, Abbate E, et al. Programmed death (PD)-1:PD-ligand 1/PD-ligand 2 pathway inhibits T cell effector functions during human tuberculosis. *J Immunol*. (2008) 181:116–25. doi: 10.4049/jimmunol.181.1.116

213. Barber DL, Mayer-Barber KD, Feng CG, Sharpe AH, Sher A. CD4 T cells promote rather than control tuberculosis in the absence of PD-1-mediated inhibition. *J Immunol*. (2011) 186:1598–607. doi: 10.4049/jimmunol.1003304

214. Lázár-Molnár E, Chen B, Sweeney KA, Wang EJ, Liu W, Lin J, et al. Programmed death-1 (PD-1)-deficient mice are extraordinarily sensitive to tuberculosis. *Proc Natl Acad Sci U.S.A*. (2010) 107:13402–7. doi: 10.1073/pnas.1007394107

215. Sable SB. Programmed Death 1 lives up to its reputation in active tuberculosis. *J Infect Dis*. (2013) 208:541–3. doi: 10.1093/infdis/jit211

216. Tousif S, Singh Y, Prasad DV, Sharma P, Van Kaer L, Das G. T cells from Programmed Death-1 deficient mice respond poorly to *Mycobacterium tuberculosis* infection. *PloS One*. (2011) 6:e19864. doi: 10.1371/journal.pone.0019864

217. Via LE, Lin PL, Ray SM, Carrillo J, Allen SS, Eum SY, et al. Tuberculous granulomas are hypoxic in Guinea pigs, rabbits, and nonhuman primates. *Infect Immun*. (2008) 76:2333–40. doi: 10.1128/IAI.01515-07

218. Belton M, Brilha S, Manavaki R, Mauri F, Nijran K, Hong YT, et al. Hypoxia and tissue destruction in pulmonary TB. *Thorax*. (2016) 71:1145–53. doi: 10.1136/thoraxjnl-2015-207402

219. Mikami Y, Grubb BR, Rogers TD, Dang H, Asakura T, Kota P, et al. Chronic airway epithelial hypoxia exacerbates injury in muco-obstructive lung disease through mucus hyperconcentration. *Sci Transl Med*. (2023) 15:eabo7728. doi: 10.1126/scitranslmed.abo7728

220. Kotov DI, Lee OV, Fattinger SA, Langner CA, Guillen JV, Peters JM, et al. Early cellular mechanisms of type I interferon-driven susceptibility to tuberculosis. *Cell*. (2023) 186:5536–5553.e22. doi: 10.1016/j.cell.2023.11.002

221. Moreira-Teixeira L, Stimpson PJ, Stavropoulos E, Hadebe S, Chakravarty P, Ioannou M, et al. Type I IFN exacerbates disease in tuberculosis-susceptible mice by inducing neutrophil-mediated lung inflammation and NETosis. *Nat Commun*. (2020) 11:5566. doi: 10.1038/s41467-020-19412-6

222. Xu G, Wang J, Gao GF, Liu CH. Insights into battles between *Mycobacterium tuberculosis* and macrophages. *Protein Cell*. (2014) 5:728–36. doi: 10.1007/s13238-014-0077-5

223. McNab F, Mayer-Barber K, Sher A, Wack A, O'Garra A. Type I interferons in infectious disease. *Nat Rev Immunol*. (2015) 15:87–103. doi: 10.1038/nri3787

224. Ji DX, Yamashiro LH, Chen KJ, Mukaida N, Kramnik I, Darwin KH, et al. Type I interferon-driven susceptibility to *Mycobacterium tuberculosis* is mediated by IL-1Ra. *Nat Microbiol*. (2019) 4:2128–35. doi: 10.1038/s41564-019-0578-3

225. Ryan GJ, Hoff DR, Driver ER, Voskuil MI, Gonzalez-Juarrero M, Basaraba RJ, et al. Multiple *M. tuberculosis* phenotypes in mouse and Guinea pig lung tissue revealed by a dual-staining approach. *PloS One*. (2010) 5:e11108. doi: 10.1371/journal.pone.0011108

226. Lin PL, Ford CB, Coleman MT, Myers AJ, Gawande R, Ioerger T, et al. Sterilization of granulomas is common in active and latent tuberculosis despite within-host variability in bacterial killing. *Nat Med*. (2014) 20:75–9. doi: 10.1038/nm.3412

227. Gideon HP, Hughes TK, Tzouanas CN, Wadsworth MH 2nd., Tu AA, Gierahn TM, et al. Multimodal profiling of lung granulomas in macaques reveals cellular correlates of tuberculosis control. *Immunity*. (2022) 55:827–846.e10. doi: 10.1016/j.immuni.2022.04.004

228. Drain PK, Bajema KL, Dowdy D, Dheda K, Naidoo K, Schumacher SG, et al. Incipient and subclinical tuberculosis: a clinical review of early stages and progression of infection. *Clin Microbiol Rev*. (2018) 31:e00021–18. doi: 10.1128/CMR.00021-18

229. Capuano SV 3rd., Croix DA, Pawar S, Zinovik A, Myers A, Lin PL, et al. Experimental *Mycobacterium tuberculosis* infection of cynomolgus macaques closely resembles the various manifestations of human *M. tuberculosis* infection. *Infect Immun*. (2003) 71:5831–44. doi: 10.1128/IAI.71.10.5831-5844.2003

230. Pena JC, Ho WZ. Monkey models of tuberculosis: lessons learned. *Infect Immun*. (2015) 83:852–62. doi: 10.1128/IAI.02850-14

231. Coleman MT, Chen RY, Lee M, Lin PL, Dodd LE, Maiello P, et al. PET/CT imaging reveals a therapeutic response to oxazolidinones in macaques and humans with tuberculosis. *Sci Transl Med*. (2014) 6:265ra167. doi: 10.1126/scitranslmed.3009500

232. Malherbe ST, Shenai S, Ronacher K, Loxton AG, Dolganov G, Kriel M, et al. Catalysis TB–Biomarker Consortium. Persisting positron emission tomography lesion activity and *Mycobacterium tuberculosis* mRNA after tuberculosis cure. *Nat Med*. (2016) 22:1094–100. doi: 10.1038/nm.4177

233. Zaidi SMA, Coussens AK, Seddon JA, Kredo T, Warner D, Houben RMGJ, et al. Beyond latent and active tuberculosis: a scoping review of conceptual frameworks. *EClinicalMedicine*. (2023) 66:102332. doi: 10.1016/j.eclinm.2023.102332

234. Gideon HP, Phuah J, Myers AJ, Bryson BD, Rodgers MA, Coleman MT, et al. Variability in tuberculosis granuloma T cell responses exists, but a balance of pro- and anti-inflammatory cytokines is associated with sterilization. *PloS Pathog*. (2015) 11:e1004603. doi: 10.1371/journal.ppat.1004603

235. Kaplan G, Post FA, Moreira AL, Wainwright H, Kreiswirth BN, Tanverdi M, et al. *Mycobacterium tuberculosis* growth at the cavity surface: a microenvironment with failed immunity. *Infect Immun*. (2003) 71:7099–108. doi: 10.1128/IAI.71.12.7099-7108.2003

236. Marakalala MJ, Raju RM, Sharma K, Zhang YJ, Eugenin EA, Prideaux B, et al. Inflammatory signaling in human tuberculosis granulomas is spatially organized. *Nat Med*. (2016) 22:531–8. doi: 10.1038/nm.4073

237. Wells G, Glasgow JN, Nargan K, Lumamba K, Madansein R, Maharaj K, et al. Micro-computed tomography analysis of the human tuberculous lung reveals remarkable heterogeneity in three-dimensional granuloma morphology. *Am J Respir Crit Care Med*. (2021) 204:583–95. doi: 10.1164/rccm.202101-0032OC

238. Wells G, Glasgow JN, Nargan K, Lumamba K, Madansein R, Maharaj K, et al. A high-resolution 3D atlas of the spectrum of tuberculous and COVID-19 lung lesions. *EMBO Mol Med*. (2022) 14:e16283. doi: 10.15252/emmm.202216283

239. Ohashi T, Terasawa K, Aoki M, Akazawa T, Shibata H, Kuze B, et al. The importance of FDG-PET/CT parameters for the assessment of the immune status in advanced HNSCC. *Auris Nasus Larynx*. (2020) 47:658–67. doi: 10.1016/j.anl.2020.01.002

240. Maiello P, DiFazio RM, Cadena AM, Rodgers MA, Lin PL, Scanga CA, et al. Rhesus macaques are more susceptible to progressive tuberculosis than cynomolgus macaques: a quantitative comparison. *Infect Immun*. (2018) 86:e00505–17. doi: 10.1128/IAI.00505-17

241. Chu Y, Chang Y, Lu W, Sheng X, Wang S, Xu H, et al. Regulation of autophagy by glycolysis in cancer. *Cancer Manag Res*. (2020) 12:13259–71. doi: 10.2147/CMAR.S279672

242. Clarke AJ, Simon A. Autophagy in the renewal, differentiation and homeostasis of immune cells. *Nat Rev Immunol*. (2019) 19:170–83. doi: 10.1038/s41577-018-0095-2

243. Dargent A, Wallet F, Friggeri A, Bohe J. Lactic alkalosis in intensive care: a red flag? *Crit Care*. (2023) 27:184. doi: 10.1186/s13054-023-04464-z

244. Quach CHT, Jung K-H, Lee JH, Park JW, Moon SH, Cho YS. Mild alkalization acutely triggers the warburg effect by enhancing hexokinase activity via voltage-dependent anion channel binding. *PloS One*. (2016) 11:e0159529. doi: 10.1371/journal.pone.0159529

245. Cumming BM, Addicott KW, Adamson JH, Steyn AJ. *Mycobacterium tuberculosis* induces decelerated bioenergetic metabolism in human macrophages. *Elife*. (2018) 7:e39169. doi: 10.7554/eLife.39169

246. Hackett EE, Charles-Messance H, O'Leary SM, Gleeson LE, Muñoz-Wolf N, Case S, et al. *Mycobacterium tuberculosis* Limits Host Glycolysis and IL-1β by Restriction of PFK-M via MicroRNA-21. *Cell Rep*. (2020) 30:124–136.e4. doi: 10.1016/j.celrep.2019.12.015

247. Olson GS, Murray TA, Jahn AN, Mai D, Diercks AH, Gold ES, et al. Type I interferon decreases macrophage energy metabolism during mycobacterial infection. *Cell Rep*. (2021) 35:109195. doi: 10.1016/j.celrep.2021.109195

248. Sbarra AJ, Karnovsky ML. The biochemical basis of phagocytosis. I. Metabolic changes during the ingestion of particles by polymorphonuclear leukocytes. *J Biol Chem*. (1959) 234:1355–62. doi: 10.1016/S0021-9258(18)70011-2

249. Lähdevirta J, Maury CP, Teppo AM, Repo H. Elevated levels of circulating cachectin/tumor necrosis factor in patients with acquired immunodeficiency syndrome. *Am J Med*. (1988) 85:289–91. doi: 10.1016/0002-9343(88)90576-1

250. Chan ED. Vulnerability to nontuberculous mycobacterial lung disease or systemic infection due to genetic / heritable disorders. In: Griffith DE, editor. *Nontuberculous Mycobacterial Disease: A Comprehensive Approach to Diagnosis and Management*. Springer Nature, Switzerland (2019). p. 89–110.

251. de Beaucoudrey L, Samarina A, Bustamante J, Cobat A, Boisson-Dupuis S, Feinberg J, et al. Revisiting human IL-12Rβ1 deficiency: a survey of 141 patients from 30 countries. *Med (Baltimore)*. (2010) 89:381–402. doi: 10.1097/MD.0b013e3181fdd832

252. Honda JR, Alper S, Bai X, Chan ED. Acquired and genetic host susceptibility factors and microbial pathogenic factors that predispose to nontuberculous mycobacterial infections. *Curr Opin Immunol*. (2018) 54:66–73. doi: 10.1016/j.coi.2018.06.001

253. Wu UI, Holland SM. Host susceptibility to non-tuberculous mycobacterial infections. *Lancet Infect Dis*. (2015) 15:968–80. doi: 10.1016/S1473-3099(15)00089-4

254. Cooper AM, Dalton DK, Stewart TA, Griffin JP, Russell DG, Orme IM. Disseminated tuberculosis in interferon gamma gene-disrupted mice. *J Exp Med*. (1993) 178:2243–7. doi: 10.1084/jem.178.6.2243

255. Flynn JL, Chan J, Triebold KJ, Dalton DK, Stewart TA, Bloom BR. An essential role for interferon gamma in resistance to *Mycobacterium tuberculosis* infection. *J Exp Med*. (1993) 178:2249–54. doi: 10.1084/jem.178.6.2249

256. Jayaraman P, Jacques MK, Zhu C, Steblenko KM, Stowell BL, Madi A, et al. TIM3 Mediates T Cell Exhaustion during *Mycobacterium tuberculosis* Infection. *PloS Pathog*. (2016) 12:e1005490. doi: 10.1371/journal.ppat.1005490

257. Kirman J, McCoy K, Hook S, Prout M, Delahunt B, Orme I, et al. CTLA-4 blockade enhances the immune response induced by mycobacterial infection but does not lead to increased protection. *Infect Immun*. (1999) 67:3786–92. doi: 10.1128/IAI.67.8.3786-3792.1999

258. Eid RE, Rao DA, Zhou J, Lo SF, Ranjbaran H, Gallo A, et al. Interleukin-17 and interferon-gamma are produced concomitantly by human coronary artery-infiltrating T cells and act synergistically on vascular smooth muscle cells. *Circulation*. (2009) 119:1424–32. doi: 10.1161/CIRCULATIONAHA.108.827618

259. Watcharanurak K, Zang L, Nishikawa M, Yoshinaga K, Yamamoto Y, Takahashi Y, et al. Effects of upregulated indoleamine 2, 3-dioxygenase 1 by interferon γ gene transfer on interferon γ-mediated antitumor activity. *Gene Ther*. (2014) 21:794–801. doi: 10.1038/gt.2014.54

260. Flynn JL, Goldstein MM, Chan J, Triebold KJ, Pfeffer K, Lowenstein CJ, et al. Tumor necrosis factor-alpha is required in the protective immune response against *Mycobacterium tuberculosis* in mice. *Immunity*. (1995) 2:561–72. doi: 10.1016/1074-7613(95)90001-2

261. Roca FJ, Whitworth LJ, Redmond S, Jones AA, Ramakrishnan L. TNF induces pathogenic programmed macrophage necrosis in tuberculosis through a mitochondrial-lysosomal-endoplasmic reticulum circuit. *Cell*. (2019) 178:1344–61. doi: 10.1016/j.cell.2019.08.004

262. Patel HJ, Patel BM. TNF-α and cancer cachexia: Molecular insights and clinical implications. *Life Sci*. (2017) 170:56–63. doi: 10.1016/j.lfs.2016.11.033

263. Hernandez-Pando R, Orozco H, Arriaga K, Pavön L, Rook G. Treatment with BB-94, a broad spectrum inhibitor of zinc-dependent metalloproteinases, causes deviation of the cytokine profile towards type-2 in experimental pulmonary tuberculosis in Balb/c mice. *Int J Exp Pathol*. (2000) 81:199–209. doi: 10.1046/j.1365-2613.2000.00152.x

264. Izzo AA, Izzo LS, Kasimos J, Majka S. A matrix metalloproteinase inhibitor promotes granuloma formation during the early phase of *Mycobacterium tuberculosis* pulmonary infection. *Tuberculosis (Edinb)*. (2004) 84:387–96. doi: 10.1016/j.tube.2004.07.001

265. Rich AR, Follis JH Jr. The effect of low oxygen tension upon the development of experimental tuberculosis. *Am Rev Tuberc*. (1942) 71:345–57.

266. Hunter L, Ruedas-Torres I, Agulló-Ros I, Rayner E, Salguero FJ. Comparative pathology of experimental pulmonary tuberculosis in animal models. *Front Vet Sci*. (2023) 10:1264833. doi: 10.3389/fvets.2023.1264833

267. Li L, Wang M, Mei Z, Cao W, Yang Y, Wang Y, et al. lncRNAs HIF1A-AS2 facilitates the up-regulation of HIF-1α by sponging to miR-153-3p, whereby promoting angiogenesis in HUVECs in hypoxia. *BioMed Pharmacother*. (2017) 96:165–72. doi: 10.1016/j.biopha.2017.09.113

268. Knight M, Stanley S. HIF-1α as a central mediator of cellular resistance to intracellular pathogens. *Curr Opin Immunol*. (2019) 60:111–6. doi: 10.1016/j.coi.2019.05.005

269. Li X, Yang Y, Zhang B, Lin X, Fu X, An Y, et al. Lactate metabolism in human health and disease. *Signal Transduct Target Ther*. (2022) 7:305. doi: 10.1038/s41392-022-01151-3

270. Mehra S, Alvarez X, Didier PJ, Doyle LA, Blanchard JL, Lackner AA, et al. Granuloma correlates of protection against tuberculosis and mechanisms of immune modulation by *Mycobacterium tuberculosis*. *J Infect Dis*. (2013) 207:1115–27. doi: 10.1093/infdis/jis778

271. Lott JS. The tryptophan biosynthetic pathway is essential for Mycobacterium tuberculosis to cause disease. *Biochem Soc Trans*. (2020) 48:2029–37. doi: 10.1042/BST20200194

272. Suzuki Y, Suda T, Asada K, Miwa S, Suzuki M, Fujie M, et al. Serum indoleamine 2,3-dioxygenase activity predicts prognosis of pulmonary tuberculosis. *Clin Vaccine Immunol*. (2012) 19:436–42. doi: 10.1128/CVI.05402-11

273. Regev D, Surolia R, Karki S, Zolak J, Montes-Worboys A, Oliva O, et al. Heme oxygenase-1 promotes granuloma development and protects against dissemination of mycobacteria. *Lab Invest*. (2012) 92:1541–52. doi: 10.1038/labinvest.2012.125

274. Silva-Gomes S, Appelberg R, Larsen R, Soares MP, Gomes MS. Heme catabolism by heme oxygenase-1 confers host resistance to Mycobacterium infection. *Infect Immun*. (2013) 81:2536–45. doi: 10.1128/IAI.00251-13

275. Kapturczak MH, Wasserfall C, Brusko T, Campbell-Thompson M, Ellis TM, Atkinson MA, et al. Heme oxygenase-1 modulates early inflammatory responses: evidence from the heme oxygenase-1-deficient mouse. *Am J Pathol*. (2004) 165:1045–53. doi: 10.1016/S0002-9440(10)63365-2

276. Yang S, Ouyang J, Lu Y, Harypursat V, Chen Y. A dual role of heme oxygenase-1 in tuberculosis. *Front Immunol*. (2022) 13:842858. doi: 10.3389/fimmu.2022.842858

277. Chinta KC, Rahman MA, Saini V, Glasgow JN, Reddy VP, Lever JM, et al. Microanatomic distribution of myeloid heme oxygenase-1 protects against free radical-mediated immunopathology in human tuberculosis. *Cell Rep*. (2018) 25:1938–1952.e5. doi: 10.1016/j.celrep.2018.10.073

278. Abdalla MY, Ahmad IM, Switzer B, Britigan BE. Induction of heme oxygenase-1 contributes to survival of *Mycobacterium abscessus* in human macrophages-like THP-1 cells. *Redox Biol*. (2015) 4:328–39. doi: 10.1016/j.redox.2015.01.012

279. Costa DL, Namasivayam S, Amaral EP, Arora K, Chao A, Mittereder LR, et al. Pharmacological inhibition of host heme oxygenase-1 suppresses *mycobacterium tuberculosis* infection *in vivo* by a mechanism dependent on T lymphocytes. *mBio*. (2016) 7:e01675–16. doi: 10.1128/mBio.01675-16

280. Rockwood N, Costa DL, Amaral EP, Du Bruyn E, Kubler A, Gil-Santana L, et al. *Mycobacterium tuberculosis* induction of heme oxygenase-1 expression is dependent on oxidative stress and reflects treatment outcomes. *Front Immunol*. (2017) 8:542. doi: 10.3389/fimmu.2017.00542

281. Vaddi A, Hulsebus HJ, O'Neill EL, Knight V, Chan ED. A narrative review of the controversy on the risk of mycobacterial infections with immune checkpoint inhibitor use: does Goldilocks have the answer? *J Thorac Dis*. (2024) 16:1601–16. doi: 10.21037/jtd-23-1395

282. Fallahi-Sichani M, Kirschner DE, Linderman JJ. NF-κB signaling dynamics play a key role in infection control in tuberculosis. *Front Physiol*. (2012) 3:170. doi: 10.3389/fphys.2012.00170

283. Iseman MD. *A Clinician's Guide to Tuberculosis. 1st ed*. Philadelphia, PA: Lippincott Williams & Wilkins (2000).

284. Balasubramanian V, Wiegeshaus EH, Taylor BT, Smith DW. Pathogenesis of tuberculosis: pathway to apical localization. *Tuber Lung Dis*. (1994) 75:168–78. doi: 10.1016/0962-8479(94)90002-7

285. Elkington PT, Friedland JS. Permutations of time and place in tuberculosis. *Lancet Infect Dis*. (2015) 15:1357–60. doi: 10.1016/S1473-3099(15)00135-8

286. Donald PR, Diacon AH, Thee S. Anton ghon and his colleagues and their studies of the primary focus and complex of tuberculosis infection and their relevance for the twenty-first century. *Respiration*. (2021) 100:557–67. doi: 10.1159/000509522

287. Hunter RL, Jagannath C, Actor JK. Pathologyt of postprimary tuberculosis in humans and mice: Contradiction of long-held beliefs. *Tuberculosis*. (2007) 87:267–78. doi: 10.1016/j.tube.2006.11.003

288. Opie EL, Aronson JD. Tubercle bacilli in latent tuberculous lesions and in the lung tissue without tuberculous lesions. *Arch Pathol Lab Med*. (1927) 4:1–21.

289. Ghesani N, Patrawalla A, Lardizabal A, Salgame P, Fennelly KP. Increased cellular activity in thoracic lymph nodes in early human latent tuberculosis infection. *Am J Respir Crit Care Med*. (2014) 189:748–50. doi: 10.1164/rccm.201311-1976LE

290. Laennec R. A treatise on diseases of the chest in which they are described according to their anatomical characters, and their diagnosis established on a new principle by means of acoustick instruments. Birmingham AL., London: T&G Underwood (1821). reprinted 1979 by The Classics of Medicine Library.

291. Virchow R. Cellular pathology as based upon physiological and pathological histology. Birmingham, AL, London: John Churchill (1860). reprinted by The Classics of Medicine Library, 1978.

292. Osler W. *The Principles and Practice of Medicine*. New York: Appleton (1920).

293. Hunter RL. Tuberculosis as a three-act play: A new paradigm for the pathogenesis of pulmonary tuberculosis. *Tuberculosis (Edinb)*. (2016) 97:8–17. doi: 10.1016/j.tube.2015.11.010

294. Hunter RL, Actor JK, Hwang SA, Karev V, Jagannath C. Pathogenesis of post primary tuberculosis: immunity and hypersensitivity in the development of cavities. *Ann Clin Lab Sci*. (2014) 44:365–87.

295. Hunter RL, Actor JK, Hwang SA, Khan A, Urbanowski ME, Kaushal D, et al. Pathogenesis and animal models of post-primary (Bronchogenic) tuberculosis, A review. *Pathogens*. (2018) 7:19. doi: 10.3390/pathogens7010019

296. Hunter RL. On the pathogenesis of post primary tuberculosis: the role of bronchial obstruction in the pathogenesis of cavities. *Tuberculosis (Edinb)*. (2011) 91 Suppl 1:S6–S10. doi: 10.1016/j.tube.2011.10.003

297. Hunter RL. Pathology of post primary tuberculosis of the lung: an illustrated critical review. *Tuberculosis (Edinb)*. (2011) 91:497–509. doi: 10.1016/j.tube.2011.03.007

298. Medlar EM. The behavior of pulmonary tuberculous lesions; a pathological study. *Am Rev Tuberc*. (1955) 71:1e244.

299. Pagel W, Simmonds F, MacDonald N, Nassau E. *Pulmonary tuberculosis, bacteriology, pathology, management, epidemiology and prevention*. London: Oxford University Press (1964).

300. Nargan K, Glasgow JN, Nadeem S, Naidoo T, Wells G, Hunter RL, et al. Spatial distribution of *Mycobacterium tuberculosis* mRNA and secreted antigens in acid-fast negative human antemortem and resected tissue. *EBioMedicine*. (2024) 105:105196. doi: 10.1016/j.ebiom.2024.105196

301. Dartois V, Dick T. A ginger root or plum model for the tuberculosis "Granuloma"? *Am J Respir Crit Care Med*. (2021) 204:505–7. doi: 10.1164/rccm.202104-1052ED

302. Chang JC, Wysocki A, Tchou-Wong KM, Moskowitz N, Zhang Y, Rom WN. Effect of *Mycobacterium tuberculosis* and its components on macrophages and the release of matrix metalloproteinases. *Thorax*. (1996) 51:306–11. doi: 10.1136/thx.51.3.306

303. Elkington P, Shiomi T, Breen R, Nuttall RK, Ugarte-Gil CA, Walker NF, et al. MMP-1 drives immunopathology in human tuberculosis and transgenic mice. *J Clin Invest*. (2011) 121:1827–33. doi: 10.1172/JCI45666

304. Elkington PT, Ugarte-Gil CA, Friedland JS. Matrix metalloproteinases in tuberculosis. *Eur Respir J*. (2011) 38:456–64. doi: 10.1183/09031936.00015411

305. Reichmann MT, Tezera LB, Vallejo AF, Vukmirovic M, Xiao R, Reynolds J, et al. Integrated transcriptomic analysis of human tuberculosis granulomas and a biomimetic model identifies therapeutic targets. *J Clin Invest*. (2021) 131:e148136. doi: 10.1172/JCI148136

306. Salgame P. MMPs in tuberculosis: granuloma creators and tissue destroyers. *J Clin Invest*. (2011) 121:1686–8. doi: 10.1172/JCI57423

307. Nedeltchev GG, Raghunand TR, Jassal MS, Lun S, Cheng QJ, Bishai WR. Extrapulmonary dissemination of *Mycobacterium bovis* but not *Mycobacterium tuberculosis* in a bronchoscopic rabbit model of cavitary tuberculosis. *Infect Immun*. (2009) 77:598–603. doi: 10.1128/IAI.01132-08

308. Kaufmann SH, Schaible UE. 100th anniversary of Robert Koch's Nobel Prize for the discovery of the tubercle bacillus. *Trends Microbiol*. (2005) 13:469–75. doi: 10.1016/j.tim.2005.08.003

309. Ganchua SKC, Cadena AM, Maiello P, Gideon HP, Myers AJ, Junecko BF, et al. Lymph nodes are sites of prolonged bacterial persistence during Mycobacterium tuberculosis infection in macaques. *PloS Pathog*. (2018) 14:e1007337. doi: 10.1371/journal.ppat.1007337

310. Chen RY, Yu X, Smith B, Liu X, Gao J, Diacon AH, et al. Radiological and functional evidence of the bronchial spread of tuberculosis: an observational analysis. *Lancet Microbe*. (2021) 2:e518–26. doi: 10.1016/S2666-5247(21)00058-6

311. Dock W. Apical localization of phthisis: its significance in treatment by prolonged rest in bed. *Am Rev Tuberc*. (1946) 53:297–305. doi: 10.1164/art.1946.53.4.297

312. Murray JF. Bill Dock and the location of pulmonary tuberculosis: how bed rest might have helped consumption. *Am J Respir Crit Care Med*. (2003) 168:1029–33. doi: 10.1164/rccm.200307-1016OE

313. Goodwin RA, Des Prez RM. Apical localization of pulmonary tuberculosis, chronic pulmonary histoplasmosis, and progressive massive fibrosis of the lung. *Chest*. (1983) 83:801–5. doi: 10.1378/chest.83.5.801

314. West JB, Luks AM. *West's Respiratory Physiology: The Essentials. 11th ed*. Philadelphia, PA: Wolters Kluwer (2020).

315. Alfarouk KO, Verduzco D, Rauch C, Muddathir AK, Adil HH, Elhassan GO, et al. Glycolysis, tumor metabolism, cancer growth and dissemination. A new pH-based etiopathogenic perspective and therapeutic approach to an old cancer question. *Oncoscience*. (2014) 1:777–802. doi: 10.18632/oncoscience.v1i12

316. López-Lázaro M. A new view of carcinogenesis and an alternative approach to cancer therapy. *Mol Med*. (2010) 16:144–53. doi: 10.2119/molmed.2009.00162

317. Sever JL, Youmans G. The relation of oxygen tension to virulence of tubercle bacilli and to acquired resistance in tuberculosis. *J Infect Dis*. (1957) 101:193–202. doi: 10.1093/infdis/101.2.193

318. Medlar EM, Sasano KT. A study of the pathology of experimental pulmonary tuberculosis in the rabbit. *Am Rev Tuberc*. (1935) 34:456–75.

319. Dock W. Effect of posture on alveolar gas tension in tuberculosis: explanation for favored sites of chronic pulmonary lesions. *Arch Intern Med*. (1954) 94:700–8. doi: 10.1001/archinte.1954.00250050014003

320. Niikawa H, Okamoto T, Ayyat KS, Itoda Y, Farver CF, McCurry KR. Better oxygenation in upper lobes than in whole lungs in marginal human donor lungs utilized for cellular ex vivo lung perfusion. *J Heart Lung Transplant*. (2019) 38:S321. doi: 10.1016/j.healun.2019.01.808

321. Haapanen JH, Kass I, Gensini G, Middlebrook G. Studies on the gaseous content of tuberculous cavities. *Am Rev Respir Dis*. (1959) 80:1–5. doi: 10.1164/arrd.1959.80.1P1.1

322. Fayyazi A, Eichmeyer B, Soruri A, Schweyer S, Herms J, Schwarz P, et al. Apoptosis of macrophages and T cells in tuberculosis associated caseous necrosis. *J Pathol*. (2000) 191:417–25. doi: 10.1002/1096-9896(2000)9999:9999<::AID-PATH664>3.0.CO;2-R

323. Dharmadhikari AS, Nardell EA. What animal models teach humans about tuberculosis. *Am J Respir Cell Mol Biol*. (2008) 39:503–8. doi: 10.1165/rcmb.2008-0154TR

324. Gupta UD, Katoch VM. Animal models of tuberculosis. *Tuberculosis (Edinb)*. (2005) 85:277–93. doi: 10.1016/j.tube.2005.08.008

325. Sakamoto K. The pathology of *Mycobacterium tuberculosis* infection. *Vet Pathol*. (2012) 49:423–39. doi: 10.1177/0300985811429313

326. Williams A, Orme IM. Animal models of tuberculosis: an overview. *Microbiol Spectr*. (2016) 4:1–12. doi: 10.1128/microbiolspec.TBTB2-0004-2015

327. Bucsan AN, Mehra S, Khader SA, Kaushal D. The current state of animal models and genomic approaches towards identifying and validating molecular determinants of *Mycobacterium tuberculosis* infection and tuberculosis disease. *Pathog Dis*. (2019) 77:ftz037. doi: 10.1093/femspd/ftz037

328. Palmer MV. *Mycobacterium bovis*: characteristics of wildlife reservoir hosts. *Transbound Emerg Dis*. (2013) 60 Suppl 1:1–13. doi: 10.1111/tbed.12115

329. Villarreal-Ramos B, Berg S, Whelan A, Holbert S, Carreras F, Salguero FJ, et al. Experimental infection of cattle with *Mycobacterium tuberculosis* isolates shows the attenuation of the human tubercle bacillus for cattle. *Sci Rep*. (2018) 8:894. doi: 10.1038/s41598-017-18575-5

330. Pesciaroli M, Alvarez J, Boniotti MB, Cagiola M, Di Marco V, Marianelli C, et al. Tuberculosis in domestic animal species. *Res Vet Sci*. (2014) 97 Suppl:S78–85. doi: 10.1016/j.rvsc.2014.05.015

331. Cardona PJ, Williams A. Experimental animal modeling for TB vaccine development. *Int J Infect Dis*. (2017) 56:268–73. doi: 10.1016/j.ijid.2017.01.030

332. Siddiqui N, Price S, Hope J. BCG vaccination of neonatal calves: potential roles for innate immune cells in the induction of protective immunity. *Comp Immunol Microbiol Infect Dis*. (2012) 35:219–26. doi: 10.1016/j.cimid.2011.11.003

333. Buddle BM, Skinner MA, Wedlock DN, de Lisle GW, Vordermeier HM, Glyn Hewinson R. Cattle as a model for development of vaccines against human tuberculosis. *Tuberculosis (Edinb)*. (2005) 85:19–24. doi: 10.1016/j.tube.2004.09.003

334. Villarreal-Ramos B, Berg S, Chamberlain L, McShane H, Hewinson RG, Clifford D, et al. Development of a BCG challenge model for the testing of vaccine candidates against tuberculosis in cattle. *Vaccine*. (2014) 32:5645–9. doi: 10.1016/j.vaccine.2014.08.009

335. McIlroy SG, Neill SD, McCracken RM. Pulmonary lesions and *Mycobacterium bovis* excretion from the respiratory tract of tuberculin reacting cattle. *Vet Rec*. (1986) 118:718–21. doi: 10.1136/vr.118.26.718

336. Wangoo A, Johnson L, Gough J, Ackbar R, Inglut S, Hicks D, et al. Advanced granulomatous lesions in *Mycobacterium bovis*-infected cattle are associated with increased expression of type I procollagen, gammadelta (WC1+) T cells and CD 68+ cells. *J Comp Pathol*. (2005) 133:223–34. doi: 10.1016/j.jcpa.2005.05.001

337. Liebana E, Marsh S, Gough J, Nunez A, Vordermeier HM, Whelan A, et al. Distribution and activation of T-lymphocyte subsets in tuberculous bovine lymph-node granulomas. *Vet Pathol*. (2007) 44:366–72. doi: 10.1354/vp.44-3-366

338. Cassidy JP, Bryson DG, Gutiérrez Cancela MM, Forster F, Pollock JM, Neill SD. Lymphocyte subtypes in experimentally induced early-stage bovine tuberculous lesions. *J Comp Pathol*. (2001) 124:46–51. doi: 10.1053/jcpa.2000.0427

339. Palmer MV, Wiarda J, Kanipe C, Thacker TC. Early Pulmonary Lesions in Cattle Infected via Aerosolized *Mycobacterium bovis*. *Vet Pathol*. (2019) 56:544–54. doi: 10.1177/0300985819833454

340. Rusk RA, Palmer MV, Waters WR, McGill JL. Measuring bovine γδ T cell function at the site of *Mycobacterium bovis* infection. *Vet Immunol Immunopathol*. (2017) 193-194:38–49. doi: 10.1016/j.vetimm.2017.10.004

341. McGill JL, Sacco RE, Baldwin CL, Telfer JC, Palmer MV, Waters WR. The role of gamma delta T cells in immunity to *Mycobacterium bovis* infection in cattle. *Vet Immunol Immunopathol*. (2014) 159:133–43. doi: 10.1016/j.vetimm.2014.02.010

342. Mikota SK. Tuberculosis in elephants. In: Fowler ME, Miller RE, editor. *Zoo and wild animal medicine, current therapy, Sixth ed*. Saunders/Elsevier, St Louis, MO (2008). p. 355–64.

343. Payeur JB, Jarnagin JL, Marquardt JG, Whipple DL. Mycobacterial isolations in captive elephants in the United States. *Ann N Y Acad Sci*. (2002) 969:256–8. doi: 10.1111/j.1749-6632.2002.tb04388.x

344. Rajbhandari RM, de la Fuente J, Karmacharya D, Mathema S, Maharjan B, Dixit SM, et al. Understanding *Mycobacterium tuberculosis* complex in elephants through a One Health approach: a systematic review. *BMC Vet Res*. (2022) 18:262. doi: 10.1186/s12917-022-03356-8

345. Miller MA, Kerr TJ, de Waal CR, Goosen WJ, Streicher EM, Hausler G, et al. *Mycobacterium bovis* infection in free-ranging african elephants. *Emerg Infect Dis*. (2021) 27:990–2. doi: 10.3201/eid2703.204729

346. Suga S, Mukai Y, Ishikawa S, Yoshida S, Paudel S, Wada T. Intensive treatment of A captive bornean elephant (*Elephas maximus borneensis*) infected with *mycobacterium caprae* in Japan. *J Zoo Wildl Med*. (2021) 51:1062–6. doi: 10.1638/2019-0152

347. Mikota SK, Peddie L, Peddie J, Isaza R, Dunker F, West G, et al. Epidemiology and diagnosis of *Mycobacterium tuberculosis* in captive Asian elephants (*Elephas maximus*). *J Zoo Wildl Med*. (2001) 32:1–16. doi: 10.1638/1042-7260(2001)032[0001:EADOMT]2.0.CO;2

348. Mikota SK, Larsen RS, Montali RJ. Tuberculosis in elephants in North America. *Zoo Biol*. (2000) 19:393e403. doi: 10.1002/1098-2361(2000)19:5<393::AID-ZOO9>3.0.CO;2-T

349. Miller MA, Buss P, Roos EO, Hausler G, Dippenaar A, Mitchell E, et al. Fatal tuberculosis in a free-ranging African elephant and one health implications of human pathogens in wildlife. *Front Vet Sci*. (2019) 6:18. doi: 10.3389/fvets.2019.00018

350. Perera BVP, Salgadu MA, de S. Gunawardena GSP, Smith NH, Jinadasa HRN. First confirmed case of fatal tuberculosis in a wild Sri Lankan elephant. *Gajah*. (2014) 41:28–31.

351. Zachariah A, Pandiyan J, Madhavilatha GK, Mundayoor S, Chandramohan B, Sajesh PK, et al. *Mycobacterium tuberculosis* in wild asian elephants, southern India. *Emerg Infect Dis*. (2017) 23:504–6. doi: 10.3201/eid2303.161741

352. Lewerin SS, Olsson SL, Eld K, Röken B, Ghebremichael S, Koivula T, et al. Outbreak of *Mycobacterium tuberculosis* infection among captive Asian elephants in a Swedish zoo. *Vet Rec*. (2005) 156:171e5. doi: 10.1136/vr.156.6.171

353. Obanda V, Poghon J, Yongo M, Mulei I, Ngotho M, Waititu K, et al. First reported case of fatal tuberculosis in a wild African elephant with past human-wildlife contact. *Epidemiol Infect*. (2013) 141:1476e80. doi: 10.1017/S0950268813000022

354. Michalak K, Austin C, Diesel S, Bacon JM, Zimmerman P, Maslow JN. Mycobacterium tuberculosis infection as a zoonotic disease: Transmission between humans and elephants. *Emerg Infect Dis*. (1998) 4:283–7. doi: 10.3201/eid0402.980217

355. Mikota SK, Maslow JN. Tuberculosis at the human-animal interface: an emerging disease of elephants. *Tuberculosis (Edinb)*. (2011) 91:208–11. doi: 10.1016/j.tube.2011.02.007

356. Oh P, Granich R, Scott J, Sun B, Joseph M, Stringfield C, et al. Human exposure following *Mycobacterium tuberculosis* infection of multiple animal species in a Metropolitan zoo. *Emerg Infect Dis*. (2002) 8:1290–3. doi: 10.3201/eid0811.020302

357. Murphree R, Warkentin JV, Dunn JR, Schaffner W, Jones TF. Elephant-to-human transmission of tuberculosis, 2009. *Emerg Infect Dis*. (2011) 17:366–71. doi: 10.3201/eid1703.101668

358. Montali RJ, Mikota SK, Cheng LI. Mycobacterium tuberculosis in zoo and wildlife species. *Rev Sci Tech*. (2001) 20:291–303. doi: 10.20506/rst.issue.20.1.16

359. Landolfi JA, Terio KA, Miller M, Junecko BF, Reinhart T. Pulmonary tuberculosis in Asian elephants (*Elephas maximus*): histologic lesions with correlation to local immune responses. *Vet Pathol*. (2015) 52:535–42. doi: 10.1177/0300985814548517

360. Stinear TP, Seemann T, Harrison PF, Jenkin GA, Davies JK, Johnson PD, et al. Insights from the complete genome sequence of *Mycobacterium marinum* on the evolution of *Mycobacterium tuberculosis*. *Genome Res*. (2008) 18:729–41. doi: 10.1101/gr.075069.107

361. Tobin DM, Ramakrishnan L. Comparative pathogenesis of *Mycobacterium marinum* and *Mycobacterium tuberculosis*. *Cell Microbiol*. (2008) 10:1027–39. doi: 10.1111/j.1462-5822.2008.01133.x

362. Berg RD, Ramakrishnan L. Insights into tuberculosis from the zebrafish model. *Trends Mol Med*. (2012) 18:689–90. doi: 10.1016/j.molmed.2012.10.002

363. Davis JM, Clay H, Lewis JL, Ghori N, Herbomel P, Ramakrishnan L. Real-time visualization of mycobacterium-macrophage interactions leading to initiation of granuloma formation in zebrafish embryos. *Immunity*. (2002) 17:693–702. doi: 10.1016/S1074-7613(02)00475-2

364. Langenau DM, Ferrando AA, Traver D, Kutok JL, Hezel JP, Kanki JP, et al. *In vivo* tracking of T cell development, ablation, and engraftment in transgenic zebrafish. *Proc Natl Acad Sci USA*. (2004) 101:7369–74. doi: 10.1073/pnas.0402248101

365. Lesley R, Ramakrishnan L. Insights into early mycobacterial pathogenesis from the zebrafish. *Curr Opin Microbiol*. (2008) 11:277–83. doi: 10.1016/j.mib.2008.05.013

366. Meijer AH, Spaink HP. Host-pathogen interactions made transparent with the zebrafish model. *Curr Drug Targets*. (2011) 12:1000–17. doi: 10.2174/138945011795677809

367. Pozos TC, Ramakrishnan L. New models for the study of *Mycobacterium*-host interactions. *Curr Opin Immunol*. (2004) 16:499–505. doi: 10.1016/j.coi.2004.05.011

368. Ramakrishnan L. Looking within the zebrafish to understand the tuberculous granuloma. *Adv Exp Med Biol*. (2013) 783:251–66. doi: 10.1007/978-1-4614-6111-1_13

369. Swaim LE, Connolly LE, Volkman HE, Humbert O, Born DE, Ramakrishnan L. *Mycobacterium marinum* infection of adult zebrafish causes caseating granulomatous tuberculosis and is moderated by adaptive immunity. *Infect Immun*. (2006) 74:6108–17. doi: 10.1128/IAI.00887-06

370. van Leeuwen LM, van der Sar AM, Bitter W. Animal models of tuberculosis: zebrafish. *Cold Spring Harb Perspect Med*. (2014) 5:a018580. doi: 10.1101/cshperspect.a018580

371. Kaufmann SH. Immune response to tuberculosis: experimental animal models. *Tuberculosis (Edinb)*. (2003) 83:107–11. doi: 10.1016/S1472-9792(02)00063-X

372. Singh AK, Gupta UD. Animal models of tuberculosis: Lesson learnt. *Indian J Med Res*. (2018) 147:456–63. doi: 10.4103/ijmr.IJMR_554_18

373. Chackerian AA, Behar SM. Susceptibility to *Mycobacterium tuberculosis*: Lessons from inbred strains of mice. *Tuberculosis*. (2003) 83:279–85. doi: 10.1016/S1472-9792(03)00017-9

374. Harper J, Skerry C, Davis SL, Tasneen R, Weir M, Kramnik I, et al. Mouse model of necrotic tuberculosis granulomas develops hypoxic lesions. *J Infect Dis*. (2012) 205:595–602. doi: 10.1093/infdis/jir786

375. Kramnik I, Dietrich WF, Demant P, Bloom BR. Genetic control of resistance to experimental infection with virulent *Mycobacterium tuberculosis*. *Proc Natl Acad Sci USA*. (2000) 97:8560–5. doi: 10.1073/pnas.150227197

376. Pichugin AV, Yan BS, Sloutsky A, Kobzik L, Kramnik I. Dominant role of the sst1 locus in pathogenesis of necrotizing lung granulomas during chronic tuberculosis infection and reactivation in genetically resistant hosts. *Am J Pathol*. (2009) 174:2190–201. doi: 10.2353/ajpath.2009.081075

377. Pan H, Yan BS, Rojas M, Shebzukhov YV, Zhou H, Kobzik L, et al. Ipr1 gene mediates innate immunity to tuberculosis. *Nature*. (2005) 434:767–72. doi: 10.1038/nature03419

378. Yan B-S, Kirby A, Shebzukhov YV, Daly MJ, Kramnik I. Genetic architecture of tuberculosis resistance in a mouse model of infection. *Genes Immun*. (2006) 7:201–10. doi: 10.1038/sj.gene.6364288

379. Smith CM, Baker RE, Proulx MK, Mishra BB, Long JE, Park SW, et al. Host-pathogen genetic interactions underlie tuberculosis susceptibility in genetically diverse mice. *Elife*. (2022) 11:e74419. doi: 10.7554/eLife.74419

380. Smith CM, Proulx MK, Lai R, Kiritsy MC, Bell TA, Hock P, et al. Functionally overlapping variants control tuberculosis susceptibility in collaborative cross mice. *mBio*. (2019) 10:e02791–19. doi: 10.1128/mBio.02791-19

381. Noll KE, Ferris MT, Heise M. The collaborative cross: A systems genetics resource for studying host-pathogen interactions. *Cell Host Microbe*. (2019) 25:484–98. doi: 10.1016/j.chom.2019.03.009

382. Smith CM, Proulx MK, Olive AJ, Laddy D, Mishra BB, Moss C, et al. Tuberculosis susceptibility and vaccine protection are independently controlled by host genotype. *mBio*. (2016) 7:e01516–16. doi: 10.1128/mBio.01516-16

383. Rhoades ER, Frank AA, Orme IM. Progression of chronic pulmonary tuberculosis in mice aerogenically infected with virulent *Mycobacterium tuberculosis*. *Tuber Lung Dis*. (1997) 78:57–66. doi: 10.1016/S0962-8479(97)90016-2

384. McCune RM, Feldmann FM, Lambert HP, McDermott W. Microbial persistence. I. The capacity of tubercle bacilli to survive sterilization in mouse tissues. *J Exp Med*. (1966) 123:445–68. doi: 10.1084/jem.123.3.445

385. Nemeth J, Olson GS, Rothchild AC, Jahn AN, Mai D, Duffy FJ, et al. Contained *Mycobacterium tuberculosis* infection induces concomitant and heterologous protection. *PloS Pathog*. (2020) 16:e1008655. doi: 10.1371/journal.ppat.1008655

386. Ordonez AA, Tasneen R, Pokkali S, Xu Z, Converse PJ, Klunk MH, et al. Mouse model of pulmonary cavitary tuberculosis and expression of matrix metalloproteinase-9. *Dis Model Mech*. (2016) 9:779–88. doi: 10.1242/dmm.025643

387. Kramnik I, Beamer G. Mouse models of human TB pathology: Roles in the analysis of necrosis and the development of host-directed therapies. *Semin Immunopathol*. (2016) 38:221–37. doi: 10.1007/s00281-015-0538-9

388. Tsai MC, Chakravarty S, Zhu G, Xu J, Tanaka K, Koch C, et al. Characterization of the tuberculous granuloma in murine and human lungs: cellular composition and relative tissue oxygen tension. *Cell Microbiol*. (2006) 8:218–32. doi: 10.1111/j.1462-5822.2005.00612.x

389. Hoff DR, Ryan GJ, Driver ER, Ssemakulu CC, De Groote MA, Basaraba RJ, et al. Location of intra- and extracellular *M. tuberculosis* populations in lungs of mice and Guinea pigs during disease progression and after drug treatment. *PloS One*. (2011) 6:e17550. doi: 10.1371/journal.pone.0017550

390. Yan BS, Pichugin AV, Jobe O, Helming L, Eruslanov EB, Gutiérrez-Pabello JA, et al. Progression of pulmonary tuberculosis and efficiency of bacillus Calmette-Guérin vaccination are genetically controlled via a common sst1-mediated mechanism of innate immunity. *J Immunol*. (2007) 179:6919–32. doi: 10.4049/jimmunol.179.10.6919

391. Dooley KE, Phillips PP, Nahid P, Hoelscher M. Challenges in the clinical assessment of novel tuberculosis drugs. *Adv Drug Delivery Rev*. (2016) 102:116–22. doi: 10.1016/j.addr.2016.01.014

392. Lai R, Gong DN, Williams T, Ogunsola AF, Cavallo K, Lindestam Arlehamn CS, et al. Host genetic background is a barrier to broadly effective vaccine-mediated protection against tuberculosis. *J Clin Invest*. (2023) 133:e167762. doi: 10.1172/JCI167762

393. Bai X, Shang S, Henao-Tamayo M, Basaraba RJ, Ovrutsky AR, Matsuda JL, et al. Human IL-32 expression protects mice against a hypervirulent strain of *Mycobacterium tuberculosis*. *Proc Natl Acad Sci U.S.A*. (2015) 112:5111–6. doi: 10.1073/pnas.1424302112

394. Bai X, Kim SH, Azam T, McGibney MT, Huang H, Dinarello CA, et al. IL-32 is a host protective cytokine against *Mycobacterium tuberculosis* in differentiated THP-1 human macrophages. *J Immunol*. (2010) 184:3830–40. doi: 10.4049/jimmunol.0901913

395. Myllymäki H, Niskanen M, Oksanen KE, Rämet M. Animal models in tuberculosis research - where is the beef? *Expert Opin Drug Discovery*. (2015) 10:871–83. doi: 10.1517/17460441.2015.1049529

396. Lurie MB. Experimental epidemiology of tuberculosis: the effect of eliminating exposure of enteric infection on the incidence and course of tuberculosis acquired by normal Guinea pigs confined with tuberculous cage mates. *J Exp Med*. (1930) 51:753–68. doi: 10.1084/jem.51.5.753

397. Lurie MB. Experimental epidemiology of tuberculosis: airborne contagion of tuberculosis in an animal room. *J Exp Med*. (1930) 51:743–51. doi: 10.1084/jem.51.5.743

398. Clark S, Hall Y, Williams A. Animal models of tuberculosis: Guinea pigs. *Cold Spring Harb Perspect Med*. (2014) 5:a018572. doi: 10.1101/cshperspect.a018572

399. Smith DW, Harding GE. Animal model of human disease. Pulmonary tuberculosis. Animal model: Experimental airborne tuberculosis in the Guinea pig. *Am J Pathol*. (1977) 89:273–6.

400. Dharmadhikari AS, Basaraba RJ, van der Walt ML, Weyer K, Mphahlele M, Venter K, et al. Natural infection of Guinea pigs exposed to patients with highly drug-resistant tuberculosis. *Tuberculosis (Edinb)*. (2011) 91:329–38. doi: 10.1016/j.tube.2011.03.002

401. Padilla-Carlin DJ, McMurray DN, Hickey AJ. The Guinea pig as a model of infectious diseases. *Comp Med*. (2008) 58:324–40.

402. Kashino SS, Napolitano DR, Skobe Z, Campos-Neto A. Guinea pig model of *Mycobacterium tuberculosis* latent/dormant infection. *Microbes Infect*. (2008) 10:1469–76. doi: 10.1016/j.micinf.2008.08.010

403. Sugawara I, Udagawa T, Aoki T, Mizuno S. Establishment of a Guinea pig model of latent tuberculosis with GFP-introduced *Mycobacterium tuberculosis*. *Tohoku J Exp Med*. (2009) 219:257–62. doi: 10.1620/tjem.219.257

404. Shang S, Shanley CA, Caraway ML, Orme EA, Henao-Tamayo M, Hascall-Dove L, et al. Activities of TMC207, rifampin, and pyrazinamide against Mycobacterium tuberculosis infection in Guinea pigs. *Antimicrob Agents Chemother*. (2011) 55:124–31. doi: 10.1128/AAC.00978-10

405. Shang S, Shanley CA, Caraway ML, Orme EA, Henao-Tamayo M, Hascall-Dove L, et al. Drug treatment combined with BCG vaccination reduces disease reactivation in Guinea pigs infected with *Mycobacterium tuberculosis*. *Vaccines (Basel)*. (2012) 30:1572–82. doi: 10.1016/j.vaccine.2011.12.114

406. Brandt L, Skeiky YA, Alderson MR, Lobet Y, Dalemans W, Turner OC, et al. The protective effect of the *Mycobacterium bovis* BCG vaccine is increased by coadministration with the *Mycobacterium tuberculosis* 72-kilodalton fusion polyprotein Mtb72F in *M. tuberculosis*-infected Guinea pigs. *Infect Immun*. (2004) 72:6622–32. doi: 10.1128/IAI.72.11.6622-6632.2004

407. Smith DW, McMurray DN, Wiegeshaus EH, Grover AA, Harding GE. Host-parasite relationships in experimental airborne tuberculosis. IV. early events in the course of infection in vaccinated and nonvaccinated Guinea pigs. *Am Rev Respir Dis*. (1970) 102:937–49. doi: 10.1164/arrd.1970.102.6.937

408. Lenaerts AJ, Hoff D, Aly S, Ehlers S, Andries K, Cantarero L, et al. Location of persisting mycobacteria in a Guinea pig model of tuberculosis revealed by r207910. *Antimicrob Agents Chemother*. (2007) 51:3338–45. doi: 10.1128/AAC.00276-07

409. Baldwin SL, D'Souza C, Roberts AD, Kelly BP, Frank AA, Lui MA, et al. Evaluation of new vaccines in the mouse and Guinea pig model of tuberculosis. *Infect Immun*. (1998) 66:2951–9. doi: 10.1128/IAI.66.6.2951-2959.1998

410. Ordway DJ, Shanley CA, Caraway ML, Orme EA, Bucy DS, Hascall-Dove L, et al. Evaluation of standard chemotherapy in the Guinea pig model of tuberculosis. *Antimicrob Agents Chemother*. (2010) 54:1820–33. doi: 10.1128/AAC.01521-09

411. Tree JA, Smith S, Baker N, Clark S, Aldwell FE, Chambers M, et al. Method for assessing IFN-γ responses in Guinea pigs during TB vaccine trials. *Lett Appl Microbiol*. (2012) 55:295–300. doi: 10.1111/j.1472-765X.2012.03292.x

412. Jeevan A, Yoshimura T, Lee KE, McMurray DN. Differential expression of gamma interferon mRNA induced by attenuated and virulent *Mycobacterium tuberculosis* in Guinea pig cells after *Mycobacterium bovis* BCG vaccination. *Infect Immun*. (2003) 71:354–64. doi: 10.1128/IAI.71.1.354-364.2003

413. Jeevan A, Yoshimura T, Ly LH, Dirisala VR, McMurray DN. Cloning of Guinea pig IL-4: reduced IL-4 mRNA after vaccination or *Mycobacterium tuberculosis* infection. *Tuberculosis (Edinb)*. (2011) 91:47–56. doi: 10.1016/j.tube.2010.11.006

414. Dirisala VR, Jeevan A, Bix G, Yoshimura T, McMurray DN. Molecular cloning and expression of the IL-10 gene from Guinea pigs. *Gene*. (2012) 498:120–7. doi: 10.1016/j.gene.2012.01.076

415. Dirisala VR, Jeevan A, Ramasamy SK, McMurray DN. Molecular cloning, expression, and in silico structural analysis of Guinea pig IL-17. *Mol Biotechnol*. (2013) 55:277–87. doi: 10.1007/s12033-013-9679-z

416. Lurie MB. The fate of human and bovine tubercle bacilli in various organs of the rabbit. *J Exp Med*. (1928) 48:155–82. doi: 10.1084/jem.48.2.155

417. Lurie MB. Heredity, constitution and tuberculosis: an experimental study. *Am Rev Tuberc*. (1941) 44:1–125.

418. Lurie MB, Abramson S, Heppleston AG. On the response of genetically resistant and susceptible rabbits to the quantitative inhalation of human-type tubercle bacilli and the nature of resistance to tuberculosis. *J Exp Med*. (1952) 95:119–34. doi: 10.1084/jem.95.2.119

419. Acosta A, Norazmi MN, Hernandez-Pando R, Alvarez N, Borrero R, Infante JF, et al. The importance of animal models in tuberculosis vaccine development. *Malays J Med Sci*. (2011) 18:5–12.

420. Converse PJ, Dannenberg AM Jr., Estep JE, Sugisaki K, Abe Y, Schofield BH, et al. Cavitary tuberculosis produced in rabbits by aerosolized virulent tubercle bacilli. *Infect Immun*. (1996) 64:4776–87. doi: 10.1128/iai.64.11.4776-4787.1996

421. Converse PJ, Dannenberg AM Jr., Shigenaga T, McMurray DN, Phalen SW, Stanford JL, et al. Pulmonary bovine-type tuberculosis in rabbits: bacillary virulence, inhaled dose effects, tuberculin sensitivity, and Mycobacterium vaccae immunotherapy. *Clin Diagn Lab Immunol*. (1998) 5:871–81. doi: 10.1128/CDLI.5.6.871-881.1998

422. Dannenberg AM Jr. Liquefaction and cavity formation in pulmonary TB: A simple method in rabbit skin to test inhibitors. *Tuberculosis*. (2009) 89:243–7. doi: 10.1016/j.tube.2009.05.006

423. Dannenberg AM Jr. Perspectives on clinical and preclinical testing of new tuberculosis vaccines. *Clin Microbiol Rev*. (2010) 23:781–94. doi: 10.1128/CMR.00005-10

424. Manabe YC, Dannenberg AM Jr., Tyagi SK, Hatem CL, Yoder M, Woolwine SC, et al. Different strains of *Mycobacterium tuberculosis* cause various spectrums of disease in the rabbit model of tuberculosis. *Infect Immun*. (2003) 71:6004–11. doi: 10.1128/IAI.71.10.6004-6011.2003

425. Subbian S, Tsenova L, O'Brien P, Yang G, Kushner NL, Parsons S, et al. Spontaneous latency in a rabbit model of pulmonary tuberculosis. *Am J Pathol*. (2012) 181:1711–24. doi: 10.1016/j.ajpath.2012.07.019

426. Dannenberg AM Jr. Cellular hypersensitivity and cellular immunity in the pathogensis of tuberculosis: specificity, systemic and local nature, and associated macrophage enzymes. *Bacteriol Rev*. (1968) 32:85–102. doi: 10.1128/br.32.2.85-102.1968

427. Dannenberg AM Jr. Pathogenesis of tuberculosis: local and systemic immunity and cellular hypersensitivity. *Bull Int Union Tuberc*. (1970) 43:177–8.

428. Dannenberg AM Jr. Delayed-type hypersensitivity and cell-mediated immunity in the pathogenesis of tuberculosis. *Immunol Today*. (1991) 12:228–33. doi: 10.1016/0167-5699(91)90035-R

429. Mantilla Galindo A, Ocampo M, Patarroyo MA. Experimental models used in evaluating anti-tuberculosis vaccines: the latest advances in the field. *Expert Rev Vaccines*. (2019) 18:365–77. doi: 10.1080/14760584.2019.1583558

430. Dorman SE, Hatem CL, Tyagi S, Aird K, Lopez-Molina J, Pitt ML, et al. Susceptibility to tuberculosis: clues from studies with inbred and outbred New Zealand White rabbits. *Infect Immun*. (2004) 72:1700–5. doi: 10.1128/IAI.72.3.1700-1705.2004

431. Ihms EA, Urbanowski ME, Bishai WR. Diverse cavity types and evidence that mechanical action on the necrotic granuloma drives tuberculous cavitation. *Am J Pathol*. (2018) 188:1666–75. doi: 10.1016/j.ajpath.2018.04.006

432. Helke KL, Mankowski JL, Manabe YC. Animal models of cavitation in pulmonary tuberculosis. *Tuberculosis (Edinb)*. (2006) 86:337–48. doi: 10.1016/j.tube.2005.09.001

433. Leong FJ, Dartois V, Dick T. *A Color Atlas of Comparative Pathology of Pulmonary Tuberculosis*. Boca Raton, FL: CRC Press (2010).

434. Gong W, Liang Y, Wu X. Animal models of tuberculosis vaccine research: an important component in the fight against tuberculosis. *BioMed Res Int*. (2020) 2020:4263079. doi: 10.1155/2020/4263079

435. Gil O, Díaz I, Vilaplana C, Tapia G, Díaz J, Fort M, et al. Granuloma encapsulation is a key factor for containing tuberculosis infection in minipigs. *PloS One*. (2010) 5:e10030. doi: 10.1371/journal.pone.0010030

436. Ramos L, Obregon-Henao A, Henao-Tamayo M, Bowen R, Lunney JK, Gonzalez-Juarrero M. The minipig as an animal model to study *Mycobacterium tuberculosis* infection and natural transmission. *Tuberculosis (Edinb)*. (2017) 106:91–8. doi: 10.1016/j.tube.2017.07.003

437. de Val Pérez B, López-Soria S, Nofrarías M, Martín M, Vordermeier HM, Villarreal-Ramos B, et al. Experimental model of tuberculosis in the domestic goat after endobronchial infection with *Mycobacterium caprae*. *Clin Vaccine Immunol*. (2011) 18:1872–81. doi: 10.1128/CVI.05323-11

438. Wedlich N, Figl J, Liebler-Tenorio EM, Köhler H, von Pückler K, Rissmann M, et al. Video endoscopy-guided intrabronchial spray inoculation of *mycobacterium bovis* in goats and comparative assessment of lung lesions with various imaging methods. *Front Vet Sci*. (2022) 9:877322. doi: 10.3389/fvets.2022.877322

439. Roy A, Risalde MA, Casal C, Romero B, de Juan L, Menshawy AM, et al. Oral vaccination with heat-inactivated *mycobacterium bovis* does not interfere with the antemortem diagnostic techniques for tuberculosis in goats. *Front Vet Sci*. (2017) 4:124. doi: 10.3389/fvets.2017.00124

440. Arrieta-Villegas C, Perálvarez T, Vidal E, Puighibet Z, Moll X, Canturri A, et al. Efficacy of parenteral vaccination against tuberculosis with heat-inactivated *Mycobacterium bovis* in experimentally challenged goats. *PloS One*. (2018) 13:e0196948. doi: 10.1371/journal.pone.0196948

441. Webb GB, Williams WW. Immunity in tuberculosis. *J AMA October*. (1911) 28:1431.

442. Webb GB, Gilbert GB. Immunity in tuberculosis: Further experiments. *J AMA*. (1914) LXIII:1098–104. doi: 10.1001/jama.1914.02570130034009

443. Schmidt LH. Some observations on the utility of simian pulmonary tuberculosis in defining the therapeutic potentialities of isoniazid. *Am Rev Tuberc*. (1956) 74:138–53. doi: 10.1164/artpd.1956.74.2-2.138

444. Barclay WR, Anacker RL, Brehmer W, Leif W, Ribi E. Aerosol-induced tuberculosis in subhuman primates and the course of the disease after intravenous BCG vaccination. *Infect Immun*. (1970) 2:574–82. doi: 10.1128/iai.2.5.574-582.1970

445. Walsh GP, Tan EV, de la Cruz EC, Abalos RM, Villahermosa LG, Young LJ, et al. The Philippine cynomolgus monkey (*Macaca fasicularis*) provides a new nonhuman primate model of tuberculosis that resembles human disease. *Nat Med*. (1996) 2:430–6. doi: 10.1038/nm0496-430

446. Reed SG, Coler RN, Dalemans W, Tan EV, DeLa Cruz EC, Basaraba RJ, et al. Defined tuberculosis vaccine, Mtb72F/AS02A, evidence of protection in cynomolgus monkeys. *Proc Natl Acad Sci U.S.A*. (2009) 106:2301–6. doi: 10.1073/pnas.0712077106

447. Via LE, Weiner DM, Schimel D, Lin PL, Dayao E, Tankersley SL, et al. Differential virulence and disease progression following *Mycobacterium tuberculosis* complex infection of the common marmoset (*Callithrix jacchus*). *Infect Immun*. (2013) 81:2909–19. doi: 10.1128/IAI.00632-13

448. Bontrop RE, Otting N, de Groot NG, Doxiadis GG. Major histocompatibility complex class II polymorphisms in primates. *Immunol Rev*. (1999) 167:339–50. doi: 10.1111/j.1600-065X.1999.tb01403.x

449. Flynn JL, Tsenova L, Izzo A, Kaplan G. . Experimental animal models of tuberculosis. In: Kaufmann SHE, Britton WJ, editors. *Handbook of Tuberculosis: Immunology and Cell Biology*. Wiley-VCH, Weinheim (2008). p. 389–417.

450. Geluk A, Elferink DG, Slierendregt BL, van Meijgaarden KE, de Vries RR, Ottenhoff TH, et al. Evolutionary conservation of major histocompatibility complex-DR/peptide/T cell interactions in primates. *J Exp Med*. (1993) 177:979–87. doi: 10.1084/jem.177.4.979

451. Lin PL, Pawar S, Myers A, Pegu A, Fuhrman C, Reinhart TA, et al. Early events in *Mycobacterium tuberculosis* infection in cynomolgus macaques. *Infect Immun*. (2006) 74:3790–803. doi: 10.1128/IAI.00064-06

452. Lin PL, Rodgers M, Smith L, Bigbee M, Myers A, Bigbee C, et al. Quantitative comparison of active and latent tuberculosis in the cynomolgus macaque model. *Infect Immun*. (2009) 77:4631–42. doi: 10.1128/IAI.00592-09

453. McLeay SC, Morrish GA, Kirkpatrick CM, Green B. The relationship between drug clearance and body size: systematic review and meta-analysis of the literature published from 2000 to 2007. *Clin Pharmacokinet*. (2012) 51:319–30. doi: 10.2165/11598930-000000000-00000

454. McShane H, Williams A. A review of preclinical animal models utilised for TB vaccine evaluation in the context of recent human efficacy data. *Tuberculosis (Edinb)*. (2014) 94:105–10. doi: 10.1016/j.tube.2013.11.003

455. Qiu CL, Yang GB, Yu K, Li Y, Li XL, Liu Q, et al. Characterization of the major histocompatibility complex class II DQB (MhcMamu-DQB1) alleles in a cohort of Chinese rhesus macaques (*Macaca mulatta*). *Hum Immunol*. (2008) 69:513–21. doi: 10.1016/j.humimm.2008.05.014

456. Scanga CA, Flynn JL. Modeling tuberculosis in nonhuman primates. *Cold Spring Harb Perspect Med*. (2014) 4:a018564. doi: 10.1101/cshperspect.a018564

457. Sharpe SA, McShane H, Dennis MJ, Basaraba RJ, Gleeson F, Hall G, et al. Establishment of an aerosol challenge model of tuberculosis in rhesus macaques and an evaluation of endpoints for vaccine testing. *Clin Vaccine Immunol*. (2010) 17:1170–82. doi: 10.1128/CVI.00079-10

458. Verreck FA, Vervenne RA, Kondova I, van Kralingen KW, Remarque EJ, Braskamp G, et al. MVA.85A boosting of BCG and an attenuated, phoP deficient *M. tuberculosis* vaccine both show protective efficacy against tuberculosis in rhesus macaques. *PloS One*. (2009) 4:e5264. doi: 10.1371/journal.pone.0005264

459. Lewinsohn DM, Tydeman IS, Frieder M, Grotzke JE, Lines RA, Ahmed S, et al. High resolution radiographic and fine immunologic definition of TB disease progression in the rhesus macaque. *Microbes Infect*. (2006) 8:2587–98. doi: 10.1016/j.micinf.2006.07.007

460. Rayner EL, Pearson GR, Hall GA, Basaraba RJ, Gleeson F, McIntyre A, et al. Early lesions following aerosol infection of rhesus macaques (*Macaca mulatta*) with *Mycobacterium tuberculosis* strain H37RV. *J Comp Pathol*. (2013) 149:475–85. doi: 10.1016/j.jcpa.2013.05.005

461. Bekara Mel A, Courcoul A, Bénet JJ, Durand B. Modeling tuberculosis dynamics, detection and control in cattle herds. *PloS One*. (2014) 9:e108584. doi: 10.1371/journal.pone.0108584

462. Sabio Y García J, Bigi MM, Klepp LI, García EA, Blanco FC, Bigi F. Does *Mycobacterium bovis* persist in cattle in a non-replicative latent state as *Mycobacterium tuberculosis* in human beings? *Vet Microbiol*. (2020) 247:108758. doi: 10.1016/j.vetmic.2020.108758

463. Cassidy JP. The pathogenesis and pathology of bovine tuberculosis with insights from studies of tuberculosis in humans and laboratory animal models. *Vet Microbiol*. (2006) 112:151–61. doi: 10.1016/j.vetmic.2005.11.031

464. Capparelli R, De Chiara F, Nocerino N, Medaglia C, Di Costanzo R, Ramunno L, et al. Heterozygosity at the A625C polymorphic site of the *MyD88* gene is associated with *Mycobacterium bovis* infection in cattle. *Infect Immun*. (2013) 81:2139–44. doi: 10.1128/IAI.01398-12

465. Neill SD, Cassidy J, Hanna J, Mackie DP, Pollock JM, Clements A, et al. Detection of *Mycobacterium bovis* infection in skin test-negative cattle with an assay for bovine interferon-gamma. *Vet Rec*. (1994) 135:134–5. doi: 10.1136/vr.135.6.134

466. Ong BL, Ngeow YF, Razak MF, Yakubu Y, Zakaria Z, Mutalib AR, et al. Tuberculosis in captive Asian elephants (*Elephas maximus*) in Peninsular Malaysia. *Epidemiol Infect*. (2013) 141:1481–7. doi: 10.1017/S0950268813000265

467. Lyashchenko KP, Greenwald R, Esfandiari J, Olsen JH, Ball R, Dumonceaux G, et al. Tuberculosis in elephants: antibody responses to defined antigens of Mycobacterium tuberculosis, potential for early diagnosis, and monitoring of treatment. *Clin Vaccine Immunol*. (2006) 13:722–32. doi: 10.1128/CVI.00133-06

468. Parikka M, Hammaren MM, Harjula SK, Halfpenny NJ, Oksanen KE, Lahtinen MJ, et al. *Mycobacterium marinum* causes a latent infection that can be reactivated by gamma irradiation in adult zebrafish. *PloS Pathog*. (2012) 8:e1002944. doi: 10.1371/journal.ppat.1002944

469. van der Sar AM, Abdallah AM, Sparrius M, Reinders E, Vandenbroucke-Grauls CM, Bitter W. *Mycobacterium marinum* strains can be divided into two distinct types based on genetic diversity and virulence. *Infect Immun*. (2004) 72:6306–12. doi: 10.1128/IAI.72.11.6306-6312.2004

470. Major S, Turner J, Beamer G. Tuberculosis in CBA/J mice. *Vet Pathol*. (2013) 50:1016–21. doi: 10.1177/0300985813482952

471. Kato-Maeda M, Shanley CA, Ackart D, Jarlsberg LGS, Shang S, Obregon-Henao A, et al. Beijing sublineages of *Mycobacterium tuberculosis* differ in pathogenicity in the Guinea pig. *Clin Vaccine Immunol*. (2012) 19:1227–37. doi: 10.1128/CVI.00250-12

472. Larenas-Muñoz F, Ruedas-Torres I, Hunter L, Bird A, Agulló-Ros I, Winsbury R, et al. Characterisation and development of histopathological lesions in a Guinea pig model of *Mycobacterium tuberculosis* infection. *Front Vet Sci*. (2023) 10:1264200. doi: 10.3389/fvets.2023.1264200

473. Willis HS, Woodruff CE. Tuberculosis in allergic and desensitized Guinea pigs: A study of histological changes. *Am J Pathol*. (1938) 14:337–46.

474. Jassal MS, Nedeltchev GG, Osborne J, Bishai WR. A modified scoring system to describe gross pathology in the rabbit model of tuberculosis. *BMC Microbiol*. (2011) 11:49. doi: 10.1186/1471-2180-11-49

475. Manabe YC, Kesavan AK, Lopez-Molina J, Hatem CL, Brooks M, Fujiwara R, et al. The aerosol rabbit model of TB latency, reactivation and immune reconstitution inflammatory syndrome. *Tuberculosis (Edinb)*. (2008) 88:187–96. doi: 10.1016/j.tube.2007.10.006

476. Gonzalez-Juarrero M, Bosco-Lauth A, Podell B, Soffler C, Brooks E, Izzo A, et al. Experimental aerosol *Mycobacterium bovis* model of infection in goats. *Tuberculosis (Edinb)*. (2013) 93:558–64. doi: 10.1016/j.tube.2013.05.006

477. Sanchez J, Tomás L, Ortega N, Buendía AJ, del Rio L, Salinas J, et al. Microscopical and immunological features of tuberculoid granulomata and cavitary pulmonary tuberculosis in naturally infected goats. *J Comp Pathol*. (2011) 145:107–17. doi: 10.1016/j.jcpa.2010.12.006

478. Gutiérrez M, García Marín JF. *Cryptococcus neoformans* and *Mycobacterium bovis* causing granulomatous pneumonia in a goat. *Vet Pathol*. (1999) 36:445–8. doi: 10.1354/vp.36-5-445

479. Liebler-Tenorio EM, Heyl J, Wedlich N, Figl J, Köhler H, Krishnamoorthy G, et al. Vaccine-induced subcutaneous granulomas in goats reflect differences in host-mycobacterium interactions between BCG- and recombinant BCG-derivative vaccines. *Int J Mol Sci*. (2022) 23:10992. doi: 10.3390/ijms231910992

480. Mehra S, Golden NA, Dutta NK, Midkiff CC, Alvarez X, Doyle LA, et al. Reactivation of latent tuberculosis in rhesus macaques by coinfection with simian immunodeficiency virus. *J Med Primatol*. (2011) 40:233–43. doi: 10.1111/j.1600-0684.2011.00485.x

481. Langermans JA, Andersen P, van Soolingen D, Vervenne RA, Frost PA, van der Laan T, et al. Divergent effect of bacillus Calmette-Guérin (BCG) vaccination on *Mycobacterium tuberculosis* infection in highly related macaque species: implications for primate models in tuberculosis vaccine research. *Proc Natl Acad Sci USA*. (2001) 98:11497–502. doi: 10.1073/pnas.201404898

482. Darrah PA, Zeppa JJ, Maiello P, Hackney JA, Wadsworth MH2nd., Hughes TK, et al. Prevention of tuberculosis in macaques after intravenous BCG immunization. *Nature*. (2020) 577:95–102. doi: 10.1038/s41586-019-1817-8

483. Pereira AHB, Lopes CAA, Pissinatti TA, Pinto ACA, Oliveira DRA, Leal GM, et al. Pulmonary granuloma is not always the tuberculosis hallmark: pathology of tuberculosis stages in new world and old world monkeys naturally infected with the *mycobacterium tuberculosis* complex. *J Comp Pathol*. (2022) 199:55–74. doi: 10.1016/j.jcpa.2022.09.011

484. Roodgar M, Ross CT, Tarara R, Lowenstine L, Dandekar S, Smith DG. Gene expression and TB pathogenesis in rhesus macaques: TR4, CD40, CD40L, FAS (CD95), and TNF are host genetic markers in peripheral blood mononuclear cells that are associated with severity of TB lesions. *Infect Genet Evol*. (2015) 36:396–409. doi: 10.1016/j.meegid.2015.10.010

485. Nogueira I, Català M, White AD, Sharpe SA, Bechini J, Prats C, et al. Surveillance of daughter micronodule formation is a key factor for vaccine evaluation using experimental infection models of tuberculosis in macaques. *Pathogens*. (2023) 12:236. doi: 10.3390/pathogens12020236

486. Beites T, O'Brien K, Tiwari D, Engelhart CA, Walters S, Andrews J, et al. Plasticity of the *Mycobacterium tuberculosis* respiratory chain and its impact on tuberculosis drug development. *Nat Commun*. (2019) 10:4970. doi: 10.1038/s41467-019-12956-2

487. Flynn JL, Gideon HP, Mattila JT, Lin PL. Immunology studies in non-human primate models of tuberculosis. *Immunol Rev*. (2015) 264:60–73. doi: 10.1111/imr.2015.264.issue-1

488. Hunter L, Hingley-Wilson S, Stewart GR, Sharpe SA, Salguero FJ. Dynamics of macrophage, T and B cell infiltration within pulmonary granulomas induced by *mycobacterium tuberculosis* in two non-human primate models of aerosol infection. *Front Immunol*. (2022) 12:776913. doi: 10.3389/fimmu.2021.776913

frontiers | Frontiers in Immunology

TYPE Review
PUBLISHED 20 January 2025
DOI 10.3389/fimmu.2024.1439434



OPEN ACCESS

EDITED BY
Enrique Hernandez-Lemus,
National Institute of Genomic Medicine (INMEGEN), Mexico

REVIEWED BY
C Gopi Mohan FRSC,
Amrita Vishwa Vidyapeetham University, India
Guillermo De Anda Jáuregui,
National Institute of Genomic Medicine (INMEGEN), Mexico

*CORRESPONDENCE
Douaa Mugahid
dmugahid@hsph.harvard.edu

RECEIVED 27 May 2024
ACCEPTED 17 December 2024
PUBLISHED 20 January 2025

CITATION
Mugahid D, Lyon J, Demurjian C, Eolin N, Whittaker C, Godek M, Lauffenburger D, Fortune S and Levine S (2025) A practical guide to FAIR data management in the age of multi-OMICS and AI. *Front. Immunol.* 15:1439434. doi: 10.3389/fimmu.2024.1439434



# A practical guide to FAIR data management in the age of multi-OMICS and AI

Douaa Mugahid[1]*, Jared Lyon[2], Charlie Demurjian[2], Nathan Eolin[2], Charlie Whittaker[2], Mark Godek[3], Douglas Lauffenburger[4], Sarah Fortune[1] and Stuart Levine[2]

[1]Department of Immunology and Infectious Diseases, T.H. Chan School of Public Health, Harvard University, Boston, MA, United States, [2]BioMicro Center, Massachusetts Institute of Technology, Cambridge, MA, United States, [3]Ragon Institute of Massachusetts General Hospital (MGH), Massachusetts Institute of Technology (MIT), and Harvard, Cambridge, MA, United States, [4]Department of Biological Engineering, Massachusetts Institute of Technology, Cambridge, MA, United States

Multi-cellular biological systems, including the immune system, are highly complex, dynamic, and adaptable. Systems biologists aim to understand such complexity at a quantitative level. However, these ambitious efforts are often limited by access to a variety of high-density intra-, extra- and multi-cellular measurements resolved in time and space and across a variety of perturbations. The advent of automation, OMICs and single-cell technologies now allows high dimensional multi-modal data acquisition from the same biological samples multiplexed at scale (multi-OMICs). As a result, systems biologists -theoretically- have access to more data than ever. However, the mathematical frameworks and computational tools needed to analyze and interpret such data are often still nascent, limiting the biological insights that can be obtained without years of computational method development and validation. More pressingly, much of the data sits in silos in formats that are incomprehensible to other scientists or machines limiting its value to the vaster scientific community, especially the computational biologists tasked with analyzing these vast amounts of data in more nuanced ways. With the rapid development and increasing interest in using artificial intelligence (AI) for the life sciences, improving how biologic data is organized and shared is more pressing than ever for scientific progress. Here, we outline a practical approach to multi-modal data management and FAIR sharing, which are in line with the latest US and EU funders' data sharing policies. This framework can help extend the longevity and utility of data by allowing facile use and reuse, accelerating scientific discovery in the biomedical sciences.

KEYWORDS

**FAIR data, systems biology, immunology, OMICs, multi-modal data, artificial intelligence, modeling, Science administration**

# Introduction

Data powers our understanding of the world around us. As the world becomes fully digitized and technology continues to develop, researchers' ability to gather different types of measurements at scale is only increasing, making the adoption of Data Science principles across all disciplines increasingly necessary. This is particularly true in biomedical research, where the race to understand the basis of life and human disease has encouraged researchers to push the boundaries of method development for decades. Most notably, the advent of high-throughput technologies such as high-content imaging, multi-parameter flow cytometry/CyToF, microarrays, next generation sequencing, and mass spectrometry has transformed biologic research into a rich multi-modal data science.

The increase in scale across the research enterprise requires careful experimental design as well as the development of novel statistical and mathematical frameworks that can help researchers synthesize all this data into meaningful, and occasionally non-intuitive biological insights. We collectively refer to these frameworks as artificial intelligence (AI). Practically, this necessitates making the data accessible and interpretable to other researchers as well as machines in ways that allow it to be used for applications beyond its original intent. In the case of human studies, this also requires deliberate efforts to ensure the data is representative of human diversity and is well-guarded to protect individuals' privacy and rights. Only then can society fully benefit from the richness and complexity of the data needed to enable AI-driven advances in the biomedical field for the benefit of all.

A term commonly used to refer to good data stewardship in the life sciences is FAIR data sharing (1). The term is an acronym for data that is findable, accessible, interoperable, and reusable, all features that extend the usability of data beyond the purposes it was generated for, thereby increasing its long-term impact. Here, we outline practical steps towards FAIR data-sharing practices that can improve the longevity and utility of biomedical data. The principles are applicable to any field in the Life Sciences.

# Why share data

Before ChatGPT made conversations about AI, multi-modal data, data and computational bias so mainstream (2, 3) the biomedical field had its taste of AI's enabling potential, yet relatively little light was shed on the central role community-wide data curation and sharing played in enabling these biomedical breakthroughs. We discuss two prominent examples below.

## AlphaFold

In the case of AlphaFold (4), which won its developers the Lasker Award in 2023 (5) and Nobel Prize in 2024 (6), years of researchers publicly depositing experimentally determined protein structures and genomic sequences was fundamental to training the underlying model (4). These data resided in public databases such as UniRef90 (7), BFD (8), Uniclust30 (9), MGnify clusters (10),and the Protein Data Bank (PDB) (11) which house some of the world's largest collections of biologic sequences and structures, respectively. Since models are only as good as the data they were trained on, it is no surprise that proteins poorly predicted by AlphaFold are often classes that are underrepresented in nature either because they lack homologues such as orphan proteins (12), or because they are highly variable such as antibodies (13). Since its release, over a million AlphaFold predicted protein structures have been shared in the public domain (14), including the proteins of bacteria rapidly developing antibiotic resistance, thereby posing an urgent threat to global health. The entirety of the AlphaFold model is also available publicly for others to explore and expand (15), which has enabled researchers to adopt it for their use-case of choice expanding its impact even further (16). Without publicly deposited data the development of AlphaFold would not have been possible, neither would much of the science enabled by it.

## NextStrain

As part of the global COVID19 response researchers worldwide rushed to sequence and share the SARS-CoV2 genomes they isolated. SARS-CoV2 genomic sequences were centralized in a repository called NextStrain (17), which also provided researchers the world over with tools that allowed tracking mutations in the viral genome, some of which threatened to be associated with changes in transmissibility, virulence, and/or clinical presentation thereby informing public health responses (18–21). Other researchers got straight to developing vaccines against the devastating virus (22). NextStrain's developers' focus on data and code sharing was central to its broad utility during the COVID19 pandemic, which was accompanied by an exponential increase in the number of citations from 19 in 2018 to over 2500 citations by May 2024. Its user-friendliness and transparency likely played a role in it featuring in several policy reports (18, 19, 21).

These two examples demonstrate how data and code sharing is fundamental to driving impactful scientific advances in the digital age. Both efforts required the development of globally accessible platforms that allowed the sharing of important, standardized biomedical data at scale. This enabled others to develop computational methods that could crunch through the massive volumes of data thereby providing more researchers with usable information on which to build. As more types of data are standardized and shared, we can only begin to imagine the scope and impact of future breakthroughs.

## The shifts in funding agency requirements

While the utility of sharing SARS-CoV2 genomic data was likely obvious to many, it is difficult to imagine that the developers of PDB or NCBI predicted the development of AlphaFold. It's even more difficult to believe that every researcher depositing their protein

structures since 1971 or sequences since 1982 understood they would be individual contributors to such a development many years down the line. Even if they did, it is no secret that the current scientific eco-system lacks a short-term mechanism for rewarding raw data sharing, which is a time-consuming and laborious process many researchers find unpleasant.

Incentive systems that reward data sharing are still under development but should be possible with the popularization of digital object identifiers (DOIs) (23), which allows users to uniquely cite papers as well as code and data in the digital sphere. In the meantime, science policy makers and funders seeking to maximize return on their and/or the public's investment in basic research have resorted to mandating data sharing. In the absence of clear mechanisms for accountability much of the enforcement currently falls to publishers. As a result, the emerging practice is for researchers to only share positive data or data that is included in a publication which means a lot of data remains unaccounted for. Another important implication is that AI algorithms are being trained disproportionately on positive data which will affect their performance and generalizability (24). That said, enforcement at publication has served science well and is arguably one of the main reasons PDB is now populated with close to 200,000 experimentally validated protein structures. Among the funders now encouraging data and code deposition are the NIH (25) and NSF (26) which are currently updating their policies following mandates from the Whitehouse Office of Science and Technology (27), as well as philanthropic organizations such as the Bill and Melinda Gates Foundation (28), and the Chan Zuckerberg Initiative (29) in the USA. In Europe, the Wellcome Trust (30) and Horizon Europe (31) mandate FAIR data sharing whenever possible.

## Key elements for responsible data use and informed reuse

### Rich metadata provides necessary context

Experimental data are most reusable when associated with rich metadata, often referred to as data about data, that help future users interpret and differentiate between data sets and individual data points. Imagine a set of hand-made Russian dolls. The smallest doll (the dataset) is nested within other dolls (the layers of metadata collected at each experimental step leading up to the data). Being hand-made, the innermost doll from a single set is made to fit the outer dolls perfectly, but might not fit within another set of Russian dolls, even if they were made by the same craftsperson, and even less so if made by another. If the craftsperson were to share the dimensions of each of the dolls, however, they could help others predict which inner dolls are combinable between sets (Figure 1). The more detailed and understandable the dimensions, the better the predicted fit, thus the need for rich and standardized metadata. In a research setting, capturing rich and understandable metadata is useful not only for researchers in the same lab, but also when re-used by others once the data is in the public domain, and is key to interoperability. Technical and biological confounders can often skew the interpretation of data and can only be accounted for if they are reported as part of the original study. This practice minimizes the chances that others will re-use the data under false assumptions leading to the generation of poorly informed hypotheses. The result is an avoidable loss of time, energy, and resources of many chasing the wrong ideas. More importantly, this contributes to the safe and cost-effective development of safer medicines for patients if such data is ever to be used in that context.

As an example, consider DNA sequencing data from a series of different tissue biopsies from a non-human primate. Each raw sequencing file is linked to a DNA library, prepared from a tissue, extracted from an animal. At the time the animal is taken into a study, it's important to assign it a unique identifier, and document its age, sex, species and geographical origins, any interventions it underwent and when, as well as the organ from which the sample was extracted, plus the time and method of extraction. Each biopsy should also receive a unique identifier and be linked to the parent animal. Similarly, the DNA library should also receive a unique identifier and be linked to the biopsy from which it was prepared, together with information about the DNA extraction kit/process (eg: the thermocycler used, the number of amplification cycles, the temperature at each step, and the sequencing primers). Finally, it's also important to note which samples were multiplexed on which chip (which should also have unique identifiers), the sequencer used, read length, and sequencing depth. If a plate-based fluorescence assay was done on cells from the same tissue, which sample was in which well, what was the analyte, antibody, and fluorophore, which plate reader was used, on which day, and what were the excitation and emission spectra. Much of this information can be captured in independent tables that serve as templates for researchers at every experimental step and can later be linked together as a set of relational databases, a simple but elegant and well-established solution in Data Science, that ensures full data provenance for single or multi-modal datasets from the same experiment. The metadata can then be shared in the public domain making the associated data truly FAIR (Figure 1).

Historically, a lot of this metadata would simply be described to various degrees of thoroughness throughout a paper, but not directly linked to a particular raw or analyzed data file. While this practice might have been sufficient to interpret one small dataset at a time, it no longer serves biology well today, and adds uncertainty where it need not exist. That is especially true when combining different datatypes within a study (vertical or multi-modal data integration; Figure 2) or across studies (horizontal integration), where the statistical uncertainty associated with data from tissues from the same animal would be different from that from different animals or studies even if the animals were treated similarly.

Open-source data management systems can be found in NextSEEK (32) which allows public metadata sharing on FAIRDOMHub (33), or the Open Science Framework (34), though the latter is currently more suited for the social sciences. A similar, but more powerful alternative is Fairspace (35) provided commercially by The Hyve which supports the cancer research community's c-Bioportal (36, 37). In principle, metadata collected as part of standard electronic notebook keeping can be easily exported when and where needed, facilitating FAIR data sharing through any of these systems.

10.3389/fimmu.2024.1439434

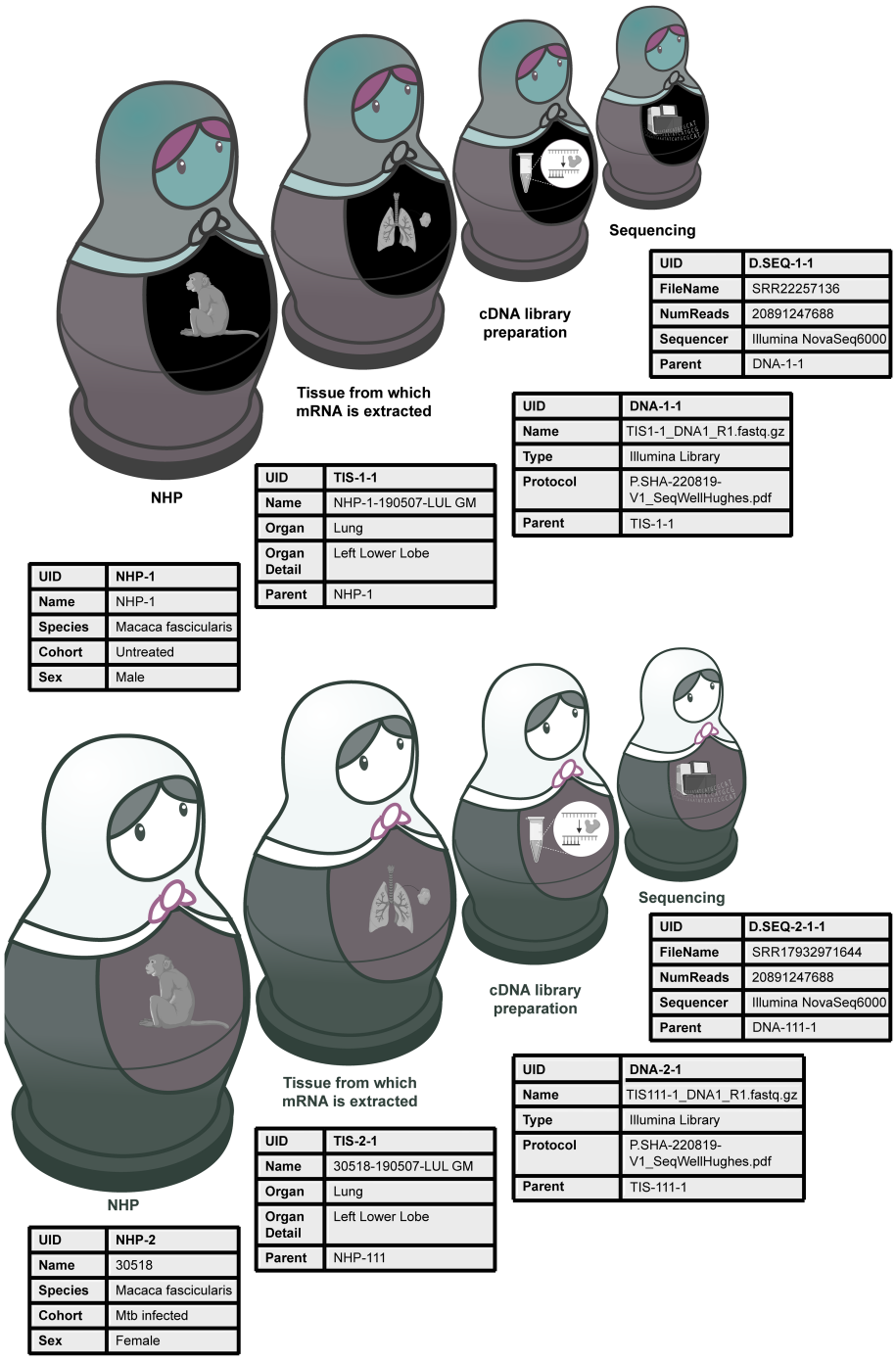


FIGURE 1
Relational databases help link metadata from multi-step experiments. Relational databases are similar to Russian dolls, nested in a particular order. They allow researchers to capture metadata at every experimental step. For example, linking sequencing data to the cDNA library, tissue (lung biopsy) and animal (non-human primate, NHP) from which it came from. The metadata for the two different sequencing files helps future users realize that the main difference between the sequenced samples is that they come from different animals that vary by sex and treatments, despite being from the same species.

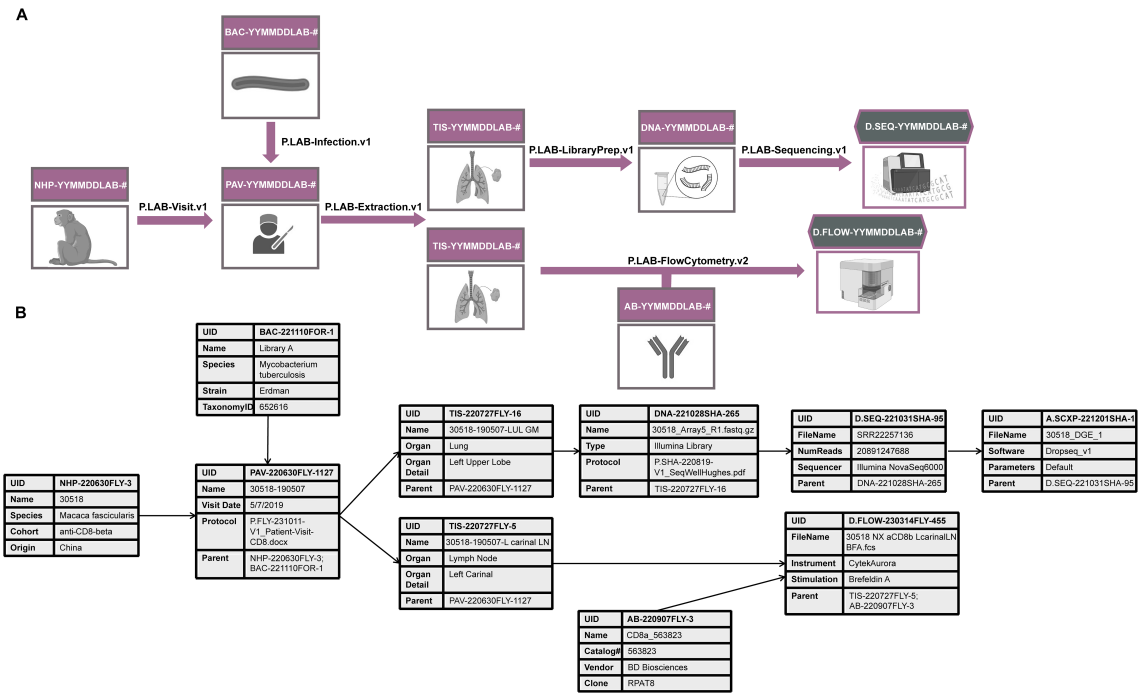


FIGURE 2
An example of how relational databases can be used to collect metadata for multi-modal data generation. **(A)** An experiment in which a lung biopsy (TIS) from a non-human primate (NHP) infected with Mycobacterium tuberculosis (BAC) is sequenced (D.SEQ) and analyzed by flow cytometry (D.Flow). DNA refers to the cDNA library sent for sequencing, AB refers to the antibody used in the flow cytometry analysis. The experimental protocol describing how each step was conducted is captured in a file denoted with a "P." suffix and referenced in the Protocol metadata field. **(B)** An example of some metadata fields to be collected in association with each step of the research process. These fields are by no means comprehensive. Find more detailed metadata fields for a similar experiment at https://fairdomhub.org/studies/1134.

## Standardization enables interoperability

Data integration has long been the focus of computational biologists, to various degrees of success (38–40) in part -some argue- because of a combination of poor data quality, experimental design and metadata availability (41–43). With the continuous increase in integratable data modalities of relevance to systems immunology, it is more important than ever to standardize how metadata is collected within and across experiments, and harmonize the vocabularies used for annotation. Unfortunately, this is no easy task. Agreeing on metadata standards for a new data type or experimental format often involves hours of discussion between experimental and computational biologists and should happen before data collection begins to avoid discrepancies down the line. This is especially true in the case of nascent technologies and requires an ability to foresee potential uses beyond what the data were originally planned for. Doing this on a field-wide level is even more challenging and requires strong vision and leadership.

For popular data types, specialist repositories often exist and some enforce the use of common data elements (44) (CDEs; pre-defined variables and acceptable values). However, these CDE are often different between repositories which makes vertical integration difficult and is further complicated by the fact that many siloed repositories offer no inherent way to link data from the same samples. This is also true in the case of inherently multi-modal measurements such as sequencing-based spatial transcriptomic technologies, which rely on a complementary set of sequencing and imaging data (45). In such cases, and in the absence of a repository for multi-modal data, the imaging data would be stored in one repository and the sequencing data in another, and would need to be linked through a public-facing database such as FAIRDOMHub (33) to be of future use (See Table 1 for examples of existing repositories for spatial transcriptomic data). Furthermore, the metadata collected by repositories is often too sparse for meaningful analysis as they tend to focus on capturing common points of variation across experiments and not much of the nuance. Generalist repositories, being data agnostic by design, are even less suited for standardized metadata collection. Thus, it is left to depositors to decide what they think is important metadata to share, and to future users to harmonize across datasets which can be very difficult without prior standardization or the release of good dictionaries with every dataset.

Data dictionaries clearly define each field as well as their possible values such that they are comprehensible to someone who was not part of the original study or is new to the field. It also facilitates standardization, which is why CDEs (44) are broadly useful. As an example, species could always be referred to by their NCBI Taxonomical ID and Latin name (73), their geographical origins by ISO 3166 codes (74), proteins by their Uniport ID (75), and antibodies by their company of source plus catalogue number, epitope, and conjugate. To avoid reinventing the wheel, researchers should reach for CDEs and standardized vocabularies in the public domain and share the ones they develop publicly for the benefit of others.

## Curation ensures data trustworthiness

Depending on the resources available, data sharing done well can be a time and labor-intensive process involving several people, especially when using infrastructure that is not built-for-purpose. Thus, it is important for researchers to focus on sharing high-quality (well annotated and from well-designed experiments) irrespective of whether their own analysis of the data supports their original hypotheses. This should be done with an eye towards enhancing reproducibility, but also the reuse of data for mechanistic modeling, machine learning (ML) and deep learning (DL) applications, which will undoubtedly increase the impact of the data on the long-term. As mentioned above, curated data should include both negative and positive data to avoid biased training datasets that do not allow the development of models that are broadly generalizable. If time is tight, researchers should prioritize multiplexed datasets (multi-parameter flow cytometry/CyToF, high-throughput sequencing of all kinds, mass spectrometry, high volume imaging data, array-based data, cytokine panels, systems serology data to name a few), which are most useful for data hungry ML/DL applications, as well as data acquired from experiments that are difficult to reproduce without an abundance of resources or access to highly specialized infrastructure.

# Code, model and parameter sharing facilitate reproducibility, interpretation, and informed reanalysis and meta analyses

Also important for reproducibility, integration, and the informed interpretation of analyzed data is capturing the complexity of data processing and computational analyses occurring post-generation of raw data. Unlike classical statistical tests familiar to many biologists [eg: the parametric and non-parametric tests pre-programmed in many available software suites such as Excel (76), Google Sheets (77), and GraphPad Prism (78)], many OMICs and most multi-OMIC analyses are far from standardized. Furthermore, compute environment, the choice of software, software version, and user-defined parameters can significantly affect the final output (1). For these reasons, researchers need to precisely document and share all aspects of a workflow including the code (including version number if using a publicly available package) and exact parameters used to analyze a particular dataset, with clear descriptions of any non-standard steps maybe as comments between blocks of code. This can be accomplished in a variety of ways but is greatly facilitated by the use of community workflows such as nf-core (79), containerized compute environments like Docker (80) and Singularity/Apptainer (81) shared in container repositories like DockerHub (82). Also useful are package and environment managers such as Bioconda (83). Jupyter (84) or Rstudio (85) notebooks shared and managed in code repositories such as Github (86) provide a method for sharing both standard and custom analyses, though this practice does not guarantee reproducibility across computing environments since Github does not enforce rigorous testing to ensure deposited packages are performant.

Researchers should also share their trained models given how time and computationally intensive this can be, in addition to the data on which they were trained to ensure full transparency and inform users' understanding of sources of bias or underperformance. Parameterized mechanistic models can be shared on BioModels (87), while their machine and deep learning equivalents can be shared and deployed on Hugging Face (88).

# Resources that enable good FAIR data stewardship

## Infrastructure

To support FAIR data practices institutions must facilitate accurate data and metadata collection with little time and effort on researchers' side. Research institutions and funders also need to account for the increasing specialization that necessitates collaboration between labs. To enable that, there is a need for a radical change in infrastructure to support an evolution to the "decentralized digital Lab with a human in the loop". In this model, laboratory infrastructure is set up such that data acquisition and import is largely automated within and between labs with the proper agreements in place, meaning scientists spend less time generating and managing data and more time curating and analyzing it. The first step towards that has been a slow-to-start but accelerating shift from paper to electronic lab notebooks (ELNs), catalyzed by the evolution of user-friendly digital platforms such as Benchling (89). Benchling's cloud-based ELN system now allows independent users anywhere in the world to share experimental templates, as well as track reagents, samples, and data through a shared registry, while linking these features through a set of relational databases ensuring data provenance is continuous and available to all who have access. Add to that the addition of features that allow the integration of lab instruments such that the data coming off them can be directly stored in the cloud, and the effort of moving data, linking to metadata, and -eventually- sharing no longer seems as daunting. Other providers such as L7 informatics are catching up (90). With more players in the Digital Lab eco-system the future of FAIR data sharing is looking promising (Figure 3). Quite importantly, this also facilitates data interpretation and saves research teams hours of lengthy discussion about how data was generated and handled.

Dedicated cloud computing platforms for biology are also emerging to compliment the shift to data-intense, decentralized and collaborative life science research, including Cirro (of the Fred Hutchinson Institute) (91), DNANexus (a techbio start up) (92), LatchBio (a techbio start up) (93), Terra (of the Broad Institute) (94), and L7 Informatics (also a techbio start up) (90). These platforms allow researchers to run complex analysis workflows in the cloud but in a more user-friendly environment than what's offered directly by cloud providers and are customized to biologists' needs. With the data already in the cloud, running such analyses is now possible without the need to duplicate and shuffle around large volumes of data between collaborators, and -in principle- facilitates analyses that respect institutional and national data governance requirements. Cloud providers vow they take data security seriously, and the likes of the NHS, FDA and NIH are beginning to trust them with data for

TABLE 1 Key data repositories useful for systems immunology.

| *Data Type* | Repository | Key Features | Number of datasets as of May 2024 | Date of establishment |
|---|---|---|---|---|
| Mass spectrometry (MS)-based Proteomics | PRIDE: PRoteomics IDEntifications Database (46) (https://www.ebi.ac.uk/pride/) | Direct submission allowed, data visualization and annotation tools. | 26847 | 2005 |
| | MassIVE (47) (https://massive.ucsd.edu/) | Direct submission allowed, data analysis tools. | 15,231 | N/A |
| | PeptideAtlas (48) (https://peptideatlas.org/) | Curated database, no data analysis tools. | N/A | 2006 |
| | Panorma (49) (https://panoramaweb.org/) | Data from targeted proteomics experiments, direct submissions allowed, tools for designing and analyzing targeted proteomics experiments. | 596 | 2014 |
| | iProX (50) (https://www.iprox.cn/) | Direct submission allowed, no data analysis tools. | 4792 Projects (3602 Public Projects) | 2019 |
| | JPOST (51) (https://repository.jpostdb.org/) | Direct submission allowed, no data analysis tools. | 2671 projects | 2017 |
| MS-based Metabolomics | MetaboLights (52) (https://www.ebi.ac.uk/metabolights) | Direct submission allowed, no data analysis tools | 1496 | 2012 |
| | National Metabolomics Data Repository (NMDR; https://www.metabolomicsworkbench.org/data/DRCCDataDeposit.php) | Direct submission allowed, no data analysis tools. | 2788 | 2020 |
| ELISA, ELISPOT, Luminex | ImmPort (53) (https://www.immport.org/) | Immunology-focused, direct submission allowed, rich metadata in relational database, no data analysis tools. | 262, 54, 61 | 2018 |
| Flow Cytometry | ImmPort (53) (https://www.immport.org/) | Immunology-focused, direct submission allowed, rich metadata in relational database, no data analysis tools. | 257 | 2018 |
| | FlowRepository (54) (https://flowrepository.org/) | Direct submission allowed, follows MIFlowCyt standard, endorsed by International Society for Advancement of Cytometry (ISAC), no data analysis tools. | ~2125 | 2012 |
| Imaging | Image Data Resource (55) (IDR; https://idr.openmicroscopy.org/) | Direct submission allowed, handles variety of image types, no data analysis tools. | 127 Studies | 2017 |
| | The Cell (CIL-CCDB) (56): (http://www.cellimagelibrary.org/) | Curated database, no data analysis. | 57 | 2012 |
| | Cancer Imaging Archive (TCIA) (57): (https://www.cancerimagingarchive.net/) | Data de-identified, allows direct submissions, no analysis tools. | N/A | 2013 |
| NGS and array data | Sequence Read Archive (58) (SRA; https://www.ncbi.nlm.nih.gov/sra) | Allows direct submissions of sequencing data, no analysis tools. | N/A | 2007 |
| | Database of Genotypes and Phenotypes (59) (dbGAP; https://www.ncbi.nlm.nih.gov/gap/) | Allows direct submissions of sequencing data, controlled access repository for human genotype/phenotype data. | 309 general use studies ie: sharable according to these (60) terms and nothing else. | 2006 |
| | The Bioinformation and DNA Data Bank of Japan (61) (DDBJ; https://www.ddbj.nig.ac.jp/) | Allows direct submissions of sequencing and array data, provides advanced search functionalities and built-in analysis tools. | 4,250,864,039 Sequences | 1987 |
| | European Nucleotide Archive (62) (ENA; (https://www.ebi.ac.uk/ena) | Allows direct submission of sequencing and data, no data analysis tools. | 4.6 billion Sequences | 1982 |
| | Gene Expression Omnibus (63) (GEO; https://www.ncbi.nlm.nih.gov/geo/) | Allow direct submissions of sequencing and MIAME-compliant array data as well | 4348 | 2000 |

*(Continued)*

TABLE 1 Continued

| *Data Type* | Repository | Key Features | Number of datasets as of May 2024 | Date of establishment |
|---|---|---|---|---|
| | | as processed data, some data analysis tools. | | |
| *Single Cell Sequencing* | Single Cell Portal: (https://singlecell.broadinstitute.org/) | Allows submission of sequencing and processed single cell data files, data visualization and analysis tools. | 670 total studies found | 2018 |
| | Single Cell Expression Atlas (64) (https://www.ebi.ac.uk/gxa/sc/home) | Curated database, data visualization and analysis. | 355 | 2018 |
| *Spatial Transcriptomics* | CROST (65) (https://ngdc.cncb.ac.cn/crost/home) | Curated database, supports different technologies, rich suite of data analysis and visualization tools. | 182 | 2024 |
| | Spatial DB (66) (http://www.spatialomics.org/SpatialDB/) | Curated database, supports different technologies, some data analysis tools. | 24 | |
| | STOmicsDB (67) (https://db.cngb.org/stomics/) | Curated database, allows direct submission, some data visualization and analysis tools. | 228 | |
| | Spatial Omics DataBase (68) (SODB; https://gene.ai.tencent.com/SpatialOmics/) | Curated database, supports different technologies, some data visualization and analysis tools. | 3145 | 2023 |
| | Aquila (69) (https://aquila.cheunglab.org) | Curated database, allows direct submission, some data visualization and analysis tools. | 110 | 2023 |
| *Single Cell Sequencing* | Single Cell Portal (70) (https://singlecell.broadinstitute.org/) | Allows submission of sequencing-based spatial transcriptomic data, data visualization and analysis tools. | 670 total studies found | 2018 |
| *Multi-modal OMICs* | Single Cell Atlas (71) (https://www.singlecellatlas.org/) | Curated database, multiple data types, data visualization and analysis. | NA | 2024 |
| *Generalist* | Zenodo – commercial (https://zenodo.org/) | 50GB dataset limit, any file type, GitHub integration, DOI creation, version control, immediate release, usage statistics. | 1,609 Projects | 2013 |
| | Figshare -commercial: (https://figshare.com/) | 20 GB per user, any file type, DOI creation, version control, private and public release, usage statistics. | N/A | 2012 |
| | BioStudies (72) (https://www.ebi.ac.uk/biostudies/) | Allows the integration of metadata, orphan data, and data found in other EBI databases and link to a paper. | 2,398,047 | 2015 |
| | FAIRDOMHub (33) (https://fairdomhub.org) | Allows the integration of metadata, orphan data, and data found in other databases and link to a paper. | 402 projects | 2017 |

megaprojects such as the UK Biobank (95) and PrecisionFDA (96) who use DNAnexus and the NIH's All of Us Research program (97) that uses Terra (Figure 3). Enticingly for the computational biologists, these platforms also provide impressive compute that scales to increasingly large and complex models, come with customizable and pre-installed pipelines that save researchers hours of set-up time, and automate log generation which allows tracking the analyses done on every dataset together with the parameters used making it easy to trace how results were derived. In addition, some of these platforms support the integration of Jupyter notebooks which, as mentioned above, allow users to run and share their own custom code within those environments and share them when needed.

Less attractive is the price for cloud storage and compute which becomes an ongoing expense liable to immense runaway costs (98), especially at the hands of less experienced users who are the majority at academic institutions today. These costs could be overcome -in part- by better training, negotiating university/funder-wide contracts with cloud platforms, and could be off-set by long-term savings in personnel, maintenance, and upgrades. However, this does leave academics at the mercy of tech oligarchs such as Amazon [providers of AWS (99)], Alphabet [providers of Google Cloud (100)], and Microsoft [providers of Azure (101)]. At the moment, it is also unclear how easy migration between any of these platforms will be if they fail to meet future user needs. That said, competition in the

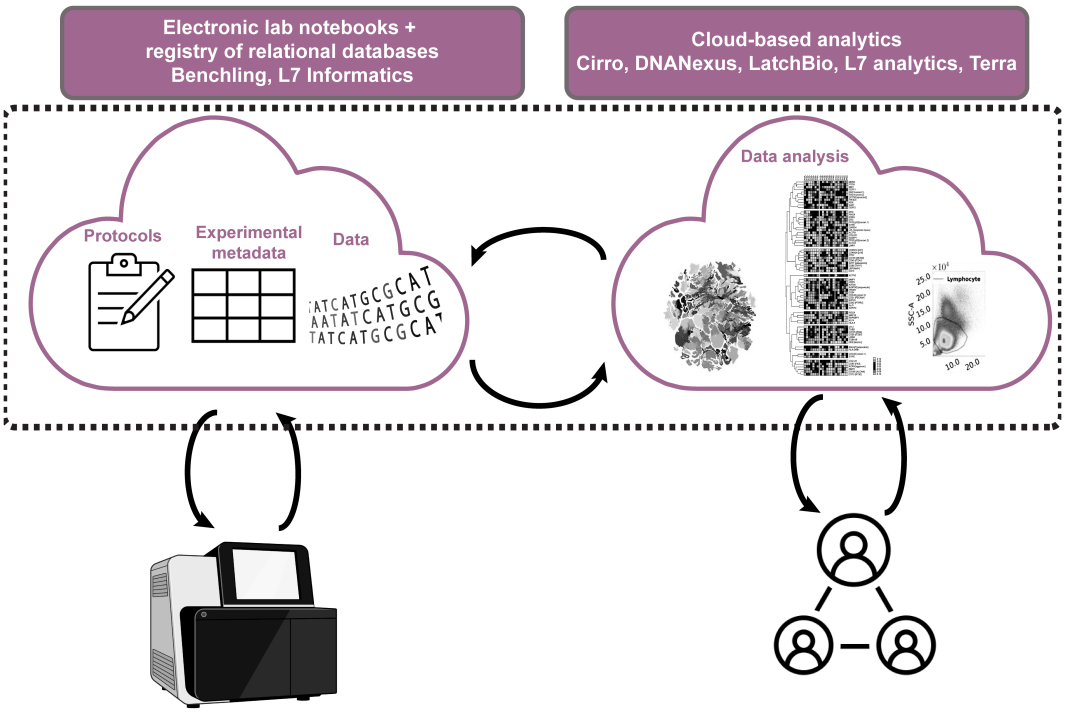


FIGURE 3
Overview of cloud-based infrastructure for digital labs with humans in the loop. Cloud-based electronic documentation systems with registries for animals, samples, reagents, equipment allow facile linking within lab notebooks. This makes experimental protocols transparent and facilitates FAIR metadata and data collection and sharing. Data from lab equipment is imported directly into the registry and can also be linked in lab notebooks saving time and effort, while minimizing human error. Metadata and data can be pushed to cloud computing platforms that allow collaborative and transparent data analysis.

infrastructure-as-a-service space is increasing because of ubiquitous demand across a variety of industries which will hopefully spur technological innovation and push prices down, democratizing access to infrastructure-as-a-service in the long-term.

The development of equally powerful open-source alternatives, continuously developed by and for the research community would be ideal. Unfortunately, funding such efforts is costly requiring a hefty upfront investment from governments or philanthropists and would take years adding more distance between them and their well-developed commercial counterparts. Once developed, long-term sustainability could be possible by licensing that allows free academic/non-profit usage and paid licensing in the case of for-profit entities similar to the Rosetta Commons approach (102).

## Personnel

With the emergence of infrastructure-as-a-service, better ELNs and digital lab management software (also referred to as LIMS), data, compute, and metadata are all now connectable and shareable with relative ease. But the transition to this new model is no easy feat, mostly because of the need for complex and often continuous change management since academic research inherently involves training inexperienced individuals and high turnover.

To facilitate this, the first kind of position universities need to create is that of the Data Officer. This individual outlines university-wide policy, and ensures it aligns with national and international mandates and legal frameworks. Together with the IT officer, they can help coordinate the roll out and adoption of the needed technology for the shift to Digital Labs across the university while vetting different vendors and platforms - all in coordination with Department Data Managers. The latter help roll out these changes within their departments and communicate the importance of FAIR data sharing to researchers of different disciplines, as well as work with them to develop and share best-practices that make FAIR data sharing a natural part of researchers' workflow with the help of enabling infrastructure. They also provide guidance regarding the choice of private storage and public data repositories depending on the types of data generated (eg: sequencing, flow cytometry, imaging), its sensitivity (eg: clinical versus pre-clinical data), and its stage in the research life cycle (pre- *vs* post-publication). On the other hand, the university/department IT officers works on optimizing on premise compute and data storage requirements to adapt to a shift to the cloud. For larger, data-intensive departments, it might be necessary to have lab data managers who work even more closely with the researchers on the day-to-day. That said, buy-in from PIs is absolutely necessary for the success of these efforts and communicating the importance of good data management practices early on in every project is immensely important for labs' long-term success. This is particularly important in academic contexts, where lab turnover is high, and data often pass multiple hands before it ends up in a paper or in the public domain.

10.3389/fimmu.2024.1439434

## Common types of data and their repositories

For systems immunologists in particular and life science researchers in general, some of the most important data types today include multiplexed flow cytometry and CyTOF, Luminex, systems serology [Luminex-based antibody profiling assays (103, 104)], single cell RNASeq, bulk RNASeq data, and imaging data, for which specialized repositories currently exist. For more nascent fields or in the case of orphan datatypes researchers are encouraged to deposit their datasets in generalist repositories, until a dedicated repository is developed (Table 1).

## Considerations for consortia

While the guidelines outlined above are broadly generalizable, they are highly relevant for interdisciplinary academic consortia which are somewhat of a special case for three main reasons: (1) data sharing between labs in almost real-time (as opposed to at the time of publication) is important for consortia to achieve their goals as experimental and biological versus mathematical and computational expertise tend to be distributed, (2) physical samples are often exchanged between labs so tracking sample as well as data provenance at scale is key to data integrity, (3) timely exchange of knowledge requires close communication across

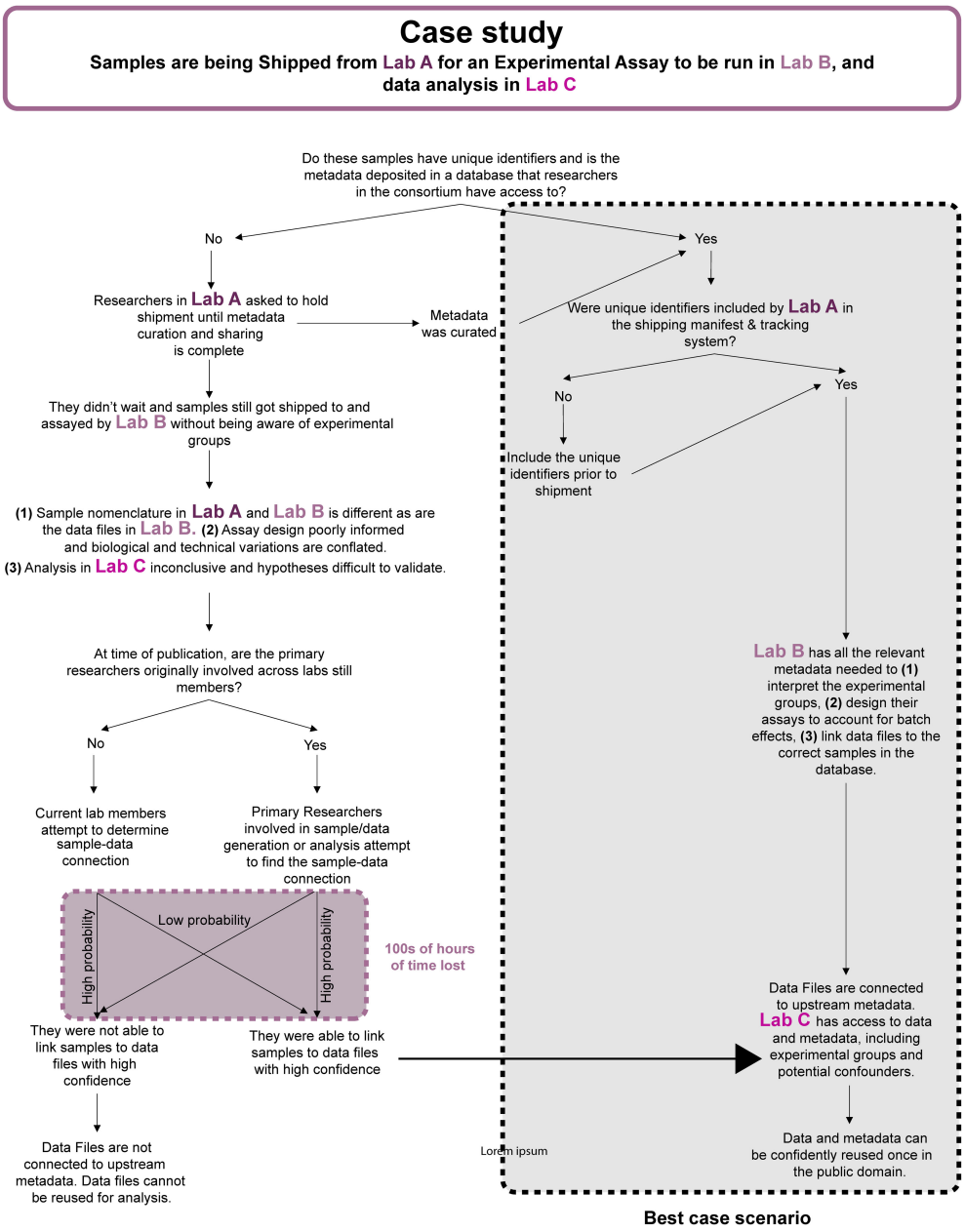


FIGURE 4
Workflow diagram describing how suboptimal practices can affect data integrity, analytical rigor, and waste valuable research time. Suboptimal practices also compromise FAIR data sharing at the end of a study.

disciplines to move project goals forward and course-correct as needed.

To address the first and second point, setting up a unified or at least interoperable, digital infrastructure at the onset is key as it allows members of the consortium to share lab notebooks, reagents, and data. Harmonization and standardization becomes easier to achieve and enforce, and analyses can also be shared. This allows for internal transparency, facilitates collaboration, troubleshooting, and corrections, and ultimately multi-modal data analysis. Eventually, sharing the data and knowledge in the public domain also becomes easier (Figure 4).

Assigning a data officer and data base manager for the consortium is key. Together they need to establish a system that allows centralized sample and data tracking and work with each lab's data manager and/or individual researchers to collate curated data and ensure the accompanying metadata is accurate, standardized, and complete. In instances when access to unified infrastructure is prohibitively expensive, individual components can be strung together. For example, they could set up a shared Dropbox or Google Drive account where all the consortium's curated data is collected until it can be shared in the appropriate repositories. Setting up a local instance of NextSEEK would facilitate metadata collection in a relational database, after researchers fill out easy to use spreadsheet-based templates. Tracking samples shipped between sites can be done using tools such as Qualtrics (105) or Google Forms (106). To facilitate early and accurate collection of metadata about samples, only samples for which unique identifiers and a comprehensive set of metadata has been collected should be shipped to other sites. Data should only be shared when all the metadata is complete, they are uploaded to a repository (privately) or a common drive, and linked in the central database. Recipients can then use the unique identifiers to look up key information about each sample/dataset in the database and find all the necessary metadata. Access to the data before it is public can be decided as needed since considerations may vary depending on project needs or data type and source, eg: human versus non-human sequencing data.

To address the third point, establishing recurrent meetings that bringing together researchers of complementary expertise to discuss experimental design, data analysis, next steps, and synthesize information is important. This helps ensure that the data is analyzed and interpreted in a meaningful way, as well as used to inform the design of appropriate follow-up experiments.

## FAIR data sharing between interdisciplinary teams is critical to the responsible development and deployment of AI

To summarize, the life sciences are on the cusp of a transformation to a data-intense field that requires experimental and computational biologists to work together and make sense of large swaths of data using mechanistic, ML and DL models. This will allow researchers to generate new insights that drive biomedical research forward in ways and at a scale previous not possible. Enabling this involves embracing a collaborative and digital-first mentality to sustain the development of data hungry, unbiased, generalizable models that are helpful to biomedical researchers. We argue that the future of such a transformation involves a shift to the Digital Lab and decentralized FAIR data sharing and compute to enable broader collaboration across disciplines. Despite the complexity of the feat, it is necessary to ensure that data is scrutinized, used, and re-used to the best extent possible, maximizing return on investment in the research enterprise for the benefit of all.

## Author contributions

DM: Conceptualization, Data curation, Investigation, Project administration, Supervision, Visualization, Writing – original draft, Writing – review & editing. JL: Investigation, Writing – review & editing. CD: Visualization, Writing – review & editing. NE: Data curation, Investigation, Writing – review & editing. CW: Writing – review & editing. MG: Writing – review & editing. DL: Supervision, Writing – review & editing. SF: Conceptualization, Supervision, Writing – review & editing. SL: Conceptualization, Supervision, Writing – review & editing, Writing – original draft.

## Funding

The author(s) declare financial support was received for the research, authorship, and/or publication of this article. All authors are funded in whole or in part with Federal funds from the National Institute of Allergy and Infectious Diseases, National Institutes of Health, Department of Health and Human Services, under Contract No. 75N93019C00071.

## Acknowledgments

We would like to thank the teams at Benchling, Cirro, LatchBio, and Terra for insightful discussions and clarifications relating to their platforms.

## Conflict of interest

The authors declare that the research was conducted in the absence of any commercial or financial relationships that could be construed as a potential conflict of interest.

## Publisher's note

# References


1. Wilkinson MD, Dumontier M, Aalbersberg J, Appleton G, Axton M, Baak A, et al. The FAIR Guiding Principles for scientific data management and stewardship. *Sci Data*. (2016) 3:160018. doi: 10.1038/sdata.2016.18

2. Tiku N, Schaul K, Chen SY. *These fake images reveal how AI amplifies our worst stereotypes. Washington Post*. Available online at: https://www.washingtonpost.com/technology/interactive/2023/ai-generated-images-bias-racism-sexism-stereotypes/ (Accessed May 20, 2024).

3. Metz C. OpenAI unveils new chatGPT that listens, looks and talks. *New York Times*. (2024).

4. Jumper J, Evans R, Pritzel A, Green T, Figurnov M, Ronneberger O, et al. Highly accurate protein structure prediction with AlphaFold. *Nature*. (2021) 596:583–9. doi: 10.1038/s41586-021-03819-2

5. Jumper J, Hassabis D. The protein structure prediction revolution and its implications for medicine: 2023 albert lasker basic medical research award. *JAMA*. (2023) 330:1425–6. doi: 10.1001/jama.2023.17095

6. *All Nobel Prizes 2024*. NobelPrize.org. Available online at: https://www.nobelprize.org/all-nobel-prizes-2024/ (Accessed December 13, 2024).

7. *Index of /pub/databases/uniprot/previous_releases/release-2020_01/uniref*. Available online at: https://ftp.ebi.ac.uk/pub/databases/uniprot/previous_releases/release-2020_01/uniref/ (Accessed May 2, 2024).

8. Steinegger S, Johannes. BFD. Available online at: https://bfd.mmseqs.com/ (Accessed May 2, 2024).

9. Mirdita M, von den Driesch L, Galiez C, Martin MJ, S ding J, Steinegger M. Uniclust databases of clustered and deeply annotated protein sequences and alignments. *Nucleic Acids Res*. (2017) 45:D170–6. doi: 10.1093/nar/gkw1081

10. Richardson L, Allen B, Baldi G, Beracochea M, Bileschi ML, Burdett T, et al. MGnify: the microbiome sequence data analysis resource in 2023. *Nucleic Acids Res*. (2023) 51:D753–9. doi: 10.1093/nar/gkac1080

11. Berman HM, Westbrook J, Feng Z, Gilliland G, Bhat TN, Weissig H, et al. The protein data bank. *Nucleic Acids Res*. (2000) 28:235–42. doi: 10.1093/nar/28.1.235

12. Chowdhury R, Bouatta N, Biswas S, Floristean C, Kharkar A, Roy K, et al. Single-sequence protein structure prediction using language models and deep learning. *Nat Biotechnol*. (2022) 40:1617–23. doi: 10.1038/s41587-022-01432-w

13. Polonsky K, Pupko T, Freund NT. Evaluation of the ability of alphaFold to predict the three-dimensional structures of antibodies and epitopes. *J Immunol*. (2023) 211:1578–88. doi: 10.4049/jimmunol.2300150

14. Varadi M, Anyango S, Deshpande M, Nair S, Natassia C, Yordanova G, et al. AlphaFold Protein Structure Database: massively expanding the structural coverage of protein-sequence space with high-accuracy models. *Nucleic Acids Res*. (2022) 50:D439–44. doi: 10.1093/nar/gkab1061

15. Google Deep Mind. (2024). Available online at: https://deepmind.google/technologies/alphafold/ (Accessed January 3, 2024).

16. Varadi M, Velankar S. The impact of AlphaFold Protein Structure Database on the fields of life sciences. *Proteomics*. (2023) 23:e2200128. doi: 10.1002/pmic.202200128

17. Hadfield J, Megill C, Bell SM, Huddleston J, Potter B, Callender C, et al. Nextstrain: real-time tracking of pathogen evolution. *Bioinformatics*. (2018) 34:4121–3. doi: 10.1093/bioinformatics/bty407

18. Chen L. *What Works to Control COVID-19? Econometric Analysis of a Cross-Country Panel*. (2020).

19. Scottish Government. Coronavirus (COVID-19) Scotland's Strategic Framework update – February 2022: evidence paper. (2022). Available online at: https://www.gov.scot/publications/evidence-paper-accompany-coronavirus-covid-19-scotlands-strategic-framework-update-february-2022/ (Accessed May 8, 2024).

20. World Health Organization. *Genomic Sequencing of SARS-CoV-2: A Guide to Implementation for Maximum Impact on Public Health, 8 January 2021*. World Health Organization (2021). Available online at: https://www.who.int/publications/i/item/9789240018440 (Accessed May 2, 2024).

21. Karmarkar EN, Blanco I, Amornkul PN, DuBois A, Deng X, Moonan PK, et al. Timely intervention and control of a novel coronavirus (COVID-19) outbreak at a large skilled nursing facility—San Francisco, California, 2020. *Infect Control Hosp. Epidemiol*. (2021) 42:1173–80. doi: 10.1017/ice.2020.1375

22. Bennett H, Stewart-Jones G, Narayanan E, Carfi A, Metkar M, Presnyak V, et al. *Coronavirus RNA vaccines and methods of use. World Intellectual Property Organization*. Cambridge University Press. (2020). WO2021159130A2.

23. *doi Handbook*. Available online at: https://www.doi.org/doi-handbook/HTML/index.html (Accessed May 8, 2024).

24. Torralba A, Efros AA. (2011). Unbiased look at dataset bias, in: *CVPR 2011*, IEEE. pp. 1521–8. doi: 10.1109/CVPR.2011.5995347

25. *NOT-OD-21-013: Final NIH Policy for Data Management and Sharing*. Available online at: https://grants.nih.gov/grants/guide/notice-files/NOT-OD-21-013.html (Accessed May 9, 2024).

26. National Science Foundation. Preparing Your Data Management Plan - Funding at NSF. (2024). Available online at: https://new.nsf.gov/funding/data-management-plan (Accessed May 8, 2024).

27. The White House. *OSTP Issues Guidance to Make Federally Funded Research Freely Available Without Delay | OSTP*. The White House (2022). Available online at: https://www.whitehouse.gov/ostp/news-updates/2022/08/25/ostp-issues-guidance-to-make-federally-funded-research-freely-available-without-delay/ (Accessed May 8, 2024).

28. Bill & Melinda Gates Foundation. *Data Sharing Requirements*. Gates Open Access Policy. Available online at: https://openaccess.gatesfoundation.org/how-to-comply/data-sharing-requirements/ (Accessed May 8, 2024).

29. Chan Zuckerberg Initiative. *Funding Scientific Research and Building Transformative Technologies*. Chan Zuckerberg Initiative. (2024). Available online at: https://chanzuckerberg.com/science/our-values-approach/.

30. Wellcome. Data, software and materials management and sharing policy - Grant Funding. (2025). Available online at: https://wellcome.org/grant-funding/guidance/policies-grant-conditions/data-software-materials-management-and-sharing-policy (Accessed January 3, 2025).

31. European Comission. Open Data, Software and Code Guidelines. Open Research Europe. Available online at: https://open-research-europe.ec.europa.eu/for-authors/data-guidelines (Accessed May 9, 2024).

32. Pradhan D, Ding H, Zhu J, Engelward BP, Levine SS. NExtSEEK: extending SEEK for active management of interoperable metadata. *J Biomolecular Techniques*. (2022) 33. doi: 10.7171/3fc1f5fe.db404124

33. Wolstencroft K, Krebs O, Snoep JL, Stanford NJ, Bacall F, Golebiewski MG, et al. FAIRDOMHub: a repository and collaboration environment for sharing systems biology research. *Nucleic Acids Res*. (2017) 45:D404–7. doi: 10.1093/nar/gkw1032

34. Foster ED, Deardorff A. Open science framework (OSF). *J Med Libr Assoc*. (2017) 105:203–6. doi: 10.5195/jmla.2017.88

35. *The Hyve*. Available online at: https://thehyve.nl/services (Accessed May 9, 2024).

36. *cBioPortal for Cancer Genomics*. Available online at: https://www.cbioportal.org/ (Accessed May 9, 2024).

37. Cerami E, Gao J, Dogrusoz U, Gross BE, Sumer SO, Aksoy BA, et al. The cBio cancer genomics portal: an open platform for exploring multidimensional cancer genomics data. *Cancer Discovery*. (2012) 2:401–4. doi: 10.1158/2159-8290.CD-12-0095

38. Izzo F, Myers RM, Ganesan S, Mekerishvili L, Kottapalli S, Prieto T, et al. Mapping genotypes to chromatin accessibility profiles in single cells. *Nature*. (2024) 629:1149–57. doi: 10.1038/s41586-024-07388-y

39. Lance C, Luecken MD, Burkhardt DB, Cannoodt R, Rautenstrauch P, Laddach A, et al. (2022). Multimodal single cell data integration challenge: Results and lessons learned, in: *Proceedings of the NeurIPS 2021 Competitions and Demonstrations Track*, PMLR. pp. 162–76. Available online at: https://proceedings.mlr.press/v176/lance22a.html.

40. Boehm KM, Aherne EA, Ellenson L, Nikolovski I, Alghamdi M, Vázquez-García IV. Multimodal data integration using machine learning improves risk stratification of high-grade serous ovarian cancer. *Nat Cancer*. (2022) 3:723–33. doi: 10.1038/s43018-022-00388-9

41. Rajendran S, Pan W, Sabuncu MR, Chen Y, Zhou J, Wang F, et al. Learning across diverse biomedical data modalities and cohorts: Challenges and opportunities for innovation. *Patterns (N Y)*. (2024) 5:100913. doi: 10.1016/j.patter.2023.100913

42. Miotto R, Wang F, Wang S, Jiang X, Dudley JT. Deep learning for healthcare: review, opportunities and challenges. *Brief Bioinform*. (2017) 19:1236–46. doi: 10.1093/bib/bbx044

43. Lipkova J, Chen RJ, Chen B, Lu MY, Barbieri M, Shao D, et al. Artificial intelligence for multimodal data integration in oncology. *Cancer Cell*. (2022) 40:1095–110. doi: 10.1016/j.ccell.2022.09.012

44. *NIH Common Data Elements (CDE) Repository*. Available online at: https://cde.nlm.nih.gov/home (Accessed May 17, 2024).

45. Williams CG, Lee HJ, Asatsuma T, Vento-Tormo R, Haque A. An introduction to spatial transcriptomics for biomedical research. *Genome Med*. (2022) 14:68. doi: 10.1186/s13073-022-01075-1

46. Perez-Riverol Y, Bai J, Bandla C, Garc a-Seisdedos D, Hewapathirana S, Kamatchinathan Selvakumar, et al. The PRIDE database resources in 2022: a hub for mass spectrometry-based proteomics evidences. *Nucleic Acids Res*. (2022) 50:D543–52. doi: 10.1093/nar/gkab1038

47. Choi M, Carver J, Chiva C, Tzouros M, Huang T, Tsai Tsung-Heng, et al. MassIVE.quant: a community resource of quantitative mass spectrometry–based proteomics datasets. *Nat Methods*. (2020) 17:981–4. doi: 10.1038/s41592-020-0955-0

48. Deutsch EW, Lam H, Aebersold R. PeptideAtlas: a resource for target selection for emerging targeted proteomics workflows. *EMBO Rep*. (2008) 9:429–34. doi: 10.1038/embor.2008.56

49. Sharma V, Eckels J, Taylor GK, Shulman NJ, Stergachis AB, Joyner SA, et al. Panorama: A targeted proteomics knowledge base. *J Proteome Res*. (2014) 13:4205–10. doi: 10.1021/pr5006636

50. Chen T, Ma J, Liu Y, Chen Zhiguang, Xiao N, Lu Yutong, et al. iProX in 2021: connecting proteomics data sharing with big data. *Nucleic Acids Res*. (2022) 50:D1522–7. doi: 10.1093/nar/gkab1081

51. Moriya Y, Kawano S, Okuda Shujiro, Watanabe Y, Matsumoto M, Takami T, et al. The jPOST environment: an integrated proteomics data repository and database. *Nucleic Acids Res*. (2019) 47:D1218–24. doi: 10.1093/nar/gky899

52. Yurekten O, Payne T, Tejera N, Amaladoss FX, Martin C, Williams M, et al. MetaboLights: open data repository for metabolomics. *Nucleic Acids Res*. (2024) 52: D640–6. doi: 10.1093/nar/gkad1045

53. Bhattacharya S, Dunn P, Thomas CG, Smith B, Schaefer H, Chen J, et al. ImmPort, toward repurposing of open access immunological assay data for translational and clinical research. *Sci Data*. (2018) 5:180015. doi: 10.1038/sdata.2018.15

54. Spidlen J, Breuer K, Rosenberg C, Kotecha N, Brinkman RR. FlowRepository: a resource of annotated flow cytometry datasets associated with peer-reviewed publications. *Cytometry A*. (2012) 81:727–31. doi: 10.1002/cyto.a.v81a.9

55. Williams E, Moore J, Li SW, Rustici G, Tarkowska A, Chessel A, et al. Image Data Resource: a bioimage data integration and publication platform. *Nat Methods*. (2017) 14:775–81. doi: 10.1038/nmeth.4326

56. Orloff DN, Iwasa JH, Martone ME, Ellisman MH, Kane CM. The cell: an image library-CCDB: a curated repository of microscopy data. *Nucleic Acids Res*. (2013) 41: D1241–1250. doi: 10.1093/nar/gks1257

57. Clark K, Vendt B, Smith K, Freymann J, Kirby J, Koppel P, et al. The cancer imaging archive (TCIA): maintaining and operating a public information repository. *J Digit Imaging*. (2013) 26:1045–57. doi: 10.1007/s10278-013-9622-7

58. Leinonen R, Sugawara H, Shumway M. The sequence read archive. *Nucleic Acids Res*. (2011) 39:D19–21. doi: 10.1093/nar/gkq1019

59. Mailman MD, Feolo M, Jin Y, Kimura M, Tryka K, Bagoutdinov R, et al. The NCBI dbGaP database of genotypes and phenotypes. *Nat Genet*. (2007) 39:1181–6. doi: 10.1038/ng1007-1181

60. NIH. *DBGAP data use certification agreement*. dbgap.ncbi.nlm.nih.gov. Available online at: https://dbgap.ncbi.nlm.nih.gov/aa/wga.cgi?page=DUC&view_pdf&stacc=phs000688.v1.p1.

61. Ara T, Kodama Y, Tokimatsu T, Fukuda A, Kosuge T, Mashima J, et al. DDBJ update in 2023: the MetaboBank for metabolomics data and associated metadata. *Nucleic Acids Res*. (2023) 52:D67–71. doi: 10.1093/nar/gkad1046

62. Burgin J, Ahamed A, Cummins C, Devraj R, Gueye K, Gupta D, et al. The european nucleotide archive in 2022. *Nucleic Acids Res*. (2022) 51:D121–5. doi: 10.1093/nar/gkac1051

63. National Center for Biotechnology Information- NCBI. NCBI GEO: archive for functional genomics data sets–update. Available online at: https://pubmed.ncbi.nlm.nih.gov/23193258/ (Accessed May 10, 2024).

64. Papatheodorou I, Moreno P, Manning J, Fuentes AM-P, George N, Fexova S, et al. Expression Atlas update: from tissues to single cells. *Nucleic Acids Res*. (2020) 48: D77–83. doi: 10.1093/nar/gkz947

65. Wang G, Wu S, Xiong Z, Qu H, Fang X, Bao Y. CROST: a comprehensive repository of spatial transcriptomics. *Nucleic Acids Res*. (2024) 52:D882–90. doi: 10.1093/nar/gkad782

66. Fan Z, Chen R, Chen X. SpatialDB: a database for spatially resolved transcriptomes. *Nucleic Acids Res*. (2020) 48:D233–7. doi: 10.1093/nar/gkz934

67. Xu Z, et al. STOmicsDB: a comprehensive database for spatial transcriptomics data sharing, analysis and visualization. *Nucleic Acids Res*. (2023) 52:D1053–61.

68. Yuan Z, Pan W, Zhao X, Zhao F, Xu Z, Li X, et al. SODB facilitates comprehensive exploration of spatial omics data. *Nat Methods*. (2023) 20:387–99. doi: 10.1038/s41592-023-01773-7

69. Zheng Y, Chen Y, Ding X, Wong KH, Cheung E. Aquila: a spatial omics database and analysis platform. *Nucleic Acids Res*. (2023) 51:D827–34. doi: 10.1093/nar/gkac874

70. Tarhan L, Bistline J, Chang J, Galloway B, Hanna E, Weitz E. Single Cell Portal: an interactive home for single-cell genomics data. *bioRxiv*. (2023). doi: 10.1101/2023.07.13.548886

71. Pan L, Parini P, Tremmel R, Loscalzo J, Lauschke VM, Maron BA, et al. Single Cell Atlas: a single-cell multi-omics human cell encyclopedia. *Genome Biol*. (2024) 25:104. doi: 10.1186/s13059-024-03246-2

72. Sarkans U, Gostev M, Athar A, Behrangi E, Melnichuk O, Ali A, et al. The BioStudies database-one stop shop for all data supporting a life sciences study. *Nucleic Acids Res*. (2018) 46:D1266–70. doi: 10.1093/nar/gkx965

73. Schoch CL, Ciufo S, Domrachev M, Hotton CL, Kannan S, Khovanskaya R, et al. NCBI Taxonomy: a comprehensive update on curation, resources and tools. *Database (Oxford)*. (2020), 2020 baaa062. doi: 10.1093/database/baaa062

74. ISO. *ISO 3166 — Country Codes*. ISO. Available online at: https://www.iso.org/iso-3166-country-codes.html (Accessed May 11, 2024).

75. UniProt Consortium. UniProt: the universal protein knowledgebase in 2023. *Nucleic Acids Res*. (2022) 51:D523–31. doi: 10.1093/nar/gkac1052

76. *Free Online Spreadsheet Software: Excel | Microsoft 365*. Available online at: https://www.microsoft.com/en-us/microsoft-365/excel (Accessed May 9, 2024).

77. *Google Sheets: Online Spreadsheet Editor | Google Workspace*. Available online at: https://www.facebook.com/GoogleDocs/ (Accessed May 9, 2024).

78. *Prism - GraphPad*. Available online at: https://www.graphpad.com/features (Accessed May 9, 2024).

79. Ewels PA, Peltzer A, Fillinger S, Patel H, Alneberg J, Wilm A, et al. The nf-core framework for community-curated bioinformatics pipelines. *Nat Biotechnol*. (2020) 38:276–8. doi: 10.1038/s41587-020-0439-x

80. *Docker: Accelerated Container Application Development* (2022). Available online at: https://www.docker.com/ (Accessed May 10, 2024).

81. *Introduction to Singularity — Singularity container 3.5 documentation*. Available online at: https://docs.sylabs.io/guides/3.5/user-guide/introduction.html (Accessed May 10, 2024).

82. *Docker Hub Container Image Library | App Containerization*. Available online at: https://hub.docker.com/ (Accessed May 10, 2024).

83. Grüning B, Dale R, Sjödin A, Chapman BA, Rowe J, Tomkins-Tinch CH, et al. Bioconda: sustainable and comprehensive software distribution for the life sciences. *Nat Methods*. (2018) 15:475–6. doi: 10.1038/s41592-018-0046-7

84. JupyterLab. (2024). Available online at: https://github.com/jupyterlab/jupyterlab (Accessed May 10, 2024).

85. Rstudio. (2024). Available online at: https://github.com/rstudio/rstudio (Accessed May 10, 2024).

86. GitHub. GitHub: Let s build from here. (2024). Available online at: https://github.com/ (Accessed May 10, 2024).

87. Malik-Sheriff RS, Glont M, Nguyen TVN, Tiwari K, Roberts MG, Xavier A, et al. BioModels-15 years of sharing computational models in life science. *Nucleic Acids Res*. (2020) 48:D407–15. doi: 10.1093/nar/gkz1055

88. *Hugging Face – The AI community building the future* (2024). Available online at: https://huggingface.co/ (Accessed May 10, 2024).

89. Benchling. *Cloud-based platform for biotech R&D*. Benchling. (2024). Available online at: https://www.benchling.com/ (Accessed May 11, 2024).

90. L7 Informatics. *Home*. L7 Informatics. Available online at: https://l7informatics.com/ (Accessed May 11, 2024).

91. Zager MA. *Cirro | Data Science Simplified*. Available online at: https://cirro.bio/./ (Accessed May 14, 2024).

92. DNAnexus®. *The Precision Health Data Cloud*. DNAnexus®. Available online at: https://www.dnanexus.com (Accessed May 11, 2024).

93. LatchBio. *LatchBio*. LatchBio. (2024). Available online at: https://latch.bio (Accessed May 11, 2024).

94. *Terra*. Available online at: https://app.terra.bio/ (Accessed May 14, 2024).

95. *Learn more about UK Biobank* (2023). Available online at: https://www.ukbiobank.ac.uk/learn-more-about-uk-biobank (Accessed May 14, 2024).

96. *precisionFDA - Overview*. Available online at: https://precision.fda.gov/ (Accessed May 14, 2024).

97. National Institutes of Health - NIH. *All of Us Research Program | National Institutes of Health (NIH). Research Program*. (2020). Available online at: https://allofus.nih.gov/future-health-begins-all-us (Accessed May 11, 2024).

98. Monica J. *Runaway Cost – Navigating the Cloud*. Thinkwgroup (2024). Available online at: https://www.thinkwgroup.com/runaway-cost/ (Accessed May 15, 2024).

99. Amazon Web Services, Inc. *Cloud Computing Services - Amazon Web Services (AWS)*. Amazon Web Services, Inc. (2024). Available online at: https://aws.amazon.com/ (Accessed May 11, 2024).

100. *Cloud Computing Services*. Google Cloud. Available online at: https://cloud.google.com/.

101. Microsoft Azure. *Cloud Computing Services*. (2024). Available online at: https://azure.microsoft.com/en-us (Accessed May 11, 2024).

102. FAQ. *RosettaCommons*. Available online at: https://www.rosettacommons.org/about/faqfaq4 (Accessed May 14, 2024).

103. Ackerman ME, Moldt B, Wyatt RT, Dugast AS, McAndrew E, Tsoukas S, et al. A robust, high-throughput assay to determine the phagocytic activity of clinical antibody samples. *J Immunol Methods*. (2011) 366:8–19. doi: 10.1016/j.jim.2010.12.016

104. Brown EP, Dowell KG, Boesch AW, Normandin E, Mahan AE, Chu T, et al. Multiplexed Fc array for evaluation of antigen-specific antibody effector profiles. *J Immunol Methods*. (2017) 443:33–44. doi: 10.1016/j.jim.2017.01.010

105. Qualtrics. Qualtrics XM - Experience Management Software. (2024). Available online at: https://www.qualtrics.com/ (Accessed May 11, 2024).

106. Workspace G. *Google Forms: Online Form Builder for Business*. Google Workspace. Available online at: https://workspace.google.com/products/forms/.

# Frontiers in Immunology

**Explores novel approaches and diagnoses to treat immune disorders.**

The official journal of the International Union of Immunological Societies (IUIS) and the most cited in its field, leading the way for research across basic, translational and clinical immunology.

## Discover the latest Research Topics

See more →


**Frontiers**

Avenue du Tribunal-Fédéral 34
1005 Lausanne, Switzerland
frontiersin.org

**Contact us**

+41 (0)21 510 17 00
frontiersin.org/about/contact